

BULGARIAN CHEMICAL COMMUNICATIONS

2014 Volume 46 / Number 4

*Journal of the Chemical Institutes
of the Bulgarian Academy of Sciences
and of the Union of Chemists in Bulgaria*

Catalytic synthesis of bis-2,3-dihydroquinazolin-4(1*H*)-ones and 2,3-dihydroquinazolin-4 (1*H*)-ones derivatives with the aid of silica-supported Preyssler nanoparticles (SPNP)

A. Gharib^{1,2*}, L. Vojdanifard³, N. Noroozi Pesyan⁴, B. R. Hashemi Pour Khorasani², M. Jahangir¹, M. Roshani¹

¹Department of Chemistry, Islamic Azad University, Mashhad, IRAN

²Agricultural Researches and Services Center, Mashhad, IRAN

³Education Ministry, Education Organization of Razavi Khorasan, Mashhad, IRAN

⁴Department of Chemistry, Faculty of Science, Urmia University, 57159 Urmia, IRAN

Received February 13, 2013; Revised July 8, 2013

One-pot three-component condensation of isatoic anhydride with primary amines or ammonium carbonate and aromatic aldehydes in refluxing ethanol in the presence of catalytic amounts of silica-supported Preyssler nanoparticles (SPNP) afforded the corresponding 2,3-dihydroquinazolin-4(1*H*)-ones in high yields. Bis-dihydroquinazolinones were synthesized for the first time by a novel pseudo five-component condensation of isatoic anhydride, a primary amine, and a dialdehyde in water. The catalyst is reusable and can be applied several times without any decrease in product yield.

Keywords: Silica-supported Preyssler nanoparticles (SPNP), Heteropolyacid, 2,3-dihydroquinazolin-4(1*H*)-ones, Bisdihydroquinazolinones, Nanocatalyst, Isatoic anhydride

INTRODUCTION

One-pot transformations, particularly multi-component reactions (MCRs) are of current interest to organic chemists [1]. Since the first MCR reported in 1850 by Strecker [2], this methodology has emerged as an especially attractive synthetic strategy for rapid and efficient library generation due to the fact that the products are formed in a single step and diversity can be achieved simply by varying the reaction components. MCRs leading to interesting heterocyclic scaffolds are particularly useful for the creation of diverse chemical libraries of drug-like molecules for biological screening [3]. 2,3-Dihydroquinazolinone derivatives are an important class of fused heterocycles that display a wide range of biological, pharmacological, and medicinal properties involving antitumor, antibiotic, antipyretic, analgesic, antihypertonic, diuretic, antihistamine, antidepressant, and vasodilating activities [4]. In addition, 2,3-dihydroquinazolinones have been shown to act as potent tubulin inhibitors with impressive antiproliferative activity against several human cancer cell lines [5]. Furthermore, these compounds can act analogously to the antimitotic agent colchicine [6].

Additionally, these compounds can easily be

oxidised to their quinazolin-4(3*H*)-one analogues [7], which are important biologically active heterocyclic compounds [8]. The usual procedure for the preparation of 2,3-dihydroquinazolin-4(1*H*)-ones involves condensation of the appropriate derivatives of anthranilamide with an aldehyde or ketone using *p*-toluenesulfonic acid as a catalyst under vigorous conditions [9]. Similar reactions have been reported to proceed under basic conditions [10]. This procedure affords dihydroquinazolinones in good yields, but requires long reaction times. The three step synthesis starting from isatoic anhydride or anthranilic acid has been reported [11] and other methods such as reductive cyclisation of *o*-nitrobenzamides with aldehydes and ketones [12], reaction of isatoic anhydride with Schiff bases [13], and reduction of quinazolin-4(3*H*)-ones [14] are also reported for the synthesis of these compounds. Due to the unique properties of nanoparticles along with their novel properties and potential applications in different fields [14], the synthesis and characterization of catalysts with lower dimensions has become an active topic of research over the last decade. As the particle size decreases, the relative number of surface atoms increases, and thus activity increases. Moreover, due to quantum size effects, nanometer-sized particles may exhibit unique properties for a wide range of applications [15]. Along this line, polyoxometalates (POMs) are attracting much attention as building blocks for functional

* To whom all correspondence should be sent:
E-mail: aligharib5@yahoo.com

composite materials because of their interesting nanosized structures [16]. They are ideal models for the construction of hybrid systems, so they are regarded as potential candidates to be transformed into nanometer-sized materials. In recent years, considerable effort has been devoted to the design and controlled fabrication of nanostructured POMs for using in green reactions. This interest has resulted in the development of numerous protocols for the synthesis of nanostructured materials over a range of sizes. Therefore, the field of nano POMs and their applications continues to attract significant attention, so the number of publications and patents continue to grow, and new researchers are entering the field. Thus, plenty of room exists for expanding the exploration of the opportunities for these materials and further exploring, so developing new POMs is still a challenge for POM chemistry. However, in spite of extensive investigations on the synthesis and characterization of Keggin-type nanocatalysts [17], the synthesis of sodium 30-tungstophosphate nanocatalysts has been largely overlooked. A Preyssler acid is a highly acidic catalyst with excellent catalytic activity in a variety of acid catalyzed reactions [18,19]. The catalyst consists of an anion with a formula of $[\text{NaP}_5\text{W}_{30}\text{O}_{110}]^{14-}$ which has unusual five-fold symmetry achieved by fusion of five $\{\text{PW}_6\text{O}_{22}\}$ groups. The central sodium ion is not lying on the equator of the anion but in a plane roughly defined by oxygen atoms of the phosphate groups. The presence of the sodium cation reduces the overall anion symmetry from D5h to C5v [20]. Silica-supported Preyssler nano structures were obtained through a micro emulsion method. Although this procedure has been reported previously, this method has never been reported for the synthesis of Preyssler nano structures with different morphologies.

EXPERIMENTAL

Instrument and chemical materials

All materials were of commercial quality and were used as received. The products purity was determined by GC-MS analysis. Mass spectra were recorded on a Shimadzu QP 1100 BX mass spectrometer. Elemental analysis was performed using an Electrothermal 9100 apparatus. IR spectra were recorded in KBr pellets on a Shimadzu IR-470 spectrophotometer. ¹H and ¹³C NMR spectra were determined on a Bruker 300 DRX Avance instrument at 300 MHz.

General procedure

Catalyst Preparation. Supported heteropolyacid catalyst was synthesized according to the literature [21] using a support in powder form (SiO₂) with an aqueous solution of the heteropolyacids. After stirring the mixture, the solvent was evaporated, dried at 120°C and calcined at 250°C in a furnace prior to use. Silica-supported Preyssler nano structures were obtained by the microemulsion method [22].

Synthesis of 2,3-dihydroquinazolin-4(1H)-ones. Silica-supported Preyssler nanoparticles heteropolyacid catalyst (SPNP) (0.03 mmol), isatoic anhydride (1 mmol), primary amine or ammonium acetate (1.1 mmol), and aromatic aldehyde (1 mmol) were added to 5 mL of water or ethanol and the mixture was stirred in a round-bottomed flask under reflux for the appropriate time (see Tables 1, 2). After completion of the reaction, which was confirmed by TLC (eluent: n-hexane/ethyl acetate: 2/1), the water was decanted, hot ethanol (5 mL) was added to the residue which was then filtered. The resulting solution was condensed under reduced pressure. Finally the crude product was filtered, and recrystallized from ethanol.

Selected spectroscopic data:

3-Ethyl-2,3-dihydro-2-(4-hydroxyphenyl)quinazolin-4(1H)-one (4c):

IR (KBr, cm⁻¹): 3440, 1680. δ_{H} (300 MHz, CDCl₃, δ /ppm): 1.00 (t, J = 7.1 Hz, 3 H, CH₃), 2.85 (dq, J = 13.6, 7.0 Hz, 1 H, CH), 3.73 (dq, J = 13.6, 7.2 Hz, 1 H, CH), 5.73 (d, J = 1.9 Hz, 1 H, CH), 6.67 (m, 4 H, ArH), 7.14 (m, 3 H, ArH), 7.24 (d, J = 1.9 Hz, 1 H, NH), 7.64 (dd, J = 7.6, 1.4 Hz, 1 H, ArH), 9.45 (s, 1 H, OH). δ_{C} (300 MHz, CDCl₃, δ /ppm): 14.5, 71.7, 115.8, 116.4, 116.7, 118.6, 128.9, 129.5, 133.0, 134.4, 148.2, 159.2, 163.3. Anal. Calcd for C₁₆H₁₆N₂O₂: C 72.31, H 4.62, N 9.91%; Found C 72.22, H 4.71, N 9.82%; HRMS (EI) Calcd. for C₁₆H₁₆N₂O₂ [M]⁺, 343.1003, Found 343.1008;

2-(4-nitrophenyl)-3-propyl-2,3-dihydroquinazolin-4(1H)-one (4i):

IR (KBr, cm⁻¹): 3420, 1680. δ_{H} (300 MHz, CDCl₃) 0.94 (t, J = 7.3 Hz, 3 H, CH₃), 1.65 (m, 2 H, CH₂), 2.79 (ddd, J = 14.1, 8.6, 5.8 Hz, 1 H, CH), 4.09 (ddd, J = 13.9, 8.7, 6.6 Hz, 1 H, CH), 5.86 (s, 1 H, CH), 7.35 (m, 8 H, ArH). δ_{C} (300 MHz, CDCl₃) 12.7, 22.4, 48.1, 71.6, 116.1, 117.5, 120.9, 125.4, 128.6, 129.5, 134.9, 145.5, 148.4, 149.3, 164.2. Anal. Calcd for C₁₇H₁₇N₃O₃: C, 65.63; H, 5.52; N, 13.56. Found: C, 65.52; H, 5.45; N, 13.49. HRMS

(EI) Calcd. for $C_{17}H_{17}N_3O_3$ $[M]^+$, 311.1002, Found 311.1005;

2-(4-chlorophenyl)-3-(4-isopropylphenyl)-2,3-dihydroquinazolin-4(1H)-one (4k):

IR (KBr, cm^{-1}): 3427, 3280, 2964, 1645, 1513, 1393, 1325, 1242, 990, 8825, 755; δ_H (300 MHz, DMSO- d_6) 7.96 (1H, d, $J=8.4$ Hz), 7.75 (1H, d, $J=6.9$ Hz), 7.64 (1H, d, $J=2.4$ Hz), 7.57 (1H, d, $J=8.4$ Hz), 7.26 (7H, m), 6.73 (2H, m), 6.27 (1H, d, $J=2.4$ Hz), 2.87 (1H, m), 1.18 (6H, d, $J=6.9$ Hz); δ_C (300 MHz, DMSO- d_6) 162.1, 146.2, 139.7, 138.5, 133.8, 132.8, 130.3, 128.9, 128.4, 127.2, 126.6, 121.5, 117.7, 115.4, 114.6, 71.7, 32.9, 23.9; HRMS (EI) Calcd. for $C_{23}H_{21}ClN_2O$ $[M]^+$, 376.1000, Found 376.1006; Anal. Calcd for $C_{23}H_{21}ClN_2O$ C 73.30, H 5.62, N 7.43%; Found C 73.11, H 5.42, N 7.31%;

3-(4-isopropylphenyl)-2-(4-methoxyphenyl)-2,3-dihydroquinazolin-4(1H)-one (4l):

IR (KBr, cm^{-1}): 3425, 3297, 2955, 1630, 1507, 1393, 1334, 1247, 1175, 1026, 835, 705; δ_H (300 MHz, DMSO- d_6) 7.76 (1H, d, $J=7.5$ Hz), 7.55 (1H, s), 7.28 (7H, m), 6.85 (2H, d, $J=8.4$ Hz), 6.75 (2H, t, $J=8.4$ Hz), 6.17 (1H, s), 3.74 (3H, s), 2.87 (1H, m), 1.19 (6H, d, $J=6.9$ Hz); δ_C (300 MHz, DMSO- d_6) 162.2, 159.3, 146.5, 145.7, 138.5, 133.6, 132.9, 127.9, 127.6, 126.4, 125.9, 117.5, 115.4, 114.8, 113.6, 72.4, 54.9, 32.9, 23.8; HRMS (EI) Calcd. for $C_{24}H_{24}N_2O_2$ $[M]^+$, 372.2003, Found 372.1007; Anal. Calcd for $C_{24}H_{24}N_2O_2$: C 77.39, H 6.49, N 7.51%; Found C 77.45, H 6.53, N 7.41%;

2-(benzo[d][1,3]dioxol-5-yl)-3-(4-isopropylphenyl)-2,3-dihydroquinazolin-4(1H)-one (4m):

IR (KBr, cm^{-1}): 3438, 2965, 1646, 1507, 1402, 1237, 1029, 757; δ_H (300 MHz, DMSO- d_6) 7.75 (1H, d, $J=7.5$ Hz), 7.59 (1H, s), 7.23 (5H, m), 6.96 (1H, s), 6.79 (4H, m), 6.19 (1H, s), 5.97 (2H, s), 2.89 (1H, m), 1.17 (6H, d, $J=6.6$ Hz); δ_C (300 MHz, DMSO- d_6) 162.4, 147.5, 147.2, 146.4, 146.0, 138.7, 134.7, 133.7, 127.9, 126.5, 125.8, 119.7, 117.5, 115.6, 114.8, 107.9, 106.7, 101.3, 72.4, 32.9, 23.9; HRMS (EI) Calcd. for $C_{24}H_{22}N_2O_3$ $[M]^+$, 386.2001, Found 386.1006; Anal. Calcd for $C_{24}H_{22}N_2O_3$: C 74.58, H 5.75, N 7.26%; Found C 74.42, H 5.81, N 7.37%;

2,3-bis(4-methoxyphenyl)-2,3-dihydroquinazolin-4(1H)-one (4q):

IR (KBr, cm^{-1}): 3425, 2938, 2835, 1637, 1512, 1393, 1442, 1245, 1176, 1027, 997, 830, 764; δ_H (300 MHz, DMSO- d_6) 7.72 (1H, d, $J=7.8$ Hz), 7.42 (1H, s), 7.28 (3H, m), 7.17 (2H, d, $J=8.7$ Hz), 6.85 (4H, m) 6.77 (2H, t, $J=7.8$ Hz), 6.17 (1H, s), 3.75 (3H, s), 3.70 (3H, s); δ_C (300 MHz, DMSO- d_6) 162.4, 159.3, 157.5, 146.7, 133.6, 132.9, 127.9, 127.8, 127.4, 117.4, 115.2, 114.6, 113.9, 113.6,

72.9, 55.1, 55.5; HRMS (EI) Calcd. for $C_{22}H_{20}N_2O_3$ $[M]^+$, 360.1004, Found 360.1008; Anal. Calcd for $C_{22}H_{20}N_2O_3$: C 73.32, H 5.58, N 7.76%; Found C 73.22, H 5.43, N 7.65%;

2,3-Dihydro-2-(3-nitrophenyl)-3-(thiazol-2-yl)quinazolin-4(1H)-one (4Z17):

IR (KBr, cm^{-1}): 3365, 3078, 2962, 1639, 1527, 1505, 1445, 1392. δ_H (300 MHz, DMSO- d_6) 7.96 (m, 10H, Ar-H), 7.50 (d, $J = 3.24$ Hz, 1H, CH), 8.33 (d, $J = 3.24$, 1H, NH). δ_C (300 MHz, DMSO- d_6) 67.8, 114.1, 116.2, 116.5, 119.2, 121.1, 123.5, 128.5, 130.4, 132.4, 135.7, 137.4, 142.3, 146.8, 148.7, 157.8, 160.9. Anal. Calcd for $C_{17}H_{14}N_4O_3S$: C 57.63, H 3.97, N 15.80%; Found C 57.52, H 3.90, N 15.72%; HRMS (EI) Calcd. for $C_{17}H_{14}N_4O_3S$ $[M]^+$, 360.1002, Found 360.1006;

2,3-Dihydro-2-(4-hydroxyphenyl)-3-(thiazol-2-yl)quinazolin-4(1H)-one (4Z18):

IR (KBr, cm^{-1}): 3346, 1638, 1614, 1511, 1453. δ_H (300 MHz, DMSO- d_6) 7.56 (m, 10H, Ar-H), 7.25 (d, $J = 3.18$ Hz, 1H, CH), 8.04 (d, $J = 3.2$ Hz, 1H, NH), 9.45 (s, 1H, OH). δ_C (400 MHz, DMSO- d_6) 68.3, 114.6, 115.6, 115.4, 116.0, 118.5, 127.4, 128.2, 130.5, 135.7, 137.5, 147.4, 157.5, 158.1, 161.2. Anal. Calcd for $C_{17}H_{15}N_3O_2S$: C 62.75, H 4.65, N 12.92%; Found C 62.81, H 4.73, N 12.82%; HRMS (EI) Calcd. for $C_{17}H_{15}N_3O_2S$ $[M]^+$, 325.1002, Found 325.1005;

2-(4,5-dihydrothiazol-2-yl)-3-p-tolyl-2,3-dihydroquinazolin-4(1H)-one (4Z19):

IR (KBr, cm^{-1}): 3406, 3045, 1635, 1507, 1453, 1393. δ_H (300 MHz, DMSO- d_6) 2.15 (s, 3 H, CH_3), 7.65 (m, 10H, Ar-H), 7.35 (d, $J = 3.27$, 1H, CH), 8.15 (d, $J = 3.27$ Hz, 1H, NH). δ_C (300 MHz, DMSO- d_6) 20.8, 68.3, 114.2, 115.8, 116.4, 118.5, 126.0, 128.6, 129.6, 135.8, 137.1, 137.6, 137.2, 147.4, 158.6, 161.3. Anal. Calcd for $C_{18}H_{17}N_3OS$: C 66.85, H 5.31, N 12.98%; Found C 66.80, H 5.22, N 12.80%; HRMS (EI) Calcd. for $C_{18}H_{17}N_3OS$ $[M]^+$, 325.1002, Found 325.1005;

2,3-Dihydro-2-(4-nitrophenyl)-3-(thiazol-2-yl)quinazolin-4(1H)-one (4Z20):

IR (KBr, cm^{-1}): 3325, 3103, 1637, 1615, 1510, 1445, 1393. δ_H (300 MHz, $CDCl_3$) 7.96 (m, 11H, Ar-H), 8.24 (s, 1H, NH). δ_C (300 MHz, $CDCl_3$) 68.4, 114.1, 116.1, 116.4, 119.1, 124.2, 127.4, 128.7, 135.4, 137.7, 146.6, 147.7, 147.7, 157.7, 160.8. Anal. Calcd for $C_{17}H_{14}N_4O_3S$: C 66.85, H 5.31, N 12.98%; Found C 66.80, H 5.22, N 12.80%; HRMS (EI) Calcd. for $C_{17}H_{14}N_4O_3S$ $[M]^+$, 354.1001, Found 354.1006;

2-(4-Chlorophenyl)-2,3-dihydro-3-(thiazol-2-yl)quinazolin-4(1H)-one (4Z21):

IR (KBr, cm^{-1}): 3360, 3333, 3078, 1624, 1613, 1508, 1433. δ_{H} (300 MHz, CDCl_3): 7.75 (m, 11H, Ar-H), 8.16 (d, $J = 3.72$ Hz, NH). δ_{C} (300 MHz, CDCl_3): 67.9, 114.1, 116.0, 116.1, 118.2, 128.0, 128.6, 129.3, 133.3, 135.5, 137.7, 139.4, 146.6, 157.6, 161.1. Anal. Calcd for $\text{C}_{17}\text{H}_{14}\text{N}_3\text{O}_2$: C, 59.38, H, 4.11, N, 12.22%; Found C 59.21, H, 4.01, N, 12.11%; HRMS (EI) Calcd. for $\text{C}_{17}\text{H}_{14}\text{N}_3\text{O}_2$ $[\text{M}]^+$, 343.1003, Found 343.1008;

2,3-Dihydro-2-[4(1,2,3,4-tetrahydro-4-oxo-3-p-tolylquinazolin-2-yl)phenyl]-3-p-tolylquinazolin-4(1H)-one (2a):

IR (KBr, cm^{-1}): 3293, 1644. δ_{H} (300 MHz, DMSO-d_6) 2.25 (s, 6 H, CH_3), 6.13 (d, $J = 1.8$ Hz, 2H, CH), 7.35-7.40 (m, 20 H, ArH), 7.55 (d, $J = 1.8$ Hz, 2 H, NH). δ_{C} (300 MHz, DMSO-d_6) 20.9, 72.5, 114.7, 115.4, 117.8, 126.4, 126.7, 127.9, 129.2, 133.8, 135.3, 138.2, 140.8, 146.5, 162.3. Anal. Calcd for $\text{C}_{36}\text{H}_{30}\text{N}_4\text{O}_2$: C, 78.50; H, 5.50; N, 10.10. Found: C, 78.41; H, 5.45; N, 9.78. HRMS (EI) Calcd. for $\text{C}_{36}\text{H}_{30}\text{N}_4\text{O}_2$ $[\text{M}]^+$, 550.2004, Found 550.1007;

3-(4-Chlorophenyl)-2-[4-[3-(4-chlorophenyl)-1,2,3,4-tetrahydro-4-oxoquinazolin-2-yl]phenyl]-2,3-dihydroquinazolin-4(1H)-one (2c):

IR (KBr, cm^{-1}): 3322, 1616. δ_{H} (300 MHz, DMSO-d_6) 6.18 (s, 2 H, CH), 7.16-7.45 (m, 22 H, $20 \times \text{ArH}$, $2 \times \text{NH}$). δ_{C} (300 MHz, DMSO-d_6) 70.9, 113.3, 113.4, 116.3, 125.5, 126.5, 126.7, 128.9, 132.7, 137.9, 139.3, 145.2, 160.8. Anal. Calcd for $\text{C}_{34}\text{H}_{24}\text{Cl}_2\text{N}_4\text{O}_2$: C, 69.0; H, 4.0; N, 9.40. Found C, 68.85; H, 3.89; N, 9.22. HRMS (EI) Calcd. for $\text{C}_{34}\text{H}_{24}\text{Cl}_2\text{N}_4\text{O}_2$ $[\text{M}]^+$, 590.2001, Found 590.1006;

2,3-Dihydro-2-[4-[1,2,3,4-tetrahydro-4-oxo-3-(thiazol-2-yl)quinazolin-2-yl]phenyl]-3-(thiazol-2-yl)quinazolin-4(1H)-one (2d):

IR (KBr, cm^{-1}): 3321, 1616. δ_{H} (300 MHz, DMSO-d_6) 6.94-7.89 (m, 20 H). δ_{C} (300 MHz, DMSO-d_6) 68.2, 114.6, 116.5, 118.8, 125.8, 126.3, 128.6, 128.7, 135.5, 137.9, 139.2, 145.6, 160.8. Anal. Calcd for $\text{C}_{28}\text{H}_{20}\text{N}_6\text{O}_2\text{S}_2$: C, 62.70, H, 3.80; N, 15.64. Found: C, 62.57; H, 3.69; N, 15.58. HRMS (EI) Calcd. for $\text{C}_{28}\text{H}_{20}\text{N}_6\text{O}_2\text{S}_2$ $[\text{M}]^+$, 536.1004, Found 536.1007;

3-Ethyl-2-[4-(3-ethyl-1,2,3,4-tetrahydro-4-oxoquinazolin-2-yl)phenyl]-2,3 dihydroquinazolin-4(1H)-one (2f):

IR (KBr, cm^{-1}): 3305, 2977, 1625. δ_{H} (300 MHz, DMSO-d_6) 1.04 (t, $J = 7.0$ Hz, 6 H, CH_3), 2.77 (dt, $J = 13.6, 7.0$ Hz, 2 H, CH), 3.83 (dt, $J = 13.6, 7.0$ Hz, 2 H, CH), 5.85 (s, 2 H, CH), 7.05-7.30 (m, 14 H, $12 \times \text{ArH}$, $2 \times \text{NH}$). δ_{C} (300 MHz, DMSO-d_6) 13.9, 69.9, 114.7, 115.5, 117.9, 126.8, 127.9, 133.7, 142.0, 146.6, 162.5. Anal. Calcd for $\text{C}_{22}\text{H}_{26}\text{N}_4\text{O}_2$:

C, 73.24; H, 6.10; N, 13.12. Found: C, 73.10; H, 5.98; N, 13.03. HRMS (EI) Calcd. for $\text{C}_{22}\text{H}_{26}\text{N}_4\text{O}_2$ $[\text{M}]^+$, 426.2004, Found 426.2009;

3-Benzyl-2-[4-(3-benzyl-1,2,3,4-tetrahydro-4-oxoquinazolin-2-yl)phenyl]-2,3-dihydroquinazolin-4(1H)-one (2g):

IR (KBr, cm^{-1}): 3290, 1644. δ_{H} (300 MHz, DMSO-d_6) 3.77 (d, $J = 15.4$ Hz, 2 H, CH), 5.25 (d, $J = 15.4$ Hz, 2 H, CH), 5.74 (d, $J = 2.3$ Hz, 2 H, CH), 7.0-7.56 (m, 22 H, ArH), 7.37 (2 H, d, $J = 2.3$ Hz, NH). δ_{C} (300 MHz, DMSO-d_6) 45.99, 68.2, 113.5, 113.4, 116.3, 125.1, 125.9, 126.2, 126.4, 127.6, 132.5, 136.3, 139.8, 145.0, 161.6. Anal. Calcd for $\text{C}_{36}\text{H}_{30}\text{N}_4\text{O}_2$: C, 78.53; H, 5.56; N, 10.14. Found: C, 78.42; H, 5.45; N, 9.92. HRMS (EI) Calcd. for $\text{C}_{36}\text{H}_{30}\text{N}_4\text{O}_2$ $[\text{M}]^+$, 550.2005, Found 550.2008;

2,3-Dihydro-2-(1,2,3,4-tetrahydro-4-oxoquinazolin-2-yl)quinazolin-4(1H)-one (3h):

IR (KBr, cm^{-1}): 3354, 3300, 1638. δ_{H} (300 MHz, DMSO-d_6) 4.83 (m, 2 H, CH), 6.89-7.70 (m, 10 H, $8 \times \text{ArH}$, $2 \times \text{NH}$), 8.44 (2 H, d, $J = 5.3$ Hz, NH). δ_{C} (300 MHz, DMSO-d_6) 67.7, 117.1, 117.5, 118.6, 126.4, 127.3, 132.4, 132.5, 144.9, 167.4. Anal. Calcd for $\text{C}_{16}\text{H}_{14}\text{N}_4\text{O}_2$: C, 65.33; H, 4.82; N, 19.06. Found: C, 65.23; H, 4.71; N, 18.89. HRMS (EI) Calcd. for $\text{C}_{16}\text{H}_{14}\text{N}_4\text{O}_2$ $[\text{M}]^+$, 294.1004, Found 294.1007;

2,3-Dihydro-2-[4-(1,2,3,4-tetrahydro-4-oxoquinazolin-2-yl)phenyl]quinazolin-4(1H)-one (2i):

IR (KBr, cm^{-1}): 3266, 3185, 1643. δ_{H} (300 MHz, DMSO-d_6) 5.75 (d, $J = 2.0$ Hz, 2 H, CH), 6.67-8.11 (m, 16 H, $12 \times \text{ArH}$, $4 \times \text{NH}$). δ_{C} (300 MHz, DMSO-d_6) 66.7, 114.9, 115.7, 117.6, 127.2, 127.8, 133.9, 142.5, 148.1, 164.6. Anal. Calcd for $\text{C}_{22}\text{H}_{18}\text{N}_4\text{O}_2$: C, 71.34; H, 4.95; N, 15.16. Found: C, 71.26; H, 4.89; N, 14.98. HRMS (EI) Calcd. for $\text{C}_{22}\text{H}_{18}\text{N}_4\text{O}_2$ $[\text{M}]^+$, 370.1001, Found 370.1006;

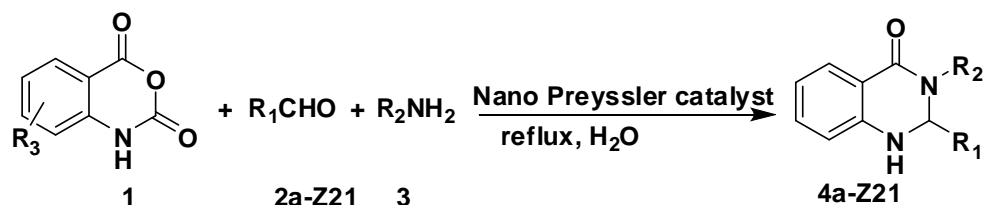
RESULTS AND DISCUSSION

We synthesized mono- and disubstituted 2,3-dihydroquinazolin-4(1H)-ones. Water as a solvent resulted in shorter reaction times than ethanol (Table 1). For the synthesis of disubstituted derivatives, isatoic anhydride, a primary amine, and an aromatic aldehyde in the presence of silica-supported Preyessler nanoparticles heteropolyacid (SPNP) were reacted in ethanol or water under reflux conditions to afford the expected products (Scheme 1).

Several aliphatic and aromatic amines were used for this reaction. Aliphatic amines afforded the

products in a shorter time compared to the aromatic analogues. Aromatic aldehydes carrying either electron-releasing or electron-withdrawing substituents afforded high yields of products. Aliphatic aldehydes could not be used in this

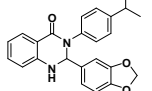
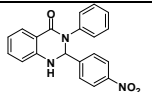
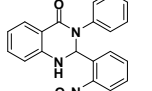
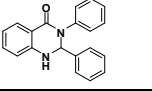
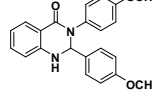
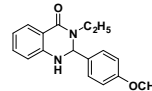
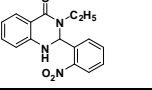
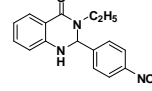
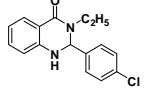
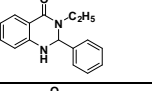
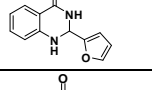
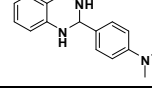
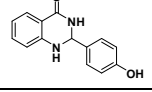
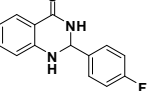
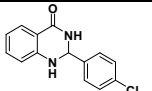
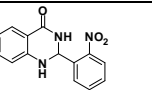
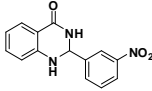
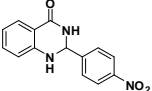
procedure because they undergo aldol condensation under the reaction conditions. After optimizing the conditions, the generality toward various amines and benzaldehydes was explored. The results obtained are listed in Table 1.

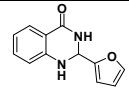
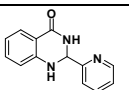
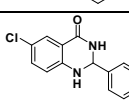
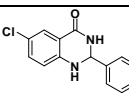
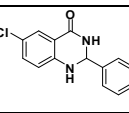
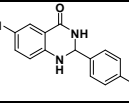
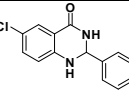
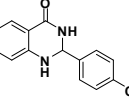
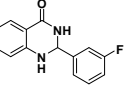
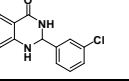
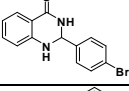
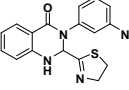
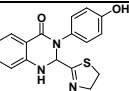
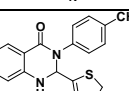
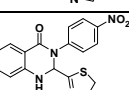
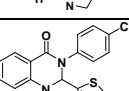


Scheme 1. Synthesized mono- and disubstituted 2,3-dihydroquinazolin-4(1H)-ones using silica-supported Preyssler nanoparticles heteropolyacid (SPNP) under reflux conditions

Table 1. Silica-supported Preyssler nanoparticles (SPNP) catalyzed synthesis of 2,3-disubstituted 2,3-dihydroquinazolin-4(1H)-one derivatives by the reaction of isatoic anhydride with primary amines and aldehydes in water and ethanol under reflux conditions in proper times

Entry	Aldehyde(2)	Amine(3)	Product(4)	Time (h)		^a Yield(%)		Mp (°C)
				EtOH	H ₂ O	EtOH	H ₂ O	
1	HCHO	NH ₃		2	1	88	92	142-145
2		C ₂ H ₅ NH ₂		425	2.5	83	87	134-137 (lit.23)
3		C ₂ H ₅ NH ₂		3	1	85	81	180-182
4				5	1.5	81	86	214-217 (lit.24)
5		CH ₃ NH ₂		2.5	1	87	80.5	188-190 (lit.23)
6		CH ₃ NH ₂		3	1.5	72	83	145-146 (lit.23)
7		CH ₃ NH ₂		1.5	3.5	74	87.5	164-165 (lit.23)
8		CH ₃ CH ₂ CH ₂ NH ₂		1	4.5	72	82.5	135-137
9		CH ₃ CH ₂ CH ₂ NH ₂		1	2.5	82.5	89.5	120-121
10				4	2	71	78.5	214-217 (lit.34)
11				2	4	89	95	190-192
12				1.5	2.5	93	97	171-172

13				m	2	4	82.5	91	210-212
14				n	1	4	70	81.5	195-197 (lit.24)
15				o	1.5	4	69	80	186-188 (lit.24)
16				p	1	3.5	68	82.5	205-208 (lit.24)
17				q	2.5	5	82	95.5	227-228
18		$C_2H_5NH_2$		r	1	4.5	89	71.5	125-128 (lit.25)
19		$C_2H_5NH_2$		s	3	5	82	95	175-178 (lit.25)
20		$C_2H_5NH_2$		t	3	4.5	82	96	157-160 (lit.25)
21		$C_2H_5NH_2$		u	1	4	82.5	89.5	134-137 (lit.25)
22		$C_2H_5NH_2$		w	1	3.5	80	89.5	136-137 (lit.25)
23		NH_3		x	2	4.5	78	79	167.2-168.5
24		NH_3		y	3	5.5	79	81	228-229 (lit.26)
25		NH_3		z	4	6	82	85	279.1-280.9 (lit.27)
26		NH_3		Z1	3.5	5	81	83	199-200 (lit.5)
27		NH_3		Z2	3	4.5	80	81.5	205-206 (lit.28)
28		NH_3		Z3	2	3	86.5	92	193-194 (lit.27)
29		NH_3		Z4	3	5	84	92	216.2-217.1 (Lit.29)
30		NH_3		Z5	3	4.5	85	91	212-214 (Lit.29)

31		NH ₃		5.5	4.5	76	79	166–167 (lit.30)
32		NH ₃		5	4	78	80	187–188 (lit.31)
33		NH ₃		5.5	3	81	83.5	249-250 (lit.32)
34		NH ₃		6	3.5	80.5	82	249-250
35		NH ₃		4.5	3	82.5	85	251, dec.
36		NH ₃		4	2.5	86	92	220-221
37		NH ₃		6	3.5	81.5	83	220 -221
38		NH ₃		5	2.5	85	89	233–234 (lit.28)
39		NH ₃		5.5	4	82	85	266-267
40		NH ₃		5	3	81	88	188-190 (lit.33).
41		NH ₃		6	3	80	84	206–207
42				5	6	81	86	164–166
43				5	2.5	74	85	260 dec
44				5	3	79	86	196–197
45				5	3	75	83.5	184–186
46				5	3.5	74.5	80	174–175

^aIsolated yields.

Following the obtained results, other derivatives of 2,3-dihydroquinazolin-4(1H)-one were synthesised by using different types of amines and aldehydes under aqueous or solvent-free conditions (Scheme 1). Aliphatic and aromatic amines as heteroaromatic model compounds also successfully afforded the desired products (Table 1).

Silica nanostructures were obtained through a sol-gel method. In this study, the gelation time is defined as the time between pouring the solution into the container and the time at which the solution ceases to discernibly flow under the influence of gravity. The conditions used are shown in Table 2 (Experimental section).

Table 2. Conditions of silica nanostructures production via sol-gel

4	C ₂ H ₅ OH/TEOS molar ratio	A
2	pH	B
12	Water/TEOS molar ratio	C
20 min	Stiring time	F
220 °C	Drying temperature	G
6 h	Drying time	H
4	C ₂ H ₅ OH/TEOS molar ratio	A

The obtained nanostructures were characterized by TEM, as shown in Figure 1. This figure shows 40-nm spheres.

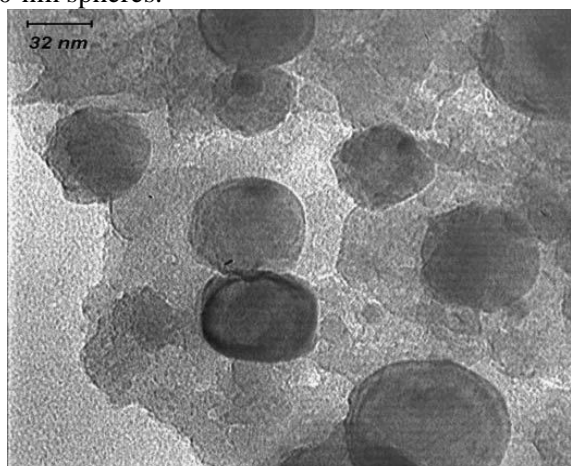


Fig. 1. TEM image of the synthesized nano-SiO₂.

The heteropolyacid H₁₄[NaP₅W₃₀O₁₁₀] in the SiO₂ nanoparticle was confirmed by infrared spectroscopy, as shown in Figure 2. The asymmetric stretching frequency of the terminal oxygen is observed at 960 cm⁻¹ and the P-O asymmetric stretching frequency is noted at 1080 and 1165 cm⁻¹. The prominent P-O bands at 960, 1080, and 1165 cm⁻¹ are consistent with a C5V symmetry anion. These bands demonstrate that H₁₄[NaP₅W₃₀O₁₁₀] is preserved in the HPA/SiO₂

nanoparticles. In addition, the protonated water of H₁₄[NaP₅W₃₀O₁₁₀] also remained in the nanoparticles at 1730 cm⁻¹. It could be confirmed that the heteropolyacid H₁₄[NaP₅W₃₀O₁₁₀] was successfully immobilized onto the SiO₂ nanoparticles since the heteropolyacid does not react with SiO₂ or with water, but it can remain in the silica nanoparticles without appreciable change of the structures.

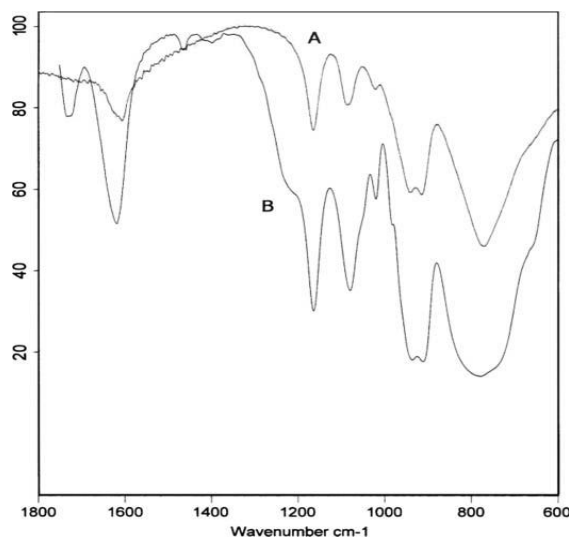
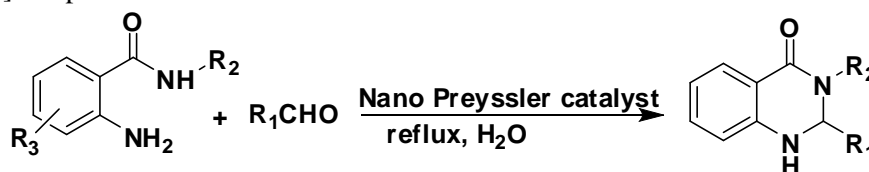
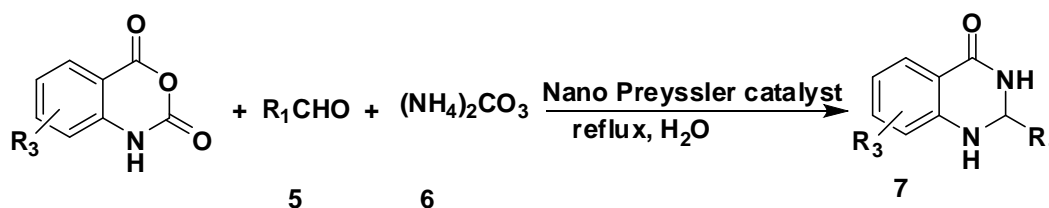


Fig. 2. Infrared spectroscopy of Preyssler heteropolyacid in bulk form (B) and nano form (A).

Considering the importance of such activities, a number of synthetic methods for their synthesis from isatoic anhydride (path 1) and anthranilamide (path 2) are reported (Schemes 1 and 2). Monosubstituted 2,3-dihydroquinazolin-4(1H)-ones were also successfully synthesized using ammonium carbonate as an ammonia source (Scheme 3).



Scheme 2. Synthesized disubstituted 2,3-dihydroquinazolin-4(1H)-ones using silica-supported Preyssler nanoparticles heteropolyacid (SPNP) under reflux conditions



Scheme 3. Synthesis of monosubstituted 2,3-dihydroquinazolin-4(1H)-ones by using ammonium carbonate and silica-supported Preyssler nanoparticles heteropolyacid (SPNP) under reflux conditions in water as solvent

The direct three-component reactions worked well with a variety of arylamines bearing either electron-donating (Table 1, entries 11-17) or -withdrawing groups (Table 1, entries 4, 42-46) and phenethylamine (Table 1, entries 8 and 9). Also the reactions with arylamines and a range of benzaldehydes carrying either electron-donating or -withdrawing groups on the benzene ring afforded the desired products 4b-h in high yields. With other primary amines having an aromatic ring, the desired products 4j-l were produced in 78.5-97% yield (Table 1, entries 10-12). These reactions provided rapid access to various 2,3-dihydroquinazolin-4(1H)-one derivatives, (Table 1, 4a-k). We also checked the reusability of the catalyst by separation and reloading in a new run and found that the catalyst could be reused several times without any decrease in the product yield. An example is shown for the reaction of ethylamine with isatoic anhydride and 3-nitrobenzaldehyde, 4g (Table 1, entry 9).

It is well known that some ammonium salts can be applied as the source of ammonia in the synthesis of nitrogen-containing heterocyclic compounds (Scheme 3).

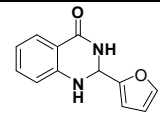
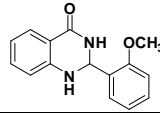
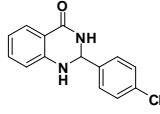
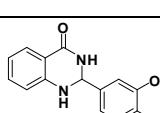
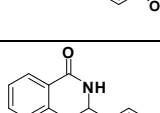
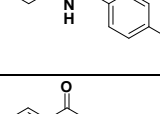
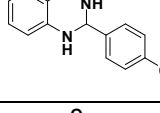
Accordingly, 2-aryl substituted 2,3-dihydroquinazolin-4(1H)-ones **7** were efficiently synthesized when ammonium carbonate (**6**), isatoic anhydride (**1**) and an aromatic aldehyde **5**, were treated with silica-supported Preyssler nanoparticles (SPNP) in ethanol under the same reaction conditions (Scheme 3, Table 3).

Some of the synthesized monosubstituted quinazolinones (Table 3, entries 2, 4, 5) have been recognized as potent anti-cancer compounds. For the preparation of our potential target compounds **2** and **3**, isatoic anhydride was treated with primary amine and terphthaldehyde (**4**) or glyoxal (**5**) in the presence of silica-supported Preyssler nanoparticles (SPNP) (Scheme 4).

All bis-dihydroquinazolinones synthesized by this pseudo five-component reaction were reported for the first time and could be considered as potentially biologically active compounds with a quinazolinone core. In addition to the above-mentioned advantages are the simple work-up

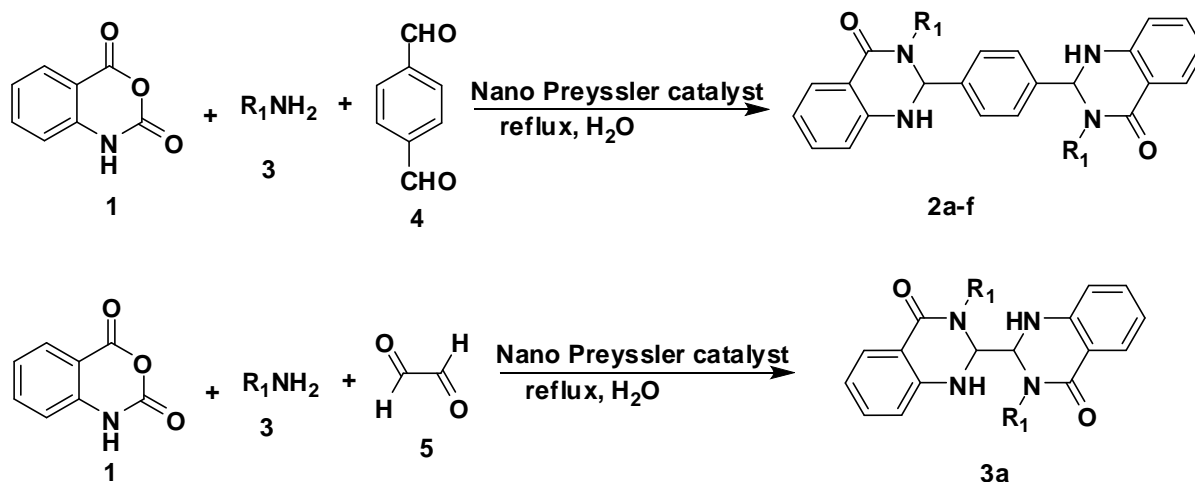
procedure, that makes this process environmentally friendly, and the easy purification, that requires only filtration of the products followed by recrystallization from ethanol (Table 4).

Table 3. Synthesis of 2-substituted 2,3-dihydroquinazolin-4(1H)-one derivatives in the presence of silica-supported Preyssler nanoparticles (SPNP) and water as solvent under reflux conditions

Entry	Product	Time (h)	^a Yield (%)	Mp (°C)
1		4.5	80	164–165 ³⁴
2		4	92	165–167 ³⁴
3		3	93	233–234 ³⁵
4		3.5	89	209–210 ³⁴
5		3	87	180–181 ³⁶
6		2.5	91	206–208 ³⁶
7		2	94.5	219–222 ³⁶

^aIsolated yield.

Different organic solvents were examined for the reaction and we found that water was the solvent of choice (Table 4). Currently the use of non-toxic and environmentally friendly solvents is of much interest. Room temperature ionic liquids are novel solvents with outstanding environmental and technical features [37]. Ethanol proved to be



Scheme 4. Synthesis of Bis-2,3-dihydroquinazolin-4(1H)-ones derivatives using Silica-Supported Preyssler Nanoparticles (SPNP) and primary amine and terphthaldehyde under reflux conditions

Table 4. Synthesis of bis-2,3-dihydroquinazolin-4(1H)-ones in the presence of silica-supported Preyssler nanoparticles (SPNP) catalyst in water and/or ethanol solvents under reflux conditions

Entry	Aldehyde	Amine	Product	Time (h)		^a Yield (%)	
				H ₂ O	EtOH	EtOH	H ₂ O
1				3	4	67	70.5
2				3	6	70	73.5
3				4	9	60	64.5
4				5.5	11.5	52	56.5
5				2.5	5	63	67
6		CH ₃ CH ₂ NH ₂		3.5	5	65	71
7				3.5	5.5	67	72.5
8		NH ₃		3.5	6	63	66.5
9		NH ₃		3.5	7.5	62.5	67.5

^a Isolated yield (%)

almost as good as water, with ethanol giving a slightly better yield than tetra-*n*-butylammonium bromide. The use of water as a solvent for organic

transformations offers several environmental benefits. In many reactions, significant rate enhancements are observed in water compared to

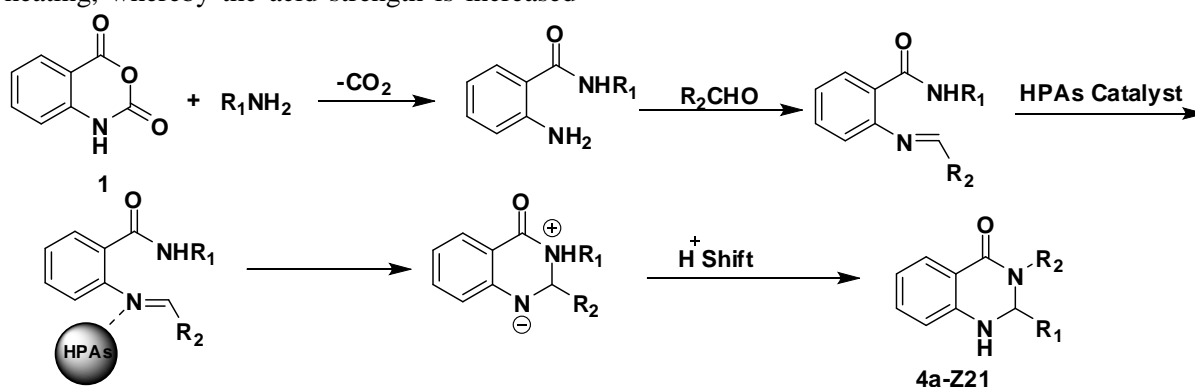
organic solvents. This acceleration has been attributed to many factors, including the hydrophobic effect, enhanced hydrogen bonding in the transition state, and the cohesive energy density of water [38]. When the reactions were conducted in water, the expected products were obtained in good yields and with better reaction times compared to organic solvents (Tables 3, 5). A part of the Preyssler heteropolyacid catalyst is solved in the water solvent. Preyssler heteropolyacid catalyst is also providing hydrogen bonding in the transition state more than ethanol in water solvent. The catalyst showed good efficiency for the synthesis of 2,3-dihydroquinazolin-4(1H)-one in water. Also, with nonpolar solvents such as carbon tetrachloride, dichloromethane and toluene, the desired adduct was not produced, likely due to insolubility of the isatoic anhydride.

Table 5. Solvent effects in the reaction of $C_2H_5NH_2$, isatoic anhydride, and terephthalaldehyde (2,2'-(1,4-phenylene)bis(3-(4-ethylphenyl)-2,3-dihydroquinazolin-4(1H)-one)) (Table 4, 2b) in the presence of silica-supported Preyssler nanoparticles catalyst (SPNP) (Table 3, entry 2).

Entry	Solvent	^b Yield (%)	Time (h)
1	H ₂ O	73.5	3
2	TBAB	61	8
3	C ₂ H ₅ OH	70	6
4	CH ₃ OH	37	12
5	CH ₃ CN	27	20
6	CH ₂ Cl ₂	-	-
7	C ₆ H ₅ CH ₃	-	-
8	CCl ₄	-	-

^bIsolated yield.

Generally, solid heteropolyacids form ionic crystals composed of heteropolyanions, counteractions (H^+ , H_3O^+ , $H_5O_2^+$, etc.) and hydration water. This water can be easily removed on heating, whereby the acid strength is increased



Scheme 5. The mechanism of synthesized mono- and disubstituted 2,3-dihydroquinazolin-4(1H)-ones using silica-supported Preyssler nanoparticles heteropolyacid (SPNP) under reflux conditions

due to the dehydration of protons. Not only water can enter and leave the heteropolyacid crystal. Misono and co-workers advanced two types of catalysis for heterogeneous acid catalysis by heteropolyacids - surface type and bulk type [39,40]. In surface type catalysis, the reactions occur on the surface of the supported heteropoly compounds and the catalytic activity usually depends on the surface acidity of the heteropolyacid. In this case, the reaction rate and the yield are parallel to the number and strength of the accessible surface acid sites. The bulk and surface type of mechanism is largely relevant to reactions of polar substrates on bulk and surface heteropoly compounds. These substrates are capable of absorbing into the catalyst bulk, and thus all protons both in the bulk and on the surface of the heteropolyacid, are suggested to participate in the catalytic reaction. Due to the flexible nature of the solid structure of some heteropolyacids, reactant molecules having polarity or basicity are readily absorbed into the solid lattice and react therein. In this case, heteropolyacid catalysts may be called “catalytically active solid solvents”.

The Preyssler type heteropolyacid, $H_{14}[NaP_5W_{30}O_{110}]$, is remarkable owing to its exclusive physicochemical properties. They include strong Brønsted acidity, reversible transformations, solubility in polar solvents, high hydrolytic stability and high thermal stability, that are very important in catalytic processes.

A plausible mechanism for this reaction is shown in Scheme 5. It is conceivable that the Preyssler heteropolyacid catalysts are coordinated to the oxygen atom of the carbonyl groups in different stages of the reaction, activating them for the nucleophilic attack of the amine and amide nitrogen atoms (Scheme 5).

CONCLUSION

In conclusion, a novel simple and environmentally friendly one-pot three-component method for the synthesis of 2,3-dihydroquinazolinones is reported. In this pseudo five-component procedure six C–N bonds are formed in a tandem one-pot process, which is comparable with other important reactions in multicomponent chemistry [41]. High yields, ease of work up procedure, use of cheap and commercially available starting materials, convenient manipulation, and mild reaction conditions are the advantages of this new method. We believe that the present methodology addresses the current trend toward green chemistry due to high yields, economy and reusability of the catalyst. By the reaction of a range of amines and dialdehydes, novel libraries of bisdihydroquinazolinones could be obtained, which would make this method a suitable candidate for combinatorial and parallel synthesis in drug discovery. Different organic solvents were examined for the reaction and we found that water was the solvent of choice. Importantly, the use of water as a solvent offers environmental benefits, as well as significant rate enhancements, likely due to several factors, including hydrophobic effect, large dielectric constant, extensive hydrogen bonding, high heat capacity, and optimum oxygen solubility. When the reactions were conducted in water, the expected products were obtained in good yields and with better reaction times compared to organic solvents or ionic liquids. This protocol will be useful for the synthesis of numerous fused heterocyclic compounds because of its non-toxicity and low-cost, short reaction time and high yield.

REFERENCES

- G. Pandey, R. P. Singh, A. Gary, V.K. Singh, *Tetrahedron Lett.*, **46**, 2137 (2005).
- A. Strecker, *Liebigs Ann. Chem.*, **75**, 27 (1850).
- A. Domling, *Curr. Opin. Chem. Biol.*, **6**, 306 (2002).
- Y. S. Sadanadam, K. R. M. Reddy, A. B. Rao, *Eur. J. Med. Chem.*, **22**, 169 (1987).
- G. M. Chinigo, M. Paige, S. Grindrod, E. Hamel, S. Dakshanamurthy, M. Chruszcz, W. Minor, M. L. Brown, *J. Med. Chem.*, **51**, 4620 (2008).
- T. Graening, H.-G. Schmalz, *Angew. Chem., Int. Ed.*, **43**, 3230 (2004).
- B. R. Baker, R. E. Schaub, J. P. Joseph, F. J. McEvoy, J. H. Williams, *J. Org. Chem.*, **18**, 133 (1953).
- J. A. Moore, G. J. Sutherland, R. Sowerby, E. G. Kelly, S. Palermo, W. Webster, *J. Org. Chem.*, 887 (1969).
- K. Ozaki, Y. Yamada, T. Oine, T. Ishizuka, Y. Iwasawa, *J. Med. Chem.*, 1985, **28**, 568-576.
- M. J. Kornet, *J. Heterocycl. Chem.*, **29**, 103 (1992).
- D. Shi, L. Rong, J. Wang, Q. Zhuang, X. Wang, H. Hu, *Tetrahedron Lett.*, **44**, 3199 (2003).
- W. Steiger, T. Kappe, E. Ziegler, E. *Monatsh. Chem.*, **100**, 146 (1969).
- S. W. Li, M. G. Nair, D. M. Edwards, R. L. Kisliuk, Y. Gaumont, I. K. Dev, D. S. Duch, J. Humphreys, G. K. Smith, R. Ferone, *J. Med. Chem.*, **34**, 2746 (1991).
- C. R. Gorla, N. W. Emanetoglu, S. Liang, W. E. Mago, Y. Lu, M. Wraback, H. Shen, *Journal of Applied Physics.*, **85**, 2595 (1999).
- J. Zhang, R. M. J. Dickson, *Physics Review Letters.*, **93**, 077402 (2004).
- B. Ding, J. Gong, J. Kim, S. Shiratori, *Nanotechnology.*, **5**, **16**, 785 (2005).
- D. P. Sawant, A. Vinu, N. E. Jacob, F. Lefebvre, S. B. Halligudi, *Journal of Catalysis.*, **235**, 2, 341 (2005).
- F. F. Bamoharram, M. M. Heravi, M. Roshani, M. Jahangir, A. Gharib, *Journal of Molecular Catalysis A: Chemical.*, **271**, 126 (2007).
- F. F. Bamoharram, M. M. Heravi, M. Roshani, A. Gharib, *Journal of the Chinese Chemical Society.*, **54**, 1017 (2007).
- A. Müller, F. Peters, M.T. Pope, D. Gatteschi, *Chemical Review.*, **98**, 239 (1998).
- M. H. Alizadeh, H. Razavi, F. F. Bamoharram, M. K. Hassanzadeh, R. Khoshnavazi, F. Mohammadi Zonoz, *Kinet. Catal.*, **44**, 524 (2003).
- M. M. Heravi, S. Sadjadi, S. Sadjadi, H. A. Oskooie, R. Hekmat Shoar, F. F. Bamoharram, *S. Afr. J. Chem.*, **62**, 1 (2009).
- V. B. Rao, P. Hanumanthu, C. V. Ratnam, *Indian J. Chem., Sect. B: Org. Chem. Incl. Med. Chem.*, **18**, 493 (1979).
- V. B. Reo, C. V. Ratnam, *Indian J. Chem.*, **18B**, 409 (1979).
- P. Salehi, M. Dabiri, M. A. Zolfigol, M. Baghbanzadeh, *Synlett.*, 1155 (2005).
- O. A. Maloshitskaya, J. Sinkkonen, V. V. Alekseyev, K. N. Zeleninb and K. Pihlajaa, *Tetrahedron.*, **61**, 7294 (2005).
- T. A. K. Smith and H. Stephen, *Tetrahedron.*, **1**, 38 (1957).
- D. Q. Shi, L. C. Rong, J. X. Wang, X. S. Wang, S. J. Tu and H. W. Hu, *Chem. J. Chin. Univ.*, **25**, 2051 (2004).
- P. Salehi, M. Dabiri, M. A. Zolfigol, M. A. Bodaghi Fard, *J. Braz. Chem. Soc.*, **15**, 773 (2004).
- M. Baghbanzadeh, P. Salehi, M. Dabiri and G. Kozehgarya, *Synlett.*, 344 (2006).
- E. S. Schipper and N. J. Clifton, *US 3316269* (1967).
- M. A. Zolfigol, M. Safaiee, *Synlett.*, 827 (2004).
- P. R. Bhalla and B. L. Walworth, *EP0058822* (1982).

34. M. Hour, L. Huang, S. Kuo, Y. Xia, K. Bastow, Y. Nakanishi, E. Hamel, K. Lee, *J. Med. Chem.*, **43**, 4479 (2000).
35. W. Su, B. Yang, *Aust. J. Chem.*, **55**, 692 (2002).
36. L. H. Yale, M. Kalkstein, *J. Med. Chem.*, **10**, 334 (1967).
37. J. S. Wilks, *J. Mol. Catal. A: Chem.*, **214**, 11 (2004).
38. L. R. Pratt, A. Pohrille, *Chem. Rev.*, **102**, 2671 (2002).
39. T. Okuhara, N. Mizuno, M. Misono, *Adv. Catal.*, **41**, 113 (1996).
40. M. Misono, *Chem. Commun.*, 1141 (2001).
41. G. Pandey, R. P. Singh, A. Gary, V. K. Singh, *Tetrahedron Lett.*, **46**, 2137 (2005).

СИНТЕЗА НА БИС-2,3-ДИГИДРОХИНАЗОЛИН-4(1H)-ОНИ И ТЯХНИ ПРОИЗВОДНИ С ПОМОЩТА НА PREYSSLER‘ОВИ НАНОЧАСТИЦИ (SPNP) ВЪРХУ ПОДЛОЖКА ОТ СИЛИЦИЕВ ДИОКСИД

А. Гариб^{1,2*}, Л. Вожданифард³, Н. Норузи Песян⁴, Б. Р. Хашеми Пур Хорасани²,
М. Джахангир¹, М. Рошани¹

¹Департамент по химия, Ислямски университет „Азад“, Маишад, Иран

²Център по земеделски изследвания и услуги, Маишад, Иран

³Образователна организация на Разави Кхорасан, Министерство на образованието, Маишад, Иран

⁴Департамент по химия, Научен факултет, Университет Урмия, Урмия, Иран

⁴Клъстер по молекулна химия, Департамент по органична химия, Университет Радбауд, Наймехен, Нидерландия

Постъпила на 13 февруари 2013 г.; коригирана на 8 юли 2013 г.

(Резюме)

Проведени са едноетапни синтети чрез три-компонентна кондензация на изатоинов анхидрид с първични амини (или амониев карбонат) и ароматни алдехиди в среда от етанол при катализатор от Preyssler‘ови наночастици (SPNP) върху подложка от силициев диоксид. Постигнати са високи добиви от 2,3-дихидрохиназолин-4(1H)-они. За пръв път са синтезирани бис-2,3-дихидрохиназолин-4(1H)-они чрез нова псевдо-пет-компонентна кондензация на изатоинов анхидрид, първичен амин и диалдехид във вода. Катализаторът може да се употребява многократно без намаляване добива на продуктите.

A computational study on the smallest exohedrally functionalized fullerenes, $C_{20}X_8$ ($X = H, F, Cl, Br, NH_2, OH$ and CN)

F. Naderi *

Department of Chemistry, Shahr-e-Qods Branch, Islamic Azad University, Tehran, Iran

Received August 9, 2013; Revised June 19, 2014

The structural stability and the electronic properties of $C_{20}X_8$ exohedrally functionalized fullerenes where $X = H, F, Cl, Br, NH_2, OH$ and CN are probed at the B3LYP level of theory. Vibrational frequency calculations show that all systems are true minima. The calculated binding energies of exohedrally functionalized fullerenes show $C_{20}(CN)_8$ followed by $C_{20}F_8$ as the most stable exohedrally functionalized fullerenes by the binding energies of 6.628 and 5.484 eV, respectively. All exohedral derivatives decrease the conductivity of fullerene through increasing their HOMO-LUMO gap and therefore enhance their stability against electronic excitations. High charge transfer on the surfaces of our stable exohedrally functionalized fullerenes, especially $C_{20}(OH)_8$ provokes further investigations on their possible application for hydrogen storage.

Keywords: Hybrid density functional theory (B3LYP); HOMO and LUMO; Exohedrally functionalized; $C_{20}X_8$; DFT.

INTRODUCTION

The discovery of C_{60} [1,2] was followed by the synthesis of other members of the fullerene family including the smallest possible fullerene cage, i.e. C_{20} [3]. The thermodynamic stability of C_{20} is different from that of C_{60} because of its extreme curvature and reactivity as it is composed of 12 pentagons and no hexagons. The angle between two adjacent bonds is 108° , much smaller than the optimal sp^2 angle of carbon, which is 120° . Therefore, it is a very strained structure. However, the fullerenes suffering from adjacent pentagons can be stabilized by forming endohedral (where the dopant is inside the cage) or exohedral (where the dopant is outside or between fullerene cages) derivatives with other groups [4]. Endohedral doping proved to be applicable in successful synthesis of $Sc_2@C_{66}$ [5], $Sc_2C_2@C_{68}$ [6], and $Sc_3N@C_{68}$ [7]. In the case of small cages, Moran *et al.* studied the equilibrium geometries and frequencies of endohedral complexes $X@C_{20}H_{20}$ where $X = H, He, Ne, Ar, Li, Li^+, Be, Be^+, Be^{2+}, Na, Na^+, Mg, Mg^+$ and Mg^{2+} [8]. Shakib *et al.* [9] found that minima fullerenes $Li^+@C_{20}H_{20}$ and $Mg^{2+}@C_{20}H_{20}$ are more stable than their isolated components. Recently, we carried out a similar study on $X@C_{12}Si_8$ complexes where $X = Li^+, Na^+, K^+, Be^{2+}, Mg^{2+}, Ca^{2+}, Al^{3+}$, and Ga^{3+} . The calculated binding energies showed the stabilization of $C_{12}Si_8$

through the inclusion of $Be^{2+}, Mg^{2+}, Al^{3+}$, and Ga^{3+} . On the other hand, the structures and electronic properties of exohedral complexes have been also of interest. $C_{54}Cl_8$ [10], $C_{56}Cl_8$, $C_{56}Cl_{10}$ [11], $C_{56}Cl_{10}$ [12], $C_{58}X_{18}$ ($X = H, F$ and Cl) [13], hept- $C_{62}X_2$ [14], $C_{64}X_4$ [15], and $C_{66}X_4$ ($X = H, F, Cl$, or Br) [16] were explored using the density functional theory. The first exohedral fullerene $C_{50}Cl_{10}$ [17] was synthesized in 2004 by Xie *et al.*, followed by the synthesis of $C_{64}H_4$ [18] and $C_{64}Cl_4$ [19]. Now, what about small fullerenes? How does exohedral doping affect the stability of the smallest fullerene cage C_{20} ? In this manner, we focused our calculations on $C_{20}X_8$ exohedrally functionalized fullerenes where $X = H, F, Cl, Br, NH_2, OH$ and CN to probe the applicability of exohedral doping in stabilization of C_{20} . The substituents are attached to eight symmetric positions of the cage in a case that none of them are adjacent to each other.

COMPUTATIONAL METHODS

Full geometry optimizations are accomplished by means of hybrid functional B3LYP [20-22] and the 6-31+G* basis set, as implemented in Gaussian 03 [23]. The applied basis set is comprised of Pople's well known 6-31G* basis set [24,25] and an extra plus due to the importance of diffuse functions [26,27]. Vibrational frequency computations confirm that the fully optimized structures are indeed minima (NIMAG = 0). To obtain more accurate energetic data, single point calculations are performed at B3LYP/6-311++G**

* To whom all correspondence should be sent:
E-mail: fnaderi2@yahoo.com

level. As a stability criterion of different configurations, binding energy per atom is calculated according to the following expression [28]:

$$E_b = (20E_C + 8E_X - E)/n$$

where E is the total energy of the $C_{20}X_8$ exohedrally functionalized fullerenes and E_X for NH_2 , OH and CN groups is equal to the sum of energy of their elements. Systems with larger binding energies are more stable. The electronic conductivity of the exohedrally functionalized fullerenes which is related to the HOMO-LUMO energy gaps were calculated at B3LYP/6-311++G**.

The nucleophilicity index, N , which was introduced by Domingo *et al.* [29], is calculated as $N = E_{HOMO(Nu)} - E_{HOMO(TTFE)}$, where tetrakis tetrafluoroethylene (TTFE) is chosen as the reference. The global electrophilicity, ω [30], is also calculated following the expression, $\omega = (\mu/2\eta)$, where μ is the chemical potential ($\mu \approx (E_{HOMO} + E_{LUMO})/2$) and η is the chemical hardness ($\eta = E_{LUMO} - E_{HOMO}$) [31]. NBO population analysis on optimized structures is also accomplished at the same level [32].

RESULTS AND DISCUSSION

Following the successful synthesis of dodecahedrane $C_{20}H_{20}$, a large number of exohedral derivatives of fullerene C_{20} have been synthesized with dodecahedrane as starting point. Among various exohedral derivatives of C_{20} , of particular interest are the polyunsaturated dodecahedranes $C_{20}R_n$ ($n = 18, 16, 14, 12, 10$; $R = H$ or other substituents) that have one to five highly bent unsaturated C=C bonds [33]. In this work first full geometry optimizations of various exohedral

derivatives of C_{20} ($C_{20}H_{10}$, $C_{20}H_{12}$, $C_{20}H_{14a}$ and $C_{20}H_{14b}$), (their figures are represented in supporting information) are performed and binding energy per atom is calculated. The binding energies are 5.19, 5.09, 5.21 and 5.22 eV/atom, respectively, while the binding energy of $C_{20}H_8$ is 5.44eV/atom. Then eight symmetrical positions of C_{20} are selected for evolution of $C_{20}X_8$ fullerenes where $X = H, F, Cl, Br, NH_2, OH$ and CN (Figure 1).

The smallest fullerene that satisfies Euler's theorem is C_{20} which is highly strained as a result of the extreme pyramidalization of the double bonds. Eight symmetrical positions of this fullerene are selected to have maximum double bond without any extra strain to have the most relative stabilities of $C_{20}X_8$.

Geometry optimizations and the resulted binding energies

The optimized geometries of C_{20} and its analogues (Figure 1) in the gas phase are listed in Table 1. Dodecahedral fullerene C_{20} does not adopt the perfect I_h symmetry due to Jahn-Teller distortion, whereas its lowest energy form is still in dispute [34-35]. The work by Chen *et al.* demonstrates that all five possible isomers of C_{20} (C_2 , C_{2h} , C_i , D_{3d} and D_{2h} symmetries) are isoenergetic (within 0.2 kcal/mol at B3LYP/6-31G*, and within 0.5 kcal/mol at MP2/6-31G*) and have essentially the same structural parameters at both B3LYP and MP2 levels [36]. The C=C bond lengths of C_i symmetry C_{20} are 1.445 Å, which is close to the sum of covalent radii of two C atoms (C: 0.76 Å). The obtained structure of C_{20} is in excellent agreement with that computed by Chen *et al.* [37].



Fig. 1. Optimized heterofullerenes at B3LYP/6-31+G*.

Table 1. Point groups (PG), total energies (E_{tot} in a.u.), ranges of C=C and X-C bond lengths (Å) and C-C-X angles (°) for the scrutinized heterofullerenes along with C₂₀ at the B3LYP/6-31+G* level.

Species	PG	E _{tot} (a.u.)	C-C	C=C	X-C	C-C-X
C ₂₀	C _i	-761.6019944	1.400-1.536		-	-
C ₂₀ H ₈	T _h	-766.7585347	1.540	1.352	1.093	118.81
C ₂₀ F ₈	T _h	-1560.8726881	1.534	1.353	1.373	118.18
C ₂₀ Cl ₈	T _h	-4443.7128301	1.531	1.351	1.797	118.60
C ₂₀ Br ₈	T _h	-21355.0790532	1.525	1.351	1.960	118.36
C ₂₀ (NH ₂) ₈	C _i	-1209.4094692	1.537-1.555	1.350-1.353	1.449-1.454	116.64-123.86
C ₂₀ (OH) ₈	C _i	-1368.6929686	1.544	1.352	1.404	120.72
C ₂₀ (CN) ₈	T _h	-1504.7670055	1.546	1.344	1.160	119.28

Introducing H atoms to C₂₀ upgrades its symmetry from C_i to T_h. This is along with the uniformity of bond lengths in C₂₀H₈. The range of 1.400-1.536 Å C=C bonds of C₂₀ is replaced with single bonds of 1.540 Å and double bonds of 1.352 Å, pretty close to typical H₃C-CH₃ and H₂C=CH₂ bonds. The H-C bond length of 1.093 Å is also completely close to a typical H-CH₃ bond length of 1.094 Å (Table 1).

Evidently, the presence of the eight sp³ carbon atoms extinguishes the electron delocalization on the surface of the cage. The same structural features are observed for all other species. However, C₂₀(NH₂)₈ does not show a fixed length for each of the single and double bonds but a narrow range. This is because it obeys C_i symmetry instead of T_h. Although the cage of C₂₀(OH)₈ is itself T_h, the overall structure obeys C_i symmetry due to the different spatial orientations of hydroxyl groups. While all species show C=C bond lengths of 1.350-1.353 Å, those of C₂₀(CN)₈ are noticeably shorter (1.344 Å) due to both inductive and mesomeric electron withdrawing of cyano groups (Table 1).

As stated by Hoffmann, Schleyer, and Schaefer, talking about the stability of a species necessitates that not only the obligatory vibrational analysis demonstrating all frequencies real, but also the computed smallest vibrational frequency (ν_{min}) should be reasonably large, i.e. more than 100 cm⁻¹ [38]. Interestingly, ν_{min} increases from 32 cm⁻¹ in C₂₀ to 474 cm⁻¹ in C₂₀H₈. This is because eight strained sp² carbon atoms are replaced with the strain-free sp³ atoms. Halogenated fullerenes show lower frequencies but those of C₂₀F₈ and C₂₀Cl₈ are still larger than 100 cm⁻¹. The ν_{min} of C₂₀Br₈ is 61

cm⁻¹ showing the weakness of C-Br bonds. While the ν_{min} of C₂₀(NH₂)₈ and C₂₀(OH)₈ bearing π-electron donor groups are satisfactorily large, the ν_{min} of C₂₀(CN)₈ with π-electron acceptor group is lower than 100 cm⁻¹ (Table 2).

Table 2. Binding energies per atom (B.E./atom) at B3LYP/6-311++G** and smallest vibrational frequencies (ν_{min}) for the scrutinized heterofullerenes along with C₂₀ at B3LYP/6-31+G*.

Species	B.E./atom (eV)	ν _{min} (cm ⁻¹)
C ₂₀	6.063	32
C ₂₀ H ₈	5.437	474
C ₂₀ F ₈	5.484	192
C ₂₀ Cl ₈	5.085	108
C ₂₀ Br ₈	4.944	61
C ₂₀ (NH ₂) ₈	5.252	157
C ₂₀ (OH) ₈	5.148	182
C ₂₀ (CN) ₈	6.628	85

The IR vibrational frequencies are computed to further provide the distinctive spectroscopic fingerprints of these probably accessible fullerenes. The simulated IR vibrational spectra of the fullerenes are illustrated in Fig.2, suggesting the prominent peaks.

These IR signatures provide useful information for their future experimental detections. It should be stressed at the outset that theoretical frequencies are almost universally overestimated compared to experimental results, even for more accurate methods, such as MP2, CCSD. It is not our intention in this study to predict absolute values of frequencies, but rather to seek for patterns in the data which might help to identify different forms of C₂₀X₈ fullerenes.

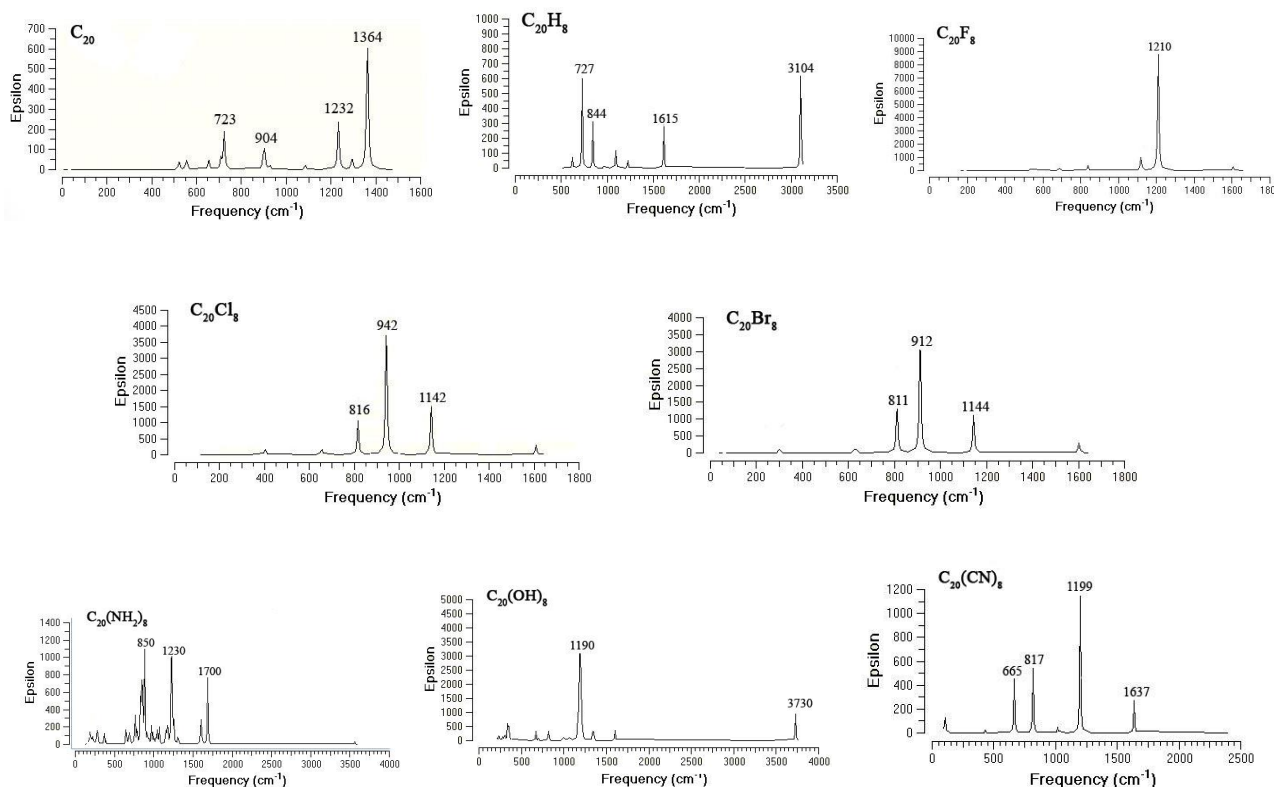


Fig. 2. Calculated IR spectra of $C_{20}X_8$ heterofullerenes at B3LYP/6-31+G*.

The binding energy of $C_{20}H_8$ is 5.437 eV which is less than that of C_{20} (6.063 eV) due to the absence of C=C bonds. From $C_{20}F_8$ to $C_{20}Br_8$ one finds a decreasing trend in binding energy due to the weakness of C–Br bonds compared to C–Cl ones and C–Cl compared to C–F. This is along with the decreasing trend of ν_{\min} among halogenated fullerene derivatives. The interesting point is the enormous stability of the fullerene bearing π -electron withdrawing group i.e. CN. The binding energy of $C_{20}(CN)_8$ is 6.628 which the highest value of all studied fullerene derivatives, consistent with the structural features (Table 2). In order to further provide distinctive spectroscopic fingerprints of probably accessible $C_{20}X_8$ fullerene derivatives, their calculated IR spectra are depicted in Figure 2.

$C_{20}X_8$ exohedrally functionalized fullerenes through NBO atomic charges

It was shown that point charges on the material's surface can improve the hydrogen storage capacity since they increase the binding energy of hydrogen [39-42]. The NBO population analysis on optimized structures is accomplished at the B3LYP/6-311++G**//B3LYP/6-31+G*.

The carbon atoms of sole fullerene bear varying charges from -0.050 to $+0.050$. In contrast, the structural uniformity of $C_{20}H_8$ is along with the electronic uniformity as all sp^3 carbons carry a

negative charge of -0.283 while the more electronegative sp^2 carbons carry a positive charge of $+0.034$. Electronegative fluoro substituent induces an overall electron density transfer and remains positively charged sp^2 and sp^3 carbons. On the other hand, electron donating characteristics of Cl and Br results in the negatively charged sp^3 carbons, i.e. this time the electron density transfer is from the exohedral substituents to the fullerene cage. Generally, since electronegativity decreases down a group of the periodic table, in $C_{20}F_8$, $C_{20}Cl_8$ and $C_{20}Br_8$, a considerable charge transfer occurs from them to the remaining carbon atoms of the cage. According to the calculated NBO atomic charges, the negative charges on F atoms are -0.354 while the charges on C atoms range from $+0.033$ to $+0.304$. The positive charges on Cl and Br atoms of $C_{20}Cl_8$ and $C_{20}Br_8$ are $+0.025$ and $+0.094$ while the charges on C atoms range from -0.131 to $+0.058$ and -0.194 to $+0.075$, respectively. Considering both stability and charge distribution on the surfaces of $C_{20}F_8$, $C_{20}Cl_8$ and $C_{20}Br_8$, it seems that $C_{20}F_8$ is possibly the best candidate for hydrogen storage.

Hydrogen and carbon atoms in $C_{20}H_8$ and $C_{20}(CN)_8$ carry a positive charge, i.e. $+0.232$ for H and $+0.276$ for C (Table 3).

Table 3. Ranges of NBO atomic charges of carbon (C) and exohedral derivatives (X) for C₂₀X₈ heterofullerenes along with C₂₀ at B3LYP/6-311++G**//B3LYP/6-31+G*.

Species	C _{sp3}	C _{sp2}	X ^a	Y ^b
C ₂₀	-	(-0.050) - (+0.050)	-	-
C ₂₀ H ₈	-0.283	+0.034	+0.232	-
C ₂₀ F ₈	+0.304	+0.034	-0.354	-
C ₂₀ Cl ₈	(-0.111) - (-0.131)	(+0.053) - (+0.080)	+0.026	-
C ₂₀ Br ₈	(-0.176) - (-0.198)	(+0.049) - (+0.076)	(+0.094) - (+0.095)	-
C ₂₀ (NH ₂) ₈	(-0.073) - (+0.046)	(-0.016) - (+0.064)	(-0.816) - (-0.869)	(+0.349) - (+0.362)
C ₂₀ (OH) ₈	(+0.188) - (+0.197)	(+0.007) - (+0.075)	(-0.703) - (-0.718)	(+0.467) - (+0.470)
^c C ₂₀ (CN) ₈	-0.221	+0.112	+0.276	-0.224

^a O in C₂₀(OH)₈, C in C₂₀(CN) and N in C₂₀(NH₂)₈

^b H in C₂₀(OH)₈ and C₂₀(NH₂)₈, and N in C₂₀(CN)₈

^c All cyano groups bear the same charges except one, the carbon and nitrogen of which bear the relative charges of +0.294 and +0.232, respectively.

The differences between their positive charges correlate with the differences between their electronegativities. However, the difference of ~ 0.350 between the electronegativities of H and C, cannot simply explain the considerable difference between their positive charges. Eventually, C₂₀(OH)₈ with -0.711 charged O and +0.197 charged C shows the highest charge separation on its surface leading to one of the highest binding energies and hence a possible candidate for hydrogen storage.

HOMO-LUMO gaps, nucleophilicity and electrophilicity of exohedrally functionalized fullerenes

The electrons donated by a molecule in a reaction should be from its HOMO, while the electrons captured by the molecule should locate on its LUMO. Furthermore, the atom on which the HOMO mainly distributes should have the ability for detaching electrons, whereas the atom with the occupation of the LUMO should gain electrons [26]. On this basis, the HOMO-LUMO gap is traditionally associated with chemical stability

against electronic excitation, with larger gap corresponding to greater stability. Note that pyramidalization of a unsaturated C=C bond remarkably reduces its energy gap between the π (bonding) and π^* (antibonding) molecular orbitals, leading to “diradical” character and, of course, much higher reactivity. The HOMO-LUMO gap of exohedrally functionalized fullerenes varies depending on the type of exohedral derivative atoms. All exohedral derivatives increase the gap leading to the enhanced stability against electronic excitations. Specifically, C₂₀H₈, and C₂₀(OH)₈ show significant stabilities with gaps of 5.670 and 5.604 eV, respectively. Interestingly, based on N and ω indices, C₂₀ is both the most nucleophilic and electrophilic species among all studied fullerenes and has a very small HOMO-LUMO gap (1.899 eV) (Table 4).

This clearly represents its huge instability resulting from extreme curvature as said before. The nucleophilicity and electrophilicity of C₂₀ is greatly influenced by substitution. After C₂₀, expectedly,

Table 4. HOMO and LUMO energies, HOMO-LUMO energy gaps (ΔE_{H-L}), nucleophilicity (N) and electrophilicity (ω) indices for the scrutinized heterofullerenes along with C₂₀ at B3LYP/6-311++G**//B3LYP/6-31+G*.

Species	HOMO (a.u.)	LUMO (a.u.)	ΔE_{H-L} (eV)	N (eV)	ω (eV)
C ₂₀	-0.20339	-0.13361	1.899	4.798	5.536
C ₂₀ H ₈	-0.24902	-0.04065	5.670	3.556	1.370
C ₂₀ F ₈	-0.31844	-0.13047	5.115	1.667	3.646
C ₂₀ Cl ₈	-0.30309	-0.11703	5.063	2.085	3.227
C ₂₀ Br ₈	-0.29229	-0.11791	4.745	2.379	3.282
C ₂₀ (NH ₂) ₈	-0.23261	-0.05123	4.936	4.003	1.511
C ₂₀ (OH) ₈	-0.26679	-0.08001	5.082	3.073	2.190
C ₂₀ (CN) ₈	-0.36080	-0.15484	5.604	0.515	4.391
TTFE	-0.37971	-0.14198	6.469	0.000	3.894

C₂₀(CN)₈ with *N* and ω values of 0.515 and 4.391 eV, respectively, is the least nucleophilic and the most electrophilic species (Table 4). Eventually, based on Pauling electronegativities, NH₂ is more nucleophilic than OH and Cl more than F.

CONCLUSION

The smallest possible fullerene cage, i.e. C₂₀, is taken into account of exohedral derivatives through our previously reported isolation strategy. The exohedral derivative atoms are replaced at eight selected symmetric positions of C₂₀. Probing exohedrally functionalized fullerenes C₂₀X₈ where X = H, F, Cl, Br, NH₂, OH and CN reveals that all these systems are true minima. Calculated binding energy of 6.628 eV shows C₂₀(CN)₈ as the most stable exohedrally functionalized fullerene followed by C₂₀F₈ with the binding energy of 5.484 eV. The binding energies of the other exohedrally functionalized fullerenes ranges from 4.944 to 5.437 eV. Exohedral derivatives lead to a high charge distribution on the surfaces of all exohedrally functionalized fullerenes with the highest distribution on C₂₀(OH)₈ with +0.197 charged carbons and -0.711 charged O atoms. These high point charges upon the exohedrally functionalized fullerenes surface can improve the storage capacity and make them worthy of investigation for hydrogen storage. All exohedral derivatives increase the HOMO-LUMO gap leading to enhanced stability against electronic excitations. Also, all exohedrally functionalized fullerenes have lower nucleophilicity and electrophilicity than C₂₀ indicating their stability compared to the unsubstituted cage.

REFERENCES

1. D.A. Bochvar, E.G. Gal'perin, *Proc. Acad. Sci. USSR*, 209, 239 (1973).
2. H.W. Kroto, J.R. Heath, S.C. O'Brien, R.F. Curl, R.E. Smalley, *Nature*, 318, 162 (1985).
3. H. Prinzbach, A. Weller, P. Landenberger, F. Wahl, J. Worth, L.T. Scott, M. Gelmont, D. Olevano, B.V. Issendorff, *Nature*, 407, 60 (2000).
4. (a) L. Türker, *Journal of Molecular Structure: THEOCHEM*, 593, 149 (2002). (b) L. Türker, *Journal of Molecular Structure: THEOCHEM*, 624, 233 (2003).
5. C.R. Wang, T. Kai, T. Tomiyama, T. Yoshida, Y. Kobayashi, E. Nishibori, M. Takata, M. Sakata, H. Shinohara, *Materials science: Nature*, 408, 426 (2000).
6. Z.Q. Shi, X. Wu, C.R. Wang, X. Lu, H. Shinohara, *Angew. Chem. Int. Ed.*, 45, 2107 (2006).
7. S. Stevenson, P.W. Fowler, T. Heine, J.C. Duchamp, G. Rice, T. Glass, K. Harich, E. Hajdu, R. Bible, H.C. Dorn, *Nature*, 408, 427 (2000).
8. (a) D. Moran, F. Stahl, E.D. Jemmis, H.F. Schaefer III, P.v.R. Schleyer, *J. Phys. Chem. A*, 106, 5144 (2002). (b) Z. Chen, H. Jiao, D. Moran, A. Hirsch, W. Thiel, P.v.R. Schleyer, *J. Phys. Chem. A*, 107, 2075 (2003).
9. F.A. Shakib, M.R. Momeni, 406,1471 (2011) .
10. X.F. Gao, Y.L. Zhao, *J. Comput. Chem.*, 28,795 (2007).
11. D.L. Chen, W.Q. Tian, J.K. Feng, C.C. *Chem. Phys. Chem.*, 8, 2386 (2007).
12. Yuan-Zhi Tan, Xiao Han, Xin Wu, Ye-Yong Meng, Feng Zhu, Zhuo-Zhen Qian, Zhao-Jiang Liao, Ming-Hui Chen, Xin Lu, Su-Yuan Xie, Rong-Bin Huang, and Lan-Sun Zheng, *J. Am. Chem. Soc.* 130, 15240 (2008).
13. D. L. Chen; W. Q.Tian; J. K.Feng; C. C.Sun , *J. Phys. Chem. B* ,111, 5167 (2007).
14. L.L. Sun, S.W. Tang, Y.F. Chang, Z.L. Wang, R.S. Wang, *J. Comput. Chem.* 29, 2631 (2008).
15. Q.B. Yan, Q.R. Zheng, G. Su, *J. Phys. Chem. C*, 111, 549 (2007).
16. Q.B. Yan, Q.R. Zheng, G. Su, *Carbon*, 45, 1821 (2007) .
17. S.Y. Xie, F. Gao, X. Lu, R.B. Huang, C.R. Wang, X. Zhang, M.L. Liu, S.L. Deng, L.S. Zheng, *Science*, 304, 699 (2004).
18. C.R. Wang, Z.Q. Shi, L.J. Wan, X. Lu, L. Dunsch, C.Y. Shu, Y.L. Tang, H. Shinohara, *J. Am. Chem. Soc.*,128, 6605 (2006) .
19. X. Han, S.J. Zhou, Y.Z. Tan, X. Wu, F. Gao, Z.J. Liao, R.B. Huang, Y.Q. Feng, X. Lu, S.Y. Xie, L.S. Zheng, *Angew. Chem., Int. Ed.*, 47, 5340 (2008).
20. A.D. Becke, *Phys. Rev. A*, 38, 3098 (1988).
21. A.D. Becke, *J. Chem. Phys.*, 98, 5648 (1993) .
22. C. Lee, W. Yang, R.G. Parr, *Phys. Rev. B* ,37,758 (1988) .
23. M.J. Frisch, et al. Gaussian 03; Revision B.02, Gaussian, Inc.: Pittsburgh, PA, (2003). See the Supporting Information for the full reference.
24. P.C. Hariharan, J.A. Pople, *Mol. Phys.* ,27,209 (1974).
25. M.M. Francl, W.J. Pietro, W.J. Hehre, J.S. Binkley, M.S. Gordon, D.J. DeFrees, J.A. Pople, *J. Chem. Phys.* ,77, 3654 (1982).
26. T. Clark, J. Chandrasekhar, G.W. Spitznagel, P.v.R. Schleyer, *J. Comput. Chem.*, 4, 294 (1983).
27. M.J. Frisch, J.A. Pople, J.S. Binkley, *J. Chem. Phys.*, 80, 3265 (1984).
28. M.R.Momeni, F.A.Shakib, *J. Chem. Phys. Letters*, 492, 137 (2010).
29. L.R. Domingo, E. Chamorro, P. Pérez, *J. Org. Chem.*,73, 4615 (2008).
30. R.G. Parr, L. Szentpaly, S. Liu, *J. Am. Chem. Soc.*, 121, 1922 (1999).
31. (a) R.G. Parr, R.G. Pearson, *J. Am. Chem. Soc.*, 105, 7512 (1983). (b) R.G. Parr, W. Yang, *Density Functional Theory of Atoms and Molecules*, Oxford University Press: New York, NY, (1989).
32. E.D. Glendening, A.E. Reed, J.E. Carpenter, F. Weinhold, NBO Version 3.1.

33. (a) H. Prinzbach, *Angew. Chem., Int. Ed. Engl.*, 32, 1722 (1993). (b) H. Prinzbach, K. Weber, *Angew. Chem., Int. Ed. Engl.*, 33, 2239 (1994). (c) M. Bertau, F. Wahl, A. Weiler, K. Scheumann, J. Wörth, M. Keller, H. Prinzbach, *Tetrahedron*, 53, 10029 (1997).
34. A. Hirsch, Z. Chen, H. Jiao, *Angew. Chem., Int. Ed.* 39, 3915, (2000).
35. Z. Chen, T. Heine, H. Jiao, A. Hirsch, W. Thiel, P.v. R. Schleyer, *Chem. Eur. J.*, 10, 963 (2004).
36. A.K. Ott, G.A. Rechtsteiner, C. Felix, O. Hampe, M.F. Jarrold, R.P.V. Duyne, K. Raghavachari, *J. Chem. Phys.*, 109, 9652 (1998).
37. X. Lu, Z. Chen, *Chem. Rev.*, 105, 3643 (2005).
38. R. Hoffmann, P.v.R. Schleyer, H.F. Schaefer *Angew. Chem. Int. Ed.*, 47, 7164 (2008).
39. G.E. Froudakis, *Nano Lett.*, 1, 531 (2001).
40. M. Menon, E. Richter, A. Mavrandonakis, G. Froudakis, A.N. Andriotis, *Phys. Rev. B*, 69, 115322 (2004).
41. A. Mavrandonakis, G.E. Froudakis, M. Schnell, M. Muhlhauser, *Nano Lett.*, 3, 1481 (2003).
42. G. Mpourmpakis, G.E. Froudakis, G.P. Lithoxoos, J. Samios, Carbon nanoscrolls: *Nano Lett.* 6, 1581 (2006).

ЧИСЛЕНО ИЗСЛЕДВАНЕ НА НАЙ-МАЛКИТЕ ЕКСОЕДРИЧНИ ФУНКЦИОНАЛИЗИРАНИ ФУЛЕРЕНИ, $C_{20}X_8$ ($X = H, F, Cl, Br, NH_2, OH$ И CN)

Ф. Надери*

Департамент по химия, Клон Шах-е-Оодс, Ислямски университет „Асад“, Техеран, Иран

Постъпила на 9 август, 2013 г.; Коригирана на 19 юли 2014 г.

(Резюме)

Изпитани са структурната стабилност и електронните свойства на ексоедрични функционализирани фулерени $C_{20}X_8$, където $X = H, F, Cl, Br, NH_2, OH$ и CN с помощта на В3LYP-ниво на теорията. Изчислените вибрационни честоти показват, че всички системи имат истински минимума. Изчислените енергии на свързване за ексоедричните функционализирани фулерени показват, че $C_{20}(CN)_8$ и след него $C_{20}F_8$ са най-стабилните с енергии на свързване съответно 6.628 и 5.484 eV. Всички ексоедрични производни намаляват проводимостта на фулерените чрез нарастването на техните НОМО-LUMO области и затова повишават тяхната стабилност срещу електронно възбуждане. Високият пренос на заряда на повърхността на нашите стабилни ексоедрични функционализирани фулерени, особено $C_{20}(OH)_8$ предизвиква следващи изследвания върху техните възможности за складиране на водород.

Synthesis and structural investigation of La₂O₃ doped anthracene nanocrystallites as an advanced dielectric material

Z. Moradinejad¹; A. Bahari²; S. M. Aghajanpour Mir³; S. N. Mousavi Kani^{3,*}

¹. Sari Second Region, Education Office, Sari, Iran

². Department of Physics, University of Mazandaran, Babolsar, Iran

³. Cellular and Molecular Biology Research Center, Babol University of Medical Sciences, Babol, Iran

Received August 30, 2013; Revised February 23, 2014

In recent years organic-inorganic hybrid nano materials have been significantly studied. These samples can prevent leakage and tunneling currents through ultra-high vacuum chambers, drug electrochemical sensors and electronic chips. Moreover, they can be used as controller gate dielectrics in nano transistor devices and memories.

In the present work, La₂O₃ doped anthracene (Ant) nano crystallites are synthesized by a sol-gel method, and their nano structural properties are studied by XRD, EDX and SEM techniques. The obtained results indicate that Ant-La₂O₃ nano particles with amorphous structure at a temperature of 300 °C are suitable as a gate dielectric for organic nano transistor devices.

Keywords: Nano, Transistors, Hybrid composite, Anthracene, La₂O₃.

INTRODUCTION

In recent years, organic-inorganic hybrid nano materials have been the subject of thorough studies. These materials are obtained by a sol-gel method [1]. The most important challenge for hybridation is the phase separation between the organic and inorganic components. Thus, to overcome this problem, strong bonds such as hydrogen bonds and especially covalent bonds have been used to increase the interaction between the two phases [2]. These nano materials combine the benefits of the organic phase such as flexibility, light weight, easy reactivity and those of the inorganic phase such as high mechanical resistance, chemical and physical stability and good optical properties. Due to their potential use in some fields such as optics, optoelectronics, electronic devices and drug electrochemical sensors, these materials are used in industry, as well as in research laboratories [3].

Pentacene as an organic material with polycyclic aromatic hydrocarbon (PAH) structure and five benzene rings is a strong gate insulator and can be the appropriate choice for research on organic electronic devices such as organic thin film transistors, organic field-effect transistors and polymer electrolyte fuel batteries [4-8]. Anthracene is a PAH compound with three benzene rings, more accessible and cheaper than pentacene with approximately the same properties. Therefore, the use of anthracene can be more affordable on

industrial scale [5].

The application of high-k dielectric materials such as Gd₂O₃ [9], Al₂O₃ [10], ZrO₂ [11], Y₂O₃ [12], CrO₂ [13], HfO₂ [14] and La₂O₃ [15-16], has been investigated in inorganic electronic devices. Among them, La₂O₃ with a high dielectric constant (K=27) [17], largest band gap and minimum energy networks is more attractive as a gate insulator than others. Moreover, La₂O₃ has a hexagonal crystal structure at low temperatures [17] and can be used as an important component in automobile exhaust-gas convectors. Also, it is a promising agent in catalytic materials and optical filters [18]. Furthermore, La₂O₃ has been employed as an antibacterial agent for water purification [19-20]. Thus, La₂O₃ has attracted much attention in recent years [21]. Therefore, we performed a series of experiments to synthesize La₂O₃-Ant nano hybrid composites by a sol-gel method and studied their nano structural properties with XRD (X-ray diffraction), SEM (scanning electron microscopy) and EDX (energy dispersive X-ray) techniques. The obtained results showed that the sample containing 0.28 g Ant, synthesized at 300 °C can be used in nano-chip devices.

EXPERIMENTAL PROCEDURE AND DETAILS

The Ant-La₂O₃ nano crystallites were prepared by a sol-gel procedure (figure 1). First, lanthanum chloride (LaCl₃·7H₂O, 5.9 g) was dissolved in 300 ml of distilled water under magnetic stirring at room temperature. Then, cetyltrimethylammonium

* To whom all correspondence should be sent:
E-mail: sn.mousavi313@gmail.com

bromide (CTAB, 2.7 g) was added to the solution at room temperature on stirring until the solution became completely transparent. Subsequently, 6.0 ml of ammonia was added to the solution to adjust the pH value between 6.0–10.0. Following the addition of ammonia, the solution turned opaque. After vigorous stirring for 2 h, Ant (0.07 g) dissolved in 2 ml of o-xylene was dropwise added and the solution was vigorously stirred for 24 h, then was dried at 80 °C for 72 h. Finally, the resultant white solid product was washed with distilled water and ethanol, centrifuged to remove the undesirable ions from the final product and dried at 80 °C. In this way Ant-La₂O₃ powder was obtained. The same procedure was performed with two more amounts of Ant (0.14 g and 0.28 g), then all products were calcined at two different annealing temperatures (300 °C and 500 °C) for studying the effect of temperature and concentration on morphology.

The crystal phases of the nano crystallites were identified by XRD analysis. Morphology analysis was performed using SEM technique. The size of nano crystallites was determined using X-powder software.

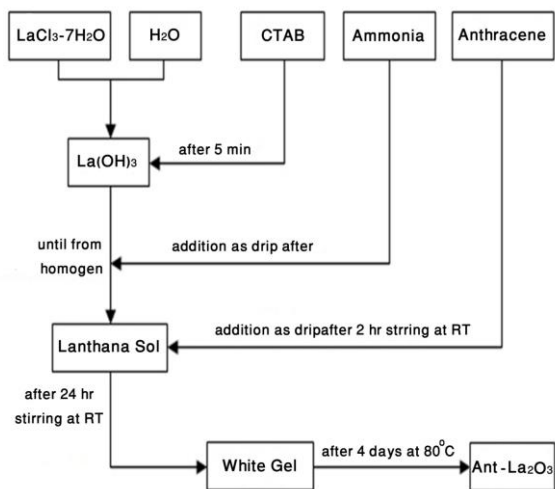


Fig. 1. Steps of Ant-La₂O₃ powders preparation

RESULTS

The structural features of the Ant-La₂O₃ nano crystallites were analyzed using XRD analysis. Figure 2 displays the XRD patterns of the calcined Ant-La₂O₃ at 300 °C. It shows that by increasing the concentration of Ant, the number of peaks decreased. Figure 3 displays the XRD patterns of Ant-La₂O₃ at two temperatures (300 and 500 °C). Here, by increasing the temperature, the quantity and intensity of peaks increases.

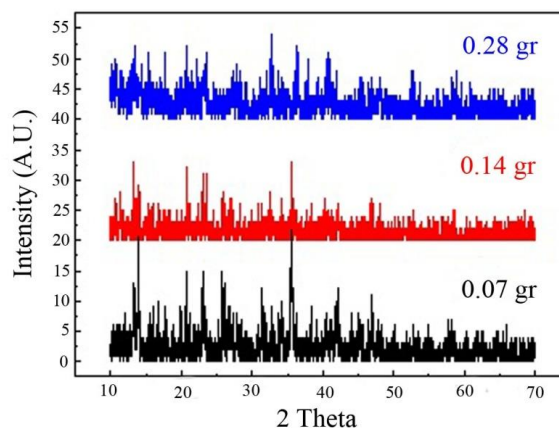


Fig. 2. XRD patterns of Ant-La₂O₃ at different Ant concentrations.

Figure 4 shows the sizes of Ant-La₂O₃ nano crystallites at 300°C and 500°C, determined by X-powder software. X-powder analysis indicated that the size of the nano crystallites increased by increasing the temperature (figure 4a and 4b) and decreasing Ant concentration (figure 4c to 4e) ranging from 30-48 nm (Table 1).

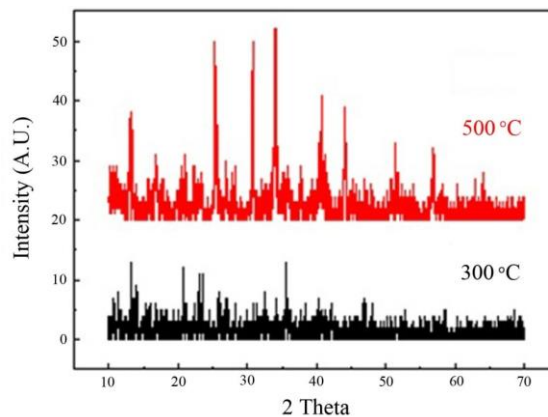


Fig. 3. XRD patterns of Ant-La₂O₃ at different temperatures (300 °C and 500 °C).

Table 1. Comparison of the size of Ant-La₂O₃ nano crystallites.

Size of nano crystallites	Calcination temperature	Sample
41 nm	300 °C	0.07 g Ant/La ₂ O ₃
48 nm	500 °C	0.07 g Ant/La ₂ O ₃
41 nm	300 °C	0.07 g Ant/La ₂ O ₃
40 nm	300 °C	0.14 g Ant/La ₂ O ₃
30 nm	300 °C	0.28 g Ant/La ₂ O ₃

The same pattern is confirmed in figure 5 which shows images obtained by the SEM technique at two different annealing temperatures. These images illustrate the micro structural alteration of the nano crystallites. On the surface of the sample calcined at 300 °C (figure 5a), no recognizable crystal particles

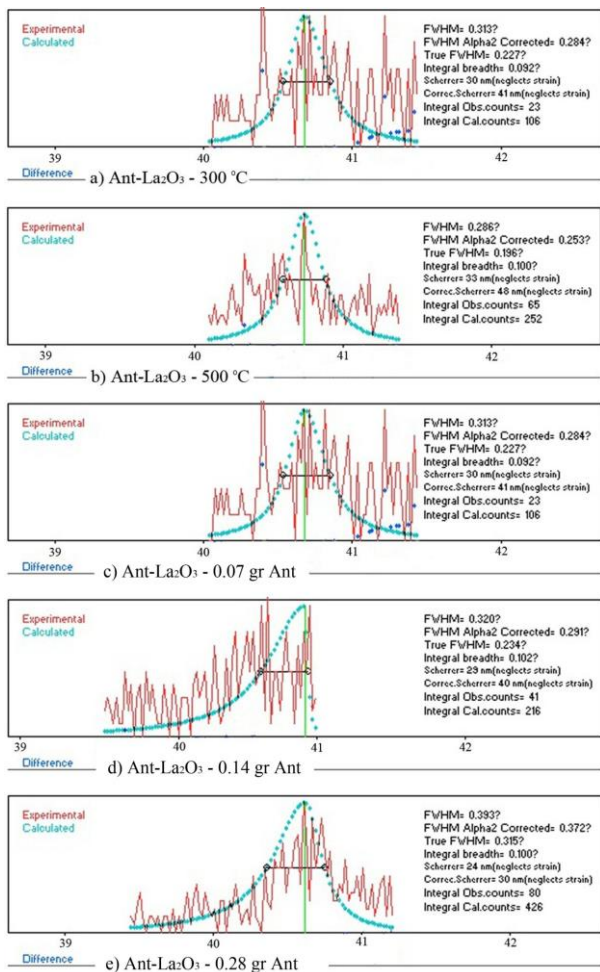


Fig. 4. Study of nano crystallite peaks using X-powder software.

are found. For the sample calcined at 500 °C (figure 5b) a regular shape of grains with clear boundaries can be seen.

Figure 6 shows the results of the EDX analysis confirming that the nano crystallites consist of La and O atoms.

DISCUSSION

According to the XRD results, at 300 °C the nano crystallites have amorphous structure and with increasing Ant concentration the amorphicity increases. On the other hand, at a temperature of 500 °C, the particles display crystalline structure.

SEM images confirmed the results of the XRD analysis and showed that La₂O₃ nano particles with Ant are in a film-layer form with amorphous structure at 300 °C, while the structural phases change. The amorphous structure of La₂O₃ at 300 °C [18] can reduce leakage and tunneling currents; moreover, upon adding Ant, the final structure at

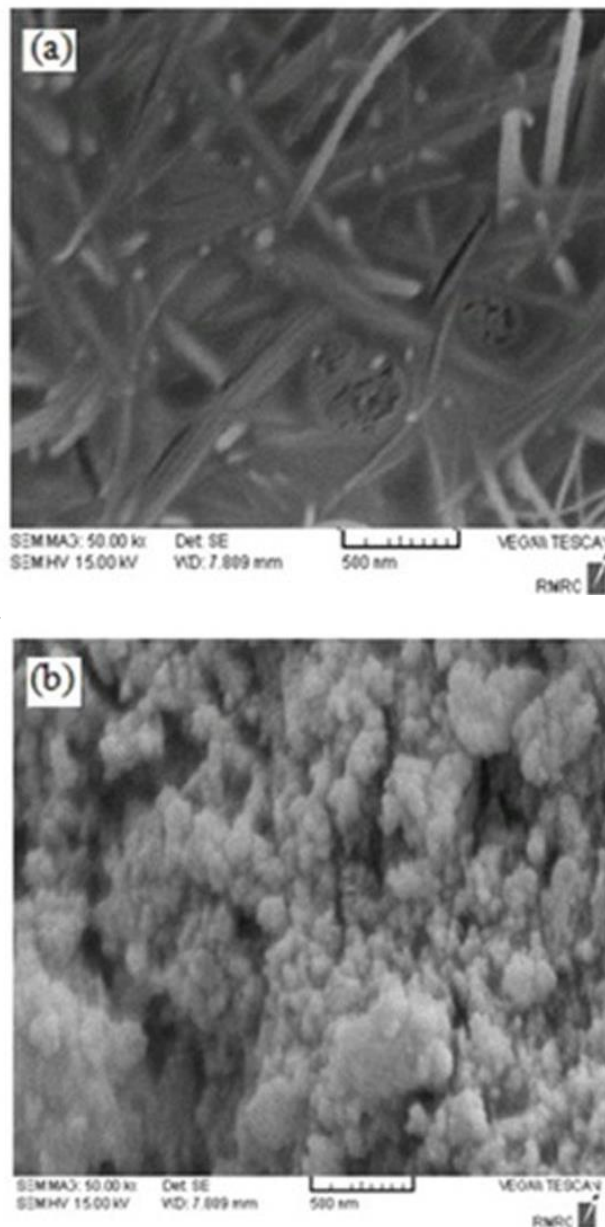


Fig. 5. SEM images of ANT-LazO₃ nano crystallites: (a) at 300 °C (b) at 500 °C.

the mentioned temperature becomes more

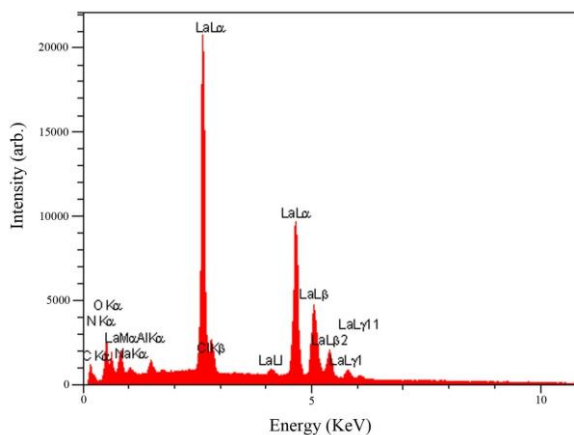


Fig. 6. EDX pattern of Ant-LazO₃.

amorphous and k-dielectric increases. As a result, La₂O₃ hybridized with Ant can be used as a good gate dielectric in nano electronic devices and organic nano transistors.

CONCLUSION

In the present work, the structural characteristics of Ant-doped La₂O₃ nano particles prepared by a sol-gel method were studied at different temperatures and concentrations. The experimental results showed that Ant-La₂O₃ with amorphous structure at 300°C can be suggested as a good gate dielectric for nano electronic devices and organic nano transistors.

REFERENCES

1. G. H. Hsiue, W. J. Kuo, Y. P. Huang, R. J. Jeng, *Polymer.*, **41**, 2813 (2000).
2. M. Xiong, S. Zhuxue, L. Wu, *Polymer.*, **45**, 8127 (2004).
3. M. Mohseni, in 2nd International Nano and Hybrid Coatings Conference, PRA Coatings Technology Centre, Hampton, Middlesex: Brussels, Belgium, (2007).
4. A. C. Yeh, *Life. Sci. J.*, **8**, 379 (2011).
5. Y. Yamashita, *Sci. Technol. Adv. Mater.*, **10**, 024313 (2009).
6. T. Hasegawa, J. Takeya, *Sci. Technol. Adv. Mater.*, **10**, 024314 (2009).
7. C. G. Choi, *SID. Symposium. Digest. Technical. Papers.*, **39**, 1239 (2008).
8. N. Koch, *Chemphyschem.*, **8**, 1438 (2007).
9. B. A. Orłowski, E. Guziewicz, E. Nossarzewska-Orłowska, A. Bukowski, R.L. Johnson, *Surf. Sci.*, **507-510**, 218 (2002).
10. S. Zafar, A. Kumar, G. Evgeni, E. Cartier, *Transactions. Device. Materials. Reliability.*, **5**, 45 (2005).
11. P. Y. Kuei, J. D. Chou, C. T. Huang, H. H. Ko, S. C. Su, *J. Crystal. Growth.*, **314**, 81 (2011).
12. J. J. Chambers, G. N. Parsons, *Appl. Phys. Lett.*, **77**, 2385 (2000).
13. A. Bahari, A. Anasari, Z. Rahmani, *J. Eng. Technol. Res.*, **3**, 203 (2011).
14. G. H. Chen, Z. F. Hou, X. G. Gong, *Comput. Mater. Sci.*, **44**, 46 (2008).
15. J. Sheng, S. Zhang, S. Lv, W. Sun, *J. Mater., Sci.*, **42**, 9565 (2007).
16. C. Hu, H. Liu, W. Dong, Y. Zhang, G. Bao, C. Lao, and Z.L. Wang, *Adv. Mater.*, **19**, 470 (2007).
17. A. Bahari, A. Ramzannejad, *Int. J. Res. Pharmac. Biomed. Sci.*, **2**, 1593 (2011).
18. A. Bahari, Z. Khorshidi, R. Gholipour, T. Taghipoor, A. Rezaeian, *Americ. J. Sci. Res.*, **54** 19 (2012).
19. L. C. Gerber, N. Moser, N. A. Luechinger, W. J. Stark, R. N. Grass, *Chem. Commun.*, **48**, 3869 (2012).
20. Y. J. Wang, R. D. Hu, D. H. Jiang, P. H. Zhang, Q. Y. Lin, Y. Y. Wang, *J. Fluoresc.*, **21**, 813(2011).
21. J. A. Ng, Y. Kuroki, N. Sugii, K. Kakushima, S.-I. Ohmi, K. Tsutsui, T. Hattori, H. Iwai, H. Wong, *Microelectron. Eng.*, **80**, 206 (2005).

СИНТЕЗ И СТРУКТУРНИ ИЗСЛЕДВАНИЯ НА АНТРАЦЕНОВИ НАНОКРИСТАЛИ, ДОТИРАНИ С La₂O₃, КАТО СЪВРЕМЕНЕН ДИЕЛЕКТРИЧЕН МАТЕРИАЛ

З. Морадинеждад¹; А. Бахари²; С.М. Агаджанпур Мир³; С.Н.Мусави Кани^{3,*}

¹ Втори район Сари, Отдел „Образование“, Сари, Иран

² Департамент по физика, Университет „Мазандаран“, Баболсар, Иран

³ Изследователски център по клетъчна и молекулярна биология, Баболски университет по медицински науки, Бабол, Иран

Постъпила на 30 август, 2013 г.; Коригирана на 23 февруари, 2014 г.

(Резюме)

През последните години интензивно са изследвани хибридни органично-неорганични наноматериали. Те могат да предотвратят изтичане и тунелни токове в камери със свръх-висок вакуум, електрохимични сензори за лекарства и електронни чипове. Освен това те могат да се използват като контролни диелектрици в нанотранзисторни прибори и памет.

В настоящата работа са синтезирани по сол-гел метода антраценови (Ant) нанокристалити, дотирани с La₂O₃. Техните нано-структурни свойства са изследвани чрез XRD, EDX и SEM методи. Получените резултати показват, че наночастиците Ant-La₂O₃ с аморфна структура са подходящи при 300°C за контролни диелектрици в органични нанотранзисторни прибори.

Synthesis and antitumor activity of some fused heterocyclic compounds based on cyclohepta[b]thiophene derivatives

K. A. El-Sharkawy,^{1,2*} M. M. Said³, G. Dardas¹

¹Department of Organic Chemistry, Faculty of Biotechnology, October University for Modern Sciences and Arts (MSA), El-Wahat Road, 6 October City, A. R. Egypt.

²Pharmaceutical Chemistry Department, Pharmacy College, Jazan University, Jazan City, Kingdom of Saudi Arabia.

³ Department of Organic Chemistry, Faculty of Pharmacy, Suez Canal University, Ismailia, A.R. Egypt.

Received September 9, 2013; Revised April 18, 2014

The reaction of 5,6,7,8-tetrahydro-4H-cyclohepta[b]thiophene derivatives 3a,b with acetic anhydride in presence of glacial acetic acid produced the acetamido derivatives 4a,b. Cyclization of the latter compounds gave the annulated products 5a,b. Compounds 3a,b reacted with one of the activated methylene groups of malononitrile (2a) and afforded compounds 7a,b through internal cyclization of the intermediates of compounds 6a,b. The latter products were reacted with the cyclic ketones 8a,b,c in presence of elemental sulphur and afforded compounds 9a-f. Compounds 3a,b reacted with different types of aldehydes 10a,b,c to produce compounds 11a-f. Finally the products 11a-f reacted with hydrazine hydrate (12) affording compounds 14a-f via the proposed intermediate formation of compounds 13a-f. The antitumor activities of the synthesized compounds were tested using three different cell lines.

Keywords: cyclohepta[b]thiophene, pyrimidine, pyridine, antitumor activity

INTRODUCTION

Thiophene and fused thiophene derivatives were studied within the frame of a comprehensive program in the last few years by our research group and others [1-4]. The biological activity of thiophene derivatives as antimicrobial [5] and antifungal agents [6] was investigated.

Cycloalkyl[b]thiophene derivatives display cytotoxic activity [7]. The activity of thienopyridine derivatives as antibacterial [8], anti-inflammatory [9], antidiabetic [10] and anti-hepatocellular carcinoma [11] agents was evaluated.

Moreover, thiophene ring fused with other heterocyclic rings like pyrimidine is known to have a wide spectrum of biological and pharmacological activities. Thus, many synthetic thienopyrimidine derivatives are considered as antibacterial [12], analgesic, anti-inflammatory agents [13], protein kinase inhibitors [14], and potential antiviral agents [15].

In this article, considering the above findings and as a continuation of the efforts directed towards the synthesis of new heterocyclic compounds with expected biological activities [16], we herein report the synthesis of some new cyclohepta[b]thiophene derivatives containing pyrimidine and pyridine moieties and the screening of their antitumor activity against three different cell lines. The

structures of the newly synthesized compounds were established using IR, ¹H-NMR and mass spectrometry techniques.

EXPERIMENTAL

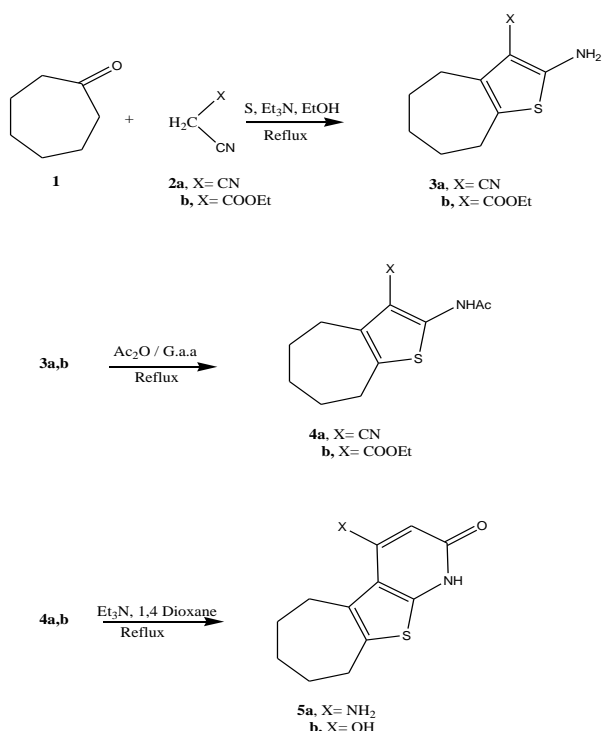
All melting points were uncorrected; the IR spectra, expressed in cm⁻¹, were recorded using KBr pellets on a Pa-9721 IR spectrometer. ¹H NMR spectra were obtained on a Varian EM-390 90 Hz spectrometer in DMSO-d₆ as solvent and TMS as internal reference. Chemical shifts (δ) are expressed in ppm. Mass spectra were recorded on Kratos (75 ev) Ms Equipment (Germany). Elemental analyses were carried out by the Microanalytical data unit at the National Research Center, Giza, Egypt and the Microanalytical data unit at the Cairo University.

Synthetic pathways are presented in Schemes 1, 2, 3 and cell growth inhibition data are presented in Table 1.

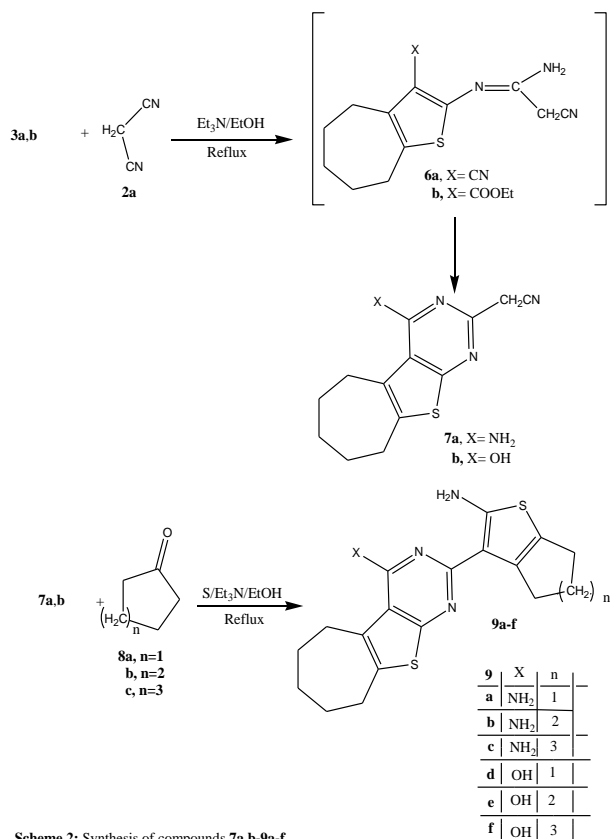
General procedure for the synthesis of: 2-Amino-5,6,7,8-tetrahydro-4H-cyclohepta [b]thiophene-3-carbonitrile (3a) and 2-Amino-5,6,7,8-tetrahydro-4H-cyclohepta[b]thiophene-3-carboxylic acid ethyl ester (3b)

The compounds (3a,b) were obtained via reaction of either malononitrile (2a) or ethylcyanoacetate (2b) with cycloheptanone and elemental sulfur according to a former described procedure [17].

* To whom all correspondence should be sent:
E-mail: karamsyn@yahoo.com

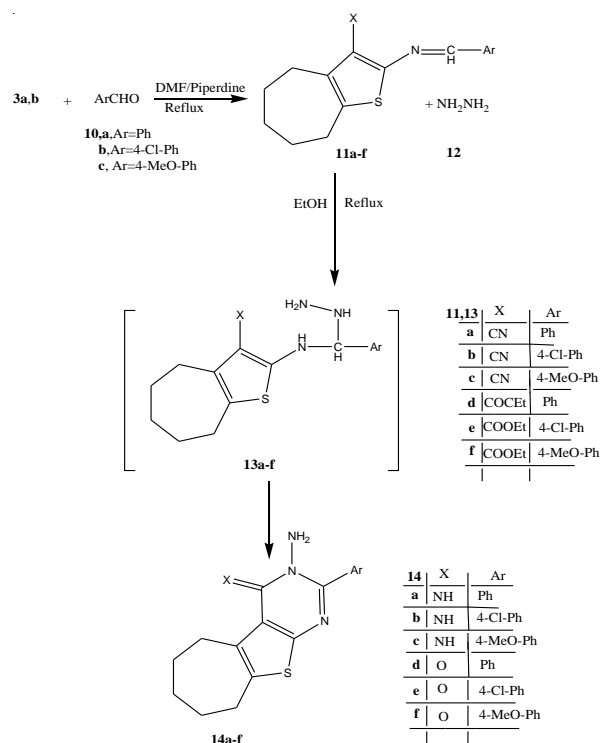


Scheme 1. Synthesis of compounds 3 a, b – 5 a, b



Scheme 2: Synthesis of compounds 7a,b-9a-f

Scheme 2. Synthesis of compounds 7 a, b – 9 a-f



Scheme 3. Synthesis of compounds 11 a-f – 14 a-f

Table 1. Effect of compounds 3a-14f on the growth of three human tumor cell lines

Compound	GI ₅₀ (μmol L ⁻¹)		
	MCF-7	NCI-H460	SF-268
3a	21.0 ± 6.8	12.0 ± 2.4	21.5 ± 5.0
3b	22.0 ± 5.4	14.0 ± 3.6	11.8 ± 4.6
4a	20.6 ± 3.8	17.1 ± 2.9	21.3 ± 2.5
4b	41.7 ± 7.9	32.2 ± 4.8	24 ± 2.8
5a	1.2 ± 0.06	0.9 ± 0.08	0.6 ± 0.05
5b	40.7 ± 7.7	33.2 ± 4.8	28.4 ± 2.8
7a	18.0 ± 1.6	24.0 ± 2.4	22.5 ± 2.5
7b	11.8 ± 2.6	24.5 ± 3.2	16.7 ± 2.4
9a	10.0 ± 1.7	20.6 ± 1.4	22.4 ± 0.8
9b	2.4 ± 0.4	4.1 ± 0.6	4.3 ± 0.4
9c	6.0 ± 0.6	4.0 ± 0.4	2.5 ± 8.0
9d	12.4 ± 1.2	11.6 ± 0.9	6.8 ± 0.5
9e	6.6 ± 2.2	4.6 ± 2.6	2.4 ± 1.8
9f	11.4 ± 1.4	12.6 ± 1.6	14.8 ± 2.2
11a	14.0 ± 0.6	12.0 ± 0.4	22.5 ± 8.0
11b	32.7 ± 7.5	40.2 ± 8.8	23.0 ± 5.0
11c	11.0 ± 0.2	16.6 ± 1.6	18.4 ± 0.6
11d	24.0 ± 1.8	24.0 ± 0.8	10.5 ± 1.1
11e	24.2 ± 10.5	20.2 ± 8.8	24.0 ± 8.0
11f	16.6 ± 2.5	10.05 ± 2.2	8.6 ± 1.6
14a	1.0 ± 0.2	3.6 ± 0.4	1.4 ± 0.8
14b	8.2 ± 0.4	6.1 ± 0.6	4.3 ± 0.5
14c	2.0 ± 0.6	1.2 ± 0.4	1.6 ± 8.0
14d	0.2 ± 0.02	0.1 ± 0.02	0.3 ± 0.04
14e	6.6 ± 22.2	4.6 ± 2.6	2.4 ± 1.8
14f	0.01 ± 0.003	0.02 ± 0.001	0.01 ± 0.001
Doxorubicin	0.04 ± 0.008	0.09 ± 0.008	0.09 ± 0.007

Results are given as concentrations causing 50 % of cell growth inhibition (GI₅₀) after an exposure of 48 h - means ± SEM of three independent experiments performed in duplicate.

N-(3-Cyano-5,6,7,8-tetrahydro-4*H*-cyclohepta[b]thiophen-2-yl)-acetamide (4a) and 2-Acetyl-amino-5,6,7,8-tetrahydro-4*H*-cyclohepta[b]thiophene-3-carboxylic acid ethyl ester (4b)

To either solution of compound (3a, 1.92 g, 0.01 mol) or (3b, 2.39 g, 0.01 mol) in glacial acetic acid (40 mL), acetic anhydride (1.04 g, 0.01 mol) was added at an acetic acid to acetic anhydride ratio of 5:1. The reaction mixture was then refluxed for 3 h, the solution was cooled, poured on an ice/water mixture containing few drops of hydrochloric acid and the formed precipitate was filtered off.

Compound 4a: Yellow crystals recrystallized from ethanol, yield 75.6%, 1.76 g, m.p.142-144 °C. IR (KBr): ν/cm^{-1} = 3321-3290 (NH), 2956 (CH₃), 2890 (CH₂), 2230 (CN), 1675 (CO), 1632 (C=C). ¹HNMR (DMSO) δ = 2.12-2.21(m, 6H, 3CH₂), 2.26-2.32 (m, 4H, 2CH₂), 2.39 (s, 3H, CH₃), δ (s, 1H, NH, D₂O-exchangeable). Calcd. for C₁₂H₁₄N₂OS (234.32): C, 61.51; H, 6.02; N, 11.96; S, 13.68%. Found: C, 61.38; H, 6.24; N, 11.74; S, 13.84 %. MS (relative intensity) m/z: 234 (M⁺, 23%), 191 (100%), 176 (48%).

Compound 4b: Pale brown crystals recrystallized from ethanol, yield 81.2%, 1.85 g, m.p. 112-114°C. IR (KBr): ν/cm^{-1} = 3346 (NH), 2977 (CH₃), 2885 (CH₂), 1795 (CO), 1667 (CONH) 1641 (C=C). ¹HNMR (DMSO) δ = 1.65 (t, 3H, CH₃), 1.98-2.11(m, 6H, 3CH₂), 2.14-2.24 (m, 4H, 2CH₂), 2.63 (s, 3H, CH₃), 4.28 (q, 2H, CH₂), 8.60 δ (s, 1H, NH, D₂O-exchangeable). Calcd. for C₁₄H₁₉NO₃S (281.37): C, 59.76; H, 6.81; N, 4.98; S, 11.40 %. Found: C, 60.02; H, 6.57; N, 4.86; S, 11.65 %.MS (relative intensity) m/z: 281 (M⁺, 16.6%), 252 (33.2%), 236 (100%).

4-Amino-1,5,6,7,8,9-hexahydro-10-thia-1-aza-benzo[*a*]azulen-2-one (5a) and 4-Hydroxy-1,5,6,7,8,9-hexahydro-10-thia-1-aza-benzo [*a*] -azulen-2-one (5b)

Either compound (4a, 1.17g, 0.005 mol) or (4b, 1.405g, 0.005 mol) was dissolved in 50 mL of 1,4-dioxane and 0.5 mL of triethylamine was added. Then the solution was refluxed for 3 h for the formation of the cyclized product. The solution was then cooled, poured on an ice/water mixture containing few drops of hydrochloric acid to enhance precipitate formation and the latter was then collected by filtration.

Compound 5a: Brown crystals recrystallized from ethanol, yield 61%, 0.714 g, m.p. 213-215°C. IR (KBr): ν/cm^{-1} = 3447, 3285, 3219, (NH₂, NH), 2885 (CH₂), 1683 (CO), 1644 (C=C). ¹HNMR (DMSO) δ = 1.78-1.94 (m, 6H, 3CH₂), 1.99-2.08 (m, 4H, 2CH₂), 5.18 (s, 2H, NH₂, D₂O-exchangeable), δ (s, 1H, pyridine ring), δ (s, 1H,

NH, D₂O-exchangeable). Calcd. for C₁₂H₁₄N₂OS (234.32): C, 61.51; H, 6.02; N, 11.96; S, 13.68 %. Found: C, 61.72; H, 6.29; N, 12.14; S, 13.55%.

Compound 5b: Yellowish brown crystals recrystallized from ethanol, yield 72.5%, 0.852 g, m.p.165-167°C. IR (KBr): ν/cm^{-1} = 3485-3380, 3225 (OH, NH), 2890 (CH₂), 1674 (C=O), 1655 (C=C), 1152 (CO). ¹HNMR (DMSO) δ = 1.88-1.97 (m, 6H, 3CH₂), 2.25-2.33 (m, 4H, 2CH₂), 6.65 (s, 1H, OH, D₂O-exchangeable), 8.25 δ (s, 1H, NH, D₂O-exchangeable). Calcd. for C₁₂H₁₃NO₂S (235.30): C, 61.25; H, 5.57; N, 5.95; S, 13.63 %. Found: C, 61.50; H, 5.84; N, 6.12; S, 13.86 %. MS (relative intensity) m/z: 235 (M⁺, 22.7%).

(4-Amino-6,7,8,9-tetrahydro-5*H*-10-thia-1,3-diazabenz[*a*]azulen-2-yl)acetonitrile (7a) and (4-Hydroxy-6,7,8,9-tetrahydro-5*H*-10-thia-1,3-diazabenz[*a*]azulen-2-yl) acetonitrile (7b)

To either solution of compound (3a, 1.92 g, 0.01 mol) or (3b, 2.39 g, 0.01 mol) in ethanol (50 ml) containing a catalytic amount of triethylamine (0.5 ml), malononitrile (2a) (0.66 g, 0.01 mol) was added. The reaction mixture was refluxed for 8 h and then cooled, poured on an ice/water mixture containing few drops of hydrochloric acid. The solid product formed was collected by filtration.

Compound 7a: Brown crystals recrystallized from ethanol, yield 52%, 1.342 g, m.p. 142-144°C. IR (KBr): ν/cm^{-1} = 3415, 3227 (NH₂), 2882 (CH₂), 2222 (CN), 1651 (C=C). ¹HNMR (DMSO) δ = 1.93-1.99 (m, 6H, 3CH₂), 2.15-2.28 (m., 4H, 2CH₂), 3.12 (s, 2H, CH₂), 4.58 (s, 2H, NH₂, D₂O-exchangeable). Calcd. for C₁₃H₁₄N₄S (258.34): C, 60.44; H, 5.46; N, 21.69; S, 12.41 %. Found: C, 60.33; H, 5.21; N, 21.88; S, 12.65%.

Compound 7b: Brown crystals recrystallized from ethanol, yield 64.5 %, 1.671 g, m.p. 191-193°C. IR (KBr): ν/cm^{-1} = 3498- 3316 (OH), 2873 (CH₂), 2227 (CN), 1660 (C=C), 1148 (CO). ¹HNMR (DMSO) δ = 1.78-1.89 (m, 6H, 3CH₂), 2.05-2.12 (m, 4H, 2CH₂), 2.98 (s, 2H, CH₂), 7.88 (s, 1H, OH, D₂O-exchangeable). Calcd. for C₁₃H₁₃N₃OS (259.33): C, 60.21; H, 5.05; N, 16.20; S, 12.36 %. Found: C, 60.02; H, 5.30; N, 16.41; S, 12.48%.

2-(2-Amino-5,6-dihydro-4*H*-cyclopenta[b]thiophen-3-yl)-6,7,8,9-tetrahydro-5*H*-10-thia-1,3-diazabenz[*a*]azulen-4-ylamine (9a), 2-(2-Amino-4,5,6,7-tetrahydro-benzo [b]- thiophen-3-yl)-6,7,8,9-tetrahydro-5*H*-10-thia-1,3-diazabenz[*a*]azulen-4-ylamine (9b), 2-(2-Amino-5,6,7,8-tetrahydro-4*H*-cyclohepta[b]thiophen-3-yl)-6,7,8,9-tetrahydro-5*H*-10-thia-1,3-diazabenz[*a*]azulen-4-ylamine (9c)

To a mixture of compound (7a, 0.774 g, 0.003 mol) and either cyclopentanone (8a, 0.252g, 0.003

mol), cyclohexanone (8b, 0.294g, 0.003 mol) or cycloheptanone (8c, 0.336g, 0.003 mol) in ethanol (50 ml) containing a catalytic amount of triethylamine (0.5 ml), elemental sulfur (0.096 g, 0.003 mol) was added. The reaction mixture was heated under reflux for 4 h. It was allowed to cool, then poured on an ice/water mixture containing few drops of hydrochloric acid. The reaction mixture was left overnight to settle and the formed solid product was collected by filtration.

Compound 9a: Brown crystals recrystallized from 1,4-dioxane, yield 66%, 0.706 g, m.p.181-183°C. IR (KBr): ν/cm^{-1} = 3442-3180 (2NH₂), 2886-2865 (CH₂), 1658 (C=N), 1645 (C=C). ¹HNMR (DMSO) δ = 1.77-1.89 (m, 10H, 5CH₂), 1.98-2.08 (m, 6H, 3CH₂), 3.95, 4.58 (2s, 4H, 2NH₂, D₂O-exchangeable). Calcd. for C₁₈H₂₀N₄S₂ (356.51): C, 60.64; H, 5.65; N, 15.72; S, 17.99 %. Found: C, 60.48; H, 5.38; N, 15.97; S, 17.74%.

Compound 9b: Pale brown crystals recrystallized from 1,4-dioxane, yield 63%, 0.7 g, m.p.152-154°C. IR (KBr): ν/cm^{-1} = 3466- 3215 (2NH₂), 2878-2862 (CH₂), 1660 (C=N), 1642 (C=C).¹HNMR (DMSO) δ = 1.86-1.93 (m, 10H, 5CH₂), 2.01-2.09 (m, 8H, 4CH₂), 4.47, 4.85 (2s, 4H, 2NH₂, D₂O-exchangeable). Calcd. for C₁₉H₂₂N₄S₂ (370.53): C, 61.59; H, 5.98; N, 15.12; S, 17.31 %. Found: C, 61.88; H, 5.77; N, 15.01; S, 17.11%.

Compound 9c: Pale brown crystals recrystallized from 1,4-dioxane, yield 58 %, 0.669 g, m.p.177-179°C. IR (KBr): ν/cm^{-1} = 3427-3263 (2NH₂), 2878-2860 (CH₂), 1657 (C=N), 1646 (C=C).¹HNMR (DMSO) δ = 1.72-1.84 (m, 12H, 6CH₂), 2.13-2.22 (m, 8H, 4CH₂), 4.63, 4.98 (2s, 4H, 2NH₂, D₂O-exchangeable). Calcd. for C₂₀H₂₄N₄S₂ (384.56): C, 62.46; H, 6.29; N, 14.57; S, 16.68 %. Found: C, 62.19; H, 6.12; N, 14.29; S, 16.42%.

2-(2-Amino-5,6-dihydro-4H-cyclopenta[b]thiophen-3-yl)-6,7,8,9-tetrahydro-5H-10-thia-1,3-diaza-benzo[a]azulen-4-ol (9d), 2-(2-Amino-4,5,6,7-tetrahydro-benzo[b]thiophen-3-yl)-6,7,8,9-tetrahydro-5H-10-thia-1,3-diaza-benzo[a]azulen-4-ol (9e), 2-(2-Amino-5,6,7,8-tetrahydro-4H-cyclohepta[b]thiophen-3-yl)-6,7,8,9-tetrahydro-5H-10-thia-1,3-di-aza-benzo[a]azulen-4-ol (9f)

To a mixture of compound (7b, 0.778 g, 0.003 mol) and either cyclopentanone (8a, 0.252g, 0.003 mol), cyclohexanone (8b, 0.294g, 0.003 mol) or cycloheptanone (8c, 0.336g, 0.003 mol) in ethanol (50 ml) containing a catalytic amount of triethylamine (0.5 ml), elemental sulfur (0.096 g, 0.003 mol) was added. The reaction mixture was heated under reflux for 3 h. It was allowed to cool

then poured on an ice/water mixture containing few drops of hydrochloric acid. The reaction mixture was left overnight to settle and the formed solid product was collected by filtration.

Compound 9d: Pale brown crystals recrystallized from 1,4-dioxane, yield 74%, 0.794 g, m.p.159-161°C. IR (KBr): ν/cm^{-1} = 3485-3194 (OH, NH₂), 2882-2860 (CH₂), 1655 (C=N), 1644 (C=C). ¹HNMR (DMSO) δ = 1.66-1.74 (m, 8H, 4CH₂), 1.89-2.06 (m, 8H, 4CH₂), 4.82 (s, 2H, NH₂, D₂O-exchangeable), 8.15 (s, 1H, OH, D₂O-exchangeable). Calcd. for C₁₈H₁₉N₃OS₂ (357.49): C, 60.47; H, 5.36; N, 11.75; S, 17.94 %. Found: C, 60.66; H, 5.28; N, 11.95; S, 17.68%.

Compound 9e: Yellowish brown crystals recrystallized from 1,4-dioxane, yield 71%, 0.791 g, m.p. 205-207°C. IR (KBr): ν/cm^{-1} = 3438- 3155 (OH, NH₂), 2878-2857 (CH₂), 1652 (C=N), 1640 (C=C). ¹HNMR (DMSO) δ = 1.88-1.97 (m, 10H, 5CH₂), 2.15-2.26 (m, 8H, 4CH₂), 5.11 (s, 2H, NH₂, D₂O-exchangeable), 7.85 (s, 1H, OH, D₂O-exchangeable). Calcd. for C₁₉H₂₁N₃OS₂ (371.52): C, 61.42; H, 5.70; N, 11.31; S, 17.26 %. Found: C, 61.68; H, 5.44; N, 11.52; S, 17.43%.

Compound 9f: Brown crystals recrystallized from 1,4-dioxane, yield 63 %, 0.729 g, m.p. 217-219°C. IR (KBr): ν/cm^{-1} = 3398-3165 (OH, NH₂), 2875-2862 (CH₂), 1653 (C=N), 1641 (C=C). ¹HNMR (DMSO) δ = 1.95-2.11 (m, 12H, 6CH₂), 2.17-2.24 (m, 8H, 4CH₂), 4.91 (s, 2H, NH₂, D₂O-exchangeable), 8.36 (s, 1H, OH, D₂O-exchangeable). Calcd. for C₂₀H₂₃N₃OS₂ (385.55): C, 62.30; H, 6.01; N, 10.90; S, 16.63 %. Found: C, 62.47; H, 5.87; N, 11.12; S, 16.86%.

2-(Benzylidene-amino)-5,6,7,8-tetrahydro-4H-cyclohepta[b]thiophene-3-carbonitrile (11a), 2-(4-Chloro-benzylidene-amino)-5,6,7,8-tetrahydro-4H-cyclohepta[b]thiophen-3-carbonitrile (11b), 2-[(4-Methoxy-benzylidene)-amino]-5,6,7,8-tetrahydro-4H-cyclo-hepta[b]thiophene-3-carbonitrile (11c)

A mixture of compound (3a, 0.96 g, 0.005mol) and either benzaldehyde (10a, 0.53 g, 0.005mol), 4-chlorobenzaldehyde (10b, 0.71 g, 0.005 mol) or 4-methoxy-benzaldehyde (10c, 0.68 g, 0.005 mol) in dry dimethylformamide (40 ml) containing a catalytic amount of piperidine (0.5 ml) was heated under reflux for 3 h, then poured on an ice/water mixture containing few drops of hydrochloric acid. The solid product formed was collected by filtration.

Compound 11a: Pale yellow crystals recrystallized from ethanol, yield 59%, 0.827 g, m.p. 208-210°C. IR (KBr): ν/cm^{-1} =3048 (CH aromatic), 2893-2864 (CH₂), 2225 (CN), 1651 (C=N), 1642 (C=C).¹HNMR (DMSO) δ = 2.12-2.18

(m, 6H, 3CH₂), 2.24-2.32 (m, 4H, 2CH₂), 6.87 (s, 1H, CH), 7.23-7.55 (m, 5H, C₆H₅). Calcd. for C₁₇H₁₆N₂S (280.39): C, 72.82; H, 5.75; N, 9.99; S, 11.44 %. Found: C, 72.99; H, 5.96; N, 9.67; S, 11.22 %. MS (relative intensity) m/z: 280 (M⁺, 21.4%).

Compound 11b: Colorless crystals recrystallized from ethanol, yield 63%, 0.989 g, m.p. 171-173°C. IR (KBr): ν/cm^{-1} = 3043 (CH aromatic), 2881-2862 (CH₂), 2223 (CN), 1655 (C=N), 1644 (C=C). ¹HNMR (DMSO) δ = 2.09-2.14 (m, 6H, 3CH₂), 2.21-2.29 (m, 4H, 2CH₂), 6.93 (s, 1H, CH), 7.18-7.45 (dd, 4H, C₆H₄). Calcd. for C₁₇H₁₅ClN₂S (314.83): C, 64.85; H, 4.80; N, 8.90; S, 10.18 %. Found: C, 65.12; H, 4.56; N, 8.63; S, 10.01%. MS (relative intensity) m/z: 314 (M⁺, 9.8 %), 316 (M⁺, 3.5 %).

Compound 11c: Yellowish white crystals recrystallized from ethanol, yield 67%, 1.039 g, m.p. 233-235°C. IR (KBr): ν/cm^{-1} = 3052 (CH aromatic), 2981 (CH₃), 2897-2872 (CH₂), 2220 (CN), 1656 (C=N), 1646 (C=C). ¹HNMR (DMSO) δ = 1.83-1.89 (m, 6H, 3CH₂), 1.92-1.97 (m, 4H, 2CH₂), 3.12 (s, 3H, CH₃), 6.38 (s, 1H, CH), 7.11-7.23 (dd, 4H, C₆H₄). Calcd. for C₁₈H₁₈N₂OS (310.41): C, 69.65; H, 5.84; N, 9.02; S, 10.33 %. Found: C, 69.89; H, 5.98; N, 9.25; S, 10.07%. MS (relative intensity) m/z: 310 (M⁺, 19.1%).

2-(Benzylidene-amino)-5,6,7,8-tetrahydro-4H-cyclohepta[b]thiophene-3-carboxylic acid ethyl ester (11d), 2-[(4-Chloro-benzylidene)-amino]-5,6,7,8-tetrahydro-4H-cyclohepta[b]thiophene-3-carboxylic acid ethyl ester (11e), 2-[(4-Methoxy-benzylidene)-amino]-5,6,7,8-tetrahydro-4H-cyclohepta[b]thiophene-3-carboxylic acid ethyl ester (11f)

A mixture of compound (3b, 1.195 g, 0.005 mol) and either benzaldehyde (10a, 0.53 g, 0.005 mol), 4-chlorobenzaldehyde (10b, 0.71 g, 0.005 mol) or 4-methoxy-benzaldehyde (10c, 0.68 g, 0.005 mol) in dry dimethylformamide (40 ml) containing a catalytic amount of piperidine (0.5 ml) was heated under reflux for 4 h, then poured on an ice/water mixture containing few drops of hydrochloric acid. The solid product formed was collected by filtration.

Compound 11d: Colorless crystals recrystallized from ethanol, yield 52%, 0.851 g, m.p. 222-224°C. IR (KBr): ν/cm^{-1} = 3057 (CH aromatic), 2965 (CH₃), 2866-2854 (CH₂), 1774 (C=O), 1661 (C=N), 1643 (C=C). ¹HNMR (DMSO) δ = 1.28 (t, 3H, J = 6.48 Hz, CH₃), 1.74-1.88 (m, 6H, 3CH₂), 2.05-2.13 (m, 4H, 2CH₂), 4.17 (q, 2H, J = 6.48 Hz, CH₂), 6.45 (s, 1H, CH), 7.34-7.53 (m, 5H, C₆H₅). Calcd. for C₁₉H₂₁NO₂S (327.44): C, 69.69; H, 6.46; N, 4.28;

S, 9.79 %. Found: C, 69.42; H, 6.25; N, 4.47; S, 10.02 %. MS (relative intensity) m/z: 327 (M⁺, 23.3%).

Compound 11e: Pale yellow crystals recrystallized from ethanol, yield 60 %, 1.086 g, m.p. 238-240°C. IR (KBr): ν/cm^{-1} = 3060 (CH aromatic), 2973 (CH₃), 2870 (CH₂), 1781 (C=O), 1663 (C=N), 1646 (C=C). ¹HNMR (DMSO) δ = 1.44 (t, 3H, J = 7.18 Hz, CH₃), 1.84-1.89 (m, 6H, 3CH₂), 2.11-2.19 (m, 4H, 2CH₂), 4.41 (q, 2H, J = 7.18 Hz, CH₂), 6.33 (s, 1H, CH), 7.41-7.56 (dd, 4H, C₆H₄). Calcd. for C₁₉H₂₀ClNO₂S (361.89): C, 63.06; H, 5.57; N, 3.87; S, 8.86 %. Found: C, 63.33; H, 5.76; N, 3.57; S, 9.07%. MS (relative intensity) m/z: 361 (M⁺, 12.7 %), 363 (M⁺, 4.6 %).

Compound 11f: Brownish white crystals recrystallized from ethanol, yield 46 %, 0.822 g, m.p. 219-221°C. IR (KBr): ν/cm^{-1} = 3055 (CH aromatic), 2988 (CH₃), 2878 (CH₂), 1786 (C=O), 1652 (C=N), 1641 (C=C). ¹HNMR (DMSO) δ = 1.49 (t, 3H, J = 8.06 Hz, CH₃), 1.87-1.94 (m, 6H, 3CH₂), 1.98-2.07 (m, 4H, 2CH₂), 2.96 (s, 3H, CH₃), 4.52 (q, 2H, J = 8.06 Hz, CH₂), 6.24 (s, 1H, CH), 7.14-7.28 (dd, 4H, C₆H₄). Calcd. for C₂₀H₂₃NO₃S (357.47): C, 67.20; H, 6.49; N, 3.92; S, 8.97 %. Found: C, 67.48; H, 6.19; N, 4.21; S, 8.68%. MS (relative intensity) m/z: 357 (M⁺, 19.8 %).

4-Imino-2-phenyl-6,7,8,9-tetrahydro-4H,5H-10-thia-1,3-diaza-benzo[a]azulen-3-yl-amine (14a), 2-(4-Chloro-phenyl)-4-imino-6,7,8,9-tetrahydro-4H,5H-10-thia-1,3-diaza-benzo[a]azulen-3-ylamine (14b), 4-Imino-2-(4-methoxy-phenyl)-6,7,8,9-tetrahydro-4H,5H-10-thia-1,3-diaza-benzo[a]azulen-3-ylamine (14c)

To either solution of compound (11a, 0.56 g, 0.002 mol), (11b, 0.63 g, 0.002 mol) or (11c, 0.62 g, 0.002 mol) in ethanol (50 ml), hydrazine hydrate (12, 0.1 ml, 0.002 mol) was added. The reaction mixture was heated under reflux for 6 h, left to cool at room temperature, then poured on an ice/water mixture containing few drops of hydrochloric acid. The solid product formed was collected by filtration.

Compound 14a: Yellow crystals recrystallized from ethanol, yield 52%, 0.323 g, m.p. 252-254°C. IR (KBr): ν/cm^{-1} = 3454-3211 (NH₂, NH), 3043 (CH aromatic), 2881 (CH₂), 1647 (C=N), 1641 (C=C). ¹HNMR (DMSO) δ = 1.91-2.08 (m, 6H, 3CH₂), 2.11-2.15 (m, 4H, 2CH₂), 4.81 (s, 2H, NH₂, D₂O-exchangeable), 7.29-7.38 (m, 5H, C₆H₅), 8.63 (s, 1H, NH, D₂O-exchangeable). Calcd. for C₁₇H₁₈N₄S (310.42): C, 65.78; H, 5.84; N, 18.05; S, 10.33 %. Found: C, 65.55; H, 5.99; N, 18.33; S, 10.52%. MS (relative intensity) m/z: 310 (M⁺, 26.8 %).

Compound 14b: Pale yellow crystals recrystallized from ethanol, yield 59%, 0.371 g, m.p. 277-279°C. IR (KBr): ν/cm^{-1} = 3378- 3235 (NH₂, NH), 3052 (CH aromatic), 2888 (CH₂), 1650 (C=N), 1643 (C=C). ¹HNMR (DMSO) δ = 1.73-1.84 (m, 6H, 3CH₂), 1.95-2.12 (m, 4H, 2CH₂), 4.42 (s, 2H, NH₂, D₂O-exchangeable), 7.46-7.62 (dd, 4H, C₆H₄), 9.35 (s, 1H, NH, D₂O-exchangeable). Calcd. for C₁₇H₁₆ClN₃OS (345.85): C, 59.04; H, 4.66; N, 12.15; S, 9.27 %. Found: C, 59.31; H, 4.89; N, 12.34; S, 9.52%. MS (relative intensity) m/z: 345 (M⁺, 24.3 %), 347 (M⁺, 8.8 %).

Compound 14c: Colorless crystals recrystallized from ethanol, yield 47%, 0.32 g, m.p. 211-213°C. IR (KBr): ν/cm^{-1} = 3426-3212 (NH₂, NH), 3056 (CH aromatic), 2945 (CH₃), 2871 (CH₂), 1653 (C=N), 1644 (C=C). ¹HNMR (DMSO) δ = 1.98-2.06 (m, 6H, 3CH₂), 2.14-2.23 (m, 4H, 2CH₂), 3.27 (s, 3H, CH₃), 4.61 (s, 2H, NH₂, D₂O-exchangeable), 7.12-7.43 (dd, 4H, C₆H₄), 9.46 (s, 1H, NH, D₂O-exchangeable). Calcd. for C₁₈H₂₀N₄OS (340.44): C, 63.50; H, 5.92; N, 16.46; S, 9.42 %. Found: C, 63.74; H, 5.64; N, 16.19; S, 9.67%. MS (relative intensity) m/z: 340 (M⁺, 33.6%).

3-Amino-2-phenyl-3,5,6,7,8,9-hexahydro-10-thia-1,3-diaza-benzo[α]azulen-4-one (14d), *3-Amino-2-(4-chloro-phenyl)-3,5,6,7,8,9-hexahydro-10-thia-1,3-diaza-benzo[α]azulen-4-one (14e)*, *3-Amino-2-(4-methoxy-phenyl)-3,5,6,7,8,9-hexahydro-10-thia-1,3-diaza-benzo[α]azulen-4-one (14f)*

To either solution of compound (11d, 0.492 g, 0.0015 mol), (11e, 0.543 g, 0.0015 mol) or (11f, 0.536 g, 0.0015 mol) in ethanol (40 ml), hydrazine hydrate (12, 0.08 ml, 0.0015 mol) was added. The reaction mixture was heated under reflux for 8 h, left to cool at room temperature, then poured on an ice/water mixture containing few drops of hydrochloric acid. The solid product formed was collected by filtration.

Compound 14d: Colorless crystals recrystallized from ethanol, yield 63 %, 0.295 g, m.p. 233-235°C. IR (KBr): ν/cm^{-1} = 3437-3266 (NH₂), 3053 (CH aromatic), 2865 (CH₂), 1672 (C=O), 1643 (C=N), 1640 (C=C). ¹HNMR (DMSO) δ = 1.80-1.87 (m, 6H, 3CH₂), 1.96-2.07 (m, 4H, 2CH₂), 4.66 (s, 2H, NH₂, D₂O-exchangeable), 7.22-7.36 (m, 5H, C₆H₅). Calcd. for C₁₇H₁₇N₃OS (311.40): C, 65.57; H, 5.50; N, 13.49; S, 10.30 %. Found: C, 65.82; H, 5.79; N, 13.31; S, 10.57%. MS (relative intensity) m/z: 311 (M⁺, 41.4 %).

Compound 14e: Yellow crystals recrystallized from ethanol, yield 66 %, 0.342 g, m.p. 203-205°C. IR (KBr): ν/cm^{-1} = 3385-3248 (NH₂), 3056 (CH aromatic), 2873 (CH₂), 1677 (C=O), 1648 (C=N), 1642 (C=C). ¹HNMR (DMSO) δ = 1.92-1.99 (m,

6H, 3CH₂), 2.12-2.24 (m, 4H, 2CH₂), 5.13 (s, 2H, NH₂, D₂O-exchangeable), 7.31-7.52 (dd, 4H, C₆H₄). Calcd. for C₁₇H₁₆ClN₃OS (345.85): C, 59.04; H, 4.66; N, 12.15; S, 9.27 %. Found: C, 59.31; H, 4.89; N, 12.34; S, 9.52%. MS (relative intensity) m/z: 345 (M⁺, 24.3 %), 347 (M⁺, 8.8 %).

Compound 14f: Pale brown crystals recrystallized from ethanol, yield 71 %, 0.364 g, m.p. 247-249°C. IR (KBr): ν/cm^{-1} = 3338-3215 (NH₂), 3057 (CH aromatic), 2976 (CH₃), 2883 (CH₂), 1678 (C=O), 1657 (C=N), 1644 (C=C). ¹HNMR (DMSO) δ = 2.09-2.15 (m, 6H, 3CH₂), 2.23-2.28 (m, 4H, 2CH₂), 3.22 (s, 3H, CH₃), 5.40 (s, 2H, NH₂, D₂O-exchangeable), 7.14-7.23 (dd, 4H, C₆H₄). Calcd. for C₁₈H₁₉N₃O₂S (341.43): C, 63.32; H, 5.61; N, 12.31; S, 9.39 %. Found: C, 63.09; H, 5.39; N, 12.59; S, 9.56%. MS (relative intensity) m/z: 341 (M⁺, 30.3 %).

RESULTS AND DISCUSSION

The reaction of 3a,b with acetic anhydride gave the acetamido derivatives 4a,b. The structures of compounds 4a,b were based on analytical and spectral data. Thus, for example, the ¹H NMR spectrum of 4a showed besides the expected regular data for the cycloheptenyl moiety, two multiplets at δ = 2.12-2.21 (6H, 3CH₂), δ = 2.26-2.32 (4H, 2CH₂), a singlet at δ = 2.39 (3H, CH₃) and a singlet at δ = (1H, NH). The structure of compounds 4a,b was confirmed through internal cyclization on heating in a basic catalyst to give 4-amino-1,5,6,7,8,9-hexahydro-10-thia-1-aza-benzo[α]azulen-2-one (5a) and 4-hydroxy-1,5,6,7,8,9-hexahydro-10-thia-1-aza-benzo[α]azulen-2-one (5b), respectively (scheme 1). Compounds 3a,b reacted with malononitrile (2a) in Et₃N/ethanol followed by internal cyclization through the proposed intermediate formation of imines 6a,b to form thienopyrimidine derivatives 7a,b. The structures of the latter products were based on analytical and spectral data. The products 7a,b readily reacted with the cyclic ketones 8a-c in presence of elemental sulfur, triethylamine and ethanol as solvent to give fused thiophene derivatives 9a-f (scheme 2). The ¹HNMR spectrum of each compound revealed, in case of 9a, two multiplets at δ = 1.77-1.89 (10H, 5CH₂), δ = 1.98-2.08 (6H, 3CH₂) and two singlets at 3.95, 4.58 (4H, 2NH₂).

Furthermore, the reaction of compounds 3a,b with different aryl aldehydes 10a-c in DMF/piperidine gave the corresponding imines 11a-f which were directed toward reaction with hydrazine hydrate (12). The final products 14a-f were obtained through internal cyclization of the proposed intermediates 13a-f (scheme 3). The

structures of compounds 14a-f were based on analytical and spectral data. Thus, for example, the ^1H NMR spectrum of 14a showed besides the expected regular data for the cycloheptenyl moiety, two multiplets at $\delta = 1.91\text{--}2.08$ (6H, 3CH_2), $\delta = 2.11\text{--}2.15$ (4H, 2CH_2), a singlet at $\delta =$ (2H, NH_2), a multiplet at $\delta = 7.29\text{--}7.38$ (5H) corresponding to aromatic protons and a singlet at $\delta =$ (1H, NH).

Antitumor activity tests

Reagents: Fetal bovine serum (FBS) and L-glutamine were from Gibco Invitrogen Co. (Scotland, UK). RPMI-1640 medium was from Cambrex (New Jersey, USA). Dimethyl sulfoxide (DMSO), doxorubicin, penicillin, streptomycin and sulforhodamine B (SRB) were from Sigma Chemical Co. (Saint Louis, USA).

Cell cultures: Three human tumor cell lines, MCF-7 (breast adenocarcinoma), NCI-H460 (non-small cell lung cancer), and SF-268 (CNS cancer) were used. MCF-7 was obtained from the European Collection of Cell Cultures (ECACC, Salisbury, UK) and NCI-H460 and SF-268 were kindly provided by the National Cancer Institute (NCI, Cairo, Egypt). They grow as a monolayer and are routinely maintained in RPMI-1640 medium supplemented with 5% heat-inactivated FBS, 2 mM glutamine and antibiotics (penicillin 100 U/mL, streptomycin 100 $\mu\text{g}/\text{mL}$), at 37°C in a humidified atmosphere containing 5% CO_2 . Exponentially growing cells were obtained by plating 1.5×10^5 cells/mL for MCF-7 and SF-268 and 0.75×10^4 cells/mL for NCI-H460, followed by 24 h of incubation. The effect of the vehicle solvent (DMSO) on the growth of these cell lines was evaluated in all experiments by exposing untreated control cells to the maximum concentration (0.5%) of DMSO used in each assay.

Tumor cell growth assay: The effect of 3a–14f on the *in vitro* growth of human tumor cell lines was evaluated according to the procedure adopted by the National Cancer Institute (NCI, USA) in the ‘*In vitro* Anticancer Drug Discovery Screen’ that uses the protein-binding dye sulforhodamine B to assess cell growth. Briefly, cells growing in 96-wellplates were then exposed for 48 h to five serial concentrations of each compound [18], starting from a maximum concentration of 150 μM . Following this exposure period adherent cells were fixed, washed, and stained. The bound stain was solubilized and the absorbance was measured at 492 nm in a plate reader (Bio-Tek Instruments Inc., Power wave XS, Wincoski, USA). For each test compound and cell line, a dose–response curve was obtained and the growth inhibition of 50% (GI_{50}),

corresponding to the concentration of the compounds that inhibited 50% of the net cell growth, was calculated as described elsewhere [19]. Doxorubicin was used as a positive control and tested in the same manner.

Effect on the Growth of Human Tumor Cell Lines

The effect of compounds 3a–14f was evaluated on the *in vitro* growth of three human tumor cell lines representing different tumor types, namely, breast adenocarcinoma (MCF-7), non-small cell lung cancer (NCI-H460) and CNS cancer (SF-268) after an exposure for 48 h. All tested compounds inhibited the growth of the tested human tumor cell lines in a dose-dependent manner (data not shown). The results presented in Table 1 revealed that the thienopyrimidine derivatives 14d and 14f showed the highest inhibitory effect against all three tumor cell lines corresponding to the reference standard material (Doxorubicin); the compounds 5a, 9b, 14a and 14c showed the highest inhibitory effect against all three tumor cell lines. On the other hand, the compounds 9a, 9c, 9e, 14b and 14e showed moderate inhibitory effects against the three cancer cell lines. The rest of the compounds 3a, b, 4a, b, 5b, 7a, b, 9d, f, 11a, b, c, d, e and f showed a low growth-inhibitory effect.

Comparing the thienopyridone derivatives 5a and 5b it was found that compound 5a with $\text{X} = \text{NH}_2$ showed a higher inhibitory effect than compound 5b, with $\text{X} = \text{OH}$. Comparing the cycloalkylthieno derivatives 9a, b, c, d, e, and f it was found that compound 9b with $\text{X} = \text{NH}_2$ and $n = 2$ showed the highest inhibitory effect among the six compounds, while compounds 9a, c and 9e with $\text{X} = \text{NH}_2$, NH_2 , OH and $n = 1, 3, 2$, respectively, showed a moderate inhibitory effect. The comparison of compounds 14a, b, c, d, e and f revealed that the presence of O instead of NH group and $\text{Ar} = \text{Ph}$ or 4-MeO-Ph only in compounds 14d and 14f increased the inhibitory effect stronger than in compounds 14a, b, c and 14e, while the presence of NH group and 4-Cl-Ph in compound 14b may be the cause for the decrease in inhibitory effect against the three tumor cell lines.

CONCLUSIONS

In this work fused heterocyclic compounds based on cyclohepta[b]thiophene derivatives were synthesized and screened for their antitumor activity against three different cell lines in comparison with the reference standard “doxorubicin”. Among the newly synthesized products, the thienopyrimidine derivatives 14d and 14f showed the highest inhibitory effect against all three tumor cell lines. Compounds 5a, 9b, 14a and 14c showed the highest inhibitory effect against all

three tumor cell lines in comparison with the other synthesized compounds.

Acknowledgment: The authors would like to thank the research group working at the Medicinal Chemistry Department of the National Research Center and the National Cancer Institute for the antitumor evaluation for the synthesized products.

REFERENCES

1. R. M. Mohareb, K. A. El-Sharkawy, S. M. Sherif, *Acta Pharm.*, **58**, 429 (2008).
2. K. A. El-Sharkawy, N. N. E. El-Sayed, M. Y. Zaki, *International Research Journal of Pure & Applied Chemistry*, **2**, 91(2012).
3. F. M. Abdelrazek, *Synthetic Commun.*, **35**, 225 (2005).
4. A. A. Fadda, E. A. bdel-Latif, R. E. El-Mekawy, *Eur. J. Med. Chem.*, **44**, 1250 (2009).
5. M. R. Shaaban, T. S. Saleh and A. M. Farag, *Heterocycles*, **78**, 151(2009).
6. G. Stefancich, R. Silvestri, A. Retico, M. Artico, G. Simonetti, *Archiv der Pharmazie*, **325**, 199 (1992).
7. B. C. Souza, T. B. Oliveira, T. M. Aquino, M. C. de Lima, I. R. Pitta, S. L. Galidino, E. O. Lima, T. S. Gonclaves, G. C. Militao, L. Scotti. M. T. Scotti, and F. J. J. r. Mendonca, *Acta Pharm.*, **62(2)**, 221 (2012).
8. J. Bompard, L. Giral, G. Malicorne, and M. Puygrenier, *Eur. J. Med. Chem.* **23**, 457(1988).
9. H. Liu, Y. Li, X. Y. Wang, B. Wang, H. Y. He, J. Y. Liu, M. L. Xiang, J. He, X. H. Wu, and L. Yang, *Bioorgan. Med. Chem. Lett.*, **23**, 2349 (2013).
10. R. H. Bahekar, M. R. Jain, P. A. Jadav, V. M. Prajapati, D. N. Patel, A. A. Gupta, A. Sharma, R. Tom, D. Bandyopadhyaya, H. Modi, and P. R. Patel, *Bioorgan. Med. Chem.*, **15**, 6782 (2007).
11. R. M.V. Abreu, I. C. F. R. Ferreira, R. C. Calhelha, R. T. Lima, M. H. Vasconcelos, F. Adegas, R. Chaves, and M.-J. R. P. Queiroz, *Eur. J. Med. Chem.*, **46**, 5800 (2011).
12. M. B. Dewal, A. S. Wani, C. Vidaillac, D. Oupický, M. J. Rybak, S. M. Firestine, *Eur. J. Med. Chem.*, **51**, 145 (2012).
13. V. Alagarsamy, S. Vijayakumar, V. Raja Solomon, *Biomed. Pharmacother.*, **61**, 285(2007).
14. A. G. Golub, V. G. Bdzhola, N. V. Briukhovetska, A. O. Balandas, O. P. Kukharensko, I. M. Kotey, O. V. Ostrynska, S. M. Yarmoluk, *Eur. J. Med. Chem.*, **46**, 870 (2011).
15. H. N. Hafez, H. A.R. Hussein, A. B.A. El-Gazzar, *Eur. J. Med. Chem.*, **45**, 4026 (2010).
16. K. A. El-Sharkawy, H. M. El-Sehrawi, and R. A. Ibrahim, *International Journal of Organic Chemistry*, **2**, 126 (2012).
17. T. Wang, X. Huang, J. Liu, B. Li, J. K. Wu Chen, W. L. Zhu, X. Y. Xu, B.B. Zeng, *Synlett.*, **9**, 1351 (2010).
18. P. Skehan, R. Storeng, D. Scudiero, A. Monks, J. McMahon, D. Vistica, J. T. Warren, H. Bokesch, S. Kenney, M. R. J. Boyd, *Natl. Cancer Inst.*, **82**, 1107 (1990).
19. A. Monks, D. Scudiero, P. Skehan, R. Shoemaker, K. Paull, D. Vistica, C. Hose, J. Langley, P. Cronise, A. Vaigro-Wolff, M. Gray-Goodrich, H. Campbell, J. Mayo, M. J. Boyd, *Natl. Cancer Inst.*, **83**, 757 (1991).

СЪЕДИНЕНИЯ ОСНОВАНИ НА ЦИКЛО-ХЕПТА[b]ТИОФЕНОВИ ПРОИЗВОДНИ

К.А. Ел-Шаркауи^{1,2*}, М.М. Саид³, Г. Дардас¹

¹Департамент по органична химия, Факултет по биотехнология, Октомврийски университет за съвременни науки и изкуства, Египет

²Департамент по фармацевтична химия, Колеж по фармация, Университет в Джасан, Кралство Саудитска Арабия

³Департамент по органична химия, Факултет по фармация, Университет „Суецки канал“, Исмаилия, Египет

Получена на 9 септември 2013 г.; коригирана на 18 април, 2014 г.

(Резюме)

Реакцията на 5,6,7,8-тетрахидро-4Н-циклохепта[b]тиофенови производни 3a,b с оцетен анхидрид в ледена оцетна киселина дава ацетамидови производни 4a,b. Циклизирането на тези съединения води до пръстенни продукти 5a,b. Съединенията 3a,b реагират с една от активирани метиленови групи в малонитрила (2a), както и съединенията 7a,b чрез вътрешно циклизиране на междинните съединения на съединенията 6a,b. Последните продукти реагират с цикличните кетони 8a,b,c в присъствие на елементарна сяра и съединенията 9a-f. Съединенията 3a,b реагират с различни типове алдехиди 10a,b,c като се получават съединенията 11a-f. Накрая продуктите 11a-f реагират с хидразин-хидрат (12), давайки съединенията 14a-f през образуването на междинните съединения 13a-f. Изпитана е антитуморната активност на синтезираните съединения използвайки три клетъчни линии.

Simple and efficient heterogeneous media for the oxidation of urazole derivatives to their corresponding triazolinediones *via in situ* generation of Cl⁺

A. Ghorbani-Choghamarani^{*,1}, G. Azadi¹ Sh. Mallakpour²

¹ Department of Chemistry, Faculty of Science, Ilam University, Ilam, Iran

² Organic Polymer Chemistry Research Laboratory, Department of Chemistry, Isfahan University of Technology, Isfahan, Iran

Received September 9, 2013; Revised May 3, 2014

A new procedure for the oxidation of urazole derivatives to their corresponding triazolinediones was developed using ZrCl₄ and polyvinylpyrrolidone-supported hydrogen peroxide (PVP-H₂O₂) in dichloromethane under very mild reaction conditions. This procedure is very simple and works efficiently at room temperature with excellent yields of products.

Keywords: Polyvinylpyrrolidone; PVP-H₂O₂; Urazole; Triazolinedione; Oxidation.

INTRODUCTION

4-Substituted-1,2,4-triazoline-3,5-diones are notable for their ability to participate in a wide range of reaction types such as [4+2] [1-2] and [2+2] [3] cycloadditions, ene reactions [4], electrophilic aromatic substitution [5], dehydrogenation [6] and oxidation of alcohols to aldehydes and ketones [7]. Oxidation of urazoles is a common way for the preparation of triazolinediones and a wide variety of methods and reagents have been reported in the literature for this purpose, such as *N,N,N,N*-tetrabromobenzene-1,3-disulfonylamide (TBBDA) or trichloromelamine (TCM) [8], Ph₃BiCO₃ [9], ICl-SiO₂ [10], periodic acid or oxone/KBr system [11], 1,4-diazabicyclo[2.2.2]octane 1,4-bis(oxide)-bis (hydrogen peroxide)/MCl_x [12], 4-(*p*-chloro) phenyl-1,2,4-triazole-3,5-dione [13] and *N*-bromo reagent [14]. However, most of the reported reagents produce byproducts, which either destroy, or are difficult to remove from the sensitive triazolinediones. Another major drawback of the older procedures is the use of reagents which are either highly toxic or impart serious disposal problems (or both) [15-18]. Therefore, the preparation of these compounds under mild conditions is of practical importance for synthetic organic chemists and is still in demand. Heterogeneous reactions facilitated by supported reagents on various solid inorganic surfaces have received attention in recent years. The advantages of these methods over conventional homogeneous

reactions are: higher selectivity, enhanced reaction rates, cleaner products, and simplicity of manipulation [19].

EXPERIMENTAL

Chemicals were purchased from Fluka, Merck and Aldrich chemical companies. The acetylated products were characterized by comparison of their spectral (IR, ¹H NMR, and ¹³C NMR) and physical data with those of authentic samples.

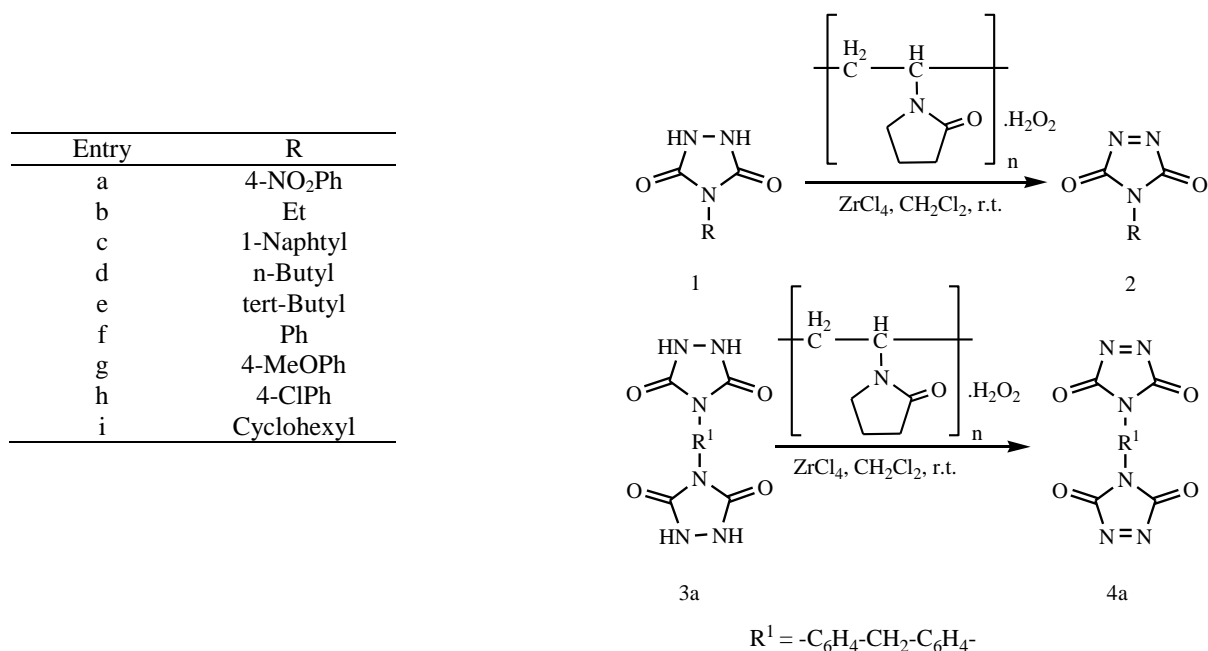
Oxidation of 4-cyclohexylurazole (1i) to 4-cyclohexyl-1,2,4-triazoline-3,5-dione (2i), as a typical experiment:

A mixture of 4-cyclohexylurazole (**1i**, 0.183 g, 1 mmol), polyvinylpyrrolidone-supported hydrogen peroxide (PVP-H₂O₂, 0.29 g), and ZrCl₄ (0.097 g, 0.417 mmol) in 5 mL dichloromethane was stirred at room temperature for 105 min and then filtered. The residue was washed with CH₂Cl₂ (20 mL). Anhydrous Na₂SO₄ (1.5 g) was added to the filtrate and then removed by filtration. Finally, evaporation of the solvent gave 4-cyclohexyl-1,2,4-triazoline-3,5-dione (**2i**). The yield of the crystalline red solid was 97%.

RESULTS AND DISCUSSION

In continuation of our ongoing work on development of environmentally benign methods using solid supported reagents [20-24], and in order to complete our studies on the functionalization of organic compounds [25-30] we investigated the

* To whom all correspondence should be sent:
E-mail: arashghch58@yahoo.com



Scheme 1. Oxidation of different types of urazoles **1** or bis-urazole **3a** to their corresponding triazolinediones **2** or **4a**

oxidation of urazole derivatives by polyvinylpyrrolidone-supported hydrogen peroxide (PVP-H₂O₂) and ZrCl₄. PVP-H₂O₂ was prepared *via* the reported procedure by Pourali and Ghanei [31]. The oxidation of different types of urazoles **1** or bis-urazole **3a** to their corresponding triazolinediones **2** or **4a** using a combination of polyvinylpyrrolidone-supported hydrogen peroxide (PVP-H₂O₂) and ZrCl₄, which *in situ* generate Cl⁺, is delineated in Scheme 1.

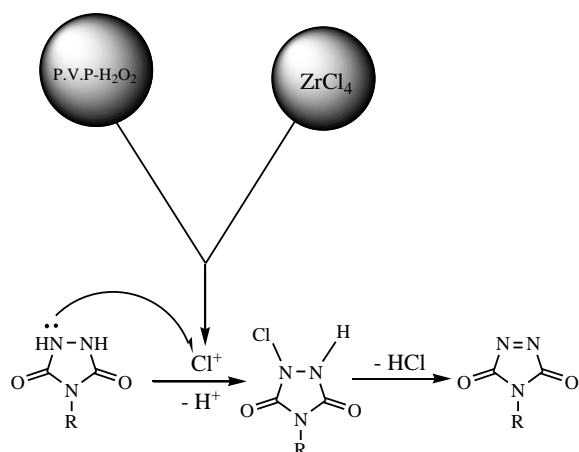
As shown in Table 1, different kinds of urazoles (**1**) and bis-urazole (**3a**) are oxidized to their corresponding triazolinediones by PVP-H₂O₂ in the

presence of ZrCl₄ and dichloromethane as a solvent under stirring the resulting heterogeneous mixture at room temperature. The triazolinediones **2** and bis(triazolinedione) **4a** are obtained by simple filtration and evaporation of the solvent. The oxidation reactions of urazoles are heterogeneous because urazoles and bis-urazole [(**1**, **3a**) white solids] are insoluble in dichloromethane whereas all triazolinediones and bis(triazolinedione) [(**2**, **4a**), red and pink, respectively] are extremely soluble in dichloromethane. A plausible mechanism of this oxidation is outlined in Scheme 2.

Table 1. Oxidation of urazole derivatives to their corresponding triazolinediones with PVP-H₂O₂ (**I**) and ZrCl₄ (**II**) in CH₂Cl₂ at room temperature

Entry	Substrate	Product	I (g)	II (mmol)	Time (min)	Yield ^a (%)
1	1a	2a	0.29	0.417	120	96
2	1b	2b	0.29	0.417	90	96
3	1c	2c	0.29	0.417	120	98
4	1d	2d	0.29	0.417	90	95
5	1e	2e	0.29	0.417	75	98
6	1f	2f	0.29	0.417	90	98
7	1g	2g	0.29	0.417	120	98
8	1h	2h	0.29	0.417	90	99
9	1i	2i	0.29	0.417	105	97
10	3a	4a	0.58	0.834	210	98

^a Isolated yield.



Scheme 2. Plausible mechanism

In conclusion, we report an efficient and versatile procedure for the oxidation of urazoles and bis-urazole with the following advantages: (a) the reagent used is inexpensive and easily handled; (b) the procedure is very simple and works efficiently without any additives at room temperature; (c) the isolation of the product is straightforward and this system could be used for the oxidation of a wide variety of urazole derivatives under mild and safe conditions.

Acknowledgment: Authors thank the research facilities of Ilam University, Ilam, Iran, for financial support of this research project.

REFERENCES

1. S.E. Mallakpour, M.A. Zolfigol, *Indian J. Chem.* 34, 183 (1995).
2. G. Desimoni, G. Faita, P.P. Righetti, A. Sulcini, D. Tsyganov, *Tetrahedron* 50, 1821 (1994).
3. J.H. Hall, G. Krishnan, *J. Org. Chem.* 49, 2498 (1984).
4. S.E. Mallakpour, G.B. Butler, H. Aghabozorg, G. Palanik, *J. Macromolecules* 18, 342 (1985).
5. S.E. Mallakpour, G.B. Butler, *J. Polym. Sci., Polym. Chem Ed*, 27, 217 (1989).
6. T. Klindert, G. Seitz, *Synth. Commun.* 26, 2587 (1996).
7. R.C. Cookson, I.D.R. Stevens, C.T. Watts, *Chem. Commun.*, 744 (1966).
8. M.A. Zolfigol, R. Ghorbani-Vaghei, S. Mallakpour, G. Chehardoli, A. Ghorbani Choghamarani, A. Hosain Yazdi, *Synthesis*, 10, 1631 (2006).
9. C. Me'nard, E. Doris and C. Mioskowski, *Tetrahedron Letters*, 44, 6591 (2003).
10. B. Karami, S. Mallakpour, and M. Farahi, *Heteroatom Chemistry*, 19, 389 (2008).
11. M. A. Zolfigol, M. Bagherzadeh, S. Mallakpour, G. Chehardoli, A. Ghorbani-Choghamarani, N. Koukabi, M. Dehghanian, M. Doroudgar, *Journal of Molecular Catalysis A: Chemical*, 270, 219 (2007).
12. M. A. Zolfigol, Peyman Salehi, S. E. Mallakpour and M. Torabi, *Bull. Chem. Soc. Jpn.*, 76, 1673 (2003).
13. M. A. Zolfigol, D. Azarifar, S. Mallakpour, I. Mohammadpour-Baltork, A. Forghaniha, B. Maleki and M. Abdollahi-Alibeik, *Tetrahedron Letters*, 47 833 (2006).
14. M. A. Zolfigol, G. Chehardoli, E. Ghaemi, E. Madrakian, R. Zare, T. Azadbakht, K. Niknam, and S. Mallakpour, *Monatsh. Chem.* 139, 261 (2008).
15. V.P. Arya, S. Shenoy, *Indian J. Chem., Sect. B: Org. Chem. Incl. Med. Chem.* 14, 883 (1976).
16. H. Warnho, K. Wald, *Org. Prep. Proced. Int.*, 7, 251 (1975).
17. S.E. Mallakpour, *J. Chem. Educ.*, 69, 238 (1992).
18. S.E. Mallakpour, M.A. Zolfigol, *J. Sci. Islamic Republic Iran*, 4, 199 (1993).
19. I. Mohammadpour-Baltork, M.M. Sadeghi, S.E. Mallakpour, A.R. Hajipour, A.H. Adibi, *Synthetic Commun.*, 32, 3445 (2002).
20. A. Ghorbani-Choghamarani, M. Nikoorazm, H. Goudarziafshar, L. Shiri, Z. Chenani, *Bull. Korean Chem. Soc.* 30, 972 (2009).
21. M.A. Zolfigol, K. Amani, A. Ghorbani-Choghamarani, M. Hajjami, R. Ayazi-Nasrabadi, S. Jafari, *Catal Commun.*, 9, 1739 (2008).
22. A. Ghorbani-Choghamarani, Z. Chenani, S. Mallakpour, *Synthetic Commun.*, 39, 4264 (2009).
23. A. Ghorbani-Choghamarani, M.A. Zolfigol, M. Hajjami, K. Darvishi, L. Gholamnia, *Collect. Czech. Chem. Commun.*, 75, 607 (2010).
24. A. Ghorbani-Choghamarani, G. Azadi, *J. Iran. Chem. Soc.*, 8, 1082 (2011).
25. M.A. Zolfigol, F. Shirini, A. Ghorbani-Choghamarani, I. Mohammadpour-Baltork, *Green Chem.*, 4, 562 (2002).
26. M.A. Zolfigol, F. Shirini, A. Ghorbani-Choghamarani, M. Hajjami, M. Sedaghat, *Mendeleev Commun.*, 15, 113 (2005).
27. M.A. Zolfigol, F. Shirini, A. Ghorbani-Choghamarani, *Synthesis*, 2043 (2006).
28. M.A. Zolfigol, M. Bagherzadeh, K. Niknam, F. Shirini, I. Mohammadpour-Baltork, A. Ghorbani-Choghamarani, M. Baghbanzadeh, *J. Iran. Chem. Soc.*, 3, 73 (2006).
29. M.A. Zolfigol, K. Amani, M. Hajjami, A. Ghorbani-Choghamarani, *Monatsh. Chem.* 139, 895 (2008).
30. A. Ghorbani-Choghamarani, M. Hajjami, H. Goudarziafshar, M. Nikoorazm, S. Mallakpour, F. Sadeghizadeh, G. Azadi, *Monatsh. Chem.*, 140, 607 (2009).
31. A.R. Pourali, M. Ghanei, *Bull. Korean Chem. Soc.*, 27, 1674 (2006).

ПРОСТИ И ЕФЕКТИВНИ ХЕТЕРОГЕННИ СРЕДИ ЗА ОКИСЛЕНИЕТО НА УРАЗОЛОВИ
ПРОИЗВОДНИ ДО СЪОТВЕТНИТЕ ТРИАЗОЛИНДИОНИ ЧРЕЗ *IN SITU* ГЕНЕРИРАНЕ
НА Cl^+

А. Горбани-Чогамарани^{*.1}, Г. Азади¹, Ш. Малакпур²

¹ Департамент по химия, Научен факултет, Иламски университет, Илам, Иран

² Изследователска лаборатория по органична и полимерна химия, департамент по химия, Технологичен университет в Исфахан, Иран

Постъпила на 9 септември, 2013 г.; Коригирана 3 май, 2014 г.

(Резюме)

Разработена е нова процедура за окисление на уразолови производни до съответните им триазолиндиони. Използвани са $ZrCl_4$ и водороден пероксид в поливинил-полипиролон ($PVP-H_2O_2$) в среда от дихлорметан при меки реакционни условия. Методът е много прост и работи ефективно при стайни температури с отличен добив на продуктите.

Effects of Hall current and rotation on unsteady MHD natural convection flow with heat and mass transfer past an impulsively moving vertical plate in the presence of radiation and chemical reaction

G. S. Seth^{1*}, S. M. Hussain², S. Sarkar¹

¹ Department of Applied Mathematics, Indian School of Mines, Dhanbad, India

² Department of Mathematics, O. P. Jindal Institute of Technology, Raigarh, India

Received September 9, 2013; Revised December 24, 2013

Effects of Hall current and rotation on unsteady MHD natural convection flow with heat and mass transfer of an electrically conducting, viscous, incompressible, chemically reacting and optically thin radiating fluid past an impulsively moving infinite vertical plate embedded in a porous medium in the presence of thermal and mass diffusion is studied. The exact solutions of momentum, energy and concentration equations, under the Boussinesq approximation, are obtained in closed form by the Laplace transform technique. The expressions for skin friction, Nusselt number and Sherwood number are also derived. The variations in fluid velocity, fluid temperature and species concentration are shown graphically whereas numerical values of skin friction, Nusselt number and Sherwood number are presented in tabular form for various values of pertinent flow parameters.

Keywords: Unsteady MHD natural convection flow, radiation, chemical reaction, Nusselt number, Sherwood number.

INTRODUCTION

Theoretical and experimental investigations of natural convection flow over vertical surfaces embedded in a porous medium have a wide range of applications in different fields of science and technology. Such configuration exists in several practical systems such as catalytic chemical reactors, thermal insulators, heat exchanger devices, nuclear waste repositories, systems for drying of porous solids, underground energy transport, enhanced recovery of oil and gas, cooling of nuclear reactors, geothermal reservoirs, etc. Considering the importance of such fluid flow problems, large amount of research works have been carried out in this field. Mention should be made of the research studies of Cheng and Minkowycz [1], Nakayama and Koyama [2], Lai and Kulacki [3], Hsieh *et al.* [4], Nield and Kuznetsov [5] and Gorla and Chamkha [6]. Comprehensive reviews of thermal/species convection in porous media are presented by Pop and Ingham [7], Vafai [8] and Nield and Bejan [9].

The problems of hydromagnetic convective flow in a porous medium have drawn the attention of several researchers in the past due to significant effects of magnetic field on many problems of physical interest, *viz.* boundary layer flow control,

plasma studies, geothermal energy extraction, metallurgy, chemical, mineral and petroleum engineering, etc. and on the performance of many engineering devices using electrically conducting fluids, namely, MHD generators, MHD pumps, MHD accelerators, MHD flow-meters, nuclear reactors, etc. Raptis and Kafousias [10] investigated steady hydromagnetic free convection flow through a porous medium bounded by an infinite vertical plate with constant suction velocity. Raptis [11] considered unsteady two-dimensional natural convection flow of an electrically conducting, viscous and incompressible fluid along an infinite vertical plate embedded in a porous medium. Chamkha [12] investigated unsteady MHD free convection flow through a porous medium supported by a surface. Chamkha [13] also studied MHD natural convection flow near an isothermal inclined surface adjacent to a thermally stratified porous medium. Aldoss *et al.* [14] investigated combined free and forced convection flow from a vertical plate embedded in a porous medium in the presence of a magnetic field. Kim [15] discussed unsteady MHD free convection flow past a moving semi-infinite vertical porous plate embedded in a porous medium with variable suction. A few representative fields of interest in which combined heat and mass transfer plays an important role are: design of chemical processing equipment; formation and dispersion of fog; distribution of temperature and moisture over agricultural fields

* To whom all correspondence should be sent:
E-mail: gsseth.ism@gmail.com

and groves of trees; damage of crops due to freezing, common industrial sight especially in power plants, etc. In view of these facts, Jha [16] considered hydromagnetic free convection and mass transfer flow past a uniformly accelerated moving vertical plate through a porous medium. Ibrahim *et al.* [17] investigated the unsteady hydromagnetic free convection flow of a micro-polar fluid and the heat transfer past a vertical porous plate through a porous medium in the presence of thermal and mass diffusion with a constant heat source. Alam and Rahman [18] considered Dufour and Soret effects on MHD free convection heat and mass transfer flow past a vertical porous flat plate embedded in a porous medium. Makinde and Sibanda [19] studied MHD mixed convective flow with heat and mass transfer past a vertical plate embedded in a porous medium with constant wall suction. Makinde [20] analyzed a hydromagnetic mixed convection flow and mass transfer over a vertical porous plate with constant heat flux embedded in a porous medium. Eldabe *et al.* [21] discussed unsteady MHD flow of a viscous and incompressible fluid with heat and mass transfer in a porous medium near a moving vertical plate with time dependent velocity.

The number of investigations of natural convection flow with thermal radiation has increased greatly during the past few decades due to its importance in many practical situations. When natural convection flows occur at high temperature, radiation effects on the fluid flow become significant. Radiation effects on the natural convection flow are important in context of furnace design, electric power generation, thermo-nuclear fusion, glass production, casting and levitation, plasma physics, cosmic flights, propulsion systems, solar power technology, spacecraft re-entry, aerothermodynamics, etc. It is worth noting that unlike convection/conduction the governing equations taking into account the effects of radiation become quite complicated. Hence, many difficulties arise while solving such equations. However, some reasonable approximations are proposed to solve the governing equations with radiative heat transfer. The textbook by Sparrow and Cess [22] describes the essential features of radiative heat transfer. Cess [23] investigated free convection flow past a vertical isothermal plate with thermal radiation using Rosseland diffusion approximation. Hossain and Takhar [24] analyzed the effects of radiation on mixed boundary layer flow near a vertical plate with uniform surface temperature using Rosseland flux model. Bakier and Gorla [25] considered the effects of radiation

on mixed convection flow over a horizontal surface embedded in a fluid-saturated porous medium. Takhar *et al.* [26] analyzed the effects of radiation on MHD free convection flow of a gas past a semi-infinite vertical plate. Chamkha [27] considered solar radiation assisted natural convection in a uniform porous medium supported by a vertical flat plate. Chamkha [28] studied thermal radiation and buoyancy effects on MHD flow over an accelerating permeable surface with heat source or sink. Azzam [29] considered the effects of radiation on MHD free and forced convection flow past a semi-infinite moving vertical plate for high temperature differences. Cooney *et al.* [30] considered the influence of viscous dissipations and radiation past an infinite heated vertical plate in a porous medium with time-dependent suction. Muthucumaraswamy and Ganesan [31] studied the effects of radiation on a flow past an impulsively started vertical plate with variable temperature. Makinde and Ogulu [32] considered the effects of radiation on the heat and mass transfer flow of a variable viscosity fluid past a vertical porous plate in the presence of a transverse magnetic field. Mahmoud Mostafa [33] investigated the effects of thermal radiation on unsteady MHD free convection flow past an infinite vertical porous plate taking into account the effects of viscous dissipation. Ogulu and Makinde [34] considered unsteady hydromagnetic free convection flow of a dissipative and radiative fluid past a vertical plate with constant heat flux. Kishore *et al.* [35] studied effects of thermal radiation and viscous dissipation on MHD heat and mass diffusion flow past an oscillating vertical plate embedded in a porous medium with variable surface conditions. Chamkha *et al.* [36] investigated radiation effects on mixed convection flow over a wedge embedded in a porous medium filled with nanofluid. Nandkeolyar *et al.* [37] investigated unsteady hydromagnetic natural convection flow of a dusty fluid past an impulsively moving vertical plate with ramped temperature in the presence of thermal radiation.

In many chemical engineering processes, there occurs chemical reaction between a foreign mass and the fluid in which the plate is moving. Chemical reactions can be classified as either heterogeneous or homogeneous processes. This depends on whether they occur at an interface or as a single phase volume reaction. These processes take place in numerous industrial applications, *viz.* polymer production, manufacturing of ceramics or glassware, food processing, etc. Afify [38] studied the effect of radiation on free convective flow and mass transfer past a vertical isothermal cone surface

with chemical reaction in the presence of a transverse magnetic field. Muthucumaraswamy and Chandrakala [39] investigated radiative heat and mass transfer effects on a moving isothermal vertical plate in the presence of chemical reaction. Ibrahim *et al.* [40] analyzed the effect of chemical reaction and radiation absorption on the unsteady MHD free convection flow past a semi-infinite vertical permeable moving plate with heat source and suction. Muthucumaraswamy *et al.* [41] considered thermal radiation effects on hydromagnetic free convection and mass transfer flow past an infinite oscillating isothermal plate in the presence of chemical reaction of first order. Rajesh [42] investigated the effects of thermal radiation and first order chemical reaction on unsteady MHD free convection and mass transfer flow of a dissipative fluid past an infinite vertical porous plate with ramped wall temperature. Sudheer Babu *et al.* [43] studied radiation and chemical reaction effects on unsteady MHD convection flow past a vertically moving porous plate embedded in a porous medium with viscous dissipation. Nandkeolyar *et al.* [44] considered unsteady hydromagnetic heat and mass transfer flow of a heat radiating and chemically reactive fluid past a flat porous plate with ramped wall temperature.

Problems of a hydromagnetic natural convection flow in a rotating medium taking into account the effects of radiation are of considerable importance in many areas of geophysics, astrophysics and fluid engineering. In view of this fact, Bestman and Adjepong [45] investigated the unsteady hydromagnetic free convection flow of an incompressible optically thick fluid with radiative heat transfer near a moving flat plate in a rotating medium by imposing time dependent perturbation on a constant plate temperature. Mbeledogu and Ogulu [46] studied the heat and mass transfer of unsteady MHD natural convection flow of a rotating fluid past a vertical porous plate in the presence of radiative heat transfer. They applied Rosseland approximation for an optically thick fluid to describe the radiative flux. Bakr [47] discussed the effects of chemical reaction on MHD free convection and mass transfer flow of a micropolar fluid with oscillatory plate velocity and constant heat source in a rotating frame of reference. Recently, Seth *et al.* [48] considered the effects of thermal radiation and rotation on unsteady hydromagnetic free convection flow past an impulsively moving vertical plate with ramped temperature in a porous medium. It is noticed that when the density of an electrically conducting fluid

is low and/or the applied magnetic field is strong, Hall current plays an important role in determining flow features of the fluid flow problem [49]. Also it is worth noting that both Hall current and rotation induce a secondary flow in the flow-field. In view of this fact, Sarkar *et al.* [50] studied the effects of Hall current on unsteady MHD free convective flow past an accelerated moving vertical plate with viscous and Joule dissipations. Anjali Devi *et al.* [51] investigated Hall effects on unsteady MHD free convection flow past an impulsively started porous plate with viscous and Joule dissipations. Farhad *et al.* [52] investigated unsteady hydromagnetic rotating flow past a moving infinite porous plate in a porous medium with slip condition taking into account the effects of Hall current.

Objective of the present investigation is to study the effects of Hall current and rotation on a hydromagnetic natural convection flow with heat and mass transfer of an electrically conducting, viscous, incompressible, chemically reacting and optically thin radiating fluid past an impulsively moving infinite vertical plate embedded in a porous medium in the presence of thermal and mass diffusion.

FORMULATION OF THE PROBLEM AND ITS SOLUTION

Consider an unsteady hydromagnetic natural convection flow with heat and mass transfer of an electrically conducting, viscous, incompressible, chemically reacting and optically thin radiating fluid past an impulsively moving infinite vertical plate embedded in a porous medium in the presence of thermal and mass diffusions. Choose the coordinate system in such a way that x' -axis is along the plate in upward direction, y' -axis normal to the plane of the plate and z' -axis perpendicular to the $x'y'$ -plane. The fluid is permeated by uniform transverse magnetic field B_0 applied in a direction parallel to the y' -axis. Both fluid and plate are in rigid body rotation with uniform angular velocity Ω about the y' -axis. Initially, i.e. at time $t' \leq 0$, both the fluid and plate are at rest and maintained at uniform temperature T'_∞ . Also the level of concentration of fluid is maintained at uniform concentration C'_∞ . At time $t' > 0$, the plate starts moving with uniform velocity u_0 in x' -direction against the gravitational field. At the same time the plate temperature is raised to uniform

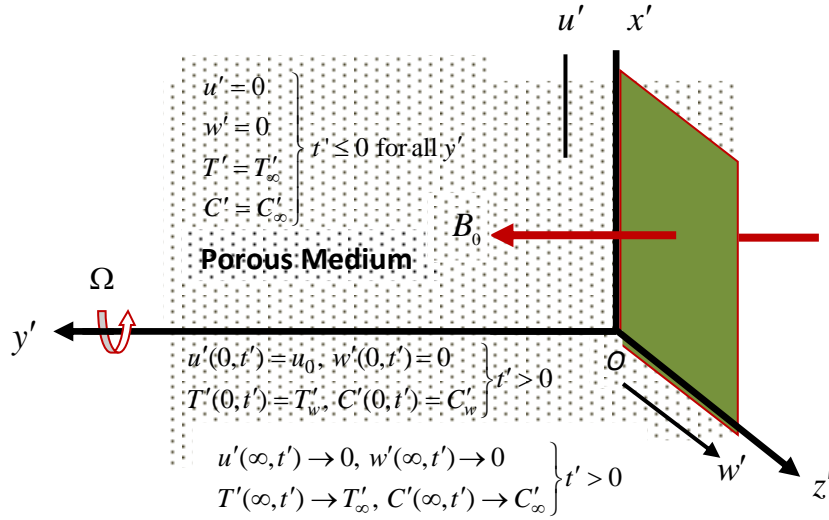


Fig. 1. Geometry of the problem

temperature T'_w and the concentration at the surface of plate is raised to uniform concentration C'_w . The fluid considered is a gray, emitting-absorbing radiation but non-scattering medium. It is assumed that there exists a homogeneous chemical reaction of first order with constant rate K'_2 between the diffusing species and the fluid. Geometry of the problem is presented in Fig. 1.

Since the plate is of infinite extent along x' and z' directions and is electrically non-conducting, all physical quantities except pressure depend on y' and t' only. The induced magnetic field generated by fluid motion is neglected in comparison to the applied one, i.e., the magnetic field $\vec{B} \equiv (0, B_0, 0)$. This assumption is justified because the magnetic Reynolds number is very

$$\frac{\partial u'}{\partial t'} + 2\Omega w' = \nu \frac{\partial^2 u'}{\partial y'^2} - \frac{\sigma B_0^2}{\rho(1+m^2)}(u' + mw') - \frac{\nu u'}{K'_1} + g\beta'(T' - T'_\infty) + g\beta^*(C' - C'_\infty), \quad (1)$$

$$\frac{\partial w'}{\partial t'} - 2\Omega u' = \nu \frac{\partial^2 w'}{\partial y'^2} + \frac{\sigma B_0^2}{\rho(1+m^2)}(mu' - w') - \frac{\nu w'}{K'_1}, \quad (2)$$

$$\rho c_p \frac{\partial T'}{\partial t'} = k \frac{\partial^2 T'}{\partial y'^2} - \frac{\partial q'_r}{\partial y'}, \quad (3)$$

$$\frac{\partial C'}{\partial t'} = D \frac{\partial^2 C'}{\partial y'^2} - K'_2(C' - C'_\infty), \quad (4)$$

Where u' , w' , ν , ρ , σ , $m = \omega_e \tau_e$, ω_e , τ_e , g , β' , β^* , T' , C' , c_p , k , K'_1 , q'_r and D

are fluid velocity in x' -direction, fluid velocity in z' -direction, kinematic coefficient of viscosity, fluid density, electrical conductivity, Hall current parameter, cyclotron frequency, electron collision

small for liquid metals and partially ionized fluids [53]. Also, no external electric field is applied so the effect of polarization of fluid is negligible and we assume the electric field $\vec{E} \equiv (0, 0, 0)$. This corresponds to the case where no energy is added or extracted from the fluid by electrical means [53].

Taking into consideration the assumptions made above, the governing equations for natural convection flow with heat and mass transfer of an electrically conducting, viscous, incompressible, chemically reacting and optically thin radiating fluid through a porous medium in the presence of thermal and mass diffusions taking Hall current into account, under Boussinesq approximation, in a rotating frame of reference are given by:

time, acceleration due to gravity, volumetric coefficient of thermal expansion, volumetric coefficient of expansion for species concentration, fluid temperature, species concentration, specific heat at constant pressure, thermal conductivity of

the fluid, permeability of the porous medium, diffusivity, respectively.
radiative flux vector and chemical molecular

Initial and boundary conditions to be satisfied are

$$\left. \begin{aligned} t' \leq 0 & : u' = 0, \quad w' = 0, \quad T' = T'_\infty, \quad C' = C'_\infty && \text{for all } y', \\ t' > 0 & : u' = u_0, \quad w' = 0, \quad T' = T'_w, \quad C' = C'_w && \text{at } y' = 0, \\ & u' \rightarrow 0, \quad w' \rightarrow 0, \quad T' \rightarrow T'_\infty, \quad C' \rightarrow C'_\infty && \text{as } y' \rightarrow \infty. \end{aligned} \right\} \quad (5)$$

The local radiant for the case of an optically thin gray gas Raptis [54] is expressed as

$$\frac{\partial q'_r}{\partial y'} = -4a^* \sigma^* (T'^4_\infty - T'^4). \quad (6)$$

where a^* is absorption coefficient and σ^* is the Stefan Boltzmann constant.

It is assumed that the temperature difference within the fluid flow is sufficiently small so that fluid temperature T'^4 may be expressed as a linear function of the temperature. This is accomplished

by expanding T'^4 in a Taylor series about the free stream temperature T'_∞ . Neglecting second and higher order terms, T'^4 is expressed as

$$T'^4 \cong 4T'^3_\infty T' - 3T'^4_\infty. \quad (7)$$

Making use of eqns. (6) and (7) in eqn. (3), we obtain

$$\rho c_p \frac{\partial T'}{\partial t'} = k \frac{\partial^2 T'}{\partial y'^2} + 16a^* \sigma T'^3_\infty (T'_\infty - T'). \quad (8)$$

Introducing non-dimensional quantities and parameters

$$\left. \begin{aligned} y &= y' / u_0 t_0, \quad u = u' / u_0, \quad w = w' / u_0, \quad t = t' / t_0, \quad \theta = (T' - T'_\infty) / (T'_w - T'_\infty), \\ C &= (C' - C'_\infty) / (C'_w - C'_\infty), \quad K^2 = \Omega \nu / u_0^2, \quad M = \sigma B_0^2 \nu / \rho u_0^2, \quad G_r = \nu g \beta' (T'_w - T'_\infty) / u_0^3, \\ G_c &= \nu g \beta^* (C'_w - C'_\infty) / u_0^3, \quad P_r = \rho \nu c_p / k, \quad S_c = \nu / D, \quad R = 16a^* \sigma \nu^2 T'^3_\infty, \quad K_1 = K'_1 u_0^2 / \nu^2 \\ &\text{and } K_2 = \nu K'_2 / u_0^2, \end{aligned} \right\} \quad (9)$$

eqns. (1), (2), (4) and (8), in non-dimensional form, become

$$\frac{\partial u}{\partial t} + 2K^2 w = \frac{\partial^2 u}{\partial y^2} - \frac{M(u + mw)}{(1 + m^2)} - \frac{u}{K_1} + G_r \theta + G_c C, \quad (10)$$

$$\frac{\partial w}{\partial t} - 2K^2 u = \frac{\partial^2 w}{\partial y^2} + \frac{M(mu - w)}{(1 + m^2)} - \frac{w}{K_1}, \quad (11)$$

$$P_r \frac{\partial \theta}{\partial t} = \frac{\partial^2 \theta}{\partial y^2} - R\theta, \quad (12)$$

$$\frac{\partial C}{\partial t} = \frac{1}{S_c} \frac{\partial^2 C}{\partial y^2} - K_2 C, \quad (13)$$

where

$K^2, M, G_r, G_c, P_r, S_c, R, K_1,$ and K_2 are rotation parameter, magnetic parameter, thermal Grashof number, solutal Grashof number, Prandtl number, Schmidt number, radiation parameter,

permeability parameter and chemical reaction parameter, respectively.

Initial and boundary conditions (5), in non-dimensional form, become

$$\left. \begin{aligned} t \leq 0 & : u = 0, \quad w = 0, \quad \theta = 0 \quad C = 0 && \text{for all } y, \\ t > 0 & : u = 1, \quad w = 0, \quad \theta = 1, \quad C = 1 && \text{at } y = 0, \\ & u \rightarrow 0, \quad w \rightarrow 0, \quad \theta \rightarrow 0, \quad C \rightarrow 0 && \text{as } y \rightarrow \infty. \end{aligned} \right\} \quad (14)$$

Combining eqns. (10) and (11), we obtain

$$\frac{\partial F}{\partial t} - 2iK^2 F = \frac{\partial^2 F}{\partial y^2} - NF - \frac{F}{K_1} + G_r \theta + G_c C, \quad (15)$$

where $F = u + iw$ and $N = \frac{M(1-im)}{(1+m^2)}$.

Initial and boundary conditions (14), in compact form, are given by

$$\left. \begin{aligned} t \leq 0 & : F = 0, \quad \theta = 0, \quad C = 0 \quad \text{for all } y, \\ t > 0 & : F = 1, \quad \theta = 1, \quad C = 1 \quad \text{at } y = 0, \\ & F \rightarrow 0, \quad \theta \rightarrow 0, \quad C \rightarrow 0 \quad \text{as } y \rightarrow \infty. \end{aligned} \right\} \quad (16)$$

Eqns. (12), (13) and (15) subject to the initial and boundary conditions (16) are solved analytically with the help of Laplace transform technique. Exact solutions for fluid velocity

$F(y,t)$, fluid temperature $\theta(y,t)$ and species concentration $C(y,t)$ are presented in the following form after simplification

$$\begin{aligned} F(y,t) = & \frac{1}{2} \left(1 + \frac{a_1}{b_1} + \frac{a_2}{b_2} \right) \left\{ e^{y\sqrt{\beta}} \operatorname{erfc} \left(\sqrt{\beta t} + \frac{y}{2\sqrt{t}} \right) + e^{-y\sqrt{\beta}} \operatorname{erfc} \left(-\sqrt{\beta t} + \frac{y}{2\sqrt{t}} \right) \right\} + \\ & + \frac{a_1}{2b_1} \left[e^{b_1 t} \left\{ e^{y\sqrt{P_r(\alpha+b_1)}} \operatorname{erfc} \left(\sqrt{(\alpha+b_1)t} + \frac{y}{2} \sqrt{\frac{P_r}{t}} \right) + e^{-y\sqrt{P_r(\alpha+b_1)}} \operatorname{erfc} \left(-\sqrt{(\alpha+b_1)t} + \frac{y}{2} \sqrt{\frac{P_r}{t}} \right) \right\} + \right. \\ & \left. - e^{y\sqrt{(b_1+\beta)}} \operatorname{erfc} \left(\sqrt{(b_1+\beta)t} + \frac{y}{2\sqrt{t}} \right) - e^{-y\sqrt{(b_1+\beta)}} \operatorname{erfc} \left(-\sqrt{(b_1+\beta)t} + \frac{y}{2\sqrt{t}} \right) \right] - e^{y\sqrt{P_r\alpha}} \times \\ & \times \operatorname{erfc} \left(\sqrt{\alpha t} + \frac{y}{2} \sqrt{\frac{P_r}{t}} \right) - e^{-y\sqrt{P_r\alpha}} \operatorname{erfc} \left(-\sqrt{\alpha t} + \frac{y}{2} \sqrt{\frac{P_r}{t}} \right) \left. \right] + \frac{a_2}{2b_2} \left[e^{b_2 t} \left\{ e^{y\sqrt{S_c(K_2+b_2)}} \times \right. \right. \\ & \times \operatorname{erfc} \left(\sqrt{(K_2+b_2)t} + \frac{y}{2} \sqrt{\frac{S_c}{t}} \right) + e^{-y\sqrt{S_c(K_2+b_2)}} \operatorname{erfc} \left(-\sqrt{(K_2+b_2)t} + \frac{y}{2} \sqrt{\frac{S_c}{t}} \right) + \\ & \left. - e^{y\sqrt{(b_2+\beta)}} \operatorname{erfc} \left(\sqrt{(b_2+\beta)t} + \frac{y}{2\sqrt{t}} \right) - e^{-y\sqrt{(b_2+\beta)}} \operatorname{erfc} \left(-\sqrt{(b_2+\beta)t} + \frac{y}{2\sqrt{t}} \right) \right\} + \\ & \left. - e^{y\sqrt{S_c K_2}} \operatorname{erfc} \left(\sqrt{K_2 t} + \frac{y}{2} \sqrt{\frac{S_c}{t}} \right) - e^{-y\sqrt{S_c K_2}} \operatorname{erfc} \left(-\sqrt{K_2 t} + \frac{y}{2} \sqrt{\frac{S_c}{t}} \right) \right], \quad (17) \end{aligned}$$

$$\theta(y,t) = \frac{1}{2} \left\{ e^{y\sqrt{P_r\alpha}} \operatorname{erfc} \left(\sqrt{\alpha t} + \frac{y}{2} \sqrt{\frac{P_r}{t}} \right) + e^{-y\sqrt{P_r\alpha}} \operatorname{erfc} \left(-\sqrt{\alpha t} + \frac{y}{2} \sqrt{\frac{P_r}{t}} \right) \right\}, \quad (18)$$

$$C(y,t) = \frac{1}{2} \left\{ e^{y\sqrt{S_c K_2}} \operatorname{erfc} \left(\sqrt{K_2 t} + \frac{y}{2} \sqrt{\frac{S_c}{t}} \right) + e^{-y\sqrt{S_c K_2}} \operatorname{erfc} \left(-\sqrt{K_2 t} + \frac{y}{2} \sqrt{\frac{S_c}{t}} \right) \right\}. \quad (19)$$

where $\alpha = R/P_r$, $a_1 = G_r/(1-P_r)$, $\beta = \left(N + \frac{1}{K_1} - 2iK^2 \right)$, $a_2 = G_c/(1-S_c)$, $b_1 = (P_r\alpha - \beta)/(1-P_r)$, $b_2 = (S_c K_2 - \beta)/(1-S_c)$.

SOLUTION IN THE CASE OF UNIT PRANDTL NUMBER AND UNIT SCHMIDT NUMBER

The solution (17) for fluid velocity is not valid for fluids with $P_r = 1$ and $S_c = 1$. Since Prandtl

number P_r is a measure of the relative strength of viscosity to thermal conductivity of the fluid and Schmidt number S_c is a measure of the relative strength of viscosity to chemical molecular diffusivity of the fluid, the case

$P_r = 1$ and $S_c = 1$ corresponds to those fluids for which viscous, thermal and concentration boundary layer thicknesses are of same order of magnitude. There are some fluids of practical interest which belong to this category [55]. Setting $P_r = 1$ and $S_c = 1$ in eqns. (12) and (13) and

following the same procedure as before, exact solutions for fluid velocity $F(y,t)$, fluid temperature $\theta(y,t)$ and species concentration $C(y,t)$ are obtained and presented in the following form

$$F(y,t) = \frac{(1-\delta_1-\delta_2)}{2} \left\{ e^{y\sqrt{\beta}} \operatorname{erfc} \left(\sqrt{\beta t} + \frac{y}{2\sqrt{t}} \right) + e^{-y\sqrt{\beta}} \operatorname{erfc} \left(-\sqrt{\beta t} + \frac{y}{2\sqrt{t}} \right) \right\} + \frac{\delta_1}{2} \left\{ e^{y\sqrt{\alpha}} \operatorname{erfc} \left(\sqrt{\alpha t} + \frac{y}{2\sqrt{t}} \right) + e^{-y\sqrt{\alpha}} \operatorname{erfc} \left(-\sqrt{\alpha t} + \frac{y}{2\sqrt{t}} \right) \right\} + \frac{\delta_2}{2} \left\{ e^{y\sqrt{K_2}} \operatorname{erfc} \left(\sqrt{K_2 t} + \frac{y}{2\sqrt{t}} \right) + e^{-y\sqrt{K_2}} \operatorname{erfc} \left(-\sqrt{K_2 t} + \frac{y}{2\sqrt{t}} \right) \right\}, \tag{20}$$

$$\theta(y,t) = \frac{1}{2} \left\{ e^{y\sqrt{\alpha}} \operatorname{erfc} \left(\sqrt{\alpha t} + \frac{y}{2\sqrt{t}} \right) + e^{-y\sqrt{\alpha}} \operatorname{erfc} \left(-\sqrt{\alpha t} + \frac{y}{2\sqrt{t}} \right) \right\}, \tag{21}$$

$$C(y,t) = \frac{1}{2} \left\{ e^{y\sqrt{K_2}} \operatorname{erfc} \left(\sqrt{K_2 t} + \frac{y}{2\sqrt{t}} \right) + e^{-y\sqrt{K_2}} \operatorname{erfc} \left(-\sqrt{K_2 t} + \frac{y}{2\sqrt{t}} \right) \right\}, \tag{22}$$

where $\delta_1 = \frac{G_r}{(\beta-\alpha)}$ and $\delta_2 = \frac{G_c}{(\beta-K_2)}$.

It is noticed from the solutions (18) and (19) that the solutions (21) and (22) may also be directly obtained by setting $P_r = 1$ and $S_c = 1$ in the solutions (18) and (19).

SKIN FRICTION, NUSSELT NUMBER AND SHERWOOD NUMBER

The expressions for the primary skin friction τ_x , secondary skin friction τ_y , Nusselt number N_u and Sherwood number S_h , which are measures of shear stress at the plate due to primary flow, shear stress at the plate due to secondary flow, rate of heat transfer at the plate and rate of mass transfer at the plate respectively, are presented in the following form

$$\begin{aligned} \tau_x + i\tau_y = & \left(1 + \frac{a_1}{b_1} + \frac{a_2}{b_2} \right) \left\{ \sqrt{\beta} \left(\operatorname{erfc}(\sqrt{\beta t}) - 1 \right) - \frac{1}{\sqrt{\pi t}} e^{-\beta t} \right\} + \frac{a_1}{b_1} \left[e^{b_1 t} \left\{ \sqrt{P_r(\alpha + b_1)} \times \right. \right. \\ & \times \left. \left(\operatorname{erfc}(\sqrt{(\alpha + b_1)t}) - 1 \right) - \sqrt{\frac{P_r}{\pi t}} e^{-(\alpha + b_1)t} - \sqrt{(\beta + b_1)} \left(\operatorname{erfc}(\sqrt{(\beta + b_1)t}) - 1 \right) + \frac{1}{\sqrt{\pi t}} e^{-(\beta + b_1)t} \right\} + \\ & - \sqrt{P_r \alpha} \left(\operatorname{erfc}(\sqrt{\alpha t}) - 1 \right) + \sqrt{\frac{P_r}{\pi t}} e^{-\alpha t} \left. \right] + \frac{a_2}{b_2} \left[e^{b_2 t} \left\{ \sqrt{S_c(K_2 + b_2)} \left(\operatorname{erfc}(\sqrt{(K_2 + b_2)t}) - 1 \right) \right. \right. \\ & - \sqrt{\frac{S_c}{\pi t}} e^{-(K_2 + b_2)t} - \sqrt{(b_2 + \beta)} \left(\operatorname{erfc}(\sqrt{(b_2 + \beta)t}) - 1 \right) + \frac{1}{\sqrt{\pi t}} e^{-(b_2 + \beta)t} \left. \right\} + \\ & \left. - \sqrt{S_c K_2} \left(\operatorname{erfc}(\sqrt{K_2 t}) - 1 \right) + \sqrt{\frac{S_c}{\pi t}} e^{-K_2 t} \right], \tag{23} \end{aligned}$$

$$N_u = \sqrt{P_r \alpha} \left(\operatorname{erfc}(\sqrt{\alpha t}) - 1 \right) - \sqrt{\frac{P_r}{\pi t}} e^{-\alpha t}, \tag{24}$$

$$S_h = \sqrt{S_c K_2} \left(\operatorname{erfc}(\sqrt{K_2 t}) - 1 \right) - \sqrt{\frac{S_c}{\pi t}} e^{-K_2 t}. \quad (25)$$

RESULTS AND DISCUSSION

In order to highlight the influence of rotation, Hall current, thermal buoyancy force, concentration buoyancy force, magnetic field, radiation, chemical reaction and mass diffusion on the flow-field in the boundary layer region, numerical values of primary and secondary fluid velocities, computed from the analytical solution (17), are displayed graphically versus boundary layer co-ordinate y in figures 2 to 9 for various values of K^2 , m , G_r , G_c , M , R , K_2 and S_c taking

$K_1 = 0.2$, $P_r = 0.71$ and $t = 0.2$. It is evident from figures 2 to 9 that the primary velocity u and secondary velocity w attain a distinctive maximum value in the vicinity of the surface of the plate and then decrease properly on increasing boundary layer coordinate y to approach free stream velocity. Fig. 2 shows the effect of rotation on the primary and secondary fluid velocities. It is revealed from Fig. 2 that primary fluid velocity u decreases whereas secondary fluid velocity w increases on increasing K^2 . This implies that rotation tends to retard fluid flow in the primary flow direction whereas it has a reverse effect on fluid flow in the secondary flow direction. This may be attributed to the fact that when the frictional layer near the moving plate is suddenly set into motion, then the Coriolis force acts as a constraint in the main fluid flow, i.e. primary flow to induce cross flow, i.e. secondary flow in the flow-field. Figs. 3 to 5 demonstrate the influence of Hall current, thermal Grashof number and solutal Grashof number on the primary and secondary fluid velocities. It is noticed from Figs. 3 to 5 that both primary and secondary fluid velocities increase on increasing either m or G_r or G_c . This implies that Hall current, thermal buoyancy force and concentration buoyancy force tend to accelerate fluid flow in both the primary and secondary flow directions. Figs. 6 to 9 display the effects of magnetic field, radiation, chemical reaction and mass diffusion on the

primary and secondary fluid velocities. It is revealed from Figs. 6 to 9 that both primary and secondary fluid velocities decrease on increasing either M or R or K_2 or S_c . This implies that magnetic field, radiation and chemical reaction tend to retard fluid flow in both the primary and secondary flow directions. Since Schmidt number S_c is a measure of relative strength of viscosity to chemical molecular diffusivity, S_c decreases on increasing chemical molecular diffusivity of the fluid. This implies that mass diffusion tends to accelerate fluid flow in both the primary and secondary flow directions.

The numerical solutions for fluid temperature and species concentration, computed from the analytical solutions (18) and (19), are depicted graphically in Figs. 10 to 13 for various values of radiation parameter R , Prandtl number P_r , chemical reaction parameter K_2 and Schmidt number S_c taking time $t = 0.2$. It is evident from Figs. 10 to 13 that fluid temperature θ and fluid concentration C are maximum at the surface of the plate and decrease properly on increasing boundary layer coordinate y to approach the free stream value. Figs. 10 and 11 illustrate the effects of radiation and thermal diffusion on fluid temperature. It is seen from Figs. 10 and 11 that fluid temperature θ decreases on increasing either R or P_r in the boundary layer region. Since P_r is a measure of the relative strength of viscosity to thermal diffusivity, P_r decreases on increasing thermal diffusivity. This implies that radiation tends to reduce fluid temperature whereas thermal diffusion has a reverse effect on it. Figs. 12 and 13 demonstrate the effects of chemical reaction and mass diffusion on species concentration. It is noticed from Figs. 12 and 13 that species concentration C decreases on increasing either K_2 or S_c . This implies that chemical reaction tends to reduce species concentration whereas mass diffusion has a reverse effect on it.

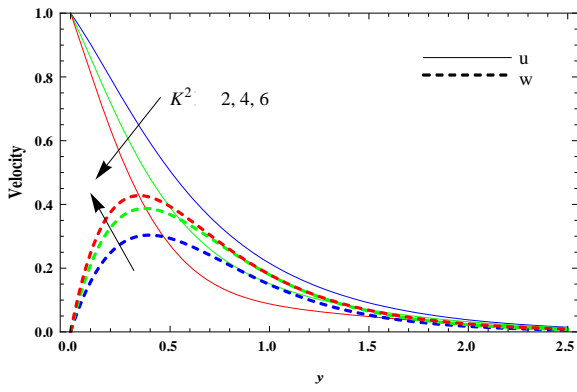


Fig. 2: Velocity profiles when $m = 1.5$, $G_r = 4$, $G_c = 5$, $M = 10$, $R = 1$, $K_2 = 0.2$ and $S_c = 0.22$

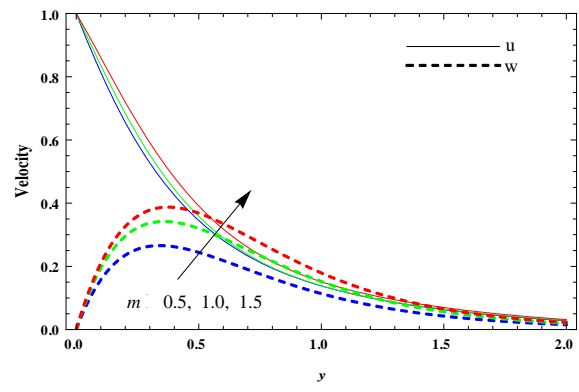


Fig. 3: Velocity profiles when $K^2 = 4$, $G_r = 4$, $G_c = 5$, $M = 10$, $R = 1$, $K_2 = 0.2$ and $S_c = 0.22$.

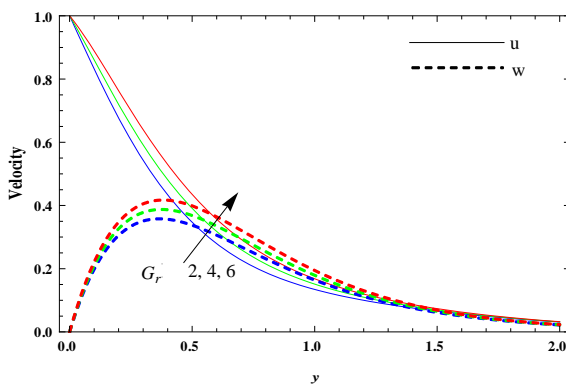


Fig. 4: Velocity profiles when $m = 1.5$, $K^2 = 4$, $G_c = 5$, $M = 10$, $R = 1$, $K_2 = 0.2$ and $S_c = 0.22$

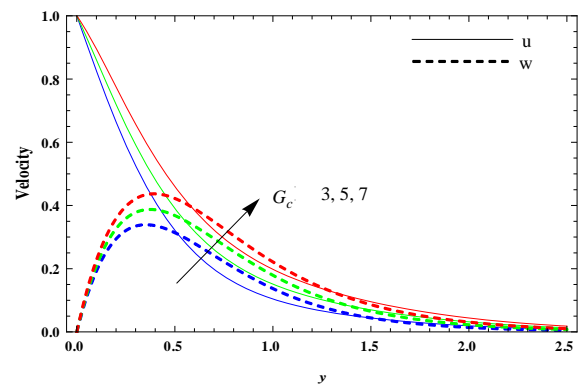


Fig. 5: Velocity profiles when $m = 1.5$, $K^2 = 4$, $G_r = 4$, $M = 10$, $R = 1$, $K_2 = 0.2$ and $S_c = 0.22$

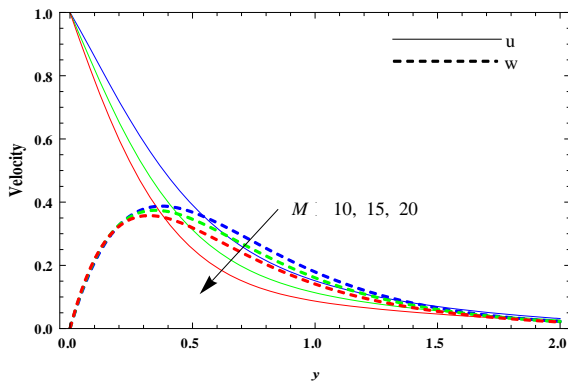


Fig. 6: Velocity profiles when $m = 1.5$, $K^2 = 4$, $G_r = 4$, $G_c = 5$, $R = 1$, $K_2 = 0.2$ and $S_c = 0.22$

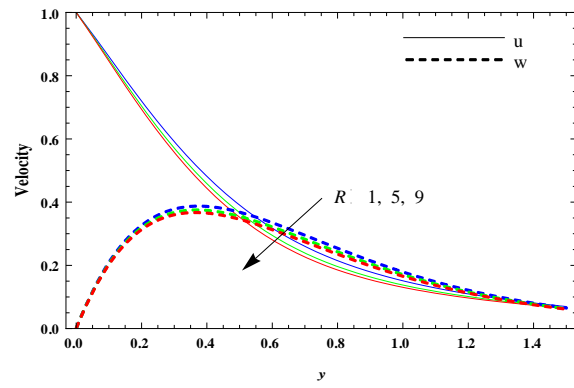


Fig. 7: Velocity profiles when $m = 1.5$, $K^2 = 4$, $G_r = 4$, $G_c = 5$, $M = 10$, $K_2 = 0.2$ and $S_c = 0.22$

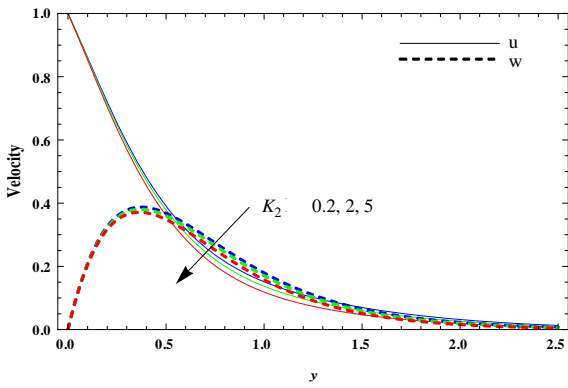


Fig. 8: Velocity profiles when $m = 1.5$, $K^2 = 4$, $G_r = 4$, $G_c = 5$, $M = 10$, $R = 1$ and $S_c = 0.22$

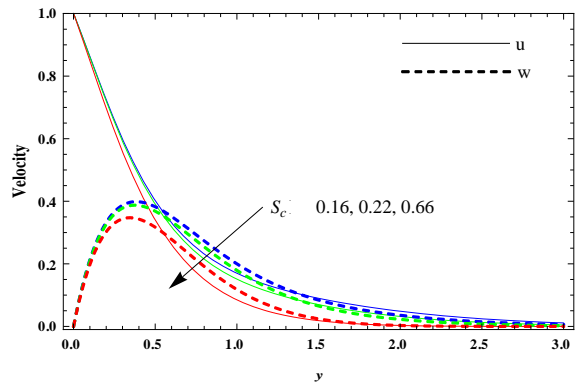


Fig. 9: Velocity profiles when $m = 1.5$, $K^2 = 4$, $G_r = 4$, $G_c = 5$, $M = 10$, $R = 1$ and $K_2 = 0.2$

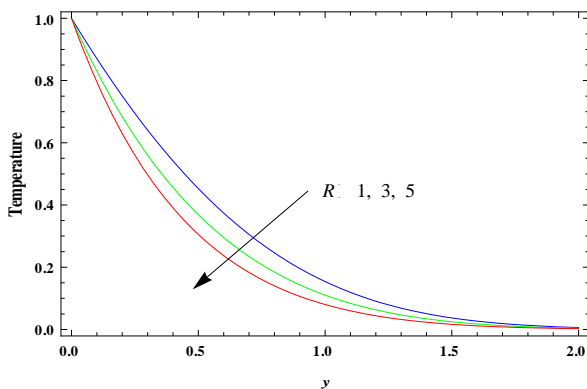


Fig. 10: Temperature profiles when $P_r = 0.71$.

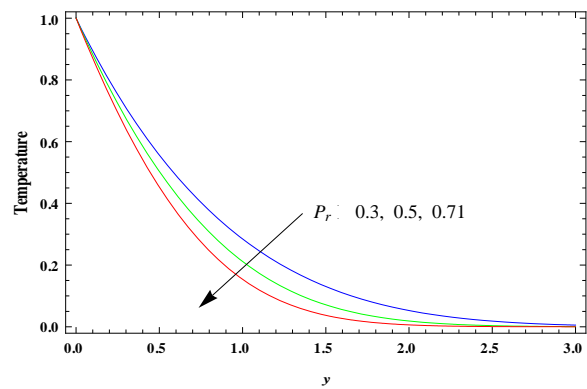


Fig. 11: Temperature profiles when $R = 1$.

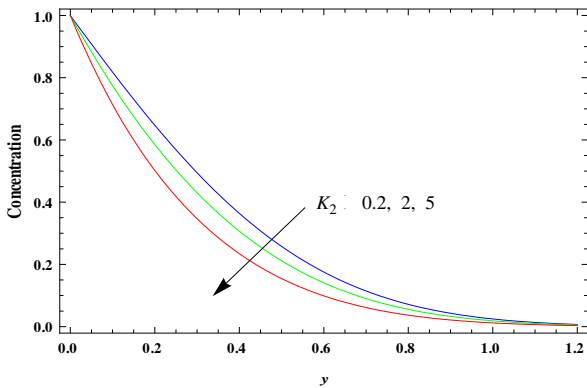


Fig. 12: Concentration profiles when $S_c = 2$.

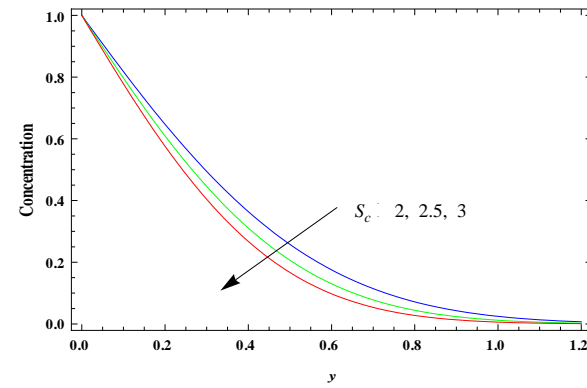


Fig. 13: Concentration profiles when $K_2 = 0.2$.

The numerical values of primary skin friction τ_x and secondary skin friction τ_z , computed from the analytical expression (23), are presented in tabular form in Tables 1 to 5 for various values of $m, K^2, K_2, S_c, G_r, G_c, M, K_1, R$ and P_r taking $t = 0.2$. It is observed from Table 1 that primary skin friction, i.e. τ_x decreases on increasing m . With an increase in m , secondary skin friction, i.e. τ_z increases, attains a maximum and then decreases when $K^2 = 2$; it increases when

$K^2 \geq 4$. τ_x and τ_z increase on increasing K^2 . This implies that Hall current tends to reduce primary skin friction whereas it has a reverse effect on secondary skin friction when $K^2 \geq 4$. Rotation tends to enhance both the primary and secondary skin frictions. It is evident from Table 2 that τ_x increases whereas τ_z decreases on increasing S_c . τ_x decreases whereas τ_z increases on increasing K_2 . This implies that mass diffusion and chemical reaction tend to reduce primary skin friction whereas these have reverse effect on secondary skin

Table 1: Primary and secondary skin frictions
when $K_1 = 0.3, K_2 = 0.2, M = 10, R = 1, P_r = 0.71, G_r = 4, S_c = 0.22$ and $G_c = 5$.

$m \downarrow K^2 \rightarrow$	$-\tau_x$			τ_z		
	2	4	6	2	4	6
0.5	2.4971	2.53666	2.70599	0.890639	1.49983	2.07509
1.0	1.98013	2.08687	2.35844	1.03103	1.77994	2.4084
1.5	1.56789	1.70466	2.04754	0.929534	1.8237	2.51996

Table 2: Primary and secondary skin frictions
when $K^2 = 4, m = 1.5, K_1 = 0.3, M = 10, R = 1, P_r = 0.71, G_r = 4$ and $G_c = 5$.

$K_2 \downarrow S_c \rightarrow$	$-\tau_x$			τ_z		
	0.16	0.22	0.66	0.16	0.22	0.66
0.2	1.652	1.70466	1.96087	1.9125	1.8237	1.41646
2.0	1.62962	1.67487	1.87401	1.98757	1.91258	1.56383
5.0	1.61981	1.65922	1.80761	2.05997	2.00076	1.73388

friction. It is noticed from Table 3 that τ_z decreases on increasing G_r whereas it increases on increasing G_c . τ_x decreases on increasing either G_r or G_c when $G_c \leq 5$. This implies that thermal buoyancy force tends to reduce secondary skin friction whereas concentration buoyancy force has a reverse effect on it. Thermal buoyancy force and concentration buoyancy force tend to reduce primary skin friction when $G_c \leq 5$. It is worth noting that there exists flow separation at the plate on increasing G_c when $G_r = 4$ and 6 and on increasing G_r when $G_c = 7$.

It is observed from Table 4 that τ_x and τ_z increase on increasing M . τ_x decreases whereas τ_z increases on increasing K_1 . This implies that magnetic field tends to enhance both primary and secondary skin frictions. Permeability of medium tends to reduce primary skin friction whereas it has a reverse effect on secondary skin friction. It is revealed from Table 5 that τ_x and τ_z decrease on increasing P_r . τ_x increases on increasing R when $P_r = 0.3$ and it decreases, attains a minimum and then increases on increasing R when $P_r \geq 0.5$. τ_z

Table 3: Primary and secondary skin frictions
when $K^2 = 4, m = 1.5, K_1 = 0.3, K_2 = 0.2, M = 10, R = 1, P_r = 0.71$ and $S_c = 0.22$.

$G_r \downarrow G_c \rightarrow$	$-\tau_x$			τ_z		
	3	5	7	3	5	7
2	1.98143	1.07968	0.177923	1.93213	1.99615	2.06018
4	1.70466	0.802902	-0.09885	1.8237	1.88773	1.95176
6	1.42788	0.526128	-0.37562	1.71528	1.77931	1.84334

Table 4: Primary and secondary skin frictions
when $K^2 = 4, m = 1.5, K_2 = 0.2, R = 1, P_r = 0.71, G_r = 4, S_c = 0.22$ and $G_c = 5$.

$M \downarrow K_1 \rightarrow$	$-\tau_x$			τ_z		
	0.1	0.3	0.5	0.1	0.3	0.5
10	2.80552	1.70466	1.42718	1.53869	1.82370	1.92827
15	3.08355	2.14366	1.92434	1.78957	2.12677	2.23223
20	3.35574	2.53327	2.35185	2.00405	2.35463	2.45468

Table 5: Primary and secondary skin frictions

when $K^2 = 4, m = 1.5, M = 10, K_1 = 0.3, K_2 = 0.2, G_r = 4, S_c = 0.22$ and $G_c = 5$.

$R \downarrow P_r \rightarrow$	$-\tau_x$			τ_z		
	0.3	0.5	0.71	0.3	0.5	0.71
1	1.54040	1.6280	1.70466	2.14126	1.96731	1.82370
5	1.58586	1.59735	1.61619	2.25045	2.17324	2.06695
9	1.65566	1.65262	1.64707	2.22303	2.2025	2.15664

Table 6: Nusselt Number N_u when $t = 0.2$.

$R \downarrow P_r \rightarrow$	N_u			
	0.3	0.5	0.71	7.0
1	1.10655	1.22687	1.34915	3.43270
3	1.74676	1.79058	1.85335	3.61987
5	2.23875	2.25505	2.28743	3.80358

increases on increasing R when $P_r \geq 0.5$ and it increases, attains a maximum and then decreases on increasing R when $P_r = 0.3$. This implies that thermal diffusion tends to enhance both the primary and secondary skin frictions. Radiation tends to enhance secondary skin friction when $P_r \geq 0.5$ and

it tends to enhance primary skin friction when $P_r = 0.3$.

The numerical values of Nusselt number N_u , computed from the analytical expression (24), are presented in Table 6 for various values of R and P_r whereas that of Sherwood number S_h , computed from the analytical expression (25), are presented in Table 7 for different values of K_2 and S_c taking

Table 7: Sherwood Number S_h when $t = 0.2$

$K_2 \downarrow S_c \rightarrow$	S_h			
	2	2.5	3	3.5
0.2	1.85502	2.07397	2.27192	2.45396
2	2.45375	2.74337	3.00521	3.246
5	3.3212	3.71321	4.06762	4.39353

$t=0.2$. It is noticed from Table 6 that Nusselt number Nu increases on increasing either R or P_r . This implies that radiation tends to enhance the rate of heat transfer at the plate whereas thermal diffusion has a reverse effect on it. It is found from Table 7 that Sherwood number S_h increases on increasing either K_2 or S_c . This implies that chemical reaction tends to enhance the rate of mass transfer at the plate whereas mass diffusion has a reverse effect on it.

CONCLUSIONS

This study presents an investigation of the effects of Hall current and rotation on hydromagnetic natural convection flow with heat and mass transfer of an electrically conducting, viscous, incompressible, chemically reacting and optically thin radiating fluid past an impulsively moving infinite vertical plate embedded in a porous medium in the presence of thermal and mass

diffusion. The significant findings are summarized below:

Rotation tends to retard fluid flow in the primary flow direction whereas it has a reverse effect on the fluid flow in the secondary flow direction. Hall current, thermal buoyancy force, concentration buoyancy force and mass diffusion tend to accelerate fluid flow in both primary and secondary flow directions. Magnetic field, radiation and chemical reaction tend to retard fluid flow in both primary and secondary flow directions. Radiation has a tendency to reduce fluid temperature whereas thermal diffusion has a reverse effect on it. Chemical reaction tends to reduce species concentration whereas mass diffusion has a reverse effect on it. Hall current tends to reduce primary skin friction whereas it has a reverse effect on secondary skin friction when $K^2 \geq 4$. Rotation tends to enhance both primary and secondary skin frictions. Mass diffusion and chemical reaction tend to reduce primary skin friction whereas these have

reverse effect on secondary skin friction. Thermal buoyancy force tends to reduce secondary skin friction whereas concentration buoyancy force has a reverse effect on it. Thermal buoyancy force and concentration buoyancy force tend to reduce primary skin friction when $G_c \leq 5$. Magnetic field tends to enhance both primary and secondary skin frictions. Permeability of medium tends to reduce primary skin friction whereas it has a reverse effect on secondary skin friction. Thermal diffusion tends to enhance both primary and secondary skin frictions. Radiation tends to enhance secondary skin friction when $P_r \geq 0.5$ and it tends to enhance primary skin friction when $P_r = 0.3$. Radiation tends to enhance the rate of heat transfer at the plate whereas thermal diffusion has a reverse effect on it. Chemical reaction tends to enhance the rate of mass transfer at the plate whereas mass diffusion has a reverse effect on it.

REFERENCES:

1. P. Cheng, W. J. Minkowycz, *J. Geophys. Res.*, **82**, 2040 (1977).
2. A. Nakayama, H. Koyama, *J. Heat Transf.*, **109**, 1041 (1987).
3. F. C. Lai, F. A. Kulacki, *J. Heat Transf.*, **113**, 252 (1991).
4. J. C. Hsieh, T. S. Chen, B. F. Armaly, *Int. J. Heat Mass Transf.*, **36**, 1485 (1993).
5. D. A. Nield, A. V. Kuznetsov, *Int. J. Heat Mass Transf.*, **52**, 5792 (2009).
6. R. S. R. Gorla, A. J. Chamkha, *Nanoscale Microscale Thermophys. Engng.*, **15**, 81 (2011).
7. I. Pop, D. B. Ingham, *Transport phenomena in porous media-II*, 1st edn., Elsevier, Oxford, U. K, 2012.
8. K. Vafai, *Handbook of porous media*, 2nd edn., Taylor and Francis Group, Florida, USA, 2005.
9. D. A. Nield, A. Bejan, *Convection in porous media*, 3rd edn., Springer, New York, USA, 2006.
10. A. Raptis, N. Kafousias, *Int. J. Energy Res.*, **6**, 241 (1982).
11. A. Raptis, *Int. J. Energy Res.*, **10**, 97 (1986).
12. A. J. Chamkha, *Fluid/Particle Separation J.*, **10**, 101 (1997).
13. A. J. Chamkha, *Int. J. Engng. Sci.*, **35**, 975 (1997).
14. T. K. Aldoss, M.A. Al-Nimr, M. A. Jarrah, B. J. Al-Shaer, *Numer. Heat Transf.*, **28**, 635 (1995).
15. Y. J. Kim, *Int. J. Engng. Sci.*, **38**, 833 (2000).
16. B. K. Jha, *Astrophys. Space Sci.*, **175**, 225 (1991).
17. F. S. Ibrahim, I. A. Hassanien, A. A. Bakr, *Canad. J. Phys.*, **82**, 775 (2004).
18. Md. S. Alam, M. M. Rahman, *J. Naval Architecture Marine Eng.*, **1**, 55 (2005).
19. O. D. Makinde, P. Sibanda, *J. Heat Transf.*, **130**, 112602 (2008).
20. O. D. Makinde, *Int. J. Numer. Methods Heat Fluid Flow*, **19**, 546 (2009).
21. N. T. M. Eldabe, E. M. A. Elbashbeshy, W. S. A. Hasanin, E. M. Elsaid, *Int. J. Energy Tech.* **3** (35) 1 (2011).
22. E. M. Sparrow, R. D. Cess, *Radiation Heat Transfer*, Brook/Cole, Belmont, California, USA, 1970.
23. R. D. Cess, *Int. J. Heat Mass Transf.*, **9**, 1269 (1966).
24. M. A. Hossain, H. S. Takhar, *Heat Mass Transf.*, **31**, 243 (1996).
25. A. Y. Bakier, R. S. R. Gorla, *Transport in Porous Media*, **23**, 357 (1996).
26. H. S. Takhar, R. S. R. Gorla, V. M. Soundalgekar, *Int. J. Num. Methods Heat Fluid Flow*, **6**, 77 (1996).
27. A. J. Chamkha, *J. Heat Transf.*, **119**, 89 (1997).
28. A. J. Chamkha, *Int. J. Engng. Sci.*, **38**, 1699 (2000).
29. G. E. A. Azzam, *Phys. Scr.*, **66**, 71 (2002).
30. C. I. Cookey, A. Ogulu, V. B. Omubo-Pepple, *Int. J. Heat Mass Transf.*, **46**, 2305 (2003).
31. R. Muthucumaraswamy, P. Ganesan, *Int. J. Appl. Mech. Engng.*, **8**, 125 (2003).
32. O. D. Makinde, A. Ogulu, *Chem. Engng. Comm.*, **195**, 1575 (2008).
33. A. A. Mahmoud Mostafa, *Canad. J. Chem. Engng.*, **87**, 47 (2009).
34. A. Ogulu, O. D. Makinde, *Chem. Engng. Comm.*, **196**, 454 (2009).
35. P. M. Kishore, V. Rajesh, S. Vijayakumar Verma, *Adv. Appl. Sci. Res.* **2**(5), 226 (2011).
36. A. J. Chamkha, S. Abbasbandi, A. M. Rashad, K. Vajravelu, *Transport in Porous Media*, **91**, 261 (2012).
37. R. Nandkeolyar, G. S. Seth, O. D. Makinde, P. Sibanda, Md. S. Ansari, *ASME J. Appl. Mech.*, **80**, p. 061003-1-9, (2013) DOI: 10.1115/1.4023959.
38. A. A. Afify, *Canad. J. Phys.*, **82**, 447 (2004).
39. R. Muthucumaraswamy, P. Chandrakala, *Int. J. Appl. Mech. Engng.* **11**, 639 (2006).
40. F. S. Ibrahim, A. M. Elaiw, A. A. Bakr, *Comm. Nonlinear Sci. Numer. Simul.*, **13**, 1056 (2008).
41. R. Muthucumaraswamy, G. Nagarajan, V. S. A. Subramanian, *Acta Tech. Corviniensis-Bull. of Engng.*, **4**, 97 (2011).
42. V. Rajesh, *Chem. Indus. Chem. Engng. Qrt.*, **17**, 189 (2011).
43. M. Sudheer Babu, P. V. Satya Narayana, T. Shankar Reddy, D. Umamaheswara Reddy, *Adv. Appl. Sci. Res.*, **2**(5), 226 (2011).
44. R. Nandkeolyar, M. Das, P. Sibanda, *Math. Prob. Engng.*, **2013**, Article ID 381806, (2013)
45. A. R. Bestman, S. K. Adjepong, *Astrophys. Space Sci.*, **143**, 73 (1998).
46. I. U. Mbeledogu, A. Ogulu, *Int. J. Heat Mass Transf.*, **50**, 1902 (2007).
47. A. A. Bakr, *Comm. Nonlinear Sci. Numer. Simul.*, **16**, 698 (2011).
48. G. S. Seth, R. Nandkeolyar, M. S. Ansari, *J. Appl. Fluid Mech.*, **6**, 27 (2013).

49. G. W. Sutton, A. Sherman, Engineering Magnetohydrodynamics. McGraw-Hill, New York 1965.
50. B. C. Sarkar, S. Das, R. N. Jana, *Int. J. Com. Appl.*, **70**, 0975 (2013)
51. S. P. Anjali Devi, K. Shailendra, C. V. Ramesan, *Int. J. Sci. Eng. Investigations*, **1**(6), 64 (2012)
52. A. Farhad, M. Norzieha, S. Sharidan, I. Khan, Samiulhaq, *Int. J. Phys. Sci.*, **7**, 1540 (2012).
53. K. R. Cramer, S. I. Pai, Magnetofluid dynamics for engineers and applied physicists. McGraw Hill Book Company, New York, USA, 1973.
54. A. Raptis, *Thermal Science*, **15**, 849 (2011).
55. T. Cebeci, Convective Heat Transfer. Horizons Publishing Inc., Long Beach, California 2002.

ЕФЕКТИ НА ТОКОВЕТЕ НА HALL И НА ВЪРТЕНЕТО В НЕСТАЦИОНАРНО
МАГНИТО-ХИДРОДИНАМИЧНО ТЕЧЕНИЕ С ЕСТЕСТВЕНИ КОНВЕКЦИИ И ТОПЛО И
МАСОПРЕНАСЯНЕ ЗАД ИМПУЛСИВНО ДВИЖЕЩА СЕ ВЕРТИКАЛНА ПЛОСКОСТ
ПРИ ИЗЛЪЧВАНЕ И ХИМИЧНА РЕАКЦИЯ

Г.С. Сет^{1*}, С.М. Хусаин², С. Саркар¹

¹ Департамент по приложна математика, Индийски минен университет, Дханбад, Индия

² Департамент по математика, Технологичен университет "О.П.Джиндал", Райгар, Индия

Постъпила на 9 септември, 2013 г.; Коригирана 24 декември, 2013 г.

(Резюме)

Изучени са ефектите на токовете на Hall и на въртенето в нестационарен магнито-хидродинамичен поток с естествени конвекции и топло-масопренасяне зад импулсивно движеща се вертикална пластина. Отчетени са термичната и молекулярната дифузия. Получени са точни решения в затворен вид на хидродинамичните уравнения, уравненията на топлопроводността и на конвективната дифузия с помощта на Лапласова трансформация в прибиблиението на Boussinesq. Получени са уравнения за коефициента на триене, числата на Nusselt и на Sherwood. Графично са представени скоростните профили, разпределението на температурата и на веществото, а коефициента на триене и числата на Nusselt и на Sherwood са показани в табличен вид в зависимост от параметрите на течението..

Silica-based sulfonic acid (SiO₂-Pr-SO₃H): an efficient catalyst in the green one-pot synthesis of 3,4-dihydropyrimidinones/thiones

G. Mohammadi Ziarani^{1,*}, A. Badiei², N. Lashgari², T. Pourjafar¹, Z. Farahani¹

¹ Department of Chemistry, Alzahra University, Tehran, Iran

² School of Chemistry, College of Science, University of Tehran, Tehran, Iran,

Received July 28, 2013; Accepted November 27, 2013

SiO₂-Pr-SO₃H efficiently catalyzes the three-component coupling of ethyl acetoacetate, aldehydes, and urea (or thiourea) under solvent-free conditions to afford the corresponding dihydropyrimidinones. Compared with the classical Biginelli reaction conditions, this protocol has the advantage of very short reaction time (2 minutes), good to excellent yields, recyclable catalyst, and simple experimental procedure.

Keywords: Sulfonic acid functionalized silica; 3,4-Dihydropyrimidinones, Biginelli reaction; Heterogeneous catalyst, Green conditions.

INTRODUCTION

Dihydropyrimidinones (DHPMs), the so called *Biginelli compounds* [1], and their derivatives are very well known for their diverse biological activities such as antifungal [2], antibacterial [3], antihypertensive [4], anti-HIV [5] and anti-tumor effects [6]. DHPMs were recently developed as calcium channel modulators, α_{1a} adrenoceptor-selective antagonists and compounds that target the mitotic machinery [7]. Moreover, several marine alkaloids with interesting biological activities containing the dihydropyrimidine-5-carboxylate core have been isolated [8, 9]. Therefore, this heterocyclic nucleus has gained great importance and several improved methodologies for the original Biginelli protocol have recently been reported in the literature [10-18]. Although these methods have their own merits, they also suffer from drawbacks such as use of solvents, expensive reagents or catalysts, drastic reaction conditions, long reaction times and unsatisfactory yields.

The development of efficient and versatile catalytic systems for the Biginelli reaction is an active ongoing research area and thus, there is scope for further improvement toward milder reaction conditions, variations of substituents in all three components, shorter reaction times, and better yields. In 2007, Paul and coworkers developed a simple procedure for the synthesis of 3,4-dihydropyrimidinones/thiones in CH₃CN using reusable covalently anchored sulfonic acid onto the

surface of silica gel solid acid catalyst with long reaction times (7-12 h) [19]. In continuation of our studies on the application of heterogeneous solid catalysts to organic synthesis [20-23], herein we developed a green, rapid, efficient and inexpensive procedure for the synthesis of 3,4-dihydropyrimidinones using SiO₂-Pr-SO₃H under solvent-free conditions.

EXPERIMENTAL

Materials

All chemicals were obtained commercially and used without further purification. Melting points were measured by the capillary tube method with an Electrothermal 9200 apparatus.

Instruments

IR spectra were recorded from KBr disks using a FT-IR Bruker Tensor 27 instrument. ¹H NMR and ¹³C NMR spectra were recorded on a Bruker DPX spectrometer (250 MHz for ¹H, 62 MHz for ¹³C) in DMSO-d₆ solutions. GC-mass analysis was performed on a model 5973/6890 network mass-selective detector (Agilent).

Preparation of catalyst: synthesis of 3-mercaptopropylsilica (MPS) and its oxidation

To 20 g of SiO₂ in dry toluene, 25 ml of (3-mercaptopropyl)trimethoxysilane was added, and the reaction mixture was refluxed for 24 h. Then, the mixture was filtered to obtain 3-mercaptopropylsilica (MPS) which was washed with acetone and dried. MPS (20 g) was oxidized with H₂O₂ (50 ml) and one drop of H₂SO₄ in methanol (20 ml) for 24 h at room temperature,

* To whom all correspondence should be sent:
E-mail: gmohammadi@alzahra.ac.ir

then the mixture was filtered and washed with H₂O and acetone to obtain SiO₂-Pr-SO₃H. The modified SiO₂-Pr-SO₃H was dried and used as a solid acid catalyst in the following reaction.

General procedure for the synthesis of 3,4-dihydropyrimidinones/thiones

SiO₂-Pr-SO₃H (0.02 g) was activated in vacuum at 100°C, and after cooling the catalyst to room temperature, aldehyde (1 mmol), urea or thiourea (1 mmol), and ethyl acetoacetate (1 mmol) were added. After completion of the reaction (monitored by TLC), the mixture was cooled to room temperature, poured into ice-water and filtered. The crude product was dissolved in EtOAc, filtered off for removing the unsolved material and the filtrate was cooled to afford the pure product.

Selected Spectral Data

5-(Ethoxycarbonyl)-6-methyl-4-phenyl-3,4-dihydropyrimidin-(1H)-one (4a)

m.p.: 203-204°C; IR (KBr): 3244, 3116, 1725, 1701, 1646 cm⁻¹; Mass: m/z (%) 260 [M⁺], 245, 231, 215, 183 (100), 169, 155; ¹H NMR (DMSO-d₆): δ = 1.10 (t, J = 5.8 Hz, 3H, CH₃-CH₂O), 2.25 (s, 3H, CH₃), 3.97 (q, J = 5.8 Hz, 2H, CH₃-CH₂O), 5.14 (d, J = 2.7 Hz, 1H, CH), 5.41 (s, 1H, NH), 7.21-7.35 (m, 5CH, ArH), 7.74 (s, 1H, NH) ppm; ¹³C NMR (DMSO-d₆): δ = 14.1, 17.8, 53.9, 59.2, 99.2, 126.2, 127.2, 128.4, 144.8, 148.3, 152.1, 165.3 ppm.

5-(Ethoxycarbonyl)-6-methyl-4-(2-thienyl)-3,4-dihydropyrimidin-(1H)-one (4c)

m.p.: 205-207°C; IR (KBr): 3333, 3245, 1700, 1650, 1594 cm⁻¹; Mass: m/z (%) 266 [M⁺], 251, 237 (100), 221, 193, 178, 110; ¹H NMR (DMSO-d₆): δ = 1.22 (t, J = 4.5 Hz, 3H, CH₃-CH₂O), 2.30 (s, 3H, CH₃), 4.11 (q, J = 7.2 Hz, 2H, CH₃-CH₂O), 5.58 (d, J = 3.5 Hz, 1H, CH), 6.88-6.96 (m, 3H, 3CH), 7.43 (s, 1H, NH), 9.02 (s, 1H, NH) ppm.

4-(4-Chlorophenyl)-5-(ethoxycarbonyl)-6-methyl-3,4-dihydropyrimidin-(1H)-one (4e)

m.p.: 210°C; IR (KBr): 3242, 3116, 1706, 1647 cm⁻¹; ¹H NMR (DMSO-d₆): δ = 1.17 (t, J = 7.0 Hz, 3H, CH₃-CH₂O), 2.34 (s, 3H, CH₃), 4.10 (q, J = 7.2 Hz, 2H, CH₃-CH₂O), 5.37 (d, J = 2.7 Hz, 1H, CH), 5.56 (s, 1H, NH), 7.23-7.31 (m, 4CH, ArH), 7.48 (s, 1H, NH) ppm.

5-(Ethoxycarbonyl)-6-methyl-4-(4-methylphenyl)-3,4-dihydropyrimidin-(1H)-one (4m)

m.p.: 211-213°C; IR (KBr): 3309, 3243, 1704, 1650 cm⁻¹; Mass: m/z (%) 274 [M⁺], 259, 245, 229, 215, 201, 215, 183 (100), 155, 91; ¹H NMR (DMSO-d₆): δ = 1.17 (t, J = 7.5 Hz, 3H, CH₃-CH₂O), 2.33 (s, 3H, CH₃), 2.45 (s, 3H, CH₃), 4.07

(q, J = 7.5 Hz, 2H, CH₃-CH₂O), 5.32 (d, J = 5.0 Hz, 1H, CH), 6.02 (s, 1H, NH), 7.08 (d, J = 7.5 Hz, 2CH, ArH), 7.20 (d, J = 7.5 Hz, 2CH, ArH), 8.05 (s, 1H, NH) ppm.

4-(4-N,N-Dimethylaniline)-5-(ethoxycarbonyl)-6-methyl-3,4-dihydropyrimidin-(1H)-one (4o)

m.p.: 248-250°C; IR (KBr): 3241, 3112, 1720, 1702, 1646 cm⁻¹; ¹H NMR (DMSO-d₆): δ = 1.18 (t, J = 7.0 Hz, 3H, CH₃-CH₂O), 2.32 (s, 3H, CH₃), 2.92 (s, 6H, 2CH₃), 4.06 (q, J = 7.0 Hz, 2H, CH₃-CH₂O), 5.25 (s, 1H, CH), 6.19 (s, 1H, NH), 6.63 (d, J = 8.5 Hz, 2CH, ArH), 7.16 (d, J = 8.5 Hz, 2CH, ArH), 8.27 (s, 1H, NH) ppm.

5-(Ethoxycarbonyl)-6-methyl-4-(2-methylphenyl)-3,4-dihydropyrimidin-(1H)-one (4q)

m.p.: 201-203°C; IR (KBr): 3237, 3104, 1702, 1642 cm⁻¹; Mass: m/z (%) 274 [M⁺], 259, 245, 229, 201, 183 (100), 155, 91; ¹H NMR (DMSO-d₆): δ = 0.97 (t, J = 5.9 Hz, 3H, CH₃-CH₂O), 2.28 (s, 3H, CH₃), 2.40 (s, 3H, CH₃), 3.86 (q, J = 4.0 Hz, 2H, CH₃-CH₂O), 5.39 (d, J = 2.1 Hz, 1H, CH), 7.09-7.16 (m, 4CH, ArH), 7.61 (s, 1H, NH), 9.14 (s, 1H, NH) ppm; ¹³C NMR (DMSO-d₆): δ = 13.9, 17.6, 18.6, 54.4, 59.0, 99.1, 126.5, 127.1, 130.0, 134.6, 143.2, 148.4, 151.5, 165.2 ppm.

5-(Ethoxycarbonyl)-6-methyl-4-(2-methoxyphenyl)-3,4-dihydropyrimidin-(1H)-one (4r)

m.p.: 258-260°C; IR (KBr): 3255, 3107, 1726, 1701 cm⁻¹; ¹H NMR (DMSO-d₆): δ = 1.10 (t, J = 7.5 Hz, 3H, CH₃-CH₂O), 2.42 (s, 3H, CH₃), 3.89 (s, 3H, CH₃), 4.05 (q, J = 7.5 Hz, 2H, CH₃-CH₂O), 5.67 (d, J = 2.5 Hz, 1H, CH), 5.89 (s, 1H, NH), 6.84-7.79 (m, 4CH, ArH), 8.46 (s, 1H, NH) ppm.

5-(Ethoxycarbonyl)-6-methyl-4-(4-methoxyphenyl)-3,4-dihydropyrimidin-(1H)-one (4s)

m.p.: 208°C; IR (KBr): 3243, 3110, 1705, 1648 cm⁻¹; Mass: m/z (%) 290 [M⁺], 261 (100), 245, 217, 183, 155, 77; ¹H NMR (DMSO-d₆): δ = 1.17 (t, J = 7.5 Hz, 3H, CH₃-CH₂O), 2.34 (s, 3H, CH₃), 3.79 (s, 3H, CH₃), 4.06 (q, J = 7.5 Hz, 2H, CH₃-CH₂O), 5.35 (d, J = 2.5 Hz, 1H, CH), 5.48 (s, 1H, NH), 6.82 (d, J = 7.5 Hz, 2CH, ArH), 7.25 (d, J = 7.5 Hz, 2CH, ArH), 7.49 (s, 1H, NH) ppm.

5-(Ethoxycarbonyl)-6-methyl-4-(2,3-dimethoxyphenyl)-3,4-dihydropyrimidin-(1H)-one (4t)

m.p.: 199-200°C; IR (KBr): 3232, 3104, 1705, 1645 cm⁻¹; ¹H NMR (DMSO-d₆): δ = 1.11 (t, J = 7.5 Hz, 3H, CH₃-CH₂O), 2.41 (s, 3H, CH₃), 3.87 (s, 3H, CH₃), 3.92 (s, 3H, CH₃), 4.04 (q, J = 7.5 Hz, 2H, CH₃-CH₂O), 5.52 (s, 1H, NH), 5.71 (d, J = 2.5 Hz, 1H, CH), 6.69-7.01 (m, 3CH, ArH), 7.53 (s, 1H, NH) ppm.

Table 1. SiO₂-Pr-SO₃H catalyzed synthesis of 3,4-dihydropyrimidinones/thiones **4** under solvent-free conditions

Entry	R	X	Product	Time (min)	^a Yield (%)	m.p (°C)	m.p. (Ref.)
1	C ₆ H ₅ -	O	4a	2	95	203-204	204-205[24]
2	2,3-Cl ₂ C ₆ H ₃ -	O	4b	2	100	236-238	244-246[25]
3	2-Thienyl-	O	4c	3	100	205-207	207-208[13]
4	4-OHC ₆ H ₄ -	O	4d	20	99	241-244	237-238[26]
5	4-ClC ₆ H ₄ -	O	4e	3	99	210	208-211[24]
6	CH ₃ -	O	4f	90	99	180-182	188-189[12]
7	2,6-Cl ₂ C ₆ H ₃ -	O	4g	1	99	230-232	226[14]
8	2-FC ₆ H ₄ -	O	4h	2	99	231-233	233-235[24]
9	2,4-Cl ₂ C ₆ H ₃ -	O	4i	7	98	235-237	238-240[27]
10	i-Pr	O	4j	2	98	198-200	194-195[27]
11	2-Furyl-	O	4k	210	95	205-208	202-204[14]
12	4-NO ₂ C ₆ H ₄ -	O	4l	2	92	209-211	209-212[24]
13	4-MeC ₆ H ₄ -	O	4m	5	85	211-213	214-215[15]
14	3-NO ₂ C ₆ H ₄ -	O	4n	2	80	228-230	226-228[12]
15	4-NMe ₂ C ₆ H ₄ -	O	4o	4	80	248-250	253-254[26]
16	3-MeC ₆ H ₄ -	O	4p	2	77	203-206	204-205[13]
17	2-MeC ₆ H ₄ -	O	4q	15	76	201-203	208-210[28]
18	2-OMeC ₆ H ₄ -	O	4r	4	70	258-260	262-265[24]
19	4-OMeC ₆ H ₄ -	O	4s	3	62	208	206-208[24]
20	2,3-OMe ₂ C ₆ H ₃ -	O	4t	8	61	199-200	New
21	3,4-OMe ₂ C ₆ H ₃ -	O	4u	2	42	188-190	192-194[29]
22	C ₆ H ₅ CH=CH-	O	4v	15	30	230-232	234-236[30]
23	4-ClC ₆ H ₄ -	S	4w	180	61	194	191-192[10]
24	C ₆ H ₅ -	S	4x	180	44	202-204	206-208[30]
25	4-OMeC ₆ H ₄ -	S	4y	180	40	151-153	153-156[10]
26	C ₆ H ₅ CH=CH-	S	4z	120	30	238-240	243-245[30]
27	3-NO ₂ C ₆ H ₄ -	S	4aa	180	20	203-205	206-207[26]
28	4-NO ₂ C ₆ H ₄ -	S	4bb	180	35	107-109	109-111[28]
29	i-Pr	S	4cc	20	30	188-190	191-192[31]

^a Isolated yield.*5-(Ethoxycarbonyl)-6-methyl-4-phenyl-3,4-dihydropyrimidin-(1H)-thione (4x)*

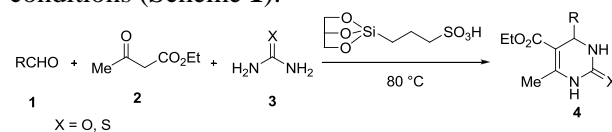
m.p.: 202-204°C; IR (KBr): 3172, 3106, 2981, 1670, 1618, 1196 cm⁻¹; Mass: m/z (%) 276 [M⁺], 247, 231, 199 (100), 171; ¹H NMR (DMSO-d₆): δ = 1.08 (t, *J* = 5.9 Hz, 3H, CH₃-CH₂O), 2.28 (s, 3H, CH₃), 4.01 (q, *J* = 5.9 Hz, 2H, CH₃-CH₂O), 5.16 (d, *J* = 3.0 Hz, 1H, CH), 7.20-7.36 (m, 5CH, ArH), 9.63 (s, 1H, NH), 10.31 (s, 1H, NH) ppm; ¹³C NMR: δ = 14.0, 17.1, 54.0, 59.6, 100.7, 126.4, 127.7, 128.5, 143.5, 145.0, 165.1, 174.2 ppm.

5-(Ethoxycarbonyl)-6-methyl-4-(4-methoxyphenyl)-3,4-dihydropyrimidin-(1H)-thione (4y)

m.p.: 151-153°C; IR (KBr): 3173, 3105, 1674, 1575 cm⁻¹; ¹H NMR (DMSO-d₆): δ = 1.17 (t, *J* = 7.0 Hz, 3H, CH₃-CH₂O), 2.34 (s, 3H, CH₃), 2.92 (s, 3H, CH₃), 4.07 (q, *J* = 7.0 Hz, 2H, CH₃-CH₂O), 5.29 (d, *J* = 3.0 Hz, 1H, CH), 7.08 (d, *J* = 8.0 Hz, 2CH, ArH), 7.17 (d, *J* = 8.0 Hz, 2CH, ArH), 8.84 (s, 1H, NH), 9.51 (s, 1H, NH) ppm.

RESULTS AND DISCUSSION

A model reaction of benzaldehyde **1a** ethyl acetoacetate **2**, and urea **3** was carried out in the presence of SiO₂-Pr-SO₃H as a highly efficient heterogeneous acid catalyst under solvent-free conditions (Scheme 1).

**Scheme 1**

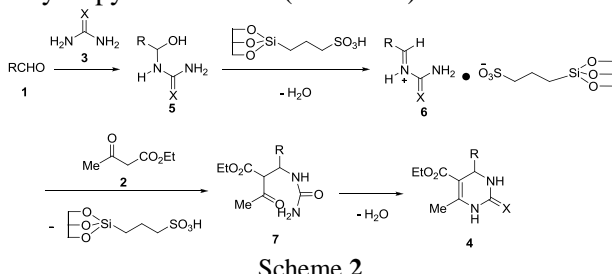
It was found that the reaction took place smoothly and the corresponding product **4a** was obtained in high yield (100%) when the mixture was stirred at 80°C for only 2 min. Encouraged by this result, various types of substituted aldehydes were examined under solvent-free conditions.

Aromatic aldehydes carrying either electron-donating or electron-withdrawing substituents reacted very well, giving moderate to excellent yields (Table 1). Even for aliphatic aldehydes, which normally show extremely poor yields in the Biginelli reaction, better yields of the

corresponding dihydropyrimidinones could be obtained.

After reaction completion (monitored by TLC), the mixture was cooled to room temperature and poured into ice-water and filtered. The crude product was dissolved in hot EtOAc, filtered for removing the unsolved material and then the filtrate was cooled to afford the pure product. The catalyst could be recycled by subsequent washing with dilute acid solution, water, and then acetone, and after drying could be reused without loss of reactivity.

The most probable mechanism of this reaction includes acid catalyzed *in situ* formation of an *N*-acyliminium ion intermediate **6** by the reaction of urea and aldehyde, which undergoes subsequent addition to ethyl acetoacetate followed by cyclization and dehydration to yield dihydropyrimidinone **4** (Scheme 2).



For preparation of the catalyst, functionalization of SiO₂ with -SO₃H group was performed by direct synthesis or post-grafting [32, 33]. SiO₂ was functionalized with (3-mercaptopropyl) trimethoxysilane (MPTS), then the thiol groups of the product were oxidized to sulfonic acid by hydrogen peroxide. The catalyst surface was analyzed by different methods such as thermogravimetric analysis (TGA), Brunauer–Emmett–Teller (BET), and CHN methods, which demonstrated that the organic groups (propyl sulfonic acid) were immobilized into the pores [34]. Pore volume and average pore diameter of SiO₂-Pr-SO₃H are smaller than those of SiO₂ due to the immobilization of organic groups (propyl sulfonic acid) into the pores.

CONCLUSIONS

In conclusion, we have developed a simple, efficient and mild protocol for the synthesis of dihydropyrimidinones in excellent yields. The use of SiO₂-Pr-SO₃H under solvent-free conditions has the advantages of being a reusable and environmentally benign catalyst. Excellent yields of the products, very short reaction times, and simplicity of the system make it an improved protocol in comparison with existing methods.

Acknowledgements: We gratefully acknowledge the financial support from the Research Council of Alzahra University and University of Tehran.

REFERENCES

1. P. Biginelli, *Gazz. Chim. Ital.*, **23**, 360 (1893).
2. O.M. Singh, S.J. Singh, M.B. Devi, L.N. Devi, N.I. Singh, S.G. Lee, *Bioorg. Med. Chem. Lett.*, **18**, 6462 (2008).
3. B. Sedaghati, A. Fassihi, S. Arbabi, M. Ranjbar, H. Memarian, L. Saghale, A. Omid, A. Sardari, M. Jalali, D. Abedi, *Med. Chem. Res.*, **21**, 3973 (2012).
4. B. Schnell, U.T. Strauss, P. Verdino, K. Faber, C.O. Kappe, *Tetrahedron: Asymmetry*, **11**, 1449 (2000).
5. A. Mai, M. Artico, G. Sbardella, S. Massa, A.G. Loi, E. Tramontano, P. Scano, P. La Colla, *J. Med. Chem.*, **38**, 3258 (1995).
6. B.R. Prashantha Kumar, G. Sankar, R.B. Nasir Baig, S. Chandrashekar, *Eur. J. Med. Chem.*, **44**, 4192 (2009).
7. C.O. Kappe, *Eur. J. Med. Chem.*, **35**, 1043 (2000).
8. A.D. Patil, N.V. Kumar, W.C. Kokke, M.F. Bean, A.J. Freyer, C. De Brosse, S. Mai, A. Truneh, D.J. Faulkner, B. Carte, A.L. Breen, R.P. Hertzberg, R.K. Johnson, J.W. Westley, B.C.M. Potts, *J. Org. Chem.*, **60**, 1182 (1995).
9. S. Sakemi, H.H. Sun, C.W. Jefford, G. Bernardinelli, *Tetrahedron Lett.*, **30**, 2517 (1989).
10. F. Shirini, K. Marjani, H.T. Nahzomi, *Arkivoc*, **2007**, 51 (2007).
11. P.G. Mandhane, R.S. Joshi, D.R. Nagargoje, C.H. Gill, *Tetrahedron Lett.*, **51**, 3138 (2010).
12. Q. Wang, W. Pei, *J. Iran. Chem. Soc.*, **7**, 318 (2010).
13. A. Debache, B. Boumoud, M. Amimour, A. Belfaitah, S. Rhouati, B. Carboni, *Tetrahedron Lett.*, **47**, 5697 (2006).
14. J.K. Joseph, S.L. Jain, B. Sain, *J. Mol. Catal. A*, **247**, 99 (2006).
15. S.L. Jain, J.K. Joseph, S. Singhal, B. Sain, *J. Mol. Catal. A*, **268**, 134 (2007).
16. M.A. Bigdeli, S. Jafari, G.H. Mahdavinia, H. Hazarkhani, *Catal. Commun.*, **8**, 1641 (2007).
17. W. Chen, S. Qin, J. Jin, *Catal. Commun.*, **8**, 123 (2007).
18. H.N. Karade, M. Sathe, M.P. Kaushik, *Molecules*, **12**, 1341 (2007).
19. R. Gupta, S. Paul, *J. Mol. Catal. A*, **266**, 50 (2007).
20. G. Mohammadi Ziarani, A. Badiei, M. Azizi, N. Lashgari, *J. Chin. Chem. Soc.*, **60**, 499 (2013).
21. G. Mohammadi Ziarani, A. Badiei, Z. Dashtianeh, P. Gholamzadeh, N. Mohtasham, *Res. Chem. Intermed.*, **39**, 3157 (2013).
22. G. Mohammadi Ziarani, A. Badiei, S. Mousavi, N. Lashgari, A. Shahbazi, *Chin. J. Catal.*, **33**, 1832 (2012).
23. G. Mohammadi Ziarani, N. Lashgari, A. Badiei, *Scientia Iranica*, **20**, 580 (2013).
24. M. Li, W.S. Guo, L.R. Wen, Y.F. Li, H.Z. Yang, *J. Mol. Catal. A*, **258**, 133 (2006).

25. F.S. Falsone, C.O. Kappe, *Arkivoc*, **2001**, 122 (2001).
26. W. Su, J. Li, Z. Zheng, Y. Shen, *Tetrahedron Lett.*, **46**, 6037 (2005).
27. Y. Ma, C. Qian, L. Wang, M. Yang, *J. Org. Chem.*, **65**, 3864 (2000).
28. N.Y. Fu, Y.F. Yuan, Z. Cao, S.W. Wang, J.T. Wang, C. Peppe, *Tetrahedron*, **58**, 4801 (2002).
29. K. Singh, J. Singh, P.K. Deb, H. Singh, *Tetrahedron*, **55**, 12873 (1999).
30. C. Liu, J. Wang, Y. Li, *J. Mol. Catal. A*, **258**, 367 (2006).
31. L. Wang, C. Qian, H. Tian, Y. Ma, *Synth. Commun.*, **33**, 1459 (2003).
32. A.P. Wight, M.E. Davis, *Chem. Rev.*, **102**, 3589 (2002).
33. M.H. Lim, C.F. Blanford, A. Stein, *Chem. Mater.*, **10**, 467 (1998).
34. G. Mohammadi Ziarani, A. Badiei, A. Abbasi, Z. Farahani, *Chin. J. Chem.*, **27**, 1537 (2009).

ЕФЕКТИВЕН КАТАЛИЗАТОР (SiO₂-Pr-SO₃H) ЗА ЕДНОСТАДИЙНА ЗЕЛЕНА СИНТЕЗА НА 3,4-ДИХИДРОПИРИМИДИНОНИ/ТИОНИ

Г.М. Зиарани^{1,*}, А. Бадиеи², Н. Лашгари², Т. Пурджафар¹, З. Фарахани¹

¹ Департамент по химия, Университет Алзахра, Техеран, Иран

² Училище по химия, Колеж за наука, Университет в Техеран, Техеран, Иран

Постъпила на 28 юли, 2013 г.; приета на 27 ноември, 2012 г.

(Резюме)

SiO₂-Pr-SO₃H ефективно катализира свързването на етил-ацетоацетат, алдехиди и карбамид (тиокарбамид) в отсъствие на разтворител за получаването на съответните дихидропиримидинони. В сравнение с класическите реакционни условия по Viginelli този протокол има предимствата на много кратко време за реакция (2 минути), добри до отлични добиви, рециклируем катализатор и проста експериментална процедура.

Catalyst-free green synthesis of urea and thiourea derivatives of tetramethylguanidine (TMG) and evaluation of biological activity

T. B. Shaik¹, S. Chennamsetty¹, S. R. Devineni¹, N. R. Shaik¹, N. D. Mundla²,
J. P. Rajkumari³, N. R. Chamarthi^{*1}

¹Department of Chemistry, Sri Venkateswara University, Tirupati, A.P., INDIA

²Department of Botany, Sri Venkateswara University, Tirupati, A.P., INDIA

³Department of Virology, Sri Venkateswara University, Tirupati, A.P., INDIA

Received September 11, 2013; Revised April 18, 2014

An expeditious green approach was developed for the synthesis of urea and thiourea derivatives of 1,1,3,3-tetramethylguanidine in high yields under catalyst-free and solvent-free conditions. The procedure has many advantages, e.g., avoiding of harmful solvents, ease of work-up, short reaction time and high purity of the products with high yields. Various reaction parameters such as catalyst effect, solvent effect and temperature conditions were optimized. Antimicrobial activity of the title compounds was evaluated and the bio-screening data disclosed that compounds **3a**, **3e** and **3g**, **3j** exhibited promising antibacterial and antifungal activities, respectively.

Keywords: Green synthesis; Solvent and catalyst-free conditions; 1,1,3,3-Tetramethyl guanidine; Urea and thiourea derivatives; Antimicrobial activity.

INTRODUCTION

It is well known that guanidine derivatives are a promising class of biologically active molecules and exhibit a great number of biological activities such as antimicrobial [1], antifungal [2], anti-inflammatory, antimalarial [3,4], antitumor [5], analgesic [6]. They have also been used as extraction agents for periodate ions [7,8]. Further, the reaction of isocyanates and isothiocyanates with various amines affords urea and thiourea molecules. The literature survey revealed that these derivatives covered a wide range of biological activities like antibacterial, antifungal, antiviral, herbicidal, inhibiting NO production, anti-HIV, anticancer, HDL-elevating activities [9] and also could be used for elimination or detoxification of super antigens from body fluids and for the treatment of haemoglobinopathies in the cases of sickle-cell anemia [10]. The investigations on urea and thiourea derivatives revealed that the high molecular recognition of urea and thiourea derivatives is due to their strong hydrogen bonding property.

Over the last few decades, the intention of the organic chemists is to develop greener and more economically competitive processes [11] for the efficient synthesis of organic molecules, intermediates or biologically active compounds

with potential application in the fields of pharmaceutical and agrochemical industries. In this connection solvent-free reactions have attained great interest not only from ecological point of view but for the afforded synthetic advantages in terms of reaction time, yield, selectivity and simple synthetic procedure [12,13]. The foremost advantages of solvent-free conditions are: reduced use of organic solvents, minimized formation of wastes and reactions occurring under mild conditions [14].

By considering the above facts and the prominence of urea and thiourea derivatives in regard of biology, we have shown significant interest to develop a new green methodology to prepare new urea and thiourea derivatives and evaluate their antimicrobial activity with good hope that the title compounds will exhibit enhanced biological activity.

EXPERIMENTAL PART

Chemicals and apparatus

All required chemicals were purchased from Sigma-Aldrich and Merck, and used without further purification. Melting points were determined in open capillaries in a Guna melting point apparatus and were uncorrected. Infrared (IR) spectra were obtained on a Nicolet 380 Fourier transform infrared (FT-IR) spectrophotometer using KBr optics. ¹H NMR and ¹³C NMR were recorded with a Bruker instrument-400 MHz (400.13 MHz

* To whom all correspondence should be sent:
E-mail: rajuchamarthi10@gmail.com

for ^1H NMR, 100.62 MHz for ^{13}C NMR) and tetramethylsilane was used as internal standard in CDCl_3 . Chemical shifts (δ) are indicated in ppm and coupling (J) in Hz. Mass spectra were recorded on an ESI-MS mass spectrometer. Elemental analyses were carried out in FLASH EA 1112.

General Procedure

Tetramethylguanidine (**1**) (1.5 mmol, 0.18 mL) and 1-isothiocyanato-4-nitrobenzene (**2f**) (1 mmol, 180 mg) were taken into a 50 mL flat-bottomed flask without solvent and catalyst. The reaction mixture was stirred for 90 min. at 60 °C and the progress of the reaction was monitored by TLC using ethylacetate:*n*-hexane (2:3). After completion of the reaction, cold water (15 mL) was added to the reaction mixture and was stirred for 10 min. Then, the reaction mixture was filtered off to obtain the product, *N*-di(dimethylamino)methylene-*N'*-(4-nitrophenyl)thiourea (**3f**). The latter was washed with cold water, air-dried and recrystallized from methanol to get the pure compound. The same procedure was adopted for the synthesis of the other title compounds (Scheme 1).

Spectral Data

***N*-di(dimethylamino)methylene-*N'*-(4-nitrophenyl)urea (3a):** Yellow solid, Yield: 85.0 %, m.p. 308-311°C. IR (KBr): ν = 3324 (NH), 1646 (-C=O), 1596 (-N=C), 1390, 1297 (OC-N-), 1044 (C-N) cm^{-1} . ^1H NMR (400 MHz, CDCl_3): δ = 8.29 (s, 1H, NH), 8.15 (d, 2H, $J_{\text{H-H}}$ = 8.0 Hz, Ar-H), 7.79 (d, 2H, $J_{\text{H-H}}$ = 8.0 Hz, Ar-H), 2.95 (s, 12H, -CH₃). ^{13}C NMR (100 MHz, CDCl_3): δ = 168.2, 164.5, 145.5, 143.1, 125.6, 118.9, 40.5. ESI-MS (m/z): 280 (M+H)⁺. Anal. Calcd. for C₁₂H₁₇N₅O₃: C, 51.60; H, 6.14; N, 25.08%. Found: C, 51.54; H, 6.20; N, 24.90%.

***N*-di(dimethylamino)methylene-*N'*-(4-fluorophenyl)urea (3b):** Colourless solid, Yield: 82.5 %, m.p. 270-274°C. IR (KBr): ν = 3285 (NH), 1606 (-C=O), 1556 (-N=C), 1392, 1293 (OC-N-), 1055 (C-N) cm^{-1} . ^1H NMR (400 MHz, CDCl_3): δ = 7.91 (s, 1H, NH), 7.19 (d, 2H, $J_{\text{H-H}}$ = 7.9 Hz, Ar-H), 6.93 (d, 2H, $J_{\text{H-H}}$ = 7.9 Hz, Ar-H), 3.03 (s, 12H, -CH₃). ^{13}C NMR (100 MHz, CDCl_3): δ = 169.3, 165.2, 161.0, 137.6, 128.9, 115.6, 41.7. ESI-MS (m/z): 253 (M+H)⁺.

***N*-di(dimethylamino)methylene-*N'*-(2-fluoro-6-nitrophenyl)urea (3c):** Reddish brown solid, Yield: 76.0 %, m.p. 298-300°C. IR (KBr): ν = 3335 (NH), 1637 (-C=O), 1590 (-N=C), 1390, 1305 (O=C-N-), 1039 (C-N) cm^{-1} . ^1H NMR (400 MHz, CDCl_3): δ = 8.18 (s, 1H, NH), 7.80-7.48 (m, 3H, Ar-H), 2.91 (s, 12H, -CH₃). ^{13}C NMR (100 MHz,

CDCl_3): δ = 165.8, 164.5, 160.5, 146.0, 129.8, 123.4, 121.9, 120.9, 39.7. ESI-MS (m/z): 298 (M+H)⁺.

***N*-di(dimethylamino)methylene-*N'*-(3,4-dichlorophenyl)urea (3d):** White solid, Yield: 85.5 %, m.p. 262-264°C. IR (KBr): ν = 3280 (NH), 1631 (-C=O), 1577 (-N=C), 1392, 1298 (OC-N-), 1053 (C-N) cm^{-1} . ^1H NMR (400 MHz, CDCl_3): δ = 8.09 (m, 1H, NH), 6.98 (s, 1H, Ar-H), 6.84-6.77 (m, 2H, Ar-H), 2.91 (s, 12H, -CH₃). ^{13}C NMR (100 MHz, CDCl_3): δ = 165.7, 159.5, 140.4, 135.5, 133.2, 130.6, 125.3, 120.8, 39.7. ESI-MS (m/z): 303 (M+H)⁺. Anal. Calcd. for C₁₂H₁₆Cl₂N₄O: C, 47.54; H, 5.32; N, 18.48%. Found: C, 47.69; H, 5.24; N, 18.55%.

***N*-di(dimethylamino)methylene-*N'*-(2,4-difluorophenyl)urea (3e):** Pale yellow solid, Yield: 88.0 %, m.p. 283-285°C. IR (KBr): ν = 3196 (NH), 1627 (-C=O), 1570 (-N=C), 1393, 1303 (OC-N-), 1044 (C-N) cm^{-1} . ^1H NMR (400 MHz, CDCl_3): δ = 8.12 (s, 1H, NH), 7.34-7.02 (m, 3H, Ar-H), 2.97 (s, 12H, -CH₃). ^{13}C NMR (100 MHz, CDCl_3): δ = 168.0, 165.7, 163.1, 159.3, 125.3, 115.8, 110.8, 103.3, 39.7. ESI-MS (m/z): 271 (M+H)⁺. Anal. Calcd. for C₁₂H₁₆F₂N₄O: C, 53.33; H, 5.97; N, 20.73%. Found: C, 53.21; H, 6.06; N, 20.61%.

***N*-di(dimethylamino)methylene-*N'*-(4-nitrophenyl)thiourea (3f):** Yellow solid, Yield: 95.0 %, m.p. 201-203°C. IR (KBr): ν = 3180 (NH), 1590 (-N=C), 1388, 1322 (SC-N), 1133 (C=S), 1030 (C-N) cm^{-1} . ^1H NMR (400 MHz, CDCl_3): δ = 7.94 (s, 1H, NH), 7.62-7.33 (m, 4H, Ar-H), 3.01 (s, 12H, -CH₃). ^{13}C NMR (100 MHz, CDCl_3): δ = 179.8, 165.2, 146.1, 145.4, 127.0, 126.4, 40.2. ESI-MS (m/z): 296 (M+H)⁺. Anal. Calcd. for C₁₂H₁₇N₅O₂S: C, 48.80; H, 5.80; N, 23.71%. Found: C, 48.72; H, 5.89; N, 23.64%.

***N*-di(dimethylamino)methylene-*N'*-(4-fluorophenyl)thiourea (3g):** White solid, Yield: 86.5 %, m.p. 178-180°C. IR (KBr): ν = 3183 (NH), 1570 (-N=C), 1390, 1294 (SC-N), 1148 (C=S), 1036 (C-N) cm^{-1} . ^1H NMR (400 MHz, CDCl_3): δ = 7.91 (s, 1H, NH), 7.44-7.40 (m, 2H, Ar-H), 6.98-6.93 (m, 2H, Ar-H), 3.01 (s, 12H, -CH₃). ^{13}C NMR (100 MHz, CDCl_3): δ = 180.5, 165.2, 164.3, 134.9, 133.2, 118.0, 39.9. ESI-MS (m/z): 269 (M+H)⁺.

***N*-di(dimethylamino)methylene-*N'*-(4-chlorophenyl)thiourea (3h):** White solid, Yield: 91.0 %, m.p. 180-184 °C. IR (KBr): ν = 3186 (NH), 1566 (-N=C), 1390, 1297 (SC-N), 1136 (C=S), 1034 (C-N) cm^{-1} . ^1H NMR (400 MHz, CDCl_3): δ = 7.98 (s, 1H, NH), 7.44-7.42 (d, 2H, $J_{\text{H-H}}$ = 8.8, Ar-H), 7.21-7.19 (d, 2H, $J_{\text{H-H}}$ = 8.8, Ar-H), 3.02 (s, 12H, -CH₃). ^{13}C NMR (100 MHz, CDCl_3): δ = 180.1, 165.5, 137.4, 135.9, 133.3, 131.3, 40.6. ESI-

MS (m/z): 285 (M+H)⁺. Anal. Calcd. for C₁₂H₁₇ClN₅S: C, 50.61; H, 6.02; N, 19.67%. Found: C, 50.69; H, 5.92; N, 19.59%.

N-di(dimethylamino)methylene-N'-phenylthiourea (3i): White solid, Yield: 92.0 %, m.p. 204-207°C. IR (KBr): ν= 3189 (NH), 1560 (-N=C), 1391, 1305 (SC-N), 1143 (C=S), 1033 (C-N) cm⁻¹. ¹H NMR (400 MHz, CDCl₃): δ= 7.91 (s, 1H, NH), 7.48-7.46 (d, 2H, J_{H-H} = 8.0, Ar-H), 7.28-7.24 (t, 2H, J_{H-H} = 8.0, Ar-H), 7.02-6.99 (t, 1H, J_{H-H} = 8.0, Ar-H), 3.02 (s, 12H, -CH₃). ¹³C NMR (100 MHz, CDCl₃): δ= 179.8, 160.2, 139.8, 131.2, 129.0, 127.5, 40.6. ESI-MS (m/z): 251 (M+H)⁺.

N-di(dimethylamino)methylene-N'-[3-(trifluoromethyl)phenyl]thiourea (3j): White solid, Yield: 93.5 %, m.p. 185-188°C. IR (KBr): ν= 3184 (NH), 1547 (-N=C), 1394, 1326 (SC-N), 1108 (C=S), 1038 (C-N) cm⁻¹. ¹H NMR (400 MHz, CDCl₃): δ= 8.03 (s, 1H, Ar-H), 7.96 (s, 1H, NH), 7.53-7.51 (d, 1H, J_{H-H} = 8.0, Ar-H), 7.37-7.34 (t, 1H, J_{H-H} = 8.0, Ar-H), 7.24-7.22 (d, 1H, J_{H-H} = 8.0, Ar-H), 3.04 (s, 12H, -CH₃). ¹³C NMR (100 MHz, CDCl₃): δ= 178.7, 168.9, 156.0, 140.7, 129.0, 122.8, 118.8, 116.0, 110.8, 40.6. ESI-MS (m/z): 319 (M+H)⁺. Anal. Calcd. for C₁₃H₁₇F₃N₄S: C, 49.04; H, 5.38; N, 17.60%. Found: C, 49.12; H, 5.30; N, 17.67%.

Biological assays

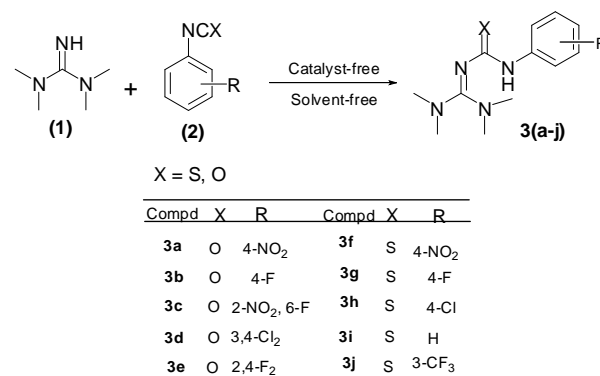
Antibacterial activity: All synthesized compounds were screened for their antibacterial activity against Gram positive bacteria, *Bacillus subtilis* (MTCC-441), *Staphylococcus aureus* (MTCC-737) and Gram negative bacteria, *Escherichia coli* (MTCC-443), *Pseudomonas aeruginosa* (MTCC-741) using a disk diffusion method [15,16]. 2 mg of the title compounds and the standard drug were dissolved in 10 mL of dimethylsulphoxide (DMSO) and further diluted to a concentration of 100 µg/mL of the tested samples. The sterile nutrient agar medium 15 mL was taken in a set of petri plates and the bacterial culture was uniformly spread with sterile inocula onto the surface of the medium. The sterile disks (6 mm diameter) previously soaked in 100 µg/mL test solutions were placed on petri plates and incubated for 24 h at 37±1°C. The zone of inhibition around the disc was measured. Ampicillin was used as a positive control and DMSO was used as a negative control. For each treatment, triplicate experiments were carried out and the average zone of inhibition was calculated in mm (Table 3).

Antifungal activity: Antifungal activity of the synthesized compounds was screened against *Aspergillus niger*, *Aspergillus flavus*, *Candida*

albicans and *Mucor indicus* by the poisoned plate technique [17]. 2 mg of the synthesized and of the standard compounds were dissolved in 10 mL of dimethylsulphoxide (DMSO) and their concentration was adjusted to 200 µg/mL by dilution before mixing with potato dextrose agar (PDA, 90 mL). The fungi were incubated in PDA at 25±1 °C for 5 days for new mycelium, 45 mm of mycelia disc was cut from the culture medium with a sterilized cork borer, inoculated in the center of the PDA plate and incubated for another 5 days at 25±1°C. Nystatin was used as a positive control while a disk poured in DMSO was used as a negative control. Triplicate experiments were carried out for each treatment and results were expressed in mm (Table 4). The inhibiting activity of the title compounds was calculated by the formula I=C-T/C, where I indicates the rate of inhibition, C indicates the diameter of fungi growth in the control and T indicates the diameter of fungi growth in treatment.

RESULTS AND DISCUSSIONS

As a result of our continuing research on the development of new methodologies for the synthesis of useful scaffolds [18], herein, we developed a green approach for the synthesis of urea and thiourea derivatives of tetramethylguanidine, as depicted in Scheme 1.



Scheme 1. Solvent- and catalyst-free synthesis of urea and thiourea derivatives of tetramethylguanidine.

Initially, the experimental conditions were optimized by taking tetramethylguanidine (1) and 1-isothiocyanato-4-nitrobenzene (2f) as models for the production of the title compound 3f. The model reaction was primarily carried out in the presence of different base catalysts, Et₃N, dimethylpiperazine and catalyst-free conditions in THF solvent (Table 1 entries 1-3). No significant yield difference was observed both in the presence of base catalyst and under catalyst-free conditions in THF solvent. Hence, the catalyst-free condition

was preferred. The model reaction was performed in different organic solvents like THF, chloroform, dichloromethane, acetonitrile as well as under solvent-free conditions (Table 1, entries 4-7) without catalyst. Interestingly, it was found that simple mixing of 4-nitrophenylisothiocyanate and 1,1,3,3-tetramethyl guanidine without solvent afforded high-purity *N*-di(dimethylamino) methylene-*N'*-(4-nitrophenyl) thiourea (**3f**) in high yield with a simple work-up procedure (filtration and recrystallization) as compared with the reactions in presence of solvents. Later, the optimized solvent-free conditions were tested at different temperatures 40°C, 50°C and 60°C (Table 1, entries 7-10) and revealed that the reaction was effective at 60 °C.

After optimization of the reaction conditions, the generality of the reaction conditions was checked by altering the substituted phenyl isocyanates and isothiocyanates to get the title compounds **3(a-j)** (Table 2). This method gave high yields of desired products in a short time with high purity using simple work-up instead of using tedious time taking column chromatography. The results revealed that isocyanates or isothiocyanates with electron withdrawing groups afforded good yields of the products as compared to those with electron donating groups. Isothiocyanates were more efficient than isocyanates to afford high yields of the products.

The structures of the title compounds **3(a-j)** were characterized using IR, ¹H NMR, ¹³C NMR, mass spectral studies and elemental analysis. IR spectra gave absorption bands in the regions of 3180-3335 cm⁻¹, 1606-1646 cm⁻¹, 1596-1547 cm⁻¹ and 1108-1148 cm⁻¹ stretching which confirmed the presence of -NH, -C=O, -C=N and -C=S functionalities in the title compounds. In the ¹H

NMR spectra, a singlet/multiplet at 8.29-7.91 ppm was assigned to NH proton in urea and thiourea derivatives and a singlet signal in the region of 2.91-3.04 ppm was ascribed to methyl groups attached to nitrogen atoms in the synthesized compounds. All phenyl protons showed signals as multiplets/triplets/doublets/singlets based on structures in the region of 6.77-7.80 ppm. The chemical shifts of carbon in the ¹³C NMR spectra, the molecular ions in the mass spectra and the elemental analytical data gave further evidence for structural elucidation of the title compounds **3(a-j)**.

BIOLOGY

The antibacterial and antifungal activities of the newly synthesized compounds **3(a-j)** were screened using disc diffusion method and poisoned plate technique, respectively. Primarily, both activities were tested at 100 µg/mL concentration of the test samples. The experiments revealed that most of the compounds exhibited potent antibacterial activity at 100 µg/mL concentration and only a few compounds exhibited moderate antifungal activity. Hence, antifungal activity of the test samples was screened at 200 µg/mL concentration. The biological data revealed that thiourea derivatives show better activity than urea derivatives against fungi whereas urea compounds showed promising activity towards bacteria. Among the screened compounds, the thiourea based analogues **3g** and **3j** exhibited good activity towards fungi which might be due to the presence of the highly lipophilic fluoro and trifluoromethyl groups, respectively (Table 3). The compounds **3a** and **3e** showed good antibacterial activity which could be related to the presence of nitro and difluoro groups on the benzene ring (Table 4).

Table-1 Optimization of the reaction conditions for the synthesis of urea and thiourea derivatives **3(a-j)**^a.

Entry	Solvent	Catalyst	Time (h)	Yield (%)
1	THF	Et ₃ N (1 equiv)	3	86.5
2	THF	DMP (1 equiv)	2.5	88.3
3	THF	No catalyst	4	86.1
4	CHCl ₃	No catalyst	6	73.2
5	DCM	No catalyst	6	78.6
6	CAN	No catalyst	7	60.9
7	Neat ^b	No catalyst	1.5	95.7
8	Neat ^c	No catalyst	4	89.3
9	Neat ^d	No catalyst	5	83.6
10	Neat ^e	No catalyst	7	79.4

^aTetramethylguanidine (1) and 1-isothiocyanato-4-nitrobenzene (2f) were selected as substances to carry out the model reaction; ^bThe model reaction was monitored by keeping the temperature at 60°C; ^cThe model reaction was monitored by keeping the temperature at 50°C; ^dThe model reaction was monitored by preserving the temperature at 40°C; ^eThe model reaction was monitored by keeping the ambient temperature conditions.

Table 2 Physical data of the newly synthesized urea and thiourea derivatives **3(a-j)**.

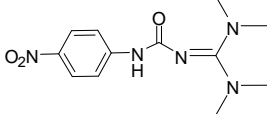
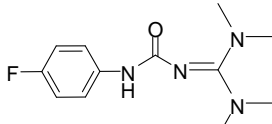
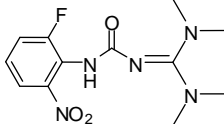
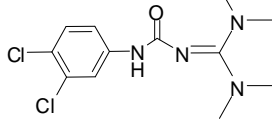
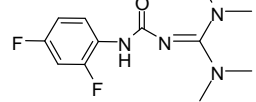
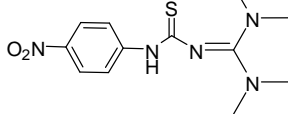
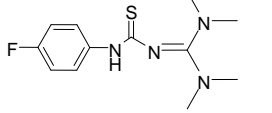
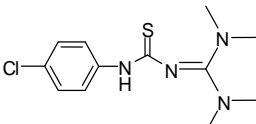
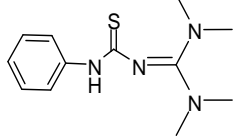
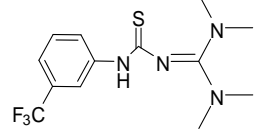
Compd.	Product	Time (h)	Yield (%)	Melting point (°C)
3a		4.0	85.0	308-310
3b		3.5	82.5	270-272
3c		6.0	76.0	298-300
3d		5.5	85.5	262-264
3e		4.5	88.0	283-285
3f		1.5	95.0	201-203
3g		1.5	86.5	178-180
3h		2.5	91.0	180-182
3i		2.0	92.0	204-206
3j		1.5	93.5	185-188

Table 3 Antibacterial Activity of the synthesized compounds **3(a-j)**

Compd.	Zone of inhibition (mm) at 100 µg/ mL			
	<i>Bacillus subtilis</i> (MTCC-441)	<i>Staphylococcus aureus</i> (MTCC-737)	<i>Escherichia coli</i> (MTCC-443)	<i>Pseudomonas aeruginosa</i> (MTCC-741)
3a	15.0 ± 0.56	12.2 ± 0.42	13.2 ± 0.45	11.4 ± 0.27
3b	10.2 ± 0.45	8.2 ± 0.33	7.5 ± 0.28	9.6 ± 0.35
3c	8.4 ± 0.21	7.6 ± 0.27	8.4 ± 0.26	8.6 ± 0.35
3d	8.6 ± 0.32	8.0 ± 0.35	8.2 ± 0.41	7.2 ± 0.24
3e	12.6 ± 0.49	11.6 ± 0.29	11.2 ± 0.33	10.8 ± 0.41
3f	N.A	N.A	N.A	N.A
3g	8.2 ± 0.12	9.1 ± 0.19	8.6 ± 0.16	8.4 ± 0.22
3h	11.5 ± 0.66	10.6 ± 0.36	10.2 ± 0.42	10.4 ± 0.25
3i	N.A	N.A	N.A	N.A
3j	N.A	N.A	N.A	N.A
Ampicillin	21	19	20	18
DMSO	N.A	N.A	N.A	N.A

(N.A: No activity)

Table 4 Antifungal activity of the synthesized compounds **3(a-j)**

Compd.	Zone of inhibition (mm) at 200 µg/ mL			
	<i>Aspergillus niger</i>	<i>Aspergillus flavus</i>	<i>Candida albicans</i>	<i>Mucorindicus</i>
3a	8.8 ± 0.25	14.4 ± 0.33	6.6 ± 0.45	8.8 ± 0.51
3b	4.4 ± 0.65	4.4 ± 0.52	4.4 ± 0.44	8.1 ± 0.47
3c	16.6 ± 0.42	14.4 ± 0.38	N.A	2.2 ± 0.52
3d	13.0 ± 0.78	12.0 ± 0.59	8.8 ± 0.47	8.8 ± 0.39
3e	11.1 ± 0.22	17.0 ± 0.39	15.6 ± 0.43	11.1 ± 0.47
3f	14.6 ± 0.56	17.7 ± 0.47	16.6 ± 0.40	6.6 ± 0.29
3g	14.4 ± 0.80	15.5 ± 0.67	13.3 ± 0.58	12.4 ± 0.61
3h	10.3 ± 0.37	4.4 ± 0.30	6.6 ± 0.25	N.A
3i	8.8 ± 0.22	6.6 ± 0.29	6.6 ± 0.34	N.A
3j	15.5 ± 0.71	15.5 ± 0.41	16.6 ± 0.49	13.3 ± 0.41
Nystatin	20	23	21	18
DMSO	N.A	N.A	N.A	N.A

(N.A: No activity)

CONCLUSION

In conclusion, we have developed a new green methodology for the synthesis of urea and thiourea derivatives in high yields under solvent-free and catalyst-free conditions. The reaction conditions like catalyst, solvent and temperature effects were optimized. The urea and thiourea derivatives of tetramethylguanidine were obtained in high yields with high purity by a simple work-up procedure like filtration and recrystallization without tedious and time taking techniques like column chromatography. The antimicrobial activity screening revealed that the urea derivatives (**3a**, **3e**) showed promising activity against bacteria while the thiourea derivatives (**3g**, **3j**) exhibited potent activity against fungi.

Acknowledgment: The author, SK. Thaslim Basha expresses thanks to UGC for financial support through UGC-JRF.

REFERENCES

1. S. M. Aldhaheeri, *Talanta*. **46**, 1613(1998).
2. C. Li, M. R. Lewis, A. B. Gilbert, M. D. Noel, D. H. Scoville, G. W. Albrann, P. B. Savage, *Antimicrob. Agents Ch.* **43**, 1347 (1999).
3. W. M. Golebiewski, M. Cholewinski, *Polish Journal of Applied Chemistry*, **47**, 137 (2003).
4. G. H. Jana, S. Jain, S. K. Arora, N. Sinha, *Bioorg. Med. Chem.Lett.* **15**, 3592 (2005).
5. M. Calas, M. Ouattara, G. Piquet, Z. Ziora, Y. Bordat, M. L. Ancelin, R. Escalé, H. Viral, *J. Med.Chem.* **50**, 6307 (2007).
6. Z. Brzozowski, F. Saczewski, J. Slawinski, *Eur. J. Med. Chem.* **42**, 1218 (2007).
7. R. N. Gacche, D. S. Gond, N. A. Dhole, B. S. Dawane, *J. Enzyme Inhib. Med. Chem.* **21**, 152 (2006).
8. E. Bramm, L. Binderup, E. Arrigoni-Martelli, *Agents Actions* **11**,402 (1981).
9. L. D. Santos, L. A. Lima, V. Cechinel-Filho, R. Correa, F. D. C. Buzzi, R. J. Nunes, *Bioorg. Med. Chem.* **16**, 8526 (2008).

10. S. A. Khan, N. Singh, K. Saleem, *Euro. J. Med. Chem.* **43**, 2272 (2008).
11. A. Corma, A. Garcia, *Chem. Rev.* **103**, 4307 (2003).
12. K. Tanaka, F. Toda, *Chem. Rev.* **100**, 1025 (2000).
13. R. S. Varma, *Green Chem.* **1**, 43 (1999).
14. A. Zare, A. Hasaninejad, M. Shekouhy, A. R. Moosayi, *Org. Prep. Proced. Int.* **40**, 457 (2008).
15. R. Cruickshank, J. P. Duguid, B. P. Marion, R. H. A. Swain *Medicinal Microbiology*, 12thed.; Churchill Livingstone: London, **2**, 196 (1975).
16. A. H. Collins, *Microbiology Methods*, 2nd ed.; Butterworth: London, 1976.
17. S. Q. Song, L. G. Zhou, D. Li, D. Tang, J. Q. Li, W. B. Jiang, *Nat. Prod. Res. Dev.* **16**, 157 (2004).
18. (a) D. SubbaRao, D. Srinivasulu, D. Rajasekhar, C. NagaRaju, *Chin. Chem. Lett.* **24**, 759 (2013); (b) D. SubbaRao, SK. ThaslimBasha, C. NagaRaju, *Der Pharmacia Lettre*, **5(3)**, 341 (2013).

ЗЕЛЕНИ, БЕЗКАТАЛИТИЧНИ ТЕХНОЛОГИИ ЗА СИНТЕЗ НА ПРОИЗВОДНИ НА КАРБАМИДА И ТИОКАРБАМИДА С ТЕТРАМЕТИЛГВАНИДИН (TMG) И ОЦЕНЯВАНЕ НА БИОЛОГИЧНАТА ИМ АКТИВНОСТ

Т.Б. Шаик¹, С. Ченнамсети¹, С.Р. Девинени¹, Н.Р. Шаик¹, Н.Д. Мундла²,
Дж.П. Раджкумари³, Н.Р. Чамартхи^{*1}

¹Департамент по химия, Университет Сри Венкатешвара, Тирупати, А.П., Индия

²Департамент по ботаника, Университет Сри Венкатешвара, Тирупати, А.П., Индия

³Департамент по вирусология, Университет Сри Венкатешвара, Тирупати, А.П., Индия

Постъпила на 11 септември, 2013 г.; Коригирана 18 април, 2014 г.

(Резюме)

Разработен е бърз зелен метод за синтезата на производни на карбамида и тиокарбамида с 1,1,3,3-тетраметилгванидин с високи добиви в отсъствие на катализатор и разтворител. Процесът има много предимства, напр. избягване на вредни разтворители, лесни и кратки операции, висока чистота с висок добив. Оптимизирани са работните условия по различни параметри. Оценена е антимикробната активност на получените съединения и е установено, че съединенията **3a**, **3e** и **3g**, **3j** проявяват обещаващи анти-бактериални и фунгицидни свойства

Microwave assisted synthesis and antimicrobial evaluation of phosphonohydrazone derivatives

R. Hajikhani ^{*1}, A. Ahmadi ², B. Nahri-Niknafs ²

¹ Department of Physiology and Microbiology, Karaj branch, Islamic Azad University, Karaj, Iran

² Department of Chemistry, Faculty of Science, Karaj branch, Islamic Azad University, Karaj, Iran

Received September 11, 2013; Revised November 30, 2013

Rapid and efficient solvent-free one-pot synthesis of dialkylamino alkyl-1-(4-bromobenzylidene) phosphonohydrazone derivatives by the condensation reaction of *N, N*-dialkylamino alkylphosphorohydrazides with *p*-bromobenzaldehyde using silica under microwave irradiation is described. The structural features of the synthesized compounds were characterized by IR, ¹H-NMR, ¹³C-NMR, mass spectroscopy and elemental analysis. The newly synthesized compounds were screened for antimicrobial activity against two Gram-positive strains (*Staphylococcus aureus* and *Bacillus subtilis*) and two Gram-negative strains (*Escherichia coli* and *Pseudomonas aeruginosa*). The results showed that some of these compounds were active against all tested bacteria.

Keywords: Antimicrobial activity, Microwave irradiation, Phosphonohydrazones, Solvent-free conditions.

INTRODUCTION

Infectious diseases are one of the leading causes of death worldwide. During the past few decades, new infectious diseases have appeared and old ones previously thought to be controlled have reemerged [1] and thus, despite of many significant developments in the antimicrobial therapy, many problems remain to be solved for most of antimicrobial drugs available [2]. Hence, discovery of novel antimicrobial agents with better pharmacological profile is still highly desirable. Hydrazones have drug and pharmaceutical properties. These compounds are widely used as anti-inflammatory [3], anticancer [4], analgesic [5], anticonvulsant [6], antituberculous [7], antiproliferative [8], antitumor [9,10], anti-HIV [11], antimycobacterial [12] and antimicrobial agents [13]. Moreover, hydrazones are used to synthesize indoles [14], 4-thiazolidin-4-ones [3], azetidines [15]. Generally, these compounds are synthesized by the condensation reaction of substituted hydrazines/hydrazides with aldehydes and ketones in organic solvents [3]. These are also synthesized by the reaction of hydrazide and carbonyl compounds in presence of polystyrene sulfonic acid in aqueous medium using microwaves [16], only microwaves [17], acidic alumina [18], ultrasound irradiation in aqueous medium [19]. There are reports for the synthesis of phosphonohydrazones, which have several

drawbacks such as use of carcinogenic solvents, long reaction time and formation of several by-products. Therefore, we have reported a new method for the preparation of phosphonohydrazones. It was found that silica supported microwave irradiation technique is capable of producing high yields of phosphonohydrazones by condensation of phosphonohydrazides with aromatic aldehydes under mild conditions. The method has advantages, such as ease of execution and work-up, fast rate of reactions, high yields, solvent-free reaction conditions and low cost. Chemically synthesized compounds like hydrazones could be prospectful for treating bacterial infections. Therefore, these compounds were synthesized and evaluated against two Gram-positive strains (*Staphylococcus aureus* and *Bacillus subtilis*) and two Gram-negative strains (*Escherichia coli* and *Pseudomonas aeruginosa*).

EXPERIMENTAL

All chemicals and solvents were obtained from E. Merck (Darmstadt, Germany), and were used without further purification. All melting points were taken with an Electrothermal melting point apparatus (Electrothermal Eng. Ltd, Essex, UK) and were uncorrected. IR spectra were recorded in KBr on a Shimadzu Dr-8031 instrument. ¹H- and ¹³C-NMR spectra of the synthesized compounds were measured in a CDCl₃ solution and TMS as the internal standard using a Varian Mercury 400 instrument at 400 and 75 MHz, respectively. All chemical shifts were reported as δ (ppm) values.

* To whom all correspondence should be sent:
E-mail: ahmadikiau@yahoo.com

The mass spectra were recorded on a LCQ ion trap mass spectrometer (Thermo Fisher, San Jose, CA, USA), equipped with an EI source. Elemental analyses were carried out using a Perkin-Elmer, CHN elemental analyzer model 2400 and were within $\pm 0.4\%$ of the theoretical values. The purity of the newly synthesized compounds was checked by TLC on plates (Merck) and spots were visualized by exposing the dry plates to iodine vapor.

General procedure for the preparation of the compounds 2(a-e):

To phosphonohydrazides (0.01M) taken in a conical flask, ground silica gel (1 g) and p-bromobenzaldehyde (0.01M) were added and mixed well. The mixture was subjected to microwave irradiation at 180 W for the appropriate time (Table 1). After complete conversion, as indicated by TLC, the mixture was extracted with petroleum ether (3 \times 50 ml) and washed with water (3 \times 50 ml). After the disappearance of the phosphonohydrazone spot on the TLC, the solvent was evaporated in vacuum and the product was purified by column chromatography.

N,N-dibutyl amino isopropyl-1-(4-bromobenzylidene) phosphonohydrazone (2a)

IR (KBr, cm^{-1}): 3366(NH), 2988(C_6H_5), 2892(C-H), 1621(C=N), 1556(C=C), 1451(C-N), 1233(P=O), 1173(P-N-N), 1089,1152 (P-N-C), 811 (C-Cl), 692 (P-C); $^1\text{H-NMR}$ (CDCl_3): δ 0.85 (t, $J = 12.75$ Hz, 6H, CH_3), 1.05 (dd, $J = 7.51$ Hz, 6H, CH_3), 1.11 (dd, $J = 7.51$ Hz, 6H, CH_3), 1.26 (m, $J = 8.31$ Hz, 4H, CH_2), 1.56 (m, $J = 8.31$ Hz, 4H, CH_2), 2.41 (m, $J^{\text{P-H}} = 20.61$ Hz, 1H, CH), 3.06 (m, $J = 8.51$ Hz, 4H, CH_2), 6.91 (d, $J^{\text{P-H}} = 23.41$ Hz, 1H, NH), 7.51 (d, 2H, Ar-H), 7.58 (d, 2H, Ar-H), 8.41 (m, 1H, CH); $^{13}\text{C-NMR}$ (CDCl_3): δ 11.50 (CH_3), 11.5 (CH_3), 14.1 (CH_3), 19.39 (CH_2), 21.84 (CH), 33.71 (CH_2), 125.4 (C-Br), 130-132 (Ar-C), 154.70 (C=N-NH); MS(m/z): 417 (M+H $^+$). Anal. Calcd for $\text{C}_{18}\text{H}_{31}\text{BrN}_3\text{OP}$: C, 51.94; H, 7.45; N, 10.10. Found: C, 51.97; H, 7.42; N, 10.10.

N,N-dibutyl amino phenyl-1-(4-bromobenzylidene) phosphonohydrazone (2b)

IR (KBr, cm^{-1}): 3340(NH), 2979 (C_6H_5), 2908 (C-H), 1617 (C=N), 1561 (C=C), 1458 (C-N), 1247 (P=O), 1181 (P-N-N), 1086, 1160 (P-N-C), 822 (C-Cl), 704(P-C); $^1\text{H-NMR}$ (CDCl_3): δ 0.92 (t, $J = 8.66$ Hz, 6H, CH_3), 1.16 (m, $J = 7.46$ Hz, 4H, CH_2), 1.56 (m, $J = 7.46$ Hz, 4H, CH_2), 2.75 (m, $J = 8.16$ Hz, 4H, CH_2), 7.10 (d, $J^{\text{P-H}} = 23.46$ Hz, 1H, NH), 7.26-

7.86 (m, $J = 7.64$ Hz, 9H, Ar-H), 8.55 (s, 1H, N=CH); $^{13}\text{C-NMR}$ (CDCl_3): δ 10.26 (CH_3), 14.53 (CH_2), 21.45 (CH_3), 31.21 (CH_2), 42.44 (CH_2), 125.4 (C-Br), 128-132 (Ar-C), 154.76 (C=N-NH); MS (m/z): 451 (M+H $^+$). Anal. Calcd. For $\text{C}_{21}\text{H}_{29}\text{BrN}_3\text{OP}$: C, 56.05; H, 6.44; N, 9.33. Found: C, 56.10; H, 6.44; N 9.35.

N,N-diisopropyl amino isopropyl-1-(4-bromobenzylidene) phosphonohydrazone (2c)

IR (KBr, cm^{-1}): 3366 (NH), 3010 (C_6H_5), 2909 (C-H), 1615 (C=N), 1535(C=C), 1432(C-N), 1246(P=O), 1175(P-N-N), 1083, 1151 (P-N-C), 815 (C-Cl), 692 (P-C); $^1\text{H-NMR}$ (CDCl_3): δ 0.94 (t, $J = 9.79$ Hz, 6H, CH_3), 1.06 (dd, $J = 7.56$ Hz, 6H, CH_3), 1.12 (dd, $J = 8.32$ Hz, 6H, CH_3), 1.33 (m, $J = 9.43$ Hz, 4H, CH_2), 2.36 (m, $J^{\text{P-H}} = 22.76$ Hz, 1H, CH), 3.06 (m, $J = 8.36$ Hz, 4H, CH_2), 6.35 (d, $J^{\text{P-H}} = 19.65$ Hz, 1H, NH), 7.79 (d, 2H, Ar-H), 7.88 (d, 2H, Ar-H), 8.41 (m, 1H, CH); $^{13}\text{C-NMR}$ (CDCl_3): δ 10.14 (CH_3), 15.62 (CH_3), 16.16 (CH_3), 21.25 (CH_2), 31.05 (CH), 42.54 (CH_2), 125.4 (C-Br), 127-130 (Ar-C), 154.78 (C=N-NH); MS (m/z): 389 (M+H $^+$). Anal. Calcd for $\text{C}_{16}\text{H}_{27}\text{BrN}_3\text{OP}$: C, 49.50; H, 6.95; N, 10.82. Found: C, 49.51; H, 6.93; N, 10.80.

N,N-diisopropyl amino phenyl-1-(4-bromobenzylidene) phosphonohydrazone (2d)

IR (KBr, cm^{-1}): 3388 (NH), 2955 (C_6H_5), 2880 (C-H), 1614 (C=N), 1546 (C=C), 1454 (C-N), 1237 (P=O), 1175 (P-N-N), 1070, 1154 (P-N-C), 809 (C-Cl), 694 (P-C), $^1\text{H-NMR}$ (CDCl_3): δ 0.82 (t, $J = 7.53$ Hz, 6H, CH_3), 1.46 (m, $J = 7.46$ Hz, 4H, CH_2), 2.73 (m, $J = 7.43$ Hz, 4H, CH_2), 6.53 (d, $J^{\text{P-H}} = 23.23$, 1H, NH), 7.30-7.66 (m, $J = 6.95$ Hz, 9H, Ar-H), 8.54 (s, 1H, CH); $^{13}\text{C-NMR}$ (CDCl_3): δ 10.46 (CH_3), 22.35 (CH_2), 46.23 (CH_2), 125.5 (C-Br), 126-133 (Ar-C), 154.71 (C=N-NH); MS (m/z): 423 (M+H $^+$). Anal. Calcd for $\text{C}_{19}\text{H}_{25}\text{BrN}_3\text{OP}$: C, 54.05; H, 5.92. N, 9.95. Found: C, 54.15; H, 5.95; N 9.98.

N,N-dibutyl amino isopropyl-1-(4-chlorobenzylidene) phosphonohydrazone (2e)

IR (KBr, cm^{-1}): 3352 (NH), 2980 (C_6H_5), 2901 (C-H), 1615(C=N), 1559(C=C), 1466(C-N), 1232(P=O), 1155 (P-N-N), 1078, 1154 (P-N-C), 816 (C-Cl), 721 (P-C); $^1\text{H-NMR}$ (CDCl_3): δ 0.71 (d, $J = 7.55$ Hz, 3H, CH_3), 0.88 (d, $J = 7.42$ Hz, 6H, CH_3), 1.06 (dd, $J = 7.91$ Hz, 6H, CH_3), 1.49 (m, $J = 7.95$ Hz, 2H, CH), 2.38 (m, $J^{\text{P-H}} = 23.72$ Hz, 1H, CH), 2.80 (m, $J = 7.57$ Hz, 4H, CH_2), 8.11 (d, $J = 24.57$ Hz, 1H, NH), 7.34-7.84 (m, 4H, Ar-H), 8.51 (s, 1H, N=CH);

^{13}C NMR (CDCl_3): δ 10.21 (CH_3), 14.76 (CH_3), 16.45 (CH_3), 16.66 (CH), 31.35 (CH_2), 33.10 (CH), 125.5 (C-Br), 128-133 (Ar-C), 154.76 (C=N-NH); MS(m/z): 417 ($\text{M}+\text{H}^+$). Anal. Calcd. For $\text{C}_{18}\text{H}_{31}\text{BrN}_3\text{OP}$: C, 51.94; H, 7.45; N, 10.10. Found: C, 51.96; H, 7.48; N, 10.10.

Screening for antibacterial activity

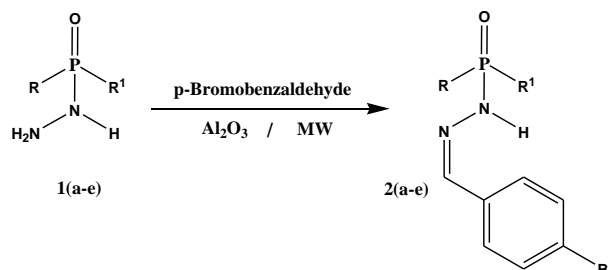
The antimicrobial activities were determined using the disc diffusion method [20] by measuring the zone of inhibition in mm. All newly synthesized compounds **2(a-e)** were screened *in vitro* for their antibacterial activity against two Gram-positive strains (*Staphylococcus aureus* and *Bacillus subtilis*) and two Gram-negative strains (*Escherichia coli* and *Pseudomonas aeruginosa*) at a concentration of 500 $\mu\text{g}/\text{ml}$. Ciprofloxacin (10 $\mu\text{g}/\text{disc}$) was used as a standard drug for antibacterial screening. All synthesized compounds exhibited satisfactory antibacterial activities. Each experiment was done in triplicate and the average reading was taken.

RESULTS AND DISCUSSION

Chemistry

We now report the synthesis of *N,N*-dialkyl alkyl-1-(4-bromo benzylidene) phosphonohydrazone **2(a-e)** from *N,N*-dialkylamino alkylphosphorohydrazides **1(a-e)** under MW and solvent-free conditions in short reaction times (Scheme). Initially, we prepared *N,N*-dialkylamino alkylphosphorohydrazides **1(a-e)** by a reported method [21]. In order to determine the optimum conditions for the synthesis of organophosphorus based hydrazone derivatives, variations in molar ratios of reagents, irradiation time and power level of the microwave set-up were investigated. After some experimentation, we found a set of conditions that generally provides products in good yields. In this regard, several reactions of *N,N*-dialkylamino

alkylphosphorohydrazides with *p*-bromobenzaldehyde were performed under different conditions. These reactions were monitored by TLC. The synthesized compounds were identified on the basis of IR, $^1\text{H-NMR}$, $^{13}\text{C-NMR}$, mass spectra and elemental analysis.



Scheme. Preparation route of the compounds

Table 1. Physical data of the newly synthesized compounds **2(a-e)**

Entry	R	R ¹	Reaction Time (min)	m. p °C	Yield (%)
2a	$^i\text{C}_3\text{H}_7$	$\text{N}(\text{C}_4\text{H}_9)_2$	4.0	144	77
2b	C_6H_5	$\text{N}(\text{C}_4\text{H}_9)_2$	5.0	165	80
2c	$^i\text{C}_3\text{H}_7$	$\text{N}(\text{C}_3\text{H}_7)_2$	4.0	137	85
2d	C_6H_5	$\text{N}(\text{C}_3\text{H}_7)_2$	5.0	162	75
2e	$^i\text{C}_3\text{H}_7$	$\text{N}(^i\text{C}_4\text{H}_9)_2$	5.0	160	76

Antimicrobial activity of compounds **2(a-e)**

To check the biological activity of the compounds, the compounds **2(a-e)** were screened for *in vitro* antimicrobial activity against a variety of bacteria, two Gram-positive strains (*Staphylococcus aureus* and *Bacillus subtilis*) and two Gram-negative strains (*Escherichia coli* and *Pseudomonas aeruginosa*). All compounds were assayed for antibacterial activity. The preliminary screening results for the compounds **2(a-e)** (Table 2) revealed that compound **2c** showed activity against all tested bacteria while **2e** was active against three bacteria (except *E. coli*). Compound **2a** and **2d** showed antimicrobial activity towards *S. aureus* and *B. subtilis* while compound **2b** showed slight activity against *S. aureus*, *B. subtilis*.

Table 2: Results for the antimicrobial activity of the tested compounds

Compound No.	Zone of inhibition in mm			
	Antibacterial activity			
	<i>S. aureus</i>	<i>B. subtilis</i>	<i>E. coli</i>	<i>P. aeruginosa</i>
2a	++	++	-	-
2b	+	+	-	-
2c	+++	+++	++	++
2d	++	++	-	-
2e	+++	++	-	+
Ciprofloxacin	+++	+++	+++	+++

Key to symbols: Highly active = +++ (inhibition zone > 12 mm); Moderately active = ++ (inhibition zone 9 – 12 mm); Slightly active = + (inhibition zone 6 – 9 mm); Inactive = - (inhibition zone < 6 mm)

CONCLUSION

In conclusion, we have synthesized a series of phosphonohydrazone derivatives **2(a-e)** by a rapid, efficient, solvent-free, one-pot procedure with excellent yields under microwave irradiation. The main advantage of this method is the clean and easy work-up. Among the synthesized compounds **2(a-e)**, compound **2c** showed excellent activity against all tested bacteria. Biological evaluation of these derivatives may furnish some other important applications.

Acknowledgment: The authors gratefully acknowledge the support from Islamic Azad University, Karaj-branch.

REFERENCES

1. P.C. Sharma, S. Jain, *Acta Pharm Scientia*, **50**, 35-40 (2008).
2. P.C. Sharma, S. Jain, *Acta Pol. Pharm.*, **65**, 551 (2008).
3. S. Rollas, S. G. Kucukguzel, *Molecules*, **12**, 1910-1939 (2007).
4. N. Terzioglu, A. Gursoy, *Eur. J. Med. Chem*, **38**, 781-786 (2003).
5. S.M. Sunidhi, M. Dinodia, A. Kumar, *Bioorg. Med. Chem.* **14**, 4657-4663 (2006).
6. H.N. Doğan, A. Duran, S. Rollas, G. Şener, Y. Armutak, M. Kayer-Uysal, *Med. Sci. Research*, **26**, 755-758 (1998).
7. K. Bedia, O. Elcin, U. Seda, K. Fatma, S. Nathalay, R. Sevim, A. Dimoglo, *Eur. J. Med. Chem.*, **41**, 1253-1261 (2006).
8. P. Vicini, M. Incerti, I. A. Doytchinova, P. Colla, B. Busonera, R. Loddo, *Eur. J. Med. Chem.* **41**, 624-632 (2006).
9. A. Andreani, S. Burnelli, M. Granaiola, *J. Med. Chem.* **51**, 809-816 (2008).
10. E. Noulisri, R. Richardson, S. Lerdwana, S. Fucharoen, T. Yamagishi, D. S. Kalinowski, K. Pattanapanyasat, *Am. J. Hematology*, **84**, 170-176 (2009).
11. L.Q. Al-Macrosaur, R. Dayam, L. Taheri, M. Witvrouw, Z. Debyser, N. Neamati, *Bioorg. Med. Chem. Lett.*, **17**, 6472-6475 (2007).
12. S. G. Kucukguzel, S. Rollas, I. Kucukguzel, M. Kiraz, *Eur. J. Med. Chem.* **34**, 1093-1100 (1999).
13. S. Rollas, N. Gulerman, H. Erdeniz, *Farmaco*, **57**, 171-174 (2002).
14. S. Kim, J.Y. Yoon, *Hydrazones*. In *Science of Synthesis: Padwa A*, Thieme; Stuttgart, New York, **27**, 671-722 (2004).
15. E. Martin-Zamora, A. Ferrete, J. M. Llera, J. M. Munoz, R. R. Pappalardo, R. Fernandez, J. M. Lassaletta, *Chem. Eur. J.* **10**, 6111-6129 (2004).
16. V. Polshettiwar, R. S. Varma, *Tetrahedron Lett.* **48**(32), 5649-5652 (2007).
17. L.V. Reddy, A. Suman, S.S. Beevi, L. N. Mangamoori, K. Mukkanti, S. Pal, *J. Braz. Chem. Soc.* **21**(1), 98-104 (2010).
18. S.I. Anson, E. V. Novikova, A. A. Iozep, *Rus. J. Appl. Chem.* **81**(4), 647-650 (2008).
19. A.C.L. Leite, D.R.M. Moreira, L.C.D. Coelho, F.D. Menezes, D. J. Brondani, *Tetrahedron Lett.* **49**(9), 1538-1541 (2008).
20. A.W. Bauer, W.M.M. Kirby, J.C. Sherris, M. Truck, *Am. J. Clin. Pathol.* **45**, 493-6 (1996).
21. P. Kavita Joshi, N. Sharma, Y.C. Joshi, *Can. J. Chem.* **88**(10), 1034-1039 (2010).

МИКРОВЪЛНОВА СИНТЕЗА И АНТИМИКРОБНА АКТИВНОСТ НА ПРОИЗВОДНИ НА ФОСФОНОХИДРАЗОНА

Р. Хаджихани^{*1}, А. Ахмади², Б. Нахри-Никнафс²

¹ Департамент по физиология и микробиология, Научен факултет, Клон Карадж, Ислямски университет „Азад“, Карадж, Иран

² Департамент по химия, Научен факултет, Клон Карадж, Ислямски университет „Азад“, Карадж, Иран

Постъпила на 11 септември, 2013 г.; Коригирана 30 ноември, 2013 г.

(Резюме)

Описана е бърза и ефективна синтеза без разтворител на диалкил-амино алкил-1-(4-брообензилиден) фосфохидазонови производни чрез кондензация *N,N*- диалкил-амино-алкил-фосфорохидразида с *p*-бромобензалдехид в присъствие на силициев диоксид при микровълново облъчване. Структурата на синтезираните съединения е охарактеризирана чрез IR, ¹H-NMR, ¹³C-NMR, мас-спектроскопия и елементен анализ. Новите съединения са скринирани за антимикробна активност срещу два Грам-положителни щамове (*Staphylococcus aureus* и *Bacillus subtilis*) и два Грам-отрицателни щамове (*Escherichia coli* и *Pseudomonas aeruginosa*). Резултатите показват, че някои от тези съединения са активни спрямо всички изпитани бактерии.

B₁₂N₁₂ nanocage as a potential adsorbent for the removal of aniline from environmental systems

M. T. Baei¹, H. Mohammadian², S. Hashemian³

¹ Department of Chemistry, Azadshahr Branch, Islamic Azad University, Azadshahr, Golestan, Iran

² Department of Physics, Mahshahr Branch, Islamic Azad University, Mahshahr, Iran

³ Department of Chemistry, Yazd Branch, Islamic Azad University, Yazd, Iran

Received December 16, 2013; Revised February 11, 2014

Density functional theory (DFT) calculations at the B3LYP/6-31G* level were performed to investigate aniline adsorption on a B₁₂N₁₂ nanocage in terms of energetic, geometric, and electronic properties. It was found that aniline is more likely adsorbed *via* its nitrogen atom on the B₁₂N₁₂ surface. The adsorption energy of aniline on the nanocage in the most stable state is -24.95 kcal/mol and about 0.34|e| is transferred from the aniline molecule to the nanocage. The calculated density of states shows that the electronic properties of the B₁₂N₁₂ nanocage are changed after the aniline adsorption process. Fermi level is dramatically changed from -4.28 eV in the pristine nanocage to higher energies after the aniline adsorption, which decreases the work function of the nanocage. The results show that the B₁₂N₁₂ nanocage can be used for adsorption of toxic aniline molecules from environmental systems.

Keywords: boron nitride nanocage, aniline, adsorbent, electronic structures

INTRODUCTION

Aniline (C₆H₅NH₂) is an important organic compound due to its wide applications in the manufacturing of dyestuffs, rubbers, pesticides, plastics and paints [1]. Aniline is released throughout the environment by industrial wastewater and/or through degradation of some of the above mentioned compounds [2-3]. Much attention should be taken concerning the contamination of groundwater because aniline is a toxic and persistent pollutant that is very harmful not only to aquatic life but also to humans [4- 5]. Aniline is toxic by inhalation of the vapor, ingestion, or contact with the skin. Therefore, it is very important to remove aniline from wastewater or environment.

In recent years, there have been several studies on the removal of aniline from wastewater [6-7]. However, these methods cannot be currently widely applied due to high cost, long duration, etc. Therefore, further study of aniline adsorption is an important task. Among different methods, using nanostructures as adsorbents is an interesting approach because of their unique physical and chemical properties including high surface/volume ratio and very sensitive electronic properties. For example, the adsorption of simple molecules on nanostructures has a considerable potential for applications in surface modification [8], fuel cells

[9], gas sensors [10] and hydrogen storage [11]. Among nanostructures, boron nitrides (BN)_x are isoelectronic to the fullerenes and have attracted considerable attention due to their high-temperature stability, low dielectric constant, large thermal conductivity, wide-band gap, and oxidation resistance [12-14]. Seifert *et al.* [15] showed that B₁₂N₁₂, B₁₆N₁₆ and B₂₈N₂₈ are magic BN fullerenes and B₁₂N₁₂ appears to be more stable than the others. Oku *et al.* [16] have synthesized B₁₂N₁₂ nanocage by laser desorption time-of-flight mass spectrometry, showing that these clusters consist of eight hexagon rings and six tetragon rings. The aim of this research is to investigate theoretically the adsorption of aniline on a B₁₂N₁₂ nanocage based on the analysis of structure, energies, stability, and electronic properties using density functional theory (DFT) calculations.

COMPUTATIONAL METHODS

Spin-unrestricted B3LYP/6-31G* level of theory was used to describe the adsorption of aniline on surfaces of B₁₂N₁₂ nanocage, specifically the geometry optimizations, energy calculations, and density of states (DOS) analysis. B3LYP is the commonly used approach for investigations of different nanostructures [17-18].

This method was used to calculate the adsorption energy (E_{ad}) of aniline on the surface of B₁₂N₁₂ nanocage as follows:

$$E_{ad} = E_{\text{aniline/B}_{12}\text{N}_{12}} - [E_{\text{B}_{12}\text{N}_{12}} + E_{\text{aniline}}] \quad \text{Eq. (1)}$$

* To whom all correspondence should be sent:
E-mail: baei52@yahoo.com

where $E_{\text{aniline}/B_{12}N_{12}}$ is the total energy of the complex (adsorbed aniline molecule on the $B_{12}N_{12}$ surface), $E_{B_{12}N_{12}}$ and E_{aniline} are the total energies of the pristine $B_{12}N_{12}$ nanocage and the aniline molecule. Negative or positive value for E_{ad} is referred to exothermic or endothermic processes, respectively. The canonical assumption for a Fermi level is that in a molecule at 0 K it lies approximately in the middle of the energy gap (E_g). Also, the chemical potential of a molecule lies in the middle of the E_g . Therefore, the chemical potential of a free gas of electrons is equal to its Fermi level as traditionally defined. Herein, the Fermi level of the considered systems is at the middle of the E_g . All calculations were carried out using the GAMESS suite of programs [19].

RESULTS AND DISCUSSION

The structure of the optimized $B_{12}N_{12}$ nanocage is shown in Fig. 1a. It is formed from eight 6-membered (hexagon) rings and six 4-membered (tetragon) rings with T_h symmetry so that the calculated electric dipole moment is zero.

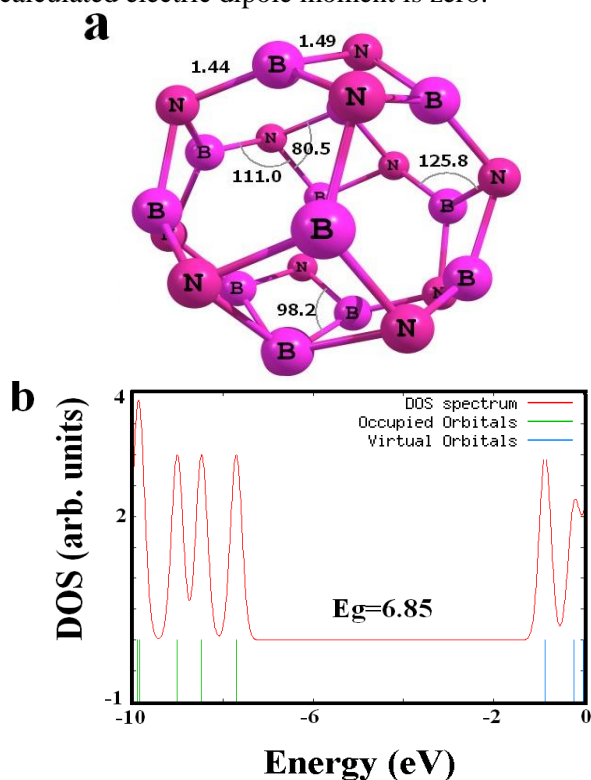


Fig. 1. Structural parameters (a) and electronic density of states (DOS) (b) for the optimized structure of the $B_{12}N_{12}$ nanocage.

Two types of B–N bonds are identified in the $B_{12}N_{12}$ nanocage, one with a bond length of 1.44 Å

which is shared between two hexagon rings, and the other with a length of 1.49 Å which is shared between a tetragon and a hexagon ring. The results are in good agreement with those obtained by Beheshtian *et al.* [20]. The natural bond orbital (NBO) population charge analysis showed a net charge transfer of 1.17 |e| from B to N atom in the nanocage, indicating an ionic nature. The angles in the 4-membered and the 6-membered rings in $B_{12}N_{12}$ nanocage vary from 80.5° to 98.2° and from 111.0° to 125.8°, respectively.

In order to find the minimum adsorption configurations of single aniline adsorbed on the $B_{12}N_{12}$ nanocage, various possible adsorption structures were considered. The molecular electrostatic potential (MEP) surfaces of single aniline are shown in Fig. 2. As can be seen, the partial negative charge on the N atom and phenyl group of aniline makes it reactive toward the Lewis acid sites of B atoms. Therefore, aniline can approach the walls of the nanocage *via* the N atom (amino group) and/or *via* the phenyl ring (π - π interaction). Finally, only two local minima structures were obtained for the adsorption of aniline *via* the phenyl group and three stable structures *via* the nitrogen atom that are shown in Figs. 3 and 4.

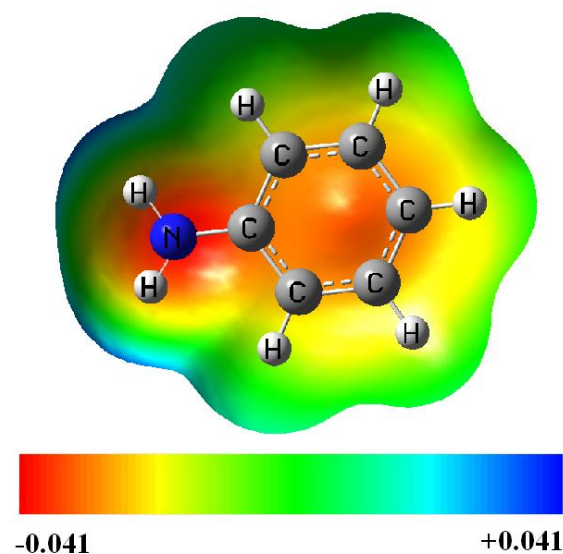


Fig. 2. Molecular electrostatic potential surface of the aniline molecule. The surfaces are defined by the 0.0004 electrons/b³ contour of the electronic density. Color ranges, in a.u.

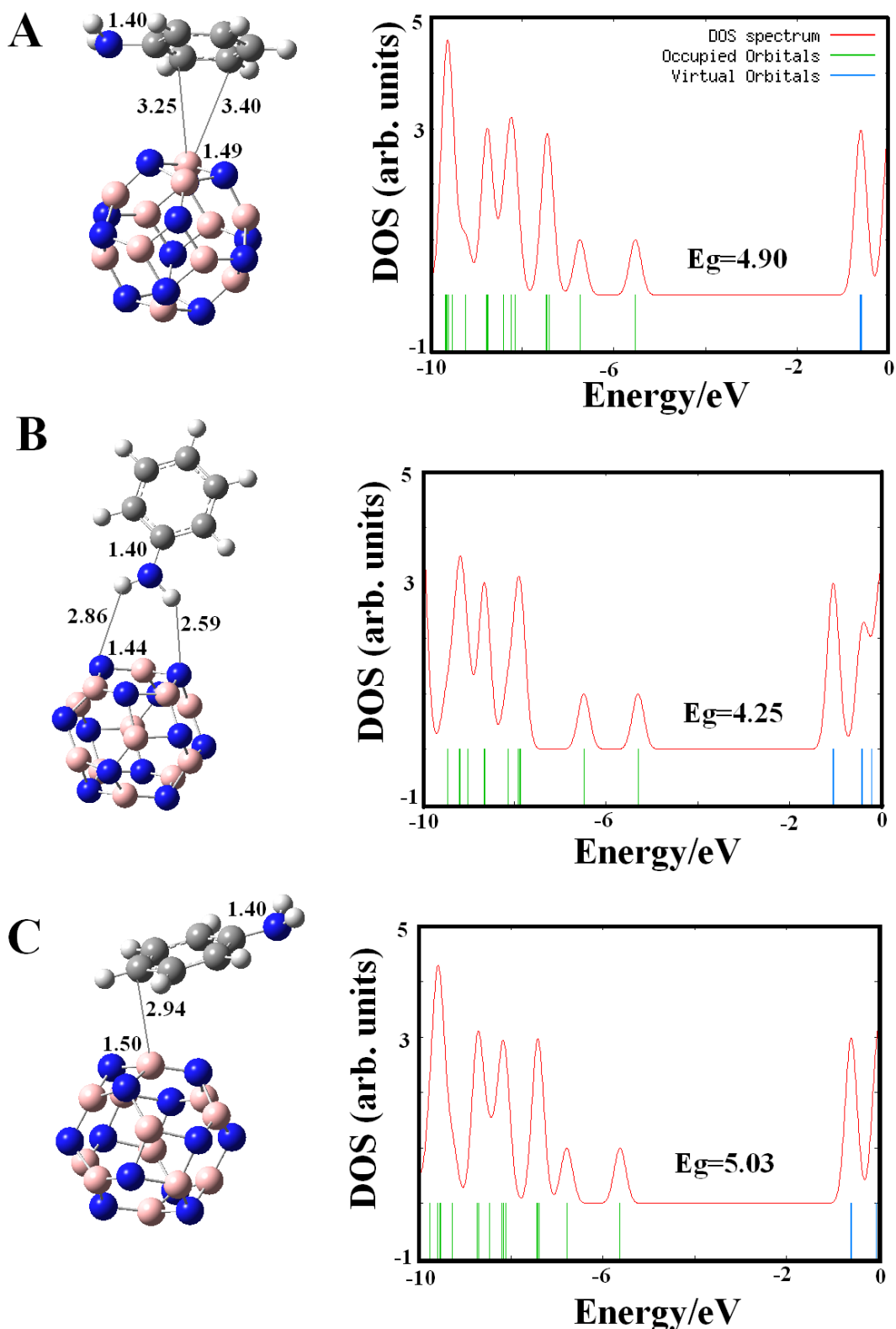


Fig. 3. Models for three different physisorption configurations and their density of states (DOS) plots. Distances are in Å.

As shown in Fig. 3, configuration A shows an interaction between the carbon atoms of aniline molecule (phenyl group) and the B atoms of a

tetragon ring of the nanocage so that the two C atoms of aniline are closer to one B atom of the nanocage with distances of 3.25 and 3.40Å. In this

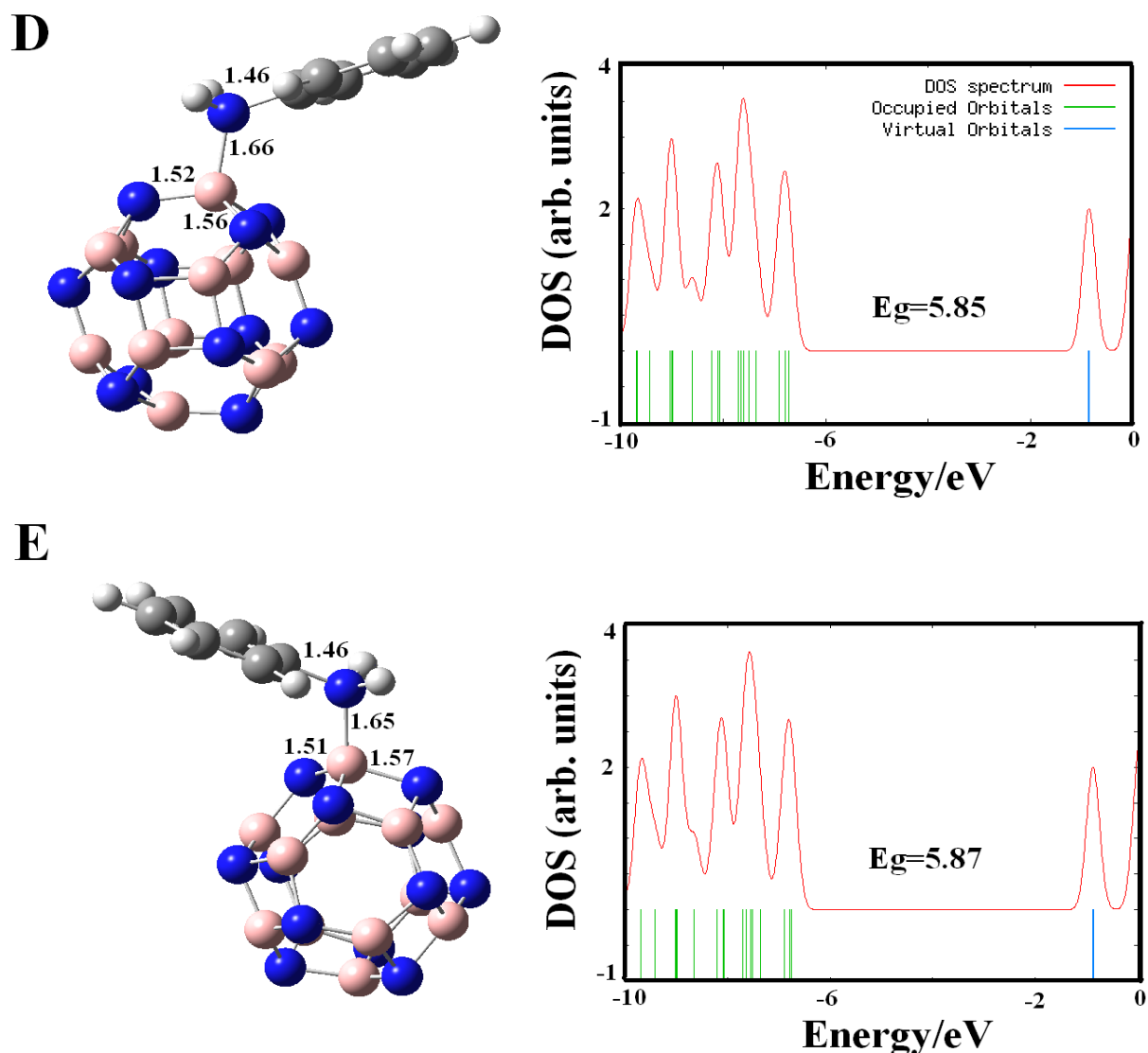


Fig.

4. Models for two different chemisorption configurations and their density of states (DOS) plots. Distances are in Å.

configuration, a net charge of 0.02 electrons is transferred from the aniline to the nanocage and E_{ad} is about -2.04 kcal/mol (Table 1). The above results indicate that this interaction is weak and should be considered as physisorption. Another aniline physisorption approach is shown in Fig. 2B in which the aniline molecule is located atop of a hexagon ring and its hydrogen atoms, so that the distances between the two H atoms of aniline and the two N atoms of the hexagon ring are 2.86 and 2.54 Å, respectively. This configuration has an E_{ad} of -2.23 kcal/mol and does not show charge transfer to take place between aniline and $B_{12}N_{12}$ nanocage. In Fig. 2, configuration C, the aniline molecule weakly interacts with the $B_{12}N_{12}$ nanocage through van der Waals forces and *via* the phenyl group. The smallest distance of the molecule to the nanocage is found to be 2.94 Å. Based on the natural bond orbital charges (NBO) analysis, a net charge of 0.04 electrons is transferred from aniline to the nanocage and its corresponding calculated E_{ad} value is -2.41 kcal/mol, indicating that the interaction is physisorption in nature. Moreover, the adsorption of aniline on the nanocage in the above complexes has no local structural deformation on both the aniline molecule and the nanocage. The small E_{ad} values and the large interaction distances in the above aniline/ $B_{12}N_{12}$ complexes indicated that aniline cannot be significantly adsorbed on the sites and undergoes weakly physical adsorption on the pristine nanocage.

Covalent functionalization is the other type of interaction between aniline and the $B_{12}N_{12}$ nanocage, so that the N atom of the molecule is bonded to one B atom of the nanocage (Fig. 4). The E_{ad} for the configuration D (-24.37 kcal/mol) is a little smaller than that of E (-24.95 kcal/mol) with a rather significant NBO charge transfer of $0.34|e|$ from the aniline to the nanocage. Therefore, the B atoms of the nanocage are a thermodynamically

more favorable site for the adsorption of aniline because the partial negative charge on the N atom of aniline makes it reactive toward the Lewis acid sites of the B atoms. The corresponding interaction distance between the B atom of the nanocage and the N atom of aniline for configurations **D** and **E** is 1.66 and 1.65 Å, respectively. Also, the electric dipole moment has increased from 0.00 Debye in the pristine nanocage to 8.35 and 8.38 Debye in the configurations **D** and **E**. Small bond length of B...N, significant change in dipole moment, and more negative E_{ad} for the applied configurations indicate that the aniline binds to the exposed B atom and can receive electrons from the lone pair orbital of nitrogen. In addition, the adsorption of aniline in these configurations shows almost local structural deformation on both the aniline molecule and the B₁₂N₁₂ nanocage. The C-N bond length of aniline increased from 1.40 Å in the isolated aniline to 1.46 Å in the adsorbed state. Also, the length of B-N bonds in the pristine B₁₂N₁₂ increased from 1.44 and 1.49 Å to 1.52 and 1.56 Å in configuration **D** and to 1.51 and 1.57 Å in configuration **E** for B-N bonds located in immediate neighborhood of the aniline molecule. All above indicates that aniline is strongly chemisorbed on B₁₂N₁₂ and the nanocage can be a promising candidate for the adsorption of aniline from environmental systems.

However, in order to investigate the effect of adsorption of the aniline molecule on the electronic properties of the B₁₂N₁₂ nanocage, the total densities of states (DOS) of aniline/B₁₂N₁₂ complexes were studied. As shown in Fig. 1b and Table 1, the calculated energy gap ($E_g = E_{LUMO} - E_{HOMO}$) of the B₁₂N₁₂ nanocage is 6.85 eV, indicating that the nanocage is an insulator. DOSs for different models of the aniline/B₁₂N₁₂ complex are shown in Figs. 2-4. In comparison to the DOS of the pristine B₁₂N₁₂ nanocage and the physisorption configurations **A**, **B**, **C**, it is found that their E_g values have changed in the range of

26.57-37.96 % after aniline adsorption. The results show that the electronic properties of the B₁₂N₁₂ nanocage are sensitive to aniline in the configurations. Also, the E_g values for the chemisorption configurations **D** and **E** have changed in the range of 14.31-15% after aniline adsorption, indicating that the changes in the electronic properties of the nanocage from physisorption to chemisorption are reduced. Also, the E_g value for all aniline/B₁₂N₁₂ complex models is reduced which might result in an electrical conductivity change of the nanocage according to the following equation [21]:

$$\sigma \propto \exp\left(\frac{-E_g}{2kT}\right) \quad \text{Eq. (2)}$$

where σ is the electric conductivity of the complexes and k is the Boltzmann's constant. According to the above equation, smaller E_g at a particular temperature leads to a higher electric conductivity. Table 1 indicates that the Fermi level energy (E_{FL}) of the aniline/B₁₂N₁₂ complex models is increased. This increase in E_{FL} with aniline adsorption leads to a decrement in the work function which is important in field emission applications. The decrement in the work function shows that the field emission properties of the complexes are improved upon aniline adsorption. The values of the induced electric dipole moment (D_M) vector obtained from these calculations increased with aniline adsorption, thus increasing the reactivity of the nanocage.

In order to interpret the aniline interaction with the B₁₂N₁₂ nanocage, we drew plots of the HOMO and LUMO for the most stable structure (configuration **E**). As shown in Fig. 5, after aniline adsorption, the HOMO is more localized on the nanocage. Energy level of HOMO in this configuration is -6.75 eV, indicating that it has become less stable upon aniline adsorption due to

Table 1 Calculated adsorption energy (E_{ad} , kcal/mol), HOMO energies (E_{HOMO}), LUMO energies (E_{LUMO}), HOMO-LUMO energy gap (E_g), and Fermi level energy (E_{FL}) of the systems in eV, sum of NBO charges on the adsorbed aniline (Q_T), and dipole moment (D_M) in Debye.

Structure	E_{ad}	E_{HOMO}	E_{LUMO}	E_g	$^a\Delta E_g(\%)$	$^bQ_T[e]$	E_{FL}	D_M
B ₁₂ N ₁₂	-	-7.71	-0.86	6.85	-	-	-4.28	0.00
A	-2.04	-5.53	-0.63	4.90	28.47	0.02	-3.08	2.72
B	-2.23	-5.30	-1.05	4.25	37.96	0.00	-3.18	2.35
C	-2.41	-5.63	-0.60	5.03	26.57	0.04	-3.12	3.52
D	-24.37	-6.72	-0.87	5.85	15.00	0.34	-3.76	8.38
E	-24.95	-6.75	-0.88	5.87	14.31	0.34	-3.82	8.40

^aChange in HOMO-LUMO gap of B₁₂N₁₂ nanocage after aniline adsorption

^b Q is defined as the total natural bond orbital charges on the aniline molecule and positive values mean charge transfer from the aniline molecule to the B₁₂N₁₂ nanocage

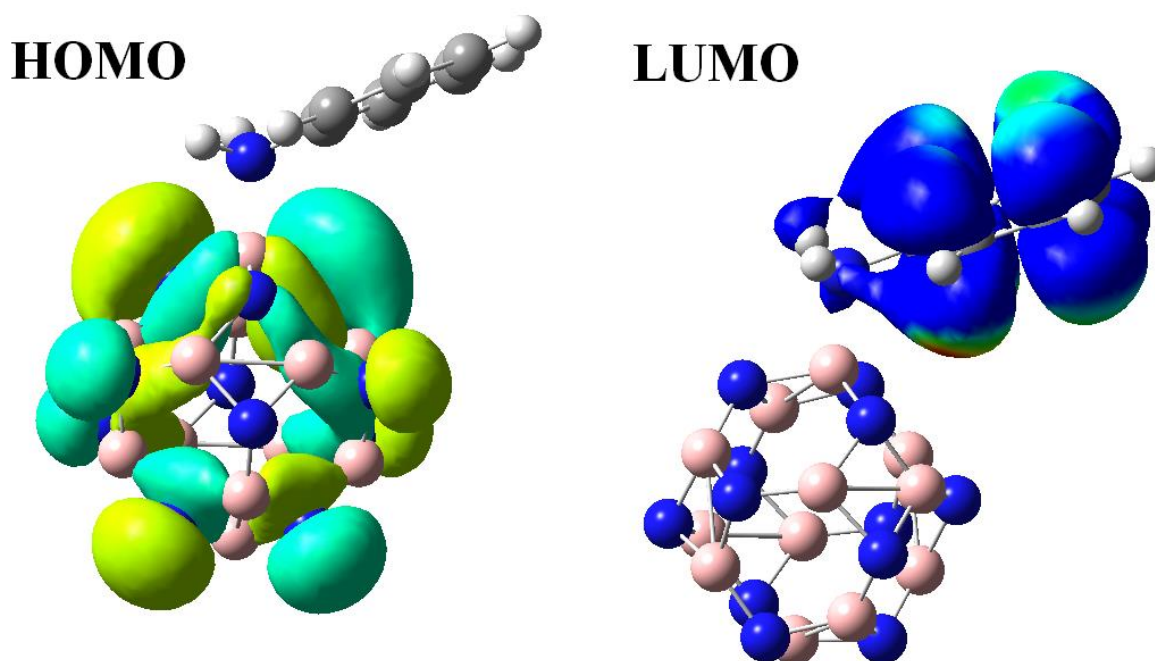


Fig. 5. HOMO and LUMO profiles of configuration E.

stronger charge transfer of aniline to the nanocage (energy level of HOMO of pristine $B_{12}N_{12}$ nanocage is -7.71 eV). On the other hand, LUMO for the configuration is localized on the aniline molecule, indicating that the LUMO has not contributed to the adsorption process. However, the study of the electronic properties of $B_{12}N_{12}$ shows that the aniline molecule is strongly chemisorbed on the $B_{12}N_{12}$ and the nanocage can be used for aniline adsorption in environmental systems.

CONCLUSIONS

Aniline is adsorbed on the $B_{12}N_{12}$ nanocage surface in molecular form through interaction of the amino group with surface active sites (B atoms). The mechanism of the intermolecular interaction between aniline and the $B_{12}N_{12}$ nanocage surface is mediated through donation of an electron lone pair from the amino group to the Lewis acid sites of the B atoms. Adsorption energy of aniline on $B_{12}N_{12}$ in the most stable configuration was calculated to be -24.95 kcal/mol with a charge transfer of $0.34|e|$ from aniline to the nanocage. The calculations also indicated that attachment of the aniline on the surface of the $B_{12}N_{12}$ nanocage induces changes in the electronic properties of the nanocage and its E_g is reduced after the adsorption process. With aniline adsorption the work function decreased which may facilitate the field electron emission from aniline to the $B_{12}N_{12}$ surface. The results showed that the

$B_{12}N_{12}$ nanocage can significantly attach aniline molecules and the pristine $B_{12}N_{12}$ nanocage can be an efficient potential adsorbent for adsorption of the aniline from environmental systems.

REFERENCES

1. Z.Z. Rappoport (ed.), *The Chemistry of Anilines: Part 1. The Chemistry of Functional Group Series*, Wiley, New York, 2007.
2. R.D. Voyksner, R. Straub, J.T. Keever, H.S. Freeman and W.N. Hsu, Determination of aromatic amines originating from azo dyes by chemical reduction combined with liquid chromatography/mass spectrometry, *Environ. Sci. Technol.*, 27 (8), 1665–1672 (1993).
3. S. Laha and R.G. Luthy, Oxidation of aniline and other primary aromatic amines by manganese dioxide, *Environ. Sci. Technol.*, 24 (3), (1990) 363–373.
4. U.S. Environmental Protection Agency, Health and Environmental Effects Profile for Aniline, Environmental Criteria and Assessment Office, Office of Health and Environmental Assessment, Office of Research and Development, Cincinnati, OH, 1985.
5. U.S. Department of Health and Human Services, Hazardous Substances Data Bank (HSDB, online database), National Toxicology Information Program, National Library of Medicine, Bethesda, MD, 1993.
6. X. Gu, J. Zhou, A. Zhang, P. Wang, M. Xiao and G. Liu, Feasibility study of the treatment of aniline hypersaline wastewater with a combined adsorption/

- bioregeneration system, *Desalination*, 227, 139–149 (2008).
7. P.C.C. Faria, J.J.M. Orfao, J.L. Figueiredo, M.F.R. Pereira, Adsorption of aromatic compounds from the biodegradation of azo dyes on activated carbon, *Appl. Surf. Sci.* 254, 3497–3503 (2008).
 8. X. Wu, W. An, X. Z. Zeng, Chemical Functionalization of Boron-nitride Nanotubes with NH₃ and Amino Functional Groups, *J. Am. Chem. Soc.* 128, 12001-12006 (2006).
 9. S. J. Hwang, J. W. Kim, S. J. Yoo, J. H. Jang, E. A. Cho, T. H. Lim, S. G. Pyo, S. K. Kim, Stabilizer-mediated Synthesis of High Activity PtFe/C Nanocatalysts for Fuel Cell Application, *Bull. Korean Chem. Soc.* 33, 699-702 (2012).
 10. O.K. Tan, W. Cao, Y. Hu, W. Zhu, Nano-structured oxide semiconductor materials for gas-sensing applications, *Ceramics International* 30, 1127–1133 (2004).
 11. P. Chen, X. Wu, J. Lin, K. L. Tan, High H₂ Uptake by Alkali-Doped Carbon Nanotubes Under Ambient Pressure and Moderate Temperatures, *Science* 285, 91-93 (1999).
 12. R.T. Paine, C.K. Narula, Synthetic routes to boron nitride, *Chem. Rev.* 90, 73–91 (1990).
 13. T. Oku, T. Hirano, M. Kuno, T. Kusunose, K. Niihare, K. Suganuma, Synthesis, atomic structures and properties of carbon and boron nitride fullerene materials, *Mater. Sci. Eng. B* 74, 206–217 (2000).
 14. T. Oku, M. Kuno, H. Kitahara, I. Nartia, Formation, atomic structures, and properties of boron nitride and carbon nanocage fullerene materials, *Int. J. Inorg. Mater.* 3, 597–612 (2001).
 15. G. Seifert, R. W. Fowler, D. Mitchell, D. Porezag, and T. Frauenheim, Boron-nitrogen analogues of the fullerenes: electronic and structural properties, *Chem. Phys. Lett.* 268, 352-358 (1997).
 16. T. Oku, A. Nishiwaki, I. Narita, Formation and atomic structure of B₁₂N₁₂ nano-cage clusters studied by mass spectrometry and cluster calculation, *Sci. Technol. Adv. Mater.* 5, 635–645 (2004).
 17. M.T. Baei, A.V. Moradi, M. Moghimi, P. Torabi, The influence of NH₃-attaching on the NMR and NQR parameters in the (6,0) zigzag single-walled BPNTs: a density functional study, *Comput. Theoret. Chem.* 967, 179-184 (2011).
 18. J. Beheshtian, M.T. Baei, A. A. Peyghan, Theoretical study of CO adsorption on the surface of BN, AlN, BP and AlP nanotubes, *Surface Science* 606, 981–985 (2012).
 19. M. Schmidt, et al., General atomic and molecular electronic structure system, *Journal of Computational Chemistry* 14, 1347 (1993).
 20. J. Beheshtian, Z. Bagheri, M. Kamfiroozi, A. Ahmadi, Toxic CO detection by B₁₂N₁₂ nanocluster, *Microelectronics Journal* 42, 1400–1403 (2011).
 21. S. S. Li (2006), *Semiconductor Physical Electronics*, 2nd ed., Springer, USA.

$B_{12}N_{12}$ -НАНОКЛЕТКА КАТО ПОТЕНЦИАЛЕН АДСОРБЕНТ ЗА ОТСТРАНЯВАНЕТО НА АНИЛИН В ОКОЛНАТА СРЕДА

М.Т. Баеи¹, Х. Мохамедиан², С. Хашемиан³

¹ Департамент по химия, Клон Азадшахр, Ислямски университет „Азад“, Азадшахр, Голестан, Иран

² Департамент по физика, Клон Машахр, Ислямски университет „Азад“, Машахр, Иран

³ Департамент по химия, Клон Язд, Ислямски университет „Азад“, Язд, Иран

Постъпила на 16 декември, 2013 г.; Коригирана 11 февруари, 2014 г.

(Резюме)

Извършени са пресмятане на the $B_{12}N_{12}$ -ниво по теорията на функционалната теория на полето (DFT) за изследване на адсорбцията на анилин в наноклетка от $B_{12}N_{12}$ като енергетични, геометрични и електронни отнасяния. Намерено е, че анилинят се адсорбира чрез своя азотен атом в молекулата си на повърхността на $B_{12}N_{12}$. Адсорбционната енергия на анилина върху наноклетката в най-стабилното си състояние е -24.95 kcal/mol и около $0.34|e|$ е пренесената от молекулата на анилина към наноклетката. Пресметнатата енергия на състоянието показва, че електронните свойства на наноклетката $B_{12}N_{12}$ се променят при адсорбцията на анилин. Нивото на Fermi се променя драстично от -4.28 eV в началната наноклетка до високи енергии след адсорбцията на анилин, които намаляват работата в наноклетката. Резултатите показват, че наноклетката $B_{12}N_{12}$ може да се използва за адсорбция на анилинови молекули в системи от околната среда.

Heat transfer and pressure drop of Al₂O₃ nanofluid as coolant in shell and helically coiled tube heat exchanger

P.C. Mukesh Kumar^{*,1}, J. Kumar², S. Sendhilnathan³, R.Tamilarasan⁴, S.Suresh⁵

¹University College of Engineering Pattukkottai, Tamilnadu, India.

²Sasurie College of Engineering, Tamilnadu, India.

³University College of Engineering Pattukkottai, Tamilnadu, India.

⁴University College of Engineering Pattukkottai, Tamilnadu, India.

⁵National Institute of Technology Trichy, India.

Received September 20, 2013; Revised March 4, 2014

In this investigation, the heat transfer and pressure drop analysis of Al₂O₃/ water nanofluid in a shell and helically coiled tube heat exchanger are studied. The Al₂O₃/water nanofluid at 0.1%, 0.4%, and 0.8% particle volume concentration was prepared by two-step method and characterized. It was found that the enhancement of experimental inner Nusselt numbers of 0.1%, 0.4% and 0.8% nanofluids are by 21%, 28% and 42%, respectively, higher than in water under laminar flow condition. This may be due to better mixing of the flow particles and higher effective thermal conductivity of the nanofluid. The inner Nusselt number correlation was proposed based on the experimental data. It is found that the deviation between the predicted and experimental Nusselt numbers in the range of ± 7.5 %. The pressure drop in 0.1 %, 0.4% and 0.8% nanofluids was by 8%, 12% and 20%, respectively higher than that in water. This is due to the improved viscosity of the nanofluids. It is concluded that the Al₂O₃ nanofluid can be applied as coolant in a helically coiled tube at 0.1% and 0.4% particle volume concentrations without significant pressure drop.

Keywords: Al₂O₃/water nanofluid, Dean number, effective thermal conductivity, helical coil, inner Nusselt number, particle volume concentration.

INTRODUCTION

As conventional heat transfer fluids have exhausted their cooling capacity, nanotechnology is trying to overcome the hurdles faced by the existing conventional heat transfer fluids. Choi [1] introduced a new class of heat transfer fluids with 1-100 nm sized suspended nanoparticles in a base fluid and conceived the concept of heat transfer nanofluids in 1995. Subsequently, it was reported that thermal performance of nanofluids is better than that of water. Wang *et al.* [2], Lee *et al.* [3], Das *et al.* [4], and Li *et al.* [5] reported the effect of a nanofluid on the friction factor. Based on the aspect of enhanced heat transfer of the nanofluid, many researchers tried recently to apply a nanofluid as coolant. The nanofluid has a higher convective heat transfer coefficient than water, which increases with increasing mass flow rate [6]. The results were validated by simulations with empirical equations. The use of CuO and TiO₂/water nanofluids can significantly enhance the convective heat transfer in laminar flow regime.

The viscosity of Al₂O₃/water nanofluids significantly decreases with increasing temperature. The viscosity of the Al₂O₃-water nanofluid is in nonlinear relation with the concentration even in the low (0.01%–0.3%) volume concentration range. It is found that the measured value of nanofluid viscosity agrees well with the values predicted by the model of Lee *et al.* [7]. They observed that the heat transfer coefficient in the nanofluids is higher than that in water. Rea *et al.* [8] found that the pressure loss for nanofluids is much higher than for pure water. They suggested that the rotational Brownian motion of nanoparticles enhances heat transfer. For a nanofluid to be an efficient coolant, the nanoparticles should have a spherical shape and higher critical dilution limit of nanoparticle volume concentration [9].

The effective viscosity of Al₂O₃/water nanofluid nonlinearly increases with the volume concentration of nanoparticles even in the very low range (0.02–0.3 vol %) and strongly depends on the ratio of the nanoparticle diameter to the tube diameter [10]. The nanofluids with low concentrations can enhance the heat transfer efficiency up to 45% in comparison with pure water

* To whom all correspondence should be sent:
E-mail: pcmukeshkumar1975@gmail.com

[11]. The use of a nanofluid gives better thermal performance than pure water [12]. A liquid metal with low melting point and high thermal conductivity is expected to act as an ideal solution for ultimate coolant [13]. An experiment with a multi-channel heat exchanger (MCHE) carried out by Jwo *et al.* [14] showed the nanofluids have a considerable potential for use in electronic chip cooling systems. Most of the studies have been done on a straight tube, as the flow pattern is simple. In case of a helically coiled tube, the flow pattern is complex. A dimensionless Dean number relates inertia force and centrifugal force in a flow through a curved pipe or channel. Dean number measures the secondary flow and the effect of curvature of bend/coil [15]. Correlations for Nusselt number (Nu), incorporating Dean number (De), and helical number (He) have been proposed by Salimpour [16]. Prabhanjan *et al.* [17] have found the helically coiled tubes are superior to straight tubes when employed in heat transfer applications using conventional fluid and the curvature of the tube plays an important role in enhancing heat transfer rate. The Reynolds number was replaced by the Dean number which takes into account the curvature effect [18]. The experiment was carried out on a residual heat removal system using helically coiled tube [19]. The friction factor of a helical coil tube was studied by Srinivasan [20] on varying the coiled tube diameter. The critical Reynolds number in a curved tube flow relates the coil pitch and the coil diameter. The formation of a secondary flow depends on the curvature radius and the Dean number. The addition of nanoparticles to the base fluid enhances the heat transfer coefficient [21]. The nanoparticles volume concentration does not affect the secondary flow, axial velocity and skin friction factor [22]. The heat transfer enhancement has a positive effect due to the presence of nanoparticles [23].

Very few works have been reported on helical coils with nanofluids. Moreover, the pressure drop plays an important role in the heat exchanger. Therefore, in this investigation, the effect of an Al₂O₃/water nanofluid on the heat transfer and pressure drop of a helically coiled tube heat exchanger is examined.

MATERIALS AND METHODS

Preparation of Al₂O₃ / water nanofluids

The Al₂O₃ nanoparticles was purchased from Alfa Aesar, USA. The Al₂O₃ nanoparticles were characterized by XRD (Rigaku Cu- k_{α1} X ray diffractometer). The average particle size was

calculated from the XRD pattern of the nanoparticles to be between 45 and 50 nm with an error within ±5 nm. In this investigation 0.1%, 0.4%, 0.8% Al₂O₃/water based nanofluids were prepared by a two-step method. The required amount of nanoparticles was dispersed in distilled water. Ultrasonic bath (Toshiba, India) generating ultrasonic pulses of 100 W at 36±3 kHz was switched on for 9 hours to get uniform dispersion and stable suspension of nanoparticles. Fig.1 illustrates the scanning electron microscope (Jeol JSM 6360 SEM) image of the agglomerated nanoparticles in the base fluid.

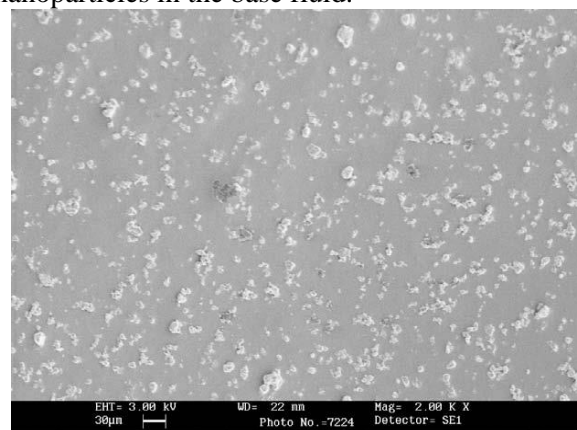


Fig. 1. SEM image of Al₂O₃ nanoparticles

The SEM image was obtained after ultrasonicated the nanoparticles to achieve stability, placing the sample on the sample holder, and rapid drying for getting solid conductive particles. The SEM image shows that the nanoparticles are uniformly dispersed, stable, less agglomerated and spherical in shape.

Experimental setup

Fig.2. illustrates the scheme of the experimental setup. The set-up has shell side loop and helical coiled tube side loop. Shell side loop handles hot water. Helical coiled tube loop handles Al₂O₃/water nanofluid. The shell side flow and the coiled tube side flow are in counter flow configuration. Shell side loop consists of a storage vessel with a heater of 1.75 kW capacity, magnetic pump and thermostat. The tube side loop consists of mono block pump, valve to control the flow on the tube side, test section, cooling unit and storage vessel of five liter capacity. The helical tube is made up of copper and shell is made up of mild steel. The temperature of the hot water in the shell side storage vessel is maintained by a thermostat. Four 'K'-type thermocouples of 0.1°C accuracy are used to measure the inlet and outlet temperatures of shell and tube side. Four 'K'-type thermocouples of

0.1°C accuracy are placed on the outer surface of the coiled tube to measure the tube wall temperatures. U-tube mercury manometer is placed across the helical tube to measure the pressure drop. The shell is insulated with fiber wool. A valve is provided in the flow pipe connecting the cooler section and the reservoir for flow rate measurements and cleaning the system between experimental runs.

The dimensions of the test section are: helical tube internal diameter (d_i) – 10 mm, external diameter of helical tube - 11.5 mm, shell external diameter - 124 mm, effective length (L) of the coil -170 mm, coil pitch (B) – 17 mm, length of calming section – 70 mm, coil diameter (D) - 93 mm.

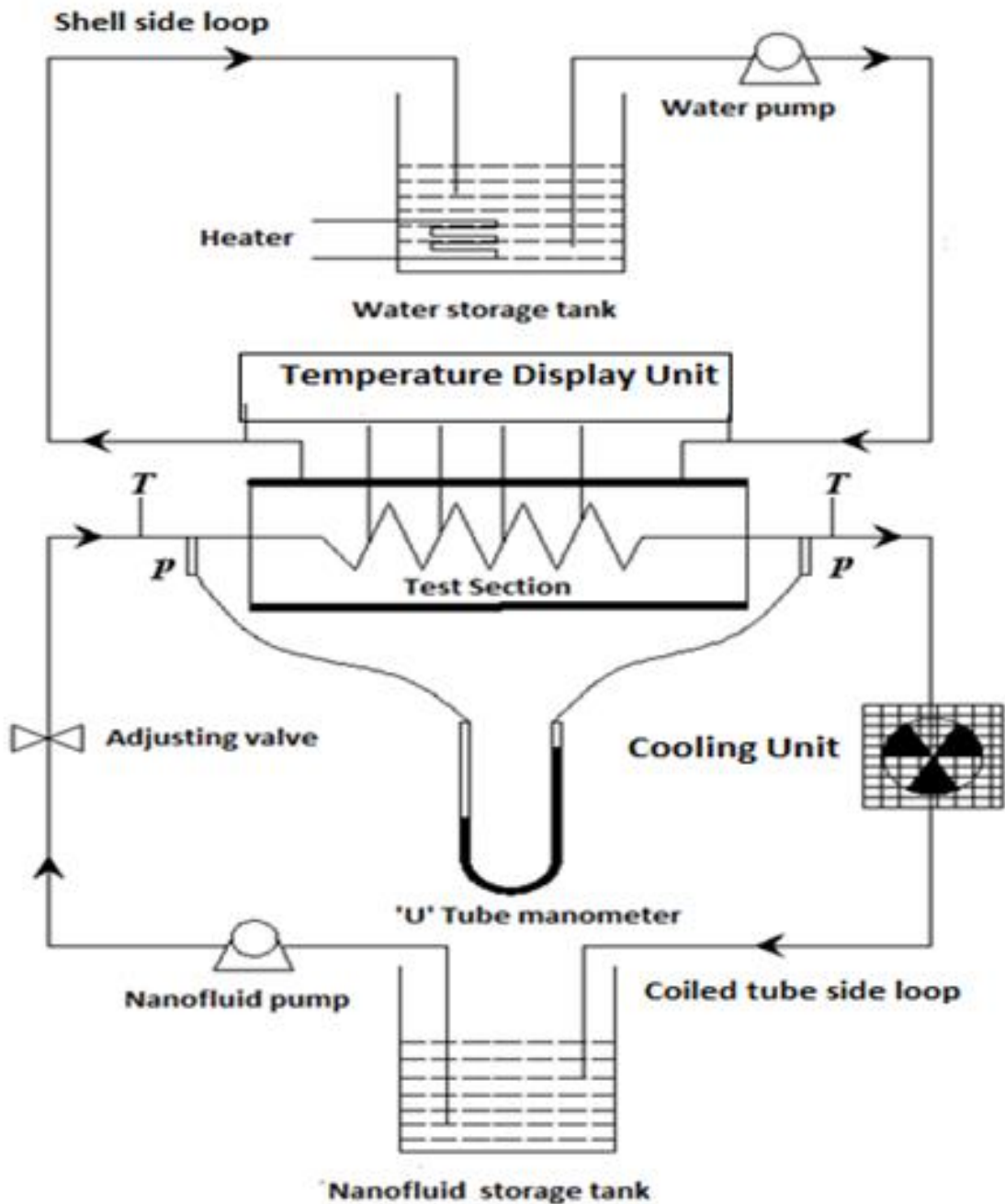


Fig. 2 . Schematic diagram of the experimental setup. T- Thermocouple, P-Pressure measuring port, Ts- Thermocouple for measuring surface temperature

Experimental procedure

Hot water and cold water were supplied to the shell side and the tube side, respectively, to check for leakages and test the accuracy of thermocouples and thermostat. Hot water was circulated to the shell side at a constant flow rate. The nanofluid with 0.1%, particle volume concentration was circulated through the tube side. The corresponding observations were made. The tube side flow was varied to attain the specified Dean number by using valve arrangement. Flow rate on the shell side was kept constant (0.15 kg/sec). The flow rate on the tube side was in the range of 0.03-0.05 kg/sec in laminar flow. The coil pitch was maintained constant throughout the test. The same procedure was followed for the 0.4% and 0.8% nanofluids. The uncertainty analysis was carried out by the Coleman and Steele method [24] and ANSI/ASME standards [25] considering measurement errors. The uncertainties involved in the measurements were about ±3% and ±2.5% for the Nusselt number and the Dean number, respectively.

Estimation of thermo-physical properties of the nanofluid

The specific heat capacity of the Al₂O₃/water nanofluid was estimated using Eqn. (1) given by Xuan and Roetzel [26].

$$(\rho c_p)_{nf} = (1 - \phi)(\rho c_p)_w + \phi(\rho c_p)_s \quad (1)$$

The thermal conductivity of Al₂O₃/water nanofluids was measured at 30°C with a KD2 Pro thermal analyzer. It is seen in Fig.3 that thermal conductivity increases with increasing particle volume concentration.

The measured thermal conductivity holds decent agreement with the estimated nanofluid thermal conductivity model proposed by Chandrasekar *et al.* [27]. The viscosity was measured at 30°C with a Brookfield cone and a plate viscometer (LVDV-I PRIME C/P). It is seen in Fig.4 that the viscosity increases with increasing particle volume concentration.

The measured viscosity holds decent agreement with the estimated viscosity of the nanofluid model proposed by Chandrasekar *et al.* [27].

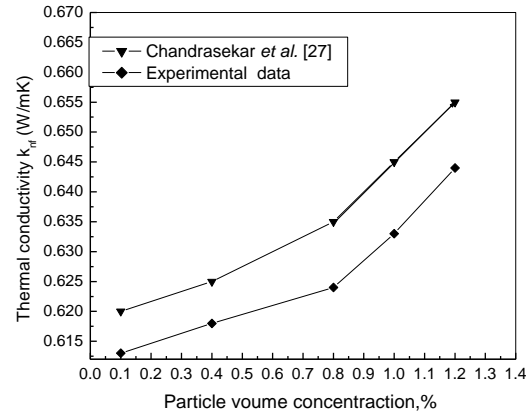


Fig. 3. Variation of the thermal conductivity of the Al₂O₃/water nanofluid with particle volume concentration

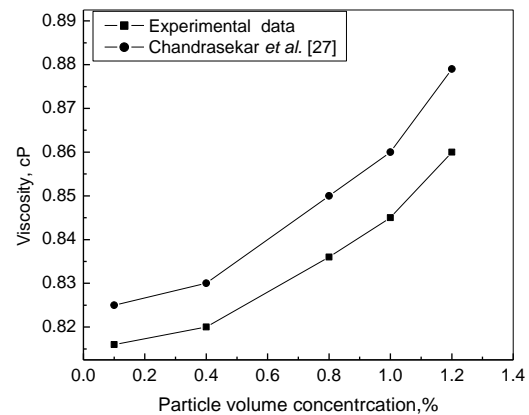


Fig. 4 Variation of viscosity with particle volume concentration.

Calculation of experimental inner Nusselt number and friction factor

The heat transfer for water and nanofluid was estimated from Eqns. (2) and (3). The inner heat transfer coefficient was calculated from Eqn. (4).

$$Q_{nf} = m_{nf} c_{p,nf} (T_{in} - T_{out})_{nf} \quad (2)$$

$$Q = h_i A_i (T_{wall} - T_{bulk}) \quad (3)$$

$$Q_w = m_w c_{p,w} (T_{in} - T_{out})_w \quad (4)$$

$$Nu_i = h_i d_i / k_{eff} \quad (5)$$

The experimental tube side Nusselt number was estimated from Eqn. (5) and it measures the convective heat transfer in the helical tube. It is a function of Dean number (De) and Prandtl number (Pr), coil pitch and curvature radius.

RESULTS AND DISCUSSION

Heat transfer coefficient

Fig.5 shows the effect of increasing the particle volume concentration on the tube side experimental Nusselt number under laminar flow.

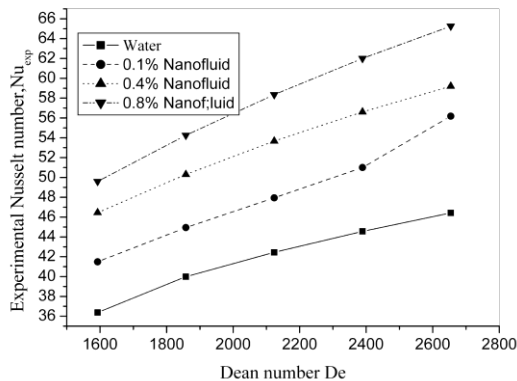


Fig. 5. Experimental inner Nusselt number *versus* inner Dean number

It is clear that the tube Nusselt number increases with particle volume concentration and Dean number. At a fixed Dean number, the enhancement of tube side experimental Nusselt number for 0.1%, 0.4% and 0.8% nanofluids is by 21%, 28% and 42% than water. This may be due to the better mixing of Al₂O₃ nanoparticles and the higher effective thermal conductivity of nanofluid. The Nusselt number increases with Dean number, as the formation of secondary flow is getting stronger and thinning of the boundary layer takes place. The increasing nanofluid conductivity and decreasing thermal boundary thickness are the reasons for enhancing heat transfer coefficient in a shell and tube heat exchanger when a nanofluid is passing through the coiled tube.

Based on the experimental data, a Nusselt number correlation (Eqn. 6) was developed for a laminar flow in the range of 1600 < De < 2700. Fig. 6 shows the comparison between experimental and predicted Nusselt number.

$$Nu_i = 1.12De^{0.45} Pr^{0.1} \delta^{0.06} \phi^{0.07} \quad (6)$$

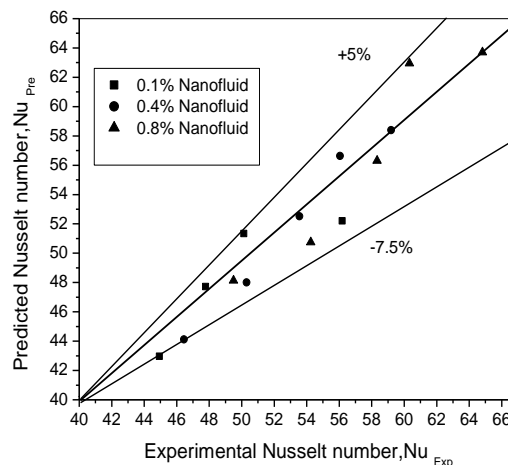


Fig. 6. Comparison between experimental and predicted inner Nusselt number

The deviation between the predicted and the experimental Nusselt number was found to be in the range of ± 7.5 under laminar flow conditions.

Effect of pressure drop

Fig. 7 shows that the pressure drop increases with increasing particle volume concentration and mass flow rate.

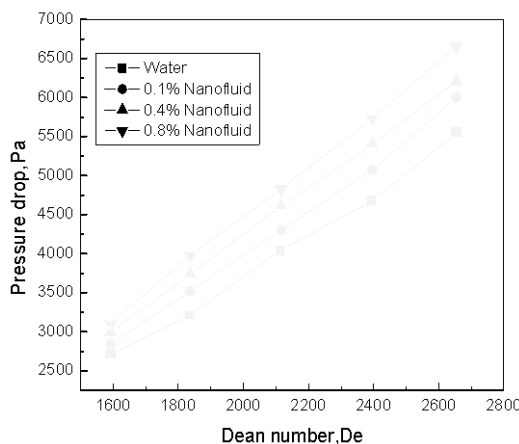


Fig. 7. Variation of experimental pressure drop with Dean number in a laminar flow

The pressure drop in 0.1 %, 0.4% and 0.8% nanofluids is higher by 8%, 12% and 20%, respectively, than in water at De = 2650. This is due to the increased density and viscosity at higher particle volume concentrations. It is observed that the rate of pressure drop increased when Dean number increased. The rate of increase of pressure drop at De = 1600 is smaller than at De = 2650 because the effect of viscosity dominates at low velocity.

CONCLUSION

In this paper, heat transfer and pressure drop studies of a shell and helically coiled tube heat exchanger with Al₂O₃/ water nanofluid were carried out under laminar flow. The increase in Nusselt number was found to be 21%, 28% and 42% at 0.1%, 0.4% and 0.8% of Al₂O₃/water nanofluid particle volume concentration respectively, when compared with water. The main reason is the higher effective thermal conductivity of nanofluid. Based on the experimental data, a Nusselt number correlation was developed for a helically coiled tube. The deviation between the predicted and experimental Nusselt number was found to be in the range of $\pm 7.5\%$. It is found that the pressure drop increases with increasing particles volume concentration and Dean number. It is concluded that the Al₂O₃/water nanofluid can be applied as coolant in a shell and helical coiled tube heat exchanger at 0.1% and 0.4% low particle volume concentration without significant pressure drop with heat transfer enhancement.

NOMENCLATURE

A	Surface area, m ²
C _p	Specific heat capacity J/kg K
d _i	Inner Diameter of tube, m
De	Dean number = $Re_i (d_i / 2R_c)^{0.5}$
h	Convective heat transfer coefficient, W/m ² K
k	Thermal conductivity, W/m K
Nu	Nusselt number = $h_i d_i / k_{eff}$
Pr	Prandtl number = $C_{p,nf} \mu_{nf} / k_{eff}$
Q	Heat transfer rate, W
Rc	Curvature radius, m
T	Temperature, K
v _i	Velocity, m/s

Greek letters

ρ	Density, kg/m ³
ϕ	Particle volume concentration (%)
μ	Dynamic viscosity, kg/m ² s
δ	Inner tube radius /mean coil radius R

Subscripts

cr	Critical
eff	Effective
in	Inlet
nf	Nanofluid
m	mean
out	Outlet
s	Surface
w	Water

REFERENCES

1. S.U.S. Choi, *ASME FED*, **66**, 99 (2006).
2. X. Wang, Xu, S.U.S. Choi, *J. Therm. Phys. and Heat trans.*, **13**, 474 (1999).
3. S. Lee, S.U.S. Choi, S. Li, J.A. Eastman, *J. Heat Trans.*, **121**, 280 (1999).
4. S.K. Das, N. Putra, P. Thiesen, W. Roetzel, *J. Heat Trans.*, **125**, 567 (2003).
5. X.F. Li, D.S. Zhu, X.J. Wang, J.W. Goa, H. Li, *Thermochim. Acta*, **469**, 98 (2008).
6. G. Huminic, A. Huminic, *Int. J. Heat and Mass Trans.*, **54**, 4280 (2011).
7. J.H. Lee, K.S. Hwang, S.P. Jang, B.H. Lee, J.H. Kim, S.U.S. Choi, C.J. Choi, *Int. J. Heat and Mass Trans.*, **51**, 2651 (2008).
8. U. Rea, T. McKrell, L.W. Hu, J. Buongiorno, *Int. J. Heat and Mass Trans.*, **52**, 2042 (2009).
9. K. Kwak, C. Kim, *Korea-Australia Rheology J.*, **17**, 35 (2005).
10. S.P. Jang, J.H. Lee, K.S. Hwang, *Appl. Phys. Lett.*, **91**, 243112 (2007).
11. S.M. Peyghambarzadeh, S.H. Hashemabadi, M.S. Jamnani, S.M. Hoseini, *Appl. Thermal Engng.*, **31**, 1833 (2011).
12. V. Vasu, K.R. Krishna, A.C.S. Kumar, *Int. J. Nanotech. Appl.*, **2**, 75 (2008).
13. K.Q. Ma, J. Liu, *Phys. Lett.*, **361**, 252 (2007).
14. C.S. Jwo, L.Y. Jeng, T.P. Teng, C.C. Chen, *J. Alloys and Compounds*, doi:10.1016/j.jallcom.2010.02.05. (2010).
15. W.R. Dean, *Philos. Mag.*, **4**, 208 (1927).
16. M.R. Salimpour, *Exp. Therm. and Fluid Sci.*, **33**, 203 (2009).
17. D.G. Prabhanjan, G.S.V. Ragavan, T.J. Rennie, *Int. Commun. in Heat and Mass Trans.*, **29**, 185 (2002).
18. Y. Moris, W. Nakayana, *Int. J. Heat and Mass Trans.*, 867 (1965).
19. J.S. Jayakumar, S.M. Mahajani, J.C. Mandal, P.K. Vijayan, R. Bhoi, *Chem. Engng. Research and Design*, **86**, 221 (2008).
20. P.S. Srinivasan, S. Nandapurkar, F.A. Holland, *Int. J. Chem. Engng. Trans.*, **48**, T156 (1970).
21. V. Kumar, K.D.P. Nigam, *Int. J. Heat Mass Trans.*, **48**, 4811 (2005).
22. A. Akbarinia, *Int. J. Heat and Fluid Flow*, **29**, 229 (2008).
23. A. Akbarinia, A. Behzadmehr, *Appl. Therm. Engng.*, **27**, 1327 (2012).
24. H.W. Coleman, W.G. Steele, *Experimental and uncertainty analysis for engineers*, Wiley, New York, (1989).
25. ANSI/ASME, 1986, Measurement of uncertainty, *PTC 19*, 1-1985 (1986).
26. Y. Xuan, W. Roetzel, *Int. J. Heat and Mass Trans.*, **43**, 3701 (2000).
27. M. Chandrasekar, S. Suresh, A. Chandra Bose, *Exp. Therm. Fluid Sci.*, **34**, 210 (2010).

АНАЛИЗ НА ТОПЛООБМЕНА И ХИДРАВЛИЧНОТО СЪПРОТИВЛЕНИЕ НА НАНОФЛУИД ОТ Al₂O₃ КАТО ОХЛАДИТЕЛ В КОЖУХО-ТРЪБНИ И СПИРАЛНИ ТОПЛООБМЕННИЦИ

П. К. Мукеш Кумар^{*1}, Дж. Кумар², С. Сендинатан¹, Р. Тамилаасан^{1*}, С. Суреш³

¹Университетски колеж по инженерство Патукотаи, Тамил Наду, Индия

²Сасури колеж по инженерство, Тамил Наду, Индия

³Национален технологичен институт. Тричи, Индия

Постъпила на 20 септември, 2013 г.; Коригирана на 4 март, 2014 г.

(Резюме)

В тази работа са изследвани топлообмена и хидравличното съпротивление на нанофлуид от Al₂O₃ като охладител в кожухо-тръбни и спирални топлообменници. Обемните концентрации на частиците от 0.1%, 0.4% и 0.8% са приготвени по двустепенен метод. Беше установено, че повишаването на числото на Нуселт за вътрешността на топлообменника спрямо водата като топлоносител са 21%, 28% and 42% при добавени съответно 0.1%, 0.4% и 0.8% нанофлуид при ламинарно течение. Това може да се дължи на по-доброто смесване и по-високата топлопроводност на нанофлуида. Предложена е корелация за числото на Нуселт на основание на експериментални данни. Установено е отклонение от $\pm 7.5\%$ между предсказаните и опитните стойности на числото на Нуселт. Хидравличното съпротивление при наличие на 0.1%, 0.4% и 0.8% нанофлуиди е с 8%, 12% и 20% по-високо, отколкото във вода. Това се дължи на повишения вискозитет на смесите с нанофлуиди. Установено е, че нанофлуидите с Al₂O₃ може да се прилагат като охлаждащи течности в спирални топлообменници без значимо повишаване на хидравличното съпротивление.

Synthesis of some new thiadiazole derivatives and their anticonvulsant activity

M. A. Rahman¹, A. K. Shakya², S. Wahab², N. H. Ansari^{3*}

¹Department of Pharm. Chemistry, Azad Institute of Pharmacy and Research Lucknow, Uttar Pradesh, India.

²Faculty of Pharmacy, Integral University, Lucknow, Uttar Pradesh, India.

³Department of Chemistry, Rajdhani College, University of Delhi, New Delhi.

Received, September 27, 2013; Revised January 3, 2014

A new series of 1,3,4-thiadiazole derivatives was synthesized and the structures of these compounds were established by means of IR, ¹H-NMR and elemental analysis. The compounds AR-5, AR-6, AR-7, AR-8 and AR-14 were screened for anticonvulsant activity on albino mice. Most of these compounds showed promising anticonvulsant activity. Structural modification of these compounds may lead to the discovery of more potent anticonvulsant agents with lower neurotoxicity.

Keywords: - I, 3, 4-thiadiazole, Anticonvulsant activity; Maximum Electroshock Seizure (MES)

INTRODUCTION

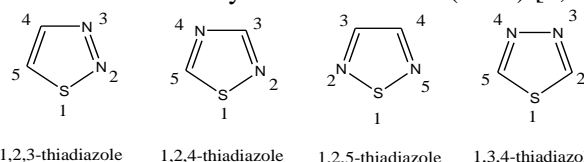
1,3,4-thiadiazoles are associated with diverse biocidal activities [1-5]. A large number of 1,3,4-thiadiazoles have been reported as anticancer, antitubercular, anti-inflammatory, and pesticide agents. These observations prompted us to synthesize the title compounds presuming that incorporation of amine derivatives would produce new compounds with significant anticonvulsant activity.

Medicinal chemistry is offering today many complicated challenges [6]. The most difficult and sometimes the most rewarding challenge is the rational design of new therapeutic agents for treating human diseases. For many years the strategy for discovering new drugs consisted of taking a lead structure and developing a chemical program for finding analogue molecules which would exhibit the desired biological properties.

After several trial-and-error cycles, the medicinal chemist would select a candidate analogue for further development. The entire process is laborious, expensive and time consuming. However, the fact is that most of the drugs that are in use today have been provided by this process.

Thiadiazole is a five-membered heterocyclic compound. It contains two nitrogen atoms and one sulfur atom. The first thiadiazole was described by Fischer (1882), but the nature of the ring system

was demonstrated by Freud and Kuhn (1890) [7, 8].



1,2,3-thiadiazole is a yellowish liquid at room temperature [10]. It boils at 157°C at normal atmospheric pressure and is soluble in alcohol, ether and water [11]. It is stable in acids but decomposes in bases with evolution of nitrogen. The compound is a weak base and forms a deliquescent hydrochloride, which get decomposed by water to its components.

1,2,4-thiadiazole is a colorless, mobile liquid, boiling at 121°C, freezing at 33°C, possessing an odor similar to that of pyridine [12,13].

1,3,4-thiadiazole is a colorless quite stable compound melting at 42°C and possessing no ultraviolet absorption maximum above 220 nm. Zinc and hydrochloric acid or 30 % hydrogen peroxide destroy the compound. 1,3,4-Thiadiazole is more stable towards the peroxide than the 1,2,4-isomer. Aqueous alkalis decompose the compound, however 1,3,4-thiadiazole is quite stable towards mineral acids [14].

1,3,4-thiadiazoles represent one of the most biologically active classes of compounds, possessing a wide spectrum of activities. A triazolo thiadiazole system may be viewed as a cyclic analogue of two very important components thiosemicarbazide and biguanide, which often display diverse biological activities, stopping multiplication of bacteria. This has made them

* To whom all correspondence should be sent:
E-mail: nizam123jmi@gmail.com

unique for the control of deadly infectious diseases caused by a variety of pathogens.

Members of the 1,3,4-thiadiazole ring system have found diverse applications as pharmaceuticals, antioxidants, cyanine dyes and metal complexing agents [8].

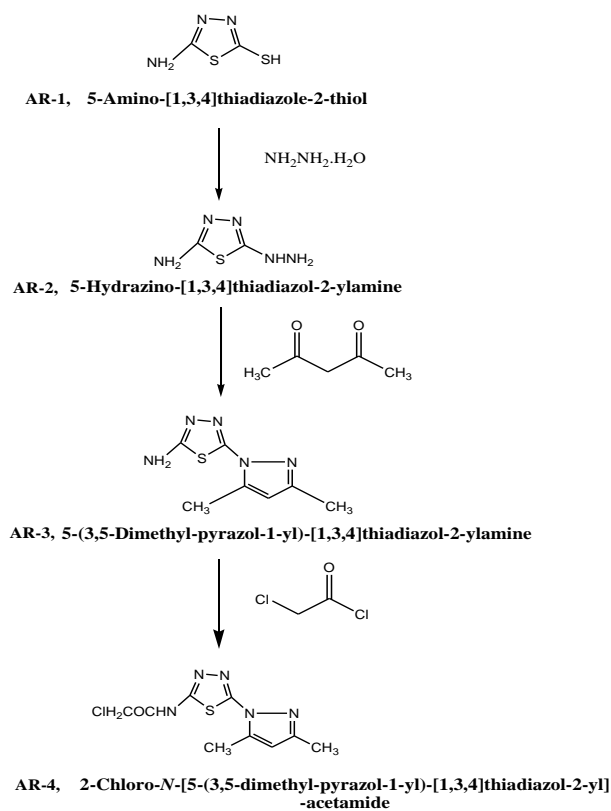
EXPERIMENTAL

General scheme for synthesis

The general methods for the synthesis of compounds bearing a five-membered heterocyclic ring for obtaining new derivatives of thiadiazoles have been used in our laboratory for a long time. Various substituted amine derivatives, piperidine, aniline, and 2-amino-oxazole derivatives were prepared.

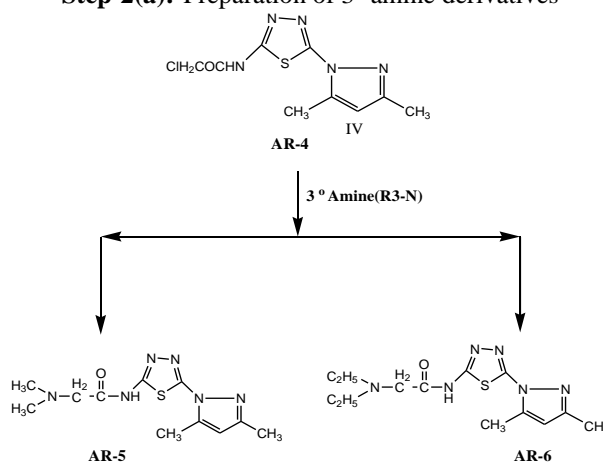
Scheme

Step-1: Preparation of intermediate

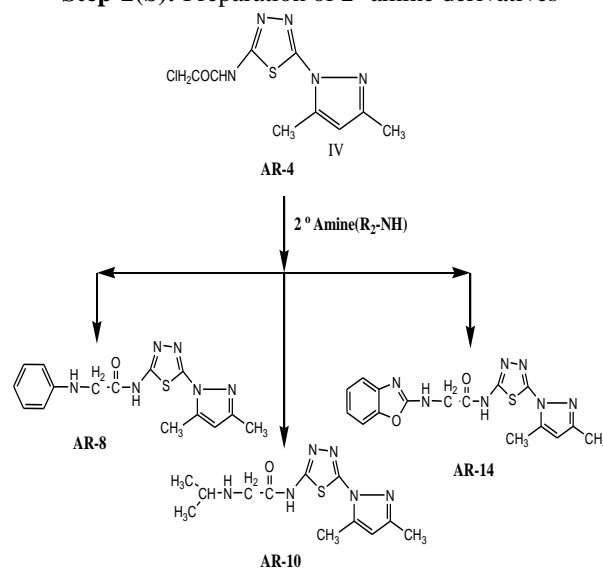


Step-2: Synthesis of derivatives:

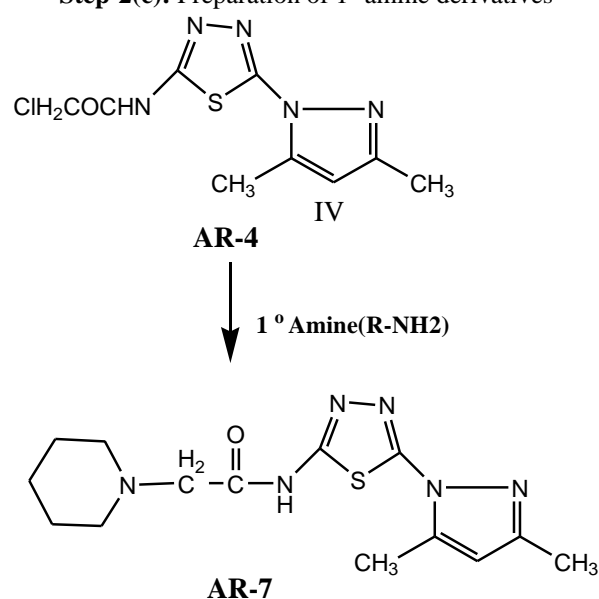
Step-2(a): Preparation of 3^o amine derivatives



Step-2(b): Preparation of 2^o amine derivatives



Step-2(c): Preparation of 1^o amine derivatives

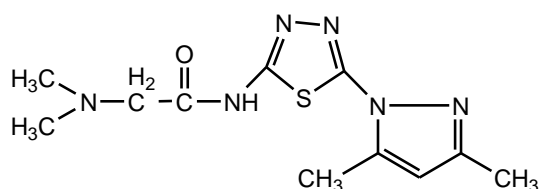


RESULTS AND DISCUSSION

The synthesis started from 2-amino-5-mercapto-1,3,4-thiadiazole (**AR-1**), the thiol group of compound **AR-1** was readily converted into the hydrazino derivative **AR-2** by heating under reflux with an ethanolic solution of hydrazine hydrate. The resulting 2-amino-5-hydrazino-1,3,4-thiadiazole was used for the synthesis of interesting derivatives as a versatile key intermediate for the synthesis of some fused heterocyclic rings. Thus, the interaction of **AR-2** with acetyl acetone and carbon disulfide gave rise to the formation of 2-amino-5-(3,5-dimethyl-1H-pyrazole-1-yl)-1,3,4-thiadiazole (**AR-3**) which reacted with an equimolar quantity of chloroacetyl chloride and produced 2-chloro-N-[5-(3,5-dimethyl-pyrazol-1-yl)-[1,3,4] thiadiazol-2-yl]-acetamide (**AR-4**). The latter, on reaction with various amines (equimolar amounts in ethanol), produced the compounds **AR-5**, **AR-6**, **AR-7**, **AR-8**, **AR-10**, and **AR-14**. The structure of the synthesized compounds was established on the basis of ¹H-NMR and IR spectral data. In all cases TLC of the product showed the presence of one single spot referring to only one product.

Spectral characterization of the compounds

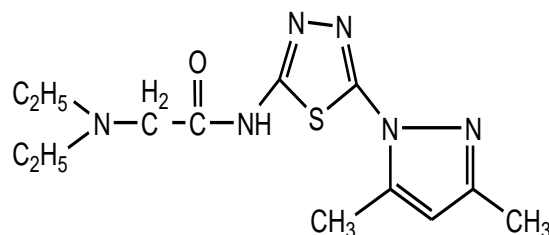
N-(5-(3,5-dimethyl-1-H-pyrazol-1-yl)-1,3,4-thiadiazol-2-yl)-2-(dimethyl amino) acetamide (**AR-5**)



IR (KBr) cm⁻¹

The spectrum of the compound showed absorption bands at: 3410 cm⁻¹ (CO-NH₂ stretching), 2984 cm⁻¹ (CH₃ stretching), 2363 cm⁻¹ (aromatic CH₃ stretching), 1728 cm⁻¹ (-NH stretching), 1600 cm⁻¹ (C=O stretching), 1437 cm⁻¹ (C=N stretching), 1295 cm⁻¹ (C-N stretching), 1104 cm⁻¹ (N-N stretching), 666 cm⁻¹ (C-S-C stretching).

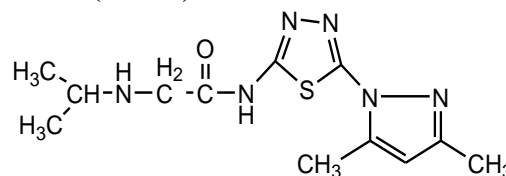
2-(Diethyl amino)-N-(3, 5-dimethyl-1H-pyrazol-1-yl)-1,3,4-thiadiazole-2-yl) acetamide (**AR-6**)



IR (KBr) cm⁻¹

The spectrum of the compound showed absorption bands at: 3423 cm⁻¹ (CO-NH₂ stretching), 2968 cm⁻¹ (aromatic CH₃ stretching), 2495 cm⁻¹ (CH₂ stretching), 1591 cm⁻¹ (C=O stretching), 1379 cm⁻¹ (C=C stretching), 1281 cm⁻¹ (C-N stretching), 1062 cm⁻¹ (N-N stretching), 667 cm⁻¹ (C-S-C stretching).

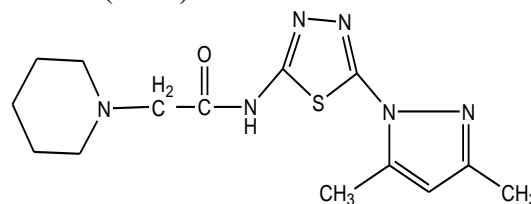
Synthesis of N-(5-(3,5-dimethyl-1H-pyrazol-1-yl)-1,3,4-thiadiazol-2-yl)-2-(isopropyl amino) acetamide (**AR-10**)



IR (KBr) cm⁻¹

The spectrum of the compound showed absorption bands at: 3410 cm⁻¹ (CO-NH₂ stretching), 2981 cm⁻¹ (aromatic CH₃ stretching), 2362 cm⁻¹ (CH₂ stretching), 1722 cm⁻¹ (C=O stretching), 1628 cm⁻¹ (C=C stretching), 1026 cm⁻¹ (N-N stretching), 667 cm⁻¹ (C-S-C stretching).

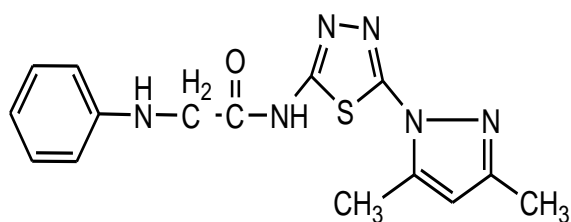
Synthesis of N-(5-(3,5-dimethyl-1H-pyrazol-1-yl)-1,3,4-thiadiazol-2-yl)-2-(piperidin-1-yl) acetamide (**AR-7**)



IR (KBr) cm⁻¹

The spectrum of the compound showed absorption bands at: 3437 cm⁻¹ (CO-NH₂ stretching), 2949 cm⁻¹ (aromatic CH₃ stretching), 2532 cm⁻¹ (CH₂ stretching), 1572 cm⁻¹ (C=O stretching), 1499 cm⁻¹ (C=N stretching), 1024 cm⁻¹ (N=N stretching), 667 cm⁻¹ (C-S-C stretching).

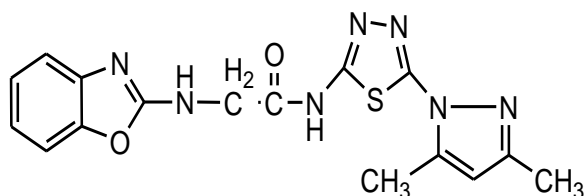
Synthesis of N-(5-(3,5-dimethyl-1H-pyrazol-1-yl)-1,3,4-thiadiazol-2-yl)-2-(phenyl amino) acetamide (**AR-8**)



IR (KBr) cm^{-1}

The spectrum of the compound showed absorption bands at: 3374 cm^{-1} (CO-NH₂ stretching), 3008 cm^{-1} (aromatic CH₃ benzene), 2365 cm^{-1} (CH₂ stretching), 1603 cm^{-1} (C=O stretching), 1562 cm^{-1} (C=N stretching), 1492 cm^{-1} (C=C stretching), 1028 cm^{-1} (N=N stretching), 667 cm^{-1} (C-S-C stretching).

Synthesis of 2-(benzo[d]oxazol-2-yl amino)-N-(5-(3,5-dimethyl-1H-pyrazol-1-yl)-1,3,4-thiadiazol-2-yl) acetamide (AR-14)



IR (KBr) cm^{-1}

The spectrum of the compound showed absorption bands at: 3776 cm^{-1} (CO-NH₂ stretching), 3429 cm^{-1} (CH₃ stretching), 3023 cm^{-1} (aromatic CH₃ benzene stretching), 2364 cm^{-1} (CH₂ stretching), 1628 cm^{-1} (C=O stretching), 1438 cm^{-1} (C=N stretching), 1022 cm^{-1} (N=N stretching), 670 cm^{-1} (C-S-C stretching).

Doses of 30, 100 and 300 mg/kg were administered i.p. The values in the table indicate the minimum dose whereby bioavailability was demonstrated in half or more of the mice. The animals were examined 0.5 and 4 h after injections were made. The dash (-) indicates an absence of activity at the maximum dose administered (300 mg/kg).

Table 1: Anticonvulsant activity of the synthesized derivatives

S.No	Compound No.	MES	
		0.5h	4h
1.	AR-5	100	300
2.	AR-6	30	100
3.	AR-8	100	100
4.	AR-14	300	300
5.	AR-7	30	100
6.	Phenytoin	30	30
7.	Carbamazepine	30	100

Table 2: Minimum motor impairment of the synthesized derivatives

S.No	Compound No.	TOXICITY SCREEN	
		0.5h	4h
1.	AR-5	100	300
2.	AR-6	30	100
3.	AR-8	300	300
4.	AR-14	30	300
5.	AR-7	30	300
6.	Phenytoin	30	30
7.	Carbamazepine	30	100

Doses of 30, 100 and 300 mg/kg were administered i.p. The figures in the table indicate the minimum dose whereby bioavailability was demonstrated in half or more of the mice. The animals were examined 0.5 and 4 h after injections were made. The dash (-) indicates an absence of activity at maximum dose administered (300mg/kg).

Anticonvulsant activity

The anticonvulsant activity was tested using a reported procedure. Albino mice (Swiss strain) of either sex weighing 20-25 g were acclimatized to their environment for at least two days before the experiment. The animals were allowed to free access to water before the test.

In order to reveal the potential anticonvulsant profile of the synthesized compounds, the MES model was employed in accordance with the anticonvulsant drug development (ADD) Protocol. The anticonvulsant activity of compounds **AR-5**, **AR-6**, **AR-7**, **AR-8** and **AR-14** in mice was evaluated at dose levels of 30, 100 and 300 mg/kg i.p. MES-maximum electroshock seizure and NT-neurotoxicity screening are summarized in tables **1** and **2** together with literature data on standard drugs (phenytoin and carbamazepine) (fig.1&2).

The compounds **AR-6**, **AR-7** exhibited fifty percent or more protection after 0.5 h at a lower dose of 30 mg/kg. These compounds showed activity comparable to phenytoin and carbamazepine. Compounds **AR-5** and **AR-8** were also active at low doses. At 100 mg/kg the compounds that showed protection were **AR-5(0.5h, 4h)**, **AR-6(0.5h, 4h)**, **AR-7(0.5h)**, and **AR-8(4h)**; compound 14 showed activity only at a higher dose level (300 mg/kg). This shows that all synthesized compounds are more or less active against the spread of seizures.

It is evident from table **2** that the compounds are less neuro-toxic than the standard drugs phenytoin and carbamazepine.

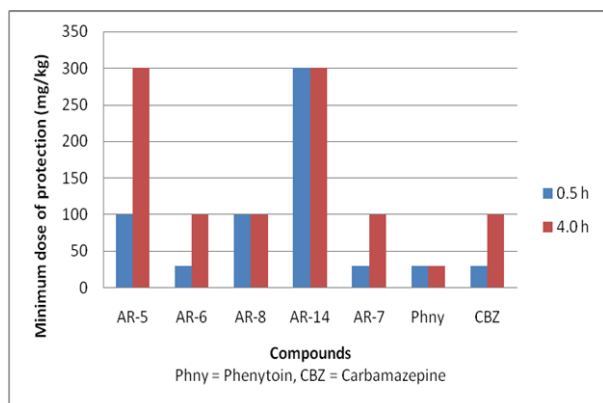


Fig. 1. Anticonvulsant activity of the synthesized compounds (AR-5,6,7,8,14)

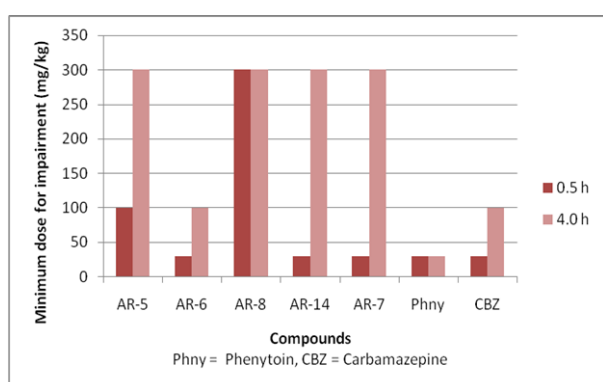


Fig. 2. Minimum motor impairment of the synthesized compounds (AR-5,6,7,8,14)

SUMMARY

The present study showed that the anticonvulsant activity of the investigated compounds depends upon the lipophilic nature of the ring due to the "S" moiety. We reported in this study the general approach for preparation of substituted 1,3,4-thiadiazole derivatives having various biological activities. The synthesized compounds were identified on the basis of their spectral data [15-17].

The results indicate that the constituents (dimethylamine, diethylamine, 2-aminobenzoxazole, aniline and piperidine) significantly affect the anticonvulsant activity. Thus, **AR-5**, **AR-8**, and **AR-14** have emerged as the lead compounds with activity in the MES test at 0.5h and 4h. The compounds **AR-6** and **AR-7** were found less neurotoxic. Structural modification of these compounds may lead to the discovery of more potent anticonvulsant agents with lower neurotoxicity.

5-amino-1, 3, 4-thiadiazole-2-thiol (AR-1)

m.p. 232 °C, R_f value 0.78

¹H-NMR (400 MHz, DMSO-d₆, TMS) ppm 7.99 (2H, s, NH₂), 12.93 (H, s, SH). FTIR (KBr) ν_{\max} cm⁻¹ 2553 (S-Hstr, thiol).

2-amino-5-hydrazino-1, 3, 4-thiadiazole (AR-2)

m.p. 242-244 °C, R_f value 0.65

IR: 3400-3250(NHNH₂), 3200, 3168(NH₂), 1600(C=N), 688(C-S). ¹H-NMR (DMSO-d₆) δ : 5.27(s, 2H, NH₂) (D₂O exchange, disappear), 6.00(s, 1H, NH) (D₂O exchange, disappear), 7.08(s, 2H, NH₂) (D₂O exchange, disappear). ¹³C-NMR (DMSO-d₆) δ : 154.7, 161.5 (thiadiazole carbons).

2-amino-5-(3, 5-dimethyl-1H-pyrazole-1-yl)-1, 3, 4-thiadiazole (AR-3)

m.p. 150-152 °C, R_f value 0.72

IR: 3300, 3250(NH₂), 3078(=CH-), 2977, 2850(CH aliphatic). ¹H-NMR (DMSO-d₆) δ : 3.32, 3.48(s, 3H, CH₃), 6.01(s, 1H, =CH-), 7.08(s, 2H, NH₂) (D₂O exchange, disappear). ¹³C-NMR (DMSO-d₆) δ : 17.6(1C, CH₃), 52.1, 56.4(2C, C-CH₃), 96.6(1C, =CH-), 152.1, 163.2 (thiadiazole carbons).

N-(5-(3, 5-dimethyl-1-H-pyrazol-1-yl)-1, 3, 4-thiadiazol-2-yl)- 2-(dimethyl amino) acetamide (AR-5)

m.p. 198-200 °C. R_f value 0.78

IR (KBr): 3410 N-H str 2984-C-H str

1670-CONH- str 1600 C=C str

1217, 1104, 1026, 866 1,3,4-thiadiazole nucleus

2-(diethyl amino)-N-(3,5-dimethyl-1H-pyrazol-1-yl)-1,3,4- thiadiazole-2-yl) acetamide (AR-6)

m.p. 210-212 °C. R_f value 0.65

3423 N-H str 2985 -C-H str.

1650 -CONH- str 1590 C=C str

1218, 1062, 99 1,3,4-thiadiazole

N-(5-(3,5-dimethyl-1H-pyrazol-1-yl)1,3,4-thiadiazol-2-(isopropyl amino) acetamide (AR-10),

M.P. 220-222 °C. R_f value 0.65

3410 N-H str, 2981 -C-H str.

1628 -CONH- str, 1600 C=C str

1218, 1026, 892 1,3,4-thiadiazole

N-(5-(3,5-dimethyl-1H-pyrazol-1-yl)-1,3,4-thiadiazol-2-(piperidin-1-yl) acetamide (AR-7),

m.p. 192-194 °C

R_f value 0.65

3410 N-H str 2981-C-H str. 1628 -CONH- str

1600 C=C str 1218, 1026, 892 1,3,4-thiadiazole
N-(5-(3,5-dimethyl-1H-pyrazol-1-yl)-1,3,4-thiadiazol-2-yl)-2-(phenyl amino) acetamide (AR-8)

m.p. 205 -207 °C.

R_f value **0.65**

3374-NH, 3008 Ar-H, 2970 -CH str.

1951, Mono substituted phenyl ring

1690-NH-CO-, 1603, 1572 C=C stretching,

1218, 1119, 1054, 999 1,3,4-thiadiazole nucleus

2-(benzo[d] oxazol-2-ylamino)-N-(5-(3,5-dimethyl-1H-pyrazol-1-yl)-1,3,4-thiadiazol-2-yl) acetamide (AR-14)

m.p. 234-235 °C.

R_f value **0.65**

3374 NH stretching, 3008 Ar-H,

2970-CH, 1951 Mono substituted phenyl ring

1690-NH-CO-, 1603, 1572 C=C stretching

1218, 1119, 1054, 999, 1,3,4-thiadiazole nucleus

Acknowledgement: The authors are grateful to Dr. Ziaur Rahman and Dr. Wasiur Rahman for providing the facilities to carry out this work.

REFERENCES

- Burger, A., Medicinal Chemistry, 3rd ed. Wiley Interscience, New York; (1970), 3.
- Hogarth, E., in Heterocyclic compounds, Chemistry of carbon compounds, IV A, Rodd, E.H. ed., Elsevier publishing company, New York, (1957), 477.
- Stolle, R., and Fehrenbach. K.J., *Prakt. Chem.*, **122**, 289 (1929).
- Rahim, N.A., Rateb, N.M., Atoom A.A., and Hamid, A.I., *Heteroatom. Chem.*, **14**, 421 (2003).
- Dogan, H.N., Duran, A., Rollas, S., Sener, G., Uysal, M.K., and Gulen, D., *Bioorg. Med. Chem.*, **10**, 2893 (2002).
- Palaska, E., Sahin, G., Kelicen, P., Tulu, N.T., and Altinok, G., *Il Farmaco*, **57**, 101 (2002).
- Mullican, M.D., Wilson, M.W., Connors, D.T., Kostlan, C.R., Schrier, D.J. and Dyer, R.D., *J. Med. Chem.*, **36**, 1090 (1993).
- Karakus, S., and Rollas, S., *Il Farmaco* **57**, 577 (2002).
- Foroumadi, A., Asadipour, A., Mirzaei, M., Karimi, J., and Emami S., *Il Farmaco* **57**, 765 (2002).
- Terzioglu, N., and Gursoy, A., *Eur. J. Med. Chem.*, **38**, 781 (2003).
- Holla, S., PooJary K.N., Rao, B.S., and Shivanada, M.K., *Eur. J. Med Chem.*, **37**, 511 (2002).
- Zou, X.J., Lai, L.H, Jin, G., and Zhang, Z.X., *J. Agric. Food Chem.*, **53**, 3757 (2002).
- Foye W.O., Principles of medicinal chemistry, II, Lea and Febiger eds., Philadelphia, (1981) 452.
- White, H.S., Woodwead, H., Franklin. M.R., Levy, R.H., Mattson, R.H., Meldrum, B.S., eds. Antiepileptic drugs. New York. Raven., **4**, 99(1995).
- Krall, R. I, Penry, J.K White, B.G., Kupferberg, H.J., Swingard, E.A., Antiepileptic drug development II. Anticonvulsant Drug Screening, *Epilepsia*, **19**, 409 (1978).
- Stables, J., Kempfer, H.J., Anticonvulsant drug development (ADD) Program. Preclinical anticonvulsant screening project, Avani, M.G., Regesta, P.T., Avoli, eds. Molecular and cellular target for antiepileptic drugs, chapter **16**, 191 (1997).
- Dimmock, J. R., Puthucode, J. M, Smith, H.M., Quail, U.P., Leechler, T., Stables, J.P., (Aryloxy) aryl semicarbazones and related compounds, a novel class of anticonvulsant agents possessing high activity in the maximum electroshock screen. *J. Med.Chem.* **39**, 3984 (1996).

СИНТЕЗА НА НЯКОИ НОВИ ТИАДИАЗОЛОВИ ПРОИЗВОДНИ ТЯХНОТО АНТИ-КОНВУЛСИВНО ДЕЙСТВИЕ

М. Атаур Рахман¹, А.К. Шакия², Ш. Уахаб², Н.Х. Ансари^{3*}

¹ Департамент по фармацевтична химия, Изследователски институт по фармация „Азад“, Лукнау, Утар Прадеш, Индия

² Факултет по фармация, Интегрален университет, Лискнов, Лукнау, Утар Прадеш, Индия

³ Департамент по химия, Колеж Радждани, Университет в Делхи, Ню Делхи, Индия

Постъпила на 27 септември, 2013 г.; Коригирана на 3 януари, 2014 г.

(Резюме)

Синтезирана е нова серия производни на 1,3,4-тиадиазол и е установена структурата им чрез IR, ¹H-NMR и елементарен анализ. Съединенията AR-5, AR-6, AR-7, AR-8 и AR-14 са изследвани за анти-конвулсивно действие върху бели мишки. Повечето от тези съединения показват обещаваща активност. Структурните модификации на тези съединения може да доведат до откриване на по-мощни анти-конвулсивни агенти с ниска невротоксичност.

Simple method for the synthesis and antibacterial activity of 2-amino-3-cyano-1,4,5,6-tetrahydropyrano[3,2-c]quinolin-5-one derivatives

A. Akbari ^{1*}, Z. Azami-Sardooei ²

¹ Department of Chemistry, Faculty of Science, University of Jiroft, Jiroft, Iran.

² Department of Corp Protection, Faculty of Agriculture, University of Jiroft, Jiroft, Iran.

Received September 20, 2013; Revised November 23, 2013

A simple method for the synthesis of 2-amino-3-cyano-1,4,5,6-tetrahydropyrano[3,2-c]quinolin-5-one derivative and biological evaluation of the antibacterial activity against *Pseudomonas syringae*, *Xanthomonas citi* and *Pectobacterium carotovorum* are reported. The structure of the isolated compounds was determined by means of ¹H/¹³C NMR and FT-IR spectroscopy. Silica supported boron trifluoride (BF₃.SiO₂) is an efficient, readily available and reusable catalyst for the synthesis of 2-amino-3-cyano-1,4,5,6-tetrahydropyrano[3,2-c]quinolin-5-one derivatives by condensation of 4-hydroxyquinolin-2(1*H*)-one, aldehyde, and malononitrile. This reaction under normal heating is very simple affording good to excellent yields products. Some of the compound showed significant inhibition of bacteria growth.

Keywords:

INTRODUCTION.

Homogeneous acidic catalysts such as H₂SO₄, HCl and BF₃ are commonly used for organic synthesis. However, the above-mentioned catalysts have several disadvantages such as corrosiveness, toxicity or volatility, and they generate large amounts of waste. Silica supported boron trifluoride, BF₃.SiO₂, which is easy to prepare and shows unusually high acidity which can be controlled by activation temperature, exhibits considerable catalytic activity [1], and enables better accessibility of the reactants to the active sites. BF₃.SiO₂ is a solid super acid and has surface species such as Al–OBF₂ and Si–OBF₂, and the ion pairs Al–OBF₃–H⁺ or Si–OBF₃–H⁺ [2]. BF₃.SiO₂ is used in several organic transformations, such as synthesis by Claisen-Schmidt condensation [3] of 14-aryl or alkyl-14*H*-dibenzo[*a,j*]xanthenes [4], 1,2,4,5-tetrasubstituted imidazoles [5], polymerization of styrene [6], polyfunctionalized piperidin-4-ones [7], α -amino phosphonates [8], quinoxalines [9], and 3,4-dihydropyrimidin-2(1*H*)-ones [10].

Pyrans constitute one of the major classes of naturally occurring compounds [11-15]. Pyran derivatives have biological activities, and photochromic properties [16-20]. Moreover, 4*H*-pyrans are useful intermediates for the synthesis of various compounds, such as pyranopyridine derivatives [21], polyazanaphthalenes [22],

pyrano[2]pyrimidines [23], and pyridin-2-ones [24]. Recently, a method has been reported for the synthesis of pyran derivatives *via* three-component condensation of 4-hydroxyquinolin-2(1*H*)-one with aldehydes and malononitrile to synthesize 2-amino-3-cyano-1,4,5,6-tetrahydropyrano[3,2-c]quinolin-5-one derivatives. A variety of catalysts such as KF–Al₂O₃ [25], ammonium acetate [26], have been employed to effect this transformation.

Pectobacterium carotovorum is a bacterium of the family *Enterobacteriaceae*; it formerly was a member of the genus *Erwinia*. The species is a plant pathogen with a diverse host range, including potato, african violet, and other agriculturally and scientifically important plant species. It causes soft rot and blackleg of potato and vegetables, as well as slime flux on many different tree species [27, 28]. *Xanthomonas* can infect a wide variety of species including pepper, rice, citrus, cotton, tomato, broccoli, cabbage, and soybeans. Some types of *Xanthomonas* cause localized leaf spot or leaf streak while others spread systemically and cause black rot or leaf blight disease [29, 30]. *Pseudomonas syringae* is responsible for causing diseases on over 180 plant species including fruit trees, vegetable crops and flowers. Pathovars of main economic importance in Europe are the pvs *syringae*, *morsprunorum*, *avii* and *persicae*, causing bacterial canker on sweet and sour cherry, plum, peach, apricot and wild cherry [31, 32].

* To whom all correspondence should be sent:
E-mail: a.akbari@ujiroft.ac.ir

EXPERIMENTAL

Preparation of $\text{BF}_3 \cdot \text{SiO}_2$

3.7 g of BF_3 (7.0 ml of $\text{BF}_3 \cdot \text{Et}_2\text{O}$) was added dropwise to a mixture of 6.3 g of silica gel and 10 ml of chloroform. The mixture was stirred for 1 h at room temperature. The resulting suspension was filtered. The obtained solid was washed with chloroform and dried in a domestic microwave oven for 20 min at power 100.

General procedure for the synthesis of 2-amino-3-cyano-1,4,5,6-tetrahydropyrano[3,2-c]quinolin-5-one derivatives:

A mixture of 4-hydroxyquinolin-2(1H)-one (0.32 g, 2 mmol) with various aldehydes (2.1 mmol), malononitrile (0.14 g, 2.1 mmol), and $\text{BF}_3 \cdot \text{SiO}_2$ (0.06 g, 0.5 mmol, 25 mol %) was heated at 60 °C. The progress of the reaction was monitored by TLC. After completion of the reaction, the mixture was washed with ethanol and filtered to recover the catalyst. The filtrate was evaporated and the crude product was recrystallized from iso-propanol to afford the pure 2-amino-3-cyano-1,4,5,6-tetrahydropyrano[3,2-c] quinolin-5-one derivatives in 85-95 % yields. All products were known and were identified by comparison of their physical and spectral data with those of authentic samples.

2-amino-3-cyano-4-(4-ethyl)-1,4,5,6-tetrahydropyrano [3,2-c] quinolin-5-one: Pink powder, m.p. >300 °C; IR (KBr) ($\nu_{\text{max}}/\text{cm}^{-1}$): 3392, 3293, 3137, 3024, 2953, 2867, 2854, 2188, 1688, 1603, 1499, 1467, 1442, 1391, 1249, 1174, 1103, 900, 754 cm^{-1} . ^1H NMR (DMSO- d_6 , 400 MHz): δ 0.60–0.75 (m, 3H), 1.45–1.85 (m, 2H), 3.47 (br s, 1H), 7.10–7.55 (m, 5H), 7.77 (d, $J = 7.0$ Hz, 1H), 11.86 (s, 1H); ^{13}C NMR (DMSO- d_6 , 100 MHz): δ 9.2, 27.0, 32.1, 54.8, 109.6, 112.5, 115.6, 121.5, 122.3, 123.1, 131.2, 138.0, 152.4, 160.8, 161.4.

2-amino-3-cyano-4-(n-propyl)-1,4,5,6-tetrahydropyrano [3,2-c] quinolin-5-one: Pink powder, m.p. >300 °C; 3391, 3293, 3137, 3024, 2952, 2867, 2853, 2188, 1688, 1603, 1499, 1466, 1442, 1391, 1249, 1174, 1103, 900, 754 cm^{-1} . ^1H NMR (DMSO- d_6 , 400 MHz): δ 0.75–0.86 (m, 3H), 1.07–1.30 (m, 2H), 1.45–1.71 (m, 2H), 3.47 (br s, 1H), 7.05–7.55 (m, 5H), 7.79 (d, $J = 7.0$ Hz, 1H), 11.84 (br s, 1H); ^{13}C NMR (DMSO- d_6 , 100 MHz): δ 14.3, 18.2, 31.0, 37.2, 55.5, 110.3, 112.5, 115.7, 120.8, 121.9, 122.3, 131.3, 138.0, 152.2, 160.7, 161.3.

2-amino-3-cyano-4-(4-nitrophenyl)-1,4,5,6-tetrahydropyrano [3,2-c] quinolin-5-one: Yellowish brown powder, m.p. >300 °C; 3549, 3426, 3329, 3001, 2951, 2857, 2191, 1670, 1643, 1588, 1516,

1438, 1378, 1352, 1250, 1173, 1107, 1015, 902, 825, 758, 707 cm^{-1} . ^1H NMR (400 MHz, DMSO- d_6): δ 4.69 (s, 1H), 7.20–7.65 (m, 7H), 7.91 (d, 1H, $J = 7.0$ Hz), 8.15 (d, 2H, $J = 5.6$ Hz), 11.79 (br s, 1H); ^{13}C NMR (100 MHz, DMSO- d_6): δ 37.2, 57.4, 108.7, 112.3, 115.9, 119.9, 122.3, 122.5, 124.1, 129.3, 131.9, 138.4, 146.8, 152.0, 152.4, 159.4, 160.9.

2-amino-3-cyano-4-(3-nitrophenyl)-1,4,5,6-tetrahydropyrano [3,2-c] quinolin-5-one: Yellowish brown powder, m.p. >300 °C; IR (KBr) ($\nu_{\text{max}}/\text{cm}^{-1}$): 3549, 3426, 3329, 3001, 2950, 2858, 2192, 1670, 1644, 1588, 1516, 1439, 1378, 1352, 1250, 1173, 1107, 1015, 902, 825, 758, 707 cm^{-1} . ^1H NMR (DMSO- d_6) δ : 4.73 (s, 1H), 7.30–7.35 (m, 2H), 7.41 (s, 2H), 7.58–7.63 (m, 2H), 7.74 (d, 1H, $J = 7.6$ Hz), 7.93 (d, $J = 8.4$ Hz, 1H), 7.95 (s, 1H), 8.10 (d, 1H, $J = 8.4$ Hz), 11.81 (s, 1H); ^{13}C NMR (100 MHz, DMSO- d_6): δ 37.2, 57.1, 108.9, 112.3, 115.9, 119.9, 122.3, 122.4, 124.1, 128.8, 129.1, 131.8, 137.9, 145.6, 151.2, 152.3, 159.4, 160.8.

2-amino-3-cyano-4-(3,4-dichlorophenyl)-1,4,5,6-tetrahydropyrano [3,2-c] quinolin-5-one: White powder, m.p. >300 °C; IR (KBr) ($\nu_{\text{max}}/\text{cm}^{-1}$): 3452, 3334, 3201, 3063, 3017, 2950, 2849, 2208, 1696, 1593, 1470, 1439, 1373, 1332, 1250, 1168, 1117, 1019, 881, 835, 738 cm^{-1} . ^1H NMR (DMSO- d_6) δ : 4.57 (s, 1H), 7.21 (d, 1H, $J = 8.4$ Hz), 7.29–7.35 (m, 4H), 7.48 (s, 1H), 7.55 (d, 1H, $J = 7.6$ Hz), 7.57–7.61 (m, 1H), 7.91 (d, $J = 8.8$ Hz, 1H), 11.79 (s, 1H); ^{13}C NMR (100 MHz, DMSO- d_6): δ 37.3, 57.1, 108.7, 112.2, 115.9, 120.0, 122.3, 122.4, 122.6, 124.1, 128.8, 129.3, 131.9, 138.4, 146.7, 141.9, 152.6, 159.4, 160.8.

2-amino-3-cyano-4-(4-methoxyphenyl)-1,4,5,6-tetrahydropyrano [3,2-c] quinolin-5-one: White powder, m.p. >300 °C; IR (KBr) ($\nu_{\text{max}}/\text{cm}^{-1}$): 3324, 3288, 3170, 2996, 2950, 2863, 2193, 1665, 1593, 1501, 1440, 1388, 1322, 1260, 1173, 1112, 1035, 815, 764 cm^{-1} . ^1H NMR (400 MHz, DMSO- d_6): δ 3.72 (s, 3H), 4.47 (s, 1H), 6.86 (d, 2H, $J = 7.4$ Hz), 7.15 (d, 2H, $J = 7.4$ Hz), 7.24 (s, 2H), 7.29 (t, 1H, $J = 7.4$ Hz), 7.35 (d, 1H, $J = 7.7$ Hz), 7.58 (t, 1H, $J = 7.3$ Hz), 7.92 (d, 1H, $J = 7.4$ Hz), 11.74 (br s, 1H); ^{13}C NMR (100 MHz, DMSO- d_6): δ 36.4, 55.5, 58.5, 110.4, 112.5, 114.2, 115.8, 120.4, 122.2, 122.4, 128.9, 131.6, 136.9, 138.2, 151.4, 158.5, 159.4, 161.0.

2-amino-3-cyano-4-(4-chlorophenyl)-1,4,5,6-tetrahydropyrano [3,2-c] quinolin-5-one: White powder, m.p. >300 °C; IR (KBr) ($\nu_{\text{max}}/\text{cm}^{-1}$): 3355, 3304, 3155, 2955, 2853, 2203, 1675, 1598, 1486, 1393, 1255, 1173, 1096, 1025, 846, 764 cm^{-1} . ^1H NMR (400 MHz, DMSO- d_6): δ 4.56 (s, 1H), 7.25–7.42 (m, 8H), 7.60 (t, 1H, $J = 7.0$ Hz), 7.95 (d, 1H,

$J = 7.2$ Hz), 11.76 (br s, 1H); ^{13}C NMR (100 MHz, DMSO- d_6): d 36.7, 57.8, 109.5, 112.4, 115.9, 120.2, 122.3, 122.4, 128.8, 129.8, 131.7, 131.8, 138.3, 143.8, 151.7, 159.4, 160.9.

2-amino-3-cyano-4-(4-bromophenyl)-1,4,5,6-tetrahydropyrano [3,2-c] quinolin-5-one: Pale yellow powder, m.p. >300 °C; IR (KBr) ($\nu_{\text{max}}/\text{cm}^{-1}$): 3324, 3310, 3150, 2950, 2853, 2197, 1680, 1593, 1486, 1383, 1327, 1291, 1260, 1163, 1107, 1004, 851, 758 cm^{-1} . ^1H NMR (400 MHz, DMSO- d_6): d 4.55 (s, 1H), 7.21 (d, 2H, $J = 7.2$ Hz), 7.25–7.43 (m, 4H), 7.50 (d, 2H, $J = 7.2$ Hz), 7.59 (t, 1H, $J = 7.4$ Hz), 7.94 (d, 1H, $J = 7.3$ Hz), 11.73 (br s, 1H); ^{13}C NMR (100 MHz, DMSO- d_6): d 36.8, 57.7, 109.4, 112.4, 115.9, 120.2, 120.2, 122.3, 122.5, 130.2, 131.7, 131.8, 138.3, 144.3, 151.7, 159.4, 160.9.

2-amino-3-cyano-4-(2-chlorophenyl)-1,4,5,6-tetrahydropyrano [3,2-c] quinolin-5-one: Pale yellow powder, m.p. >300 °C; IR (KBr) ($\nu_{\text{max}}/\text{cm}^{-1}$): 3324, 3288, 3170, 2996, 2950, 2863, 2193, 1665, 1593, 1501, 1440, 1388, 1322, 1260, 1173, 1112, 1035, 815, 764 cm^{-1} . ^1H NMR (400 MHz, DMSO- d_6): d 5.03 (s, 1H), 7.15–7.41 (m, 8H), 7.57 (t, 1H, $J = 6.8$ Hz), 7.92 (d, 1H, $J = 7.4$ Hz), 11.70 (br s, 1H); ^{13}C NMR (100 MHz, DMSO- d_6): d 34.5, 57.0, 108.9, 112.3, 115.9, 119.9, 122.3, 122.4, 128.0, 128.8, 129.9, 130.7, 131.8, 132.8, 138.4, 142.0, 152.3, 159.4, 160.8.

2-amino-3-cyano-4-(2,4-dichlorophenyl)-1,4,5,6-tetrahydropyrano [3,2-c] quinolin-5-one: Pale yellow powder, mp >300 °C; IR (KBr) ($\nu_{\text{max}}/\text{cm}^{-1}$): 3344, 3307, 3170, 2950, 2958, 2197, 1670, 1634, 1583, 1480, 1383, 1317, 1260, 1183, 1112, 1045, 850, 748 cm^{-1} . ^1H NMR (400 MHz, DMSO- d_6): d 5.01 (s, 1H), 7.20 (d, 1H, $J = 7.9$ Hz), 7.25–7.38 (m, 5H), 7.52 (s, 1H), 7.58 (t, 1H, $J = 7.4$ Hz), 7.90 (d, 1H, $J = 7.7$ Hz), 11.67 (br s, 1H); ^{13}C NMR (100 MHz, DMSO d_6): d 34.2, 56.4, 108.4, 112.3, 115.9, 119.7, 122.3, 122.5, 128.2, 129.2, 131.8, 132.1, 132.3, 133.7, 138.4, 141.1, 152.3, 159.4, 160.7.

2-amino-3-cyano-4-(3,4-dimethoxyphenyl)-1,4,5,6-tetrahydropyrano [3,2-c] quinolin-5-one: White powder, mp >300 °C; IR (KBr) ($\nu_{\text{max}}/\text{cm}^{-1}$): 3355, 3314, 3160, 3068, 3001, 2964, 2884, 2197, 1680, 1593, 1496, 1440, 1378, 1245, 1168, 1112, 1035, 912, 856, 774 cm^{-1} . ^1H NMR (DMSO- d_6) d: 4.43 (s, 1H), 5.96 (s, 2H), 6.67 (d, 2H, $J = 8.4$ Hz), 6.74 (s, 1H), 6.81 (d, 1H, $J = 8.0$ Hz), 7.22 (s, 2H), 7.27–7.34 (m, 2H), 7.55–7.59 (m, 1H), 7.90 (d, $J = 8.4$ Hz, 1H), 11.75 (s, 1H); ^{13}C NMR (100 MHz, DMSO- d_6): d 36.4, 55.5, 57.5, 58.5, 110.4, 112.5, 114.2, 115.8, 120.4, 122.2, 122.4, 128.9, 128.8,

130.7, 131.6, 136.9, 138.2, 151.4, 158.5, 159.4, 161.0.

2-amino-3-cyano-4-(4-cyanophenyl)-1,4,5,6-tetrahydropyrano [3,2-c] quinolin-5-one: Yellowish brown powder, m.p. >300 °C; 3355, 3304, 3155, 2955, 2853, 2225, 2203, 1675, 1598, 1486, 1393, 1255, 1173, 1025, 846, 763 cm^{-1} . ^1H NMR (DMSO- d_6 , 400 MHz): d 4.63 (s, 1H), 7.27 (t, 1H, $J = 7.3$ Hz), 7.34 (d, 1H, $J = 8.0$ Hz), 7.38 (s, 2H), 7.43 (d, 2H, $J = 7.5$ Hz), 7.57 (t, 1H, $J = 7.0$ Hz), 7.75 (d, 2H, $J = 7.5$ Hz), 7.91 (d, 1H, $J = 7.6$ Hz), 11.78 (br s, 1H); ^{13}C NMR (DMSO- d_6 , 100 MHz): d 37.4, 57.2, 108.8, 110.0, 112.4, 115.9, 119.3, 120.0, 122.3, 122.5, 129.1, 131.9, 132.9, 138.4, 150.4, 152.0, 159.4, 160.9.

2-amino-3-cyano-4-(phenyl)-1,4,5,6-tetrahydropyrano [3,2-c] quinolin-5-one: White powder, m.p. >300 °C; IR (KBr) ($\nu_{\text{max}}/\text{cm}^{-1}$): 3392, 3293, 3137, 3024, 2854, 2188, 1688, 1603, 1499, 1442, 1391, 1249, 1174, 1103, 900, 754 cm^{-1} . ^1H NMR (400 MHz, DMSO- d_6): d 4.52 (s, 1H), 7.21–7.32 (m, 8H), 7.35 (d, 1H, $J = 8.2$ Hz), 7.58 (t, 1H, $J = 7.7$ Hz), 7.93 (d, 1H, $J = 7.7$ Hz), 11.77 (br s, 1H); ^{13}C NMR (100 MHz, DMSO- d_6): d 37.2, 58.2, 110.0, 112.5, 115.8, 120.3, 122.2, 122.4, 127.2, 127.8, 128.8, 131.7, 138.2, 144.8, 151.7, 159.4, 160.9.

2-amino-3-cyano-4-(4-fluorophenyl)-1,4,5,6-tetrahydropyrano [3,2-c] quinolin-5-one: Pale yellow powder, m.p. >300 °C; 3354, 3304, 3155, 2954, 2853, 2203, 1675, 1598, 1486, 1393, 1255, 1248, 1173, 1025, 846, 764 cm^{-1} . ^1H NMR (400 MHz, DMSO- d_6): d 4.52 (s, 1H), 7.05–7.35 (m, 8H), 7.56 (t, 1H, $J = 7.2$ Hz), 7.89 (d, 1H, $J = 7.4$ Hz), 11.75 (br s, 1H); ^{13}C NMR (100 MHz, DMSO- d_6): d 36.5, 58.1, 109.8, 112.4, 115.4, 120.2, 122.3, 122.4, 129.8, 129.8, 131.7, 138.3, 141.0, 151.6, 159.4, 160.3, 160.9.

2-amino-3-cyano-4-(4-hydroxyphenyl)-1,4,5,6-tetrahydropyrano [3,2-c] quinolin-5-one: White powder, m.p. >300 °C; 3403, 3324, 3310, 3150, 3058, 2950, 2920, 2853, 2197, 1680, 1620, 1593, 1486, 1383, 1327, 1291, 1260, 1163, 1107, 1004, 851, 758 cm^{-1} . ^1H NMR (400 MHz, DMSO- d_6): d 4.40 (s, 1H), 6.67 (d, 2H, $J = 8.3$ Hz), 7.01 (d, 2H, $J = 8.3$ Hz), 7.18 (s, 2H), 7.27 (t, 1H, $J = 7.6$ Hz), 7.33 (d, 1H, $J = 8.2$ Hz), 7.55 (t, 1H, $J = 7.6$ Hz), 7.90 (d, 1H, $J = 8.0$ Hz), 11.74 (br s, 1H); ^{13}C NMR (100 MHz, DMSO- d_6): d 36.3, 58.7, 110.6, 112.6, 115.5, 115.8, 120.5, 122.2, 122.4, 128.9, 131.5, 135.2, 138.2, 151.3, 156.7, 159.4, 161.0.

In vitro antibacterial screening: Preparation of plates and microbiological assays:

Inoculation of test bacteria (*X. campestris* pvs, *P. syringae* and *P. carotovorum*) was carried out by inoculating a loopful of organism in a 10 ml nutrient broth and incubated at 37°C for 24 h till a moderate turbidity was developed. 0.10 ml of each suspension was thoroughly mixed with 25 ml of nutrient agar medium in a pre-sterilized petri plate and was set aside. After cooling, the seeded agar plate was used for testing compounds by the disc diffusion method. Sterilized paper discs were dipped in each compound solution. These discs were placed equidistant in the plates. The central disc without any compound was taken as control. The petri plates were then incubated at 37°C for 24 h, after which the zones of inhibition were measured. After solidification of the medium, 0.10 ml of spore suspension was spread by a sterilized spreader in a specific zone. The compounds were dissolved in DMSO solvent at 200 ppm concentration. The paper discs were dipped in each compound solution for 5 min. Then the paper discs were placed equidistant in the plates. The central disc dipped in DMSO solvent without compound was used as control. The petri plates were kept for incubation at 28°C for 3 days, after the completion of recommended period, the zones of inhibition were measured (Table 3).

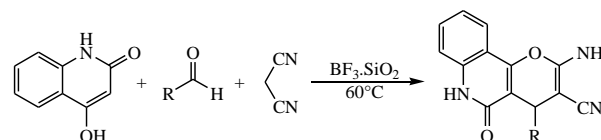
RESULTS AND DISCUSSION

In continuation of our investigations on the application of solid acids in organic synthesis, we investigated the synthesis of 2-amino-3-cyano-1,4,5,6-tetrahydropyrano [3,2-c]quinolin-5-one

derivatives in the presence of $\text{BF}_3 \cdot \text{SiO}_2$ under normal heating. Herein, we report that $\text{BF}_3 \cdot \text{SiO}_2$ is an efficient and reusable catalyst for the synthesis of 2-amino-3-cyano-1,4,5,6-tetrahydropyrano[3,2-c]quinolin-5-one derivatives. The reaction of 4-hydroxyquinolin-2(1*H*)-one (0.32 g, 2 mmol) with 4-nitrobenzaldehyde (0.32 g, 2.1 mmol) and malononitrile (0.14 g, 2.1 mmol) was investigated for optimization of the reaction conditions (Table 1). Reaction at different temperatures and various molar ratios of substrates in the presence of $\text{BF}_3 \cdot \text{SiO}_2$ revealed that the best conditions were solvent-free at 60 °C and a ratio of 4-hydroxyquinolin-2(1*H*)-one (mmol): 4-nitrobenzaldehyde (mmol): malononitrile (mmol): 37% $\text{BF}_3 \cdot \text{SiO}_2$ of 2 : 2.1 : 2.1 : 0.5 (Table 1).

The applicability of the present method to a large-scale process was examined with 4-hydroxyquinolin-2(1*H*)-one (3.22 g, 20 mmol), 4-nitrobenzaldehyde (3.17 g, 21 mmol), and malononitrile (1.39 g, 21 mmol) under thermal conditions which gave 2-amino-3-cyano-4-(4-nitrophenyl)-1,4,5,6-tetrahydropyrano[3,2-c]quinolin-5-one in (6.70 g, 93%) yield.

4-hydroxyquinolin-2(1*H*)-one, malononitrile and various aldehydes were used as substrates for the synthesis of 2-amino-3-cyano-1,4,5,6-tetrahydropyrano[3,2-c]quinolin-5-one derivatives under normal heating, (Scheme 1 and Table 2).



Scheme 1

Table 1. Optimization of conditions for the synthesis of 2-amino-3-cyano-4-(4-nitrophenyl)-1,4,5,6-tetrahydropyrano [3,2-c]quinolin-5-one

Entry	Catalyst (mol %)	Solvent	Conditions	Time (min)	Yield ^a %
1	$\text{BF}_3 \cdot \text{SiO}_2$ (25)	Chloroform	r.t.	30	scarce
2	$\text{BF}_3 \cdot \text{SiO}_2$ (25)	Chloroform	Reflux	30	62
3	$\text{BF}_3 \cdot \text{SiO}_2$ (25)	Ethanol	r.t.	30	scarce
4	$\text{BF}_3 \cdot \text{SiO}_2$ (25)	Ethanol	Reflux	30	75
5	$\text{BF}_3 \cdot \text{SiO}_2$ (25)	Water	r.t.	30	scarce
6	$\text{BF}_3 \cdot \text{SiO}_2$ (25)	Water	Reflux	30	58
7	$\text{BF}_3 \cdot \text{SiO}_2$ (25)	Solvent-free	r.t.	30	scarce
8	$\text{BF}_3 \cdot \text{SiO}_2$ (25)	Solvent-free	50°C	30	77
9	$\text{BF}_3 \cdot \text{SiO}_2$ (25)	Solvent-free	50°C	12	60
10	$\text{BF}_3 \cdot \text{SiO}_2$ (25)	Solvent-free	60°C	8	72
11	$\text{BF}_3 \cdot \text{SiO}_2$ (30)	Solvent-free	60°C	12	95
12	$\text{BF}_3 \cdot \text{SiO}_2$ (20)	Solvent-free	60°C	12	90
13	$\text{BF}_3 \cdot \text{SiO}_2$ (25)	Solvent-free	60°C	12	95
14	$\text{BF}_3 \cdot \text{SiO}_2$ (25) 2 nd run	Solvent-free	60°C	12	93
15	$\text{BF}_3 \cdot \text{SiO}_2$ (25) 2 nd run	Solvent-free	60°C	12	93

^a Isolated yield

Table 2. Synthesis of 2-amino-3-cyano-1,4,5,6-tetrahydropyrano[3,2-c]quinolin-5-one derivatives via Scheme 1

Entry	R ^b	Time (min)	Yield ^c %	Ref
1	CH ₃ CH ₂	25	87	20
2	CH ₃ CH ₂ CH ₂	25	89	20
3	4- O ₂ N-C ₆ H ₄	12	95	20
4	3- O ₂ N-C ₆ H ₄	12	95	19
5	3,4-Cl ₂ -C ₆ H ₄	12	94	20
6	4-MeO-C ₆ H ₄	15	93	20
7	4-Cl-C ₆ H ₄	15	92	20
8	4-Br-C ₆ H ₄	15	92	20
9	2-Cl-C ₆ H ₄	15	92	19
10	2,4-Cl ₂ -C ₆ H ₄	15	92	19
11	3,4-CH ₃ O-C ₆ H ₄	15	90	20
12	4-CN-C ₆ H ₄	15	90	20
13	C ₆ H ₅	15	90	20
14	4-F-C ₆ H ₄	18	85	20
15	4-HO-C ₆ H ₄	18	85	20

^a4-hydroxyquinolin-2(1*H*)-one (2 mmol) and malonitrile (2.1 mmol) were stirred with various aldehydes (2.1 mmol) in the presence of 0.5 mmol of freshly prepared 37% BF₃.SiO₂ under neat conditions at 60 °C ^ball products are known and were characterized by IR and ¹H-NMR and by comparison of their physical properties with those reported in the literature.

^cIsolated yield

The *in vitro* antibacterial activity of the synthesized novel class of 2-amino-4*H*-pyran derivatives was tested against some important bacteria by the disc diffusion method [33, 34] using Mueller-Hinton agar No. 2 as the nutrient medium.

Table 3. Analytical and antibacterial activity of compounds

Entry	R	Molecular Formula	Molecular weight	Zone of inhibition (mm)		
				<i>X.campest-rispvs</i>	<i>P. syringae</i>	<i>P. carotovorum</i>
1	CH ₃ CH ₂	C ₁₅ H ₁₃ N ₃ O ₂	267.28	22± 0.9	19± 1.0	17± 1.1
2	CH ₃ CH ₂ CH ₂	C ₁₆ H ₁₅ N ₃ O	281.31	19± 1.0	20± 1.1	18± 1.2
3	4-O ₂ N-C ₆ H ₄	C ₁₉ H ₁₂ N ₄ O	360.32	18± 0.4	14± 0.6	16± 0.9
4	3-O ₂ N-C ₆ H ₄	C ₁₉ H ₁₂ N ₄ O ₄	360.32	17± 0.8	18± 1.0	20± 1.0
5	3,4-Cl ₂ -C ₆ H ₃	C ₁₉ H ₁₁ Cl ₂ N ₃ O ₃ O ₂	384.22	33± 1.1	28± 1.1	35± 0.7
6	4-MeO-C ₆ H ₄	C ₂₀ H ₁₆ N ₃ O ₃ O ₂	345.35	19± 1.1	19± 0.9	14± 1.3
7	4-Cl-C ₆ H ₄	C ₁₉ H ₁₂ ClN ₃ O ₂₄	349.77	28± 0.4	29± 1.2	30± 1.2
8	4-Br-C ₆ H ₄	C ₁₉ H ₁₂ BrN ₃ O ₂₄	394.22	23± 1.8	25± 0.4	22± 1.1
9	2-Cl-C ₆ H ₄	C ₁₉ H ₁₂ ClN ₃ O ₂	349.77	31± 0.9	29± 1.0	32± 0.8
10	2,4-Cl ₂ -C ₆ H ₄	C ₁₉ H ₁₁ Cl ₂ N ₃ O ₃	384.22	34± 1.1	32± 1.2	36± 1.2
11	3,4-MeO-C ₆ H ₃	C ₂₁ H ₁₇ N ₃ O ₄	375.38	18± 1.4	12± 1.1	12± 0.9
12	4-CN-C ₆ H ₄	C ₂₀ H ₁₂ N ₄ O ₂ O ₂	340.33	21± 1.1	25± 1.2	23± 1.4
13	C ₆ H ₅	C ₁₉ H ₁₃ N ₃ O ₂	315.33	22± 1.2	24± 0.9	22± 1.8
14	C ₁₉ H ₁₂ FN ₃ O ₂	C ₂₄ H ₂₀ O ₂	332.32	23± 1.2	24± 1.1	21± 1.5
15	4-HO-C ₆ H ₄	C ₁₉ H ₁₃ N ₃ O ₃	331.32	27± 1.1	29± 1.3	26± 1.2

In vitro antibacterial assay was performed against *X. campestris pvs*, *P. syringae* and *P. carotovorum*. The results obtained as zone of inhibition (mm) are presented in Table 3.

The current method for the synthesis of 2-amino-3-cyano-1,4,5,6-tetrahydropyrano[3,2-c]quinolin-5-one is simple, efficient, and less time-consuming. The materials were purchased from Sigma–Aldrich and Merck and were used without additional purification. The compounds gave satisfactory analytical and spectroscopic data. A Bruker (DRX-400 Avance) NMR apparatus was used to record the ¹H NMR and ¹³C NMR spectra. All NMR spectra were recorded in DMSO-d₆ at ambient temperature. Melting points were measured on an Electrothermal apparatus. All products are known and were characterized by ¹H NMR, ¹³C NMR and comparison of their physical properties with those reported in the literature.

In conclusion, we have demonstrated a simple method for the synthesis of 2-amino-3-cyano-1,4,5,6-tetrahydropyrano[3,2-c]quinolin-5-one using BF₃.SiO₂ as an eco-friendly, inexpensive and efficient reagent. Short reaction times, high yield, simplicity of operation and easy work-up are some of the advantages of this method.

Acknowledgments: The support for this study by the Research Council of University of Jiroft and Yazd University is gratefully acknowledged.

REFERENCES

1. K. Wilson, J. H. Clark, *Chem. Commun.*, 2135 (1998).
2. T. M. Klapotke, F. Mc Monagle, R. R. Spence, J. M. Winfield, *J. Fluorine Chem.*, **127**, 1446 (2006).
3. B. Sadegi, B. F. Mirjalili, M. M. Hashememi, *Tetrahedron Lett.*, **49**, 2575 (2008).
4. B. F. Mirjalili, A. Bamoniri, A. Akbari, *Tetrahedron Lett.*, **49**, 6454 (2008).
5. B. Sadegi, B. F. Mirjalili, M. M. Hashemi, *J. Iran. Chem. Soc.*, **5**, 694 (2008).
6. K. V. K. Boodhoo, W. A. E. Dunk, M. Vicevic, R. J. Jachuck, V. Sage, D. J. Macquarrie, J. H. Clark, *J. Applied Polymer Science*, **101**, 8 (2006).
7. S. D. Dindulkar, P. Parthiban, Y. T. Jeong, *Monatsh Chem.*, **143**, 113 (2012).
8. M. V. Reddy, S. D. Dindulkar, Y. T. Jeong, *Tetrahedron Lett.*, **52**, 4764 (2011).
9. B. F. Mirjalili, A. Bamoniri, A. Akbari, *Chem. Heterocycl. Compd.*, **47**, 487 (2011).
10. B. F. Mirjalili, A. Bamoniri, A. Akbari, *J. Iran. Chem. Soc.*, **8**, 135 (2011).
11. Y. Tang, J. Oppenheimer, Z. Song, L. You, X. Zhang, R. P. Hsung, *Tetrahedron*, **62**, 10785 (2006).
12. T. C. McKee, R. W. Fuller, C. D. Covington, J. H. Cardellina, R. J. Gulakowski, B. L. Krepps, J. B. McMahon, M. R. Boyd, *J. Nat. Prod.* **59**, 754 (1996).
13. T. C. McKee, C. D. Covington, R. W. Fuller, H. R. Bokesch, S. Young, J. H. Cardellina, M. R. Kadushin, D. D. Soejarto, P. F. Stevens, G. M. Cragg, M. R. Boyd, *J. Nat. Prod.*, **61**, 1252 (1998);
14. S.-J. Wu, I.-S. Chen, *Phytochemistry*, **34**, 1659 (1993).
15. E. J. Jung, B. H. Park, Y. R. Lee, *Green Chem.*, **12**, 2003 (2010).
16. S. Kumar, D. Hernandez, B. Hoa, Y. Lee, J. S. Yang, A. McCurdy, *Org. Lett.*, **10**, 3761 (2008).
17. M. Rawat, V. Prutyay, W. D. Wulff, *J. Am. Chem. Soc.*, **128**, 11044 (2006).
18. O. A. Fedorova, F. Maure, A. V. Chebunkova, Y. P. Strokach, T. M. Valova, L. G. Kuzmina, J. A. K. Howard, M. Wenzel, K. Gloe, V. Lokshin, A. Samat, *J. Phys. Org. Chem.*, **20**, 469 (2007).
19. J. D. Hepworth, B. M. Heron, *Prog. Heterocycl. Chem.*, **17**, 33 (2005).
20. S. Delbaer, J.-C. Micheau, G. Vermeersch, *J. Org. Chem.*, **68**, 8968 (2003).
21. Q. Ren, W.-Y. Siau, Z. Du, K. Zhang, J. Wang, *Chem. Eur. J.*, **17**, 7781 (2011).
22. A. H. Adbel-Fattah, A. M. Hesien, S. A. Metwally, M. H. Elnagdi, *Liebigs Ann. Chem.*, 585 (1989).
23. J. M. Quintela, C. Peinador, M. J. Moreira, *Tetrahedron*, **51**, 5901 (1995).
24. S. Srivastava, S. Batra, A. P. Bhaduri, *Indian J. Chem. Sect. B.*, **35**, 602 (1996).
25. X. Wang, Z. Zeng, D. Shi, X. Wei, Z. Zong, *Synth. Commun.*, **34**, 3021 (2004).
26. M. Lei, L. Mab, L. Hu, *Tetrahedron Lett.*, **52**, 2597 (2011).
27. E.-J. Park, P. M. Gray, S.-W. Oh, J. Kronenberg, D.-H. Kang, *J. Food. Sci.*, **73**(6), M278 (2008).
28. I. K. Toth, K. S. Bell, M. C. Holeva, P. R. J. Birch, *Mol. Plant Pathol.*, **4** (1), 17 (2003).
29. J. W. Yang, H.-S. Yi, H. Kim, B. Lee, S. Lee, S.-Y. Ghim, C.-M. Ryu, *J. Ecol.*, **99**(1), 46 (2011).
30. J. Boch, U. Bonas, *Annu. Rev. Phytopathol.*, **48**, 419 (2010).
31. Z. Ivanovic, S. Zivkovic, M. Starovic, D. Josic, S. Stankovic, V. Gavrilovic, *Arch. Boil. Sci.*, **61**(4), 863 (2009).
32. J. Rodrigo, *Sci. Hortic.*, **85**(3), 155 (2000).
33. S. Lemriss, B. Marquet, H. Ginestet, L. Lefeuvre, A. Fassouane, P. Boiron, *J. Mycol. Med.*, **13**, 189 (2003).
34. A. Rahman, M. I. Choudhary, W. J. Thomsen, Harwood Academic Publishers, Amsterdam, 2001, p. 14.

ПРОСТ МЕТОД ЗА СИНТЕЗА И АНТИБАКТЕРИАЛНА АКТИВНОСТ НА 2-АМИНО-3-ЦИАНО-1,4,5,6-ТЕТРАГИДРОПИРАНО[3,2-С] ХИНОЛИН-5-ОН ПРОИЗВОДНИ

А. Акбари^{1*}, З. Азами-Сардуеи²

¹ Департамент по химия, Научен факултет, Университет в Джирофт, Джирофт, Иран

² Департамент по защита на растенията, Агрономически факултет, Университет в Джирофт, Джирофт, Иран

Постъпила на 20 септември, 2013 г.; Коригирана на 23 ноември, 2014 г.

(Резюме)

Съобщава се за прост метод за синтеза на 2-амино-3-циано-1,4,5,6-тетрахиdropирано[3,2-с] хинолин-5-он производни и оценката на тяхната антибактериална активност спрямо *Pseudomonas syringae*, *Xanthomonas citi* и *Pectobacterium carotovorum*. Структурата на изолираните съединения е определена с помощта на ¹H/¹³C ЯМР и FT-IR спектроскопия. Борният трифлуорид, фиксиран със силициев диоксид (BF₃.SiO₂) е ефикасен, лесно достъпен и многократно използваем катализатор за синтезата на is an efficient, readily available and reusable catalyst for the synthesis of 2-амино-3-циано-1,4,5,6-тетрахиdropирано[3,2-с] хинолин-5-он'ови производни чрез кондензацията на 4-хидроксихинолин-2(1H)-он, алдехид и малонитрил. Тази реакция е много проста при леко нагряване и дава добри до отлични добиви. Някои от тези продукти показват значително инхибиране на микробния растеж.

Voltammetric behavior of lercanidipine and anodic adsorptive stripping voltammetric method for assay in pharmaceutical dosage forms and biological fluids

F. Öztürk^{1,*}, D. Koyuncu Zeybek², E. Kilic³

¹Namik Kemal University, Faculty of Arts and Science, Department of Chemistry, Tekirdağ, Turkey

²Dumlupınar University, Faculty of Arts and Science, Department of Chemistry, Kütahya, Turkey

³Ankara University, Faculty of Science, Department of Chemistry, Ankara, Turkey

Received September 24, 2013; Revised December 4, 2013

Electrochemistry of lercanidipine (LCN) was investigated and its optimal conditions were evaluated based on the irreversible and diffusion-controlled electrochemical oxidation signal (+ 0.93 V) of a carbon paste electrode (CPE) versus Ag/AgCl in Britton Robinson buffer (BR) and ethanol mixture of pH 4.5. Electrochemical determination was performed by square wave anodic adsorptive stripping voltammetry (SWAAdSV). Linear range was found to be between 3.3×10^{-7} mol L⁻¹ and 4.5×10^{-5} mol L⁻¹ in two different regions; preconcentration potential and time were found to be 0.0 V and 150 s, respectively. In this method, the limit of quantification (LOQ) was found to be 2.0×10^{-8} mol L⁻¹ (0.012 mg L⁻¹). The method was applied to determine the content of LCN in a commercial pharmaceutical preparation, spiked human serum and spiked human urine. The method was found to be highly accurate and precise, having a relative standard deviation of less than 10% for all applications.

Keywords: Carbon paste electrode, human urine, human serum, lercanidipine, pharmaceuticals.

INTRODUCTION

LCN (Fig.1), 2-[(3,3-diphenylpropyl) methylamino]-1,1-dimethylethylmethyl-1,4-dihydro-2,6-dimethyl-4-(3-nitrophenyl)-3,5-pyridine dicarboxylic ester is an antihypertensive drug which belongs to the dihydropyridine derivatives known as calcium antagonists. Similar to other calcium antagonist drugs, LCN blocks the influx of calcium ions through L-type calcium channels in cell membranes and reduces the blood pressure [1, 2].

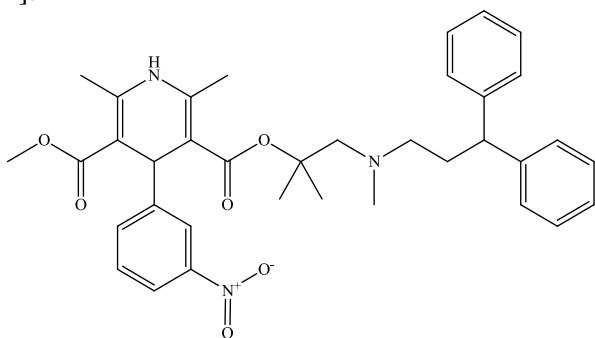


Fig. 1. Chemical structure of LCN

LCN and other 1,4-dihydropyridines have been determined in pharmaceutical samples by spectrophotometric [3], liquid chromatographic/tandem mass spectrometric [4], capillary

electrophoresis [5, 6], high performance liquid chromatography with UV detection, high performance liquid chromatography with electrochemical detection [7], high performance liquid chromatography with amperometric detection [8] and electrochemical methods [9-11]. Electrode modification and alternation of working electrodes is of great importance in electroanalysis. To the best of our knowledge, no study based on the oxidation of LCN at modified electrodes and CPE has been applied to pharmaceutical samples and human body fluids. Only Altun *et al.* [11], studied the electrooxidative behavior and redox properties of LCN using a boron-doped diamond electrode. CPE is becoming a popular electrode material in electrochemical studies [12, 13].

The aim of this study is to investigate the oxidation properties of LCN on a CPE and to develop an adsorptive stripping voltammetric method for its determination.

EXPERIMENTAL

Apparatus and reagents

All electrochemical studies were carried out using a BAS 100B electrochemical analyzer in a single-compartment three-electrode cell system (BAS C3 Cell Stand). For cyclic voltammetry (CV), square wave voltammetry (SWV) with and without anodic adsorptive stripping mode experiments, a CPE with 3 mm internal diameter,

* To whom all correspondence should be sent:

E-mail: fozanozturk@yahoo.com

Ag/AgCl electrode (BAS MF-2052 RE-5B, 3.0 mol L⁻¹ KCl) and platinum wire electrode (BAS MW-1034) were used as the working, reference and counter electrode, respectively. The bulk electrolysis was performed by a glassy carbon sieve (approximately 65 cm² area) as a working electrode, coiled platinum wire as a counter electrode (23 cm) (BAS MW-1033) and Ag/AgCl (BAS MF-2052 RE-5B, 3.0 mol L⁻¹ KCl) reference electrode.

All pH measurements were performed using Thermo Orion Model 720A pH-ion meter with an Orion combined glass pH electrode (912600). Ultrapure water (18.2 MΩ cm) was obtained from ELGA Purelab Classic water purification system. All data were obtained at room temperature (23±2 °C).

Standard LCN (99.0 %) was supplied from Fako drug manufacturing company, Turkey and a stock LCN solution (1.0×10⁻³ mol L⁻¹) in ethanol was prepared. The calibration solutions were prepared by diluting the stock solution with a mixture of ethanol and Britton-Robinson buffer (BR) in a volume ratio of 20:80 as solvent-supporting electrolyte mixture. The pH values of these solutions were adjusted using 0.2 mol L⁻¹ NaOH solutions. All LCN solutions were protected from light and used within a day to avoid photochemical decomposition.

BR buffer was prepared and pH of the working solutions was adjusted as described in literature [10].

Preparation of CPE

The carbon paste was prepared by hand mixing of graphite powder and paraffin oil in a mass ratio of 5:3 until a homogeneous paste was obtained. A portion of the paste was placed firmly into a cavity of a polyetheretherketone (PEEK) rod electrode body (with 3 mm internal diameter) and a brass wire was introduced into the opposite end of the electrode body to establish an electrical contact. Then the CPE surfaces were smoothed. The resulting CPE was used as a working electrode.

Preparation and Analysis of Samples

Lercadip® tablets containing LCN (10 mg per tablet) manufactured by Fako were used as the pharmaceutical dosage form. Ten tablets were weighed, finely powdered and mixed in a mortar. The average mass per tablet was determined and then the powder equivalent to one tablet was weighed and transferred to a 100.0 mL calibrated flask containing about 50 mL of ethanol. After sonication for 30 min, the volume was filled up with ethanol. The solution was centrifuged at 1500

rpm for 30 min. For preparation of the stock solution, a 10.0 mL sample was diluted to 100.0 mL with ethanol-BR buffer mixture. It was stored at +4 °C in dark. Appropriate volumes of this solution were transferred to the electrochemical cell containing 10.0 mL solvent-supporting electrolyte mixture, then pH was adjusted to the desired value and LCN was determined by the calibration curve method.

The spiked human serum and urine samples were analyzed in the same manner. The samples obtained from healthy persons were kept frozen until analysis. After melting, an aliquot of serum (or urine) sample was appended to the electrochemical cell containing 10.0 mL of solvent-supporting electrolyte mixture and appropriate volumes (0.01 mL, 0.02 mL, 0.025 mL, and 0.03 mL) of standard LCN solutions were transferred to the cell. After the solution was deaerated for 10 min with argon, measurements were performed to determine the LCN content.

Voltammetric procedure

All voltammetric experiments were performed in a cell containing 10.0 mL of LCN solution prepared in a solvent-supporting electrolyte mixture. The CPE was placed into the cell and the solution was purged with purified argon (99.99 % purity) for 10 min before the first run and for 30 s between runs. The voltammograms were recorded by anodic sweeping from 0.00 V to +1.10 V.

RESULTS AND DISCUSSION

Electrochemical Behavior of LCN

Electrochemical behavior, diffusion and adsorption properties of LCN were investigated by cyclic voltammetry (CV), square wave voltammetry (SWV), and bulk electrolysis (BE). Fig. 2 shows the voltammograms of CPE in the ethanol-BR mixture in absence (Fig. 2a) and presence (Fig. 2b) of 5×10⁻⁵ M LCN at pH 4.5. As can be seen, there is a single irreversible oxidation peak at about +0.93 V in presence of LCN, and no peak in absence of LCN. It can be hence concluded that the oxidation peak is due to the oxidation of LCN molecules on CPE.

The effects of the scan rate (between 0.005 – 2.0 Vs⁻¹) on the anodic peak potential ($E_{p,a}$) and anodic peak current ($i_{p,a}$) for 5×10⁻⁵ M LCN were investigated. The peak potential shifts to more positive values and the peak current increases with

increasing the scan rate (Fig. 3 (A)), indicating that the electrooxidation steps are not reversible

from 0.0 V to 0.7 V and from 30 s to 180 s, respectively. As can be seen from Fig. 5(A), the maximum values for the peak current are established at 0.0 V and peak current decreases with more positive potential values. The maximum peak current in the deposition step was observed for a deposition time of 150 s in the SWAAdSV (Fig 5(B)). In a further stripping assay, deposition potential and deposition time were employed as 0.0 V and 150 s, respectively.

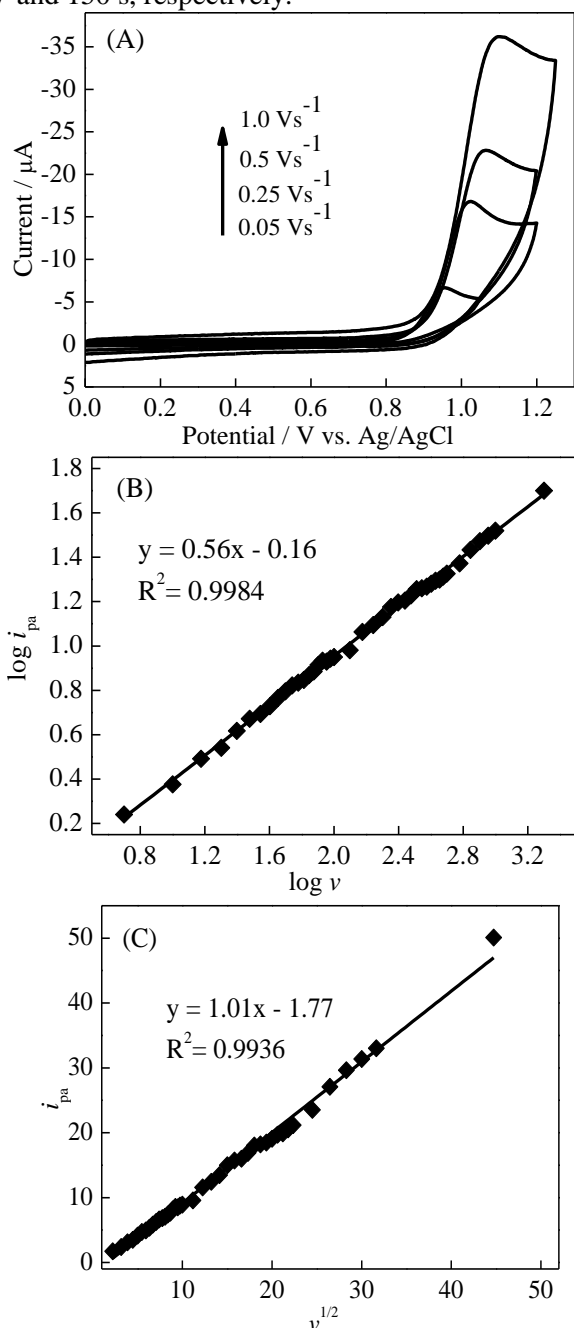


Fig. 3. Cyclic voltammograms of 5×10^{-5} M LCN at different scan rates: (A) plot of the logarithm of the peak current versus the logarithm of the scan rate; (B) plot of the peak current versus the square root of the scan rate; (C) EtOH–BR buffer solution at pH 4.5.

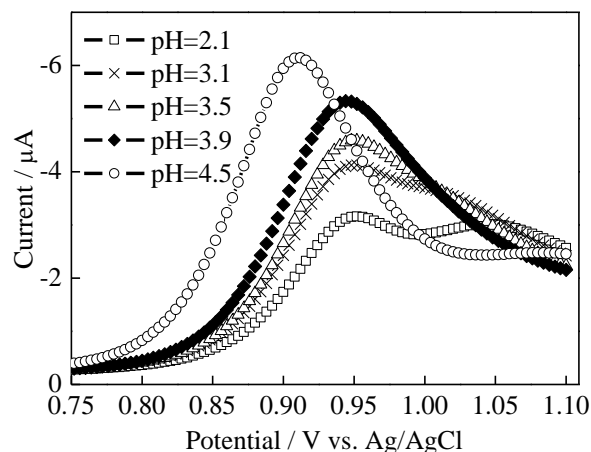


Fig. 4. Influence of different pH on square wave voltammograms of 5×10^{-5} mol L⁻¹ LCN

In order to determine the linearity range of LCN in the proposed method, standard solutions containing LCN in the range from 3×10^{-7} mol L⁻¹ to 4.5×10^{-5} mol L⁻¹ were used. For each concentration, three replicate measurements were performed and the mean of these measurements was used in the plot of the calibration curve for the corresponding concentration.

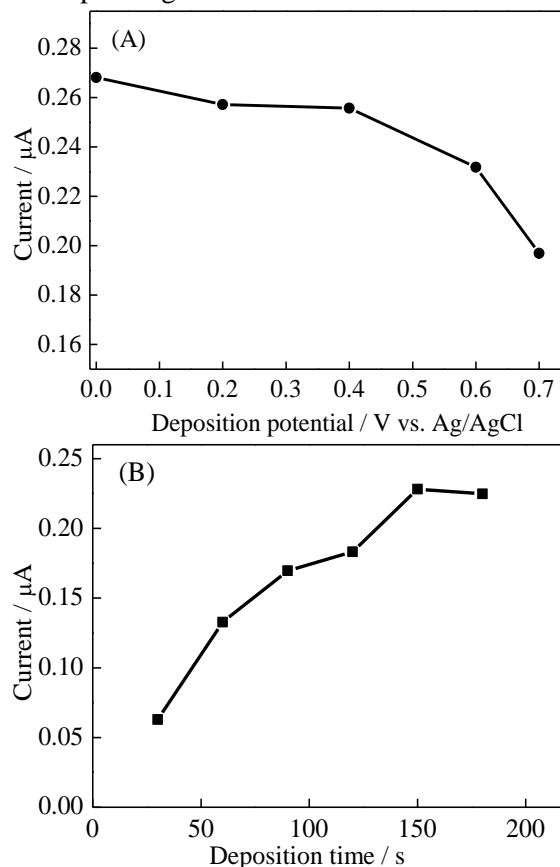


Fig. 5. Effect of deposition potential (A) and deposition time (B) on peak current of 6.5×10^{-7} mol L⁻¹ LCN at pH 4.5 in SWAAdSV (deposition potential: 0.0 V, deposition time: 150 s).

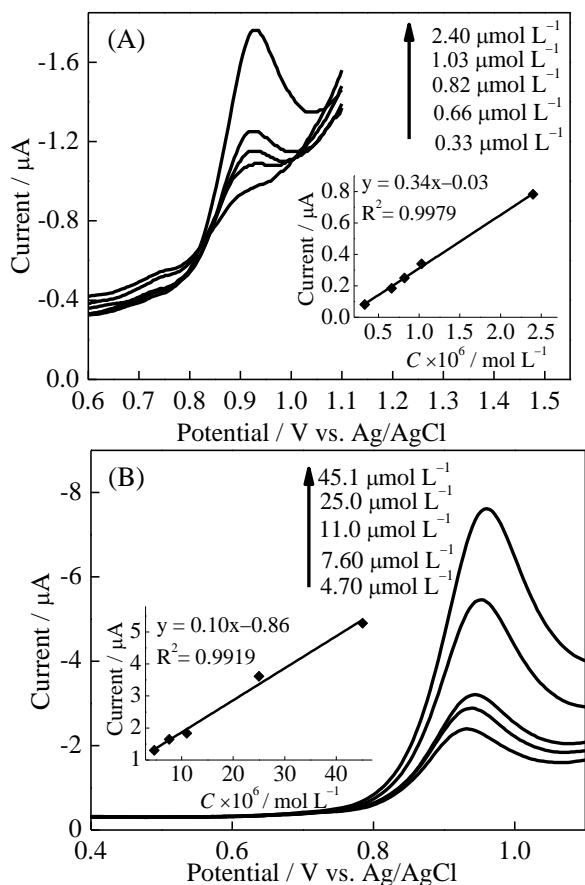


Fig. 6. SWAAdSVs of LCN at different concentrations (inset: calibration curve for the corresponding concentrations), first (A) and second (B) linear range

The currents of the oxidation peaks were linear with LCN concentration in two regions. The first linear range was from $3.3 \times 10^{-7} \text{ mol L}^{-1}$ to $2.4 \times 10^{-6} \text{ mol L}^{-1}$ with a regression equation of $i_{p(\mu A)} = 0.34 \times C_{\text{LCN}} (\times 10^6 \text{ mol L}^{-1}) - 0.03$ ($R^2 = 0.9979$) (Fig. 6 (A)) and the second one was from $4.7 \times 10^{-6} \text{ mol L}^{-1}$ to $4.5 \times 10^{-5} \text{ mol L}^{-1}$ with a regression equation of $i_{p(\mu A)} = 0.10 \times C_{\text{LCN}} (\times 10^6 \text{ mol L}^{-1}) - 0.86$ ($R^2 = 0.9919$) (Fig. 6 (B)).

The characteristics of the calibration plots are summarized in Table 1.

Table 1. Regression data of the calibration curve for assay of LCN by SWAAdSV

Calibration Parameter	First Linear Region	Second Linear Region
Linearity Range, mol L^{-1}	$(0.33 - 2.4) \times 10^{-6}$	$(4.7 - 45) \times 10^{-6}$
Calibration Equation	$i_{p(\mu A)} = 0.34 \times C_{\text{LCN}} (\times 10^6 \text{ mol L}^{-1}) - 0.03$	$i_{p(\mu A)} = 0.10 \times C_{\text{LCN}} (\times 10^6 \text{ mol L}^{-1}) - 0.86$
Slope of Calibration Curve, $\text{A mol}^{-1}(\text{m})$	0.34	0.10
Intercept, A	-2.89×10^{-8}	8.70×10^{-7}
SD (Standard Deviation) of Calibration, A	1.92×10^{-9}	1.73×10^{-7}
SD of Slope, A mol^{-1}	1.20×10^{-3}	5.18×10^{-3}
SD of Intercept, (s), A	6.78×10^{-10}	6.12×10^{-8}
Limit of Detection (LOD), mol L^{-1}	6.0×10^{-9}	1.83×10^{-6}
Limit of Quantification (LOQ) mol L^{-1}	2.0×10^{-8}	6.11×10^{-6}
Regression Coefficient, R^2	0.9979	0.9919
Repeatability of peak current ^a , (RSD, %)	2.93	7.46
Repeatability of peak potential ^a , (RSD, %)	0.25	0.25

^a Calculated for 5 replicate measurements

Application of the Proposed Method: The Dosage Form and Biological Samples

The determination of LCN in commercial tablets (labeled as 10 mg of LCN per tablet) was performed using the calibration curve method and the validity of the proposed SWAAdSV method was evaluated. Pretreatment procedures such as extraction or evaporation were not required for sample preparation. The amount of LCN determined using the proposed method is presented in Table 2. The applicability of the proposed method was also checked for spiked human urine and spiked human serum as described in the Experimental section. The obtained results are presented in Table 3. The accuracy of the proposed method was determined by its recovery values.

Validation of Method

The validation of an analytical method aims at demonstrating that the analytical procedure is suitable for the intended use. It involves determination of accuracy, precision, repeatability, intermediate precision, reproducibility, specificity, detection limit, quantitation limit, linearity range and robustness of the method [21]. The results of the validation studies are given in the above sections. Limit of detection (LOD) and limit of quantification (LOQ) values were calculated as described in [22] and were found to be $6 \times 10^{-9} \text{ mol L}^{-1}$ and $2 \times 10^{-8} \text{ mol L}^{-1}$, respectively. The accuracy of the measurement by means of the described procedure was checked by calculating the recovery of a known concentration of LCN following the proposed method. Recovery values ranged from 99.51 % to 102.55 % for tablet analysis, from 100.42 % to 105.48 % for urine analysis and from 98.06 % to 100.63 % for serum analysis (Tables 2 and 3).

Table 2. Results of proposed method for determination of LCN from the solution of lercadip® tablets

Sample ^a	Labeled value per tablet, mg	Found values per tablet, mg	Recovery value ^b , %	RSD ^c , %
I	10	10.19, 10.28, 10.30	102.56 ± 1.46	0.57
II	10	9.65, 9.93, 10.27	99.50 ± 7.71	3.12

^a Sample I is in the first linear region and II is in the second linear region

^b Results of recovery values are given as mean ± ts/√N (at 95 % confidence level)

^c RSD is relative standard deviation

Table 3. Results of the proposed method for determination of spiked standard LCN solution into various biological media

Sample ^a	Spiked, µg	Found, µg	Recovery value ^b	RSD ^c , %
Standard in Urine I	101.79	108.32, 107.02, 106.76	105.48 ± 1.98	0.78
Standard in Urine II	152.69	156.43, 152.06, 151.50	100.42 ± 4.39	1.76
Standard in Serum I	101.79	100.89, 100.51, 98.05	98.06 ± 3.76	1.54
Standard in Serum II	203.58	213.47, 201.79, 199.33	100.63 ± 9.22	3.69

^a Samples given in linear regions

^b Results of recovery values are given as mean ± ts/√N (at 95 % confidence level)

^c RSD is relative standard deviation

CONCLUSION

In the present study, for the first time the electrooxidation behavior of LCN was studied on a CPE. It was demonstrated that LCN has one oxidation peak at the CPE at +0.93 V. The proposed method was used for determination of LCN in pharmaceutical tablets without pretreatment. The method developed in this study has a high potential to be applied in determining the content of LCN in commercial pharmaceutical preparations, spiked human serum and spiked human urine due to its high accuracy and precision (RSD < 10%).

Acknowledgement: The authors wish to thank to Prof. Nevin Erk from Ankara University, Faculty of Pharmacy, because of her kindly help to provide the standard LCN.

REFERENCES

1. K. J. McClellan, B. Jarvis, *Drugs*, **60**, 1123 (2000).
2. V. Barrios, C. Escobar, Á. Navarro, L. Barrios, J. Navarro-Cid, A. Calderón, *Int. J. Clin. Pract.*, **60**, 1364 (2006).
3. M. A. Abu El-Enin, D. R. El-Wasseef, D. T. El-Sherbiny, S. M. El-Ashry, *Int. J. Biomed. Sci.*, **5**, 261 (2009).
4. C. A. Mueller, A. B. B. González, W. Weinmann, *J. Mass Spectrom.*, **39**, 639 (2004).
5. T. Christians, D. Diewald, C. Wessler, Y. Otte, J. Lehmann, U. Holzgrabe, *J. Chromatogr., A*, **853**, 455 (1999).
6. T. Christians, U. Holzgrabe, *Electrophoresis*, **21**, 3609 (2000).
7. A. Álvarez-Lueje, S. Pujol, J. A. Squella, L. J. Núñez-Vergara, *J. Pharm. Biomed. Anal.*, **31**, 1 (2003).
8. A. B. Baranda, R. M. Jiménez, R. M. Alonso, *J. Chromatogr., A*, **1031**, 275 (2004).
9. A. Álvarez-Lueje, S. Pujol, L. J. Núñez-Vergara, J. A. Squella, *J. AOAC Int.*, **85**, 1247 (2002).
10. F. Öztürk, I. H. Taşdemir, D. A. Erdoğan, N. Erk, E. Kiliç, *Acta Chimica Slovenica*, **58**, 830 (2011).
11. Y. Altun, B. Uslu, S. A. Ozkan, *Anal. Lett.*, **43**, 1958 (2010).
12. M. A. T. Gilmartin, J. P. Hart, *Analyst*, **120**, 1029 (1995).
13. I. Švancara, K. Vytrás, K. Kalcher, A. Walcarius, J. Wang, *Electroanalysis*, **21**, 7 (2009).
14. R. S. Nicholson, I. Shain, *Anal. Chem.*, **36**, 706 (1964).
15. J. Wang, Study of Electrode Reactions and Interfacial Properties. In *Analytical Electrochemistry*, John Wiley & Sons, Inc.: 2006; pp 29.
16. Z. Mandić, B. Nigović, B. Šimunić, *Electrochim. Acta*, **49**, 607 (2004).
17. N. Menek, Y. Karaman, *Dyes Pigm.*, **68**, 101 (2006).
18. J. A. Squella, A. E. Iribarren, J. C. Sturm, L. J. Núñez-Vergara, *J. AOAC Int.*, **82**, 1077 (1999).
19. G. Altiokka, D. Dogrukol-Ak, M. Tunçel, H. Y. Aboul-Enein, *Arch. Pharm.*, **335**, 104 (2002).
20. R. N. Goyal, S. Bishnoi, *Bioelectrochemistry*, **79**, 234 (2010).
21. 2A. E. Bretnall, G. S. Clarke, 11 - Validation of Analytical Test Methods. In *SS&T*, Satinder, A.; Stephen, S., Eds. Academic Press: 2011; Vol. Volume 10, pp 429.
22. F. Ozturk, I. H. Tasdemir, Z. Durmus, E. Kilic, *Collect. Czech. Chem. Commun.*, **75**, 685 (2010).

ВОЛТАМПЕРОМЕТРИЧНИ ОТНАСЯНИЯ НА ЛЕРКАНИДИПИН И АНОДНО-АДСОРБЦИОНЕН ВОЛТАМПЕРОМЕТРИЧЕН МЕТОД ЗА АНАЛИЗ НА ФАРМАЦЕВТИЧНИ ДОЗИРОВКИ И БИОЛОГИЧНИ ФЛУИДИ

Ф. Йозтюрк^{1,*}, Д. Коюнджу Зейбек², Е. Килич³

¹ Департамент по химия, Факултет за изкуства и наука, Университет Намък Кемал, Текирдаг, Турция

² Департамент по химия, Факултет за изкуства и наука, Университет Думлупънар, Кютахия, Турция

³ Департамент по химия, Факултет за наука, Университет в Анкара, Анкара, Турция

Постъпила на 24 септември, 2013 г.; коригирана на 4 декември, 2014 г.

(Резюме)

Изследвани са електрохимичните отнасяния на лерканидипин (LCN) и са определени оптималните условия за необратима и дифузионно-контролирана окислителна реакция при потенциал (+ 0.93 V) при електрод от въглеродна паста (CPE) спрямо Ag/AgCl - електрод в буфер на Britton Robinson (BR) и водно-етанолова смес при рН 4.5. Електрохимичните изследвания са извършени при анодно-адсорбционна волтамперометрия с правоъгълни импулси (SWAAdSV). Намерена е линейна област между 3.3×10^{-7} и 4.5×10^{-5} mol L⁻¹ в две различни области; потенциалът и времето на пред-концентриране са намерени съответно 0.0 V and 150 s. По този метод е намерена границата на чувствителност като 2.0×10^{-8} mol L⁻¹ (0.012 mg L⁻¹). Методът е използван за определянето на съдържанието на LCN в търговски фармацевтични препарати човешки серум и човешка урина. Методът е много точен и чувствителен със стандартно отклонение под 1% във всички изследвани случаи.

Preliminary geochemical investigation of karst barré from eastern Serbia Sokobanja basin

D. M. Djordjević^{1,*}, A. R. Radivojević², M. A. Pavlović³, M. G. Djordjević¹, M. N. Stanković¹, I. M. Filipović², S. I. Filipović⁴

¹Laboratory for Geochemistry, Cosmochemistry and Astrochemistry, University of Niš, Serbia

²Department of Geography, Faculty of Science, University of Niš, Serbia

³Faculty of Geography, University of Belgrade, Serbia

⁴Faculty of Science, University of Niš, Serbia

Received September 30, 2013; Revised December 27, 2013

Karst barré is a hydrogeological phenomenon which denotes a karst terrain of limited area completely surrounded by rocks of low permeability, i.e. whose lower part is enclosed and bordered by more or less impervious rocks impeding ground water flowing out of the karst area. Sokobanja basin is one of the first localities where this kind of karst was detected. This study represents a preliminary geochemical analysis of karst barré samples from this locality. Atomic absorption spectrometric analysis shows that the studied samples are composed predominantly of Ca and contain minor amounts of Mg, probably in form of carbonate minerals obtained by dissolving with mineral acids. There are no detailed geochemical data about karst barré from this or any other locality in the available literature to date.

Keywords: karst, karst barré, Sokobanja basin, geochemical analysis, AAS.

INTRODUCTION

Karst and karst barré. Karst is the term used to describe a special style of landscape containing caves and extensive underground water systems that is developed on particularly soluble rocks such as limestone, marble and gypsum [1]. Soluble rocks with extremely high primary porosity (~30-50%) usually have poorly developed karst. Karst barré denotes an isolated karst that is impounded by impermeable rocks. Stripe karst is a barré subtype where a narrow band of limestone, crops out in a dominantly clastic sequence, usually with a stratal dip that is very steep or vertical [2].

In Eastern Serbia karst belongs to the Carpatho-Balkan geotectonic unit. It is characterized by isolated limestone areas separated by Neogene basins whose sediments cover the borders of the limestone areas. Some of the limestone masses are separated by Tertiary volcanic rocks. The thickness of limestone mass is not uniform, though the average thickness is 500 m. Karst is developed on mountain plateaus of various altitudes, starting from 500 to 700 m (on Miroč, Kalafat, Tresibaba Mts.), mostly situated at elevations from 1000 to 1100 m a.s.l. (at Beljanica, Devica, Ozren,

Tupižnica, Vidlič, Tresibaba and Kučaj Mts.), and finally at 1500 - 1600 m a.s.l. (at Suva planina) [3].

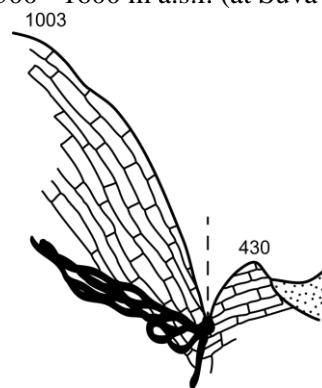


Fig. 1. Karst barré of the SB basin (based on Petrović and Petrović [4])

Soko Banja (SB) basin is the first locality on the Balkan peninsula where the karst barré (Fig. 1) has been detected by Cvijić [5]. This hydrogeological phenomenon can be recognised by lowering the spring under influence of groundwater which surrounds the karst. This phenomenon can represent a serious industrial problem with drinking water springs for water supply of population, considering the unpredictability of the spring.

* To whom all correspondence should be sent:
E-mail: dragance73@yahoo.com

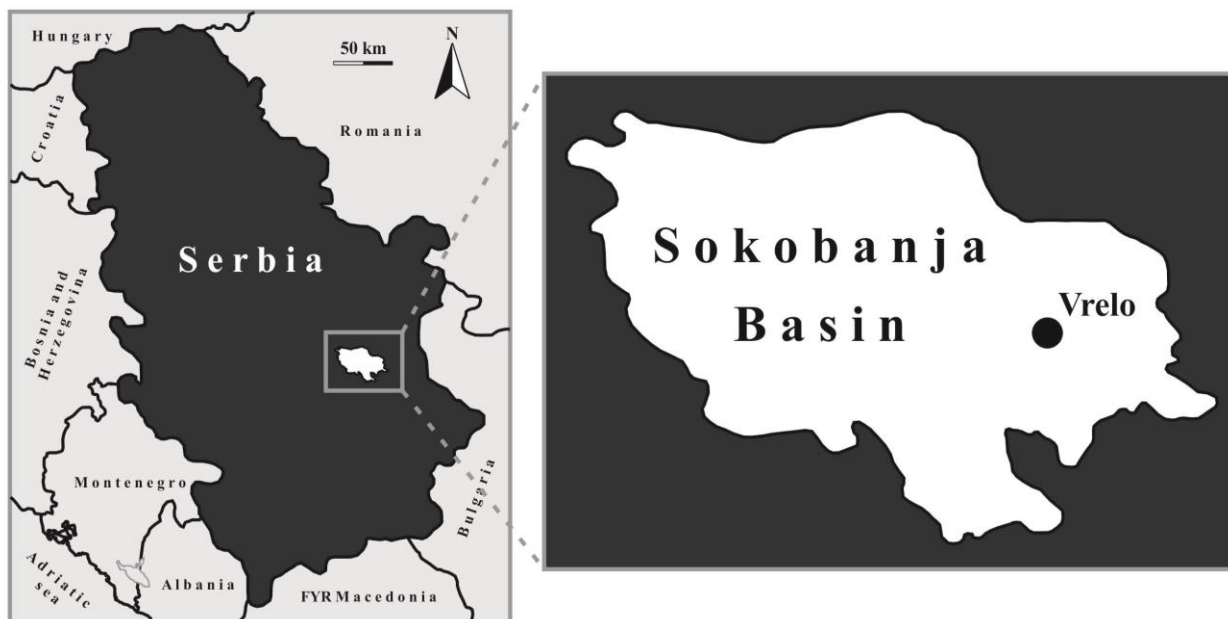


Fig. 2. Geographical location of SB basin

The aim of this preliminary study was to investigate the limestone facies and obtain more information of their geochemical composition.

Geographical location

The intermontane Sokobanja basin is located 250 km south-east of Belgrade (Fig. 1), and covers about 250 km². The Sokobanja basin is a north-south elongated tectonic depression with a maximum length of 29 km and width of 16 km. The basin was filled up by 1500 m thick limnic sediments, which had been accumulated during the time interval from the lower Palaeogene to the upper Miocene age [6,7]. The karst barré is most prominent at the east of the SB basin. The studied samples were collected from different locations of the SB (Fig. 2).

Geological setting

The complex tectonic evolution of the SB basin caused that it contains the rocks of various geological formations and compositions. The basement of the Sokobanja basin is composed of Proterozoic schist, Devonian schist and sandstone, Carboniferous schist and claystone with a thin coal bed, Permian sandstone, Triassic sandy limestone, Upper Jurassic dolomite and limestone, and Upper Cretaceous limestone (Fig 3) [8].

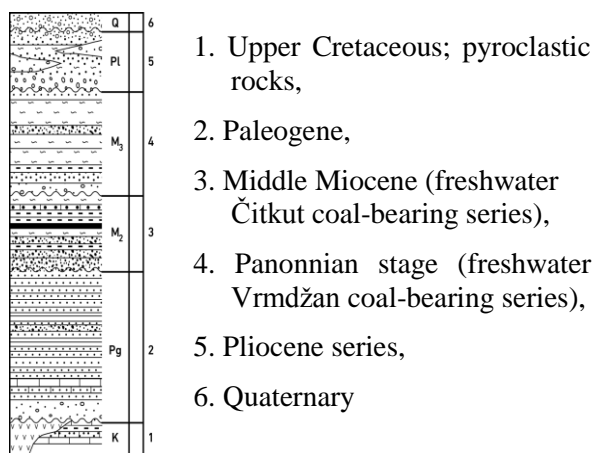


Fig. 3. Lithostratigraphic column of the SB basin (based on the Geological annals of the Balkan Peninsula [9])

These are mostly sedimentary formations, followed by crystalline shale and volcanic rocks, whose age is estimated at more than a billion years. Low-metamorphic Proterozoic shale of Bukovik and Rožanj formed the western rim of the basin, as well as the basal Tertiary sediments (Fig. 4, 5). The Carboniferous formations in the southern part of the basin are represented by conglomerates, quartz sandstones and shales with thin layers of coal. The Permian red sandstone, bedded limestones and dolomites are most common in the western part of the basin.

Eastern, northern and southern edges of the SB basin are mainly built of sediments of the Mesozoic age. The mountain massifs of Rtanj, Krastatac, Devica, Ozren and Leskovik are built of upper

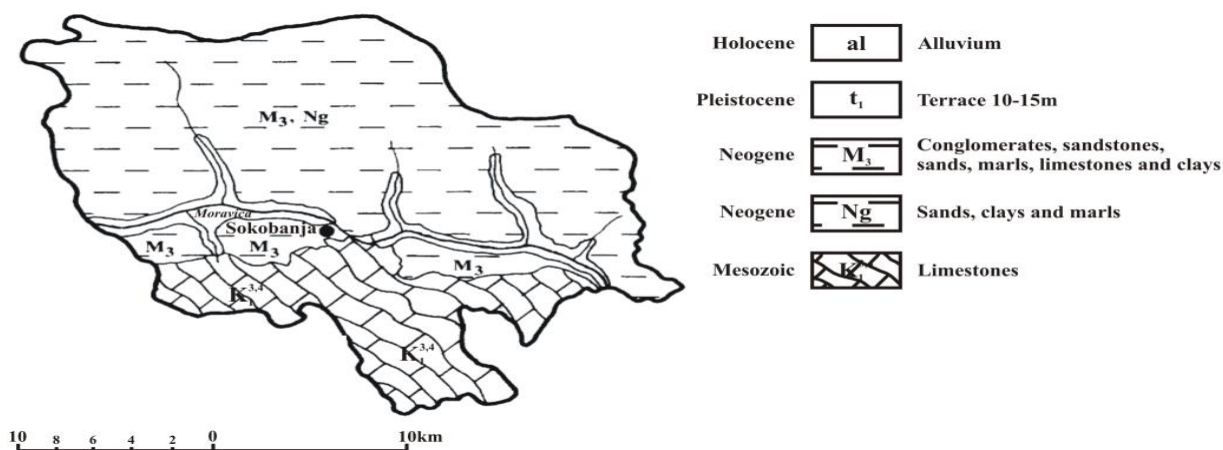


Fig. 4. Geological map of the SB basin (based on the Geological Guide [10])

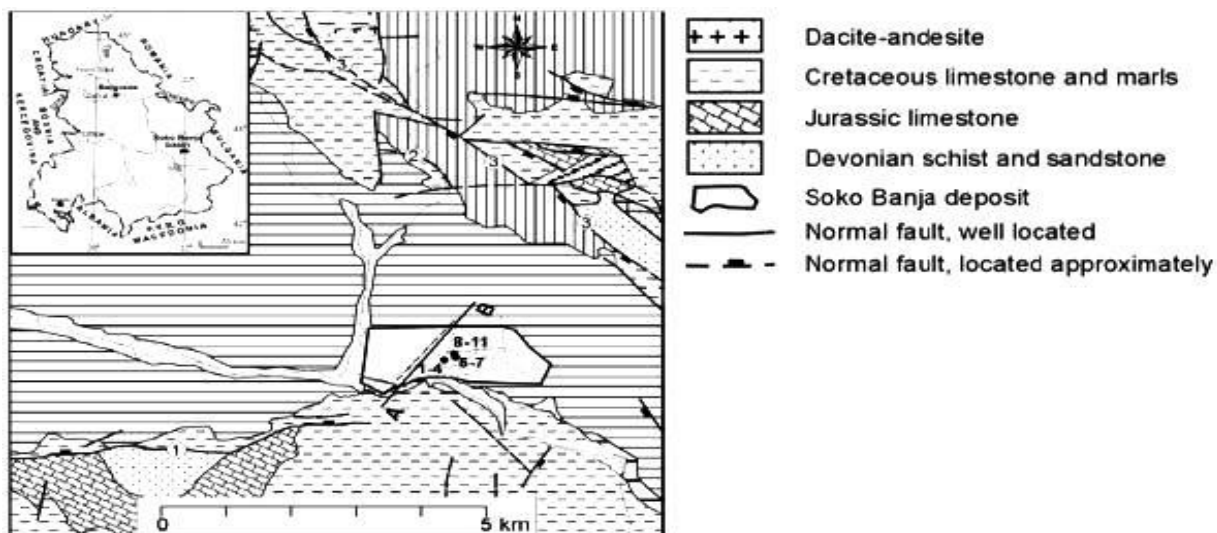


Fig. 5. Simplified tectonic map of the Soko Banja basin (modified after the Basic Geologic Map of the SFRY (modified after Novković et al. [6])).

Jurassic oolitic laminar and stratified limestone and dolomite. Four series [6] of sediments are recognized:

1. The Lower Palaeogene Series
2. The Čitluk Series
3. The Vrmdža Series
4. The Upper Series

The most important Soko Banja, Vrmdža, and Rtanj-Krstatac faults strike E–W, WNW–ESE, NW–SE, respectively [7]. There are also minor faults running N–S, which, together with the previously mentioned, control both the general contour and the shape of the basin.

EXPERIMENTAL

Six samples of karst barré from Sokobanja valley were investigated. (Fig. 1) Samples were collected from the surface of the SB. Three samples

were collected from Vrelo locality (43° 38' 03"N, 21° 59' 57"E) (samples 1, 2 and 3). The other samples were collected from the flow of the river Moravica (4,5,6).

Fractionation procedure

Pre-treatment. Before treatment with mineral acids, the samples were grinded in a vibrating mill to a particle size of 100 µm. The fractionation procedure was similar to that used by Premović *et al.* [11]. The flow chart in Fig. 6 outlines the major steps in preparing the two fractions of samples from SB basin.

Dissolution in acetate buffer. The powdered sample (1 g) was added in small amounts to 25 mL of 1 M acetate buffer (CH₃COOH/CH₃COONa, pH 4.8). After that the solution was mixed on a magnetic stirrer, without heat, for 12 h, then

centrifuged and rinsed with distilled water to a negative reaction to acetate. The residue was dried in an electric oven at 105 °C and weighed. The difference between the masses of untreated sample and insoluble residue, equals the percentage of fractions soluble in acetate buffer. The soluble material constitutes the carbonate fraction.

Dissolution in hydrochloric acid. The insoluble residue was further demineralized by repeated treatment with cold 6 M HCl. This acid solution removed most of the metal oxides. After rinsing and drying, the remainder was weighed and the fractions soluble in cold HCl were determined. The soluble material constitutes the fraction of metal oxides and hardly soluble carbonates.

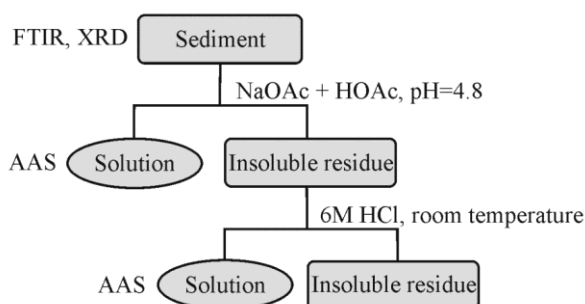


Fig 6. Flow chart of fractionation procedure

X-ray powder diffraction (XRPD) analysis

XRD analyses of the whole sample and the carbonate-free fraction were performed using a powder diffractometer SIEMENS D500 equipped with a scintillation counter, using Ni-filtered Cu radiation ($\lambda = 1.54184 \text{ \AA}$) at 35 kV and 20 mA. The diffractograms of the samples were recorded in the range from 4 to 75° 2 θ with 0.02° step and retention time of 0.5 s at each step. Program Search/Match was used for comparison of the diffractograms of the recorded samples to a database for identification of the crystalline phases in the samples. Analyses were performed in the Laboratory for Materials (Institute of Nuclear Sciences, Vinča).

Fourier Transform Infrared (FTIR) spectroscopy

The functional groups available in the untreated samples were detected by the KBr technique using

FTIR spectroscopy (Bomem, Hartman & Braun MB-100 spectrometer). The spectra were recorded at room temperature in the range from 4000 to 400 cm⁻¹. The KBr pellets were prepared from 1.5 mg finely powdered samples dispersed in 150 mg of anhydrous KBr. The obtained FTIR spectra were analyzed using Win Bomem Easy software. FTIR analyses of whole samples were performed in the Spectroscopy Laboratory (Faculty of Technology, Leskovac).

Atomic absorption spectrometry (AAS) analysis

The concentrations of metal ions (Ca, Mg and Fe) in the soluble residues were determined on a flame atomic absorption spectrometer Varian Spectra A-20 (Mulgrave, Victoria, Australia). Analyses were performed in the Laboratory for Applied and Industrial Chemistry (Faculty of Science, University of Niš).

RESULTS AND DISCUSSION

Sequential demineralization analysis showed that karst barré samples from the SB basin are completely dissolved after treating with acetate buffer (55.20 % of the sediment) and cold HCl (44.80 %) implying the absence of clay and other silicate minerals, as well as organic matter.

A typical FTIR spectrum of untreated sample is shown in Fig. 7. Similar spectra were recorded for all studied samples with bands characteristic for calcite and no bands that would indicate the presence of some other mineral phases. The carbonates in the samples were confirmed by the strong absorption bands between 3050-2850 cm⁻¹, 2650-2500 cm⁻¹, 1500-1400 cm⁻¹, and at 1800 cm⁻¹, 878 cm⁻¹, and 714 cm⁻¹ (Fig. 7, Table 1). Dolomite displays characteristic FTIR absorption bands at 3020 cm⁻¹, 2626 cm⁻¹ and 730 cm⁻¹, and the presence of these bands would indicate the presence of this mineral. However, the spectra of the investigated samples showed no presence of dolomite, probably owing to the low content of this mineral.

Table 1. Assignment of absorption bands to characteristic vibrations in the FTIR spectra of karst barré samples

Assignment	Sample	
	Wavenumber (cm ⁻¹)	
v(OH) stretching	2514	Calcite
v(C=O) stretching	1800	Calcite
v ₃ (CO ₃ ²⁻) asymm. stretching	1426	Calcite
v ₂ (CO ₃ ²⁻) out-of-plane	878	Calcite
v ₄ (CO ₃ ²⁻) planar stretching	714	Calcite

The X-ray diffraction analysis made it possible to identify the main crystalline phases in the studied samples. According to the interplanar distance values characteristic for each crystal, only one mineral has been found, calcite (CaCO_3), Figs. 8a/b. The chemical analysis of each sample (Table 2) showed that the studied samples also contain Mg carbonate, probably in form of dolomite, but the crystalline phases for this mineral were not identified due to the low content of this mineral in all studied samples. By AAS analysis only Ca^{2+} , Mg^{2+} and Fe^{3+} ions (in form of oxides in Table 2) were detected in the solutions after dissolution with mineral acids. The se metals are probably present as carbonate minerals in the sample.

Table 2. Results of the geochemical analysis of karst barré samples from the SB basin.

	Acetate buffer [wt %]	Cold HCl [wt %]
Solubility	54.8-55.4	44.6-45.2
CaO	48.3-53.6	35.8-39.4
MgO	2.7-4.0	0.9-2.4
Fe_2O_3	/	0-0.1

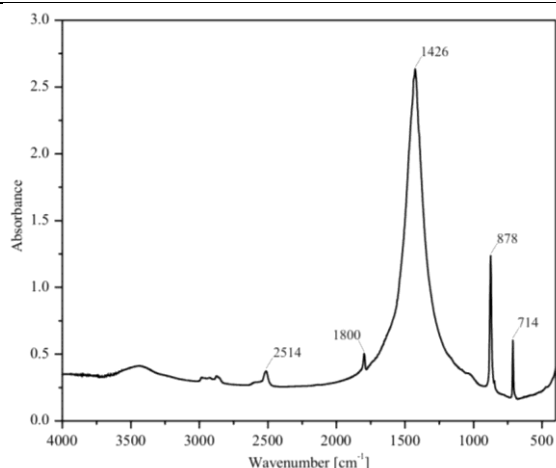


Fig. 7. FTIR spectrum of untreated sample

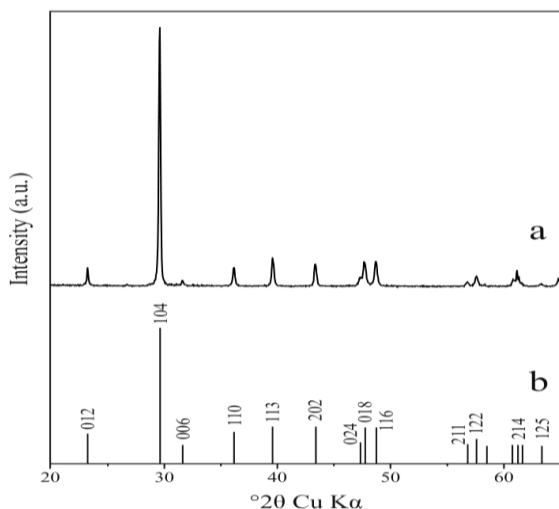


Fig. 8. a) XRPD patterns of untreated sample; (b) standard diffraction pattern for calcite (JCPDS card No. 83-0578).

The stereo-microphotographs of fine-grained raw (Fig. 9a) and acetate buffer treated (Fig. 9b) karst barré samples show that the material is homogenous calcite with no presence of organic matter and non-carbonate minerals.

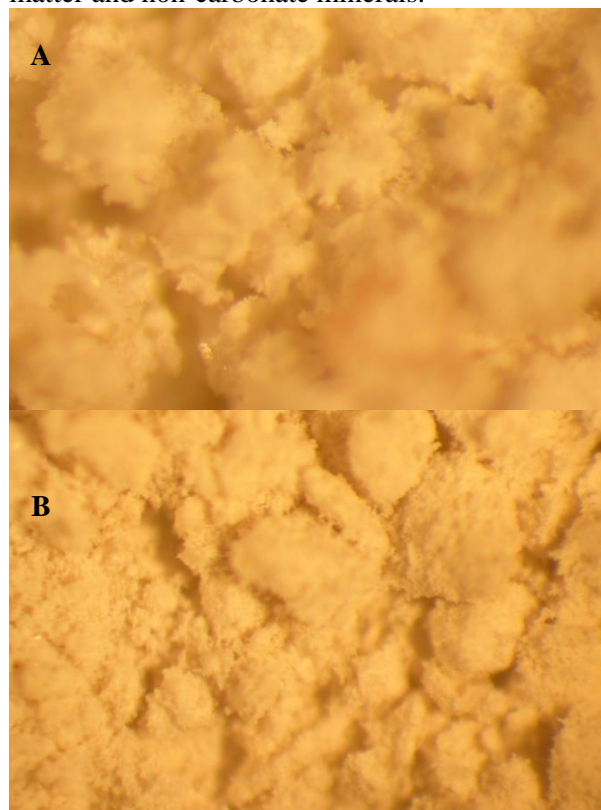


Fig. 9. Stereo-microphotographs (magnification up to 180×) of A) raw sample, and B) acetate buffer treated sample from SB basin.

CONCLUSION

Sokobanja basin is the first locality where karst barré has been detected. Karst barré as a hydrogeological phenomenon can be recognised by lowering the spring under influence of groundwater which surrounds the karst. This phenomenon can present serious problems with springs for municipal drinking water supply, considering the unpredictability of the spring behaviour.

The mineralogical analyses by XRD and FTIR techniques imply that the investigated samples are composed of pure calcite. Other mineral phases are not detected (probably because their contents are below the detection limits). The results of sequential demineralization procedure and atomic absorption spectrometric analysis show that the studied samples are composed predominantly from CaCO_3 and contain minor amounts of $\text{MgCO}_3/\text{CaMg}(\text{CO}_3)_2$, which is in correspondence with the chemical composition of karst. No clay, other silicate minerals, or organic matter were detected in the samples. The hydrogeological

phenomenon that accompanies the karst confirmed the assumption that the samples from the investigated locality belong to the karst barré.

Acknowledgements: This paper is the result of the project OI 176008 funded by the Ministry of Education and Science of the Republic of Serbia.

REFERENCES

1. D. Ford, P. Williams, Karst Hydrogeology and Geomorphology, John Wiley & Sons, West Sussex, 2007.
2. A. Kranjc, in: About the Name Kras (Karst) in Slovenia (Proc. 26th Brazilian Congr. Speleol.), Brasília 2001.
3. M. Zukorlica-Mandić, J. Čalić-Ljubojević, *Acta Cars.*, **28/1**, 149 (1999).
4. D. Petrović, B. J. Petrović, Morfologija i hidrologija krasa, Zavod za udžbenike i nastavna sredstva, Beograd, 1997.
5. J. Cvijić, Das Karstphänomen. Versuch einer morphologischen Monographie, Geographische Abhandlungen, Wien, 1893.
6. M. Novković, B. Milaković, D. Cvetković, in: The Geology of Serbia: Fossil Fuels, V. Aksin, B. Maksimović (eds.), VII, Belgrade, 1975 (in Serbian).
7. M. Marović, I. Đoković, D. Đinović, *Annales Geol. de la Penin. Balkanique* **54**, 145 (1990).
8. D. Životić, H. Wehner, O. Cvetković, B. Jovančićević I. Gržetić, G. Scheeder, A. Vidal, A. Šajnović, M. Ercegovac, V. Simić, *Inter. J. Coal Geol.*, **73**, 285 (2008).
9. Geological annals of the Balkan Peninsula, Belgrade, 1958.
10. Geological guide for journal Boljevac and Aleksinac, Faculty of Mining and Geology, Belgrade, 1975 (in Serbian).
11. P. I. Premović, G. S. Nikolić, M. P. Premović, I. R. Tonsa, *J. Serb. Chem. Soc.* **65**, **4**, 229 (2000).

ПРЕДВАРИТЕЛНО ГЕОХИМИЧНО ИЗСЛЕДВАНЕ НА КАРСТОВА КОТЛОВИНА В БАСЕЙНА НА СОКОБАНИЯ В ИЗТОЧНА СЪРБИЯ

Д.М. Джорджевич^{1,*}, А.Р. Радожоевич², М.А. Павлович³, М.Г. Джорджевич¹, М.Н. Станкович¹, И.М. Филипович², С.И. Филипович⁴

¹Лаборатория по геохимия, космохимия и астрохимия, Университет в Ниш, Сърбия

²Департамент по география, Научен факултет, Университет в Ниш, Сърбия

³Географски факултет, Университет в Белград, Сърбия

⁴Научен факултет, Университет в Ниш, Сърбия

Постъпила на 30 септември, 2013 г.; коригирана на 27 декември, 2014 г.

(Резюме)

Карстовите котловини (karst barré) са хидрогеологично явление, което се характеризира с ограничен карстов терен, заобиколен от скали с ниска пропускливост (ниските им части са ограничени от непроницаеми скали, пречещи на изтичането на подземните води). Басейнът Сокобаня е едно от първите места, където са открити такива карстови образувания. Това изследване представя предварителен геохимичен анализ на проби от това място. Анализът с атомно-абсорбционна спектрофотометрия показва, че изследваните проби са съставени главно от калций и съдържат малки количества от магнезий, вероятно като карбонати. Досега не са известни подробни геохимични данни за такива обекти на други места.

Effect of modification of zeolite A using sodium carboxymethylcellulose (CMC)

P. Padhi^{1,*}, S. K. Rout², D. Panda¹

¹Research and Development Center, Hi-Tech Medical College and Hospital, India

²Department of Chemistry Konark Institute of Science and Technology, India

Received November 3, 2013; Revised May 19, 2014

Structural modification of zeolite A was carried out using sodium carboxymethylcellulose (CMC). The product was characterized by XRD, FTIR, FESEM, EDAS and HRTEM. As a result of the modification reaction carried out at a temperature of 80°C, the particle size of zeolite A was reduced to 668.1 nm. The particle shape changed as a result of calcination after sonication.

Keywords: Zeolite A, adsorbent, sodium carboxymethylcellulose (CMC), ultrasonication, crystal and centrifugation.

INTRODUCTION

Structurally, zeolite is a framework of aluminosilicate which is based on infinitely extending three-dimensional AlO_4 and SiO_4 tetrahedra linked to each other sharing the oxygen [1-2]. Zeolite is a crystalline hydrated aluminosilicate of group I and II elements, in particular, sodium, potassium, calcium, magnesium, strontium and barium. More than 150 synthetic and 40 naturally occurring zeolites are known [3]. They can be represented by the empirical formula $\text{M}_{2/n}\text{O} \cdot \text{Al}_2\text{O}_3 \cdot x\text{SiO}_2 \cdot y\text{H}_2\text{O}$. In this oxide formula, x is generally equal to or greater than 2, since tetrahedral AlO_4 join only tetrahedral SiO_4 and n is the valency of the cation. Initially, only natural zeolites were used, but more recently, modified and synthetic forms have been made on an industrial scale giving rise to tailor-made zeolites. The properties that make zeolites unique and under a separate category are [4]:

- Cations within the cavities are easily replaced with a large number of cations of different valency which exert electrostatic or polarizing forces across the smallest dimension of the cavity [4].
- The cations introduced into the cavities by ion exchange have separate activities; this facilitates the opportunity of dual function catalysis involving acidity along with other activities [4].
- Zeolite has a well-defined highly crystalline structure with cavities in the aluminum silicate framework which are occupied by large ions and water molecules. The openings of the

cavities range from 0.8 to 1.0 nm in diameter which is of the order of molecular dimensions. The size and shape of these pores determine which molecules would enter the cavities and which not. So they are called molecular sieves [4].

The general chemical formula of zeolite A is $\text{Na}_{12} [\text{AlO}_2 \cdot \text{SiO}_2]_{12} \cdot 27\text{H}_2\text{O}$. According to the database of zeolite structure [5], zeolites of type A are classified into three dimensional grades, 3A, 4A and 5A, all of the same general formula but with a different cation type. When 75% of sodium is replaced by potassium, it is referred to as zeolite (3A). Alternatively, replacing of sodium by calcium gives rise to zeolite (5A). Zeolite is commercially produced from hydro gels of sodium aluminate and silicate [6]. Faujasite zeolite is obtained from KanKara Kaolin clay [7] and zeolite NaX - from Kerala Kaolin [8]. Because of the presence of a large volume of micro pores and the high thermal stability of the zeolite, this material is used for purification of waste water, and soil remediation [9,10]. Synthetic zeolites are widely used as industrial adsorbents for various gases and vapors [8] and as catalysts in petroleum industry [11]. They are also used for drying of gases and liquids of low humidity content where they show a higher adsorption capacity than other adsorbents. Further, they have a high tendency to adsorb water and other polar compounds like NH_3 , CO_2 , H_2S and SO_2 and a good capacity at very low temperatures compared with other adsorbents. Pressure swing adsorption (PSA) is one of the techniques which can be applied for the removal of CO_2 from gas streams. Zeolite has shown promising results in the separation of CO_2 from gas mixtures and can potentially be used in a PSA process [12-14].

* To whom all correspondence should be sent:
E-mail: payodharpadhi@gmail.com

Perfect defect-free zeolite crystalline structures are not readily available or easy to prepare. Therefore, most of the zeolite material has defects and spaces between crystals which are larger than the pore sizes in the crystalline structures. To control the pore size different methods have been adopted for modification of zeolite [9-10, 15-21]. A lot of work has already been done in chemical modification to prepare composite membranes for gas separation. No extensive works have been done for physical modification of zeolite.

The present study focuses on the physical modification of zeolite A to reduce particle size, as well as to achieve uniform distribution. There are different types of polymer hydrogels having temperature dependent gelation behavior, i.e., they convert to gel at elevated temperature and turn back to solution at room temperature. Further, the hydrogel has a three-dimensional network structure. Sodium carboxymethylcellulose (CMC) is a polymer that is cheap, economical, water-soluble, eco-friendly and adheres onto zeolite A. This helps to reduce the crystal size of the zeolite. Hence, CMC was used as a modifying agent for the zeolite.

EXPERIMENTAL METHOD

Materials

Raw zeolite A purchased from NALCO, India was used as the starting material for the modification experiments. The chemical composition was determined by atomic absorption spectroscopy (AAS) using Perkin Elmer AAnalyst 200/400, as shown in Table 1. Ignition loss and pH (1% in water) were found to be 21.84% and 10.3, respectively.

Table 1. Composition of Zeolite A

Molar composition: (Based on chemical analysis)	Average Chemical Composition (%)
1.0 ± 0.2 Na ₂ O	Na ₂ O 16.5-17.5
1.0 Al ₂ O ₃	Al ₂ O ₃ 27.5-28.5
1.85 ± 0.5 SiO ₂	SiO ₂ 32.5-33.5
6.0 (Max.) H ₂ O	

CMC was purchased from Central Drug House (CDH), India with the specification of technical purity (99.5 %).

Modification of zeolite

About 7.5 g of CMC was taken in a beaker, 150 mL of de-ionized water was added and ultrasonic dispersion was carried out for 5 min to make a homogeneous solution. Then 5 g of zeolite A was added to the solution. Ultrasonic dispersion was carried out for 3 h at 80°C. Finally, the zeolite was recovered from the mother liquor by repeated

cycles of centrifugation, decanting and ultrasonic redispersion in pure water until CMC was completely washed away (no bubbles observed). Modified zeolite was dried at 100°C for 3 h and calcined at 4 h at 600°C.

Characterization

The crystalline structure of the modified zeolite A was determined by X-ray diffraction using a PANalytical XPERT-PRO diffractometer with Cu-K α radiation ($\lambda=1.5406\text{\AA}$). Diffraction measurements were performed over the 2θ range from 5-80°.

The functional groups present after modification of zeolite A were determined by Fourier transform infrared spectroscopy (FTIR) using a Perkin Elmer SPECTRUM-GX FTIR spectrometer in the 4000-400 cm⁻¹ region using pellets of 0.5 mg powdered samples mixed with 250 mg of KBr.

The microstructure and the morphology of size reduction of the modified zeolite A were examined using field emission scanning electron microscopy (FESEM model ZEISS EM910).

The composition of the modified zeolite A was examined by energy dispersive X-ray spectroscopy (EDAS model ZEISS EM910).

The particle size of modified zeolite A was determined using high resolution transmission electron microscopy (HRTEM model ZEISS EM910) operated at 100 Kv, with a 0.4 nm point-to-point resolution side entry goniometer attached to a CCD Mega Vision III image processor.

RESULTS AND DISCUSSION

The powder X-ray diffraction patterns of a raw, water treated and modified zeolite A are shown in Fig. 1 (a), (b) and (c), respectively.

The patterns are plots of the X-ray intensity scattered from the sample *versus* the scattering angle (Bragg angle, 2θ). The positions and intensities of the peaks in the diffraction pattern are a fingerprint of the crystalline components present in the sample. In the samples Na₂O, Al₂O₃ and SiO₂ planes are present in the orthorhombic, rhombohedral and hexagonal unit cells, respectively. The faces [6 0 0], [6 2 2], [6 4 2], [6 4 4] are with higher intensities than [2 0 0], [2 2 0], [2 2 2], [4 2 0]. When treated with CMC, it anchored to faces [6 0 0], [6 2 2], [6 4 2], [6 4 4]. This is evident from the lowering of peak intensities. The peaks in the XRD pattern of zeolite A treated with CMC are slightly broadened, as compared to those of raw zeolite A and zeolite A treated with water. This points to a decrease in the crystallite size of the modified zeolite A.

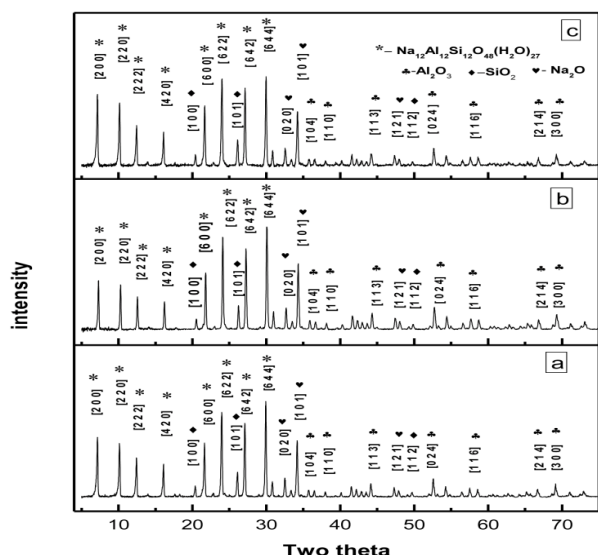


Fig.1. X-ray diffraction patterns of (a) raw zeolite A, (b) zeolite A treated with water and (c) zeolite A modified with CMC.

During modification, the temperature does not exceed 80°C. It is found that during sonication, the local heat caused by inter-particle collisions (for ~10 μm particles) could reach 2600-3400°C [22]. Thus, it is possible that the modification of the supplied zeolite A could take place at a lower macroscopic temperature because of the extremely high local temperatures generated during sonication. It is observed that sub-micro particles cannot be separated by stirring. Sonication is one of the most effective methods for dispersing the particles; however a stabilization technique like centrifugation must be used to prevent high agglomeration once sonication stopped. Higher temperature might de-mature the CMC structure and interaction is prompted at elevated temperature. That is why we picked up 80°C as a reaction temperature well below the boiling point of the solution. Calcination does not change crystallinity, and 600°C calcination cannot remove the anchored CMC from the zeolite faces, which is evident from the low-intensity peaks [1 0 1], [6 4 4], [6 2 2], [6 4 2], [1 0 1].

The FTIR spectra of raw zeolite A treated with water and modified with CMC are shown in Fig. 2(a), 2(b) and 2(c), respectively.

The absorption peaks are discussed individually. A characteristic strong and broad band at 3400 cm⁻¹ is seen due to O-H stretching vibrations [23]. The band at 2100 cm⁻¹ is due to Si-H stretching, vibration [24,25]. The deformation band at 1640 cm⁻¹ confirming the presence of bound water [23], pre-dominant in Fig. 2 (b), is related to the (H-O-H) bending vibration of water molecules adsorbed on zeolite. The band at 1150 cm⁻¹ appears because of

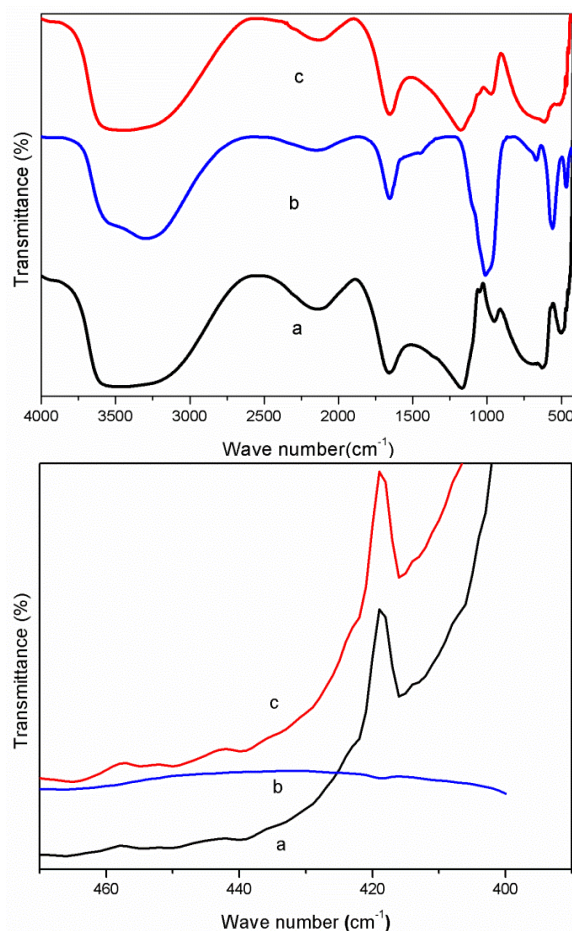


Fig. 2. FTIR spectra of (a) raw zeolite A, (b) zeolite A treated with water and (c) zeolite A modified with CMC.

Si-O-Si asymmetric stretching [26] which is insignificant in Fig. 2(b) due to the presence of excess water molecule in the pores of zeolite A treated with water. The band appearing at 1034 cm⁻¹ [27] related to T-O-T (T=Si and/or Al) stretching is more intense in zeolite A treated with water as shown in Fig. 2 (b) because of the excess of water molecules. The asymmetric Al-O stretch of Al₂O₃ is located at 950 cm⁻¹ [28]. The bands at 557 cm⁻¹ and 620 cm⁻¹ (in the region of 500 - 650 cm⁻¹) are related to the presence of double rings (D4R and D6R) in the framework structure of these zeolites [28]. The band at 557 cm⁻¹ also could represent the beginning of the crystallization of a zeolite with double rings [29]. The bands at 420 cm⁻¹ and 490 cm⁻¹ (in the region of 420-500 cm⁻¹) are related to internal tetrahedral vibrations of Si-O and Al-O in SiO₂ and Al₂O₃ [28]. The two most intense bands of the zeolite usually occur at 860-1230 cm⁻¹ and 420-500 cm⁻¹, as shown in Fig.2. The first is assigned to an asymmetric stretching mode and the second one to a bending mode of a T-O bond. All these bands are more or less dependent on the crystal structure. The mid regions of the spectra contain the

fundamental framework vibration of Si (Al) O₄ groupings [30]. The bands in the region 400-420 cm⁻¹ are related to the pore opening or motion of the tetrahedral rings, which form the pore opening of the zeolite [1]. This is shown in the case of raw zeolite A and zeolite treated with CMC but in the case of water-treated zeolite the bands are missing, which is clearly evident from the spectra. The noise level of the bands in the region 400-420 cm⁻¹ decreased in the case of zeolite A treated with CMC which indicates that the rough zeolite surface is smoothed by the application of CMC.

The FESEM studies of raw zeolite A, zeolite A treated with water and that modified with CMC are shown in Fig. 3 (a), 3 (b) and 3 (c), respectively. The particle size of the raw zeolite A is in the range

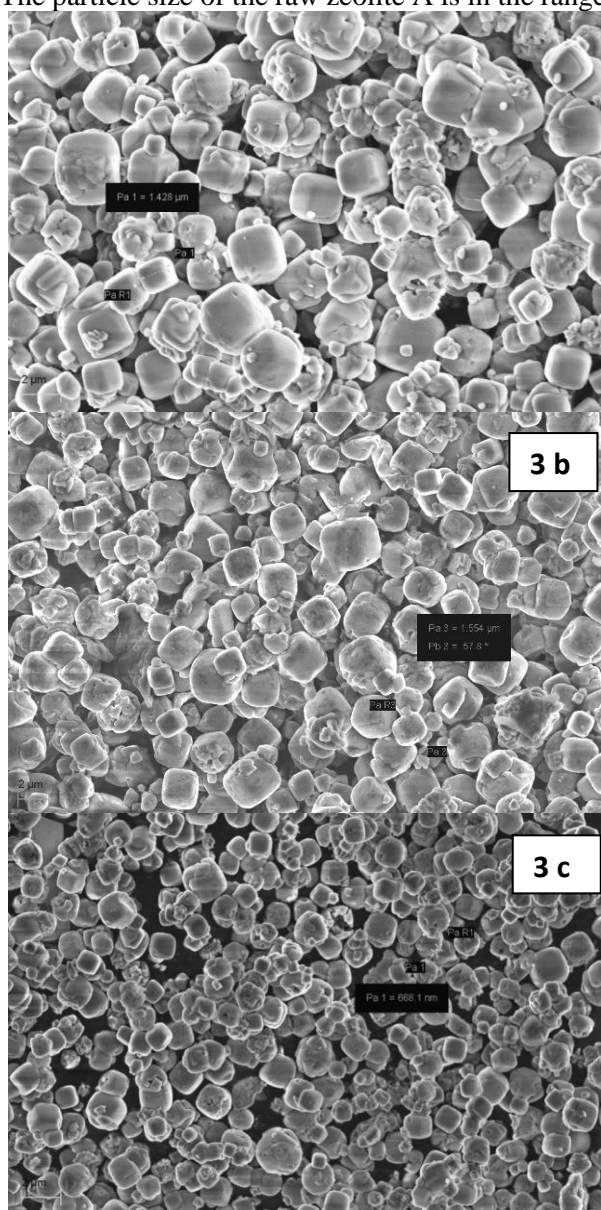


Fig.3. FESEM micrographs of (a) raw zeolite A, (b) zeolite A treated with water and (c) zeolite A modified with CMC.

of 2.5-3.5 μm with high agglomeration, which remains unchanged in case of zeolite A treated with water. After modification with CMC the particle size was found to be lower than 2 μm, in some cases being from 668.1 nm to 1 μm with better dispersion. Also the shape of the modified particles changed to slightly spherical one, as observed in Fig. 3 (b). This may be a result of calcination.

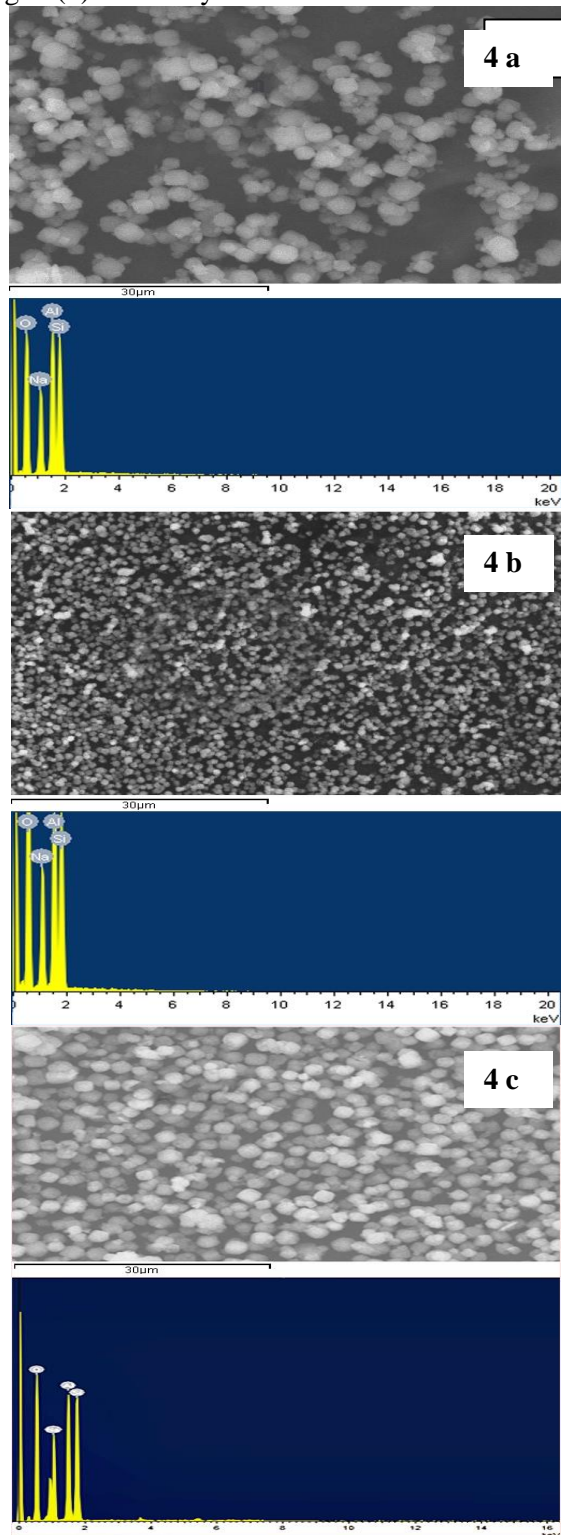


Fig.4. EDAS of (a) raw zeolite A, (b) zeolite A treated with water and (c) zeolite A modified with CMC.

The EDAS studies of raw zeolite A, zeolite A treated with water and that modified with CMC are shown in Fig.4 (a), 4 (b) and 4 (c), respectively.

The EDAS was done to determine any change of composition of both raw and modified zeolite. It is seen from Table 2 that the composition, weight and atomic percentage are changing slightly. Oxygen percentage is increasing whereas Na, Al, and Si percentages are decreasing after modification. This may be due to the particle size reduction after calcination. Further, it should be noted that in both raw zeolite A and zeolite A treated with water, the distribution of the particles is not uniform, whereas in the modified one, the particle distribution is uniform and with very few agglomerations.

The HRTEM micrograph studies of raw zeolite A, zeolite A treated with water and that modified with CMC are shown in Fig. 5 (a), 5 (b) and 5 (c), respectively.

It is seen that the particle size is in the range of 2.5-3.5 μm for zeolite A (as supplied) and remains unchanged in case of zeolite A treated with water. After modification with CMC, the particle size is found to be lower than 2 μm , which confirms the reduction of the size and shape of the zeolite.

CONCLUSIONS

It is found in the present study that modification of zeolite A using CMC is possible. As a result of CMC modification, the particle size is reduced from 3 μm to 1 μm and in some cases to 668.1 nm with better dispersion. The modified zeolite A may be used for purification of waste water, soil remediation, as a catalyst, molecular sieve, ion exchanger, adsorbent and for the removal of CO_2 from gas streams.

Acknowledgments: The authors acknowledge the Ministry of Environment and Forest (MOEF), Govt. of India for its financial support with sanction letter no 19-17/2008-RE and NALCO, Govt. of India for supplying zeolite A powder.

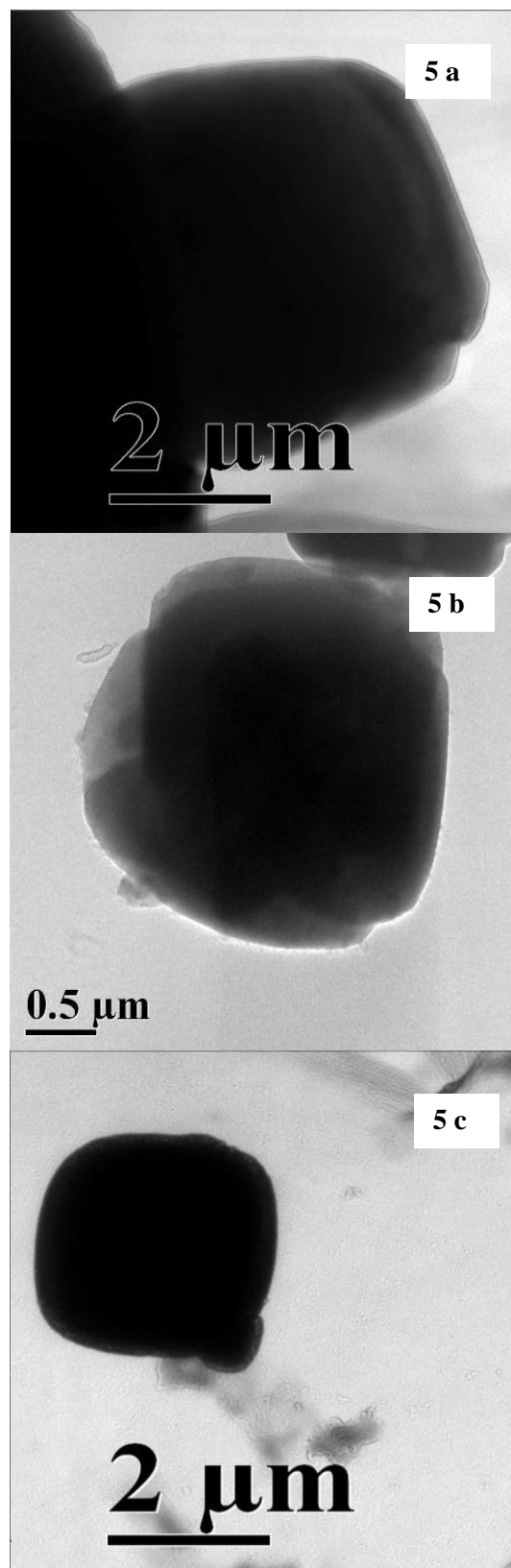


Fig. 5. HRTEM micrographs of (a) raw zeolite A, (b) zeolite A treated with water and (c) zeolite A modified with CMC.

Table 2. Elemental composition of raw zeolite A, zeolite A treated with water and that modified with CMC.

Elements	Raw Zeolite A		Zeolite A treated with water		Zeolite A modified with CMC	
	Weight %	Atomic %	Weight %	Atomic %	Weight%	Atomic%
O	50.01	62.01	19.79	37.97	56.98	68.31
Na	14.03	12.10	8.22	10.98	12.47	10.40
Al	16.98	12.48	11.57	13.16	14.87	10.57
Si	18.98	13.40	11.45	12.52	15.68	10.71
Total	100					

REFERENCES:

1. D.W. Breck; Zeolite Molecular Sieves: Structure, Chemistry and Uses, John Wiley, New York. (1974).
2. J.T. Richardson, Principles of Catalysts Developments, Plenum Press, New York and London. (1989).
3. B.K. Marcus and W.E. Cormier: Going Green with Zeolites. *Chem. Eng. Progress.* **95**, 47 (1999).
4. J.R. Ugal, K.H. Hassan and I.H. Ali, Preparation of Type 4A Zeolite from Iraqi Kaolin. Characterization and properties measurements. *J. Association of Arab Universities for Basic and Applied Sciences.* **9**, 1 (2010).
5. Database of Zeolite Structures, (2002) /www.zeolites.ethz.ch/zeolites/stdAtlas.htm.
6. R.G. Copperwaite, G.T. Hutching and M. Vander Riet: Preparation and Evaluation of a Synthetic zeolite Catalyst. *J. Chem Edu* **7**, 632 (1986).
7. A.Y. Atta, O.A. Ajayi and S.S. Adefila Synthesis of Faujasite Zeolites from Kankara Kaolin Clay. *J. Appl. Sci. Res.* **3**, 1017 (2007).
8. S. Chandrasekhar and P.N. Pramada Investigation on the synthesis of Zeolites NaX from Kerala Kaolin. *Journal of Porous Materials.* **6**, 283 (1999).
9. C. J. Rhodes, Properties and applications of zeolites. *Sci. Prog.* **93**, 223-84 (2010).
10. G. B. Gholikandi, M. M. Baneshi, E. Dhghanifard, S. Salehi, A. R. Yari Natural Zeolites Application as Sustainable Adsorbent for Heavy Metals Removal from Drinking Water. *Indian J. Toxicology.* **3**, 3 (2010).
11. J.G. Speight, The chemistry and technology of petroleum, Marcel Dekker Inc, New York. 1999.
12. K. Cheu, K. Jong-Nam, Y. Yun-Jong and C. Soon-Haeng, Fundamentals of Adsorption, Proc. Int. Conf, D. Levan (ed), Kluwer Academic Publishers: Boston. MA. 203 (1996).
13. R.V. Siriwardane, M. Shen, E.P. Fisher and J.P. Poston, Adsorption of CO₂ on molecular sieves and activated carbon. *Energy Fuels.* **15**, 279 (2001).
14. F. Dong, H. Lou, M. Goto and T. Hirose, A new PSA process as an extension of the Petlyuk distillation concept. *Sep. Purif. Technol.* **15**, 31 (1999).
15. S. Mishar, G. U. Rani, G. Sen, Microwave initiated synthesis and application of polyacrylic acid grafted carboxymethyl cellulose. *Carbohydrate Polym.* **87**, 2255-2262 (2012).
16. K. M. Jae, O. T. Hwan, H. S. Soo, J. S. Woo, J. H. Yong, C. D. Wook, Preparation of poly (vinyl alcohol) /silver-zeolite composite hydrogels by UV-Irradiation *Fibers and Polymers.* **15**, 101-107 (2014).
17. M. Ugrina, N. V. Medvidović and A. Daković: Characterization and environmental application of iron-modified zeolite from the Zlatokop deposit. *Desalination and Water Treatment* .1-13 (2013).
18. T. Haixiang, L. Changlin, R. Jiawen, W. Yanqin, L. Guanzhong: Synthesis of mesoporous zeolite single crystals with cheap porogens. *J. Solid State Chem* , **184**, 1820– 1827 (2011).
19. H. Long and J. L. Zuo: Effect of heat modification and bio-film on zeolite adsorption properties. *Key Eng. Materials.* **439-440** , 956-959 (2010).
20. Y. Tang, D. Zhou, and J. Zhang: Novel Polyvinyl Alcohol/Styrene Butadiene Rubber Latex/Carboxymethylcellulose Nanocomposites Reinforced with Modified Halloysite Nanotubes. Hindawi Publ. Corp. *J. Nanomaterials*, **8**, (2013).
21. H. Peng, G. Ma, W. Ying, A. Wand, H. Huang, Z. Lei, In situ synthesis of polyaniline/sodium carboxymethyl cellulose nanorods for high-performance redox supercapacitors. *J. Powder Sources*, **211**, 40-45 (2012).
22. S.J. Doktycz and K.S. Suslick, Inter particle collisions driven by ultrasound. *Science.* **247**, 1067 (1990).
23. H. Dogan and N.D. Hilmiglu, Zeolite-filled regenerated cellulose membranes for pervaporative dehydration of glycerol. *Vacuum.* **84**, 1123 (2010).
24. F. Ruiz, C.V-Lopez, J.G-Hernandez; D.D. Allred, G.R-Paredes, R.P-Sierra and G.T-Delgado, Meso structure of Photo Luminescent porous silicon. *J. Vacuum Sci. and Technol.* **A12**, 25 (1994).
25. R.R. Koropecski and R. Arce, Infrared study of the kinetics of oxidation in porous amorphous Silicon. *J. Appl. Phys.* **60**, 1802 (1986).
26. K.L. Pong, S.C. Chen and K.W. Cheah, Photo luminescence of laser ablated silicon, *Solid State Communications*, **99**, 887 (1996).
27. S.S. Rayalu, Estimation of crystallinity in fly ash-based Zeolite-A using XRD and IR Spectroscopy. *Current Science.* **89**, 25 (2005).
28. C.A. Rios, C.D. Williams and M.A. Fullen, Nucleation and growth history of zeolite LTA synthesized from ualinite by two different methods. *Appl. Clay Sci.* **42**, 446 (2009).
29. M. Alkan, C. Hopa, Z. Yilman and H. Guler, The effect of alkali concentration and solid/liquid ratio on the hydrothermal synthesis of zeolite NaA from natural Kaolinite, *Macroporous Mesoporous Materials*, **86**, 176 (2005).

P. Padhi et al.: Effect of Modification of Zeolite A using Sodium Carboxy Methyl Cellulose (CMC)

30. K. Ojha, N. C. Pradhan, A. N. Samanta, Zeolite from fly ash: synthesis and characterization, *Bull. Mater. Sci.* **27**, 555 (2004).

ЕФЕКТ НА МОДИФИКАЦИЯТА НА ЗЕОЛИТ А С НАТРИЕВА СОЛ НА КАРБОКСИМЕТИЛЦЕЛУЛОЗА (СМС)

П. Падхи^{1,*}, С.К. Рут², Д. Панда¹

¹Център за изследвания и развитие, Хай-тек медицински колеж и болница, Индия
Департамент по химия, Научно-технологичен институт „Конарк“, Индия

Постъпила на 3 ноември, 2013 г.; коригирана на 19 май, 2014 г.

(Резюме)

Извършена е структурна модификация на зеолит А с помощта на натриевата сол на карбоксиметилцелулоза (СМС). Продуктът е охарактеризиран с XRD, FTIR, FESEM, EDAS и HRTEM. В резултат на реакцията, протекла при 80°C размерите на частиците на зеолита са намалени до 668.1 nm. Формата на частиците се променя в резултат на калциниране след звукова обработка.

Influence of pH and aeration on 2,3-butanediol production from glucose by *Klebsiella pneumoniae* G31

F. V. Tsvetanova, K. K. Petrov*

Institute of Chemical Engineering, Bulgarian Academy of Sciences, Sofia, Bulgaria

Received October 8, 2013; Accepted October 26, 2013

The strain *Klebsiella pneumoniae* G31, an extra-producer of 2,3-butanediol (2,3-BD) from glycerol, was tested in glucose fermentation. Key factors affecting the fermentation, such as pH and aeration regime were optimized. The best conditions favorable for 2,3-BD production were found to be pH 6.0, air flow 1.45 vvm and agitation speed of 500 rpm. Thereby, after 18 h of fermentation, the concentration of 2,3-BD reached a maximum of 30.4 g/l with productivity of 1.69 g/l h and yield of 0.32 g/g. The efficiency of the process demonstrates the potential industrial application of *K. pneumoniae* G31 as a 2,3-BD producer from glucose-containing feedstock.

Keywords: 2,3-butanediol, glucose, *Klebsiella pneumoniae*, pH, aeration.

INTRODUCTION

The growing interest in 2,3-BD production in recent years is due to the wide range of industrial applications of diols. 2,3-BD and its derivatives as 1,3-butadiene, ethylketone and many others, are extensively used in many industrial sectors: manufacturing of printing ink, perfumes, explosives, softening agents, plasticizers, foods and pharmaceuticals [1,2,3]. In addition, its high octane rating makes 2,3-BD a potential aviation fuel [4].

2,3-butanediol can be produced *via* the mixed acid-alcohol fermentation pathway from carbohydrates. In certain conditions 2,3-BD is the major product, but accumulation of acids, ethanol and carbon dioxide cannot be avoided. The most preferable carbon source is glucose, although 2,3-BD can be produced naturally from different hexoses, pentoses, disaccharides or glycerol [5,6]. As the final price of the product strongly depends on the raw material cost, recently the focus is on the use of cheaper and abundant raw materials as molasses, whey, Jerusalem artichoke, crude glycerol, lignocellulosic materials, food industry residues or wood hydrolysates [2,7,8].

Although many species can generate 2,3-BD, only the strains of *Klebsiella pneumoniae* and *Klebsiella oxytoca* are capable of producing it in quantities high enough for industrial application. Of

significant importance for the process efficiency are the fermentation conditions. The key role to enhance 2,3-BD yield and productivity, as well as to decrease by-product formation is played by the medium composition and pH and the oxygen supply. Since 2,3-BD is produced *via* mixed acid fermentation, usually the higher the pH of the media, the greater are the amounts of acids produced. On the other hand, lower values of pH lead to lower biomass formation and consumption rate. Hence, the highest 2,3-BD concentration, productivity and conversion rate could be obtained at different pH conditions. The oxygen supply also has a contradictory effect on 2,3-BD production. Jansen *et al.* [9] found that higher aeration rates increase biomass formation, but decrease 2,3-BD accumulation. On the opposite, lower oxygen supply decreases both conversion rate and cell density. Thus, aiming at shifting the metabolic flux toward 2,3-BD, a lot of new strategies of oxygen supply control [10], pH control [11], and medium optimization [12] were developed. In any case, the optimum values of the air flow, pH and agitation speed control are strain specific and should be experimentally determined.

MATERIALS AND METHODS.

Strain. For the present experimental work the strain *Klebsiella pneumoniae* G31 was used, an extra-producer of 2,3-BD from glycerol [11,13], isolated from active slime [14] and deposited in the

* To whom all correspondence should be sent:
E-mail: kaloian04@yahoo.com

Bulgarian National Collection for Microorganisms and Cell Cultures under registration № 8650.

Media and cultivation conditions. The strain used for seed preparation was preserved at a temperature of -20°C with addition of 20% glycerol. The fermentation medium used for both inoculums and batch processes was previously optimized for 2,3-BD production from glucose [15]. Content (g/l): (NH₄)₂HPO₄, 4.91; Na-acetate, 3; KCl, 0.4; MgSO₄·7H₂O, 0.2; FeSO₄·7H₂O, 0.02; MnSO₄·7H₂O, 0.01; yeast extract, 5; ZnSO₄·7H₂O, 0.001. Inoculum cultures were supplemented with 30 g/l glucose, as 100 ml media were grown on a rotary shaker in 500 ml flasks at 37°C, agitation 200 rpm for 24 h. The batch fermentations were performed in a 1 l stirred bioreactor (Biostat® A plus, Sartorius Stedim Biotech, Goettingen, Germany). The media for all batch experiments were supplemented with 100 g/l glucose and sterilized at 105 °C for 15 min. Temperature was set to 37 °C and 1% (v/v) of inoculum was added. The aeration regime and pH of the medium were the subjects of optimization. The air flow and agitation speed control were varied between 0 and 1.6 l/min (up to 1.6 vvm) and 200 – 700 rpm, respectively. The pH was adjusted by 5 M NaOH.

Analytical methods. Glucose, 2,3-butanediol, ethanol, acetic, lactic and succinic acid concentrations were determined using high-performance liquid chromatography (HPLC). The metabolites were separated using a Bio-Rad column for organic acids analysis (Aminex Ion Exclusion HPX-87H) at 65°C and detected by RI detector (Perkin-Elmer series 10 HPLC). As a mobile phase

Table 1. Glucose consumption and products formation after 18 h of fermentation in batch processes with different pH control. Air flow 1.00 vvm, agitation 200 rpm.

Conditions	Glucose consumed (g/l)	2,3-BD (g/l)	Yield of 2,3-BD (g/g)	Acetic acid (g/l)	Lactic acid (g/l)	Ethanol (g/l)	Succinic acid (g/l)	Biomass (OD ₆₀₀)
uncontrolled pH	40.82	16.11	0.39	1.67	2.01	3.44	1.37	2.013
pH=5.5	62.81	19.20	0.31	-	7.08	4.65	3.54	2.150
pH=6.0	73.77	22.72	0.31	0.49	8.27	5.63	3.13	2.353
pH=7.0	97.06	19.21	0.20	4.84	21.04	8.62	3.85	2.678

Table 2. Glucose consumption and products formation after 18 h of fermentation in batch processes with different aeration. All fermentations were conducted without pH control.

Aeration		Glucose consumed (g/l)	2,3-butanediol (g/l)	Acetic acid (g/l)	Lactic acid (g/l)	Ethanol (g/l)	Succinic acid (g/l)	Biomass (OD ₆₀₀)
Air flow (vvm)	Agitation (rpm)							
1.0	200	40.82	16.11	1.67	2.01	3.44	1.37	2.013
1.15	500	50.97	21.80	1.80	0.39	2.62	1.14	2.150
1.45	500	65.00	24.15	1.70	0.15	2.30	1.05	2.425
1.60	500	60.78	23.46	1.47	-	2.19	0.90	2.637
1.60	700	5.1	2.08	1.50	-	-	-	2.986

0.005 M sulphuric acid at an elution rate of 0.6 ml/min was used. Cell growth was estimated by measurement of the optical density of the broth at 600 nm (OD₆₀₀) with a UV-1600PC spectrophotometer (VWR).

RESULTS

pH optimization.

The pH was optimized in batch processes under microaerobic conditions (1.0 l/min sterile air supply and agitation at 200 rpm). The pH was maintained at 5.5, 6.0, 7.0 or not controlled. The results showed that the higher pH maintained, the greater was the extent of biomass formation and the conversion rate. At pH 7.0 after 18 h of fermentation, almost the entire amount of 100 g/l glucose was consumed, but the main product was lactic acid (21.04 g/l). In all other cases the main product was 2,3-BD, and the lower the pH of the medium, the higher was the conversion of glucose to 2,3-BD. Nevertheless, the highest 2,3-BD concentration (22.72 g/l) was obtained at pH 6.0, because at lower pH values the glucose consumption sharply decreased. Thus, when pH was not controlled (pH decreased to 4.5), the highest conversion of glucose to 2,3-BD was obtained (0.39 g 2,3-BD / g glucose consumed), but the maximum concentration was only 16.11 g/l (Table 1).

Aeration regime optimization.

Batch fermentations with different air flow (1.0 - 1.6 vvm) and agitation speed (200 – 700 rpm) were investigated at non-controlled pH conditions. The results are given in Table 2.

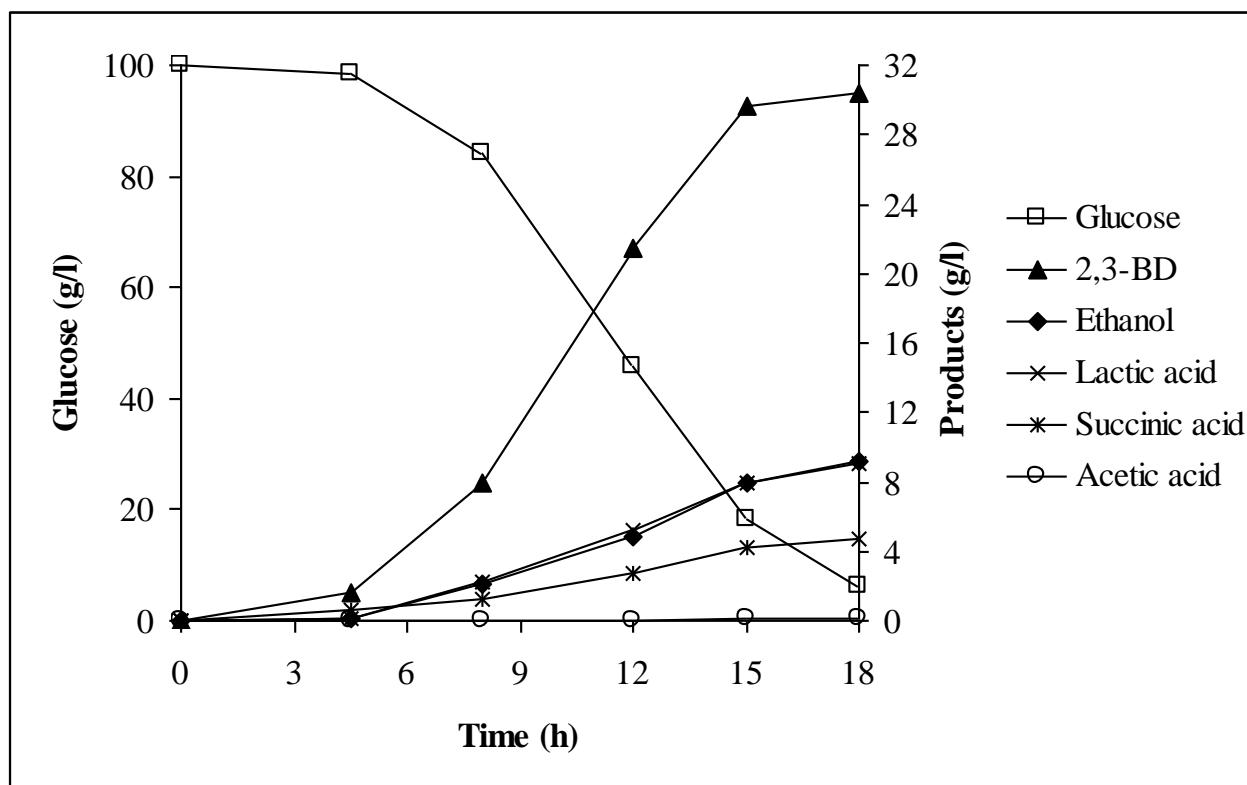


Fig. 1. Time courses of glucose consumption and products accumulation in batch fermentation. pH 6.0, air flow 1.45 vvm, agitation 500 rpm.

The titers of the soluble metabolites revealed that the highest aeration regime (air flow 1.6 vvm and agitation 700 rpm) is favorable only for biomass accumulation ($OD_{600}=2.986$ at 18 h). Glucose consumption completely ceased after few hours of fermentation, producing 2.08 g/l 2,3-BD and 1.5 g/l acetic acid. No other metabolites were detected. The highest concentration of 2,3-BD was obtained at an air flow of 1.45 (vvm) and agitation of 500 rpm – 24.15 g/l (productivity 1.34 g/l h) with an yield of 0.37 g/g glucose.

Batch fermentation in optimal conditions. Batch fermentation with presumed optimal pH and aeration was conducted (pH 6.0, air flow 1.45 vvm and agitation 500 rpm). After 18 h of fermentation 94 g/l glucose was consumed and 30.4 g/l 2,3-BD was accumulated (Fig. 1). The productivity was 1.69 g/l h and yield of 0.32 g/g glucose.

DISCUSSION

The pH control and the aeration regime are the most significant factors determining the shift of the metabolic pathways in mixed acid fermentations. Most anaerobic processes are coupled with organic acids formation. Thus, in the course of the fermentation the medium acidifies and the growth

and conversion of substrate gradually cease thus inactivating the culture by its own products [4].

Our observation is that extreme pH values are not suitable for 2,3-BD production. Considering the optimal pH for 2,3-BD production, the general opinion is that it is in the range between 5.0 and 6.0 [4,7,8]. Our results showed that at pH 7.0 the metabolic flux was shifted to acids production, especially in anaerobic conditions (Fig. 2).

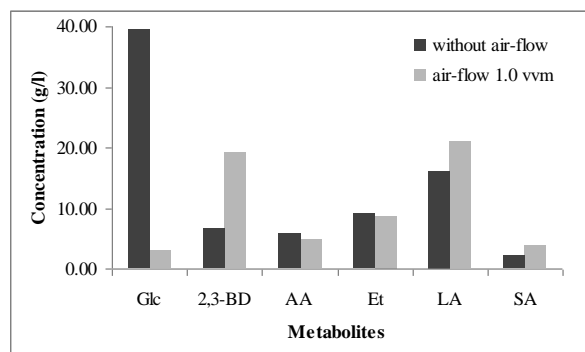


Fig. 2 Comparison of the residual glucose and products formation in batch processes with or without aeration after 18 h of fermentation. Initial concentration of glucose – 100 g/l. Glc – glucose, 2,3-BD – 2,3-butanediol, AA – acetic acid, Et – ethanol, LA – lactic acid, SA – succinic acid.

In contrary, the decrease of the maintained pH of the medium led to diminishing of the acid production and enhanced the 2,3-BD yield. The conversion of glucose to 2,3-BD reached its maximum at pH below 5.5, but at the same time, the substrate consumption sharply decreased because of weak biomass formation. This is the reason for the final 2,3-BD titer decrease at pH above 6.0.

The moderate enhancement of the oxygen supply also turns the metabolic flux towards 2,3-BD. Results revealed that at the highest aeration regimes the consumption rate decreased and the carbon flux shifted only towards cells formation. The explanation is based on *Klebsiella pneumoniae* metabolism. This species is a facultative anaerobe and can get energy by two different pathways: respiration and fermentation [4]. When the oxygen supply is limited, both pathways are simultaneously active, therefore, its minimizing would increase 2,3-BD yield. On the other hand, when oxygen supply is too low, the accumulated biomass is negligible and this results in decreased yield of 2,3-BD. In anaerobic conditions, the strain cannot survive when pH is not controlled. The combination of low pH (below 4.8-5.0) and absence of oxygen is lethal for the culture (data not shown).

CONCLUSIONS

Aiming at maximum 2,3-BD production, the optimum values of pH and aeration were investigated. The experimental results revealed that for *K. pneumoniae* G31, the maximum concentration and productivity (30.4 g/l, 1.69 g/lh) were obtained at pH 6.0, sterile air supply of 1.45

vvm and agitation speed of 500 rpm after 18 h of batch fermentation. These results are promising for 2,3-BD production on an industrial scale and prove the high potentialities of *K. pneumoniae* G31, comparable with the best known to date.

REFERENCES

1. A.V. Tran, R.P. Chambers, *Biotechnol. Bioeng.*, **29**, 343 (1987).
2. M.J. Syu, *Appl. Microbiol. Biotechnol.* **55**, 10 (2001).
3. S.J. Garg, A. Jain, *Bioresour. Technol.* **51**, 103, (1995).
4. E. Celińska, W. Grajek, *Biotechnol. Adv.* **27**, 715, (2009).
5. K.B. Ramachandran, G. Goma, *J. Biotechnol.* **9**, 39, (1998).
6. J. Qin, Z.J. Xiao, C.Q. Ma, N.Z. Xie, P.H. Lio, P. Xu. Chinese, *J. Chem. Eng.* **14**, 132, (2006).
7. L.-H. Sun, X.-D. Wang, J.-Y. Dai, Z.-L. Xiu, *Appl. Microbiol. Biotechnol.* **82**, 847, (2009)
8. X.-J. Ji, H. Huang, P.-K. Ouyang, *Biotechnol. Adv.* **29**, 351, (2011).
9. N.B. Jansen, M.C. Flickinger, G.T. Tsao, *Biotechnol. Bioeng.* **26**, 362, (1984).
10. X.-J. Ji, H. Huang, J. Du, J.-G. Zhu, L.-J. Ren, N. Hu, S. Li, *Bioresour. Technol.* **100**, 3410, (2009).
11. K. Petrov, P. Petrova, *Appl. Microbiol. Biotechnol.* **87**, 943, (2010).
12. C. Ma, A. Wang, J. Qin, L. Lin, X. Ai, T. Jiang, H. Tang, P. Xu, *Appl. Microbiol. Biotechnol.* **82**, 49, (2009).
13. K. Petrov, P. Petrova, *Appl. Microbiol. Biotechnol.* **84**, 659 (2009)
14. P. Petrova, K. Petrov, V. Beschkov, *Compt. rend. Acad. Bulg. Sci.*, **62**, 233 (2009).
15. F.V. Tsvetanova, K.K. Petrov, V.N. Beschkov, *J. Int. Sci. Publ. Ecology and Safety*, **7**, 257 (2013).

ВЛИЯНИЕ НА рН И АЕРАЦИЯТА ВЪРХУ ПОЛУЧАВАНЕТО НА 2,3-БУТАНДИОЛ ОТ ГЛЮКОЗА ЧРЕЗ *Klebsiella pneumoniae* G31

Ф.В. Цветанова, К.К. Петров *

Институт по инженерна химия, Българска академия на науките, София, България

Постъпила на 8 октомври, 2013 г.; приета на 26 октомври, 2013 г

(Резюме)

Щамът *Klebsiella pneumoniae* G31, екстра-продуцент на 2,3-butanediol (2,3-BD) от глицерол, е изпитан за ферментация при субстрат глюкоза. Оптимизирани са ключовите фактори, влияещи на ферментацията (рН и аерацията). Най-добрите условия, благоприятстващи получаването на 2,3-BD са намерени при рН 6.0, степен на аерация 1.45 vvm и обороти на бъркачката 500 об/мин. При това след 18 часа на ферментация концентрацията на 2,3-BD достига максимум от 30.4 g/l с производителност 1.69 g/l.ч добив от 0.32 g/g. Ефективността на процеса демонстрира потенциалното промишлено приложение на *K. pneumoniae* G31 като продуцент на 2,3-BD от глюкоза като суровина

Mineral composition, phenolic profile, antioxidant and antimicrobial activities of *Corchorus depressus* roots extracts

T. H. Bokhari^{1*}, M. A. Aslam¹, S. Hina², N. B. Rizvi³, N. Rasool¹, M. J. Saif⁴, M. Zubair¹, A. I. Hussain⁴, S. A. Shahid chatha⁴, M. Raiz¹

¹Department of Chemistry, Government College University, Faisalabad, Pakistan

²Department of Bioinformatics and Biotechnology, Government College University, Faisalabad, Pakistan

³Institute of Chemistry, New Campus, University of the Punjab, Lahore

⁴Department of Applied Chemistry and Biochemistry, Government College University, Faisalabad, Pakistan

Received November 29, 2013; Revised February 28, 2014

The present study was carried out to examine the mineral contents, phenolic profile, antioxidant and antimicrobial activities of *Corchorus depressus* roots extracts. The ground roots were extracted with the following solvents: n-hexane, ether, acetone, ethanol and methanol. The *Corchorus depressus* roots extracts contained the following metals: cobalt, nickel, copper, chromium, zinc, lead, and iron. Total phenolic contents (9.64-40.14 mg/100 g of dry matter were measured as Gallic Acid Equivalent), and total flavonoid contents (8.08-37.04 mg/100 g of dry matter) were measured as Catechin Equivalent). *Corchorus depressus* roots extracts showed very good DPPH radical scavenging of 56.31 % inhibition. The GC-MS analysis of the essential oils from the roots showed 13 compounds with n-butyl acetate (12.48%), 2,3,3-trimethyl octane (16.36%) and *cis*-methyl hexadecimal compounds (9.15%) as major components. All results of *Corchorus depressus* roots extracts and essential oils demonstrated significant ($P < 0.05$) variations.

Keywords: *Corchorus depressus*, DPPH, total phenolics, total flavonoids, MIC, GC-MS.

INTRODUCTION

An important phenomenon attracting the attention of many scientists is oxidation. Free radicals are considered to initiate oxidation which leads to aging and causes diseases in human beings. Oxidation widely occurs in food systems. It is mediated by oxygen free radicals or reactive oxygen species. Among organic compounds, lipids are prone to auto-oxidation reactions with oxygen. Lipid peroxidation is a major reaction of food deterioration which is responsible for significant changes in texture and nutritive value. Excessive amounts of free radicals are produced during the oxidation process with contribute to the progression of many clinical diseases. Dietary antioxidants might play positive role in delaying or inhibiting oxidation reactions [1].

Antioxidants play an important role in scavenging free radicals both *in vivo* and *in vitro*. The use of synthetic antioxidants such as butylated hydroxytoluene, butylated hydroxyanisol, propylgallate and *tert.* butylhydroquinone promotes negative health effects [2].

There is worldwide interest in replacing

synthetic antioxidants with natural ones. It has been observed that synthetic antioxidants are carcinogenic, pathogenic and toxic. Enzymes, lipids and reproductive processes are affected by them [3].

At present, plant-based natural antioxidants like phenols, flavonoids and tocopherols are gaining high recognition due to their antioxidant activities. They show anti-carcinogenic potential and various health-promoting effects. Food manufacturers prefer natural antioxidants to synthetic antioxidants as additives to healthy foods [4].

Some earlier chemical analyses and biological studies of various plants have been made [5-9] and more research work is required to study the unexplored plants.

Corchorus depressus belongs to the family *Mavaceae* (formally under *Tiliaceae*) and the genus is *Corchorus*. The common name of this plant is Bauphali. It is a perennial herb. It occurs in Pakistan, India, Africa and Cape Verde Islands. It grows from sea level to an altitude of 1000 m in arid and semi-arid regions throughout Pakistan [10]. It is 6-9 inches in length. The roots are diffusely branched. Its leaves are ecliptic, 4-18 mm long and 2-9 mm wide. Its flowers are yellowish, 1 mm long. The growth of leaves and fruits is stunted in saline and rocky soils [11]. This plant is regarded

* To whom all correspondence should be sent:
E-mail: tanveer.bokhari@yahoo.com

as a good sand binder in the desert. Its seeds are minute and their color is like chocolate. Its fruits are capsule-like with length in the range of 8-15 mm. Its branches are radiating from a woody crown [12]. It is reported that *Corchorus depressus* contains triterpenoids, sterols, phenolics, fatty acids, cardiac glycosides and carbohydrates [13]. Approximately 100 species of *corchorus* are found. South Africa is richest in species of *corchorus* (16), followed by Tanzania (13 species), Ethiopia (12 species), Kenya (11 species) and Pakistan (6 species). Wild species are mostly found in Africa, America, Brazil, Mexico, Bolivia, Venezuela, West Indies, Australia, China, Taiwan, India, Japan and Sri Lanka [14].

EXPERIMENTAL

Collection of Sample

Corchorus depressus roots were collected from Nankana District, Pakistan. The sample was identified and authenticated by Dr. Muhammad Naem, Assistant professor in the Botany Department of Government College University Faisalabad, Pakistan. The collected roots were dried under ambient temperature and crushed to powder in a mortar.

Chemicals and Reagents

Gallic acid, 2,2-diphenyl-1-picrylhydrazyl radical (90.0 %), folin-ciocalteu reagent, butylated hydroxytoluene (99.0 %), linoleic acid, ascorbic acid, aluminum chloride, ferric chloride, ferrous chloride, sodium nitrite, trichloroacetic acid, potassium ferricyanate were purchased from Sigma Chemicals Co (St, Louis, MO, USA). All other analytical grade chemicals such as ammonium thiocyanate, methanol and anhydrous sodium carbonate were obtained from Merck (Darmstadt, Germany).

Preparation of *Corchorus depressus* Extract

Extracts of *Corchorus depressus* roots were prepared using solvents of increasing polarity: methanol, ethanol, acetone, ether and n-hexane.

Determination of Total Phenolic Contents (TPC) and Total Flavonoid Contents (TFC)

Folin-ciocalteu reagent was used to determine the total phenolic contents following an already reported method [15].

Antioxidant activity in a linoleic acid system

The antioxidant activity was determined in terms of percentage inhibition of the peroxidation of a linoleic acid system using a method reported by Riaz et al. and Yen et al. [16,17]. The

percentage inhibition of linoleic acid peroxidation was calculated by the following equation:

$$\% \text{ inhibition of peroxidation} = 100 - \left[\frac{\text{Abs. increase of sample at 175h}}{\text{Abs. increase of control at 175h}} \times 100 \right]$$

DPPH Free Radical Scavenging Assay

The 2,2-diphenyl-1-picrylhydrazyl radical (DPPH) assay was carried out spectrophotometrically as reported in [18]. The IC₅₀ values were calculated. Three replicates were recorded for each sample. The percentage scavenging activity was calculated by the following equation:

$$\text{Inhibition (\%)} = 100 \times \left(\frac{A_{\text{blank}} - A_{\text{sample}}}{A_{\text{blank}}} \right)$$

Reducing Power

The reducing power of the extracts was determined by the method reported in [16,17]. The plant extracts containing 2.5-10 mg/ml of dry matter were mixed with sodium phosphate buffer (5.0 mL, 0.2 M, pH 6.6) and potassium ferricyanide (5.0 mL, 1.0 %); the mixture was incubated at 50°C for 20 min. Then 5 mL of 10 % trichloroacetic acid was added, centrifuged at 980xg for 10 min at 5°C in a refrigerated centrifuge. The upper layer of the solution (5.0 mL) was diluted with 5.0 mL of distilled water. 1 mL of 0.1 % ferric chloride was added and the absorbance was measured at 700 nm.

Antimicrobial Activity

The antimicrobial activity of the plant extracts was studied against the bacterial strains, *Pasturella multocida* (locally isolated), *Escherichia coli*, *Bacillus subtilis* and *Staphylococcus aureus* and the fungal strains *Aspergillus niger*, *Aspergillus flavus*, *F. solani* and *Rhizopus solani* by the disc diffusion method [19]. The minimum inhibitory concentration (MIC) was determined as described in [20,21] with some modifications.

Statistical Analysis

The experiments were carried out in triplicate and statistical analysis of the data was performed by analysis of variance, using STATISTICA 5.5. The probability value $p \leq 0.05$ was considered to denote a statistically significance evaluation. All results were presented as mean \pm SD.

RESULTS AND DISCUSSION

Percentage yield of roots extracts

The present study shows that the percentage yield extracts in the different solvents was in the range of 2.89 -5.69% in (Table 1)

Table 1. Percentage yield of different extracts of *corchorus depressus* roots

Extracts of roots	% Yield (g/100g dry matter)
Methanol	5.69
Ethanol	5.27
Acetone	3.29
Ether	3.19
n-Hexane	2.89

Total Phenolic Contents (TPC)

The folin-ciocalteu method was used for the determination of the quantity of TPC in the *Corchorus depressus* extracts. This method was preferred because of its higher sensitivity, lower interference and rapidity in comparison with other test [22]. Table 2 presents the amounts of TPC (mg/100 mg of dry weight as GAE).

Table 2. Total phenolic contents (TPC) of *Corchorus depressus* roots

Extract	TPC (mg/100 g of dry matter measured as GAE)
Methanol	40.14±1.02
Ethanol	40.32±1.07
Acetone	26.62±0.06
Ether	11.20±1.02
n-Hexane	9.64±0.07

The present results for TPC in *Corchorus depressus* roots using pure methanol as a solvent were in close agreement with those (38.60 mg GAE/100g fresh weight) reported for the antioxidant activity of phenolic fractions in *Corchorus depressus* roots in methanol using an FTC model (HUDA) [23].

Table 3 presents the amount of total flavonoid contents (mg/100 g of dry weight as CE) of the roots extracts of *Corchorus depressus*. The present

results for TFC of *Corchorus depressus* roots are in the range of 8.08-37.04 (mg/100g of CE).

Table 3. Total Flavonoid Contents (TFC) of *Corchorus depressus* roots

Extract	TFC (mg/100 g dry matter measured as (CE)
Methanol	37.04±0.07
Ethanol	28.14±1.02
Acetone	26.07±0.09
Ether	24.34±1.03
n-Hexane	8.08±0.06

DPPH Radical Scavenging Activity

The free radical DPPH is stable and has a deep violet color in the range of 515-528 nm. As DPPH accepts a proton from proton-donating species, especially phenols, its color changes from deep violet to yellow. The DPPH scavenging activity increases as the concentration and degree of hydroxylation increases. In the transformation of DPPH to its reduced form DPPH-H, the extracts behave as donors of protons or electrons. In a concentration- dependent manner, the free radical scavenging capacity of the extracts increased. Table 4 shows that the *Corchorus depressus* root extracts display excellent radical scavenging activity.

Table 4: DPPH free radical scavenging activity of *Corchorus depressus* roots

Extract	IC ₅₀ (µg/ml)
Methanol	69.01±0.09
Ethanol	68.04±0.12
Acetone	58.06±0.16
Ether	36.11±0.12
n-Hexane	19.23±0.16
BHT	76.30±0.08

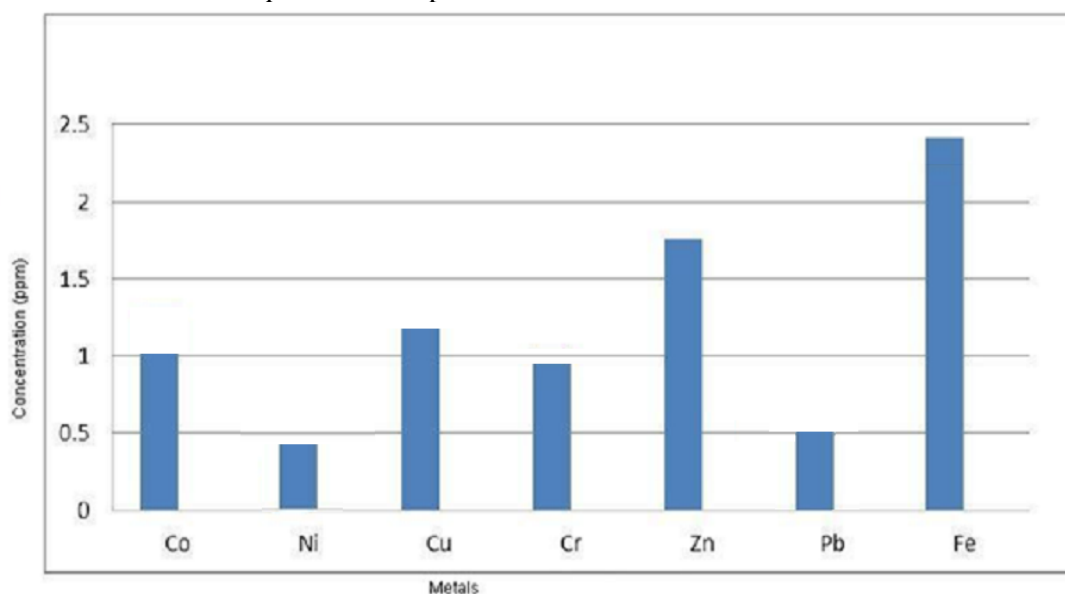


Fig. 1 Concentration of metals in *Corchorus depressus* roots

Pure methanol exhibits the highest scavenging activity but slightly lower antioxidant activity when compared with the synthetic antioxidant BHT. Our result is comparable with those reported for the plant extract [18]. The scavenging activity of *Corchorus depressus*, was significantly ($p < 0.05$) lower than that of BHT which showed an IC_{50} value of 19.23 $\mu\text{g/mL}$.

Percentage Inhibition of Peroxidation in Linoleic Acid System

As antioxidants have the ability to prevent oxidation, the percentage inhibition of linoleic acid was employed to check the antioxidant activity of *Corchorus depressus* roots extracts, (Table 5). Linoleic acid gives upon oxidation peroxides which oxidize Fe^{+2} to Fe^{+3} . According to statistical analysis, the variation in percentage inhibition of the oxidation in linoleic acid by roots extracts was significant ($p < 0.05$) depending on the solvent system. The % inhibition of *corchorus depressus* using absolute methanol solvent system was found to be comparable with that of the synthetic antioxidant BHT (93.09%). Our results are in good agreement with the reported value of up to 70.60% for linoleic acid inhibition of peroxidation [24].

Concentration of metals in *Corchorus depressus* roots are presented in Fig. 1.

Table 5: Percentage inhibition of linoleic acid peroxidation by *Corchorus depressus* roots

Extract	% Inhibition
Methanol	56.31±1.03
Ethanol	49.71± 1.06
Acetone	42.32±0.09
Ether	16.20±0.06
n-Hexane	11.24±1.02
BHT	93.09±1.6

Reducing Power

The trends in the reducing power of *Corchorus depressus* roots extracts are presented in Fig. 2; the greater the color intensity, the greater is the absorption and, correspondingly, the antioxidant activity. The absorbance of the sample was measured out spectrophotometrically; the antioxidant activity increased when the concentration of the extracts increased. The extracts having higher concentration of phenolics and higher antioxidant activity also showed good reducing power of the phytochemical constituents [25]. Therefore, the reducing power may be used in the evaluation of antioxidant activity of plant extracts.

Antimicrobial Activity

The antimicrobial activity of the extracts against selected microorganisms is presented in Tables 6-7. The *Corchorus depressus* roots showed significant antimicrobial potential against most of the fungal and bacterial strains ($p < 0.05$). The *n*-hexane fraction showed the lowest activity against all tested fungal strains with zones of inhibition (mm) against *B. subtilis* (7.21 mm), *S. aureus* (6.18 mm), *P. multocida* (9.73 mm), *E. coli* (9.71 mm) respectively. The results indicated that the methanol extracts showed good activity against fungal strains. The lowest inhibition zones were registered against *F. solani* (15.44 mm). The *n*-hexane fraction showed the lowest activity against all tested fungal strains with zones of inhibition against *R. solani* (9.08 mm), *F. solani* (7.44 mm), *A. flavus*(8.66 mm) and *A. niger* (6.92 mm). It was

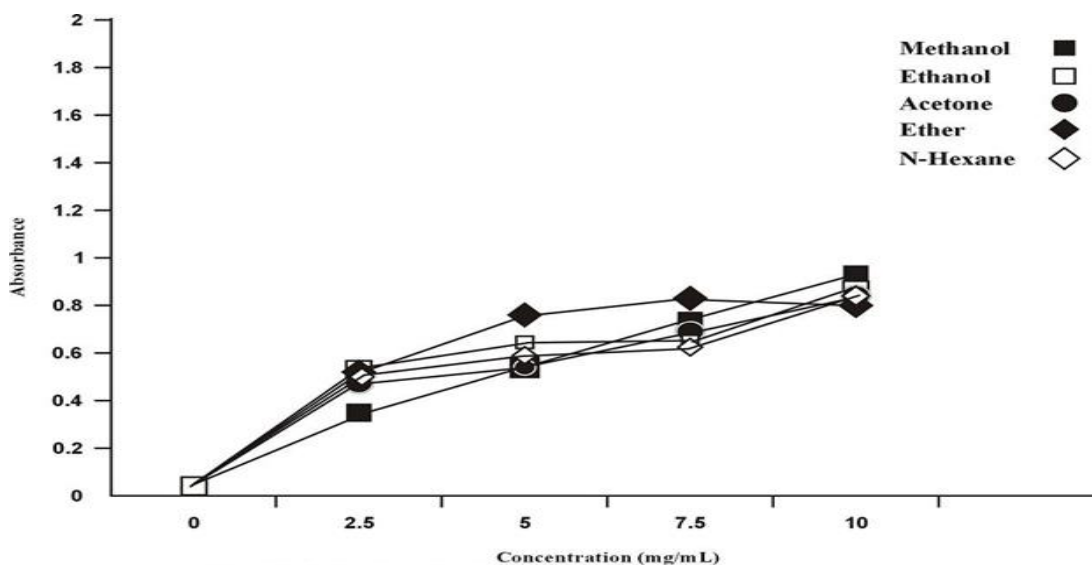


Fig: 2 Reducing potential of *Corchorus depressus* roots extracts

earlier reported that the phytochemical constituents in plants, which are active against microorganisms, are aromatic or saturated organic compounds, and are most often obtained through methanol extraction [26,27]. Refampicine and terbinafine were used as positive controls for bacterial and fungal strains, respectively. The standard showed higher activity on the organisms than the tested

extracts (Tables 6-7). In our studies all extracts (methanol, ethanol, acetone, ether and n-hexane) were active against the tested fungal strains and methanol extract of *Corchorus depressus* roots was used to cure diseases caused by bacterial and fungal strains in the present research. The plants may contain organic compounds like steroids, tannins,

Table 6: Antifungal activity of *Corchorus depressus* roots by zone of inhibition determination (mm)

Extracts	<i>A. niger</i>	<i>A. flavus</i>	<i>F. solani</i>	<i>R. solani</i>
Methanol	18.24±0.16	15.62±0.21	15.44±0.41	14.62±0.15
Ethanol	16.29±0.29	14.86±0.26	12.26±0.37	13.86±0.26
Acetone	13.54±0.17	13.22±0.31	11.06±0.26	12.62±0.23
Ether	13.24±0.24	14.24±0.24	9.12±0.28	11.12±0.16
n-Hexane	6.92±0.51	8.66±0.29	7.44±0.13	9.08±0.39
Terbinafine	18.56±0.44	19.16±0.5	20.16±0.45	18.24±0.31

Table 7: Antibacterial activity of *Corchorus depressus* roots by zone of inhibition determination (mm)

Extracts	<i>P. multocida</i>	<i>E. coli</i>	<i>B. subtilis</i>	<i>S. aureus</i>
Methanol	17.41±0.11	16.21±0.16	15.06±0.02	14.22±0.07
Ethanol	14.23±0.24	15.46±0.19	13.47±0.03	13.66±0.02
Acetone	14.48±0.62	13.24±0.26	11.66±0.17	11.28±0.03
Ether	12.66±0.33	11.66±0.24	8.43±0.12	10.24±0.14
n-Hexane	9.73±0.06	9.71±0.07	7.21±0.04	6.18±0.04
Rifampicine	20.82±0.13	21.14±0.52	21.63±0.48	19.82±0.51

Table 8: Antibacterial activity of *Corchorus depressus* roots by minimum inhibitory concentration (MIC, mg/mL)

Extracts	<i>P. multocida</i>	<i>E. coli</i>	<i>B. subtilis</i>	<i>S. aureus</i>
Methanol	0.065±0.03	0.084±0.02	0.052±0.02	0.062±0.002
Ethanol	0.072±0.02	0.076±0.03	0.061±0.02	0.058±0.002
Acetone	0.044±0.02	0.065±0.12	0.071±0.04	0.047±0.004
Ether	0.041±0.04	0.019±0.16	0.047±0.12	0.049±0.03
n-hexane	0.043±0.05	0.016±0.13	0.018±0.14	0.039±0.002
Rifampicine	0.62±0.02	0.92±0.02	0.52±0.003	0.065±0.003

Table 9: Antifungal activity of *Corchorus depressus* roots by minimum inhibitory concentration (MIC, mg/mL)

Extracts	<i>A. niger</i>	<i>A. flavus</i>	<i>F. solani</i>	<i>R. solani</i>
Methanol	0.176±0.006	0.058±0.005	0.056±0.002	0.076±0.004
Ethanol	0.162±0.005	0.082±0.005	0.047±0.004	0.062±0.002
Acetone	0.153±0.004	0.147±0.004	0.052±0.003	0.059±0.003
Ether	0.154±0.005	0.141±0.004	0.039±0.004	0.047±0.004
n-Hexane	0.121±0.007	0.151±0.002	0.092±0.002	0.037±0.006

Table 10: Gas chromatographic and mass spectral data for the essential oil from *Corchorus depressus* roots

Sr. No	Retention time(min)	Compound Name	% Composition
1	6	P-xylene	2.89
2	7	n-Butylacetate	12.48
3	7.65	2,4,6 Trimethylheptane	5.06
4	9.40	2,3,3, Trimethyloctane	16.36
5	11.55	5- Methyl octadecane	2.61
6	12.35	4- Chloro-2,6-dioxadmantane	2.33
7	13.80	Plamitic acid, methyl ester	3.36
8	14.94	Cis-9- hexadecenal	9.15
9	17.16	Roridin A	1.12
10	17.35	Tetradecamethylhexasiloxane	0.56
11	20.13	Lupeol	1.44
12	22	Octadecamethyl	0.84
13	24	Uridine	0.71

saponins, flavonoids, alkaloids, anthraquinone. These compounds have been reported to exhibit antimicrobial activity in [3]. The phytochemicals may have antimicrobial property through different mechanisms. The antimicrobial studies performed in [28] showed that the extracts tested were active against the fungal strains. These observations support the use of *Corchorus depressus* in herbal cure remedies. The traditional medicine uses this plant in the treatment of various diseases [29]. Table 8 and 9 represent antibacterial and antifungal activities of *Corchorus depressus* roots by minimum inhibitory concentration (MIC, mg/mL) respectively.

GC-MS Analysis of *Corchorus depressus* roots essential oil

GC-MS analysis of the essential oil from the stem was performed. The chemical composition of *R. equisetiformis* essential oils is presented in Table 10. The major compounds with their percentage are 2,3,3-trimethyloctane (16.36 %), n-butyl acetate (12.48 %), cis-9-hexadecenal (9.15%). It was found that the biological activities such as antioxidant potential are similar to those of some phyto-components [10,29].

CONCLUSION

The *Corchorus depressus* extracts and essential oil showed significant antioxidant potential in terms of scavenging free radicals. The extracts showed antimicrobial properties against selected bacterial and fungal strains. The roots contain some metals with maximum content of iron.

REFERENCES

1. M. H. Abdille, R. P. Singh, G. K. Jayaprakasha, B. S. Jena, *Food Chem.* **90**, 891 (2005).
2. M. Namiki, *Crit. Rev. Food Sci. Nutr.* **29**, 273 (1990).
3. I. Sasidharan, N. A. N. Menon, *Journal of Food Sciences and Technology* **48**, 366 (2011).
4. S. Iqbal, M. I. Bhangar, F. Anwar, *LWT-Food Science and Technology* **40**, 361 (2007).
5. S. Adeel, F. Rehman, T. Gulzar, I. A. Bhatti, S. Qaiser, A. Abid, *Asian J. Chem.* **25**, 2739 (2012).
6. F. Batool, S. Adeel, M. Azeem, A. A. Khan, I. A. Bhatti, A. Ghaffar, N. Iqbal, *Radiation Physics and Chemistry* **89**, 33 (2013).
7. F. Rehman, S. Adeel, M. Zuber, I. A. Bhatti, S. Qaiser, M. Shahid, *Radiation Physics and Chemistry* **81**, 1752 (2012).
8. K. Rehman, S. Ashraf, U. Rashid, M. Ibrahim, S. Hina, T. Iftikhar, S. Ramzan, *Pak. J. Bot.* **45**, 391 (2013).
9. M. Zubair, S. Hassan, K. Rizwan, N. Rasool, M. Riaz, M. Zia-Ul-Haq, V. D. Feo, *The Scientific World Journal* **2013**, 1 (2013).
10. F. Aslam, N. Rasool, M. Riaz, M. Zubair, K. Rizwan, M. Abbas, T. H. Bukhari, I. H. Bukhari, *Int. J. Phytomed.* **3**, 567 (2011).
11. K. M. Soliman, R. I. Badeaa, *Food Chemistry Toxicology* **40**, 1669 (2002).
12. M. Sokmen, J. Serkedjieva, D. Daferera, M. Gulluce, M. Polissiou, B. Tepe, *J. Agri. Food Chem.* **52**, 3309 (2004).
13. M. A. Hanif, M. Y. Al-maskari, A. Al-maskari, A. Al-shukaili, A. Y. Al-maskari, J. N. Al-sabahi, *J. of Med. Plants Res.* **5**, 751 (2011).
14. Y.-I. Chew, J.-k. Goh, Y.-y. Lim, *Food Chem.* **116**, 13 (2009).
15. M. Riaz, N. Rasool, I. Bukhari, M. Shahid, F. Zahoor, M. Gilani, M. Zubair, *Afri. J. Microbiol. Res.* **6**, 5700 (2012).
16. M. Riaz, N. Rasool, I. H. Bukhari, K. Rizwan, F. Javed, A. A. Altaf, H. M. A. Qayyum, *Oxi. Commun.* **36**, 272 (2013).
17. G. C. Yen, P. D. Duh, D. Y. Chuang, *Food Chem.* **70**, 437 (2000).
18. M. Riaz, N. Rasool, I. H. Bukhari, M. Shahid, M. Zubair, K. Rizwan, U. Rashid, *Molecules* **17**, 14275 (2012).
19. Y. Y. Soong, P. J. Barlow, *Food Chem.* **97**, 524 (2006).
20. M. Riaz, N. Rasool, S. Rasool, U. Rashid, I. H. Bukhari, M. Zubair, M. Noreen, M. Abbas, *Asian J. Chem.* **25**, 5479 (2013).
21. S. D. Sarker, L. Nahar, Y. Kumarasamy, *Methods* **42**, 321 (2007).
22. M. Lateef, L. Iqbal, N. Fatima, K. Siddiqui, N. Afza, M. Zia-ul-Haq, M. Ahmad, *Pak. J. Pharma. Sci.* **25**, 99 (2012).
23. E. M. Abdallah, A. E. Khalid, *Int. J. Chem. Biochem. Sci.* **1**, 1 (2012).
24. N. M. A. Hassimotto, M. I. Genovese, F. M. Lajolo, *J. Agri. Food Chem.* **53**, 2928 (2005).
25. N. Huda-Faujan, A. Noriham, A. S. Norrakiah, A. S. Babji, *Afr. J. Biotechnol.* **8**, 484 (2011).
26. S. N. Hsu, S. Yonekura, Y. Lwai, T. Uemura, H. M. Robertson, C. H. Lee, A. Chiba, *A Drosophila Research Conference* **47** : , 609 (2006).
27. P. G. Waterman, S. Mole, *Blackwell Scientific Publications Oxford* **238**, 210 (1994).
28. P. Siddhuraju, K. Becker, *Food Chem.* **101**, 10 (2007).
29. P. Kumar, S. Kumaravel, C. Lalitha, *Afr. J. Biochem. Res.* **4**, 191 (2010).

МИНЕРАЛЕН СЪСТАВ, ФЕНОЛЕН ПРОФИЛ, АНТИОКСИДАНТНА И АНТИМИКРОБНА АКТИВНОСТ НА ЕКСТРАКТИ ОТ КОРЕНИ НА *Corchorus depressus*

Т.Х. Бохари^{1*}, М.А. Аслам¹, С. Хина², Н.Б. Ризви³, Х. Расуул¹, М. Дж. Саиф⁴, М. Зубаир¹, А.И. Хусаин⁴, Ш.А.Шахид Чатха⁴, М. Риаз¹

¹Департамент по химия, Правителствен университетски колеж, Файсалабад, Пакистан

²Департамент по биоинформатика и биотехнология, Правителствен университетски колеж, Файсалабад, Пакистан

³Институт по химия, Нов кампус, Университет в Пунджаб, Лахор, Пакистан

⁴Департамент по приложна химия и биохимия, Правителствен университетски колеж, Файсалабад, Пакистан

Постъпила на 29 ноември, 2013 г.; коригирана на 28 февруари, 2014 г.

(Резюме)

В настоящата работа се изследват минералният състав, фенолен профил, антиоксидантна и антимикробна активност на екстракти от корени на *Corchorus depressus*. Корените се третираат със следните екстрагенти: *n*-хексан, етер, ацетон, етанол и метанол. Екстрактите от корените на *Corchorus depressus* съдържат следните метали: кобалт, никел, мед, хром, цинк, олово и желязо. Общото фенолно съдържание е между 9.64-40.14 mg/100 g сухи вещества като еквивалент на галова киселина, а общото съдържание на флавоноиди (8.08-37.04 mg/100 g сухи вещества) е измерено като катехинов еквивалент. Екстрактите от корените на *Corchorus depressus* показват много добра DPPH радикал-премахваща активност, като 56.31 % инхибиране. GC-MS-анализът на есенциалните масла от корените притежават 13 съединения с *n*-бутилацетат (12.48%), 2,3,3-триметил октан (16.36%) и *cis*-метил хексадецимални съединения (9.15%) като главни компоненти. Всички резултати за екстрактите от корени на *Corchorus depressus* и есенциални масла показват значителна дисперсия ($P < 0.05$).

Synthesis, characterization and biological activities of some novel isatin derivatives

A.M. Amani

Department of Chemistry, Shiraz University of Technology, Shiraz, Iran

Received October 22, 2013; Revised January 4, 2014

A series of novel (arylimino-2-oxo-2,3-dihydro-indol-1-yl)-acetic acid N'-(4-aryl-2-yl)-hydrazide derivatives (**5a-g**) were synthesized. The structures of the newly synthesized compounds were characterized by elemental analysis, FT-IR, ^1H -, ^{13}C -NMR and mass spectroscopy. The compounds were screened *in vitro* for antibacterial and antifungal activities against some human pathogenic microorganisms by the disc diffusion technique. Some of the compounds showed moderate to good biological activities when compared with commercially available drugs.

Keywords: isatin; 1,3-thiazole; antibacterial, antifungal

INTRODUCTION

A new class of antibacterial and antifungal agents is needed, especially against drug-resistant bacteria and fungi such as gram-positive and gram-negative strains, which are responsible for a number of serious infections in the acute and chronic care units in hospitals. Isatin or 1*H*-indole-2,3-dione is an indole derivative. The compound was first obtained by Erdmann [1] and Laurent [2] in 1841 as a product from the oxidation of indigo dye by nitric acid and chromic acids. The compound is found in many plants, such as *Isatis tinctoria*, *Calanthe discolor* and *Couroupita guianensis* [3]. Schiff bases of isatin are investigated for their pharmaceutical properties [4]. Isatin forms a blue dye (indophenin) when mixed with sulfuric acid and crude benzene. The formation of indophenin was long believed to be a result of the reaction with benzene. Victor Meyer was able to isolate the substance responsible for

this reaction from crude benzene. This new heterocyclic compound was thiophene [5]. Isatin is commercially available. It may be prepared by cyclicizing the condensation product of chloral hydrate, aniline and hydroxylamine in sulfuric acid. This reaction is called the Sandmeyer isonitrosoacetanilide isatin synthesis (**Fig. 1**) and was discovered by Traugott Sandmeyer in 1919 [6,7].

Another classic reaction, the Sandmeyer diphenylurea isatin synthesis (Sandmeyer 1903), starts from diphenylthiourea, potassium cyanide, and lead carbonate [7]. Isatin can be made from the corresponding indole in good yield by a mixture of InCl_3 and IBX in an acetonitrile/water solution at 80°C [8]. Literature survey revealed that isatin possesses diverse biological activities such as antibacterial [9], antifungal [10], antiviral [11], antimycobacterial [12], anticancer [13], anti-inflammatory [14] and anticonvulsant [15]

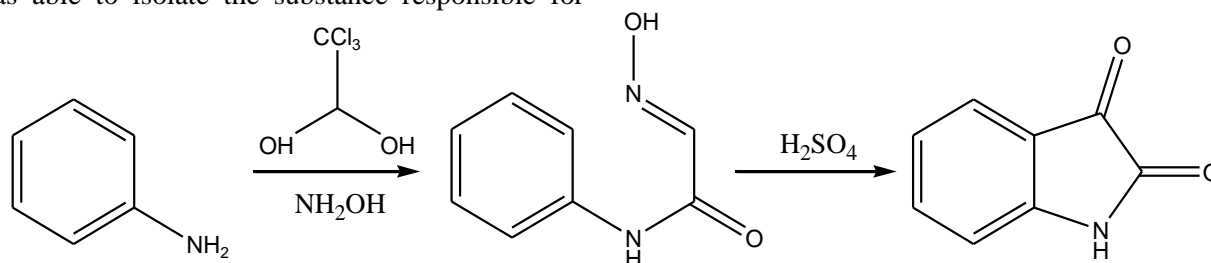
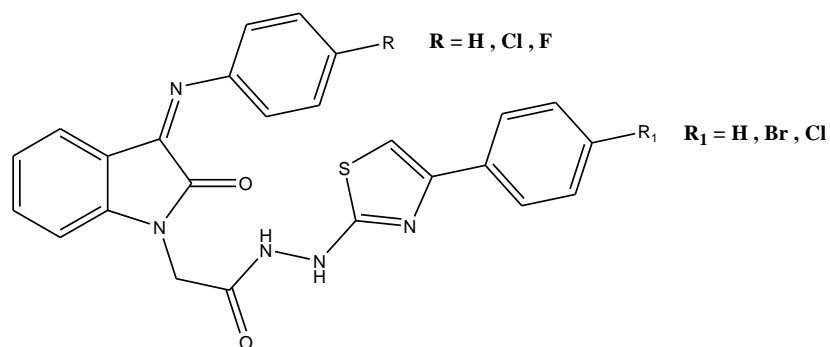


Fig. 1. Isatin synthesis according to Sandmeyer method

* To whom all correspondence should be sent:
E-mail: amani@sutech.ac.ir



Compound	R	R ₁
5a	H	H
5b	H	Br
5c	Cl	Br
5d	Cl	H
5e	H	Cl
5f	F	H
5g	F	Cl

Fig. 2. Structure of target compounds (**5a-g**)

activities. The thiazole moiety also displays diverse pharmacological activities like anti-microbial [16], anti-inflammatory [17], anti-viral [18], antipsychotic [19], antiarrhythmic and anticoagulant [20] activities. The study of the above pharmacophores reveals that the combination of these two entities may result in increased antimicrobial activity. In view of the biological importance of these two moieties, it was planned to synthesize a new series of isatin containing 1,3-thiazole derivatives and to evaluate the new compounds for their biological activities (**Fig. 2**)

EXPERIMENTAL

Material and Equipments

All chemicals and solvents were obtained from E. Merck and Sigma-Aldrich and used without further purification. All melting points were taken

with an Electrothermal melting point apparatus (Electrothermal Eng. Ltd, Essex, UK) and were uncorrected. IR spectra were recorded in KBr on a Shimadzu Dr-8031 instrument. The ¹H and ¹³C-NMR spectra of the synthesized compounds were measured in DMSO-d₆ or CDCl₃ solution with TMS as the internal standard using a Varian Mercury 400, 400MHz instrument. All chemical shifts were reported as δ (ppm) values. The mass spectra were recorded on a LCQ ion trap mass spectrometer (Thermo Fisher, San Jose, CA, USA), equipped with an EI source. Elemental analyses were carried out using a Perkin-Elmer, CHN elemental analyzer.

Synthesis of Compounds

The synthetic route of intermediates and target compounds is given in **Fig. 3**.

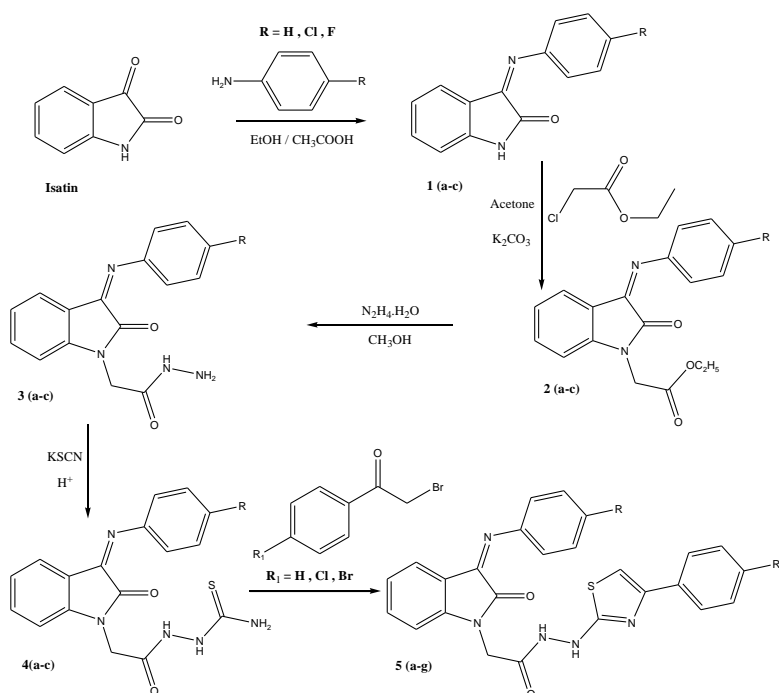


Fig. 3. Schematic synthesis of intermediates and target compounds

General procedure for the preparation of the compounds 1(a-c)

These intermediates were prepared according to ref. [21] with some modifications.

A mixture of isatin (1.47 g, 0.01 mol) and an appropriate aniline (0.01 mol) in absolute ethanol (20 ml) was refluxed for one hour in the presence of 2-3 drops of glacial acetic acid. Crystals were separated out, filtered and re-crystallized from ethanol to give **1(a-c)**.

General procedure for the preparation of the compounds 2(a-c)

These intermediates were prepared according to ref. [22] with some modifications.

A mixture of the corresponding 3-phenylimino-1*H*-indol-2,3-dione **1(a-c)** (0.01 mol), ethyl chloroacetate (1.22 ml, 0.01 mol) and potassium carbonate (2.2 g, 0.015 mol) in dry acetone was refluxed for 20 h. The reaction mixture was poured onto crushed ice. The separated solid was filtered, washed with water and re-crystallized from methanol to give **2(a-c)**.

General procedure for the preparation of the compounds 3(a-c)

These intermediates were prepared according to ref. [23] with some modifications.

A mixture of the corresponding 3-phenylimino-2-oxo-1-indole-ethylacetate **2(a-c)** (0.01 mol) and hydrazine hydrate (99%, 0.5 ml, 0.01 mol) in methanol (20 mL) was refluxed for about 5 h on a steam bath. After completion of the reaction (monitored by TLC), the mixture was cooled and the resulting solid was filtered, dried and re-crystallized from ethanol to give **3(a-c)**.

General procedure for the preparation of the compounds 4(a-c)

These intermediates were prepared according to ref. [18] with some modifications.

A mixture of the corresponding 3-phenylimino-2-oxo-1-indole-acetylhydrazide **3(a-c)** (0.01 mol) was refluxed with 10 ml of 10% HCl and potassium thiocyanate (0.015 mol) for 4 h. The reaction mixture was allowed to cool to room temperature. The solid formed was collected by filtration, washed with water, dried and re-crystallized from ethanol to give **4(a-c)**.

General procedure for the preparation of the new compounds 5(a-g)

A mixture of the corresponding 3-phenylimino-2-oxo-1-indole-acetylthiosemicarbazide **4(a-c)**

(0.01 mol) and phenacyl bromide (0.01 mol) was refluxed in ethanol (50 mL) for 10 h. The separated solid was filtered off and re-crystallized from DMF to give **5(a-g)**.

(2-Oxo-3-phenylimino-2,3-dihydro-indol-1-yl)-acetic acid N'-(4-phenyl-thiazol-2-yl)-hydrazide (5a)

Cream powder; Yield 71 %; m.p. 248-250 °C; IR (KBr, cm⁻¹): 1052, 1320, 1610, 1658, 2560, 3075 cm⁻¹; ¹H-NMR (δ, ppm): 4.3 (s, 2H, N-CH₂), 6.7 (thiazole CH), 7.1-8.00 (m, 14H, Ar-H), 9.62 (s, H, CS-NH), 10.32 (s, H, CO-NH); ¹³C-NMR (δ, ppm): 56, 110.5, 123.5, 134, 152, 155, 159, 165, 170; Anal. Calcd. for C₂₅H₁₉N₅O₂S: C, 66.21; H, 4.22; N, 15.44 %. Found: C, 66.11; H, 4.18; N, 15.48 %. MS (m/z, regulatory intensity, %): 453 (100), 454 (30), 131 (18), 77 (22).

(2-Oxo-3-phenylimino-2,3-dihydro-indol-1-yl)-acetic acid N'-[4-(4-bromo-phenyl)-thiazol-2-yl]-hydrazide (5b)

Light reddish powder; Yield 75%; m.p. 256-258 °C; IR (KBr, cm⁻¹): 670, 1062, 1330, 1622, 1651, 2568, 3100 cm⁻¹; ¹H-NMR (δ, ppm): 4.2 (s, 2H, N-CH₂), 6.8 (thiazole CH), 7.3-8.05 (m, 13H, Ar-H), 9.70 (s, H, CS-NH), 10.40 (s, H, CO-NH); ¹³C-NMR (δ, ppm): 58, 111.5, 122, 125.5, 133.5, 156, 158, 159.5, 165.5, 171; Anal. Calcd. for C₂₅H₁₈BrN₅O₂S: C, 56.40; H, 3.41; N, 13.15 %. Found: C, 56.31; H, 3.45; N, 13.10 %. MS (m/z, regulatory intensity, %): 533 (100), 531 (98), 532 (18).

[3-(4-Chloro-phenylimino)-2-oxo-2,3-dihydro-indol-1-yl]-acetic acid N'-[4-(4-bromo-phenyl)-thiazol-2-yl]-hydrazide (5c)

Light yellowish powder; Yield 70 %; m.p. 218-220 °C; IR (KBr, cm⁻¹): 650, 820, 1055, 1328, 1640, 1657, 2582, 3090 cm⁻¹; ¹H-NMR (δ, ppm): 4.2 (s, 2H, N-CH₂), 6.8 (thiazole CH), 7.05-7.95 (m, 12H, Ar-H), 9.60 (s, H, CS-NH), 10.25 (s, H, CO-NH); ¹³C-NMR (δ, ppm): 55.5, 113.5, 123.5, 126.5, 131.5, 134.5, 157, 159.5, 160.5, 166, 169; Anal. Calcd. for C₂₅H₁₇BrClN₅O₂S: C, 52.97; H, 3.02; N, 12.35 %. Found: C, 53.05; H, 2.96; N, 12.29 %. MS (m/z, regulatory intensity, %): 567 (100), 565 (97), 568 (38).

[3-(4-Chloro-phenylimino)-2-oxo-2,3-dihydro-indol-1-yl]-acetic acid N'-(4-phenyl-thiazol-2-yl)-hydrazide (5d)

Yellowish powder; Yield 72 %; m.p. 260-262 °C; IR (KBr, cm⁻¹): 835, 1065, 1328, 1655, 1668, 2575, 2988 cm⁻¹; ¹H-NMR (δ, ppm): 4.23 (s, 2H, N-CH₂), 6.75 (thiazole CH), 7.10-8.05 (m, 13H, Ar-H), 9.68 (s, H, CS-NH), 10.40 (s, H, CO-NH); ¹³C-

NMR (δ , ppm): 54.5, 114.5, 122.5, 126, 132.5, 135.5, 158.5, 159, 161.5, 167.5, 170; Anal. Calcd. for $C_{25}H_{18}ClN_5O_2S$: C, 61.54; H, 3.72; N, 14.35 %. Found: C, 61.47; H, 3.66; N, 14.39 %. MS (m/z, regulatory intensity, %): 487 (100), 488 (28), 489 (36).

(2-Oxo-3-phenylimino-2,3-dihydro-indol-1-yl)-acetic acid N'-[4-(4-chloro-phenyl)-thiazol-2-yl]-hydrazide (**5e**)

Yellowish powder; Yield 74 %; m.p. 229-231 °C; IR (KBr, cm^{-1}): 830, 1050, 1331, 1642, 1673, 2580, 3000 cm^{-1} ; 1H -NMR (δ , ppm): 4.25 (s, 2H, N-CH₂), 6.65 (thiazole CH), 7.10-7.95 (m, 13H, Ar-H), 9.50 (s, H, CS-NH), 10.38 (s, H, CO-NH); ^{13}C -NMR (δ , ppm): 52, 111.5, 124.5, 128.5, 133.5, 137.5, 159.5, 160, 162.5, 168.5, 171; Anal. Calcd. for $C_{25}H_{18}ClN_5O_2S$: C, 61.54; H, 3.72; N, 14.35 %. Found: C, 61.58; H, 3.76; N, 14.29 %. MS (m/z, regulatory intensity, %): 487 (100), 488 (28), 489 (36), 453 (17), 398 (19), 376 (18), 268 (100).

[3-(4-Fluoro-phenylimino)-2-oxo-2,3-dihydro-indol-1-yl]-acetic acid N'-(4-phenyl-thiazol-2-yl)-hydrazide (**5f**)

Grayish powder; Yield 69 %; m.p. 225-227 °C; IR (KBr, cm^{-1}): 1060, 1250, 1333, 1653, 1675, 2588, 2950 cm^{-1} ; 1H -NMR (δ , ppm): 4.33 (s, 2H, N-CH₂), 6.73 (thiazole CH), 7.15-8.05 (m, 13H, Ar-H), 9.45 (s, H, CS-NH), 10.45 (s, H, CO-NH); ^{13}C -NMR (δ , ppm): 53.5, 113.5, 126.5, 129.5, 138.5, 158.5, 162, 163.5, 168.5, 169, 171; Anal. Calcd. for $C_{25}H_{18}FN_5O_2S$: C, 63.68; H, 3.85; N, 14.85 %. Found: C, 63.61; H, 3.87; N, 14.79 %. MS (m/z, regulatory intensity, %): 471 (100), 472 (30).

[3-(4-Fluoro-phenylimino)-2-oxo-2,3-dihydro-indol-1-yl]-acetic acid N'-[4-(4-chloro-phenyl)-thiazol-2-yl]-hydrazide (**5g**)

Yellowish powder; Yield 68 %; m.p. 239-241 °C; IR (KBr, cm^{-1}): 825, 1065, 1262, 1344, 1659,

1701, 2562, 2985 cm^{-1} ; 1H -NMR (δ , ppm): 4.45 (s, 2H, N-CH₂), 6.69 (thiazole CH), 7.05-8.10 (m, 12H, Ar-H), 9.56 (s, H, CS-NH), 10.48 (s, H, CO-NH); ^{13}C -NMR (δ , ppm): 52.5, 112.5, 128.5, 129, 139.5, 157.5, 163.5, 166.5, 168.5, 169, 170.5; Anal. Calcd. for $C_{25}H_{17}ClFN_5O_2S$: C, 59.35; H, 3.39; N, 13.84 %. Found: C, 59.31; H, 3.32; N, 13.90 %. MS (m/z, regulatory intensity, %): 505 (100), 506 (30), 507 (36).

Biological Evaluation

In vitro antibacterial and antifungal activity

All compounds were evaluated for their *in vitro* anti-bacterial activity against *S. aureus*, *B. subtilis*, *E. coli*, *P. vulgaris* and antifungal activity against *C. albicans*, *A. niger* standard strains using the disc diffusion method [24, 25]. Each disc contained 200 μ g/ml of the tested compounds. The paper disc diffusion method was performed using Mueller-Hinton (Hi-Media) agar (antibacterial) and potato dextrose (Hi-Media) agar (antifungal). Suspensions of each microorganism were prepared to contain approximately 10^6 colony forming units (cfu)/ml and applied to plates. The surface of the medium was allowed to dry. The 200 μ g/ml (in DMSO) compound-impregnated discs were applied to the surface of the inoculated plates. The petri plates were incubated at 37°C for 18-24 h for antibacterial activity, and at 26°C for approx. 48-72 h for antifungal activity (Table 1) [26].

Minimum Inhibitory Concentration Determination:

The solutions of the newly synthesized compounds and standard drugs were prepared at 500, 250, 125, 62.5, 31.25, 15.63, 7.8, 3.9, 1.95, 0.98, 0.48, 0.24, 0.12 mg/ml concentrations in the wells of micro plates by dilution with the liquid

Table 1: Biological activities of the compounds **5a-g** at a concentration of 200 μ g/ml

Compound	Zone of inhibition (mm)					
	Antimicrobial activity (200 μ g/ml)				Antifungal activity (200 μ g/ml)	
	<i>S. aureus</i>	<i>B. subtilis</i>	<i>E. coli</i>	<i>P. vulgaris</i>	<i>C. albicans</i>	<i>A. niger</i>
5a	Not Seen	7.5	Not Seen	Not Seen	7.12	Not Seen
5b	Not Seen	7.85	8.9	Not Seen	7.5	7.5
5c	6.85	9.62	9.95	9.1	8.5	8.5
5d	6.72	8.2	10.5	8.5	8.5	7.5
5e	6.85	7.5	8.2	7.5	7.5	8.5
5f	7.1	11.1	11.5	10.5	8.5	7.5
5g	7.6	9.5	12.8	9.5	7.5	7.5
Ampicilin	14.8	8.8	16.5	17.5	-	-
Norfloracin	8.6	12.5	12.2	12.5	-	-
Fluconazole	-	-	-	-	10.5	12.5

Table 2: MIC value of compounds **5a-g**

Compound	Minimum Inhibitory Concentration ($\mu\text{g/ml}$)					
	<i>S. aureus</i>	<i>B. subtilis</i>	<i>E. coli</i>	<i>P. vulgaris</i>	<i>C. albicans</i>	<i>A. niger</i>
5a	-	250	-	-	250	-
5b	-	250	125	-	125	250
5c	125	62.5	62.5	125	125	125
5d	125	125	62.5	125	125	125
5e	125	125	125	62.5	250	250
5f	125	62.5	31.25	62.5	125	250
5g	62.5	62.5	31.25	62.5	125	125
Ampicilin	0.48	0.48	3.9	3.9	-	-
Norfloxacin	0.12	0.12	0.12	0.12	-	-
Fluconazole	-	-	-	-	0.98	1.95

double stranded nutrient broth. The bacterial suspensions of 10^5 cfu/ml used for inoculation were prepared by diluting fresh cultures at McFarland 0.5 density (10^7 cfu/ml). Suspensions of the bacteria at 10^5 cfu/ml concentration were inoculated to the two-fold diluted solution of the compounds. There were 10^4 cfu/ml bacteria in the wells after inoculations. Nutrient broth was used for diluting the bacterial suspension and for two-fold dilution of the compound. DMSO, pure microorganisms and pure media were used as control wells. A $10 \mu\text{l}$ bacterial inoculum was added to each well of the micro dilution trays. The trays were incubated at 37°C in a humid chamber and MIC endpoints were read after 24 h of incubation. For antifungal activity, the same procedure was used. The lowest concentration of the compound that completely inhibits macroscopic growth was determined and the minimum inhibitory concentrations (MICs) were reported (Table 2)

RESULTS AND DISCUSSION

Chemistry

In the present work, nucleophilic addition of 4-substituted aniline to indole-2,3-dione yielded 3-(4-arylimino)-indol-2-one **1(a-c)** which on further treatment with ethyl chloroacetate underwent alkylation reaction in presence of anhydrous K_2CO_3 in dry acetone and yielded 3-(4-arylimino)-2-oxo-1-indole-ethylacetate **2(a-c)**. The latter was converted to 3-(4-arylimino)-2-oxo-1-indole-acetylthiazide **3(a-c)** through reaction with hydrazine hydrate. Further, thiosemicarbazone formation from compounds **3(a-c)** in presence of KSCN and 10 % HCl, yielded 3-phenylimino-2-oxo-1-indole-acetylthiosemicarbazides **4(a-c)**. Compounds **4(a-c)**, refluxed in ethanol in the presence of phenacyl bromide or substituted phenacyl bromide, yielded

(arylimino-2-oxo-2,3-dihydro-indol-1-yl)-acetic acid N'-(4-aryl-2-yl)-hydrazide analogues **5(a-g)**. The IR spectrum of the final compounds **5(a-g)** showed isatin carbonyl ($\text{C}=\text{O}$ str.), 2° NH str., amide $\text{C}=\text{O}$ str., $\text{C}=\text{N}$ str., S-C str., C-X str., which confirmed the formation of the final compound. In the $^1\text{H-NMR}$ spectrum of **5(a-g)**, as representative compounds of the series, all protons were seen according to the expected chemical shift and integral values. The structure of the compounds **5(a-g)** was confirmed by physical data, elemental analysis, spectral data, IR, ^1H -, ^{13}C -NMR and mass spectroscopy.

Biological activities

The compounds **5f**, **5g** with fluoro substitution at the R position were found to be highly active against *S. aureus* and *B. subtilis*. Compounds **5d** with Cl substitution at R and **5e** with Cl substitution at R_1 were found to be moderately active against *S. aureus* and *B. subtilis*.

In the case of gram-negative bacteria *E. coli*, *P. vulgaris*, the compounds **5f** with fluoro substituent at R position and **5g** with fluoro and chloro substituents at R and R_1 position, respectively, were found to be highly active. **5d** was moderately active against *E. coli* and **5e** was moderately active against *P. vulgaris*. All compounds showed moderate activity for *C. albicans* and *A. niger*. All screened compounds showed significant antimicrobial activity.

CONCLUSIONS

In conclusion, the present method may be considered as a practical route for the synthesis of a series of new (arylimino-2-oxo-2,3-dihydro-indol-1-yl)-acetic acid N'-(4-aryl-2-yl)-hydrazide analogues from 3-(4-arylimino)-2-oxo-1-indole-acetylthiosemicarbazide in ethanol in the presence

of phenacyl bromide or substituted phenacyl bromides. The procedure has the advantages of high yield, mild reaction conditions, simple experimental work-up and may be an acceptable method for the preparation of isatin containing 1,3-thiazole derivatives. Our studies clearly demonstrated that the novel synthesized compounds have prospectful pharmaceutical properties and can be used for the development of new drugs in the future.

REFERENCES

1. O.L. Erdmann, *J. Prakt. Chem.*, **19(1)**, 321 (1840).
2. A. Laurent, *Annales de Chimie et de Physique*, **3(3)**, 393 (1840).
3. J.F.M. da Silva, S.J. Garden, A.C. Pinto, *J. Braz. Chem. Soc.*, **12 (3)**, 273 (2001).
4. A.A. Jarrahpour, D. Khalili, *Molbank*, **4**, M437 (2005).
5. W.C. Sumpter, *Chem. Rev.*, **34 (3)**, 393 (1944).
6. C.S. Marvel, G.S. Hiers, *Org. Synth.*, **5(71)**, 327 (1925).
7. T. Sandmeyer, *Helvetica Chimica Acta*, **2(1)**, 234 (1919).
8. J.S. Yadav, B.V.S. Reddy, Ch.S. Reddy, A. Krishna, *Synthesis*, **5**, 693 (2007).
9. S.N. Pandeya, D. Sriram, G. Nath, E. De Clercq, *Eur. J. Pharm. Sci.*, **9**, 25 (1999).
10. K. Mirjana, M.M. Saric, M. Morvin, D. Maysinger, *J. Pharm. Sci.*, **68**, 459 (2006).
11. S.N. Pandeya, D. Sriram, G. Nath, E. De Clercq, *Pharm. Acta Helv.*, **74**, 11 (1999).
12. S.K. Sridhar, S.N. Pandeya, S.K. Bajpai, H. Manjula, *Indian Drugs*, **36(6)**, 412 (1999).
13. V. SLakshmi, A. Pandeya, S.N. Pandeya, *Indian J. Pharm. Sci.*, **65(3)**, 213 (2003).
14. Y. Teitz, ELadizensky, N. Barko, E. Burstein, *Antimicrob. Agents Chem. Ther.*, **37**, 2483 (1993).
15. V. Alagarsamy, S. Meena, S. Vijayakumar, K.V. Ramseshu, Revathi R. *Pharmazie*, **58**, 233 (2003).
16. H. Pajouhesh, R. Parson, F.D. Popp, *J. Pharm. Sci.*, **72(3)**, 318 (1983).
17. B.F. Abdel-Wahab, H.A. Abdel-Aziz, E.M. Ahmed. *Eur. J. Med. Chem.*, **44**, 2632 (2009).
18. H.N. Hafez, A.B.A. El-Gazzar, *Bioorg. Med. Chem.*, **18**, 5222 (2009).
19. O. I. el-Sabbagh, M.M. Baraka, S.M. Ibrahim, C. Pannecouque, G. Andrei, R. Snoeck, J. Balzarini, A.A. Rashad, *Eur. J. Med. Chem.*, **44(9)**, 3746 (2009).
20. K.V.G. Chandra, V. Rao, R.K. Vyas, M. Murali Krishna Kumar, *Bioorg. Med. Chem. Lett.*, **18**, 6054 (2008).
21. S.B. Bari, A.O. Agrawal, U.K. Patil, *J. Sci. Islamic Rep. Iran.*, **19(3)**, 217 (2008).
22. P.V. Frank, K. S. Girish, B. Kalluraya, *J. Chem. Sci.*, **119(1)**, 41 (2007).
23. S. George, M.K. Parameshwaran, A.R. Chakraborti, T.K. Ravi, *Acta Pharma.*, **58**, 119 (2008).
24. A.W. Bauer, W.M. Kirby, J.C. Sherris, M. Turck, *Am. J. Clin. Pathol.*, **45**, 493 (1996).
25. National Committee for Clinical Laboratory Standards. Reference method for broth dilution antifungal susceptibility testing of yeasts; Approved Standard. NCCLS Document M27-A2, 2nd ed. Vol. 22 No. 15; National Committee for Clinical Laboratory Standards: 940 West Valley Road, Suite 1400, Wayne, Pennsylvania 19087-1898 USA (2002).

СИНТЕЗА, ОХАРАКТЕРИЗИРАНЕ И БИОЛОГИЧНА АКТИВНОСТ НА НЯКОИ НОВИ ИЗАТИНОВИ ПРОИЗВОДНИ

А.М. Амани

Департамент по химия, Технологичен университет, Шираз, Иран

Постъпила на 22 октомври, 2013 г.; коригирана на 4 януари, 2014 г.

(Резюме)

Синтезирани са серия от нови производни (арил имино-2-оксо-2,3-дихидро-индол-1-ил)-оцетнакиселина N¹-(4-арил-2-ил)-хидразид. Структурите на новосинтезираните съединения са охарактеризирани чрез елементарен анализ, FT-IR, ¹H-, ¹³C-NMR и мас-спектроскопия. Съединенията са изследвани *in vitro* за антибактериална и фунгицидна активност спрямо някои патогенни за човека микроорганизми чрез диск-дифузионна техника. Някои от съединенията показват умерена до добра биологична активност в сравнение с търговски достъпните препарати.

Mechanism of mercury removal by a novel hydrazine hydrate-modified pectin

Jj. Guo^{1,2}, Jy. Zhang², Y. Yue¹, Y. Guo^{1,*}

¹ Key Laboratory for Natural Medicine of Gansu Province, Key laboratory of Chemistry of Northwestern Plant Resources, Lanzhou Institute of Chemical Physics, Chinese Academy of Sciences, Lanzhou 730000, China

² College of Petro Chemical Engineering, Lanzhou University of Technology, Lanzhou 730050, China

Received October 29, 2013; Revised December 12, 2013

This paper describes a novel hydrazine hydrate-modified pectin for the removal of Hg²⁺. The modified pectin was characterized by elemental analysis and FT-IR spectroscopy which indicated that hydrazine hydrate was successfully grafted on the side chains of pectin. In addition, the reaction mechanism between modified pectin and Hg²⁺ was studied by X-ray diffraction (XRD) and X-ray photoelectron spectroscopy (XPS). The results revealed that the removal effect was probably due to the form of the coordination bonds between Hg²⁺ and N/O atoms. Under optimized experimental conditions, the efficiency of removal Hg²⁺ by the modified pectin reached 74.8%, which was far higher than the 30.5% obtained with unmodified pectin.

Keywords: Pectin, modification, mercury, hydrazine hydrate, mechanism

INTRODUCTION

The discharge of toxic heavy metal ions into the environment is a serious pollution problem. Major sources of water pollution with heavy metals are plating plants, mining and metal finishing manufacturing [1]. With the wastewater discharge, heavy metals enter into water, soil and atmosphere in various forms. Through the food chain they are further transferred to plants, animals, and even humans. Furthermore, heavy metals can be enriched in the body, causing serious harm. Mercury, one of the most toxic metals, has drawn much attention on account of its toxicity and impact on the public health. It is well known that Hg²⁺ has a very high tendency to bind proteins, mainly causing damage to the renal and nervous systems [2]. The main anthropogenic sources contributing to mercury contamination include wastewater discharges and atmospheric depositions from mining activities, oil and coal combustion, chlor-alkali industries, cement production, municipal waste and sewage sludge combustion, and manufacture of batteries [3-6]. Because of its high toxicity, mercury has been included in the list of priority pollutants by U.S. EPA [7]. In the early 1950s, the minamata disease broke out in Kumamoto, Japan, and after that the problem of mercury pollution has extensively aroused public attention.

Natural pectin is a vegetable polymer of L, D-

galacturonic acid partially esterified with methoxy groups. It is widely used as a coagulant additive in foods and pharmaceutical applications, as well as in some industrial productions [8, 9]. At the same time, since the first report on pectin as an efficient antidote for heavy metals poisoning, it has been found to suppress the absorption of strontium into the bone structure of rats [10]. Pectin has been widely used as a gelling agent in foodstuffs, but its application in heavy metals removal from wastewater has not been fully recognized [11,12]. Although pectin has several reactive groups, such as esterified carboxyl groups, free carboxyl groups and hydroxyl, there are still some limitations such as low removal efficiency, low resistance to acid and base, impact of the environment on the performance, and other practical issues. The performance of heavy metal ions removal by pectin can be improved through physical or chemical modification. For example, introducing functional groups with stronger combining ability can enhance the removal efficiency to heavy metals. Moreover, pectin can be extracted from fruit peels which are abundant, cheap and environmentally safe. Therefore, modified pectin has good prospects for heavy metals removal from aqueous solutions.

In this work a new approach of modified pectin preparation and its uptake capacity to heavy metal ions, especially Hg²⁺, is studied. The concentration of Hg²⁺ ions in the filtrate was determined by the dithizone-acetonitrile UV-vis method. Compared with the national standard method, the improved method was more rapid and avoided extraction.

* To whom all correspondence should be sent:
E-mail: guoyong@licp.cas.cn

EXPERIMENTAL

All reagents were of chemical grade and purchased from National medicine group chemical reagent co., LTD. Pectin with high methoxy content (HMP, esterification degree of 70%) was purchased from USA. Ultrapure water was used throughout.

(1) Modified pectin (HHA-HMP) was prepared by dissolving 5 g of HMP in 300 mL of ultrapure water and stirring until it was homogeneous, followed by gradual addition of 75 mL of 80% hydrazine hydrate. Finally, the mixture was stirred and refluxed at 80 °C for 12 h and then cooled to room temperature. After reaction, the viscous gel substance was washed 4–5 times with absolute ethyl alcohol, dried in a freeze-drier for 11 h and ground to powder for use. The preparation process is shown in Scheme 1. The HHA-HMP was characterized by elemental analysis and FT-IR spectroscopy.

(2) The modified pectin was used for Hg²⁺ removal. 100 mL of Hg²⁺ solution (1 mmol L⁻¹) and modified pectin (0.3 g L⁻¹) were vigorously stirred at pH=4 for 30 min at room temperature. The complex of Hg-HHA-HMP is water-insoluble, so the flocculent precipitate was separated through centrifuging. The supernatant was analyzed by dithizone-acetonitrile ultraviolet spectrophotometry. The flocculent precipitate was washed 3-4 times with ultrapure water, dried in a freeze-drier for 5 h and ground to powder for use.

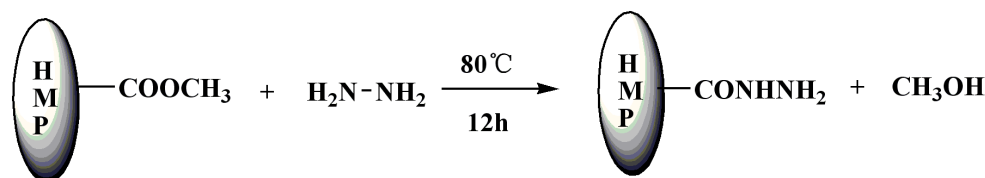
(3) The properties of dithizone are well-known, and works about using dithizone for metal analysis are largely published [13]. Unfortunately, extraction with an organic solvent is needed, preventing the choice of dithizone-based methods for on-line measurements. Other colorimetric methods for the determination of Hg²⁺ were proposed [14-17], but all of them require complex and time-consuming sample pretreatment. The

method described in this work was rapid and without extraction, using dithizone dissolved in acetonitrile. This method can directly determine the content of Hg²⁺ in the aqueous phase. Dithizone-acetonitrile spectrophotometric determination of low concentrations of Hg²⁺ is based on the formation of an orange-red complex between dithizone and Hg²⁺ under acidic conditions in a homogeneous medium, the absorption of which is measured at 480 nm. Various concentrations of Hg²⁺ (0-8.33 μmol L⁻¹) were mixed with dithizone (1 mmol L⁻¹) in acetonitrile solution (pH=2). The absorption values were measured at 480 nm and 600 nm by UV-vis spectrometry.

RESULTS AND DISCUSSION

The elemental analysis (E.A.) results of HMP and HHA-HMP are shown in Table 1. Compared with HMP, the nitrogen content of HHA-HMP increased after modification, indicating that the –CONHNH₂ groups were grafted to the pectin.

IR analysis is used to identify some characteristic functional groups, and the spectra of HMP and HHA-HMP are shown in Fig. 1 (a, b). In the HMP spectrum, the broad and intense absorption peak at 3423 cm⁻¹ corresponds to O-H stretching vibration. The peak at 2922 cm⁻¹ can be attributed to the C-H stretching vibration of methyl, methylene and methoxy groups. The peaks at 1721 cm⁻¹ and 1622 cm⁻¹ in the HMP spectrum are usually representative of ester carbonyl (C=O) groups and carboxylate ions (COO⁻) stretching bands, respectively [18]. The bands in the range of 1300-1000 cm⁻¹ can be assigned to the C-O stretching vibration of carboxylic acids and alcohols [19]. The IR spectrum of HHA-HMP



Scheme 1. Preparation process of HHA-HMP.

Table 1. Results of E. A. of the sample (wt %)

Sample	C (%)	H (%)	O (%)	N (%)
HMP	38.12	6.05	55.44	0.39
HHA-HMP	35.90	6.25	53.31	4.54

shows various distinctive absorption peaks: the broad bands in the region 3326 cm^{-1} can be attributed to the stretching of -OH groups of HHA-HMP and overlapping stretching bands of -NH. In addition, a sharp peak appeared at 1601 cm^{-1} , corresponding to the C=O stretching vibration of the amide group (-CONH₂) [20]. It indicates that the ester carbonyl (C=O) groups switch to amide group (C=O). Besides, the peaks at 1468 cm^{-1} and 1360 cm^{-1} can be attributed to N-H bending vibration and C-N stretching vibration, respectively. Thus, these results confirm that HHA-HMP was successfully obtained.

Dithizone-acetonitrile UV-vis spectrophotometry is an improved method based on the national standard method. The ultraviolet absorption spectra

are presented in Fig. 2a. The new absorption peak of the dithizone-Hg²⁺ chelate was measured at 480 nm. The calibration curve (absorption ratio ($A_{480\text{ nm}}/A_{600\text{ nm}}$) versus concentration) covered a linear range from 0.83 to 8.33 $\mu\text{mol L}^{-1}$ (Fig. 2b). The experiments were carried out at room temperature with 30 min reaction (HHA-HMP=0.3 g L^{-1} , [Hg²⁺]=1 mmol L^{-1} , pH=4), and the removal efficiency of HHA-HMP toward Hg²⁺ was 74.8% (the binding capacity of modified pectin is 2.49 mmol g^{-1}). It was far higher than the 30.5% removal efficiency of HMP (1.02 mmol g^{-1}). The higher removal efficiency was mainly due to the participation of N atoms, which enhanced the coordinating effect between Hg²⁺ and HHA-HMP.

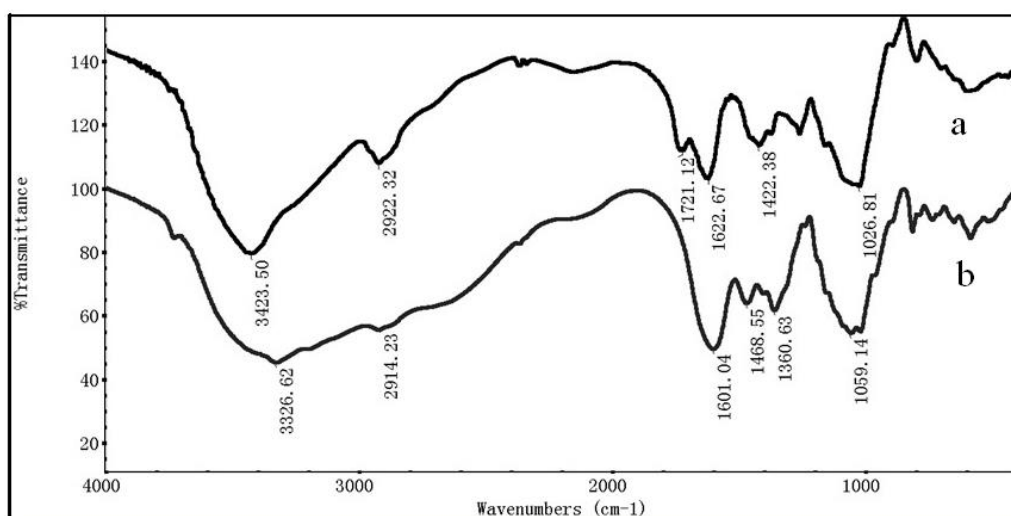


Fig. 1. IR spectra of HMP (a) and HHA-HMP (b).

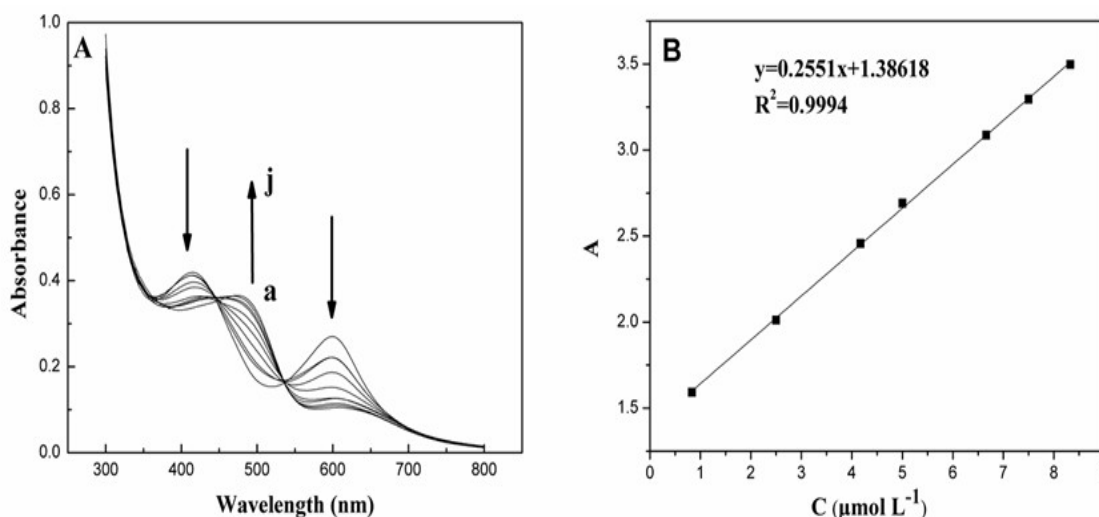


Fig. 2. (A) Absorption change of dithizone (1 mmol L^{-1}) upon addition of different Hg²⁺ concentrations (a-j): 0, 0.17, 0.50, 0.83, 2.50, 4.17, 5.00, 6.67, 7.50, 8.33 $\mu\text{mol L}^{-1}$ in acetonitrile solution (pH=2); (B) Calibration curve (absorption ratio ($A_{480\text{ nm}}/A_{600\text{ nm}}$) vs Hg²⁺ concentration (0.83-8.33 $\mu\text{mol L}^{-1}$).

Variation of the metal uptake with pH is shown in Fig. 3. The binding capacity of HHA-HMP does not increase at pH above 4-5, which is due to fact that the formation of the species $Hg(OH)_2$ achieves 100% at pH about 5 [21]. It follows from this result that the most favorable pH providing the best uptake effectiveness, is pH 4 where Hg^{2+} is present mostly in cationic form.

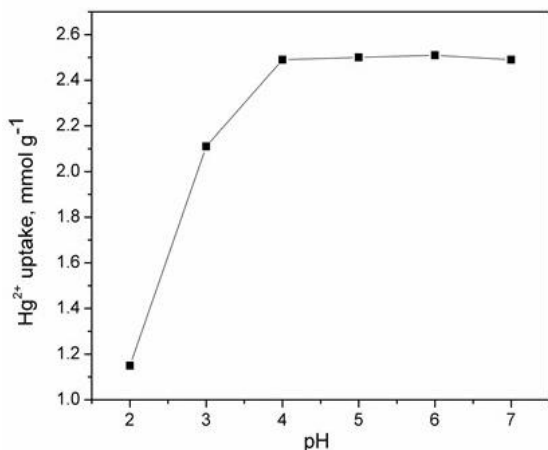


Fig. 3. Effect of pH on the uptake of Hg^{2+} by HHA-HMP (100 mL, 0.3 g L⁻¹ HHA-HMP; 100 mL, 1 mmol L⁻¹ Hg^{2+} ; 25°C; 30 min).

The XRD patterns are shown in Fig. 4.

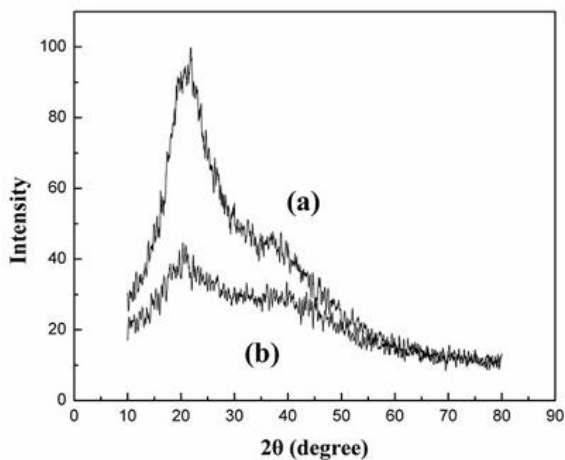


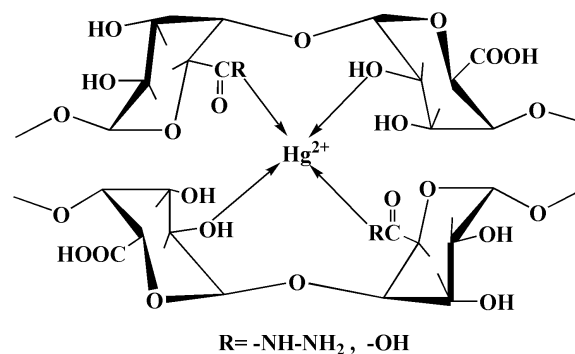
Fig. 4. XRD diffraction pattern of HHA-HMP (a) and HHA-HMP- Hg^{2+} (b).

As illustrated in Fig. 4a, the peak of HHA-HMP is remarkably sharp and the peak intensity near $2\theta=20^\circ$ indicates that HHA-HMP has a crystalline area, which is primarily ascribed to intramolecular hydrogen bonding. However, the XRD pattern of HHA-HMP- Hg^{2+} (Fig. 4b) shows that the

crystallization peak significantly decreases at around 20° which is due to the decreased intramolecular hydrogen bonding and the increased steric hindrance between the molecules. The XRD results showed that coordination bonds are formed between HHA-HMP and Hg^{2+} .

XPS provides identification of the sites involved in the accumulation of metals, as well as the species on the biopolymer [22]. The surface element electron binding energy data of HHA-HMP and HHA-HMP- Hg^{2+} are displayed in Table 2. The electron binding energies of C atoms before and after complexation are unchanged, indicating that the C atoms of the chemical environment on the HHA-HMP ligand surface are not different. However, the electron binding energies of N, O and Hg have changed. The changes show an apparent decrease in the binding energy of Hg4f and correspondingly an increase in the electron binding energy of N1s and O1s [23]. The results suggest that the removal of Hg^{2+} can be considered as a result of the complexation between Hg^{2+} and N/O atoms. The N and O atoms have a tendency of losing electrons and the Hg atoms have a tendency of getting electrons or sharing electron pairs, so it may be considered that the N and O atoms provide lone electron pairs to the empty orbits of the Hg atoms.

According to this, the reaction mechanism of HHA-HMP and Hg^{2+} involves the formation of coordination bonds of Hg^{2+} with N and O. The possible reaction mechanism of HHA-HMP with Hg^{2+} is shown in Scheme 2.



Scheme 2. Possible mechanism of the reaction of HHA-HMP with Hg^{2+} .

Table 2. Comparison of the electron binding energies of HHA-HMP and HHA-HMP- Hg^{2+} (ev)

Samples	C(1s)	N(1s)	O(1s)	Hg(4f)
HHA-HMP	284.88	398.77	531.06	
Hg^{2+}				101.56
HHA-HMP- Hg^{2+}	284.88	399.28	531.29	99.88

CONCLUSION

This study presents a novel hydrazine hydrate-modified pectin. On the basis of this study, a possible schematic mechanism for mercury uptake by HHA-HMP was proposed. Removal of Hg^{2+} by HHA-HMP from aqueous solutions is due to the complexation between Hg^{2+} and N/O atoms on the polymer matrix. So, the modified pectin has good prospects for the removal of heavy metals from aqueous solutions.

Acknowledgment: This work was supported by Special Plan of modern agricultural industry technology system "Waste utilization of potato processing and pollution control" of Gansu Province (nucytx-15).

REFERENCES

1. P. Bose, M.A. Bose, S. Kumar, *Adv. Environ. Res.*, **7**, 179 (2002).
2. E.P. Lai, B. Wong, V.A. VanderNoot, *Talanta*, **40**, 1097 (1993).
3. E. Pacyna, J. Pacyna, *Water, Air, and Soil Pollut.*, **137**, 149 (2002).
4. K.H. Nam, S. Gomez-Salazar, L.L. Tavlarides, *Ind. Eng. Chem. Res.*, **42**, 1955 (2003).
5. Q. Wang, D. Kim, D.D. Dionysiou, G.A. Sorial, D. Timberlake, *Environ. Pollut.*, **131**, 323 (2004).
6. J. Aguado, J.M. Arsuaga, A. Arencibia, *Ind. Eng. Chem. Res.*, **44**, 3665 (2005).
7. R.E. Cameron, *Superfund Risk Assessment in Soil Contamination Studies*, **1158**, 1 (1992).
8. C.D. May, *Carbohydr. Polym.*, **12**, 79 (1990).
9. B.R. Thakur, R.K. Singh, A.K. Handa, *Crit. Rev. Food Sci.*, **37**, 47 (1997).
10. I. Eliaz, A.T. Hotchkiss, M.L. Fishman, D. Rode, *Phytother. Res.*, **20**, 859 (2006).
11. M. Minamisawa, H. Minamisawa, S. Yoshida, *Green Chem.*, **7**, 595 (2005).
12. R.P. Dhakal, K.N. Ghimire, K. Inoue, *Sep. Purif. Technol.*, **42**, (3), 219 (2005).
13. B.W. Budesinsky, M. Sagat, *Talanta*, **20**, 228 (1973).
14. H.B. Singh, B. Kumar, R.L. Sharma, *Analyst*, **114**, 853 (1989).
15. N.S. Murcia, E.G. Lundquist, S.O. Russo, *J. Chem. Educ.*, **67**, 608 (1990).
16. B. Raman, V.M. Schinde, *Analyst*, **115**, 93 (1990).
17. M.M. Seleim, K.A. Idriss, M.S. Saleh, H. Sedaira, *Analyst*, **112**, 1685 (1987).
18. R. Gnanasambandam, A. Proctor *Food Chem.*, **68**, 327 (2000).
19. G. Guibaud, N. Tixier, A. Bouju, M. Baudu, *Chemosphere*, **52**, 1701 (2003).
20. A. Li, R.F. Liu, A.Q. Wang, *J. Appl. Polym. Sci.*, **98**, 1351 (2005).
21. S. Cataldo, A. Gianguzza, A. Pettignano, I. Villaescusa, *React. Funct. Polym.*, **73**, 207 (2013).
22. L. Dambies, C. Guimon, S. Yiacoumi, E. Guibal, Characterization of metal ion interactions with chitosan by X-ray photoelectron spectroscopy, *Colloids and Surfaces A: Physicochem. Eng. Aspects*, **177**, 203 (2000).
23. J.A. Taylor, G.M. Lancaster, J.W. Rabalais, Chemical reactions of N_2^+ ion beams with group IV elements and their oxides, *J. Electron. Spectrosc. Relat. Phenom.*, **13**, 435-444 (1978).

МЕХАНИЗЪМ ЗА ОТСТРАНЯВАНЕ НА ЖИВАК ЧРЕЗ ЕДИН НОВ МОДИФИЦИРАН С ХИДРАЗИН ХИДРАТ- ПЕКТИН

Дж. Гуо^{1,2}, Дж. Жанг², И. Юе¹, И. Гуо^{1,*}

¹ Лаборатория по природна медицина в провинция Гансу, Лаборатория по химия на североизточните растителни ресурси, Институт по химична физика Ланжу, Китайска академия на науките, Ланжу Китай

² Колеж по нефтохимично инженерство, Технологичен университет в Ланжу, Ланжу, Китай

Постъпила на 20 октомври, 2013 г.; коригирана 12 декември, 2013 г.

(Резюме)

В тази работа се описва нов пектин, модифициран с хидразин-хидрат, изследван за отстраняването на Hg^{2+} . Модифицираният пектин е охарактеризиран чрез елементен анализ и FT-IR спектроскопия, която показва, че хидразин-хидратът успешно се присажда към страничната верига на пектина. Освен това механизмът на реакцията между модифицирания пектин и Hg^{2+} е изследван чрез рентгеноструктурен анализ и рентгенова фотоелектронна спектроскопия (XPS). Резултатите показват, отстраняването на живачни йони се дължи на координационни връзки между Hg^{2+} и азотните и кислородните атоми. Ефективността на отстраняване на живака с модифициран пектин достига 74.8% при оптимизирани условия, което много над известните 30.5%, получени при природния пектин.

Validated UHPLC-DAD method for quantification of cholesteryl-succinyl-5-fluorouracil conjugate

F. K. Alanazi¹, A.A. Radwan¹, N. Haq^{2,3}, I. A. Alsarra^{2,3}, F.Shakeel^{2,3*}

¹*Kayyali Chair for Pharmaceutical Industry, Department of Pharmaceutics, College of Pharmacy, King Saud University, Riyadh, Saudi Arabia*

²*Center of Excellence in Biotechnology Research (CEBR), King Saud University, Riyadh, Saudi Arabia*

³*Department of Pharmaceutics, College of Pharmacy, King Saud University, Riyadh, Saudi Arabia*

Received October 29, 2013; Revised January 7, 2014

The aim of the present study was to develop and validate an UHPLC-DAD method for quantification of cholesteryl-succinyl-5-fluorouracil conjugate in a standard sample, a lipid nanoemulsion and dissolved samples. The separation of the conjugate was carried out on Hypersil GOLD 50 X 2.1 mm RP C₁₈ column packed with 1.9 μm packing as a stationary phase. The mobile phase was methanol:water (80:20 % v/v) at a flow rate of 0.3 ml/min with DAD detection at 276 nm. The proposed method was found to be precise, accurate, robust, sensitive and specific for quantification of the conjugate. The utility of the proposed method was checked by the assay of conjugate in a lipid nanoemulsion and in dissolved samples. High assay value of conjugate in the lipid nanoemulsion was observed (99.25 %). *In vitro* dissolution of the cholesteryl-succinyl-5-fluorouracil conjugate in the lipid nanoemulsion was observed as 78.1% after 24 h. The conjugate was found to be sufficiently degraded under acid, base and thermal stress conditions. The developed method successfully resolved the drug conjugate peak in the presence of its degradation products. These results indicated that the developed UHPLC-DAD method can successfully be used for routine analysis of drug conjugates in pharmaceutical formulations.

Keywords: UHPLC-DAD, Cholesteryl-succinyl-5-fluorouracil, Dissolution, Lipid nanoemulsion, Validation.

INTRODUCTION

The 5-fluorouracil (5-FU) is a well known antitumor drug which belongs to the antimetabolite class of anticancer drugs and is recommended clinically for the treatment of various types of tumors such as colorectal, breast and ovarian tumor either alone or in combination with other antitumor drugs [1, 2]. Nevertheless, due to incomplete and erratic bioavailability profile upon oral administration, it has been administered *via* intravenous injection whereby the drug plasma concentration could not be maintained for long time because of rapid metabolism of drug [3, 4]. In the last few decades, the prodrug/conjugation approach has been successfully applied for enhancing therapeutic efficacy and reducing adverse effects associated with 5-FU [5-7]. Therefore, in the present study, the cholesteryl ester conjugate of 5-FU (cholesteryl-succinyl-5-fluorouracil with molecular weight of 598.38, Figure 1) was synthesized in order to improve its therapeutic efficacy of 5-FU and to reduce oral/parenteral adverse effects.

For quantification of 5-FU, various analytical methods such as gas chromatography, capillary electrophoresis, spectrophotometry, colorimetry and high performance liquid chromatography (HPLC) have been reported [8-21]. Ultra high performance liquid chromatography (UHPLC) is a relatively newly developed liquid chromatographic technique which offered several advantages over routine HPLC method such as high sensitivity, high analytical speed, improved resolution and short analysis run time [22-24]. Nevertheless, no UHPLC methods have been reported for the quantification of 5-FU or any of its conjugate/derivative or prodrug in literature so far. Therefore, in the present study, attempts were made to develop and validate a rapid, facile, precise, accurate, robust and stable UHPLC method coupled with diode array detector (DAD) for rapid analysis of the newly synthesized conjugate cholesteryl-succinyl-5-fluorouracil conjugate utilizing isocratic elution, taking into consideration the test conditions recommended by the International conference on harmonization (ICH) [25]. The developed method is completely novel for the cholesteryl-succinyl-5-fluorouracil conjugate. The developed method was applied for the assay of cholesteryl-succinyl-5-fluorouracil conjugate in a lipid nanoemulsion and

* To whom all correspondence should be sent:
E-mail: faiyazs@fastmail.fm

in vitro dissolved samples of the lipid nanoemulsion.

EXPERIMENTAL

Chemicals and reagents

5-FU was donated by Alfa Aesar (Ward Hill, MA). Cholesteryl-succinyl-5-fluorouracil conjugate (Mol. Wt. 598.38, Figure 1) was synthesized and characterized in the laboratory. HPLC grade methanol, hydrochloric acid (HCl), sodium hydroxide (NaOH) and hydrogen peroxide (H₂O₂) were purchased from BDH Laboratory supplies (Liverpool, UK).

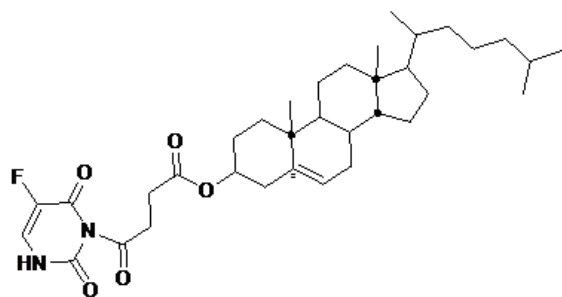


Figure 1 Molecular structure of cholesteryl-succinyl-5-fluorouracil conjugate (mol. wt. 598.38)

Cholesterol, cholesteryloleate, phosphatidylcholine and glycerol trioleate (triolein) were purchased from Sigma Aldrich (St. Louis, MO). Ultra-pure water was obtained from a ELGA water purification system (Wycombe, Bucks, UK). All other chemicals and reagents were of analytical reagent grade.

Instrumentation and chromatographic conditions

Chromatographic identification of the cholesteryl-succinyl-5-fluorouracil conjugate was performed at room temperature (22±1°C), with a Thermo Scientific UHPLC system (Thermo Scientific, Germany) equipped with a 3000 LC pump, 3000 autosampler, binary pumps, programmable DAD detector, Ultimate 3000 column oven, Ultimate 3000 controller and an online vacuum degasser. Chromeleon software (version 6.8) was used for data analysis. Chromatographic identification of the conjugate was performed on a Thermo Hypersil GOLD 50 × 2.1 mm RP C₁₈ column (Thermo Scientific, Germany) with a 1.9 μm packing as a stationary phase. The mobile phase consisted of methanol: water (80:20 % v/v). The elution was performed at a flow rate of 0.3 ml/min with diode array detection (DAD) detection at 276 nm. Samples (1 μl) were

injected using an Ultimate 3000 series Thermo auto sampler.

Preparation of cholesteryl-succinyl-5-fluorouracil conjugate stock solution

The calibration curve for the cholesteryl-succinyl-5-fluorouracil conjugate was plotted in the concentration range of 1 to 50 μg/ml. Stock solution of 100 μg/ml was prepared. Serial dilutions were made from the stock solution by diluting the required aliquots with the mobile phase to get concentrations in the range of 1 to 50 μg/ml.

Method development

Various solvent systems were checked as mobile phase for the development of a suitable UHPLC-DAD method for the quantification of cholesteryl-succinyl-5-fluorouracil conjugate in its standard drug compound. The selection of mobile phase was mainly based on assay sensitivity, retention time, peak parameters, suitability for stability studies, ease of preparation and cost effectiveness of the solvents. Based on these criteria, several mobile phases such as acetonitrile-water, acetonitrile-phosphate buffer, methanol-water, methanol-phosphate buffer, ethanol-water and ethanol-phosphate buffer at different proportions were used. Finally, the combination of methanol-water (80:20 % v/v) was selected as an eluent for the further studies.

Validation studies

The proposed UHPLC-DAD method was validated for various parameters such as linearity, accuracy, precision, sensitivity, robustness and specificity according to ICH guidelines [25].

Freshly prepared linearity solutions in the concentration range of 1-50 μg/ml were used for construction of the calibration curves. The mobile phase consisting of methanol-water (80:20 % v/v) was delivered at a rate of 0.3 ml/min for column equilibration; the baseline was continuously monitored during this process. The chromatographic detection was performed at 276 nm. The prepared dilutions were injected in triplicate; peak areas were recorded using the UHPLC system for each dilution and concentration was plotted against peak area.

The accuracy of the proposed method was assessed by a previously reported standard addition method [26]. The standard cholesteryl-succinyl-5-fluorouracil conjugate solution (10 μg/ml) was spiked with 0, 50, 100 and 150 % of extra standard drug solution and was reanalyzed by the proposed method. Percent recovery (%), percent relative

standard deviation (%RSD) and standard error for each concentration were calculated.

The precision of the proposed UHPLC-DAD method was determined as repeatability (intraday precision) and interday (intermediate precision). Intraday precision of the proposed method was measured by quantification of four different concentrations of cholesteryl-succinyl-5-fluorouracil conjugate (10, 15, 20 and 25 µg/ml) in triplicate on the same day. Intermediate precision was measured by repeating the studies on three different days.

Limit of detection (LOD) and limit of quantification (LOQ) of the proposed method were determined by the signal to noise ratio (S/N ratio) method as reported previously using the following equations:

$$\text{LOD} = 3.3 \times \text{S/N} \text{ and } \text{LOQ} = 10 \times \text{S/N}$$

The robustness of the proposed method was determined to evaluate the effect of deliberate variation of chromatographic conditions on the determination of the cholesteryl-succinyl-5-fluorouracil conjugate. A target concentration of 10 µg/ml of the conjugate was selected for this purpose. The robustness of the proposed method was determined by changing the mobile phase flow rate from 0.3 ml/min to 0.35 and 0.25 ml/min; the wavelength of detection from 276 to 280 and 272 nm and the concentration of methanol in the mobile phase from 80 to 85 and 75 %.

Forced degradation studies

Forced degradation studies were performed under various stress conditions such as acid stress, base stress, oxidative stress and thermal stress. These studies were performed to evaluate the stability and specificity of the proposed UHPLC-DAD method.

For acid- and base-induced degradation, the target concentration (10 µg/ml) of cholesteryl-succinyl-5-fluorouracil conjugate was freshly prepared in the mobile phase. An aliquot (1 ml) of this solution was exposed to acid and base hydrolysis by adding 4 ml of 0.1M HCl or 4 ml of 0.1M NaOH, respectively. Acid and base treated mixtures were kept in a hot-air oven for 48 h at 60°C and then analyzed by the proposed method for determination of cholesteryl-succinyl-5-fluorouracil conjugate in the presence of its acid and base degradation products, respectively.

The same procedure was adopted for oxidative degradation studies using 3% H₂O₂ as an oxidant.

For thermal degradation, an aliquot of the target concentration of cholesteryl-succinyl-5-fluorouracil conjugate (10 µg/ml) was exposed to a hot-air oven

for 48 h at 60°C and then analyzed by the proposed method for determination of cholesteryl-succinyl-5-fluorouracil conjugate in the presence of its thermal degradation products.

Preparation and characterization of a lipid nanoemulsion

A lipid nanoemulsion of cholesteryl-succinyl-5-fluorouracil conjugate was prepared according to the method reported by Moura and coworkers [27]. Briefly, the lipid phase was emulsified with the aqueous phase (deionized water) by prolonged ultrasonic irradiation followed by two-step ultracentrifugation with density adjustment by addition of KBr to obtain a lipid nanoemulsion [28]. The composition of the lipid phase was as follows: 40 mg of cholesteryloleate, 20 mg of phosphatidylcholine, 1 mg of triolein and 0.5 mg of cholesterol. 6 mg of cholesteryl-succinyl-5-fluorouracil conjugate was solubilized in ethanol and introduced into the lipid nanoemulsion. The prepared lipid nanoemulsion was then sonicated, dialyzed and filtered as reported previously [27, 28].

The lipid nanoemulsion of cholesteryl-succinyl-5-fluorouracil conjugate was characterized for droplet size, PI, viscosity and RI. The droplet size and PI were determined using Malvern Mastersizer (Malvern Instruments Ltd., Worcestershire, UK) at room temperature (25°C) at a scattering angle of 90°. The procedure for the measurement of droplet size and PI was similar to that reported in our previous article [29]. Viscosity and RI of the cholesteryl-succinyl-5-fluorouracil loaded lipid nanoemulsion were determined using Brookfield viscometer (Brookfield Engineering Laboratories, Inc, Middleboro, MA) and Abbes type refractometer (Precision Standard Testing Equipment Corporation, Germany), respectively, at 25±1°C as reported in ref. [29].

Assay of cholesteryl-succinyl-5-fluorouracil conjugate in the lipid nanoemulsion

The utility of the proposed UHPLC-DAD method was checked by applying this method for the quantification of cholesteryl-succinyl-5-fluorouracil conjugate in the lipid nanoemulsion. For determination of the cholesteryl-succinyl-5-fluorouracil conjugate content in the lipid nanoemulsion (containing 6 mg/ml of cholesteryl-succinyl-5-fluorouracil conjugate), 1 ml of the formulation was suitably diluted with mobile phase (methanol:water-80:20) to obtain 100 ml of stock solution [30]. The stock solution was sonicated for about 1 h and subjected to UHPLC analysis for

determination of the cholesteryl-succinyl-5-fluorouracil conjugate content after suitable dilution with mobile phase. The possible interactions between the components of the lipid nanoemulsion and the cholesteryl-succinyl-5-fluorouracil conjugate were also studied.

Dissolution studies of the lipid nanoemulsion

The utility of the proposed method was also checked by applying the method in dissolution/drug release studies of cholesteryl-succinyl-5-fluorouracil conjugate from the lipid nanoemulsion. Dissolution studies were performed in 500 ml of deionized water using the United States Pharmacopoeia (USP) XXIV method at a speed of 100 rpm at $37 \pm 0.5^\circ\text{C}$ [28]. One ml of the formulation was placed in a dialysis bag (MWCO 12,000 g/mol; Spectrum Medical Industries, Mumbai, India). Samples (1 ml) were withdrawn at different intervals of time (0, 1, 2, 3, 6, 18 and 24 h) and were replaced by the same amount of fresh deionized water. The samples were analyzed for the cholesteryl-succinyl-5-fluorouracil conjugate content by the proposed method.

RESULTS AND DISCUSSION

Method development

During method development step, the use of ethanol-water and ethanol-phosphate buffer as the mobile phases resulted in an asymmetric peak with a high tailing. Further, acetonitrile-water and acetonitrile-phosphate buffer were tried at different proportions at a flow rate of 0.3 ml/min. These also resulted in a very poor peak with high tailing. Further, methanol-water and methanol-phosphate buffer were tried as mobile phases. Finally, the proportions of methanol and water were adjusted to obtain a rapid and simple assay method for cholesteryl-succinyl-5-fluorouracil conjugate with a reasonable run time, suitable retention time and acceptable tailing or asymmetry factor. Of several compositions of methanol and water and methanol and phosphate buffer investigated, the binary proportion at 80:20 % v/v was found yield a sharp peak with suitable retention time and good asymmetry. Finally, the proportions of methanol and water were adjusted to obtain a rapid and simple assay method for cholesteryl-succinyl-5-fluorouracil conjugate with a reasonable run time, suitable retention time (0.60 ± 0.001 min) and acceptable tailing or asymmetry factor (Figure 2a).

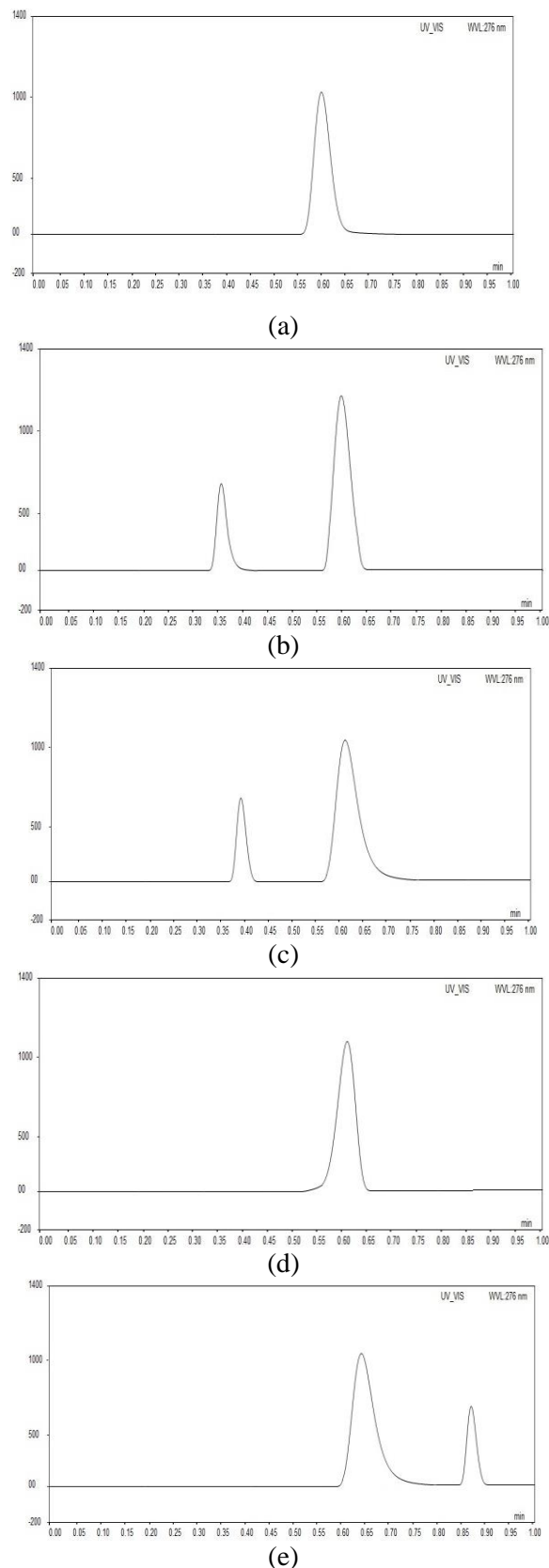


Fig. 2. UHPLC-DAD chromatogram of cholesteryl-succinyl-5-fluorouracil conjugate (a) and chromatograms in the presence of 0.1M HCl (b), 0.1M NaOH (c), 3% H_2O_2 (d) and under thermal condition (e)

Method validation

The calibration curve was plotted as a dependence of UHPLC peak areas on concentration. The data were evaluated by linear least square analysis. The calibration curve was found to be linear in the concentration range of 1–50 µg/ml. The regression equation was $Y = 0.021X + 0.041$ with a correlation coefficient (R^2) of 0.999 ± 0.001 (Table 1).

Table 1. Linear regression data for the calibration curve of cholesteryl-succinyl-5-fluorouracil conjugate ($n=3$)

Parameters	Values
Linearity range	1– 50 µg/ml
Correlation coefficient ($R^2 \pm SD$)	0.999 ± 0.001
Regression equation	$Y = 0.021X + 0.041$
Slope \pm SD	0.021 ± 0.001
Confidence interval of slope*	0.018–0.023
Standard error of slope	0.00057
Intercept \pm SD	0.041 ± 0.003
Confidence interval of intercept*	0.033–0.048
Standard error of intercept	0.00173

* 95% confidence interval

No significant difference was observed in the slopes/intercepts of calibration curves (ANOVA, $p > 0.05$). The linear regression data for calibration curve of cholesteryl-succinyl-5-fluorouracil conjugate are listed in Table I.

The accuracy of the proposed UHPLC-DAD method was determined as % recovery and the results are listed in Table 2.

Good recoveries (98.12–99.60 %) of the spiked cholesteryl-succinyl-5-fluorouracil conjugate were obtained with lower values of %RSD and standard errors at each concentration level. The high recoveries pointed to the good accuracy of the developed UHPLC-DAD method.

Table 2. Accuracy of the UHPLC-DAD method (% recovery, $n = 3$)

% of conjugate added to analyte	Theoretical concentration (µg/ml)	Measured concentration (µg/ml) \pm SD	RSD (%)	Standard error	% Recovery
0	10	9.86 ± 0.16	1.62	0.09	98.60
50	15	14.73 ± 0.21	1.42	0.12	98.20
100	20	19.92 ± 0.28	1.40	0.16	99.60
150	25	24.53 ± 0.34	1.38	0.19	98.12

Table 3. Precision of UHPLC-DAD method ($n = 3$)

Concentration (µg/ml)	Repeatability (Intra-day precision)			Intermediate precision (Inter-day)		
	Mean area \pm SD	RSD (%)	Standard error	Mean area \pm SD	RSD (%)	Standard error
10	0.2614 ± 0.0044	1.68	0.0025	0.2702 ± 0.0047	1.73	0.0027
15	0.3856 ± 0.0071	1.84	0.0040	0.3907 ± 0.0076	1.94	0.0043
20	0.4808 ± 0.0082	1.70	0.0047	0.4771 ± 0.0072	1.50	0.0041
25	0.5819 ± 0.0088	1.51	0.0050	0.5789 ± 0.0083	1.43	0.0047

The results of intra-day and intermediate precision were expressed in terms of % RSD and are listed in Table 3.

The results indicated that the proposed UHPLC-DAD method was precise as the % RSD values for intraday and intermediate precision were in the range of 1.51–1.84 and 1.43–1.94, respectively. Moreover, the low values of % RSD indicated the good precision of the proposed UHPLC-DAD method.

The LOD and LOQ for the proposed UHPLC-DAD method were determined by the S/N ratio method and were found to be 0.50 and 1.50 µg/ml, respectively. The low values of LOD and LOQ indicated the good sensitivity of the proposed method.

For robustness, the SD, % RSD and standard error of the peak areas for all parameters (mobile phase composition, wavelength of detection and flow rate) at a concentration level of 10 µg/ml were determined. The results are shown in Table 4.

The low values of % RSD and standard error obtained after introducing small deliberate changes in the mobile phase composition, wavelength of detection and flow rate indicated the robustness of the proposed method.

Forced degradation studies

Forced degradation studies were performed to evaluate the stability and the specificity of the proposed method. Forced degradation of cholesteryl-succinyl-5-fluorouracil conjugate was determined by exposing a target concentration under various stress conditions. The results of the forced degradation studies are listed in Table 5 and Figures 2b–e.

Table 4. Robustness of the UHPLC-DAD method (n = 3)

Parameters	Mean area ± SD	RSD (%)	Standard error	Retention time ± SD	RSD (%)	Standard error
Mobile phase composition (85:15 % v/v)	0.2788±0.0048	1.72	0.0027	0.586 ± 0.004	0.68	0.0023
(75:25 % v/v)	0.2594±0.0039	1.50	0.0022	0.632 ± 0.007	1.10	0.0040
Mobile phase flow rate (0.35 ml/min.)	0.2509±0.0034	1.35	0.0019	0.575 ± 0.005	0.86	0.0028
(0.25 ml/min.)	0.2745±0.0046	1.67	0.0026	0.674 ± 0.008	1.86	0.0046
Detection wavelength (nm) 272	0.2642±0.0033	1.24	0.0019	0.604 ± 0.005	0.82	0.0028

Table 5. Results of forced degradation studies (n = 3)

Stress condition	Mean area ± SD	RSD (%)	Standard error	Number of degradation products (R _t)	5-FU conjugate remaining (µg/ml)	Amount recovered (%)
0.1M HCl	0.1787±0.0031	1.73	0.0017	1 (0.362)	6.55	65.57
0.1M NaOH	0.1573±0.0028	1.78	0.0016	1 (0.390)	5.53	55.38
3% H ₂ O ₂	0.2452±0.0042	1.71	0.0024	-	9.72	97.23
Thermal	0.2104±0.0037	1.75	0.0021	1 (0.893)	8.06	80.66

65.57% of the cholesteryl-succinyl-5-fluorouracil conjugate was found to remain in the acid induced sample and 34.43% was degraded (Figure 2b). The acid degradation product (peak 1 in Figure 2b) was found to be eluted with a retention time of 0.362 min (Table V). It was also found to be degraded sufficiently in the presence of 0.1M NaOH solution (alkaline condition). 55.38% of cholesteryl-succinyl-5-fluorouracil conjugate was remaining in the alkaline stress sample and 44.62% was degraded within 48 h (Figure 2c). The base-induced degradation product (peak 1 in Figure 2c) was found to be eluted with a retention time of 0.390 min. However, 97.23% of cholesteryl-succinyl-5-fluorouracil conjugate remained in the H₂O₂ induced sample and only 2.77% degraded (Figure 2d). Therefore, cholesteryl-succinyl-5-fluorouracil conjugate was found to be sufficiently stable under oxidative stress conditions. On the other hand, 19.34% of cholesteryl-succinyl-5-fluorouracil conjugate was found to be degraded under thermal conditions and 80.66% was remaining in the solution after 48 h (Figure 2e). The thermal-induced degradation product (peak 2 in Figure 2e) was found to be eluted with a retention time of 0.893 min. Therefore, cholesteryl-succinyl-5-fluorouracil conjugate was found to be stable under oxidative stress conditions while it degraded sufficiently under acid, base and thermal stress conditions. Generally, the forced degradation studies indicated that the proposed method was specific and stable.

Characterization of the lipid nanoemulsion

Lipid nanoemulsion formulation of cholesteryl-succinyl-5-fluorouracil conjugate was successfully

prepared and characterized in terms of droplet size, polydispersity index (PI), viscosity and refractive index (RI). The results of the characterization studies are listed in Table 6.

Table 6. Physicochemical characterization of cholesteryl-succinyl-5-fluorouracil loaded lipid nanoemulsion

Parameters	Value
Droplet size (nm) ^a	71.210±5.870
PI	0.287
Viscosity (cp) ^a	152.130±8.210
RI ^a	1.343±0.002

Polydispersity index (PI); Refractive index (RI); mean ± SD, n=3

The mean droplet size of the lipid nanoemulsion was 71.21±5.87 nm with a low value of PI (0.287) which indicated the proper development of lipid nanoemulsion. However, the viscosity of the lipid nanoemulsion was found to be 152.13±8.21 cp (Table VI). The RI of the lipid nanoemulsion was 1.343±0.002 which is close to the RI of water (1.33). The lower values of droplet size, PI, viscosity and RI supported the proper development of the lipid nanoemulsion formulation of cholesteryl-succinyl-5-fluorouracil conjugate.

Assay of cholesteryl-succinyl-5-fluorouracil conjugate in the lipid nanoemulsion

According to the validation studies, the proposed UHPLC-DAD method is rapid, precise, accurate and sensitive for the quantification of the cholesteryl-succinyl-5-fluorouracil conjugate. Therefore, the developed UHPLC-DAD method was applied for the quantification of cholesteryl-succinyl-5-fluorouracil conjugate in a lipid nanoemulsion. The assay value of cholesteryl-succinyl-5-fluorouracil conjugate in the lipid

nanoemulsion was found to be $99.25 \pm 1.97\%$. This assay value was found to be highly acceptable according to the regulatory guidelines of ICH. The % RSD in the assay of cholesteryl-succinyl-5-fluorouracil conjugate was 1.98% which was also within the limits. High assay value and low % RSD of cholesteryl-succinyl-5-fluorouracil conjugate in the lipid nanoemulsion indicated that the proposed UHPLC-DAD method could be applied for routine analysis of derivatives/conjugates/prodrugs of 5-FU in lipid nanoemulsions and other formulations. No interactions between cholesteryl-succinyl-5-fluorouracil and nanoemulsion excipients were observed. The UHPLC-DAD chromatogram of cholesteryl-succinyl-5-fluorouracil conjugate extracted from the lipid nanoemulsion was found to be the same as that of standard cholesteryl-succinyl-5-fluorouracil conjugate, indicating the purity of the peak in the lipid nanoemulsion.

Dissolution studies of the lipid nanoemulsion

In vitro drug release (dissolution) profile of cholesteryl-succinyl-5-fluorouracil conjugate from the lipid nanoemulsion was also determined by the proposed method. The results of the *in vitro* drug release (dissolution) profile of cholesteryl-succinyl-5-fluorouracil conjugate from the lipid nanoemulsion are presented in Figure 3. About 68% of cholesteryl-succinyl-5-fluorouracil conjugate was found to be released from the lipid nanoemulsion after 6 h, as shown in Figure 3.

Initially, the release profile was of the rapid/immediate type. After a period of 6 h, the lipid nanoemulsion showed a sustained release profile of cholesteryl-succinyl-5-fluorouracil conjugate. The % dissolution of cholesteryl-succinyl-5-fluorouracil conjugate after 24 h was found to be 78.1%. Drug release studies showed that the proposed UHPLC-DAD method could also be applied for dissolution/release studies of pharmaceutical dosage forms containing 5-FU derivatives as the active ingredients.

CONCLUSION

The proposed UHPLC-DAD method for quantification of cholesteryl-succinyl-5-fluorouracil conjugate is simple, accurate, precise, robust, sensitive and stable. High assay value of cholesteryl-succinyl-5-fluorouracil conjugate was obtained in a developed lipid nanoemulsion. The drug release profile of cholesteryl-succinyl-5-fluorouracil conjugate from lipid nanoemulsion was within the acceptable limits. The method was found to be economic and efficient. These factors make the proposed method superior for routine analysis

of cholesteryl-succinyl-5-fluorouracil conjugate in standard drugs, pharmaceutical formulations and dissolution samples. Because of its stability, the proposed UHPLC-DAD method can be utilized for the prediction of half life and shelf life of cholesteryl-succinyl-5-fluorouracil conjugate in pharmaceutical formulations.

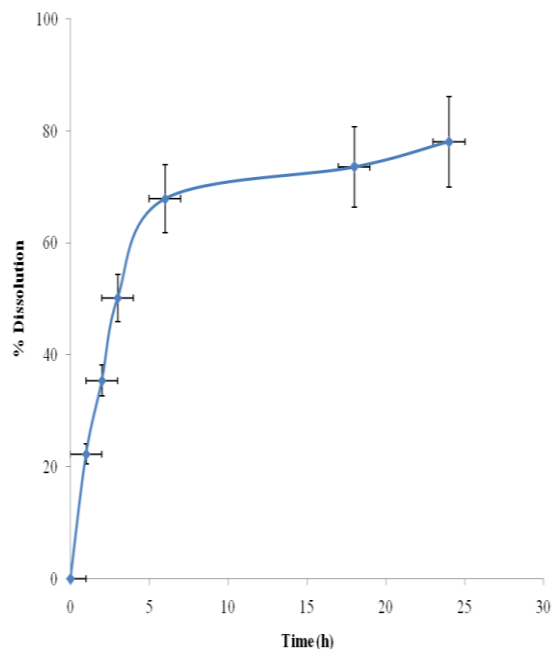


Fig. 3. *In vitro* dissolution (drug release) profile of cholesteryl-succinyl-5-fluorouracil conjugate from the lipid nanoemulsion through dialysis membrane

Acknowledgment: The authors are highly thankful to the National Plan for Science, Technology and Innovation for the generous financial support (Grant No. 11 NAN 1286-02).

CONFLICT OF INTEREST

The authors report no conflict of interest related with this manuscript.

REFERENCES

1. P. Rossella, B. Massimo, G. Simona, A.J. Christopher, *J. Pharm. Biomed. Anal.* **38** (2005) 738-745.
2. Z. Dong, W. Zheng, Z. Xu, Z. Yin, *J. Appl. Polym. Sci.* **130** (2013) 927-932.
3. C.A. Presant, J. Jacobson, W. Wolf, V. Waluch, I.C. Weitz, J.S. Macdonald, *Invest. New Drugs* **20** (2002) 369-376.
4. D.B. Longley, D.P. Harkin, P.G. Johnston, *Nature Rev. Cancer* **3** (2003) 330.
5. S. Kuzuhara, N. Ohkoshi, K. Kanemaru, H. Hashimoto, T. Nakanishi, Y.J. Toyokura, *Neurol.* **234** (1987) 365-370.
6. E. Casado, P. Pfeiffer, J. Feliu, M. Gonzalez-Baron, L. Vestermark, H.A. Jensen, *Ann. Oncol.* **19** (2008) 1371-1378.

7. G.V. Koukourakis, V. Kouloulis, M.J. Koukourakis, G.A. Zacharias, H. Zabatis, J. Kouvaris, *Molecules* **13** (2008) 1897-1922.
8. Y. Morimoto, M. Akimoto, K. Sugibayashi, T. Nadai, Y. Kato, *Pharmazie* **36** (1981) 155-156.
9. S.K. Banerjee, A. Sumathi, *Ind. J. Pharm. Sci.* **56** (1994) 42-44.
10. G. Micoli, R. Turci, M. Arpellin, C. Minoia, *J. Chromatogr. B.* **750** (2001) 25-32.
11. L. Yang, J.S. Chu, J.A. Fix, *Int. J. Pharm.* **235** (2002) 1-15.
12. H.J. Lu, Y.L. Guo, H. Zhang, Q.Y. Ou, *J. Chromatogr. B.* **788** (2003) 291-296.
13. I.A. Alsarra, M.N. Alarifi, *J. Chromatogr. B.* **804** (2004) 435-439.
14. F. Casale, R. Canaparo, L. Serpe, E. Muntoni, C.D. Pepa, M. Costa et al, *Pharmacol. Res.* **50** (2004) 173-179.
15. O.T. Fahmy, M.A. Korany, H.M. Maher, *J. Pharm. Biomed. Anal.* **34** (2004) 1099-1107.
16. A. Di-Paolo, R. Danesi, L. Ciofi, F. Vannozzi, G. Bocci, M. Lastella et al, *Ther. Drug Monit.* **27** (2005) 362-368.
17. F.K. Alanazi, A.E. Yassin, M. Elbadry, H.A. Mowafy, I.A. Alsarra, *J. Chromatogr. Sci.* **47** (2009) 558-563.
18. V.R. Sinha, R.V. Kumar, R. Bhinghe, *Ind. J. Pharm. Sci.* **71** (2009) 630-637.
19. L.D. Vainchtein, H. Rosing, J.H. Schellens, J.H. Beijnen, *Biomed. Chromatogr.* **24** (2010) 374-386.
20. G. Yuan, L. Rong, S. Duanyun, L. Changxiao, *Trans. Tianjin Uni.* **16** (2010) 167-173.
21. N. Haq, F. Shakeel, F.K. Alanazi, A.A. Radwan, M. Ali, I.A. Alsarra, *Asian J. Chem.* **25** (2013) 7177-7182.
22. A. Kaufmann, P. Butcher, K. Maden, M. Widmer, *Anal. Chim. Acta* **586** (2007) 13-21.
23. W. Dong, P. Wang, X. Meng, H. Sun, A. Zhang, W. Wang et al, *Phytochem. Anal.* **23** (2012) 657-667.
24. S. Strano-Rossia, L. Anzillotti, E. Castrignanò, F.S. Romolo, M. Chiarottia, *J. Chromatogr. A.* **1258** (2012) 37-42.
25. ICH. Stability Testing of New Drug Substances and Products Q1A (R2), International Conference on Harmonization, IFPMA, Geneva, 2003.
26. P. Alam, M. Ali, R. Singh, Madhurima, S. Ahmad, F. Shakeel, *J. Chromatogr. Sci.* **47** (2009) 910-913.
27. J.A. Moura, C.J. Valduga, E.R. Tavares, I.F. Kretzer, D.A. Maria, R.C. Maranhão, *Int. J. Nanomed.* **6** (2011) 2285-2295.
28. R.C. Maranhão, T.B. César, S.R. Pedroso-Mariani, M.H. Hirata, C.H. Mesquita, *Lipids* **28** (1993) 691-696.
29. S. Shafiq, F. Shakeel, S. Talegaonkar, F.J. Ahmad, R.K. Khar, M. Ali, *Eur. J. Pharm. Biopharm.* **66** (2007) 227-243.
30. N. Haq, F. Shakeel, M. Ali, M. Elbadry, F.K. Alanazi, I.A. Alsarra, *J. Liq. Chromatogr. Rel. Technol.* (2013) DOI: 10.1080/10826076.2012.758150.

ВАЛИДИРАН УНPLC-DAD МЕТОД ЗА КОЛИЧЕСТВЕНО ОПРЕДЕЛЯНЕ НА ХОЛЕСТЕРИЛ-СУКЦИНИЛ-5-ФЛУОРОАЦИЛОВИ КОНЮГАТИ

Ф.К. Аланази¹, А.А. Радуан¹, Н. Хак^{2,3}, И.А. Алсарра^{2,3}, Ф. Шакийл^{2,3*}

¹Катедра по фармацевтична промишленост "Каяли", Департамент по фармация, Колеж по фармация, Университет "Крал Сауд", Риад, Саудитска Арабия

²Център за върхови постижения по биотехнологични изследвания (CEBR), Университет "Крал Сауд", Риад, Саудитска Арабия

³Департамент по фармация, Колеж по фармация, Университет "Крал Сауд", Риад, Саудитска Арабия

Постъпила на 29 октомври, 2013 г.; коригирана 7 януари, 2014 г.

(Резюме)

Целта на настоящата работа е да се разработи и валидира УНPLC-DAD метод за количествено определяне на холестерил-сукцинил-5-флуороацилови конюгати в стандартни проби, наноемулсии и разтворени проби. Разделянето на конюгатите е извършвано на колона Hypersil GOLD 50 X 2.1 mm RP C₁₈ с размери на частиците 1.9 µm като неподвижна фаза. Подвижната фаза е смес от метанол и вода (80:20 % об.) при дебит 0.3 мл/мин. С детектор DAD при 276 nm. Установено е че предложеният метод е прецизен, точен, стабилен, чувствителен и специфичен за количественото определяне на конюгатите. Приложимостта на предложения метод е изпитана при анализа на конюгати в липидни наноемулсии и в разтворени проби. Установени са високи съдържания на конюгати в наноемулсиите (99.25 %). Наблюдавано е *in vitro* разтваряне на холестерил-сукцинил-5-флуороациловите конюгати до 78.1% след 24 часа. Установено е, че конюгатите се разтварят достатъчно при стресови въздействия с киселина, основа или повишена температура. Разработеният метод успешно определя пика на лекарствения конюгат в присъствие на неговите разпадни продукти. Тези резултати показват, че разработеният УНPLC-DAD мерод може да бъде използван успешно за рутинни анализи на конюгати на лекарства във фармацевтични препарати.

Recycling of silver-plated brass for production of high purity copper and ultrafine silver powder for electric contacts

S. P. Dimitrijević¹, Z. Anđić², Ž. Kamberović³, S. B. Dimitrijević⁴, N. Vuković⁵

¹Innovation Center Faculty of Technology and Metallurgy, University of Belgrade, Beograd, Serbia

²Faculty of Chemistry, University of Belgrade, Beograd, Serbia

³Faculty of Technology and Metallurgy, University of Belgrade, Beograd, Serbia

⁴Mining and Metallurgy Institute Bor, Bor, Serbia

⁵Faculty of Mining and Geology, University of Belgrade, Beograd, Serbia

Received November 20, 2013; Revised February 16, 2014

The paper presents an improved process for recycling of silver-plate brass housing. Silver and copper are recovered with a purity of 99.99 % and 99.90 %, respectively, with the aim of obtaining materials of higher value using additional procedures based on the same process and equipment. The novel approach with subsequent electrorefining yields copper of 99.99 % purity with BS EN 1978:1998 (Cu-CATH-1) quality and is referred to as LME grade A. Additional processing of silver results in superfine, micro-sized Ag powder with particle size from 0.14 to 1.13 μm and purity of 99.999 %. Copper electrorefining tests were performed using 1.50 dm³ of synthetic electrolyte in a 2 dm³ electrolytic cell. Effects of current density and electrolyte composition were investigated. Optimal current density for the first and second refining was 120 A/m² and 200 A/m², respectively. Additional refining of silver was performed by chemical reduction from an aqueous solution. Optimal results were obtained with ascorbic acid as a reduction agent in concentration of 0.1 mol/dm³ and polyvinylpyrrolidone as a protective agent in concentration of 2 % by mass. The investigation results could be adopted into production.

Key words: recycling, copper, electrorefining, silver, micro-sized powder.

INTRODUCTION

Recycling of silver-plated brass has some specific issues when compared with conventional e-waste (waste electrical and electronic equipment, WEEE) processing. The recovery fundamentally aims at separating the three main metals in the material: copper, zinc and silver. The main goal of the present investigation was to obtain materials of higher value and to lower the cost of waste processing. Another result that was planned and realized was to obtain materials that can be reused with the same or similar purpose. Although the process of metal separation has been already applied in production [1], small changes in the process could yield copper and silver of higher purity.

Additional electrorefining (ER) leads to standard electrolytic copper quality, 99.99 %, with no more than 65 ppm of total impurities, of which maximum 25 ppm of silver [2]. Even higher purity of copper (99.999%) could be obtained from copper previously refined by electrolysis. Silver refinement is a common process and easily achieves 99.99 % metal purity. The disadvantage of the basic

hydrometallurgical process of refinement is that non-uniform, relatively coarse silver powder is obtained. ER could produce silver of uniform particle size of about 30 μm [3].

A hydrometallurgical process could be developed using a flexible technology with a full range of extractive metallurgic methods, such as pyro-, electro-, and hydrometallurgic processes. Pyrometallurgy is used barely for separation but primarily for anode casting. ER has given positive results in copper and zinc separation from pure brass [1]. It can be performed as either electrowinning or classical ER. Since no source of fresh electrolyte is available, combination of the two methods is used. Copper concentration decreases since the anodic dissolution compensates only part of the copper deposited on the cathode. Frequent corrections of the electrolyte are thus necessary. The process used in the study is basically a combination of EW and classical ER. Optimal parameters are similar to those in ER but with lower current density and higher concentrations of copper at the start of the process. Lower concentrations of copper and higher current densities have been used for similar recycling processes [4] but they were not confirmed. Subsequent ER was performed with a higher

* To whom all correspondence should be sent:
E-mail: stevad@gmail.com

current density, 200 A/m² and with higher concentrations of Cu²⁺, sulfuric acid and additives. Possibilities of using higher current densities are indicated in several papers [5–7] but the research leaves only a small margin for it owing to the relatively high content of silver in the cathode copper of the second ER. The primary goal was to obtain copper of 99.99 % purity, but the results indicated the possibility of obtaining copper of higher purity in two consecutive electrolytic refining runs. Copper of 99.999 % purity could be recovered with lower current densities only from the first cathodic cycle in an experiment with three cathodic cycles.

Fine silver powder is extensively used in various industries for different applications. Despite the high purity of silver (99.99 %) obtained by classical chemical reduction of AgNO₃ with hydrazine hydrate, the aim of the research was to obtain fine particles for general industrial use with possibility of reuse. Synthesis of silver nanoparticles is a well-developed process for small size production and is of interest for mass-scale production. Silver nanoparticles can be prepared using different methods which could be categorized as [8]:

- 1) Chemical reduction from aqueous solutions;
- 2) Non-aqueous chemical reduction;
- 3) Electrochemical reduction;
- 4) Photoinduced or photocatalytic reduction;
- 5) Irradiation reduction;
- 6) Ultrasonic assisted reduction;
- 7) Microwave assisted synthesis;
- 8) Microemulsion methods and
- 9) Biochemical methods.

Subject of the present research was the production of micro-sized uniform spherical Ag powders that are commonly used in electrically conductive pastes, solid oxide fuel cells, chemical catalysts, etc. [9]. At first electrical contact alloys were considered. Because of their high electrical and thermal conductivity, silver alloys are frequently used materials in the industry. They also have high corrosion resistance, excellent solderability, resistance to abrasive wear, mechanical strength and reasonable price [10–12]. Alloying elements (Cd, Mg, Sn, C, W and Ni) are selected in order to improve the mechanical properties without significantly increasing the electrical resistance. The oldest and best known alloy of this type is Ag-CdO which meets the above requirements [10]. However, while using the electrical contacts of Ag-CdO, dissociation of CdO in Cd (vapor state) and O₂ occurs, which, due to the toxicity of cadmium, is considered extremely harmful to human health [13]. For environmental

reasons and toxicity of the material, there is interest to find a suitable replacement for Ag-CdO. The most promising material is Ag-SnO₂ [11, 14]. Its potential as substitute for Ag-CdO contacts is virtually complete for direct current applications, but not complete for alternating current. It is known that the functional properties of Ag-SnO₂ electrical contact materials can be improved by the addition of metal oxide components which increase the dispersion of the main oxide (SnO₂) in the silver matrix and contribute to the activation of the sintering process [15–16]. The influence of SnO₂ nanoparticles and the method of their introduction into the silver matrix on the microstructure and physical properties of the material have been examined. The highest hardness has been registered for the sample prepared using soluble starch as a template [17].

Silver powders constituted of non-agglomerated micron/submicron crystalline particles with a narrow size distribution were found to be ideal for thick film conductive pastes [18]. Chemical reduction with formaldehyde in base solutions was used with similar results [19] by using silver nitrate as metal source, ascorbic acid as reducing agent and arabic gum as dispersant.

In this paper, silver particles were synthesized from silver nitrate or silver ammonium chloride, using ascorbic acid as a reducing agent and polyvinylpyrrolidone as a protecting agent, by a traditional chemical reduction method. This method was chosen because it requires no specific experimental equipment or working conditions. It may be efficiently scaled-up for mass production [20] which was the primary objective.

EXPERIMENTAL

Silver-plated brass housings were processed by a combination of pyrometallurgical, electrometallurgical and hydrometallurgical processes on laboratory and semi-industrial scale. Final products of the recycling were standard cathode copper Cu-CATH-1 (LME Grade A, European Standard EN 1978:1998) or Cu-CATH-2 grade [2] and 99.99% to 99.999% purity submicronic silver powder.

Analysis methods

Inductively coupled plasma optical emission spectrometry (ICP-OES) and atomic absorption spectrometry (AAS)

Inductively coupled plasma optical emission spectrometer (ICP-OES, Spectro, model: Ciris Visio, detection limits: <0.0001 g/dm³) and atomic absorption spectrometer (AAS, Perkin-Elmer,

model 403, detection limits: $< 0.0001 \text{ g/dm}^3$) were used for determination of the chemical composition of silver-plated housing and final products of refining.

Scanning electron microscopy (SEM) with energy-dispersive spectrometry (EDS)

Scanning electron microscope (SEM model: JOEL JSM- 6610LV operated at 20 keV) was used for determination of the chemical composition (with EDS), particle size and morphology of the silver powder. Chemical composition was determined using energy dispersive X-ray spectroscopy (EDS). The EDS spectra for silver powder were recorded using a X-ray spectrometer attached to the scanning electron microscope. The EDS image shows the place where the chemical composition of the silver powder was determined. Granulometric composition (particle size distribution; particle size analysis for SEM) of powders were determined by SEM software ImageJ (National Institutes of Health USA). ImageJ was able to measure distances directly from the image. The morphology of the silver powder was studied using SEM imaging.

Reagents

For the electrolyte preparation and its correction the following chemicals were used: copper sulfate pentahydrate p.a. (Zorka, Serbia); hydrochloric acid p.a. (Merck, Germany); sulfuric acid p.a. (Merck, Germany), thiourea p.a. (Kemika, Croatia) and gelatin powder pharmaceutical grade, Ph. Eur. (Merck, Germany).

For silver reduction and AgCl dissolution the following chemicals were used: nitric acid p.a. (Merck, Germany), ammonium hydroxide p.a. (Zorka, Serbia), hydrazine hydrate p.a. (Merck, Germany), ascorbic acid p.a. (Merck, Germany), polyvinylpyrrolidone, PVP K30 (trade name Plasdone[®] K-29/32) was of pharmaceutical grade (USP/NF) produced by ISP, sodium dodecyl sulfate (SDS) was of pharmaceutical grade (Ph. Eur.) produced by Cognis (trade name Texapon K12 P PH). Absolute ethanol p.a. (Zorka, Serbia) for silver powder rinsing was used. Deionized or double distilled water (max. conductivity $1 \mu\text{S/cm}$) was used in all experiments.

Experimental apparatus

Electrolytic laboratory type PP cell with approximately 2 dm^3 volume (1.50 dm^3 of electrolyte) was used for electrorefining. Electrorefining was performed with common open-tank parallel-plate electrode design, using

monopolar electrodes with parallel connection. A system of three anodes and four cathodes was used. Potentiostat Bank STP 84, with 6 A maximal electric current output was used as the electric current source. For electric measurements an HP 3466a multimeter was used, with 0.025Ω external shunt for currents above 2 A.

Analytical balance (Radwag AS 220/C/2) with a maximum load of 220 g and $d=0.1 \text{ mg}$ was used for the mass measurements of each anode and cathode and of the chemicals. High-precision laboratory balance (Kern EG 620-3NM) with maximum load of 620 g and $d=1 \text{ mg}$ was used for silver brass housing measurements.

The apparatus used for anode slime treatment experiments included: temperature-adjustable magnetic stirrer, with $\pm 1.0^\circ\text{C}$ deviation, various laboratory glassware, erlenmeyer flasks and beakers from 400 to 1000 ml, Büchner (vacuum) flask and electrical laboratory drier.

Recycling methods

Electrolytic refining

Electrolytic refining of anodes obtained by melting of silver-plated brass housing is realized through three anode periods. In the electrolytic refining of copper brass anode, the electrolyte concentration of copper decreases and the concentration of zinc increases. For this reason, during the process, the concentrations of copper and zinc should be daily monitored and adjusted. Correction of electrolyte was carried out twice a day every 12 h. Complete replacement of the electrolyte at the end of each cathode period was required. Waste electrolyte could be purified by zinc cementation or electrochemically decopperised to achieve environmental regulations [21].

Chemical refining of anode slime

Anode slime from copper electrorefining process consists mainly of silver (approx. 60%) with copper, lead, iron, cadmium and other impurities. Chemical refining could produce silver powder of 99.99% purity. This hydrometallurgical process has several stages, and is based on anode slime dissolving in dilute nitric acid, followed by precipitation with sodium chloride. The final stage is silver/lead separation by hydrazine reduction from ammonia solution. Recrystallization of silver is required to obtain a smaller particle size.

RESULTS AND DISCUSSION

Silver-plated brass housing in a quantity of 1846.574 g was the starting material for recycling. At the start, it was melted in an induction furnace.

Reducing atmosphere in the furnace was provided to prevent oxidation and evaporation of silver. Nine anodes with total mass of 1833.3833 g were made by casting. Anode dimensions were 60×80×5 mm. The chemical composition of the silver-plated brass and the anodes was different (Table 1). However, the differences are very small and are mainly due to metal evaporation, since refining does not take place during the anode casting. Nevertheless, even with small evaporation, higher silver concentration is obtained in the casted anodes.

Table 1. Chemical composition of silver-plated brass housing and brass anodes obtained from it

Composition, %	Silver-plated brass housing	Casted brass anodes
Copper (Cu)	59.41	59.53
Zinc (Zn)	34.85	33.77
Lead (Pb)	2.17	2.02
Cadmium (Cd)	0.018	0.023
Silver (Ag)	2.42	2.75
Iron (Fe)	0.64	0.97
Nickel (Ni)	0.38	0.56
Tin (Sn)	0.12	0.10
Silicon (Si)	0.00	0.28

Electrolytic refining

Metal recovery and separation start with the electrolytic refining. It is the first step of the process. The main goal of electrolysis is to obtain high-purity copper from the material with recovery as close as possible to 100%. The process is essentially brass electrolysis, since about 93% of the anode consists of copper and zinc. The electrolytic process is based on the large difference in the standard electrode potentials of copper and zinc. The potential difference between the copper and zinc half-cells is 1.10 V. It is more than enough for metal separation but due to the heterogeneous composition and variable concentration of ions in the electrolyte, several issues should be considered. The most important aspect is the constant increase in zinc concentration simultaneously with the reduction of copper concentration in the electrolyte. This affects the composition of the electrolyte as an important technological parameter and has to be adjusted during operation. Current density is important for both the quality of the cathode and the anode slime composition.

Electrolytic refining (ER) was realized in three independent experiments similar to the anodic periods in industrial-scale process. The first anodic period had two consecutive cathodic cycles, the second anodic period had three cathodic cycles and the third had two cathodic cycles. The first and second anodic periods had identical current density for determination of the influence of the electrolyte

composition and the third had higher current density for determination of the influence of that parameter. Refining the same anode material on a larger scale in a pilot plant requires minimum two and preferably three cathodic cycles to obtain copper purity higher than 99% to eventually 99.9% [1]. In large-scale production (refining) three cathodic cycles result in better cathode copper quality. However, two cathodic cycles were found as the optimum compromise, since one cycle leads to a high concentration of zinc that exceeds the experimentally determined maximum level to obtain copper of 99% purity while more than two cycles raise the expenses and are very demanding in industrial conditions because of the need of handling a lot of material. Finally, the number of cathodic cycles primarily depends on the required quality of copper; higher purity like 99.99% or 99.999% could be obtained only by re-refining using two subsequent electrorefining processes. This is cost-effective especially if the copper cathode from the last (second or third) cathode cycle is used. Variable concentrations of copper and zinc in the electrolyte require their constant monitoring and correction of the electrolyte composition based on analysis. Electrolyte corrections require a daily addition of 10 g of copper sulfate pentahydrate and 10 ml of concentrated sulfuric acid.

First experiment (anodic period)

For electrolytic treatment three brass anodes with total weight of 613.7987g were used in one electrolytic cell. Cathode starting sheets were made from "grade A" (purity of 99.97% or more) copper sheets with dimensions 80×60×0.5mm. The process duration was 140 h: 80 h for the first cathodic period and 60 h for the second cathodic period. The first period is longer on purpose, as is the usual practice in electrorefining of copper with two cathodic cycles. Organization of electrodes in the cells was cathode - anode - cathode, so that the cell had 4 cathodes and 3 anodes with parallel configuration. The last two cathodes were placed next to the cell wall and had only one active side, so the anode and cathode surfaces were practically identical. Inter-electrode axial distance was 20 mm, current level was maintained in the range of 3.45 to 3.60 A which corresponds to a current density of 120 to 125 A/m². Electrolyte temperature was maintained within 55±2 °C. Circulation system for the electrolyte was provided. Due to the specifics of the process, the composition of the electrolyte was determined on every 24 h from the beginning of each cycle and at the end, as shown in Table 2.

Table 2. Chemical composition of the electrolyte for the first anodic and both cathodic periods

Concentration, g/dm ³	First cathodic cycle					Second cathodic cycle			
	Start, 0h	24h	48h	72h	End, 80h	Start, 0h	24h	48h	End, 60h
Cu	37.05	33.18	32.09	30.44	29.11	36.93	34.84	33.26	31.47
Zn	0	21.56	44.20	67.18	73.57	0	21.83	43.66	54.43
H ₂ SO ₄	180.5	177.2	178.3	181.6	175.9	180.2	184.0	182.4	172.8
Ag, ppm	0	0	0	0.8	1.6	0	1.2	1.8	2.7
Fe	0	0	0	1.08	1.46	0	0	0.87	1.82

Voltage measurements were done and cell voltage ranged within the limits of 180 - 220 mV. The obtained copper cathode had purity of 99.63 % by weight for the first cathodic cycle and 99.56% for the second one. Silver content was 0.058 % and 0.077 %, respectively. The corresponding concentrations of zinc were 19 ppm and 24 ppm.

Second anodic period

For electrolytic treatment three brass anodes with total weight of 610.2755 g were used in the electrolytic cell. The process duration was 144 h. All three cathodic periods were of 48 h and the end of ER was adjusted for their equalization. Configuration of the electrodes in the cells was identical to that in the first anodic period. Current level was maintained in the same range with corresponding current density of 125 to 150 A/m². Electrolyte temperature was 55±2°C. Circulation of electrolyte was provided. The composition of the electrolyte was determined on every 24 h and is shown in Table 3. Voltage measurements were

done and cell voltage ranged within the limits of 175 - 210 mV. The purity of the obtained copper cathode for all three cycles is shown in Table 4

It is obvious that the fresh electrolyte directly influences the purity of cathode copper.

Third anodic period

For electrolytic treatment three brass anodes with total weight of 609.3091 g were used in one electrolytic cell. The process duration was 106 h: 60 h for the first cathodic period and the remaining 46 h for the second cathodic period. The first period was longer, as in the first experiment with two cathodic cycles. Organization of electrodes in the cells was the same as in the previous two experiments. Current level was maintained in the range of 4.60 to 4.75 A which corresponds to a current density of 160 to 165 A/m². Electrolyte temperature and other parameters were the same as in the previous two anodic periods. Sampling of the electrolyte was also identical and its chemical composition is shown in Table 5.

Table 3. Chemical composition of the electrolyte for the second anodic and all three cathodic periods

Concentration, g/dm ³	First cathodic cycle			Second cathodic cycle			Third cathodic cycle		
	Start, 0h	24h	48h	Start, 0h	24h	48h	Start, 0h	24h	48h
Cu	37.02	34.04	30.43	37.05	36.32	29.64	36.89	38.80	33.67
Zn	0	22.00	43.68	0	21.75	44.11	0	21.59	42.90
H ₂ SO ₄	180.0	181.2	178.6	180.3	182.2	176.5	179.7	176.0	173.4
Ag, ppm	0	0	0.8	0	0	2.3	0	0.6	1.5
Fe	0	0	0	0	0	0	0	0	0

Table 4. Chemical content of the copper cathode in the second anodic period

Concentration of metals, ppm	First cathodic cycle	Second cathodic cycle	Third cathodic cycle
Copper (Cu), %	99.95	99.92	99.89
Silver (Ag)	166.7	297.4	432.5
Zinc (Zn)	3.0	4.8	10.5
Lead (Pb)	86.3	98.1	134.9
Cadmium (Cd)	< 1.0	< 1.0	1.1
Tin (Sn)	28.4	27.6	39.8
Nickel (Ni)	41.6	49.9	58.2
Iron (Fe)	72.5	121.7	144.3

Table 5. Chemical composition of the electrolyte for the third anodic and both cathodic periods

Concentration, g/dm ³	First cathodic cycle				Second cathodic cycle		
	Start, 0h	24h	48h	Stop, 60h	Start, 0h	24h	48h
Cu	37.01	37.50	35.66	33.13	36.95	38.23	34.74
Zn	0	29.86	59.39	74.22	0	30.27	57.88
H ₂ SO ₄	180.1	182.0	177.2	170.6	179.6	181.3	174.5
Ag, ppm	0	0	2.0	3.3	0	0	2.8
Fe	0	0	1.31	2.02	0	0	1.50

The correction of the electrolyte required an addition of 15.0 g of copper sulfate pentahydrate and 15.0 ml of concentrated sulfuric acid per day. Larger correction of electrolyte composition was necessary due to the higher current density. Cell voltage ranged within the limits of 190 - 235 mV. The obtained copper cathode had a purity of 99.37 % by weight for the first cathodic cycle and 99.25 % for the second one. Silver content was 0.094 % and 0.135 % respectively. Concentrations of zinc were 33 ppm for the first cathodic cycle and 41 ppm for the second. When comparing the results with those of the first anodic period, a direct influence of current density is clear.

Second stage of electrolysis

Since "grade A" purity of copper was not achieved in any of the three experiments, cathode copper was used as anode for subsequent electrorefining to produce copper metal of 99.99% purity or more. Electrorefining is a very efficient process and could reduce impurities by an order of magnitude but rarely more, especially when copper has high a concentration of silver - a metal with higher allowed concentration in cathode copper [2]. Therefore, the cathode copper with the second maximum purity (obtained in the second cathodic cycle of the second anodic period) was refined. The starting electrolyte was synthetic (p.a. chemicals) and all impurities came from the anode, in this case cathode copper with Cu-CATH-2 quality. Cathodes from the second cathodic cycle were used.

No special adjustment of the process was necessary. Minor corrections of the electrolyte composition were: higher concentration of Cu^{2+} ions, 40–45 g/dm^3 and H_2SO_4 , 200–220 g/dm^3 while the concentrations of additives (thiourea, gelatin and chloride ions) were not significantly higher than is normal for the process. As silver was the main impurity, chloride ions concentration was monitored and kept in the narrow limits of 50 mg/dm^3 , as silver chloride is not favorable for the further recovery and refining of silver. Thiourea and gelatin were of initial concentration of 10 mg/dm^3 and 5 mg/dm^3 of both were added per day; current density was set to 200 A/m^2 partly because of equipment limitations but essentially near the optimal level although higher values are also possible. Results confirmed that there was not much room for increasing this parameter. Temperature was a little bit higher than in the previous electrorefining and was kept at 60 ± 2 °C. There was only one cathodic cycle.

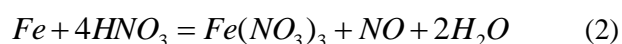
The obtained copper cathode had a purity of 99.99% with 13 ppm of silver. This purity meets

the requirements of BS EN 1978:1998 standard (LME Grade A) [2].

Hydrometallurgical refining of anode slime

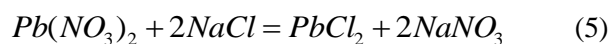
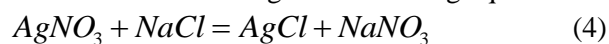
Anode slime with 57.81% silver content was refined by the technological process shown in Figure 1. Anode slime also contained lead, iron, cadmium and other contaminants. The goal of anode slime refining was to obtain silver with purity of 99.99% in powder form which can be used in sinter metallurgy and especially for electrical contact alloys.

The first phase of the anode slime processing is its dissolution in dilute nitric acid (1:1 vol.). The solution contains silver and many impurities like iron, nickel, copper, zinc and lead. During sludge dissolution, the following reactions (1) to (6) occurred:



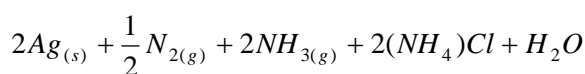
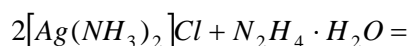
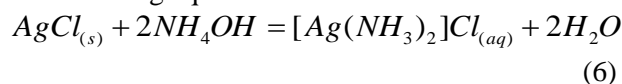
where M are metals giving two-valent nitrates: Cu, Pb, Zn and Ni.

Silver was separated from the impurities in the nitrate solution by precipitation with sodium chloride. Lead is also precipitated as a chloride with silver. Precipitation of silver and lead in the form of chlorides occurs through the following equation:



The white precipitate after the above reactions is a mixture of lead and silver chlorides. It was washed with hot water until a negative reaction for the Pb^{2+} ions (test with SO_4^{2-}).

Silver chloride was dissolved with the addition of ammonium hydroxide (12.5% mass) and reduced to elemental silver by hydrazine hydrate, according to the following equations:



The obtained silver powder was filtered, rinsed with distilled water and 96% ethanol (absolute ethanol or high purity 2-propanol) and dried at 110 °C for two hours.

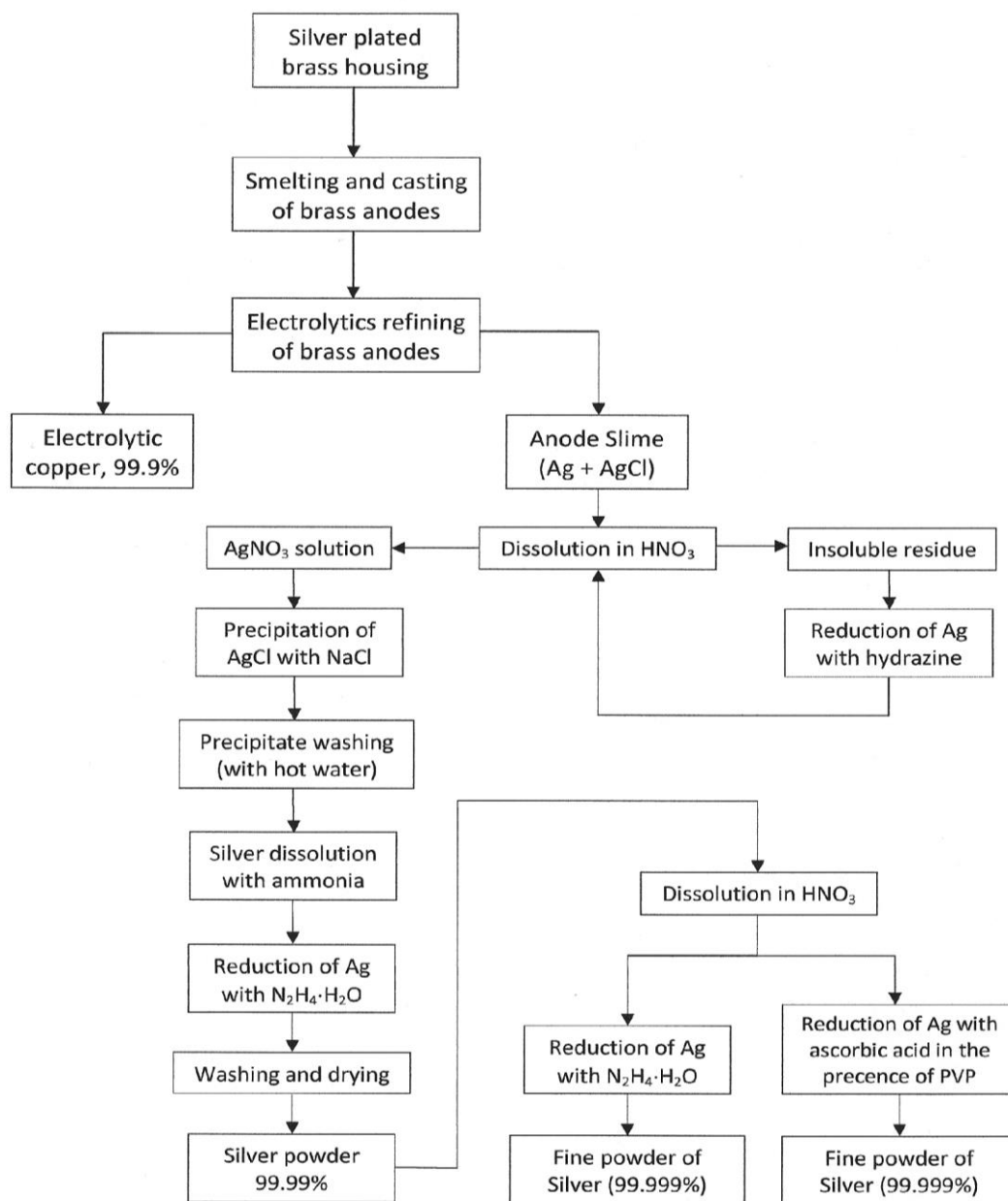


Fig. 1. Flow sheet of anode slime processing

Morphology and size of the silver particles

Classical chemical reduction could result in microsized silver crystals, especially when re-precipitated at an appropriate pH. Reducing agent (hydrazine solution) should be added slowly, drop by drop, with vigorous mixing. The obtained silver powder particles were under 5 μm , non-uniform [1], some particles reaching up to 50 μm [18]. Traditional electrochemical methods easily produce uniform but coarse particles with an average size of about 30 μm [3]. Certainly, there are a number of ECh methods for obtaining silver nano particles, as discussed above, but they have specific requirements and are not suitable for mass production.

For the synthesis of nano silver particles a variety of chemical reduction methods were developed.

Wet-chemical reduction route is preferred due to the controllable size and shape of the particles obtained [9]. Various reducing agents and templates or protecting agents are used depending on the required particle morphology [8]. The same principles with little modification of the conditions lead to micro sized Ag particles. Ascorbic acid is a commonly used reducing agent [22-24] for preparation of fine silver powder, silver microcrystals and silver nanoparticles. Ascorbic acid (AA) has been chosen as reducing agent due to the positive experience in gold and silver reduction

on its usage. Silver ions are reduced to metal silver by ascorbic acid (C₆H₈O₆) according to the following reaction [25]:



This easily controlled process yielding high purity metals was a real alternative for hydrazine for all but very dilute solutions.

The morphology of the silver microcrystals is affected by the modifiers used in the reduction process. They are mainly surfactants or polymers and are used to prevent particles from aggregation. Polyvinylpyrrolidone (PVP) is a most commonly used protecting agent not only in chemical reduction but in other methods as well [8]. Therefore, PVP was selected for this investigation. It is common for the nanoparticles production that ascorbic acid reaction with AgNO₃ is performed in dilute solutions (10⁻² mol/dm³ or less for both) but for obtaining of fine microcrystals a higher concentration is used, like: 0.2 M of AgNO₃ and AA [22] or 60 g/dm³ AgNO₃ and 40 g/dm³ AA [26]. For reduction by formaldehyde (CH₂O) the concentrations of AgNO₃ are even higher (up to 0.865 M) [9].

In this research, concentration of 0.1 M of both, silver nitrate and AA was used. The concentration was set conservatively to be between ideal for nanoparticles and microcrystal structure. Detailed influence of different parameters was not investigated since the main goal was the production on a moderate scale in a pilot plant.

Fine silver powder preparation

After silver reduction with hydrazine hydrate (HH) from nitric acid solution, fine powder with purity of 99.99 % was obtained. Reduction was performed with an excess of reduction agent. The hydrazine/silver molar ratio was 5:1. For the preparation of fine silver powder, silver was recrystallized after dissolution in nitric acid and evacuation of the nitrous oxides from the solution. Two methods for silver reduction from the solution were used: by HH and by AA. Reduction with HH was used as a control method. In both cases silver with purity of 99.999 % was obtained, but the use of HH without a protecting agent gave less uniform and larger particles.

Table 6. Statistical analysis of the particle sizes given in Figure 2

Reduction agent and type of reduction	Average particle size, μm	Corrected sample standard deviation, μm
Hydrazine, one reduction	0.800	0.391
Hydrazine, two consecutive reductions of silver	0.627	0.271
Hydrazine reduction followed by ascorbic acid reduction in presence of PVP	0.423	0.210

Starting solution was 0.1 M AgNO₃ and the solution was thermostated at 25.0±0.5°C. Reductions were performed by dropwise adding the reduction solution. Reduction solutions were of the same volume as the AgNO₃ solution and the reducing agent/silver molar ratio was 2:1 in both cases (0.1 M AA and 0.1 M HH).

Since the SEM images showed layers of particles without clear grain boundaries, the software for granulometric analysis ImageJ was not usable. An alternative method was then used, direct measurement of the grain size on SEM images with ImageJ software (which automatically takes resolution in account). A hundred of grains for each experiment was measured from several SEM images and the result for the particle size is given in Figure 2. Since little differences were found between the smallest and the largest grain, as well in size distribution, one of the figures was taken as representative: Figure 3 for single reduction with hydrazine hydrate (HH), Figure 4 for double reduction with HH and Figure 5 for the reduction of the powder shown on Figure 3 with AA in the presence of the PVP as protecting agent.

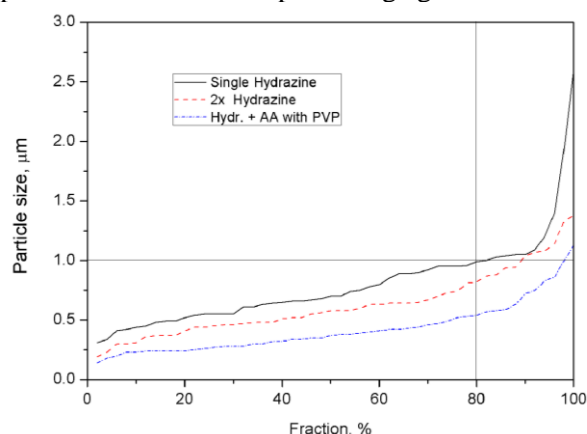


Fig. 2. Distribution of the particle size for the different reduction agents used for the reduction of Ag

The line marked with "Single hydrazine" refers to the reduction with hydrazine and the other two - to the two consecutive reductions with two different reduction agents, as pointed in the introduction.

Basic statistical data for the three sets of data are given in Table 6.

It is clear that double reduction leads to smaller size and better uniformity of the particles; if reduction by hydrazine is performed carefully, small and uniform silver grains can be obtained. The line in Figure 2 outlines that exactly 80% of the silver particles are smaller than 1.0 μm after the first reduction with hydrazine hydrate. This is due to the slow process and the great amount of the reduction agent. The obtained silver was of 99.99% purity.

Recrystallization of silver resulted in improved purity of silver and morphology of the particles. Gains in reducing the size of the particles are relatively small but the uniformity is significantly better, as shown in Figure 4.

The additive, PVP, improves the surface smoothness and compactness of the particles while the particle size is more influenced by mild reducing agents such as ascorbic acid.

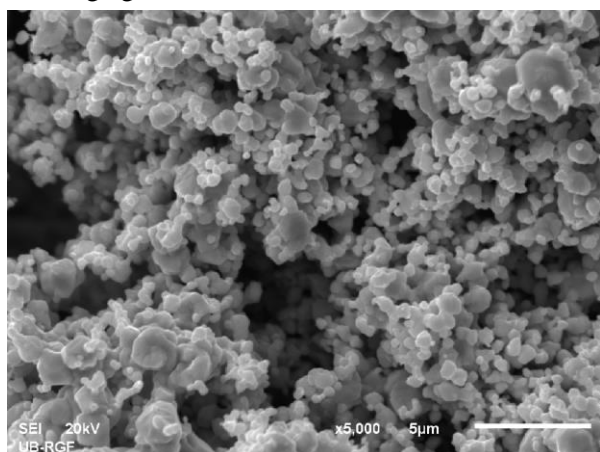


Fig. 3. SEM image of silver powder obtained by one reduction with hydrazine

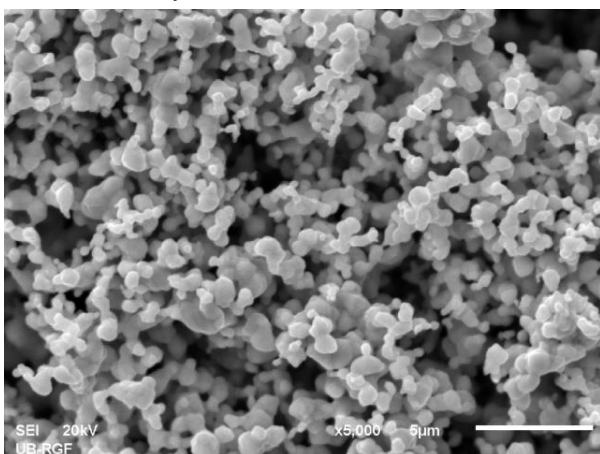


Fig. 4. SEM image of silver powder obtained by double reduction with hydrazine

First reduction with hydrazine produced very fine powder (Figure 3) which can be used in many applications including silver source for contact alloys. As Figure 2 shows, 80% of the particles are

smaller than 1.0 μm ; Figure 3 shows that there are several large and many small (even smaller than the average in Figure 4) particles, but due to aggregation larger secondary particles with fair uniformity are formed. Consecutive reduction with hydrazine is more efficient in terms of better silver purity and uniformity of the particles than in decreasing their size.

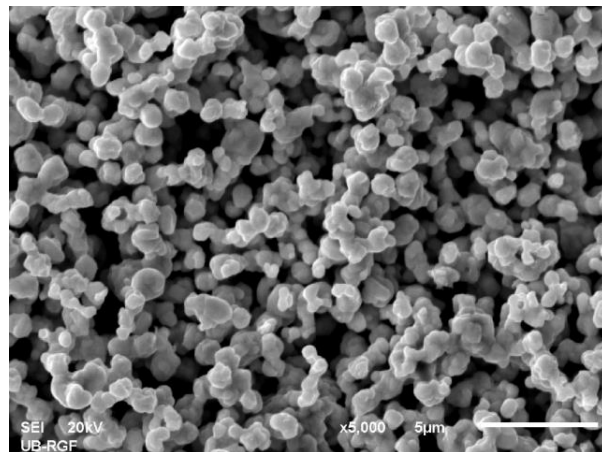


Fig. 5. SEM image of silver powder obtained by one reduction with hydrazine followed by reduction with AA in the presence of PVP

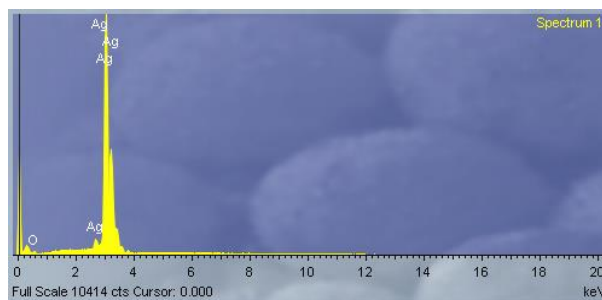


Fig. 6 EDS spectrum of the silver powder obtained by secondary reduction with AA with PVP

Reduction with AA and PVP as a protecting agent improved the morphology of the particles. They are more spherical, smaller and with much better uniformity in size ($0.423 \mu\text{m} \pm 0.210 \mu\text{m}$). The obtained powder has particles sized under micrometer. EDS analysis points to silver purity of 100.00 %; ICP-OES as a more precise method shows “5N” quality (99.999 %) with total impurities content lower than 7.3 ppm. EDS of the other two silver powders were practically the same as that in Figure 6 (100.00 % of silver) and are not shown. Purity of the silver powder, determined by ICP-OES, with one HH reduction was 99.99 % and for the double reduction with HH little higher purity was obtained than for the second reduction with AA. AAS showed only 4.8 ppm of total impurities and higher silver powder purity (99.9995 %).

CONCLUSIONS

The results presented in this paper show a possibility of recycling silver-plated brass for the production of high-purity copper and fine silver powder for electric contacts. Both investigated parameters, electrolyte composition (EC) and current density (CD), primarily need to be stable and with small variations from the optimal values (concentration of important ingredients). With increasing current density the quality of the cathode copper decreased; the optimal current density was as low as possible and technologically acceptable - about 120 A/m². The influence of electrolyte composition shows optimal Cu²⁺ and H₂SO₄ concentrations of 35–40 g/dm³ and 180±10 g/dm³, respectively. For the additional (consecutive) electrorefining the optimal parameters are slightly different: higher current density is acceptable, 200 A/m² and electrolyte composition needs adjustment, since the optimal concentrations of Cu²⁺ and sulphuric acid need to be higher, 40–45 g/dm³ and 200–220 g/dm³, respectively. The concentration of additives (thiourea, gelatin and chloride ions) should be raised.

Reduction of silver by the process shown in Figure 1 can produce micro-sized Ag powder with purity of 99.99%. Additional reduction is necessary for silver of higher purity "5N" up to 99.9995%. Reducing agents with a higher standard redox potential such as ascorbic acid and protective surface-active agents like polyvinylpyrrolidone reduce the particle size and improve its morphology. Fine submicronic Ag powder was prepared without special working conditions and the process could be useful in large-scale production.

Acknowledgment: This work has resulted from the project funded by the Ministry of Education and Science of the Republic of Serbia, No 34033 to which the authors want to thank.

REFERENCES

1. S. B. Dimitrijević, S. Dragulović, Z. Ljubomirović, V. Trujić, Z. Stanojević-Simšić, R. Marković, B. Trumić, 2nd International Symposium on Environmental and Material Flow Management "EMFM 2012" Zenica, B&H, Recycling of silver and copper from housing plated with silver, Proceedings, **07–09**, 59–65, (2012).
2. British Standard, BS EN 1978:1998, Copper and copper alloys – Copper cathodes, BSI publication, 1998.
3. A. Ivanović, S. B. Dimitrijević, S. P. Dimitrijević, B. Trumić, V. Marjanović, J. Petrović, N. Vuković,

Optoelectronics and advanced materials-Rapid communications, **6**(3–4), 1454–1464, (2012).

4. A. Ehsani, E. Yazıcı, H. Deveci, The Influence of Impurity Ions on The Electrowinning of Copper from Waste PCBs Leaching Solutions, XIII International Mineral Processing Symposium-IMPS 2012, Proceedings, pp. 443–449, (2012).
5. M. Stelter, H. Bombach, Process optimization in Copper Electrorefining, *Advanced Engineering Materials*, Wiley, **6**(7), (2004).
6. M. Moats, J. Hiskey, D. Collins, *Hydrometallurgy*, **56**, 255–268, (2000).
7. Y. Run-lan, L. Qing-ming, Q. Guan-zhou, F. Zheng, Tan Jian-xi, Y. Peng, *Trans. Nonferrous Met. Soc. China*, **18**, 1280–1284, (2008).
8. W. Zhang, X. Qiao, J. Chen, *Materials Science and Engineering: B*, **142**(1), 1–15, (2007).
9. A. Bing, C. Xiong-hui, W. Feng-shun, W. Yi-ping, *Transactions of Nonferrous Metals Society of China*, **20**, 1550–1554, (2010).
10. T. Nowicki, C. Carbonnaux, J. *De Physique IV, Colloque C7, Supl. J. De Physique III*, **3**, 509-518, (1993).
11. V. Behrens, W. Weise, Contact materials, Landolt-Bornstein, New Series VIII/2AI, p.10.1-10.27., 2003.
12. M. Filipović, Ž. Kamberović, E. Romhanji, *MJoM Metalurgija – Journal of Metallurgy*, **14**(3), 169-178, (2008).
13. M. Schwert, Removing Cadmium from Relays and Switches, TTI Inc, May 24, 2004.
14. V. Čosović, N. Talijan, D. Živković, D. Minić, Ž. Živković, *Journal Mining Metallurgy, Sect. B-Metall.* **48**(1), 131–141, (2012).
15. K. Wojtasik, W. Missol, PM helps develop cadmium-free electrical contacts, Elsevier Ltd, 2004.
16. Lungu M., Gavrilu S., Canta T., Lucaci M., Enescu E. *Journal of optoelectronics and advanced materials*, **8**, 576–581, (2006).
17. V. Čosović, A. Čosović, N. Talijan, D. Živković, D. Manasijević, D. Minić, *Journal of Alloys and Compounds*, **567**, 33–39, (2013).
18. N. Moudirab, Y. Boukennoub, N. Moulai-Mostefaac, I. Bozetineb, M. Maoudjb, N. Kameld, Z. Kameld, D. Moudird, Preparation of silver powder used for solar cell paste by reduction process, TerraGreen 13th International Conference 2013 – *Advancements in Renewable Energy and Clean Environment, Energy Procedia* **36**, 1184–1191, (2013).
19. Z. Liu, X. Qi, H. Wang, *Adv. Powder Technogy*, **23**, 250–255, (2012).
20. W. Songping, M. Shuyuan, *Materials Chemistry and Physics*, **89**, 423–427, (2005).
21. V. Trujić, S. Dragulović, S. Dimitrijević, Z. Ljubomirović, D. Simonović, Electrochemical deposition of Cu, Pt, Pd and Rh from waste sulphur acidic solution obtained in anode slime decoperisation, *Metalurgia International*, **2**, 11–15, (2012).

22. J. Yang, L. Qi, D. Zhang, J. Ma, H. Cheng, *Crystal Growth & Design*, **4**(6), 1371–1375, (2004).
23. N. Elizondo, Paulina Segovia, V. Coello, J. Arriaga, S. Belmares, A. Alcorta, F. Hernández, R. Obregón, E. Torres, F. Paraguay, *Green Chemistry - Environmentally Benign Approaches*, Chapter 8 *Green Synthesis and Characterizations of Silver and Gold Nanoparticles*, *Intech*, 139–157, (2012).
24. A. Stroia, C. Matei, B. S. Vasile, O. Oprea, C. Covaliu, I. Jitaru, *U.P.B. Sci. Bull., Series B*, **74**(3), 7–18, (2012)
25. G.G. Rao, T.V.S. Rao, *Indian Scientific Journal*, **8**(1), 137–146, (1942).
26. X. Tang, Y. Wu, Y. Yao, Z. Zhang, *Materials Science Forum*, **743–744**, 903–909, (2013).

РЕЦИКЛИРАНЕ НА ПОСРЕБРЕН МЕСИНГ ЗА ПОЛУЧАВАНЕТО ЧИСТА МЕД И СВРЪХ-ФИН СРЕБЪРЕН ПРАХ ЗА ЕЛЕКТРИЧЕСКИ КОНТАКТИ

С.П. Димитриеви¹, З. Андийч², Ж. Камберович³, С.Б. Димитриеви⁴, Н. Вукович⁵

¹ Иновационен център, Факултет по технология и металургия, Университет в Белград, Белград, Сърбия

² Химически факултет, Университет в Белград, Белград, Сърбия

³ Факултет по технология и металургия, Университет в Белград, Белград, Сърбия

⁴ Минен и металургичен институт, Бор, Сърбия

⁵ Минно-геоложки факултет, Университет в Белград, Белград, Сърбия

Постъпила на 20 ноември, 2013 г.; коригирана на 16 февруари, 2014 г.

(Резюме)

В работата се представя подобрен процес за рециклиране на облицовки от посребрен месинг. Среброто и медта се оползотворяват с чистота съответно от 99.99 % и 99.90 %. Целта е да се получат материали с висока стойност при същите процес и апаратура. Новият подход с последващо електрорафинаване дава мед с чистота от 99.99 % с качество по стандарта BS EN 1978:1998 (Cu-CATH-1) и се отнася към LME – степен А. Допълнителната преработка на среброто дава свръх-фин, микро-размерен сребърен прах с размер на частиците между 0.14 и 1.13 μm и чистота от 99.999 %. Изпитанията за електрорафинация за медта са проведени със синтетичен електролит с обем 1.50 dm^3 в електролизна клетка с обем 2 dm^3 . Изследвани са ефектите на плътността на тока и състава на електролита. Оптималните плътности на тока за първата и втората рафинация са съответно 120 A/m^2 и 200 A/m^2 . Допълнителната рафинация на среброто се извършва с химична редукция от воден разтвор. Оптимални резултати са получени при използване на аскорбинова киселина като редуктор с концентрация 0.1 mol/dm^3 и поливинилпирилодон като защитен агент с концентрация 2 % (мас.). Получените резултати може да се внедрят в производството.

Solvent-free (neat) synthesis of stable phosphorus ylides using alkyl phenylcarbamates

R. Hajinasiri*, A. Gholami Orimi

Chemistry Department, Qaemshahr Branch, Islamic Azad University, Qaemshahr, Iran

Received November 20, 2013; Revised February 12, 2014

Efficient synthesis of dimethyl 2-[(alkoxycarbonyl)anilino]-3-(1,1,1-triphenyl- λ^5 -phosphanylidene) succinate derivatives with good yields is described. The method involves three-component reaction between triphenylphosphine, dimethyl acetylenedicarboxylates and alkyl phenylcarbamate under solvent-free conditions at room temperature.

Keywords: alkyl phenylcarbamate, phosphorus ylides, solvent-free condition, triphenylphosphine.

INTRODUCTION

Phosphorus ylides are important reagents in synthetic organic chemistry, especially in the synthesis of naturally occurring products, and compounds with biological and pharmacological activity [1-6]. The prominent role of these compounds is to convert the carbonyl groups to carbon-carbon double bonds [7-8]. Many methods have been reported on the preparation and structural analysis of phosphorus ylides [9-14]. From the large number of methods available, the most important ones involve reaction of a phosphonium salt with a base [15-16]. There are many studies on the reaction between trivalent phosphorus nucleophiles and α,β -unsaturated carbonyl compounds in the presence of a proton source such as OH, CH, NH or SH [17-31]. Here we describe an efficient synthetic route for the preparation of stable phosphorus ylides **3** using triphenylphosphine, dimethyl acetylenedicarboxylates **2** and alkyl phenylcarbamate **1** under solvent-free conditions at room temperature (Scheme 1).

EXPERIMENTAL

General

Melting points were taken on a Kofler hot stage apparatus and are uncorrected. ^1H NMR and ^{13}C NMR spectra were obtained with a Bruker FT-500 spectrometer in CDCl_3 , using tetramethylsilane (TMS) as an internal standard. Mass spectra were recorded with a Finnigan Mat TSQ-70 spectrometer. Infrared (IR) spectra were acquired on a Nicolet Magna 550-FT spectrometer. Elemental analyses were carried out with a Perkin-Elmer model 240-C apparatus. The results of the elemental analyses (C,

H, N) were within $\pm 0.4\%$ of the calculated values. Dimethyl acetylenedicarboxylates and triphenyl phosphine were obtained from Fluka and were used without further purification.

General procedure for the preparation of compounds 3a-g

To a magnetically stirred mixture of an alkyl phenylcarbamate **1** (2 mmol) and dimethyl acetylenedicarboxylate **2** (2 mmol) triphenylphosphine (2 mmol) was slowly added, and the reaction mixture was stirred for 4 h at room temperature. After completion of the reaction, as indicated by TLC, the residue was purified by chromatography over silica gel (Merck 230-400 mesh) using an *n*-hexane-AcOEt mixture (2:1) as eluent, to afford the pure adducts.

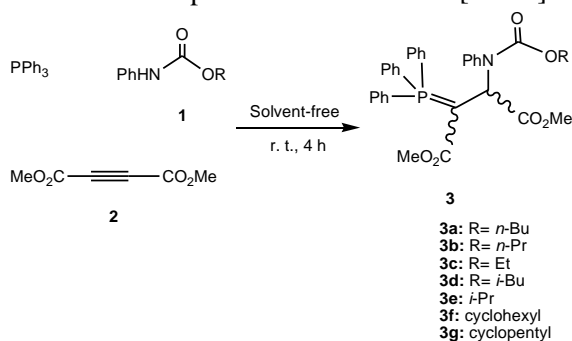
RESULTS AND DISCUSSION

The reaction between alkyl phenylcarbamate **1**, dimethyl acetylenedicarboxylates **2** and triphenylphosphine proceeded smoothly under solvent-free conditions at room temperature to produce dimethyl 2-[(alkoxycarbonyl)anilino]-3-(1,1,1-triphenyl- λ^5 -phosphanylidene)succinate derivatives **3** in 90 – 95 % yield (Scheme 1).

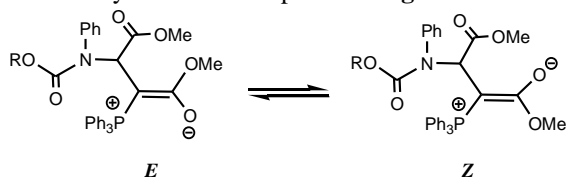
The structures of compounds **3a-g** were determined by elemental analysis, mass, IR, ^1H , ^{13}C , and ^{31}P NMR spectra. The ^1H , ^{13}C , and ^{31}P NMR spectra revealed that the ylides **3a-g** are mixtures of two isomers. According to the structure of the stable phosphorus ylides determined by X-ray [32-33], the ylide moiety of these compounds is strongly conjugated with the adjacent carbonyl group, and the rotation about the partial double bond in **E**, **Z** geometrical isomers is low on the NMR time scale at ambient temperature (Scheme 2). Conformational

* To whom all correspondence should be sent:
E-mail: rhhajinasiri@yahoo.com

isomers in phosphoranes have been previously established and reported in the literature [34-37].



Scheme 1. Synthesis of compounds **3a-g**.



Scheme 2. Geometrical isomers of **3a-g**.

The ^1H NMR spectrum of compound **3a** showed two singlets at δ 3.73 and 3.82 ppm for two methoxy groups and 3.82 for the major isomer (*Z*-isomer), along with a signal for the methine proton at δ 4.96 ppm which appeared as a doublet ($^3J_{\text{PH}} = 17.8$ Hz). This spectrum also exhibited signals at δ 0.80, 1.10-1.14, 1.28-1.32 and 3.86 ppm for the butyl moiety in the major isomer.

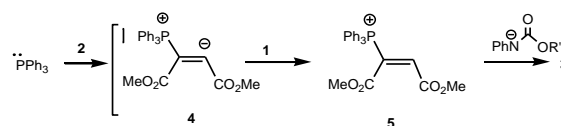
The corresponding signals for the minor isomer (*E*-isomer) were two signals at δ 3.70 and 3.80 ppm for methoxy groups and a doublet at δ 4.83 ppm ($^3J_{\text{PH}} = 16.8$ Hz) for the methine proton. Four signals appeared at δ 0.84, 1.15-1.21, 1.33-1.38 and 4.02 ppm assigned to the butyl moiety in this isomer.

The ^{13}C NMR spectrum of **3a** displayed signals agreeing with the mixture of two geometrical isomers of *Z* and *E*. Although the presence of the ^{31}P nucleus complicates both the ^1H and ^{13}C NMR spectra of **3a**, it helps in the assignment of signals by long range spin-spin couplings with ^1H and ^{13}C nuclei. The ^1H NMR and ^{13}C NMR spectral data for compounds **5b-g** are consistent with the geometrical isomers.

On the basis of the well-established chemistry of trivalent phosphorus nucleophiles, it is reasonable to assume that the phosphorus ylide **3** results from the initial addition of triphenylphosphine to the dimethyl acetylenedicarboxylates and subsequent protonation of the 1:1 adduct by the phenylcarbamate to form **3** (Scheme 3) [38-41].

In conclusion, the reaction between dimethyl acetylenedicarboxylates, phenylcarbamates, and triphenylphosphine provides a simple one-pot

synthesis of stable phosphorus ylides of potential synthetic interest.



Scheme 3. Possible mechanism for the formation of compounds **3**.

The present procedure has the following advantages: (i) the reaction is performed under solvent-free conditions, and (ii) the starting material can be used without any activation or modification. The procedure described here provides an acceptable method for the preparation of phosphoranes with variable functionalities.

Dimethyl-2-[(butoxycarbonyl)anilino]-3-(1,1,1-triphenyl- λ^5 -phosphanylidene)succinate (3a)

Yellow oil, yield, 1.13 g (95%). IR (KBr) ($\nu_{\text{max}}/\text{cm}^{-1}$): 2958 (CH), 1752 (C=O), 1692 (C=O), 1434, 1102, 996 (P-Ph). **NMR data for the major isomer (Z) (60 %):** ^1H NMR (500 MHz, CDCl_3): δ 0.80 (t, 3H, $J = 6.8$ Hz, $\text{O}(\text{CH}_2)_3\text{CH}_3$), 1.10-1.14 (m, 2H, $\text{O}(\text{CH}_2)_2\text{CH}_2\text{CH}_3$), 1.28-1.32 (m, 2H, $\text{OCH}_2\text{CH}_2\text{CH}_2\text{CH}_3$), 3.73 (s, 3H, OCH₃), 3.82 (s, 3H, OCH₃), 3.86 (t, 2H, $J = 6.9$ Hz, $\text{OCH}_2(\text{CH}_2)_2\text{CH}_3$), 4.96 (d, 1H, $J_{\text{PH}} = 17.8$ Hz, H-2), 7.23-7.42 (m, 20H, ArH) ppm. ^{13}C NMR (125 MHz, CDCl_3): δ 13.7 ($\text{O}(\text{CH}_2)_3\text{CH}_3$), 18.8 ($\text{O}(\text{CH}_2)_2\text{CH}_2\text{CH}_3$), 29.7 ($\text{OCH}_2\text{CH}_2\text{CH}_2\text{CH}_3$), 41.3 (d, $^1J_{\text{PC}} = 134.0$ Hz, C-3), 52.1 (OCH₃), 52.3 (OCH₃), 60.9 (d, $^2J_{\text{PC}} = 16.0$ Hz, C-2), 64.9 ($\text{OCH}_2(\text{CH}_2)_2\text{CH}_3$), 126.4 (d, $^1J_{\text{PC}} = 98.0$ Hz, C-*ipso*), 128.6, 128.7, 128.9 (d, $^3J_{\text{PC}} = 8.0$ Hz, C-*meta*), 132.0, 132.2 (d, $^4J_{\text{PC}} = 2.0$ Hz, C-*para*), 133.5 (d, $^2J_{\text{PC}} = 10.0$ Hz, C-*ortho*), 139.1, 155.4 (C=O), 168.5 (d, $^2J_{\text{PC}} = 13.0$ Hz, C=O), 173.5 (d, $^3J_{\text{PC}} = 10.0$ Hz, C=O) ppm. ^{31}P NMR (202 MHz, CDCl_3): δ 24.76 (PPh₃) ppm. **NMR data for the minor isomer (E) (40 %):** ^1H NMR (500 MHz, CDCl_3): δ 0.84 (t, 3H, $J = 7.1$ Hz, $\text{O}(\text{CH}_2)_3\text{CH}_3$), 1.15-1.21 (m, 2H, $\text{O}(\text{CH}_2)_2\text{CH}_2\text{CH}_3$), 1.33-1.38 (m, 2H, $\text{OCH}_2\text{CH}_2\text{CH}_2\text{CH}_3$), 3.70 (s, 3H, OCH₃), 3.80 (s, 3H, OCH₃), 4.02 (t, 2H, $J = 6.8$ Hz, $\text{OCH}_2(\text{CH}_2)_2\text{CH}_3$), 4.83 (d, 1H, $^3J_{\text{PH}} = 16.8$ Hz, H-2), 7.49-7.66 (m, 20H, ArH) ppm. ^{13}C NMR (125 MHz, CDCl_3): δ 13.8 ($\text{O}(\text{CH}_2)_3\text{CH}_3$), 18.9 (m, 2H, $\text{O}(\text{CH}_2)_2\text{CH}_2\text{CH}_3$), 30.2 ($\text{OCH}_2\text{CH}_2\text{CH}_2\text{CH}_3$), 42.2 (d, $^1J_{\text{PC}} = 137.2$ Hz, C-3), 48.8 (OCH₃), 49.5 (OCH₃), 61.8 (d, $^2J_{\text{PC}} = 17.0$ Hz, C-2), 64.8 ($\text{OCH}_2(\text{CH}_2)_2\text{CH}_3$), 126.7 (d, $^1J_{\text{PC}} = 92.0$ Hz, C-*ipso*), 128.5, 128.6, 129.1 (d, $^3J_{\text{PC}} = 8.0$ Hz, C-*meta*), 132.0, 132.1 (d, $^4J_{\text{PC}} = 2.0$ Hz, C-*para*), 133.7 (d, $^2J_{\text{PC}} = 10.0$ Hz, C-*ortho*), 139.4, 154.0 (C=O), 173.5 (d, $^2J_{\text{PC}} = 13.0$ Hz, C=O), 174.1 (d, $^3J_{\text{PC}} = 9.0$ Hz, C=O) ppm. ^{31}P NMR (202 MHz, CDCl_3): δ 29.11 (PPh₃) ppm. MS (EI, 70 eV) m/z (%): 597 (M^+ , 2),

538 (12), 405 (38), 335 (15), 262 (42), 192 (51). Anal. Calcd for $C_{35}H_{36}NO_6P$: C 70.34; H 6.07; N 2.34; found: C 70.36; H 6.05; N 2.37.

Dimethyl-2-[(propoxycarbonyl)anilino]-3-(1,1,1-triphenyl- λ^5 -phosphanylidene)succinate (3b)

Yellow oil, yield: 1.08 g (93%). IR (KBr) (ν_{max}/cm^{-1}): 2961 (CH), 1754 (C=O), 1695 (C=O), 1432, 1105, 995 (P-Ph). **NMR data for the major isomer (Z) (63 %):** 1H NMR (500 MHz, $CDCl_3$): δ 1.04 (t, 3H, $J = 6.9$ Hz, $(OCH_2)_2CH_3$), 1.67 (s, 2H, $J = 7.0$ Hz, $(OCH_2CH_2CH_3)$), 3.68 (s, 3H, OCH_3), 3.77 (s, 3H, OCH_3), 3.80 (t, $J = 6.8$ Hz, $(OCH_2CH_2CH_3)$), 4.80 (d, $^3J_{PH} = 18.0$ Hz, H-2), 7.17-7.38 (m, 20H, ArH) ppm. ^{13}C NMR (125 MHz, $CDCl_3$): δ 11.4 ($(OCH_2)_2CH_3$), 23.0 ($OCH_2CH_2CH_3$), 41.5 (d, $^1J_{PC} = 134.5$ Hz, C-3), 52.1 (OCH_3), 52.3 (OCH_3), 61.0 (d, $^2J_{PC} = 17.2$ Hz, C-2), 64.7 ($OCH_2CH_2CH_3$), 126.5 (d, $^1J_{PC} = 99.0$ Hz, C-*ipso*), 128.5, 128.6, 128.7 (d, $^3J_{PC} = 8.0$ Hz, C-*meta*), 132.0, 132.2 (d, $^4J_{PC} = 2.0$ Hz, C-*para*), 133.5 (d, $^2J_{PC} = 9.5$ Hz, C-*ortho*), 140.0, 155.3 (C=O), 168.4 (d, $^2J_{PC} = 13.2$ Hz, C=O), 173.3 (d, $^3J_{PC} = 10.0$ Hz, C=O) ppm. ^{31}P NMR (202 MHz, $CDCl_3$): δ 24.73 (PPh₃) ppm. **NMR data for the minor isomer (E) (37 %):** 1H NMR (500 MHz, $CDCl_3$): δ 1.00 (t, 3H, $J = 7.0$ Hz, $(OCH_2)_2CH_3$), 1.63 (s, 2H, $J = 7.1$ Hz, $(OCH_2CH_2CH_3)$), 3.70 (s, 3H, OCH_3), 3.74 (s, 3H, OCH_3), 4.10 (t, 2H, $J = 6.8$ Hz, $(OCH_2CH_2CH_3)$), 4.88 (d, 1H, $^3J_{PH} = 17.0$ Hz, H-2), 7.43-7.61 (m, 20H, ArH) ppm. ^{13}C NMR (125 MHz, $CDCl_3$): δ 11.0 ($(OCH_2)_2CH_3$), 23.2 ($OCH_2CH_2CH_3$), 42.1 (d, $^1J_{PC} = 136.0$ Hz, C-3), 48.7 (OCH_3), 49.5 (OCH_3), 61.6 (d, $^2J_{PC} = 16.8$ Hz, C-2), 64.6 ($OCH_2CH_2CH_3$), 126.8 (d, $^1J_{PC} = 95.0$ Hz, C-*ipso*), 128.3, 128.5, 128.6 (d, $^3J_{PC} = 8.0$ Hz, C-*meta*), 131.8, 132.1 (d, $^4J_{PC} = 2.0$ Hz, C-*para*), 133.7 (d, $^2J_{PC} = 9.8$ Hz, C-*ortho*), 139.6, 154.2 (C=O), 173.1 (d, $^2J_{PC} = 13.0$ Hz, C=O), 174.0 (d, $^3J_{PC} = 9.0$ Hz, C=O) ppm. ^{31}P NMR (202 MHz, $CDCl_3$): δ 29.10 (PPh₃) ppm. MS (EI, 70 eV) m/z (%): 583 (M^+ , 3), 524 (15), 405 (38), 321 (17), 262 (41), 178 (54). Anal. Calcd for $C_{34}H_{34}NO_6P$: C 69.97; H 5.87; N 2.40; found: C 69.96; H 5.88; N 2.37.

Dimethyl-2-[(ethoxycarbonyl)anilino]-3-(1,1,1-triphenyl- λ^5 -phosphanylidene)succinate (3c)

Yellow oil, yield: 1.08 g (95%). IR (KBr) (ν_{max}/cm^{-1}): 2955 (CH), 1756 (C=O), 1697 (C=O), 1431, 1108, 997 (P-Ph). **NMR data for the major isomer (Z) (64 %):** 1H NMR (500 MHz, $CDCl_3$): δ 1.04 (t, 3H, $J = 6.9$ Hz, OCH_2CH_3), 3.64 (s, 3H, OCH_3), 3.72 (s, 3H, OCH_3), 3.97 (q, 2H, $J = 6.9$ Hz, OCH_2CH_3), 4.87 (d, 1H, $^3J_{PH} = 17.8$ Hz, H-2), 6.73-7.30 (m, 20H, ArH) ppm. (125 MHz, $CDCl_3$): δ 14.6 (OCH_2CH_3), 41.4 (d, $^1J_{PC} = 134.0$ Hz, C-3), 52.2 (OCH_3), 52.4 (OCH_3), 60.1 (OCH_2CH_3), 61.8

(d, $^2J_{PC} = 16.2$ Hz, C-2), 126.3 (d, $^1J_{PC} = 92.0$ Hz, C-*ipso*), 128.6, 128.7, 128.8 (d, $^3J_{PC} = 8.0$ Hz, C-*meta*), 132.0, 132.1 (d, $^4J_{PC} = 2.0$ Hz, C-*para*), 133.7 (d, $^2J_{PC} = 9.6$ Hz, C-*ortho*), 139.4, 154.1 (C=O), 168.6 (d, $^2J_{PC} = 13.0$ Hz, C=O), 173.6 (d, $^3J_{PC} = 14.0$ Hz, C=O) ppm. ^{31}P NMR (202 MHz, $CDCl_3$): δ 24.68 (PPh₃) ppm. **NMR data for the minor isomer (E) (36 %):** 1H NMR: (500 MHz, $CDCl_3$): δ 1.15 (t, 3H, $J = 7.0$ Hz, OCH_2CH_3), 3.62 (s, 3H, OCH_3), 3.73 (s, 3H, OCH_3), 3.85 (t, 2H, $J = 6.9$ Hz, OCH_2CH_3), 4.80 (d, 1H, $^3J_{PH} = 16.7$ Hz, H-2), 7.35-7.56 (m, 20H, ArH) ppm. ^{13}C NMR (125 MHz, $CDCl_3$): δ 14.5 (OCH_2CH_3), 42.0 (d, $^1J_{PC} = 136.8$ Hz, C-3), 48.9 (OCH_3), 49.5 (OCH_3), 60.9 (OCH_2CH_3), 61.0 (d, $^2J_{PC} = 16.0$ Hz, C-2), 126.6 (d, $^1J_{PC} = 92.0$ Hz, C-*ipso*), 128.5, 128.6, 128.9 (d, $^3J_{PC} = 8.0$ Hz, C-*meta*), 131.9, 132.0 (d, $^4J_{PC} = 2.0$ Hz, C-*para*), 133.5 (d, $^2J_{PC} = 9.0$ Hz, C-*ortho*), 139.3, 155.3 (C=O), 170.6 (d, $^2J_{PC} = 13.0$ Hz, C=O), 173.8 (d, $^3J_{PC} = 13.0$ Hz, C=O) ppm. ^{31}P NMR (202 MHz, $CDCl_3$): δ 29.13 (PPh₃) ppm. MS (EI, 70 eV) m/z (%): 569 (M^+ , 4), 496 (10), 405 (36), 307 (17), 262 (43), 164 (48). Anal. Calcd for $C_{34}H_{34}NO_6P$: C 69.59; H 5.66; N 2.46; found: C 69.60; H 5.63; N 2.42.

Dimethyl-2-[(isobutoxycarbonyl)anilino]-3-(1,1,1-triphenyl- λ^5 -phosphanylidene)succinate (3d)

Yellow oil, yield: 1.07 g (90%). IR (KBr) (ν_{max}/cm^{-1}): 2958 (CH), 1752 (C=O), 1692 (C=O), 1434, 1102, 996 (P-Ph). **NMR data for the major isomer (Z) (63 %):** 1H NMR (500 MHz, $CDCl_3$): δ 1.21 (d, 6H, $J = 6.9$ Hz, $OCH_2CH(CH_3)_2$), 1.83 (heptet, 1H, $J = 7.0$ Hz, $OCH_2CH(CH_3)_2$), 3.67 (s, 3H, OCH_3), 3.70 (s, 3H, OCH_3), 3.79 (d, 2H, $J = 6.8$ Hz, $OCH_2CH(CH_3)_2$), 4.96 (d, 1H, $^3J_{PH} = 18.0$ Hz, H-2), 6.80-7.43 (m, 20H, ArH) ppm. ^{13}C NMR (125 MHz, $CDCl_3$): δ 18.9 ($OCH_2CH(CH_3)_2$), 19.1 ($OCH_2CH(CH_3)_2$), 29.6 ($OCH_2CH(CH_3)_2$), 41.3 (d, $^1J_{PC} = 134.1$ Hz, C-3), 52.1 (OCH_3), 52.3 (OCH_3), 60.9 (d, $^2J_{PC} = 14.6$ Hz, C-2), 71.1 ($OCH_2CH(CH_3)_2$), 126.7 (d, $^1J_{PC} = 92.0$ Hz, C-*ipso*), 128.6, 128.7, 128.8 (d, $^3J_{PC} = 7.8$ Hz, C-*meta*), 132.0, 132.2 (d, $^4J_{PC} = 2.0$ Hz, C-*para*), 133.7 (d, $^2J_{PC} = 9.7$ Hz, C-*ortho*), 138.9, 154.1 (C=O), 168.5 (d, $^2J_{PC} = 13.0$ Hz, C=O), 170.1 (d, $^3J_{PC} = 17.0$ Hz, C=O) ppm. ^{31}P NMR (202 MHz, $CDCl_3$): δ 24.73 (PPh₃) ppm. **NMR data for the minor isomer (E) (37 %):** 1H NMR (500 MHz, $CDCl_3$): δ 1.23 (d, 6H, $J = 6.9$ Hz, $OCH_2CH(CH_3)_2$), 1.60 (heptet, 1H, $J = 7.0$ Hz, $OCH_2CH(CH_3)_2$), 3.66 (s, 3H, OCH_3), 3.73 (s, 3H, OCH_3), 3.78 (d, 2H, $J = 6.8$ Hz, $OCH_2CH(CH_3)_2$), 4.80 (d, 1H, $^3J_{PH} = 16.8$ Hz, C-2), 7.45-7.63 (m, 20H, ArH) ppm. ^{13}C NMR (125 MHz, $CDCl_3$): δ 18.8 ($OCH_2CH(CH_3)_2$), 19.0 ($OCH_2CH(CH_3)_2$), 30.8 ($OCH_2CH(CH_3)_2$), 42.2 (d,

$^1J_{PC} = 136.5$ Hz, C-3), 48.8 (OCH₃), 49.5 (OCH₃), 61.8 (d, $^2J_{PC} = 13.0$ Hz, C-2), 71.2 (OCH₂CH(CH₃)₂), 126.4 (d, $^1J_{PC} = 90.0$ Hz, C-*ipso*), 128.5, 128.6, 128.7 (d, $^3J_{PC} = 8.0$ Hz, C-*meta*), 131.9, 132.1 (d, $^4J_{PC} = 2.0$ Hz, C-*para*), 133.5 (d, $^2J_{PC} = 9.8$ Hz, C-*ortho*), 139.1, 154.3 (C=O), 173.5 (d, $^2J_{PC} = 13.0$ Hz, C=O), 174.1 (d, $^3J_{PC} = 16.0$ Hz, C=O) ppm. ^{31}P NMR (202 MHz, CDCl₃): δ 29.09 (PPh₃) ppm. MS (EI, 70 eV) m/z (%): 597 (M⁺, 3), 538 (13), 405 (43), 335 (21), 262 (43), 192 (55). Anal. Calcd for C₃₅H₃₆NO₆P: C 70.34; H 6.07; N 2.34; found: C 70.36; H 6.05; N 2.37.

Dimethyl-2-[(isopropoxycarbonyl)anilino]-3-(1,1,1-triphenyl- λ^5 -phosphanylidene)succinate (3e)
Yellow oil, yield: 1.10 g (95%). IR (KBr) (ν_{max}/cm^{-1}): 2960 (CH), 1753 (C=O), 1695 (C=O), 1435, 1103, 994 (P-Ph). **NMR data for the major isomer (Z) (65 %):** 1H NMR (500 MHz, CDCl₃): δ 1.22 (d, 6H, $J = 6.9$ Hz, OCH(CH₃)₂), 3.72 (s, 3H, OCH₃), 3.76 (s, 3H, OCH₃), 3.84 (heptet, $J = 6.8$ Hz, OCH(CH₃)₂), 4.82 (d, $^3J_{PH} = 17.9$ Hz, H-2), 7.13-7.35 (m, 20H, ArH) ppm. ^{13}C NMR (125 MHz, CDCl₃): δ 21.8 (OCH(CH₃)₂), 41.5 (d, $^1J_{PC} = 134.0$ Hz, C-3), 52.2 (OCH₃), 52.4 (OCH₃), 61.2 (d, $^2J_{PC} = 17.2$ Hz, C-2), 64.6 (OCH(CH₃)₂), 126.5 (d, $^1J_{PC} = 99.0$ Hz, C-*ipso*), 128.4, 128.6, 128.7 (d, $^3J_{PC} = 8.0$ Hz, C-*meta*), 132.0, 132.2 (d, $^4J_{PC} = 2.0$ Hz, C-*para*), 133.5 (d, $^2J_{PC} = 9.5$ Hz, C-*ortho*), 140.0, 155.3 (C=O), 168.4 (d, $^2J_{PC} = 13.2$ Hz, C=O), 173.3 (d, $^3J_{PC} = 10.0$ Hz, C=O) ppm. ^{31}P NMR: δ 24.75 (PPh₃) ppm. **NMR data for the minor isomer (E) (35 %):** 1H NMR (500 MHz, CDCl₃): δ 1.19 (d, 6H, $J = 6.8$ Hz, OCH(CH₃)₂), 3.71 (s, 3H, OCH₃), 3.74 (s, 3H, OCH₃), 3.81 (heptet, 1H, $J = 6.8$ Hz, OCH(CH₃)₂), 4.78 (d, 1H, $^3J_{PH} = 16.9$ Hz, H-2), 7.37-7.56 (m, 20H, ArH) ppm. ^{13}C NMR (125 MHz, CDCl₃): δ 21.6 (OCH(CH₃)₂), 42.2 (d, $^1J_{PC} = 136.2$ Hz, C-3), 48.8 (OCH₃), 49.4 (OCH₃), 61.8 (d, $^2J_{PC} = 17.2$ Hz, C-2), 64.8 (OCH(CH₃)₂), 126.8 (d, $^1J_{PC} = 95.0$ Hz, C-*ipso*), 128.3, 128.5, 128.6 (d, $^3J_{PC} = 8.0$ Hz, C-*meta*), 131.9, 132.1 (d, $^4J_{PC} = 2.0$ Hz, C-*para*), 133.7 (d, $^2J_{PC} = 9.8$ Hz, C-*ortho*), 139.6, 154.2 (C=O), 173.0 (d, $^2J_{PC} = 13.0$ Hz, C=O), 174.1 (d, $^3J_{PC} = 9.0$ Hz, C=O) ppm. ^{31}P NMR (202 MHz, CDCl₃): δ 29.11 (PPh₃) ppm. MS (EI, 70 eV) m/z (%): 583 (M⁺, 3), 524(13), 405 (39), 321 (20), 262 (43), 178 (58). Anal. Calcd for C₃₄H₃₄NO₆P: C 69.97; H 5.87; N 2.40; found: C 69.95; H 5.85; N 2.41.

Dimethyl-2-[(cyclohexyloxycarbonyl)anilino]-3-(1,1,1-triphenyl- λ^5 -phosphanylidene)succinate (3f)
Yellow oil, yield, 1.14 g (92%). IR (KBr) (ν_{max}/cm^{-1}): 2958 (CH), 1752 (C=O), 1691 (C=O), 1434, 1105, 996 (P-Ph). **NMR data for the major isomer (Z) (64 %):** 1H NMR (500 MHz, CDCl₃): δ 1.60-

1.64 (m, 2H, CH₂), 1.71-1.75 (m, 4H, 2CH₂), 1.90-1.96 (m, 4H, 2CH₂), 3.74 (s, 3H, OCH₃), 3.85 (s, 3H, OCH₃), 4.21 (m, 1H, OCH), 4.93 (d, 1H, $^3J_{PH} = 18.0$ Hz, H-2), 7.21-7.40 (m, 20H, ArH) ppm. ^{13}C NMR (125 MHz, CDCl₃): δ 23.4 (2CH₂), 25.4 (CH₂), 32.0 (2CH₂), 41.2 (d, $^1J_{PC} = 134.5$ Hz, C-3), 52.2 (OCH₃), 52.4 (OCH₃), 60.9 (d, $^2J_{PC} = 16.5$, C-2), 64.8 (OCH), 126.4 (d, $^1J_{PC} = 98.0$ Hz, C-*ipso*), 128.6, 128.7, 128.9 (d, $^3J_{PC} = 8.0$ Hz, C-*meta*), 132.0, 132.2 (d, $^4J_{PC} = 2.0$ Hz, C-*para*), 133.5 (d, $^2J_{PC} = 10.0$ Hz, C-*ortho*), 139.1, 155.4 (C=O), 168.5 (d, $^2J_{PC} = 13.0$, C=O), 173.5 (d, $^3J_{PC} = 10.0$, C=O) ppm. ^{31}P NMR (202 MHz, CDCl₃): δ 24.77 (PPh₃) ppm. **NMR data for the minor isomer (E) (36 %):** 1H NMR (500 MHz, CDCl₃): δ 1.56-1.59 (m, 2H, CH₂), 1.69-1.73 (m, 4H, 2CH₂), 1.82-1.90 (m, 4H, 2CH₂), 3.72 (s, 3H, OCH₃), 3.81 (s, 3H, OCH₃), 4.23 (m, 1H, OCH), 4.90 (d, 1H, $^3J_{PH} = 17.0$ Hz, H-2), 7.42-7.53 (m, 20H, ArH) ppm. ^{13}C NMR (125 MHz, CDCl₃): δ 23.2 (2CH₂), 25.5 (CH₂), 32.2 (2CH₂), 42.1 (d, $^1J_{PC} = 136.1$ Hz, C-3), 48.7 (OCH₃), 49.6 (OCH₃), 61.3 (d, $^2J_{PC} = 16.0$ Hz, C-2), 65.2 (OCH), 126.7 (d, $^1J_{PC} = 92.0$ Hz, C-*ipso*), 128.5, 128.6, 129.1 (d, $^3J_{PC} = 8.0$ Hz, C-*meta*), 132.0, 132.1 (d, $^4J_{PC} = 2.0$ Hz, C-*para*), 133.7 (d, $^2J_{PC} = 10.0$ Hz, C-*ortho*), 139.4, 154.0 (C=O), 173.5 (d, $^2J_{PC} = 13.0$ Hz, C=O), 174.1 (d, $^3J_{PC} = 9.0$ Hz, C=O) ppm. ^{31}P NMR (202 MHz, CDCl₃): δ 29.12 (PPh₃) ppm. MS (EI, 70 eV) m/z (%): 623 (4) [M]⁺, 496 (11), 405 (41), 361 (18), 262 (35), 218 (47). Anal. Calcd for C₃₇H₃₈NO₆P: C 71.25; H 6.14; N 2.25; found: C 71.20; H 6.12; N 2.27.

Dimethyl-2-[(cyclopentylloxycarbonyl)anilino]-3-(1,1,1-triphenyl- λ^5 -phosphanylidene)succinate (3g)
Yellow oil, yield, 1.14 g (92%). IR (KBr) (ν_{max}/cm^{-1}): 2953 (CH), 1754 (C=O), 1695 (C=O), 1432, 1102, 998 (P-Ph). **NMR data for the major isomer (Z) (64 %):** 1H NMR (500 MHz, CDCl₃): δ 1.46-1.56 (m, 4H, 2CH₂), 1.63-1.76 (m, 4H, 2CH₂), 3.76 (s, 3H, OCH₃), 3.84 (s, 3H, OCH₃), 4.19 (m, 1H, OCH), 4.81 (d, 1H, $^3J_{PH} = 18.0$ Hz, H-2), 6.91-7.42 (m, 20H, ArH) ppm. ^{13}C NMR (125 MHz, CDCl₃): δ 24.4 (2CH₂), 33.6 (2CH₂), 41.1 (d, $^1J_{PC} = 134.0$ Hz, C-3), 52.1 (OCH₃), 52.3 (OCH₃), 61.1 (d, $^2J_{PC} = 17.0$ Hz, C-2), 64.9 (OCH), 126.7 (d, $^1J_{PC} = 92.0$ Hz, C-*ipso*), 128.6, 128.7, 128.8 (d, $^3J_{PC} = 7.8$ Hz, C-*meta*), 132.0, 132.2 (d, $^4J_{PC} = 2.0$ Hz, C-*para*), 133.7 (d, $^2J_{PC} = 9.7$ Hz, C-*ortho*), 138.9, 154.1 (C=O), 168.5 (d, $^2J_{PC} = 13.0$ Hz, C=O), 170.1 (d, $^3J_{PC} = 17.0$, C=O) ppm. ^{31}P NMR (202 MHz, CDCl₃): δ 24.76 (PPh₃) ppm. **NMR data for the minor isomer (E) (36 %):** 1H NMR (500 MHz, CDCl₃): δ 1.57-1.68 (m, 4H, 2CH₂), 1.77-1.89 (m, 4H, 2CH₂), 3.74 (s, 3H, OCH₃), 3.86 (s, 3H, OCH₃), 4.17 (m, 1H, 2CH₂), 4.78 (d, 1H, $^3J_{PH} = 17.0$ Hz, H-

2), 7.42-7.58 (m, 20H, ArH) ppm. ^{13}C NMR (125 MHz, CDCl_3): δ 24.5 (2CH_2), 33.8 (2CH_2), 42.0 (d, $^1J_{\text{PC}} = 136.2$ Hz, C-3), 48.8 (OCH_3), 49.6 (OCH_3), 61.9 (d, $^2J_{\text{PC}} = 17.0$ Hz, C-2), 64.5 (OCH), 126.4 (d, $^1J_{\text{PC}} = 90.0$ Hz, C-*ipso*), 128.5, 128.6, 128.7 (d, $^3J_{\text{PC}} = 8.0$ Hz, C-*meta*), 131.9, 132.1 (d, $^4J_{\text{PC}} = 2.0$ Hz, C-*para*), 133.5 (d, $^2J_{\text{PC}} = 9.8$ Hz, C-*ortho*), 139.1, 154.3 (C=O), 173.5 (d, $^2J_{\text{PC}} = 13.0$ Hz, C=O), 174.1 (d, $^3J_{\text{PC}} = 16.0$ Hz, C=O) ppm. ^{31}P NMR (202 MHz, CDCl_3): δ 29.20 (PPh_3) ppm. MS (EI, 70 eV) m/z (%): 609 (M^+ , 2), 96 (14), 405 (33), 347 (18), 262 (37), 204 (45). Anal. Calcd for $\text{C}_{36}\text{H}_{36}\text{NO}_6\text{P}$: C 70.92; H 5.95; N 2.30; found: C 70.90; H 5.097; N 2.27.

REFERENCES

1. D. E. C. Corbridge, *Phosphorus: An Outline of The Chemistry, Biochemistry and Uses*, Elsevier: Amsterdam, 1995.
2. P. J. Murphy, *Organophosphorus Reagents*, Oxford University Press: Oxford, 2004.
3. R. Engel, J. I. Cohen, *Synthesis of Carbon-Phosphorus Bonds*, CRC Press: Boca Raton, FL, 2004.
4. A. W. Johnson, *Ylide Chemistry*, Academic Press: London, 1966.
5. G. Wittig, *Science*, **210**, 500 (1980).
6. O. I. Kolodiazny, *Phosphorus Ylides: Chemistry and Application in Organic Synthesis*, Wiley-VCH: Weinheim, 1999.
7. B. E. Maryanoff, A. B. Reitz, *Chem. Rev.* **89**, 863 (1989).
8. M. G. Russell, S. J. Warren, *Chem. Soc. PerkinTrans 1*, 505 (2000).
9. M. R. Islami, M. A. Amrollahi, M. Iranmanesh, *Arkivoc*, **x**, 35 (2009).
10. A. Ramazani, F. Sadri, *Phosphorus Sulfur Silicon Relat. Elem.*, **184**, 3126 (2009); A. Ramazani, A. R. Kazemizadeh, *Curr. Org. Chem.*, **15**, 3986 (2011); A. Ramazani, A. R. Kazemizadeh, E. Ahmadi, N. Noshiranzadeh, A. Souldozi, *Curr. Org. Chem.*, **12**, 59 (2008).
11. A. Ramazani, N. Noshiranzadeh, A. Ghamkhari, K. Šlepokura, T. Lis, *Helv. Chim. Acta*, **91**, 2252 (2008); N. Noshiranzadeh, A. Ramazani, K. Šlepokura, T. Lis, *Synth. Commun.*, **38**, 1560 (2008).
12. A. Ramazani, A. Souldozi, *Phosphorus Sulfur Silicon Relat. Elem.*, **178**, 1325 (2003); A. Ramazani, A. Souldozi, *Phosphorus Sulfur Silicon Relat. Elem.*, **178**, 1329 (2003); A. Ramazani, A. Souldozi, *Phosphorus Sulfur Silicon Relat. Elem.*, **179**, 529 (2004).
13. A. R. Kazemizadeh, F. Marandi, *Phosphorus, Sulfur Silicon Relat. Elem.*, **180**, 1541 (2005); A. Ramazani, A. Souldozi, *Phosphorus, Sulfur Silicon Relat. Elem.* **178**, 2663 (2003); A. Ramazani, Souldozi, N. Noshiranzadeh, *Phosphorus, Sulfur Silicon Relat. Elem.*, **181**, 587 (2006); A. Ramazani, G. R. Fattahi-Nujokamberi, *Indian J. Chem.*, **41b**, 407 (2002).
14. A. Ramazani, A. Souldozi, *Phosphorus Sulfur Silicon Relat. Elem.*, **181**, 2373 (2006); A. Ramazani, A. Souldozi, *Phosphorus Ylides. Phosphorus Sulfur Silicon Relat. Elem.*, **184**, 536 (2009); A. Ramazani, A. Momeni-Movahhed, F. Gouranlou, *Phosphorus Sulfur Silicon Relat. Elem.*, **177**, 903 (2002).
15. M. R. Islami, F. Mollazehi, A. Badiei, H. Sheibani, *Arkivoc* **xv**, 25 (2005).
16. R. Greenwald, M. Chaykovsky, E. J. Corey, *J. Org. Chem.*, **28**, 1128 (1963).
17. L. Fitjer, U. Quabeck, *Synth. Commun.*, **15**, 855 (1985).
18. H. R. Hudson, *Nucleophilic Reactions of Phosphines*, ch .11 in *The Chemistry of Organophosphorus Compounds, Primary, Secondary, and Tertiary Phosphates and Heterocyclic Organophosphorus III Compounds*, Hartely, F. R., Ed., Wiley: New York, 1. 1990.
19. B. E. Maryanoff, A. B. Reitz, *Chem. Rev.*, **89**, 863 (1989).
20. K. C. Nicolaou, M. W. Harter, J. L. Gunzner, A. Nadin, *Liebigs Ann.*, **7**, 1283 (1997).
21. Y. Shen, *Acc. Chem. Res.*, **31**, 584 (1998).
22. L. D. Quin, *A Guide to Organophosphorus Chemistry*, Wiley-Interscience: New York, 2000.
23. I. Yavari, A. A. Esmaili, *J. Chem. Res.*, 714 (1998).
24. M. R. Islami, F. Mollazehi, A. Badiei, H. Sheibani, *Arkivoc* **xv**, 25 (2005).
25. I. Yavari, M. R. Islami, *J. Chem. Res.* 166 (1998).
26. I. Yavari, A. Esmaili, S. Asghari, H. R. Bijanzadeh, *J. Chem. Res.* 368 (1999).
27. M. Kalantari, M. R. Islami, Z. Hassani, K. Saidi, *Arkivoc*, **x**, 55 (2006).
28. Z. Hassani, M. R. Islami, H. Sheibani, M. Kalantari, K. Saidi, *Arkivoc*, **i**, 89 (2006).
29. M. T. Maghsoodlou, N. Hazeri, S. M. Habibi Khorassani, L. Saghatforoush, M. K. Rofouei, M. Rezaie, *Arkivoc*, **xiii**, 117 (2006).
30. M. T. Maghsoodlou, S. M. Habibi Khorassani, N. Hazeri, M. Nassiri, *Phosphorus, Sulfur, and Silicon*, **181**, 1363 (2006).
31. N. Hazeri, M. T. Maghsoodlou, S. M. Habibi Khorassani, M. Nassiri, Z. Afarini, *J. Chem. Res.* 97 (2008).
32. M. T. Maghsoodlou, S. M. Habibi Khorassani, M. Nassiri, S. R. Adhamdoust, J. Salehzadeh, *J. Chem. Res.* 79 (2008).
33. M. T. Maghsoodlou, S. M. Habibi-Khorassani, R. Heydari, A. Hassankhani, G. Marandi, M. Nassiri, E. Mosaddeg, *Mol. Divers.*, **11**, 87 (2007).
34. G. Marandi, N. Akbarzadeh Torbati, R. Heydari, N. Hazeri, S. M. Habibi Khorassani, M. T. Maghsoodlou, B. Adrom, B. W. Skelton, M. Makha, *Phosphorus, Sulfur, and Silicon*, **187**, 1450, (2012).
35. H. J. Bestmann, G. Joachim, T. Lengyel, J. F. Oth, R. Merenyi, H. Weitkamp, *Tetrahedron Lett.*, **7**, 3355 (1966).
36. H. J. Bestmann, J. P. Snyder, *J. Am. Chem. Soc.*, **89**, 3963 (1967).

37. D. L. Hooper, S. Garagan, *J. Org. Chem.*, **59**, 1126 (1994).
38. M. R. Islami, I. Yavari, A. M. Tikdari, L. Ebrahimi, S. Razee, H. R. Bijanzadeh, *Russ. Chem. Bull.*, **51**, 2244 (2002).
39. M. Shahraki, S. M. Habibi-Khorassani, A. Ebrahimi, M. Maghsoodlou, *Y. Struct. Chem.* **24**, 623 (2013).
40. S. M. Habibi-Khorassani, M. T. Maghsoodlou, A. Ebrahimi, S. Sameh-Salari, F. Vasheghani-Farahani, M. A. Kazemian, *Concepts in Magnetic Resonance Part A*, **42**, 107 (2013).
41. M.A. Kazemian, S. M. Habibi-Khorassani, A. Ebrahimi, M. T. Maghsoodlou, P. M. Jahani, M. Ghahramaninezhad, *J. Mol. Model.* **18**, 5075 (2012).
42. S. M. Habibi-Khorassani, M. T. Maghsoodlou, A. Ebrahimi, M. Mohammadi, M. Shahraki, E. Aghdaei, *J. Mol. Model.* **18**, 1328 (2012).

СИНТЕЗ НА СТАБИЛНИ ФОСФОРНИ ИЛИДИ С АЛКИЛ-ФЕНИЛКАРБАМАТИ БЕЗ РАЗТВОРИТЕЛ

Р. Хаджинасири*, А. Голами Орими

Департамент по химия, Клон Каемшахр, Ислямски университет "Азад", Иран

Постъпила на 20 ноември, 2013 г.; коригирана на 12 февруари, 2014 г.

(Резюме)

Описана е ефикасна синтеза на производни на диметил 2-[(алкоксикарбонил)анилино-3-(1,1,1-трифенил- λ^5 -фосфанилиден) сукцинат с добър добив. Методът включва три-компонентна реакция между трифенилфосфин, диметил-ацетилен-дикарбоксилати и алкил-фенилкарбамати без разтворител и при стайна температура.

GC-MS profiling, antioxidant, and antimicrobial studies of various parts of *Carissa grandiflora*

M. Abbas¹, N. Rasool^{1,*}, M. Riaz², M. Zubair¹, M. Abbas³, Noor-Ul-Haq¹, N. Hayat¹

¹Department of Chemistry, Government College University Faisalabad 38000, Pakistan

²Department of Chemistry, University of Sargodha Women Campus, Faisalabad, Pakistan

³Department of Chemistry and Biochemistry, University of Agriculture, Faisalabad 38040, Pakistan

Received, November 5, 2013; Revised January 2, 2014

The present research work was carried out to evaluate the bioactivity of methanol extracts of leaves, roots and stems of *Carissa grandiflora* and their fractions in solvents of different polarity (*n*-hexane, chloroform, ethyl acetate and *n*-butanol). The extracts and their fractions contained appreciable levels of total phenolic contents (TPC) ranging from 31.17 to 349.43 Gallic Acid Equivalent (GAE mg/100 g) of dry matter (leaves), 38.85 to 269.81 GAE, mg/100 g of dry matter (roots) and 40.18 to 241.11 GAE, mg/100 g of dry matter (stems). Total flavonoid contents were found to be from 59.14 to 284.99, 32.27 to 199.74 and 21.37 to 158.56 Catechin Equivalent (CE mg/100 g) of dry matter for leaves, roots and stems, respectively. IC₅₀ values in case of DPPH radical scavenging activity of leaves, roots and stems were from 20.89 to 578.9, 12.28 to 325.31 and 6.15 to 941.4 µg/mL respectively. The percentage inhibition of peroxidation in a linoleic acid system was from 11.34 to 46.7, 15.56 to 41.31 and 18.14 to 50.46 for leaves, roots and stems, respectively. The methanol extracts of all three parts exhibited the maximum reducing activity in comparison to other fractions. Maximum antibacterial activity was shown by the ethyl acetate fraction of stems against *S. aureus*, its *n*-butanol fraction against *E. coli* and its methanol extract against *S. epidermidis*. *C. albicans* revealed the highest resistance against the ethyl acetate fraction of roots. GCMS analysis of the *n*-hexane fraction of roots revealed that this part of the plant is enriched with the maximum number of bioactive compounds.

Keywords: *Carissa grandiflora*, linoleic acid, phenolics, flavonoids, DPPH, gallic acid

INTRODUCTION

Plants containing a wide variety of ingredients are being used in traditional medicines. These medicines are used to treat infectious, as well as chronic diseases. The medicinal plants contain some secondary metabolites which produce a characteristic physiological action on the human body [1]. The most significant compounds present in plants are phenolic compounds like tannins, flavonoids and alkaloids [2].

Carissa grandiflora is a shrub of high ornamental value. Its large, lush green, thick, shiny leaves are very showy and attractive and the white star-shaped flowers are fragrant. It can be grown in containers and makes an ideal container specimen. It can also be used as a large dense security hedge or barrier due to its large thorns which are practically impenetrable. Its oval to elliptical shaped radish fruits are edible and are very delicious in taste. The cranberry-flavoured fruits are used in sauces, cakes, desserts, jams, jellies, yogurt and ice cream. The plant is also used to make graceful and elegant bonsai specimen [3]. Plants belonging to this family are of immense medicinal

importance. Several authors have analyzed the chemical and biological properties of some of these plants [4-6] and more research work should be dedicated to the unexplored plants.

In the present research work we have made an attempt to analyze the biological (antioxidant and antimicrobial) activity of methanol extracts of leaves, roots and stems of *Carissa grandiflora*.

EXPERIMENTAL

Collection of plant

The selected plant *Carissa grandiflora* was collected from the Madina Nursery Tehsil Pattoki District Kasur and was identified by Dr. R.B. Tareen from the Department of Botany, University of Balochistan, Quetta, Pakistan. A voucher specimen (CG-NR-05) was deposited in the herbarium/collection of the Department of Botany, University of Balochistan, Quetta, Pakistan.

Preparation of methanol extracts

Plant extracts from leaves, roots and stems were prepared by the soaking method. According to this method, portions of finely ground leaves (488 g), roots (156 g) and stems (466 g) were placed in separate flasks and measured volumes of methanol

* To whom all correspondence should be sent:
E-mail: nasirhej@yahoo.co.uk

were added to each flask. Then the flasks were kept at room temperature for 4 to 5 days and were shaken at regular intervals. Vacuum rotary evaporator (Eyela, Tokyo Rikakikai Co., Ltd Japan) was used to evaporate the solvent under vacuum at 45°C. In this way, viscous extracts were obtained which were dried and stored at -4°C. Sufficient amounts of methanol extracts (18.02 g leaves, 8.06 g roots and 16.67 g stems) were obtained by repeating the extraction process thrice. The methanol extracts of leaves, roots and stems were dissolved in distilled water separately and then fractionation was carried out using solvents of different polarity. The solvents used for fractionation of the methanol extracts were *n*-hexane, chloroform, ethyl acetate and *n*-butanol [7].

Phytochemical analysis

Phytochemical screening of the methanol extracts of leaves, roots and stems was performed according to a previously described method [8,9]

Total Phenolic Contents (TPC)

TPC of leaves, roots and stems extracts of the plant and their fractions were determined using the Follin-Ciocalteu reagent method [10,11].

Total Flavonoid Contents (TFC)

TFC of extracts/fractions of leaves, roots and stems were determined spectrophotometrically following a previously reported method [12].

DPPH radical scavenging assay

The 2,2-diphenyl-1-picrylhydrazyl radical (DPPH) assay was carried out spectrophotometrically as described in [13]. Stock solution was prepared by dissolving 100 mg of each extract or fraction in 100 mL of methanol. From the stock solution concentrations in the range 0.2-1 mg/mL were made. To each concentration, 5 mL of freshly prepared DPPH of concentration 0.025 g/L (0.0050 g DPPH in 200 mL CH₃OH) was added. After 10 min, the absorbance of the resulting solution and the blank (5 mL DPPH + 1 mL methanol) was measured at 515 nm. Three replicates were recorded for each sample. The inhibitory effect of DPPH was calculated according to the following equation:

$$\text{Inhibition (\%)} = 100 \times (A_{\text{blank}} - A_{\text{sample}} / A_{\text{blank}})$$

where A_{blank} is the absorbance of the control (containing all reagents except the test samples), and A_{sample} is the absorbance of the test samples. IC₅₀ value (mg/mL), defined as the concentration at which the scavenging activity was 50% and caused

50% neutralization of DPPH radicals, was measured from the plot of concentration *versus* percentage inhibition.

Determination of reducing power

The reducing power of methanol extracts and fractions of leaves, roots and stems was evaluated spectrophotometrically [11,14]. Stock solution was prepared by dissolving 100 mg of each extract or fraction in 100 mL of methanol. From the stock solution different concentrations in the range of 0.2-1 mg/mL were made. To 1 mL of each concentration, 2 mL phosphate buffer and 2 mL potassium ferricyanide (1%) were added. The mixture was incubated at 50°C for 20 min. Then 2 mL of 10% trichloroacetic acid were added and the mixture was centrifuged at 3000 rpm for 10 min at 5°C. The upper layer of the solution was removed. Finally, 5 mL deionised water and 1 mL FeCl₃ were added. The absorbance of the reaction mixture was measured at 700 nm using a spectrophotometer. Three replicates were measured for each sample.

Antioxidant activity determination in a linoleic acid system

The antioxidant potential of the extracts/fractions of leaves, roots and stems was estimated following an already reported method [15,14].

Antimicrobial assay of plant extracts (leaves, roots and stems) and their fractions

Disc Diffusion Method

Antimicrobial activity of the methanol extracts and different fractions was examined by the disc diffusion method [16,17]. The discs (5 mm diameter) were impregnated with 10 mg/mL extracts/fractions (50 µL/disc) and were placed on inoculated agar under aseptic conditions. Discs injected with 100 µL of the respective solvent served as negative controls; Amikacin (50 µL/disc) and Terbinaline (50 µL/disc) were employed as positive references for bacteria and fungi, respectively. The petri dishes were incubated at 37 ± 0.1°C for 20-24 hours and at 28±0.3°C for 40-48 hours for bacteria and fungi, respectively. The inhibition zones formed around each disc were measured at the end of the specified period with a zone reader. Zone inhibition diameter (ZID) values were directly related with the antimicrobial activity of the extracts/fractions. Determination of the inhibitory properties was carried out in triplicate.

Resazurin Microtitre-Plate Assay of minimum inhibitory concentration MIC

The minimum inhibitory concentration (MIC) of

the plant extracts/fractions was determined by the resazurin microtitre-plate assay reported in [7,18].

Sample Preparation for GC-MS analysis

An amount of 100 g of the dried and ground plant was extracted with *n*-hexane in a Soxhlet apparatus for the GC-MS analysis [1].

Gas Chromatography/Mass Spectrometry Analysis

The GC-MS analysis of the *n*-hexane fractions of leaves, roots and stems were carried out using a GC 6850 Network gas chromatographic system equipped with 7683 B series auto injector and 5973 inert mass selective detector (Agilent Technologies USA). The compounds were separated on an HP-5 MS capillary column using 5% phenyl polysiloxane as stationary phase, column length 30.0 m, internal diameter 0.25 mm and film thickness 0.25 µm. The injector temperature was 300°C. 1.0 µL of the sample was injected in split mode with a split ratio of 30:1. Helium with a flow rate of 1.5 mL/min was used as a carrier gas. The temperature program was: initial temperature 150°C, hold for 1 min at this temperature; ramp at a rate of 10°C/min up to 290°C, hold for 5 min at this temperature. The temperature of the MSD transfer line was 300°C. Mass spectra were recorded in electron ionization (EI) mode with ionization energy of 70 eV; the mass range scanned was 3–500 *m/z*. The temperature of the ion source was 230°C and that of the MS quadrupole 150°C. The identification of the components was based on comparison of their mass spectra with those of the NIST mass spectral library with some modification [19,20].

RESULTS AND DISCUSSION

Phytochemical Analysis

The phytochemical constituents of the methanol extracts were analyzed and the results are given in Table 1. Alkaloids and terpenoids were found to be present in all parts of the plant. There were no flavonoids in the leaves while steroids and tannins were found in leaves and roots, respectively.

Table 1: Phytochemical analysis of methanol extracts

Plant part	Alkaloid	Steroid	Flavonoid	Tannin	Terpenoid
	s	s	s	s	s
Leaves	+	+	-	-	+
Roots	+	-	+	+	+
Stems	+	-	+	-	+

Percent yields of methanol extracts and different fractions of leaves, roots and stems of *Carissa grandiflora*

The percent yields of the plant methanol extracts and organic fractions are shown in Table 2.

Table 2: Percent yield of methanol extracts and various organic fractions of leaves, roots and stems

Extracts/Fractions	Yield (g/100g)		
	Leaves	Roots	Stems
Methanol	13.69	10.06	12.58
<i>n</i> -Butanol	3.87	3.62	4.54
Ethyl acetate	3.54	4.34	2.47
Chloroform	4.63	2.49	2.36
<i>n</i> -Hexane	1.82	1.2	2.48

The highest amounts were extracted with methanol from all parts of the plant followed by the chloroform fraction of the leaves (4.6 g) and *n*-butanol fraction of the stems (5.45 g). *n*-Hexane was found to be the least effective solvent. The amount of substances that can be extracted from a plant depends upon the nature and amount of solvent and the mixing procedure used. Sample to sample variation in extracted material is possible [11].

We determined the total phenolic contents (TPC) and the total flavonoid contents (TFC) in the methanol extracts and different fractions of *C. grandiflora* roots, leaves and stems. Total phenolic contents were expressed as gallic acid equivalents (GAE), mg/100 g of dry matter. The amounts of TPC extracted from leaves, roots and stems were in the ranges of 31.17 to 349.4, 38.85 to 269.81 and 40.18 to 241.11 GAE (mg/100 g of dry matter), respectively (Table 3). Total flavonoid contents were expressed as mg catechin equivalents (CE) per 100 g of dry matter. The quantities of TFC obtained from leaves, roots and stems were in the range of 59.14 to 284.99, 32.27 to 199.74 and 21.37 to 158.56 CE (mg/100 g of dry matter), respectively.

Effect of polarity on the extraction of TPC and TFC has been illustrated in numerous reports. Soil and growing conditions have drastic effects on the amount of TPC which can be extracted from the plant. The capability of a given solvent to dissolve endogenous substances determines the amounts of TPC and TFC extracted from the plant. The highest quantity of phenolic compounds was extracted by methanol while *n*-hexane, owing to its non-polar nature, was found to be the least effective solvent for extraction of phenolics.

DPPH scavenging assay

We investigated the free radical scavenging activity of methanol extracts and fractions of *Carissa grandiflora* leaves, roots and stems. Free radical scavenging activities were measured by DPPH assay. The methanol extracts and various fractions of the plant showed excellent radical quenching activities having IC₅₀ values of 20.89 to 578.9, 12.28 to 325.31 and 6.25 to 941.4 mg/mL for

Table 3: Phytochemical and antioxidant studies of methanol extracts and different fractions of leaves, roots and stems of *Carissa grandiflora*

Assay	Extract and fractions	Part		
		Stems	Roots	Leaves
TPC (GAE, mg/100g)	Methanol	241.11 ± 1.35 ^c	269.81 ± 1.64 ^b	349.43 ± 2.23 ^a
	<i>n</i> -Butanol	163.63 ± 1.36 ^f	184.24 ± 1.18 ^e	211.29 ± 0.48 ^d
	Ethyl acetate	105.58 ± 0.40 ⁱ	135.69 ± 0.71 ^g	117.23 ± 0.58 ^h
	Chloroform	59.36 ± 0.39 ^k	103.05 ± 0.53 ⁱ	69.87 ± 0.49 ^j
	<i>n</i> -Hexane	40.18 ± 0.27 ^l	38.85 ± 0.39 ^l	31.17 ± 0.20 ^m
TFC (CE, mg/100g)	Methanol	158.56 ± 1.14 ^c	199.74 ± 1.20 ^b	284.99 ± 1.69 ^a
	<i>n</i> -Butanol	83.43 ± 0.68 ^h	132.21 ± 0.76 ^d	156.9 ± 0.87 ^c
	Ethylacetate	75.78 ± 0.29 ⁱ	91.54 ± 0.52 ^g	114.44 ± 0.76 ^e
	Chloroform	62.27 ± 0.29 ^j	52 ± 0.59 ^k	101.79 ± 0.69 ^f
	<i>n</i> -Hexane	21.37 ± 0.15 ^m	32.27 ± 0.25 ^l	59.14 ± 0.33 ^j
IC ₅₀	Methanol	6.15 ± 0.02 ^m	12.28 ± 0.35 ^l	20.89 ± 0.40 ⁱ
	<i>n</i> -Butanol	18.27 ± 0.01 ^j	14.68 ± 0.04 ^k	72.94 ± 0.16 ^e
	Ethyl acetate	26.09 ± 0.13 ^h	29.74 ± 0.34 ^g	76.8 ± 0.11 ^d
	Chloroform	28.49 ± 0.25 ^g	41.45 ± 0.14 ^f	78.43 ± 0.32 ^d
	<i>n</i> -Hexane	941.4 ± 0.80 ^a	325.31 ± 0.64 ^c	578.9 ± 0.90 ^b
% Inhibition of linoleic acid peroxidation	Methanol	50.46 ± 0.27 ^a	41.31 ± 0.49 ^c	46.47 ± 0.27 ^b
	<i>n</i> -Butanol	39.96 ± 0.38 ^c	33.2 ± 0.18 ^e	37.89 ± 0.33 ^d
	Ethyl acetate	33.1 ± 0.52 ^e	31.34 ± 0.68 ^f	31.84 ± 0.25 ^e
	Chloroform	28.57 ± 0.26 ^g	23.82 ± 0.12 ⁱ	26.21 ± 0.17 ^h
	<i>n</i> -Hexane	18.14 ± 0.24 ^j	15.56 ± 0.48 ^k	11.34 ± 0.09 ^l

The values are the average of triplicate samples (n=3) ± S.D., ($p < 0.05$)

The superscript alphabets showed significant differences.

leaves, roots and stems, respectively. Methanol extracts of leaves, roots and stems exhibited the lowest IC₅₀ values (20.89, 12.28 and 6.25 µg/mL) followed by *n*-butanol fractions (72.94, 14.68 and 18.27 µg/mL), ethyl acetate (76.8, 29.7 and 20.09 µg/mL), chloroform (78.43, 41.45 and 28.49 µg/mL) and *n*-hexane (578.9, 325.31 and 941.4 µg/mL), respectively. IC₅₀ values indicated that the methanol extracts display the highest free radical scavenging activity while *n*-hexane fractions display the lowest one.

Percent inhibition of linoleic acid peroxidation

The percent inhibition of linoleic acid peroxidation by crude extracts/fractions of leaves, roots and stems is shown in Table 3. The values are in the range of 18.14% to 50.46% for stems, 15.56% to 41.31% for roots and 11.34% to 46.47% for leaves. The methanol extract and the *n*-butanol fraction of leaves exhibited excellent inhibition of linoleic acid oxidation, i.e. 46.47 and 37.89, respectively. Other fractions also showed reasonable inhibition. The methanol extracts of all three parts exhibited the highest inhibition of linoleic acid oxidation followed by *n*-butanol, ethyl acetate, chloroform and *n*-hexane fractions. On comparing the three plant parts, the methanol extract and fractions obtained from stems showed better inhibition than those of the other two parts.

Reducing power

Antioxidant activity can be determined by evaluating the reducing power of methanol extracts of leaves, roots and stems of plant and different fractions. The reducing potential of leaves, roots and stems was measured at a concentration of 0.2-1.0 mg/mL. The results showed that the absorbance increases with concentration. The assay of the reducing power of all fractions of the three parts showed a linear increase of absorbance with concentration. Maximum absorbance values (1.73, 1.82 and 1.82) were shown by the methanol extracts of leaves, roots and stems compared with other fractions.

The values for the methanol extracts of leaves, roots and stems range from 0.83 to 1.73, 0.94 to 1.82 and 0.97 to 1.82, respectively. *n*-Hexane fractions of all three parts exhibited the lowest reducing activity.

Antimicrobial Activity

Antimicrobial activity of methanol extracts and different fractions of leaves, roots and stems against a panel of pathogenic microorganisms was assessed by the disc diffusion method. The results are given in Table 4. The extracts and fractions of stems, roots and leaves were tested against three bacterial and one fungal strain. The different fractions and methanol extracts of all parts of the plant revealed a broad spectrum of activities by forming clear zones

Table 4: Antimicrobial activity of methanol extracts and different fractions of leaves, roots and stems of *Carissa grandiflora*

Strain	Extract and fractions	Plant part		
		Stems	Roots	Leaves
<i>S. aureus</i>	Methanol	7.81 ± 0.01 ^g	7.73 ± 0.02 ^{gh}	6.82 ± 0.02 ^l
	<i>n</i> -Butanol	7.52 ± 0.02 ⁱ	8.65 ± 0.02 ^c	8.27 ± 0.01 ^e
	Ethyl acetate	8.73 ± 0.02 ^c	7.69 ± 0.02 ^h	7.15 ± 0.02 ^j
	Chloroform	8.53 ± 0.01 ^d	6.56 ± 0.04 ^m	6.23 ± 0.01 ⁿ
	<i>n</i> -Hexane	7.17 ± 0.02 ^j	6.63 ± 0.02 ^m	6.95 ± 0.02 ^k
	Amikacin	13.55 ± 0.05 ^a	9.41 ± 0.01 ^b	8.41 ± 0.01 ^f
<i>E. coli</i>	Methanol	7.49 ± 0.04 ^{jk}	7.33 ± 0.01 ^{kl}	8.42 ± 0.02 ^e
	<i>n</i> -Butanol	9.03 ± 0.03 ^d	7.28 ± 0.01 ^l	7.65 ± 0.01 ⁱ
	Ethyl acetate	7.93 ± 0.01 ^h	7.57 ± 0.01 ^{ij}	8.10 ± 0.04 ^{fg}
	Chloroform	8.41 ± 0.01 ^e	8.25 ± 0.06 ^f	8.05 ± 0.03 ^{gh}
	<i>n</i> -Hexane	7.45 ± 0.04 ^{jk}	7.20 ± 0.04 ^l	7.51 ± 0.01 ^{ij}
	Amikacin	10.72 ± 0.02 ^c	11.03 ± 0.04 ^b	12.34 ± 0.04 ^a
<i>S. epidermidis</i>	Methanol	10.82 ± 0.04 ^d	10.27 ± 0.01 ^e	9.68 ± 0.05 ^h
	<i>n</i> -Butanol	9.52 ± 0.01 ⁱ	9.93 ± 0.03 ^g	9.22 ± 0.04 ^j
	Ethyl acetate	9.56 ± 0.02 ^{hi}	8.82 ± 0.02 ^k	7.64 ± 0.02 ⁿ
	Chloroform	8.65 ± 0.02 ^l	10.09 ± 0.04 ^f	8.19 ± 0.03 ^m
	<i>n</i> -Hexane	9.3 ± 0.01 ^j	9.88 ± 0.02 ^g	8.53 ± 0.02 ^l
	Amikacin	11.15 ± 0.02 ^c	11.69 ± 0.01 ^b	12.47 ± 0.05 ^a
<i>C. albicans</i>	Methanol	10.67 ± 0.03 ⁱ	13.72 ± 0.02 ^d	10.9 ± 0.04 ^{hi}
	<i>n</i> -Butanol	10.78 ± 0.01 ^{hi}	12.57 ± 0.05 ^f	13.2 ± 0.12 ^e
	Ethyl acetate	15.17 ± 0.06 ^a	8.16 ± 0.04 ^m	11.12 ± 0.05 ^{gh}
	Chloroform	10.17 ± 0.02 ^j	10.12 ± 0.02 ^j	9.53 ± 0.02 ^k
	<i>n</i> -Hexane	8.64 ± 0.03 ^l	10.16 ± 0.02 ^j	11.53 ± 0.23 ^g
	Terbinaline	15.73 ± 0.06 ^b	14.44 ± 0.06 ^c	14.51 ± 0.14 ^c

The values are the average of triplicate samples (n=3) ± S.D., (p < 0.05)

The superscript alphabets showed significant differences.

The methanol extract and fractions were analyzed at 5 mg/ml and Terbinaline at 1 mg/ml

of inhibition against strains. Results indicated that the *n*-butanol fraction of roots and the ethyl acetate fraction of stems showed good activity against *S. aureus* with inhibition zones of 8.65 and 8.73 mm, respectively. Maximum activity against *E. coli* was displayed by the methanol extract of leaves and the *n*-butanol fraction of stems with inhibition zones of 8.42 and 9.03 mm, respectively. Methanol extracts of leaves, roots and stems were found to be more effective against *S. epidermidis*, as compared to other fractions with inhibition zones (10.82, 10.27, 9.68 mm, respectively). Highest potential against *C. albicans* was shown by the ethyl acetate fraction of stems with inhibition zone of 15.73 mm. The antimicrobial activity for stems was found to be in the range of 7.17 (*n*-hexane) to 15.73 mm (ethyl acetate). For roots, the range was from 6.56 (*n*-hexane) to 13.72 mm (*n*-butanol) and for leaves from 6.23 (chloroform) to 13.2 mm (*n*-butanol). All extracts and fractions showed considerable activity against these strains. Methanol extract of roots and ethyl acetate fraction of stems showed strong activity against *C. albicans* with ZID values of 13.73 and 15.83 mm, respectively. The *n*-hexane, chloroform and *n*-butanol fractions of leaves

exhibited moderate values of ZID with a maximum value for *n*-butanol (13.2 mm against *C. albicans*). The *n*-hexane fraction of roots showed poor activity with a maximum ZID value of 10.16 mm against *C. albicans*. Chloroform fraction of leaves showed minimum activity (6.23 mm) against *S. aureus*. All extracts and fractions were found particularly effective against *C. albicans* with inhibition zones ranging from 8.16 to 15.73 mm. The ethyl acetate fraction of stems exhibited specifically strong activity against *C. albicans* with ZID of 15.73 mm.

Minimum Inhibitory Concentration

Minimum inhibitory concentration (MIC) is the minimum concentration that could inhibit the growth of pathogens. The MIC activity of methanol extracts and different fractions of leaves, roots and stems of *C. grandiflora* against one fungal and three bacterial strains was evaluated using a modified resazurin microtitre-plate assay. MIC values were found to be inverse to the antimicrobial activity values. The MIC values are presented in mg/mL (Table 5).

Methanol extracts and fractions of stems, roots and leaves displayed MIC values in the range of

Table 5: Minimum inhibitory concentration (MIC), mg/ml, of methanol extracts and different fractions of leaves, roots and stems of *Carissa grandiflora*

Strains	Extract and fractions	Plant part								
		Stems			Roots			Leaves		
<i>S. aureus</i>	Methanol	1.41	±	0.03 ^g	0.89	±	0.01 ⁱ	1.35	±	0.02 ^{gh}
	<i>n</i> -Butanol	1.55	±	0.03 ^d	0.82	±	0.01 ^{de}	0.67	±	0.02 ^{de}
	Ethyl acetate	1.31	±	0.03 ^{ab}	1.23	±	0.01 ^b	0.88	±	0.01 ⁱ
	Chloroform	1.35	±	0.02 ^a	1.7	0±	0.01 ^c	1.46	±	0.05 ^{de}
	<i>n</i> -Hexane	1.72	±	0.03 ^f	1.43	±	0.01 ^{ef}	1.24	±	0.02 ^{de}
	Amikacin	0.95	±	0.02 ^{hi}	0.51	±	0.01 ^j	0.43	±	0.02 ^j
<i>E. coli</i>	Methanol	1.83	±	0.02 ^c	0.74	±	0.02 ^{klm}	0.39	±	0.01 ^{jkl}
	<i>n</i> -Butanol	0.73	±	0.01 ^{fg}	0.85	±	0.02 ^{ef}	0.89	±	0.01 ^e
	Ethyl acetate	1.52	±	0.02 ^{hij}	0.63	±	0.01 ^d	0.65	±	0.01 ^{gh}
	Chloroform	1.24	±	0.07 ^b	0.56	±	0.02 ^e	0.76	±	0.02 ^{ijk}
	<i>n</i> -Hexane	5.52	±	0.07 ^a	0.91	±	0.01 ^e	0.93	±	0.01 ^{hi}
	Amikacin	0.27	±	0.01 ^{lm}	0.23	±	0.01 ^m	0.31	±	0.01 ^{klm}
<i>S. epidermidis</i>	Methanol	1.88	±	0.06 ^d	0.24	±	0.01 ^j	0.56	±	0.02 ⁱ
	<i>n</i> -Butanol	2.41	±	0.01 ^{de}	0.92	±	0.02 ^{gh}	0.78	±	0.01 ^h
	Ethyl acetate	2.19	±	0.01 ^c	0.97	±	0.01 ⁱ	0.95	±	0.02 ^f
	Chloroform	2.69	±	0.01 ^b	0.90	±	0.01 ^{fg}	0.87	±	0.02 ⁱ
	<i>n</i> -Hexane	2.61	±	0.02 ^a	0.94	±	0.01 ^f	0.82	±	0.02 ^{gh}
	Amikacin	1.75	±	0.01 ^e	0.23	±	0.01 ^j	0.27	±	0.01 ^j
<i>C. albicans</i>	Methanol	0.84	±	0.01 ^g	0.23	±	0.02 ⁱ	1.02	±	0.01 ^g
	<i>n</i> -Butanol	0.74	±	0.02 ^f	0.81	±	0.01 ^{de}	0.76	±	0.01 ^{ef}
	Ethyl acetate	0.55	±	0.02 ^{cd}	0.97	±	0.01 ^g	0.98	±	0.01 ^a
	Chloroform	0.86	±	0.02 ^d	0.91	±	0.01 ^{bc}	1.24	±	0.01 ^g
	<i>n</i> -Hexane	0.95	±	0.01 ^{ef}	0.87	±	0.01 ^{ab}	0.81	±	0.01 ^{de}
	Terbinaline	0.39	±	0.01 ^h	0.21	±	0.01 ⁱ	0.25	±	0.01 ⁱ

The values are the average of triplicate samples (n=3) ± S.D., (p <0.05)

The superscript alphabets showed significant differences.

0.52 to 5.52, 0.23 to 1.83 and 0.39 to 1.46 mg/mL respectively. *n*-Hexane fraction of stems exhibited the maximum MIC value (5.52 mg/mL). Methanol extracts of stems, roots and leaves showed maximum antimicrobial activity and the range of their MIC values was found to be from 0.23 to 1.88 mg/mL which means that it might show antimicrobial activity at this low concentration. MIC ranges of the *n*-hexane fraction were 0.91–1.43 mg/mL for roots, 0.53 –1.44 mg/mL for leaves and 0.75-5.52 mg/mL for stems. The MIC values revealed that the greater the antimicrobial activity, the lower would be the MIC value.

The minimum inhibitory concentration of the methanol extracts of roots showed the lowest value of MIC against *S. epidermidis* (0.24 mg/mL) and the highest value against *S. aureus* (0.89 mg/mL). The *n*-butanol fraction of stems showed the lowest value of MIC against *E. coli* (0.73 mg/mL) and the highest value against *S. epidermidis* (1.83 mg/mL). The *n*-hexane fraction of stems showed the highest value of MIC against *E. coli* (5.52 mg /mL) while the chloroform fraction of leaves showed the lowest value of MIC against *E. coli* (0.45 mg/mL). The ethyl acetate fraction of stems showed the maximum value of MIC against *S. epidermidis* (2.19 mg/mL).

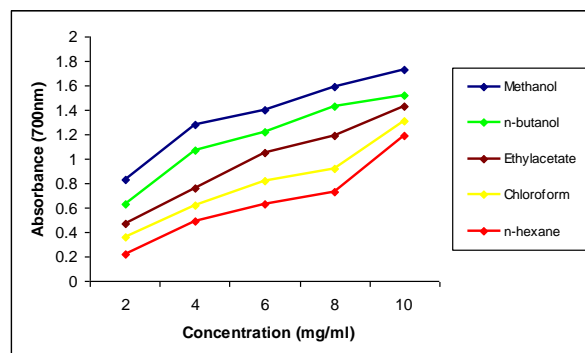


Fig. 1. Comparison of the reducing power activity of methanol extract and different fractions of leaves

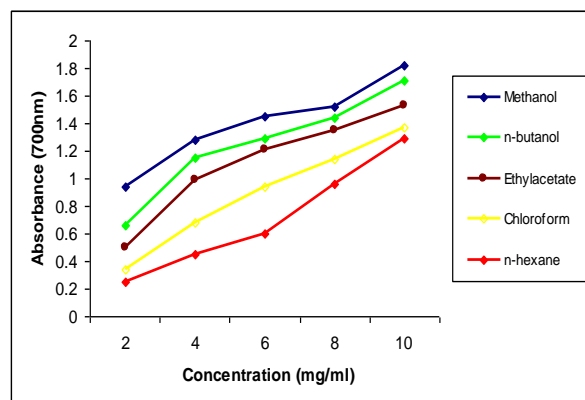


Fig. 2. Comparison of the reducing power activity of methanol extract and different fractions of roots

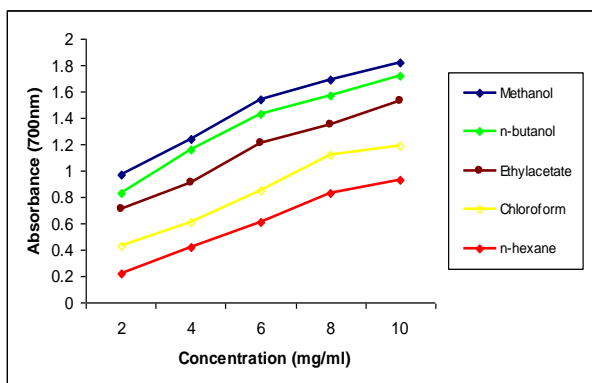


Fig. 3. Comparison of the reducing power activity of methanol extract and different fractions of stems

GC-MS Analysis

The GC-MS analysis of the *n*-hexane fractions of leaves, stems and roots from methanol extracts confirmed the presence of chemical components. The GC-MS chromatograms are shown in Figures (4-6) and results are presented in Tables (6-8). The volatile and non volatile fractions consisted of a mixture of different classes of compounds. In the *n*-hexane fraction of leaves 8 components representing 60.47% of the total fraction content were identified. The major constituents in the *n*-hexane fraction of leaves were found to be urs-12-en-24-oic acid 3-oxo-methyl ester (21.09%), urs-12-en-3 β -ol-ethanoate, (17.58%), heneicosane (9.61%). The *n*-hexane fraction of stems revealed the presence of urs-12-en-24-oic acid 3-oxo-methyl ester (22.03%), 12-oleanen-3 α -yl (8.74%) and β -amyryn (1.19%) as significant components. Hexadecanoic acid (3.02%), zeirone (5.46%), 12-oleanen-3-yl-ethanoate (15.6%) were found to be the dominant components in the *n*-hexane fraction of roots.

Abundance

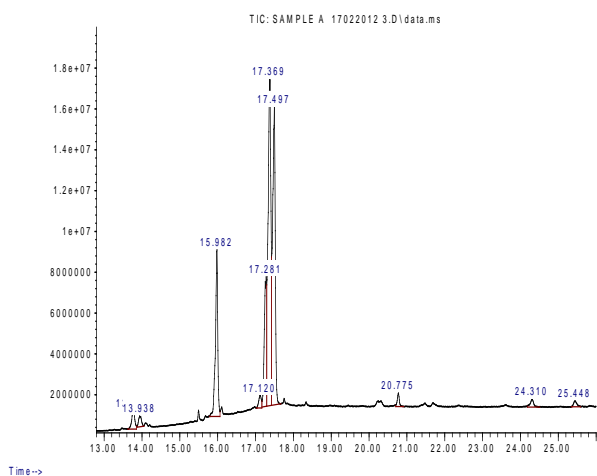


Fig 4. GC-MS chromatogram of the *n*-hexane fraction of plant leaves

Table 6: GC-MS analysis of the *n*-hexane fraction of plant leaves

Retention Time (min.)	Name of Compound	% Area
13.762	β -Amyryn; Olean-12-en-3 β -ol	1.281
13.938	α -Amyryn; Urs-12-en-3 β -ol	0.898
15.982	12-Oleanen-3 α -yl-ethanoate	8.772
17.281	Vasicionolone	0.784
17.369	Urs-12-en-24-oic acid, 3-oxo-methyl ester (+)	21.095
17.497	Urs-12-en-3 β -ol-ethanoate	17.584
20.775	Heneicosane	9.615
24.310	Not identified	6.000
25.448	Stigmasterol	0.446

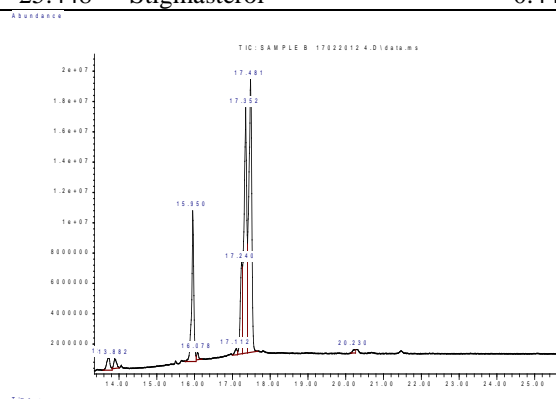


Fig. 5 GC-MS chromatogram of the *n*-hexane fraction of plant stems

Table 7: GC-MS analysis of the *n*-hexane fraction of plant stems

Retention Time (min.)	Name of Compound	% Area
13.882	Urs-12-en-3 β -ol	0.821
15.95	12-Oleanen-3 α -yl	8.748
16.078	Olean-12-en-3 β -ol-ethanoate	0.349
17.112	Urs-12-en-3 β -ol-ethanoate	0.405
17.352	12-Oleanen-3 α -ethanoate	5.24
17.481	Urs-12-en-24-oic acid 3-oxo-methyl ester (+)	22.031
20.230	β -Amyryn	1.198

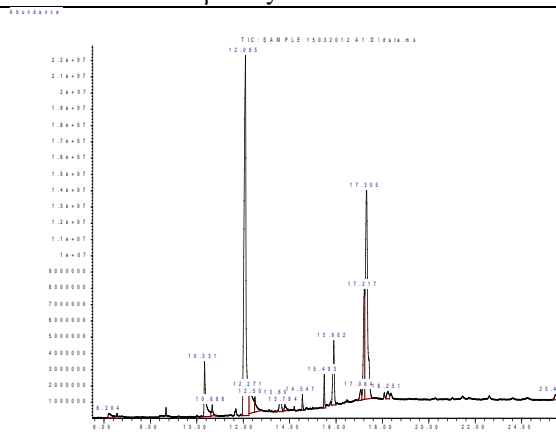


Fig. 6. GC-MS chromatogram of the *n*-hexane fraction of plant roots

Table 8. GC-MS analysis of the *n*-hexane fraction of plant roots

Retention Time (min.)	Name of Compound	% Area
6.204	Dodecanoic acid	0.589
10.331	Hexadecanoic acid	3.02
10.668	Eicosane	0.501
12.095	9,12-Octadecadienoic acid	0.331
13.61	Vimalolol	1.016
13.794	α -Amyrin	0.378
14.547	Pyrrolidin-2-one 5-[2-butyrylethyl]	0.403
15.493	Di-(2-ethylhexyl)phthalate	0.839
17.06	Urs-12-en-24-oic acid 3-oxo- methyl ester (+)	0.628
17.217	Zierone	5.465
17.305	12-Oleanen-3 α -yl-ethanoate	15.616
18.251	Friedooleanan-3-one	0.552
25.472	2-Amino-4-(3,4-dimethylphenyl) thiophene-3-carboxylic acidpropy ester	0.165

Acknowledgements: The authors are highly thankful to Dr. Muhammad Athar Abbasi, Assistant Professor, Department of Chemistry, GC University Lahore, Pakistan, for providing the facility for GC-MS analysis.

REFERENCES

1. F. Aslam, N. Rasool, M. Riaz, M. Zubair, K. Rizwan, M. Abbas, T. H. Bukhari, I. H. Bukhari, *Int. J. Phytochem.* **3**, 567 (2011).
2. M. R. Ahsan, K. M. Islam, M. E. Haque, M. A. Mossaddik, *World Journal of Agricultural Sciences* **5**, 617 (2009).
3. J. Sparrow, H. Gil, *Subtropical Plants: A Practical Gardening Guide*. Timber Press, Inc, Portland, Oregon, 2002.
4. E. M. Abdallah, A. E. Khalid, *Int. J. Chem. Biochem. Sci.* **1**, 1 (2012).
5. S. Adeel, F. Rehman, T. Gulzar, I. A. Bhatti, S. Qaiser, A. Abid, *Asian J. Chem.* **25**, 2739 (2012).
6. K. Rehman, S. Ashraf, U. Rashid, M. Ibrahim, S. Hina, T. Iftikhar, S. Ramzan, *Pak. J. Bot.* **45**, 391 (2013).
7. M. Riaz, N. Rasool, S. Rasool, U. Rashid, I. H. Bukhari, M. Zubair, M. Noreen, M. Abbas, *Asian J. Chem.* **25**, 5479 (2013).
8. H. O. Edeoga, D. E. Okwu, B. O. Mbaebie, *J. Biotechnol.* **4**, 685 (2005).
9. T. Okuda, *Phytochem.* **66**, 2012 (2005).
10. A. Chaovanalikit, R. E. Wrolstad, *J. Food Sci.* **69**, 67 (2004).
11. M. Riaz, N. Rasool, I. Bukhari, M. Shahid, F. Zahoor, M. Gilani, M. Zubair, *Afr. J. Microbiol. Res.* **6**, 5700 (2012).
12. V. Dewanto, X. Wu, K. K. Adom, R. H. Liu, *J. Agri. Food Chem.* **50**, 3010 (2002).
13. B. Bozin, D. Micica, N. Simin, G. Anackov, *J. Agric. Food Chem.* **54**, 1822 (2006).
14. G. C. Yen, P. D. Duh, D. Y. Chuang, *Food Chem.* **70**, 437 (2000).
15. T. Osawa, M. Namiki, *Agric. Biol. Chem.* **45**, 735 (1981).
16. NCCLS, Performance standards for antimicrobial disk susceptibility test by National Committee for Clinical Laboratory Standards (NCCLS), 6th ed. Wayne PA, M2-A6., 1997.
17. A. U. Rahman, M. I. Choudhary, *Pure Appl. Chem.* **73**, 555 (2001).
18. S. D. Sarker, L. Nahar, Y. Kumarasamy, *Methods* **42**, 321 (2007).
19. E. Derwich, Z. Benziane, R. Taouil, *Chemical Bulletin of "Politehnica" University of Timisoara, Romania* **55**, 103 (2010).
20. M. Riaz, N. Rasool, I. H. Bukhari, M. Shahid, M. Zubair, K. Rizwan, U. Rashid, *Molecules* **17**, 14275 (2012).

GC-MS ПРОФИЛИРАНЕ, АНТИОКСИДАНТНО И АНТИМИКРОБНО ИЗСЛЕДВАНЕ НА РАЗЛИЧНИ ЧАСТИ НА РАСТЕНИЕТО *Carissa grandiflora*

М. Абас¹, Н. Расул^{1,*}, М. Риаз², М. Зубаир¹, М. Аббас³, Нур-ул-Хак¹, Н. Хаят¹

¹ Департамент по химия, Правителствен университетски колеж, Файсалабад 38000, Пакистан

² Катедра по химия в Университет на Саргода, Район на Жените, Файсалабад, Пакистан

³ Департамент по химия и биохимия, Агрономически университет, Файсалабад 38040, Пакистан

Постъпила на 5 ноември, 2013 г.; коригирана на 2 януари, 2014 г.

(Резюме)

В настоящата работа се оценява биологичната активност на метанолови екстракти от листа, корени и стебла на растението *Carissa grandiflora* и техни фракции в разтворители с различна полярност (*n*-хексан, хлороформ, етилацетат и *n*-бутанол). Екстрактите и техните фракции съдържат значителни нива на общи фенолни производни (TPC) в интервала от 31.17 до 349.43 GAE, mg/100 g сухи вещества (листа), 38.85 до 269.81 еквивалент на галова киселина (GAE), mg/100 g сухи вещества (корени) и 40.18 до 241.11 GAE, mg/100 g сухи вещества (стебла). Общото съдържание на флавоноиди е от 59.14 до 284.99, 32.27 до 199.74 и 21.37 до 158.56 CE, mg/100 g сухи вещества съответно за листа, корени и стебла. Стойностите на IC₅₀ в случай на DPPH радикал-премахваща активност за листа, корени и стебла са от 20.89 до 578.9, 12.28 до 325.31 и 6.15 до 941.4 mg/mL съответно. Процентното инхибиране на пероксидация по линоленова киселина е съответно от 11.34 до 46.7, 15.56 до 41.31 и 18.14 до 50.46 за листа, корени и стебла. Метаноловите екстракти от всички части на растенията показват най-висока редукционна активност в сравнение с другите фракции. Максимална антибактериална активност спрямо *S. aureus* показват екстрактите от стебла с етилацетат; фракцията с *n*-butanol спрямо *E. coli* и метаноловите екстракти спрямо *S. epidermidis*. Щамът *C. albicans* показва най-голяма резистентност спрямо екстракта в етил ацетат от корени. GCMS-анализът на хексановата фракция от корени показва, че в тази част на растението е обогатена с максимален брой биологично активни съединения.

Determination of the trace element content in Bulgarian bottled potable waters by total reflection X-ray fluorescence analysis

R. H. Georgieva¹, A. K. Detcheva^{1*}, M. G. Karadjov², S. E. Mitsiev¹,
J. H. Jordanov¹, E. H. Ivanova¹

¹ Institute of General and Inorganic Chemistry, Bulgarian Academy of Sciences, Sofia, Bulgaria

² Geological Institute, Bulgarian Academy of Sciences, Sofia, Bulgaria

Received January 13, 2014; Revised February 28, 2014

The content of S, Cl, K, Ca, Mn, Fe, Ni, Cu, Zn, As, Br, Rb and Ba in several brands of Bulgarian bottled potable waters (“Savina” table, “Gorna Banya” mineral, “Bankya” mineral, “Kom” mineral, “Thorn Spring” mineral, “Hissar” mineral, “Devin” spring and mineral and “Mihalkovo” spring and mineral) was determined by total reflection X-ray fluorescence (TXRF) analysis using gallium as internal standard. The spring waters generally displayed lower mineralization (total dissolved solids, TDS content) than the mineral waters, even those originating from the same location. The content of S, Cl, K and Ca was at the mg L⁻¹ level, while that of Mn, Fe, Ni, Cu, Zn, As, Br, Rb and Ba - at the lower µg L⁻¹ level. The trace element content of the mineral waters did not considerably change (less than ±30 % difference) over a storage period of approx. 2.5 years after bottling.

Keywords: Bulgarian bottled potable waters; total reflection X-ray fluorescence analysis; essential and toxic elements

INTRODUCTION

Bulgaria is one of the countries in the world richest in mineral and spring waters (more than 850 boreholes and springs) [1]. At present, more than 50 brands of bottled mineral, spring and table waters are offered on the Bulgarian market. The major components of bottled Bulgarian drinking waters, such as K, Na, Ca, Mg, and Fe are monitored in accordance with European legislation, e.g. [2,3], whereas only limited data are available about their trace element content. Information on the location, physico-chemical characteristics, element content, and medical applications of Bulgarian mineral and spring waters can be found in [1,4-6].

During the last two decades the total reflection X-ray fluorescence (TXRF) has turned out to be a well-established analytical tool and has found many applications owing to the fact that quantification procedures are very simple and practically no sample preparation is required [7,8]. Further benefits of TXRF are: no need of external calibration; multi-element analysis including halogenides; low analytical operation and maintenance costs; portability. TXRF methods for trace element analysis in different kinds of natural waters including mineral waters after separation and preconcentration of the analytes [9,10], as well

as direct TXRF methods [11-15] are reported in the literature. In a former work of the present authors [16], the conditions for the direct TXRF determination of both major and trace elements in mineral waters of total dissolved solids (TDS) content in a broad range – from 160 to 2900 mg L⁻¹ were optimized.

The purpose of the present work was to apply the optimized TXRF procedure [16] for direct trace element analysis of several brands of bottled potable waters offered on the Bulgarian market: the mineral waters “Hissar” and “Bankya”, the spring waters “Devin” and “Mihalkovo” and the table water “Savina”. Furthermore, the trace element content in the formerly analyzed mineral waters “Gorna Banya”, “Kom”, “Devin”, “Thorn Spring” and “Mihalkovo” [16] was again determined in the present work in order to find out whether any changes have taken place in their composition and characteristics over a storage period of approx. 2.5 years after bottling.

EXPERIMENTAL

Instrumentation

The TXRF analyser S2 PICOFOX (BRUKER AXS GmbH Karlsruhe, Germany) was used for the measurements. This instrument was equipped with an air-cooled low power X-ray tube (Mo target), a Ni/C monochromator with 80% reflectivity and a liquid nitrogen-free Silicon Drift Detector (SDD) of 10 mm² area with an energy resolution of < 159 eV

* To whom all correspondence should be sent:
E-mail: albena@svr.igic.bas.bg

(Mn K α). The sample holders were quartz optical plates of 30 mm diameter and 3 mm thickness (Perspex Distribution LTD, UK). The power was 50 kV and the current was 1000 μ A. Prior to each series of measurements gain correction was performed to compensate for the drift of the channel/energy dependence by measuring at As K α – 10.53 keV.

Cleaning of the lab ware

The quartz plates used as sample holders were cleaned with 10% (v/v) nitric acid (p.a., Merck, Darmstadt, Germany) at a temperature of 80 °C for 1 h on a hot plate. They were subsequently flushed with water from a Cole-Parmer deionizer model 01503-20, Germany, conductivity 15 M Ω /cm, and were let to dry in the air.

Sample preparation and analysis

Sample preparation was performed according to [16]. The water sample (1.0 mL) was transferred to an Eppendorf[®] tube of 1.5 mL volume and was mixed with 20 μ L of the internal standard (a 10 mg L⁻¹ Ga solution). Three aliquots (each of 5 μ L) of the water sample, mixed with the internal standard, were consecutively pipetted and dried on a siliconized quartz holder. The dry residue was measured for 1000 s at two perpendicular positions of the sample holder. Several blank quartz holders were measured to determine the blank value.

For the evaluation of the TXRF spectra, the Spectra 5.1[®] software (Bruker AXS Microanalysis GmbH, Berlin, Germany) was used. The quantification was performed as described in [17].

RESULTS AND DISCUSSION

Several brands of bottled Bulgarian mineral, spring and table waters were selected for analysis. Some of the characteristics of the waters, as given on the bottle labels, are presented in Table 1.

As can be seen, all selected waters are neutral to slightly alkaline (pH from 7.2 to 9.0) and of low mineralization (TDS content between 50 and 240 mg L⁻¹). The waters were analyzed within one year after bottling. As Table 1 shows, the spring waters are of lower TDS content than the mineral waters. The lowest TDS content is manifested by the “Savina” table water, which may be attributed to its treatment by reverse osmosis prior to bottling. The TDS content of the mineral waters analyzed in [16] was as follows: “Gorna Banya” ~160 mg L⁻¹, “Kom” and “Devin” ~260 mg L⁻¹, “Thorn Spring” ~420 mg L⁻¹ and “Mihalkovo” ~2900 mg L⁻¹. In the present work the pH values of these waters were measured again ~2.5 years after bottling. No changes in the pH values of these waters with respect to the original values were registered, except for the “Mihalkovo” mineral water: the presently measured pH value was ~ 7 (original value 6.4). This increase in pH was attributed to the removal of CO₂, naturally contained in the “Mihalkovo” mineral water, which diffused out of the bottle during the prolonged storage.

It was further of interest that mineral and spring waters from the same location displayed different TDS values, e.g., “Mihalkovo” mineral water (2900 mg L⁻¹) – “Mihalkovo” spring water (72 mg L⁻¹); “Devin” mineral water (260 mg L⁻¹) – “Devin” spring water (82 mg L⁻¹).

The content of the trace elements S, Cl, K, Ca, Mn, Fe, Ni, Cu, Zn, As, Br, Rb (K α line) and Ba (L α line) in the water samples was determined. Light elements (Li, Na, Be, B) were not detectable in the water samples with the present instrumentation [18]. Ag, Cd, Sb, Sr, Mo were excluded from the list of analytes as discussed in [16]. The TXRF lower limits of detection (LLD), determined according to the 3 σ criterion [18] in low- and high-TDS waters, are shown in Table 2.

Table 1. Characteristics of bottled mineral, spring and table waters, analyzed in the present work, according to the certificates of the Ministry of Health of Bulgaria, given on the bottle labels. Bottle volume is 0.5 L.

Characteristic	“Savina” table water	“Hissar” mineral water	“Bankya” mineral water	“Devin” spring water	“Mihalkovo” spring water
Bottled in	10.2012	03.2012	09.2012	11.2012	11.2012
TDS content, mg L ⁻¹	< 50	240	247	82	72
pH	7.2-7.6	9.0	8.9	7.8	7.4
Source	Busmanci (Sofia district)	Hissar (Plovdiv district)	Ivanyane (Sofia district)	Devin (Smolian district)	Mihalkovo (Smolian district)
Na, mg L ⁻¹	< 0.002	60.3	53.0	5.4	2.8
K, mg L ⁻¹		1.1	0.67		11.3
Ca, mg L ⁻¹		2.7	4.61	7.14	5.1

Table 2. TXRF lower limits of detection (LLD, $\mu\text{g L}^{-1}$) of the analytes in waters of low and high TDS content, obtained under the conditions given in the Experimental.

Analyte	LLD, $\mu\text{g L}^{-1}$ for low-TDS waters (TDS <50-420 mg L^{-1})	LLD, $\mu\text{g L}^{-1}$ for high-TDS waters (TDS 2900 mg L^{-1})
S	90	970
Cl	70	800
K	20	300
Ca	18	200
Mn	2	20
Fe	2	14
Ni	1	10
Cu	2	10
Zn	2	9
As	1	7
Br	1	6
Rb	1	7
Ba	14	100

As can be seen, the LLD values in high-TDS waters are higher by a factor of 5-15 than those in low-TDS waters, which may be related to the increased X-ray excitation scattering and the higher background in the former case.

The results for the trace element content in the analyzed table, spring and mineral waters are shown in Table 3. S, Cl, K and Ca are at the mg L^{-1} level; Fe, Cu, Zn and Br are at the $\mu\text{g L}^{-1}$ level, while Mn, As, Ni and Ba are not detected (below the corresponding LLD). Rb is detected only in the “Hissar” mineral water, which agrees with literature data for waters of the same location [1].

The results for the trace element content in mineral waters, stored for approx. 2.5 years after bottling, are shown in Table 4.

The upper values refer to the analysis carried out in 2011 [16], while the lower ones are obtained in the present work. As can be seen, the concentrations of the analytes are not significantly changed over the period of 2.5 years (differences below $\pm 30\%$). This is an evidence for the stability of the trace element content of the bottled waters during prolonged storage.

The precision of the TXRF results for the trace element content in the analyzed waters is characterised by an RSD of 5–16%.

Table 3. Data for the trace element content in bottled table, mineral and spring waters of low TDS content (50-260 mg L^{-1}). The results are presented as mean \pm SD of six replicates.

Analyte	“Savina” table water	“Hissar” mineral water	“Bankya” mineral water	“Devin” spring water	“Mihalkovo” spring water
S, mg L^{-1}	0.20 ± 0.01	6.3 ± 1.1	14 ± 1	0.80 ± 0.05	2.6 ± 0.4
Cl, mg L^{-1}	2.2 ± 0.2	6.2 ± 0.8	9.8 ± 1.2	1.2 ± 0.2	1.4 ± 0.2
K, mg L^{-1}	1.1 ± 0.1	1.7 ± 0.1	0.7 ± 0.1	1.5 ± 0.2	10.6 ± 0.3
Ca, mg L^{-1}	6.1 ± 0.5	3.6 ± 0.2	6.1 ± 0.7	7.9 ± 1.3	5.7 ± 0.8
Mn, $\mu\text{g L}^{-1}$	< 2	< 2	< 2	< 2	< 2
Fe, $\mu\text{g L}^{-1}$	18 ± 3	19 ± 1	20 ± 3	15 ± 2	16 ± 2
Ni, $\mu\text{g L}^{-1}$	< 1	< 1	< 1	< 1	< 1
Cu, $\mu\text{g L}^{-1}$	12 ± 2	19 ± 2	9 ± 1	8 ± 1	7 ± 1
Zn, $\mu\text{g L}^{-1}$	15 ± 2	29 ± 2	9 ± 1	9 ± 1	12 ± 2
As, $\mu\text{g L}^{-1}$	< 1	< 1	< 1	< 1	< 1
Br, $\mu\text{g L}^{-1}$	6 ± 1	30 ± 3	76 ± 6	9 ± 1	9 ± 1
Rb, $\mu\text{g L}^{-1}$	< 1	19 ± 1	< 1	< 1	< 1
Ba, $\mu\text{g L}^{-1}$	< 14	< 14	< 14	< 14	< 14

Table 4. Data for the trace element content in bottled mineral waters. The first row of values is obtained in the year of bottling [16]; the second one – approx. 2.5 years after bottling. The results are presented as mean \pm SD of six replicates.

Analyte	“Gorna Banya” mineral water	“Kom” mineral water	“Thorn Spring” mineral water	“Devin” mineral water	“Mihalkovo” mineral water
S, mg L ⁻¹	7.9 \pm 0.4	8.9 \pm 0.2	2.8 \pm 0.4	5.1 \pm 0.8	123 \pm 13
	6.4 \pm 0.5	8.8 \pm 0.3	2.2 \pm 0.3	4.5 \pm 0.4	96 \pm 6
Cl, mg L ⁻¹	2.4 \pm 0.2	1.2 \pm 0.1	2.9 \pm 0.4	3.4 \pm 0.2	47 \pm 7
	1.8 \pm 0.2	0.9 \pm 0.1	2.2 \pm 0.3	3.1 \pm 0.2	45 \pm 7
K, mg L ⁻¹	0.35 \pm 0.02	1.3 \pm 0.2	1.2 \pm 0.2	0.6 \pm 0.1	48 \pm 7
	0.31 \pm 0.05	1.0 \pm 0.1	1.5 \pm 0.2	0.6 \pm 0.1	46 \pm 6
Ca, mg L ⁻¹	1.3 \pm 0.2	1.4 \pm 0.2	78 \pm 8	1.5 \pm 0.1	215 \pm 25
	1.5 \pm 0.2	1.7 \pm 0.2	80 \pm 6	1.3 \pm 0.1	217 \pm 29
Mn, μ g L ⁻¹	< 2	< 2	< 2	< 2	48 \pm 7
	< 2	< 2	< 2	< 2	38 \pm 5
Fe, μ g L ⁻¹	25 \pm 4	10 \pm 1	6.8 \pm 0.8	15 \pm 2	15 \pm 2
	24 \pm 3	7.9 \pm 1.0	8.0 \pm 1.0	13 \pm 2	15 \pm 2
Ni, μ g L ⁻¹	3.0 \pm 0.5	12 \pm 1	5.0 \pm 0.8	4.0 \pm 0.5	14 \pm 2
	< 1	10 \pm 1	4.0 \pm 0.5	3.0 \pm 0.5	13 \pm 2
Cu, μ g L ⁻¹	6.0 \pm 0.5	6.0 \pm 0.5	< 2	3.0 \pm 0.5	< 10
	4.8 \pm 0.5	4.8 \pm 0.1	< 2	3.0 \pm 0.5	< 10
Zn, μ g L ⁻¹	6.0 \pm 0.5	47 \pm 4	10 \pm 1	< 2	< 9
	4.9 \pm 0.5	50 \pm 4	13 \pm 2	3.0 \pm 0.5	< 9
As, μ g L ⁻¹	3.0 \pm 0.5	12 \pm 2	2.5 \pm 0.2	< 1	< 7
	3.0 \pm 0.5	9.0 \pm 1.0	< 1	< 1	< 7
Br, μ g L ⁻¹	8.0 \pm 1.0	37 \pm 5	15 \pm 2	6.0 \pm 0.5	400 \pm 50
	6.5 \pm 1.0	32 \pm 3	13 \pm 2	6.0 \pm 0.5	350 \pm 50
Rb, μ g L ⁻¹	5.0 \pm 0.5	4.0 \pm 0.5	< 1	< 1	163 \pm 25
	4.0 \pm 0.5	4.0 \pm 0.5	< 1	< 1	160 \pm 25
Ba, μ g L ⁻¹	45 \pm 7	30 \pm 5	28 \pm 4	38 \pm 5	< 100
	36 \pm 1	26 \pm 4	23 \pm 2	35 \pm 2	< 100

CONCLUSIONS

The trace element content in several brands of bottled Bulgarian potable waters (“Savina” table, “Gorna Banya” mineral, “Bankya” mineral, “Kom” mineral, “Thorn Spring” mineral, “Hissar” mineral, “Devin” spring and mineral and “Mihalkovo” spring and mineral) was determined by direct TXRF analysis using gallium as internal standard. The spring waters generally displayed a lower TDS content than the mineral waters, even those from the same location. The trace elements S, Cl, K and Ca were found to be at the mg L⁻¹ level, while Mn, Fe, Ni, Cu, Zn, As, Br, Rb and Ba - at the lower μ g L⁻¹ level. It was of interest that the trace element content of the examined mineral waters remained rather constant over a period of storage of 2.5 years (differences below \pm 30 %). The natural purity and the stable trace element content of Bulgarian mineral, spring and table waters make them a high-quality product on the Bulgarian and the European market of potable waters. It follows from the obtained results that TXRF is a suitable method for the routine trace element analysis (including S, Cl and Br) of bottled potable waters of various type and mineral composition.

Acknowledgement: The authors thank the National Science Fund at the Ministry of Education, Youth and Science of Bulgaria for the financial support (Contract DTK 02-5/2010).

REFERENCES

1. E.N. Pentcheva, L. Van't dack, E. Veldeman, V. Hristov, R. Gijbels, Hydrogeochemical characteristics of geothermal systems in South Bulgaria, Universiteit Antwerpen (UIA), 1997.
2. Deutsches Institut für Normung Standards DIN 38406 Part 3 Cations (1982); DIN 38405 Part 19 Anions (1988); DIN 38405 Part 20 Anions (1989).
3. Natural Potable Mineral Waters, *Bulgarian Governmental Standard* BDS 14947 (1980).
4. L. Vladeva, D. Kostadinov, Bulgarian mineral potable waters, Part 1. M-8-M Publ. House, Sofia, 1996.
5. L. Vladeva, D. Krasteva, J. Jordanov, D. Kostadinov, Guide on Bulgarian Mineral Waters, Nauka i Technika Publ. House, Stara Zagora, 2000.
6. L. Vladeva, D. Kostadinov, Bulgarian mineral potable waters, Part 2. M-8-M Publ. House, Sofia, 2007.
7. R. Klockenkämper, Total-reflection X-ray Fluorescence Analysis, Wiley, New York, 1997.
8. C. Strelu, *Appl. Spectrosc. Rev.*, **41**, 473 (2006).
9. N. Kallithrakas-Kontos, *X-Ray Spectrom.*, **33**, 12 (2004).

10. W. Gerwinski, D. Schmidt, *Spectrochim. Acta Part B*, **53**, 1355 (1998).
11. A.M. Alvarez, J.R.E. Alvarez, R.P. Alvarez, *J. Radioanal. Nucl. Chem.*, **273**, 427 (2007).
12. G.A. Tavares, E. Almeida, J.G.G. De Oliveira, J.A. Bendassolli, V.F. Nascimento Filho, *J. Radioanal. Nucl. Chem.*, **287**, 377 (2011).
13. S. Dhara, N.L. Misra, *J. Phys.*, **76**, 361 (2011).
14. S. Kunimura, J. Kawai, *Anal. Sci.*, **23**, 1185 (2007).
15. F. Cataldo, *J. Radioanal. Nucl. Chem.*, **293**, 119 (2012).
16. R. Georgieva, A. Detcheva, M. Karadjov, J. Jordanov, E. Ivanova, *Intern. J. Environ. Anal. Chem.* **93**, 1043 (2013).
17. H. Hoefler, C. Strel, P. Wobrauschek, M. Ovari, Gy. Zaray, *Spectrochim. Acta Part B*, **61**, 1135 (2006).
18. H. Stosnach, Lab Report XRF 425 Bruker AXS Microanalysis GmbH, Berlin, Germany (2007)

ОПРЕДЕЛЯНЕ НА СЛЕДИ ОТ ЕЛЕМЕНТИ В БЪЛГАРСКИ БУТИЛИРАНИ ПИТЕЙНИ ВОДИ С ПОМОЩТА НА РЕНТГЕНОФЛУОРЕСЦЕНТЕН АНАЛИЗ С ПЪЛНО ВЪТРЕШНО ОТРАЖЕНИЕ

Р. Х. Георгиева¹, А. К. Дечева¹, М. Г. Караджов², С. Е. Мициев¹, Ю. Х. Йорданов¹, Е. Х. Иванова¹

¹Институт по обща и неорганична химия, Българска академия на науките, ул. Акад. Георги Бончев бл.11, 1113, София, България

²Геологически институт, Българска академия на науките, ул. Акад. Георги Бончев бл.24, 1113, София, България

(Резюме)

Съдържанието на S, Cl, K, Ca, Mn, Fe, Ni, Cu, Zn, As, Br, Rb и Ba в различни марки български бутилирани питейни води ("Савина" трапезна, "Горна баня" минерална, "Банкя" минерална, "Ком" минерална, "Трънска баня" минерална, "Хисар" минерална, "Девин" изворна и минерална и "Михалково" изворна и минерална) е определено чрез рентгенофлуоресцентен анализ с пълно вътрешно отражение с вътрешен стандарт галий. Изследваните изворни води са с по-ниска обща минерализация от минералните води, дори от едно и също находище. Съдържанието на S, Cl, K и Ca е на ниво mg L⁻¹, а това на Mn, Fe, Ni, Cu, Zn, As, Br, Rb и Ba – на ниво µg L⁻¹. Установено е, че съдържанието на елементи в минералните води не се променя съществено (по-малко от ± 30 %) при съхранението им за период от 2.5 години след бутилиране.

The 2nd Asia-Pacific Conference on Engineering Technology (APCET 2014)

The study of TiO₂-ZrO₂ preparation and its elimination efficiency on triclosan

Xu Han, Lei Cai, Huiping Deng, Jun Shi*

Key Laboratory of Yangtze River Water Environment, Ministry of Education, Tongji University, 1239 Siping Road, 200092 Shanghai, P.R.China

Received April 19, 2014

Abstract. Titania zirconia (TiO₂-ZrO₂) photocatalyst were successfully synthesized using the sol-gel impregnation method containing commercial titania and zirconium (IV) oxide chloride as precursor. X-ray powder diffraction was used to characterize the phases of the photocatalyst, the rutile type was not detected even at 700°C. Photocatalytic degradation of triclosan was employed to test photoactivity of the catalyst on different molar ratios of Ti/Zr and calcination temperatures, respectively. TiO₂-ZrO₂ catalysts were more photoactive than commercial TiO₂. Photodegradation efficiency of removing triclosan was close on molar ratio of Ti/Zr 1/20 and 1/1 and the highest removal was observed at 500 °C.

Key words: TiO₂-ZrO₂, triclosan, photocatalysis

INTRODUCTION

Triclosan(5-chloro-2-(2,4-dichlorophenoxy) phenol, TCS), known as one of pharmaceutical and personal care products (PPCPs), has been widely used in a variety of consumer products, including tooth paste, detergent, soap, shampoos, skin care creams and cosmetics[1, 2]. Triclosan, which is hard to be decomposed against hydrolysis, has been detected in the aquatic environment (waste water, surface water and lake sediments) [3-5] and even be found in human milk and fatty tissues [6, 7]. In addition, carcinogenic dioxins might arise in the manufacture of triclosan reported by the Environmental Protection Agency of United States, and it has been reported that dioxins can be formed when the triclosan-contaminated natural waters are exposed to the sunlight [8]. Due to its widely existing and carcinogenic effects, the presence of triclosan in the aquatic environment and its potential adverse impacts on ecological and public health has been concerned increasingly. The removal of triclosan from natural waters has drawn extensive interests [2, 9-11].

Adsorbents (activated carbon, zeolites, soil, etc.), thermal destruction and biodegradation as traditional

methods, which are used to remove recalcitrant organic chemicals, suffer the drawbacks such as requiring long period of treatment, large energy input or only transferring the contaminants from one phase to another. Photocatalysis, one of advanced oxygen technologies and promising technologies, can provide a cost-saving alternative method removing organic substrates from water [12-14]. Titanium dioxide (TiO₂) is applied in heterogenous photocatalysis because of excellent physical and chemical properties. Under UV irradiation, TiO₂ can be photoactivated, and generate hydroxyl radicals ($\cdot\text{OH}$) which can mineralize most organic compounds for its strong oxidation. Titanium and zirconium have similar physicochemical properties as they are in the same group (IVB) and both oxides TiO₂ and ZrO₂ are n-type semiconductors with similar physicochemical properties. The combination of TiO₂ and ZrO₂ has been investigated for its advantages such as strong acid-base, extended specific surface area and mechanical strength [15-17].

The paper reports the physicochemical properties of TiO₂-ZrO₂ prepared by sol-gel impregnation and the influence of the molar ratio and calcination temperature of TiO₂/ZrO₂.

* To whom all correspondence should be sent.

EXPERIMENTAL

Reagents

Triclosan(5-chloro-2-(2,4-dichlorophenoxy)phenol, TCS 97%), titania (TiO₂ 99.8% 40nm anatase) and zirconium (IV) oxide chloride (ZrO₂ 36%) were purchased from Aladdin (Shanghai China). Ammonia and sodium hydroxide were purchased from Sinopharm Chemical Reagent Co., Ltd (China) and used in the experiments were of analytical grade.

Preparation of ZrO₂-TiO₂ particles

ZrO₂-TiO₂ catalysts on different Ti/Zr molar ratios (1/20, 1/4, 1/2 and 1/1) were prepared by means of sol-gel impregnation method using ZrOCl₂·8H₂O and TiO₂ (99.8% 40nm anatase) as precursors [18]. The ZrO₂-TiO₂ binary semiconductor was obtained by precipitation of TiO₂ on ZrOCl₂·8H₂O solution in deionized water, using ammonia as precipitating agent which was dropped slowly into the suspension until at pH 10. The gel was filtered and washed with plenty of deionized water for eliminating Cl⁻, and finally dried in oven at 110 °C overnight and calcined at 500, 600 and 700 °C for 2h respectively. Samples were named TZ500-a, TZ500-b, TZ500-c and TZ500-d (500 means calcined at 500°C, a, b, c and d are Ti/Zr molar ratios 1/20, 1/4, 1/2 and 1/1, respectively).

XRD characterization

X-ray powder diffraction (XRD) patterns were recorded on a Bruker D8 Advance diffraction spectrometer (Germany) using Cu K_α radiation. Data were collected from 2θ = 10~90° in a step-scan mode (step 0.02°, time per step 0.1 s). Qualitative phase analysis was performed with software MID Jade 5.0 [19].

Photocatalytic experiments

Experiments were carried out in a home-made laboratory reactor (500ml) using a high pressure 250 W Hg lamp (250W×365nm, TianMai Light Source Co., China) as light source. Aqueous solution 400 ml volume of TCS, pH value of 10.8~11.2 was selected to increase the solubility of TCS with 1mol/L sodium

hydroxide, was filled in the reactor. The initial concentration of 50 mg/L TCS was used in the experiments. Before each experiment, 40mg catalyst was dispersed in the solution and stirred with magnetic stirrer for 20min to reach adsorption equilibrium in the dark prior to illumination. All the experiments were performed at ambient temperature (18°C). At pre-selected time intervals, 2ml aliquots were taken from the suspension and put into glass vials.

The concentration of TCS was analyzed by high performance liquid chromatography (Agilen1200-HPLC, Agilent Co., America) consisting of Diode Array Detector. The mobile phase methanol/ water (90:10, v/v) with a shim-pack reverse phase column (250mm×4.6mm) were used. Injection volume was 20μl, a flow rate was 1ml/min, and 35°C column temperature and detection wavelength of 280 nm was applied. All the samples collected were filtered through micro syringe filters (0.45μm).

RESULTS AND DISCUSSIONS

X-ray powder diffraction (XRD)

XRD patterns of samples calcined at 500-700 °C on 1/2 molar ratio of Ti/Zr were shown in Fig.1. Both of anatase and zirconia phase were observed; the diffraction peak area of zirconia was larger for its higher amount. No trace diffraction of rutile structure was detected for ZrO₂ doped TiO₂ after heat treatment at 700 °C.

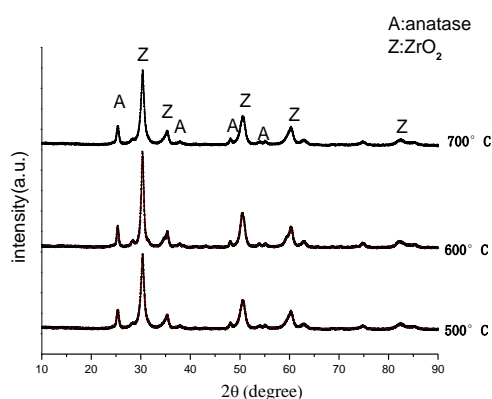


Fig.1. XRD of TZ-c photocatalyst calcined at 500, 600 and 700 °C.

Zirconium as a stabilization agent could suppress the transformation from anatase to rutile when the

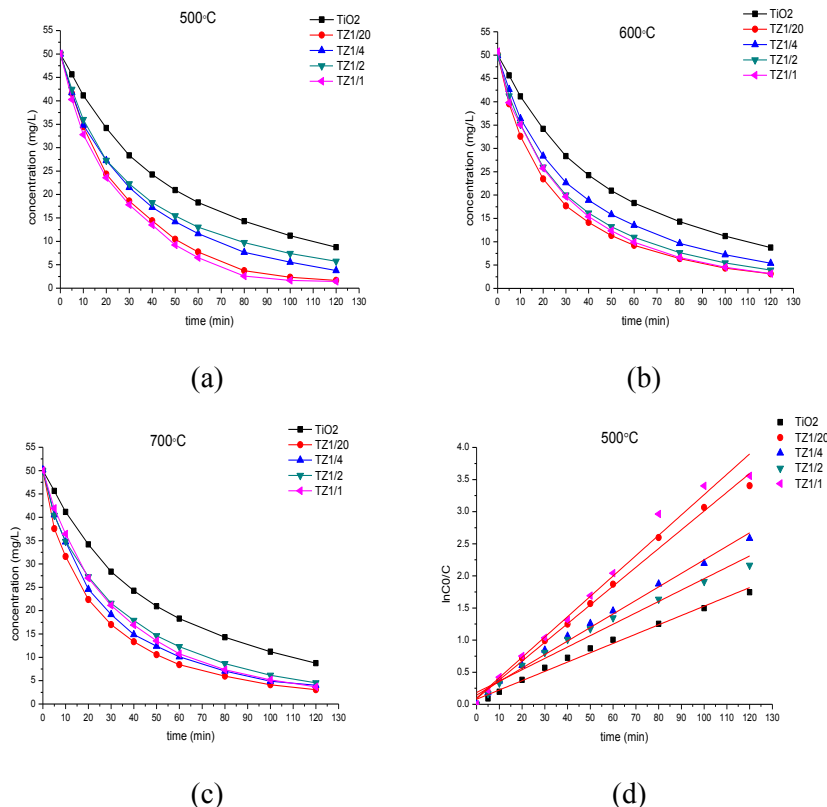


Fig. 2. Photocatalytic degradation of TCS and kinetic of photodegradation of TCS at photocatalyst calcined at 500 °C (a) 600 °C (b) 700 °C (d) kinetics at 500 °C.

calcination temperature increased to 600 and 700 °C, while the temperature of anatase to rutile was 550-600 °C [20, 21]. Zr^{4+} is considered to retard the transformation by forming interstitial Ti^{3+} cations that suppress atomic transport in the anatase structure [22].

Photocatalytic experiments

The experiment of photocatalytic degradation of TCS in aqueous suspensions of the $\text{TiO}_2\text{-ZrO}_2$ photocatalysts at various calcined temperatures and Ti/Zr molar ratios were shown in the Fig.2.

The photocatalytic behavior of commercial TiO_2 was measured as a reference. It could be clearly seen from Fig.2a, Fig.2b and Fig.2c that all the degradations of TCS by composite semiconductors were better than that of commercial TiO_2 via modified by ZrO_2 . In the TiO_2 photocatalytic degradation, the concentration of TCS dropped by 63.4% after UV irradiation for 60min. As for $\text{ZrO}_2\text{-TiO}_2$ photocatalytic process, TZ500-d sample exhibited a much higher efficiency in photocatalytic

degradation. The concentration decreased rapidly during 120 min from 50.09 mg/L to 1.43 mg/L, and 87.02 % TCS was removed after 60 min and nearly completely degraded in 120 min of irradiation.

The removal of TCS decreased with the decreasing of Ti/Zr molar ratio was shown in the Fig.2. ZrO_2 could raise the surface area of the samples that had been reported [23]. The surface area was becoming smaller that could provide surface sites which could adsorb reactants molecules such as TCS and hydroxyl group which was favor for forming hydroxyl radicals ($\cdot\text{OH}$) to enhance photocatalytic activity was becoming smaller. Simultaneously, ZrO_2 could be a charge separation centre to enhance the charge trapping and inhibit the e^-/h^+ pair recombination [23]. However, the degradation efficiency on Ti/Zr 1/20 was higher than Ti/Zr 1/4 and 1/2. It might be two possible reasons for this phenomenon: one was that surface sites was provided by doping with much more amount of ZrO_2 that was mentioned above; the other was that the recombination of electron and hole was decreased

doping excess amount of ZrO₂. It is known that separation of electron and hole might take place in the binary oxide of TiO₂ and ZrO₂ [24]. In this process, electrons and holes produced both by TiO₂ and ZrO₂ would be recombined with each other to reduce the photocatalytic activity. However, comparing with Ti/Zr 1/4 and 1/2, there was much more electrons and holes left to enhance the photocatalytic efficiency after recombined with that produced by TiO₂ in the condition of excess amount of ZrO₂.

The plots of ln(C₀/C) versus irradiation time are shown in Fig.2b, and they give straight lines. TCS photodegradation followed the pseudo-first-order kinetics with respect to different samples of Ti/Zr molar ratios that demonstrated by experimental data and the rate constant and coefficient were shown in Table 1. The calcination temperature also influences the photocatalytic efficiency. The degradation of TCS was a little decreasing with the elevation of calcination temperatures at the same Ti/Zr molar ratio, which maybe was because of the growth of particle size that had been proved by XRD.

CONCLUSIONS

Triclosan, as one of PPCPs have been detected in aquatic environment and have been harmful for human health. Photocatalysis, as one of promise advanced oxygen technologies, has good degradability for triclosan.

Photocatalyst of TiO₂-ZrO₂ was successfully prepared by wet impregnation method. A series of Ti/Zr molar ratios at different calcination temperatures was applied to photocatalytic degradation of target contaminant. The synthesized photocatalysts were more efficient than commercial TiO₂. The most photoactive catalyst was calcined at 500°C at 1:20 and 1:1 molar ratio of Ti/Zr, respectively

ZrO₂ doping TiO₂ can improve the ability of photodegradation probably due to mutually working effects that the surface area are enhanced by doping with Zr⁴⁺ which is also as a charge separation centre for electrons trapping to improve the degradation of tricolsan.

Table 1. Kinetic constant for sample at different calcination temperatures

Sample	Calcination temperature (°C)	Rate constant (k)	R ²
TiO ₂	18°C	0.0145	0.9893
TZ-1/20	500°C	0.0292	0.9932
	600°C	0.0225	0.9776
	700°C	0.0225	0.9776
TZ-1/4	500°C	0.0210	0.9912
	600°C	0.0182	0.9842
	700°C	0.0182	0.9842
TZ-1/2	500°C	0.0177	0.9741
	600°C	0.0208	0.9823
	700°C	0.0208	0.9823
TZ-1/1	500°C	0.0316	0.9819
	600°C	0.0227	0.9872
	700°C	0.0227	0.9872

Acknowledgements: This work was supported by National Science and Technology Major Project for Water Pollution Control and Treatment of PR China (Grant No.2008ZX07425-007).

REFERENCES

1. K. Aranami, J.W. Readman, *Chemosphere*, **66**, 1052 (2007).
2. G.G. Ying, X.Y. Yu, R.S. Kookana, *Environ. Pollution*, **150**, 300 (2007).
3. H. Singer, S. Muller, C. Tixier, L. Pillonel, *Environ. Sci. Technol.*, **36**, 4998 (2002).
4. D.W. Kolpin, E.T. Furlong, M.T. Meyer, E.M. Thurman, S.D. Zaugg, L.B. Barber, H.T. Buxton, *Environ. Sci. Technol.*, **36**, 1202 (2002).
5. A. Lindstrom, I.J. Buerge, T. Poiger, P.A. Bergqvist, M.D. Muller, H.R. Buser, *Environ. Sci. Technol.*, **36**, 2322 (2002).
6. M. Allmyr, M. Adolfsson-Erici, M.S. McLachlan, G. Sandborgh-Englund, *Sci. Total Environ.*, **372**, 87 (2006).
7. A.D. Dayan, *Food. Chem. Toxicol.*, **45**, 125 (2007).
8. K.N. Knust, M.P. Foley, M.S. Mubarak, S. Skljarevski, K. Raghavachari, D.G. Peters, *J. Electroanal. Chem.*, **Vol 638**, 100-108 (2010).
9. I. Sires, N. Oturan, M.A. Oturan, R.M. Rodriguez, J.A. Garrido, E. Brillas, *Electrochim. Acta*, **52**, 5493 (2007).
10. Z.L. Chen, Q.J. Song, G.Q. Cao, Y.F. Chen, *Chem. Papers*, **62**, 608 (2008).

11. L. Sanchez-Prado, R. Barro, C. Garcia-Jares, M. Llompарт, M. Lores, C. Petrakis, N. Kalogerakis, D. Mantzavinos, E. Psillakis, *Ultrason. Sonochem.*, **15**, 689 (2008).
12. W. Choi, M.R. Hoffmann, Abstracts of Papers - American Chemical Society Publications, 200-209 (1995).
13. M.R. Hoffmann, S.T. Martin, W.Y. Choi, D.W. Bahnemann, *Chem. Rev.*, **95**, 69 (1995).
14. J.C. Yu, J.G. Yu, W.K. Ho, Z.T. Jiang, L.Z. Zhang, *Chem. Mater.*, **14**, 3808 (2002).
15. G.H. Tian, K. Pan, H.G. Fu, L.Q. Jing, W. Zhou, *J. Hazard. Mater.*, **166**, 939 (2009).
16. X.Z. Fu, L.A. Clark, Q. Yang, M.A. Anderson, *Environ. Sci. Technol.*, **30**, 647 (1996).
17. X.J. Chen, H.P. Wang, B.A. Wang, Proc. International conference on advanced fibers and polymer materials, Vol. 1/2, 211 (2007).
18. M.C. Hidalgo, G. Colon, J.A. Navio, A. Macias, V. Kriventsov, D.I. Kochubey, M.V. Tsodikov, *Catal. Today*, **128**, 245 (2007).
19. M. Sato, H. Shibata, H. Sakai, M. Abe, M. Matsumoto, *Trans. Mater. Res. Soc.*, **33**, 111 (2008).
20. X.Z. Ding, X.H. Liu, *J. Mater. Res.*, **13**, 2556 (1998).
21. J. Wu, C.Y. Yeh, *J. Mater. Res.*, **16**, 615 (2001).
22. K. Okada, N. Yamamoto, Y. Kameshima, A. Yasumori, K. MacKenzie, *J. Am. Ceram. Soc.*, **84**, 1591 (2001).
23. Y.M. Wang, S.W. Liu, M.K. Lu, S.F. Wang, F. Gu, X.Z. Gai, X.P. Cui, J. Pan, *J. Mol. Catal. A-Chem.*, **215**, 137 (2004).
24. X.Z. Fu, L.A. Clark, Q. Yang, M.A. Anderson, *Environ. Sci. Technol.*, **30**, 647 (1996).

ИЗСЛЕДВАНЕ НА ПРЕПАРАТ ОТ TiO₂-ZrO₂ И ОПРЕДЕЛЯНЕ НЕГОВАТА ЕФЕКТИВНОСТ СПРЯМО ТРИКЛОЗАН

Ксу Хан, Лей Кай, Хуипинг Денг, Джун Ши*

Лаборатория по водната среда в река Янцизъ, Министерство на образованието, Университет Тонгдзю, Шанхай, Китай

Постъпила на 19 април, 2014 г

(Резюме)

Успешно е синтезиран фотокатализатор от титанов диоксид и циркониев диоксид (TiO₂-ZrO₂) с помощта на зол-гел метода и съдържащи търговски титанов диоксид и циркониев диоксид - хлорид като прекурсор. Използвана е прахова рентгенова дифракция за да се охарактеризират фазите в катализатора. Не е открит рутил дори при 700°C. Използвано е фотокаталитичното разпадане на триколзан за да се изпита активността на катализатора при различни моларни отношения Ti/Zr и температури на калциниране. Смесеният катализатор TiO₂-ZrO₂ е по-активен от търговския TiO₂. Фотодеградационната активност бе близо до моларното съотношение Ti/Zr 1/20 и 1/1. Най-високо разпадане бе наблюдавано при 500 °C.

Synthesis and antimicrobial activity of some new 1 β -methylcarbapenem derivatives having pyrrolidine or piperidine moieties

Xudong Jiang^{1,2}, Zhedong Yuan^{2*}, Xiong Yu², Weicheng Zhou²

¹ Department of Biological and Chemical Engineering, Guangxi University of Science and Technology, 545006 Liuzhou, China;

² State Key Lab of New Drug and Pharmaceutical Process, Shanghai Institute of Pharmaceutical Industry, 200437 Shanghai, China

Submitted April 19, 2014

A series of 1 β -methylcarbapenems having pyrrolidine or piperidine moieties were synthesized and in vitro antibacterial activities against both Gram-positive and Gram-negative bacteria were tested and the effect of substituent on the pyrrolidine ring or piperidine ring was investigated. The antibacterial activity of these carbapenem, **6b** and **6g** showed good results, and were worth further studying.

Key words: synthesis; 1 β -Methylcarbapenem; antibacterial activity

INTRODUCTION

The rising emergence of bacteria resistant to existing antimicrobial therapy is responsible for the prevailing interest in new agents for the fight against these threats to human health [1]. Carbapenem is a novel class of β -lactam antibiotics developed in 1970's, which have used in clinical treatment of severe bacterial infections caused by multidrug resistant strains [2]. Carbapenems are one of the most potent types of antimicrobial agents and are among those used as last resort against infections in the clinical field [3], imipenem, panipenem, meropenem, biapenem, doripenem and tebipenem have already been clinically used. In the cases of meropenem, biapenem and ertapenem, doripenem and tebipenem introduction of a 1 β -methyl group to the carbapenem skeleton enhances metabolic stability to renal dehydropeptidase-I (DHP-I) and leads to high antimicrobial potency.

The carbapenem compounds which have a 1 β -methylcarbapenem skeleton having a potential antimicrobial activity against Gram-negative and Gram-positive bacteria and are useful as medicines or as intermediates for compounds possessing antimicrobial activity, studies on the carbapenem derivatives have been widely develop. We have studied on the synthesis of a variety of 1 β -methylcarbapenem derivatives and found that the

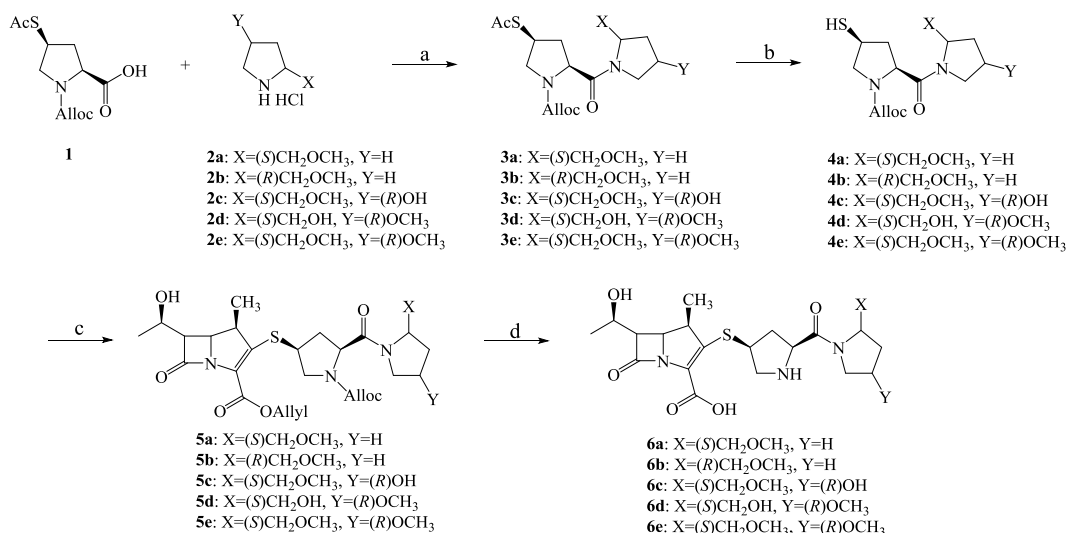
carbapenem compounds having (3S)-pyrrolidin-3-ylthio group at the C-2 position show good antimicrobial, and a large number of derivatives have been synthesized and investigated [4-9].

In this paper, we described the synthesis and antimicrobial activity of new 1 β -methylcarbapenems having 5'-pyrrolidine and piperidine derivatives substituted pyrrolidin-3'-ylthio group as C-2 side chain and our approach to improve the antimicrobial activity of the carbapenems is discussed.

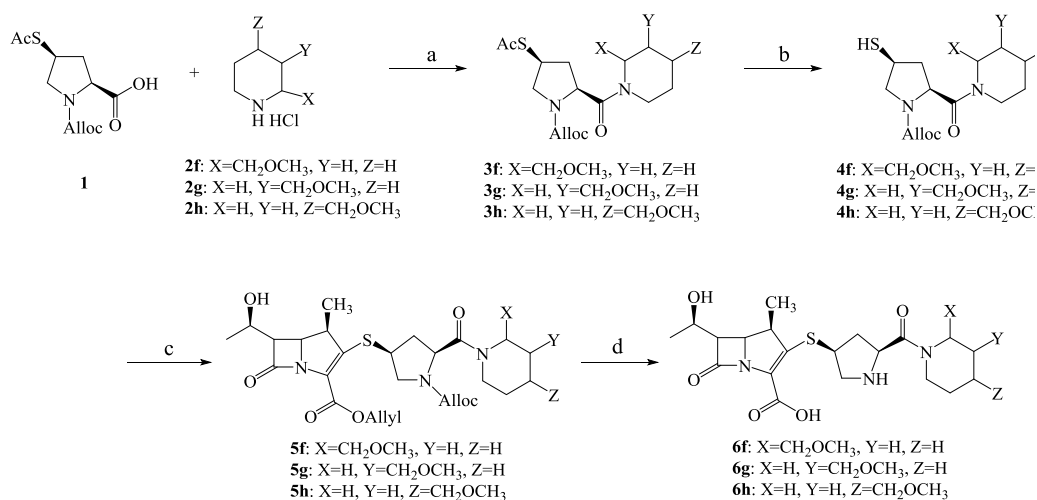
INVESTIGATIONS AND RESULTS

Synthesis of the target compounds was conducted as shown in Scheme 1 and Scheme 2. The starting material (compound 1), (2S, 4R)-4-acetylthio-1-(allyloxycarbonyl)pyrrolidine-2-carboxylic acid was prepared according to the literature [10]. The starting material, compounds (2a-h) was prepared according to the literature [11-13]. The preparation of compounds (3a-h) was achieved by using followed the method described, Compound 1 was activated with ethyl chloroformate followed by reaction with compounds (2a-h) to afford. Then the compounds

* To whom all correspondence should be sent.
E-mail: xudong_j@126.com



Scheme 1. Scheme of synthesis of 1β-Methylcarbapenem compounds **6a-e** (a) ethyl chloroformate/Et₃N/THF/-5°C/5h; (b) 4N NaOH/MeOH/0-5°C/3h; (c) DIPEA/DCM/-5°C/5h; (d) NDMBA/Ph₃P/Pd(PPh₃)₄/THF/-5-0°C/6h.



Scheme 2. Scheme of synthesis of 1β-Methylcarbapenem compounds **6f-h** (a) ethyl chloroformate/Et₃N/THF/-5°C/5h; (b) 4N NaOH/MeOH/0-5°C/3h; (c) DIPEA/DCM/-5°C/5h; (d) NDMBA/Ph₃P/Pd(PPh₃)₄/THF/-5-0°C/6h.

were readily hydrolyzed with 4N NaOH aqueous in methanol to give mercaptan compounds (**4a-h**), which were used in the next reaction without purification. A mixture of 1β-methylcarbapenem nucleus allyl (1R, 5S, 6S)-2-(diphenylphosphoryloxy)-6-[(R)-1-hydroxy-ethyl]-1-methylcarbapen-2-em-3-carb-oxylate was prepared according to the literature [14] and mercaptan compounds (**4a-h**) in the presence of diisopropylethylamine gave the corresponding carbapenem esters (**5a-h**) in 22.7%–29.3% total yield from compound **1**. Removal of the protecting groups of these compounds by treatment of 1, 3-dimethyl- barbituric acid (NDMBA), Tetrakis-(triphenylphosphine)-palladium(0) (Pd(PPh₃)₄) and Ph₃P gave corresponding carbapenems (**6a-h**) [15, 16]. In accordance with the standard agar dilution method, we obtained antimicrobial activity of the derivatives. The in vitro antimicrobial activity of

new 1β-methylcarbapenems **6a-h** having pyrrolidine or piperidine moieties are shown in Table 1. The minimal inhibitory concentrations (MIC) of these compounds were compared with meropenem(MPM) as positive controls. All the compounds exhibited superior antimicrobial activity. Some of the target compounds possess similar or superior activity against some Gram-positive organisms or Gram-negative bacteria than MPM. Against most Gram-positive organisms or Gram-negative bacteria, **6b**, **6h** exhibited interesting antimicrobial activities compared to MPM, but poorer against *Pseudomonas aeruginosa*. As to the substituent of the C-5 on the pyrrolidine side chain, the compounds containing introduction of a pyrrolidine or piperidine moieties slightly lower antimicrobial activity than MPM in most cases, presumably due to increased sterics hindrance to penicillin-binding proteins.

Table 1. In vitro antimicrobial activity (MIC, μ g/ml) of the carbapenem derivatives

	6a	6b	6c	6d	6e	6f	6g	6h	MPM
<i>Staphylococcus aureus</i> 26003	0.78	0.39	0.78	3.13	0.39	0.78	6.25	0.39	0.39
<i>pneumococcal pneumonia</i> 31002	0.098	0.098	0.195	0.78	0.39	0.098	1.56	0.098	0.098
<i>Staphylococcus albus</i> 26101	0.78	0.39	1.56	3.13	0.78	1.56	6.25	0.39	0.39
<i>Enterococcus</i> 32220	0.39	0.39	0.195	0.195	0.39	3.13	12.5	6.25	6.25
<i>gamma streptococcus</i> 32206	6.25	12.5	12.5	12.5	12.5	6.25	25	12.5	6.25
<i>Staphylococcus epidermidis</i> 26069	0.78	0.39	1.56	3.13	0.78	0.78	3.13	0.39	0.195
<i>Shigella boydii</i> 51313	0.098	<0.049	0.098	0.195	0.098	0.195	0.39	<0.049	<0.049
<i>Proteus mirabilis</i> 49005	0.098	0.098	0.195	0.195	0.098	0.195	0.78	<0.049	<0.049
<i>Proteus vulgaris</i> 49085	0.195	<0.049	0.195	0.195	0.195	0.195	0.78	<0.049	<0.049
<i>Morgan proteus</i> 49086	0.098	<0.049	0.098	0.195	0.098	0.195	0.39	<0.049	<0.049
<i>Pseudomonas aeruginosa</i> 10124	>25	6.25	>25	12.5	>25	>25	>25	6.25	0.78
<i>Pneumobacillus</i> 46101	0.39	0.195	0.195	0.39	0.39	0.39	0.78	0.098	<0.049
<i>Salmonella enteritidis</i> 50041	0.098	<0.049	0.098	0.195	0.195	0.195	0.39	<0.049	<0.049
<i>Salmonella typhi</i> 50097	0.098	<0.049	0.098	0.195	0.098	0.195	0.39	<0.049	<0.049
<i>Citrobacter</i> 48017	0.098	<0.049	0.098	0.195	0.098	0.39	0.39	<0.049	<0.049
<i>Aerobacter aerogenes</i> 45102	0.195	<0.049	0.39	0.78	0.39	0.78	0.78	<0.049	<0.049
<i>Serratia marcescens</i> 41002	0.195	<0.049	0.195	0.195	0.39	0.78	0.78	<0.049	<0.049
<i>Shigella sonnei</i> 51081	0.098	<0.049	0.195	0.195	0.098	0.195	0.39	<0.049	<0.049
<i>Shigella flexneri</i> 51573	0.098	<0.049	0.098	0.098	0.098	0.098	0.39	<0.049	<0.049
<i>Escherichia Coli</i> 44102	0.098	<0.049	0.39	0.195	0.195	0.195	0.39	<0.049	<0.049

EXPERIMENTAL

All reagents were purchased from commercial sources such as SCRC (www.reagent.com.cn), Aladdin (www.aladdin-reagent.com) and used without further purification. The $^1\text{H-NMR}$ spectra (400 MHz) were measured on a DRX-400 spectrometer using DMSO-*d*₆ or CDCl₃ or D₂O as solvent and TMS as an internal standard. Chemical shifts were expressed in ppm units. Multiplicities were recorded as s (singlet), brs (broad singlet), d (doublet), t (triplet), q (quartet), m (multiplet). Mass spectra were obtained on a LC-MSD 1100 spectrometer with ESI.

Spectra data of compounds **6a-6h**: the titled compounds were new compounds and their structures were fully confirmed by $^1\text{H NMR}$ and ESI-MS. **6a**: Yield: 33.1% $^1\text{H-NMR}$ (400Hz, D₂O): δ 1.16 (d,3H, *J*=7.2Hz, β -CH₃), 1.24(d,3H,*J*=6.4Hz, CH₃CHOH), 1.77~1.94 (m,5H, pyrrolidine H), 3.03~3.10(m, 1H, pyrrolidine H), 3.25~3.33(m,4H, -CH₂O- and pyrrolidine H and H₆), 3.42~3.65(m, 6H, and pyrrolidine H and -OCH₃), 3.80~3.84(m,2H, pyrrolidine H), 3.94~3.98(m, 2H, H₁ and pyrrolidine H), 4.10~4.16 (m,2H, H₅ and H₈); ESI-MS: *m/z* = 454.12 [M+H]⁺. **6b**: Yield: 34.8%; $^1\text{H-NMR}$ (400Hz, D₂O): δ 1.22 (d,3H,*J*=7.2Hz, β -CH₃), 1.30(d,3H,*J*=6.4Hz, CH₃CHOH), 1.88~2.06 (m,5H, pyrrolidine H), 3.04~3.11(m,1H, pyrrolidine H), 3.32~3.39(m,4H, -CH₂O- and pyrrolidine H and H₆), 3.45~3.61(m,6H,

pyrrolidine H and -OCH₃), 3.75~3.79(m,2H, pyrrolidine H), 4.01~4.06(m,2H, H₁ and pyrrolidine H), 4.23~4.28(m, 2H, H₅ and H₈) ; ESI-MS: *m/z* = 454.17 [M+H]⁺. **6c**: Yield: 37.3%; $^1\text{H-NMR}$ (400Hz, D₂O): δ 1.13(d,3H,*J*=7.2Hz, β -CH₃), 1.24(d,3H, *J*=6.4Hz,CH₃CHOH), 1.82-1.99 (m, 3H), 2.93-2.98(m, 1H, pyrrolidine H), 3.22-3.27(m, 2H, -CH₂O-), 3.39-3.46(m,3H, pyrrolidine H and H₆), 3.45(s, 3H, -OCH₃), 3.59-3.63(m, 2H, pyrrolidine H), 3.71-3.74(m, 1H, pyrrolidine H), 3.90-3.95(m, 2H, pyrrolidine H), 4.08-4.13(m, 2H, H₁ and pyrrolidine H), 4.28-4.33(m, 2H, H₅ and H₈). ESI-MS: *m/z* = 470.22 [M+H]⁺. **6d**: Yield: 45.1%; $^1\text{H-NMR}$ (400Hz, D₂O): δ 1.13(d,3H, *J*=7.2Hz, β -CH₃), 1.24(d,3H, *J*=6.4Hz, CH₃CHOH), 2.09-2.23(m, 3H), 2.99-3.06(m, 1H, pyrrolidine H), 3.14-3.23 (m, 2H, -CH₂O-), 3.25(s, 3H, -OCH₃), 3.40-3.48(m,3H, pyrrolidine H and H₆), 3.60-3.74(m, 3H, pyrrolidine H), 3.79-3.86(m, 2H, pyrrolidine H), 4.03-4.06(m, 2H, H₁ and pyrrolidine H), 4.20-4.27(m, 2H, H₅ and H₈). ESI-MS: *m/z* = 470.23 [M+H]⁺. **6e**: Yield: 42.3%; $^1\text{H-NMR}$ (400Hz, D₂O): δ 1.13(d,3H,*J*=7.2Hz, β -CH₃), 1.18(d,3H,*J*=6.4Hz,CH₃CHOH), 1.76-1.99 (m, 3H, pyrrolidine H), 2.84-2.89(m, 1H, pyrrolidine H), 3.18~3.32(m,5H, -CH₂O- H and -OCH₃), 3.39-3.46(m,6H, and pyrrolidine H and -OCH₃ and H₆), 3.57-3.66(m, 3H, pyrrolidine H), 3.87-3.90(m, 2H,

pyrrolidine H), 3.94-4.00(m, 2H, H₁ and pyrrolidine H), 4.09-4.15(m, 2H, H₅ and H₈). ESI-MS: $m/z=484.23$ [M+H]⁺. **6f**: Yield: 39.6%; ¹H-NMR(400Hz, D₂O): δ 1.21(d, 3H, $J=7.6$ Hz, β -CH₃), 1.30(d, 3H, $J=6.0$ Hz, CH₃CHOH), 1.47~1.58(m, 1H, piperidine H), 1.73~1.85(m, 4H, piperidine H), 2.85~3.04(m, 2H, pyrrolidine H), 3.15~3.22(m, 4H, -CH₂O- and pyrrolidine H and H₆), 3.42~3.57(m, 6H, -OCH₃ and piperidine H), 3.59~3.64(m, 1H, pyrrolidine H), 3.73~3.78(m, 2H, pyrrolidine H), 3.87~4.02(m, 2H, H₁ and pyrrolidine H), 4.10~4.17(m, 2H, H₅ and H₈); ESI-MS: $m/z=468.21$ [M+H]⁺. **6g**: Yield: 35.4%; ¹H-NMR(400Hz, D₂O): δ 1.24(d, 3H, $J=7.2$ Hz, β -CH₃), 1.32(d, 3H, $J=6.4$ Hz, CH₃CHOH), 1.51~1.57(m, 1H, piperidine H), 1.78~2.02(m, 4H, piperidine H), 2.98~3.13(m, 2H, pyrrolidine H), 3.16~3.26(m, 1H, H₆), 3.34~3.46(m, 7H, -OCH₃ and piperidine H and -CH₂O-), 3.48~3.52(m, 2H, piperidine H), 3.61~3.71(m, 1H, pyrrolidine H), 3.76~3.83(m, 2H, pyrrolidine H), 4.05~4.12(m, 2H, H₁ and pyrrolidine H), 4.16~4.30(m, 2H, H₅ and H₈); ESI-MS: $m/z=468.17$ [M+H]⁺. **6h**: Yield: 41.2%; ¹H-NMR(D₂O): δ 1.14(d, 3H, $J=6.8$ Hz, β -CH₃), 1.22(d, 3H, $J=7.6$ Hz, CH₃CHOH), 1.62~1.82(m, 5H, pyrrolidine H), 2.72~2.78(m, 1H, pyrrolidine H), 3.04~3.09(m, 3H, pyrrolidine H and -CH₂-NHSO₂NH₂), 3.18~3.21(m, 1H, H₆), 3.56~3.64(m, 3H, pyrrolidine H), 3.77~3.83(m, 2H, pyrrolidine H), 3.93~3.97(m, 2H, H₁ and pyrrolidine H), 4.09~4.16(m, 2H, H₅ and H₈); ESI-MS: $m/z=468.27$ [M+H]⁺.

CONCLUSIONS

A series of 1 β -methylcarbapenems having pyrrolidine or piperidine moieties have been prepared from (2*S*, 4*R*)-4-acetylthio-1-(allyloxycarbonyl) pyrrolidine-2-carboxylic acid (**1**) in the reaction with the corresponding pyrrolidine or piperidine derivatives (**2a-h**). Obtained derivatives were determined their antimicrobial activity by the standard agar dilution method. Then the MIC values

were calculated and compared with standard (MPM). We have found the derivatives exhibited superior antimicrobial activity, among these compounds **6b** and **6h** have antimicrobial activities higher than others, and were worth further studying. Due to increased sterics hindrance to penicillin-binding proteins, the derivatives slightly lower antimicrobial activity than MPM in most cases.

Acknowledgements: This work was financially supported by National Major New Drug Creation Program (2009JX090301-007), Shanghai outstanding academic leaders Plan (09XD1423100) and Guangxi education department science research Foundation (201106LX396).

REFERENCES

1. I. Kawamoto, *Drugs Future*, **2**, 181 (1998).
2. M. Doddareddy, Cha J., Cho Y., et al., *Biorg. Med. Chem.*, **13**, 3339 (2005).
3. C. Okereke, *Current Therapeutic Research*, **61**, 289 (2000).
4. S. Ahn, Jeon H., Choi J., et al., *Arch. Pharm.*, **339**, 67 (2006).
5. G. Bonfiglio, G. Russo, G. Nicoletti *Expert opinion on investigational drugs*, **11**, 529 (2002).
6. Oh C., Lee S., Cho J., *Eur. J. Med. Chem.*, **38**, 751 (2003).
7. Lee J., Lee K., Kang Y. et al., *Bioorg. Med. Chem. Lett.*, **13**, 4399 (2003).
8. Lee K.S., Lim J.H., Kang Y.K., et al., *Eur. J. Med. Chem.*, **41**, 1347 (2006).
9. Jeon H.C. KJ-W, Hong J.H., *Eur. J. Med. Chem.*, **41**, 1201 (2006).
10. X.D. Jiang, Lan Liao, *Guangdong Cem. Ind.*, **252**, 207 (2013)
11. H. Sakashita, F. Akahoshi, H. Kitajima, et al., *Biorg. Med. Chem.*, **14**, 3662 (2006).
12. A. Mollica, M.P. Paradisi, K. Varani et al., *Biorg. Med. Chem.*, **14**, 2253 (2006).
13. N. Ohtake, O. Okamoto, S. Kato, et al., *J. Antibiot.*, **50**, 586 (1997).
14. X.D. Jiang, X.F. Cao, Z.D. Yuan, et al., *Chin. J. Antibiot.*, **36**, 132 (2011).
15. M. Reggelin, V. Brenig, C. Zur, *Org. Lett.*, **2**, 531 (2000).
16. I. Kawamoto, Y. Shimoji, O. Kanno, et al., *J. Antibiot.*, **56**, 565 (2003).

СИНТЕЗА И АНТИ-МИКОТИЧНА АКТИВНОСТ НА НЯКОИ НОВИ 1 β -МЕТИЛ-КАРБАПЕНЕМ‘ОВИ ПРОИЗВОДНИ С ПИРОЛИДИНОВИ ИЛИ ПИПЕРИДИНОВИ ПОЛОВИНИ

Ксудонг Джианг^{1,2}, Жедонг Юан^{2*}, Ксионг Ю², Уейченг Жу²

¹ Департамент по биологично и химично инженерство, Научно-технологичен университет Гуангкси, Люжун, Китай

² Държавна лаборатория за нови лекарства и фармацевтични процеси, Институт за фармацевтична индустрия в Шанхай, Шанхай, Китай

(Резюме)

Постъпила на 19 април, 2014 г.

Синтезирани са серия от 1 β -метил-карбапенем с пирролидинови или пиперидинови половини. Изследвана е *in vitro* антибактериалната им активност спрямо Грам-положителни и Грам-отрицателни бактерии. Изследван е ефектът на заместителите в пирролидиновите или пиперидиновите пръстени. Антибактериалната активност на карбапенемите **6b** и **6g** показва добри резултати и си струва бъдещи изследвания.

Spin-glass behavior and magnetic studies of nickel-iron multi-metal Prussian blue complexes $\text{Ni}_{0.75}\text{Cu}_{0.75}[\text{Fe}(\text{CN})_6] \cdot 6.3\text{H}_2\text{O}$

Qing Lin^{1,2}, Zhimin Ji¹, Haifu Huang^{1,3}, Yun He^{1,*}, Jianmei Xu²

¹College of Physics and Technology, Guangxi Normal University, 541004, Guilin, China

²Department of Information Technology, Hainan Medical College, 571199, Haikou, China

³Department of Physics, Nanjing University, Nanjing 210093, China

Submitted April 22, 2014

A multi-metal Prussian blue compound $\text{Ni}_{0.75}\text{Cu}_{0.75}[\text{Fe}(\text{CN})_6] \cdot 6.3\text{H}_2\text{O}$ was prepared by co-precipitation method. The temperature-dependent magnetic susceptibilities of the compound were measured. The Curie-Weiss constants are $C = 1.79 \text{ cm}^3 \cdot \text{K} \cdot \text{mol}^{-1}$, $\theta = 21.53 \text{ K}$. These results indicate that there exists a ferromagnetic exchange interaction in the complexes. It undergoes a paramagnetic to ferromagnetic transition at 20 K. The observed value of coercive field (H_c) and remanent magnetization (M_r) for the compound are 1.12 KOe and $0.92 \mu_B$. This value of H_c is much higher than that for reported most Prussian blue analogues. In addition, there exist a spin-glass behaviour in the compound. This behaviour of χ' and χ'' is typical of a spin glass state, both the in-phase and out-of-phase signals, χ' and χ'' , go through a maximum with strong frequency dependence.

Key words: Prussian blue analogue, molecular alloys magnet, magnetic transition, ferromagnetic, spin glass

INTRODUCTION

In recent years, design and synthesis of molecule-based magnets, involving many fields such as chemistry, physics, materials and life sciences, has become one of the hot research projects on the physics and chemistry nowadays^[1-5]. The Ni-Fe cyanides, whose chemical formula is $A_x\text{Ni}[\text{Fe}(\text{CN})_6]_y \cdot z\text{H}_2\text{O}$ ($A = \text{K}, \text{Mn}, \text{Cs}, \text{Cu}$), have been attracting renewed interest of the material scientists. Prussian Blue analogues are very promising in terms of multi-functionality^[6-9]. Prussian Blue analogues $C_n\text{A}_p[\text{B}(\text{CN})_6]_q \cdot x\text{H}_2\text{O}$ (Molecular structure of Prussian blue analogue compound as show in figure 1) are molecular-based materials with a 3-D network structure which are strongly bridged by cyano groups and exhibit interesting properties like electric field-induced conductance switching, photo-induced magnetization, etc. Hashimoto^[3] have prepared a series of molecular alloy magnet $[\text{A}^{\text{II}}_x\text{B}^{\text{II}}_{1-x}]_y[\text{Cr}^{\text{III}}(\text{CN})_6] \cdot n\text{H}_2\text{O}$, which magnetic parameters like saturation magnetization (M_s), magnetization (M), coercive field (H_c), transition temperature (T_c), compensation temperature (T_{comp}), etc., can be controlled through changing the value of x or metal cations. Ni-Cu-ferro-cyanides have been getting much interest in the contemporary research. At the same time, it is likely to bring a breakthrough in the field of magnetic materials, due to the infinity of molecular synthesis and the diversity of selection for the ions and ligand. So this ideas of synthesis for the type of molecule-based magnets can provide a new way to overcome some difficulties on the study of molecular-based magnet. In this context, we have prepared a multi-metal Prussian blue compound $\text{Ni}_{0.75}\text{Cu}_{0.75}[\text{Fe}(\text{CN})_6] \cdot 6.3\text{H}_2\text{O}$ by co-

precipitation method and the magnetic properties of this compound have been studied.

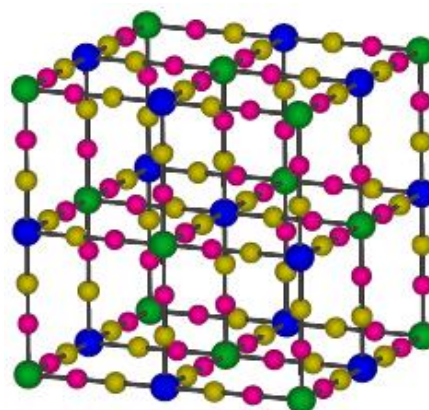


Fig. 1. Structure of Prussian Blue analogs

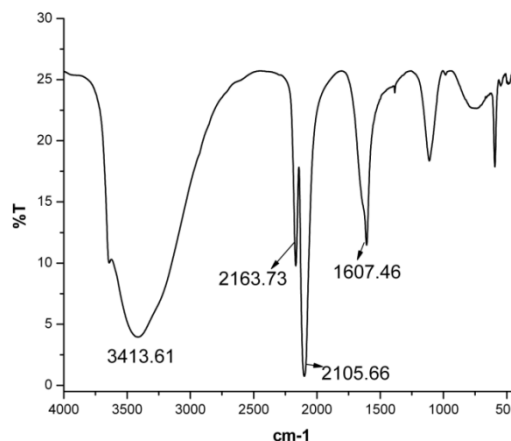


Fig. 2. FT-IR spectrum of the compound

* To whom all correspondence should be sent:
E-mail: yunhe_gxnu@163.com

EXPERIMENTAL

Materials and physical measurements

Material. $\text{NiCl}_2 \cdot 6\text{H}_2\text{O}$, $\text{CuSO}_4 \cdot 6\text{H}_2\text{O}$ and $\text{K}_3\text{Fe}(\text{CN})_6$ are reagent grade, and without further purification. Elemental analysis (Perkin Elmer Corporation PE2400 II), Fourier transform infrared spectroscopy (Perkin Elmer Corporation PE Spectrum One FT-IR spectrometer, KBr pellet) with the radiation spectrum of the $400\text{--}4000\text{ cm}^{-1}$. Magnetization measurements were measured on a Quantum Design MPMS-7 magnetometer in the scope of $2\text{--}300\text{ K}$.

Synthesis of $\text{Ni}_{0.75}\text{Cu}_{0.75}[\text{Fe}(\text{CN})_6] \cdot 6.3\text{H}_2\text{O}$

Polycrystalline compound $\text{Ni}_{0.75}\text{Cu}_{0.75}[\text{Fe}(\text{CN})_6] \cdot 6.3\text{H}_2\text{O}$ was prepared by co-precipitation method. To a solution of $\text{NiCl}_2 \cdot 6\text{H}_2\text{O}$ (1.5mmol, 0.3565g) in water (150 ml) was mixed 150ml $\text{CuSO}_4 \cdot 6\text{H}_2\text{O}$ (1.5mmol, 0.5456g) solution. Then a solution of $\text{K}_3\text{Fe}(\text{CN})_6$ (2mmol, 0.6585g) in water (100 ml) was slowly added to the mixed solution of $\text{NiCl}_2 \cdot 6\text{H}_2\text{O}$ and $\text{CuSO}_4 \cdot 6\text{H}_2\text{O}$, and a solid was precipitated immediately. After sitting for 48 h, the precipitates were filtered, washed repeatedly with water and dried at 45°C . Elemental analysis to measure C, H, N mass ratio: Found: C, 16.94%; H, 3.14%; N, 20.53%; Calc: C, 17.27%; H, 3.04%; N, 20.15%.

IR SPECTRUM ANALYSIS

The IR spectrum of the compound has been recorded over the $400\text{--}4000\text{ cm}^{-1}$ range, and shown in Fig. 2. It shows two bands at 2105.66 and 2163.73 cm^{-1} indicating the existence of two types of cyanide groups in the crystal lattice of the compound. Compared to the compound $\text{K}_3\text{Fe}(\text{CN})_6$ ($\nu_{\text{CN}}=2121.29\text{ cm}^{-1}$), $\text{Ni}_{0.75}\text{Cu}_{0.75}[\text{Fe}(\text{CN})_6] \cdot 6.3\text{H}_2\text{O}$ shows two bands (2105.66 and 2163.73 cm^{-1}) in $2200\text{--}2000\text{ cm}^{-1}$ range, which are consistent with the formation of bridging cyanide groups and there are two different coordination environment, which may due to the change in the spin states and valence states of metal ions. The broad peak at 3413.61 cm^{-1} and 1607.46 cm^{-1} are assigned to the $\nu(\text{O-H})$ of the crystal water stretching vibrations.

MAGNETIC MEASUREMENT

DC magnetic susceptibility

Figure 3 depicts the field-cooled magnetization (M) versus temperature (T) curve at 1 kOe magnetic field (H) in the temperature range $2\text{--}300\text{ K}$. A sharp rise in M is observed around 20 K. Magnetic transition temperature ($T_c=20\text{ K}$) of the compound was estimated from minima of dM/dT vs. T curve, which corresponds to the steepest rise of magnetization with decreasing temperature (as shown in Figure 4). The compound undergoes a paramagnetic to ferro/ferrimagnetic type phase transition at 20 K which is lower than that for the

parent compound, $\text{Ni}_{1.5}[\text{Fe}(\text{CN})_6] \cdot x\text{H}_2\text{O}$ ($T_c=23.6\text{ K}$) [18].

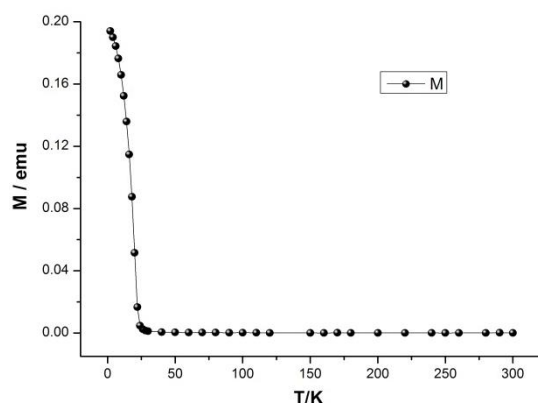


Fig. 3. Temperature dependence of magnet for the compound

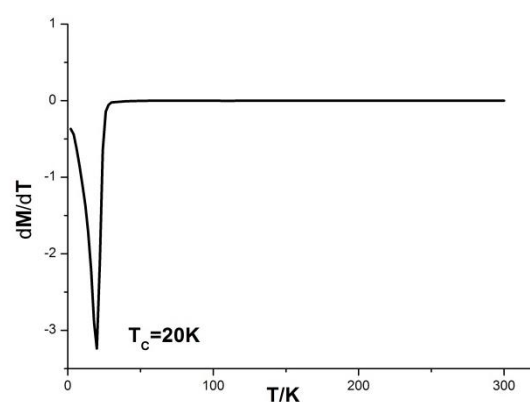


Fig. 4. dM/dT vs T for the compound

The inverse susceptibility as a function of temperature in the paramagnetic state is shown in Fig. 5. The curve rises slowly till the temperature is lowered from 25 to 300 K. The in-phase susceptibility χ_m of $\text{Ni}_{0.75}\text{Cu}_{0.75}[\text{Fe}(\text{CN})_6] \cdot 6.3\text{H}_2\text{O}$ shows a sharp maximum at 2 K. This kind of behaviour is a characteristic of a ferromagnet

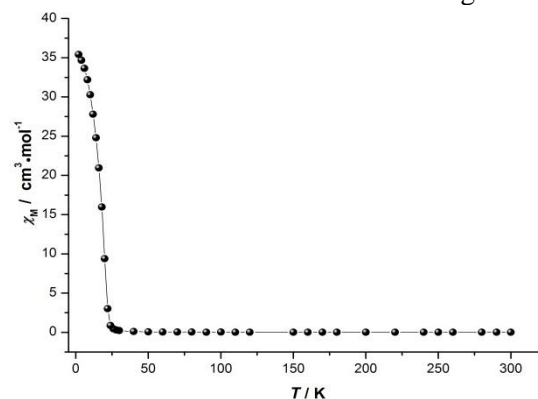


Fig. 5. Temperature dependence of χ_m for the compound.

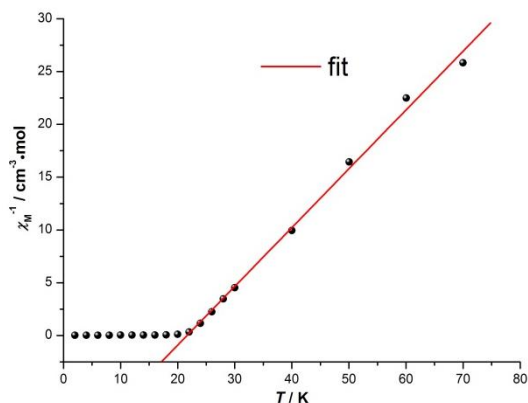


Fig. 6. χ_m^{-1} vs T for the compound.

The magnetic order results from combined ferromagnetic and neighbouring anti-ferromagnetic interactions. High temperature dc susceptibility ($\chi_m=M/H$) is found to obey the Curie-Weiss law. Fig. 6 shows temperature dependence of χ_m^{-1} in the temperature range 2–80 K. The Curie constant, C, and the Curie-Weiss temperature, θ , are determined from a linear fitting of $1/\chi = (T-\theta)/C$ (Curie-Weiss law) to the linear region [10-14]. Fitting yielded that the Curie constant $C=1.79 \text{ cm}^3 \cdot \text{K} \cdot \text{mol}^{-1}$, paramagnetic curie temperature $\theta = 21.53 \text{ K}$. The positive value of θ indicates the existence of a predominant ferromagnetic interaction. The positive value of θ indicates the existence of a predominant ferromagnetic interaction. The values of T_c , θ and C in 100 Oe are different from those values for ferrimagnet $\text{Ni}_{1.5}[\text{Fe}(\text{CN})_6] \cdot x\text{H}_2\text{O}$ [18] and $\text{Cu}_3[\text{Fe}(\text{CN})_6]_2 \cdot 11.6\text{H}_2\text{O}$ ($T_c=18.1 \text{ K}$) [10].

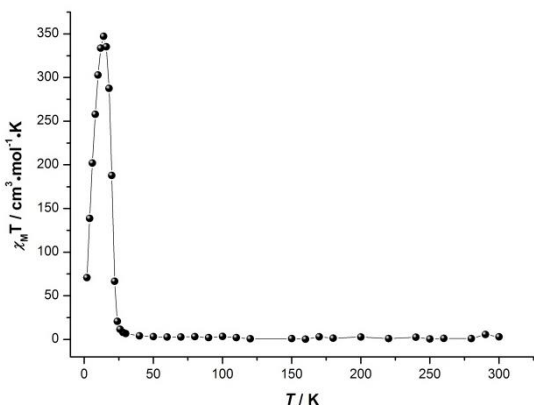


Fig. 7. $\chi_m T$ versus T plot of the compound.

A curve of $\chi_m T$ vs T is shown in Figure.7, the μ_{eff} value at room temperature is $2.82 \text{ cm}^3 \cdot \text{K} \cdot \text{mol}^{-1} \cdot T$. Upon lowering the temperature, and then sharply increase after 25 K with a further decrease of the temperature. The $\chi_m T$ of $\text{Ni}_{0.75}\text{Cu}_{0.75}[\text{Fe}(\text{CN})_6] \cdot 6.3\text{H}_2\text{O}$ shows a sharp maximum value of $350 \text{ cm}^3 \cdot \text{K} \cdot \text{mol}^{-1} \cdot T$ at 14 K, and then finally decreases more rapidly on further

cooling. For a ferrimagnetic compound $\chi_m T$ vs. T curve undergoes to a minima before rising around magnetic ordering temperature [15-18]. As shown in Fig. 8, it goes up in a mild way in the temperature range of 2–300 K, followed by a sharp increase at 25 K. With further lowering of the temperature, μ_{eff} drops down sharply, reaching the minimum values at 2 K, which could be attributed to an intermolecular antiferromagnetic interaction and/or a zero-field splitting (ZFS) effect. This kind of behaviour is a characteristic of a ferrimagnet [18-19].

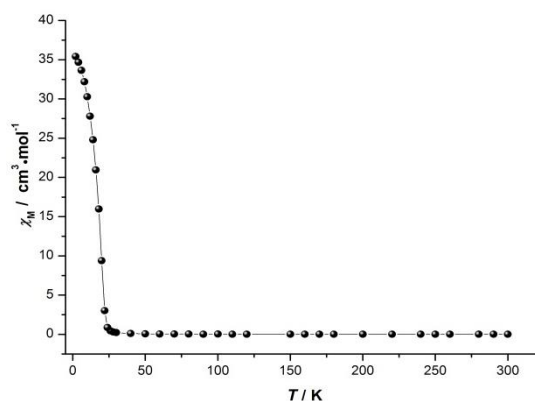


Fig. 5. Temperature dependence of χ_m for the compound.

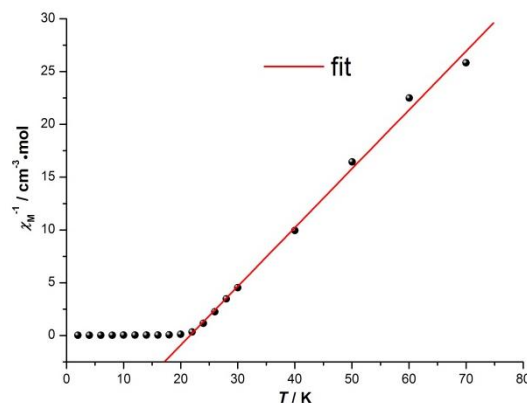


Fig. 6. χ_m^{-1} vs T for the compound.

The magnetic order results from combined ferromagnetic and neighbouring anti-ferromagnetic interactions. High temperature dc susceptibility ($\chi_m=M/H$) is found to obey the Curie-Weiss law. Fig. 6 shows temperature dependence of χ_m^{-1} in the temperature range 2–80 K. The Curie constant, C, and the Curie-Weiss temperature, θ , are determined from a linear fitting of $1/\chi = (T-\theta)/C$ (Curie-Weiss law) to the linear region [10-14]. Fitting yielded that the Curie constant $C=1.79 \text{ cm}^3 \cdot \text{K} \cdot \text{mol}^{-1}$, paramagnetic curie temperature $\theta = 21.53 \text{ K}$. The positive value of θ indicates the existence of a predominant ferromagnetic interaction. The positive value of θ indicates the existence of a predominant ferromagnetic interaction. The values of T_c , θ and C in 100 Oe are different from those values for

ferrimagnet $\text{Ni}_{1.5}[\text{Fe}(\text{CN})_6]_x \cdot x\text{H}_2\text{O}$ [18] and $\text{Cu}_3[\text{Fe}(\text{CN})_6]_2 \cdot 11.6\text{H}_2\text{O}$ ($T_c=18.1\text{K}$) [10].

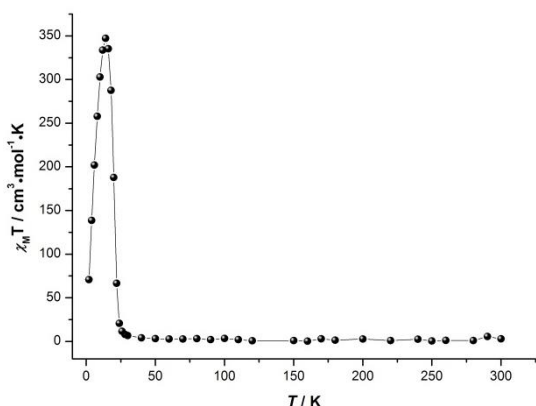


Fig. 7. $\chi_m T$ versus T plot of the compound

A curve of $\chi_m T$ vs T is shown in Figure.7, the μ_{eff} value at room temperature is $2.82 \text{ cm}^3 \cdot \text{K} \cdot \text{mol}^{-1} \cdot T$. Upon lowering the temperature, and then sharply increase after 25 K with a further decrease of the temperature. The $\chi_m T$ of $\text{Ni}_{0.75}\text{Cu}_{0.75}[\text{Fe}(\text{CN})_6] \cdot 6.3\text{H}_2\text{O}$ shows a sharp maximum value of $350 \text{ cm}^3 \cdot \text{K} \cdot \text{mol}^{-1} \cdot T$ at 14 K, and then finally decreases more rapidly on further cooling. For a ferrimagnetic compound $\chi_m T$ vs. T curve undergoes to a minima before rising around magnetic ordering temperature [15-18]. As shown in Fig. 8, it goes up in a mild way in the temperature range of 2–300 K, followed by a sharp increase at 25 K. With further lowering of the temperature, μ_{eff} drops down sharply, reaching the minimum values at 2 K, which could be attributed to an intermolecular anti-ferromagnetic interaction and/or a zero-field splitting (ZFS) effect. This kind of behaviour is a characteristic of a ferrimagnet [18-19].

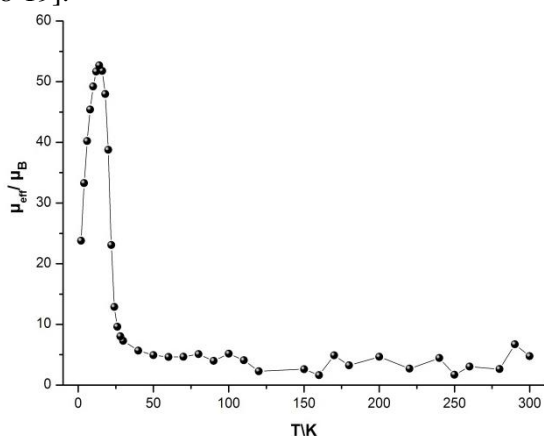
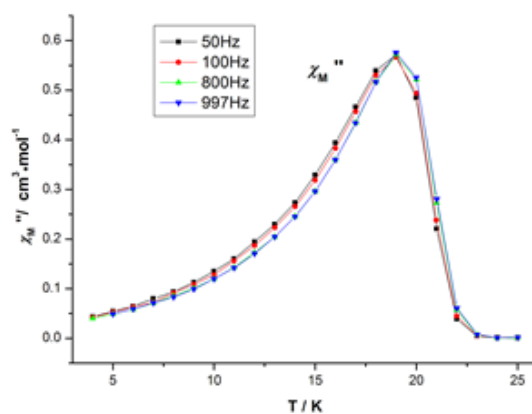


Fig. 8. μ_{eff} versus T plot of for the compound

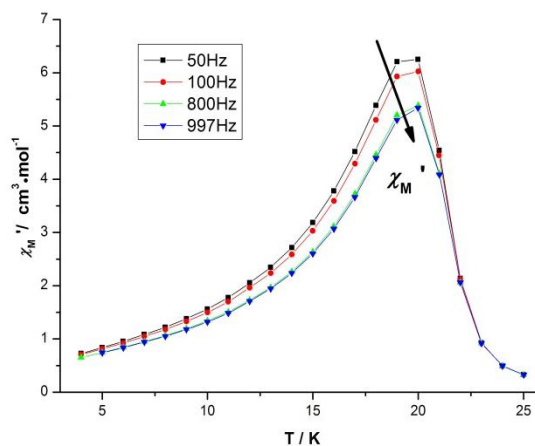
4.2. Ac magnetic susceptibility

At a fixed temperature and a zero dc field or a certain applied field, the χ' and χ'' values were also measured as a function of the ac frequency, f ,

ranging from 50 to 997 Hz (as shown in Figure 9). It is also confirmed that there exist a spin-glass behave in the compound through ac magnetization curves. The temperature dependence of zero-static field ac magnetic susceptibilities show that the in-phase component (χ') has the maximum at about 19 K for frequencies of 50, 100, 800, and 997 Hz and that a significant out-of-phase component (χ'') appears, confirming the long-range ferrimagnetic ordering. The ac susceptibility measurements for the compound also confirm the magnetic phase transition in both complexes, showing a peak in the in-phase (χ') signal and out-of-phase (χ'') signal that is non-zero below 23 K, defining T_c for this magnet. Surprisingly, both the in-phase and out-of-phase signals, χ' and χ'' , go through a maximum with strong frequency dependence.



(a)



(b)

Fig. 9. χ' (T) (Fig. 9b) and χ'' (T) (Fig. 9a) curves of ac magnetic susceptibility of the sample with different frequencies.

On decreasing temperature, the in-phase signals χ' behave: increase abruptly at around 20 K, reach the maximum at about 18 K, and then decrease slowly toward zero. The out-of-phase signals χ'' increase steadily to the maximum around

18-20 K, and then decrease slowly. Although there is no frequency dependence for both the χ'' and χ' , obvious frequency dependence was observed at lower temperatures for both samples (as shown in Figure 10). The frequency dependence of ac magnetic susceptibilities suggests the presence of a degree of spin-glass behavior. The relative shift of frequency (c) is $c = \frac{\Delta T_f}{T_f \Delta \log w}$, which fall within the range typical for the conventional spin-glass system (10^{-2} - 10^{-3}).

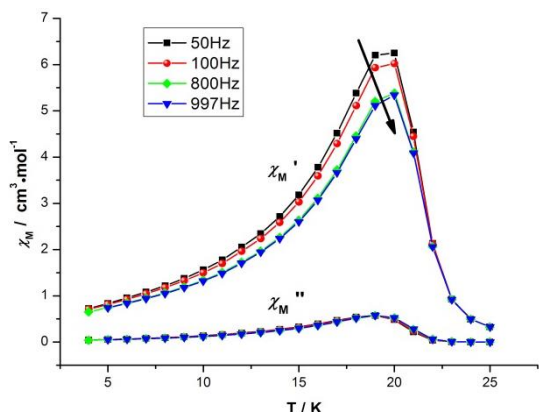


Fig.10. $\chi(T)$ curves of the sample.

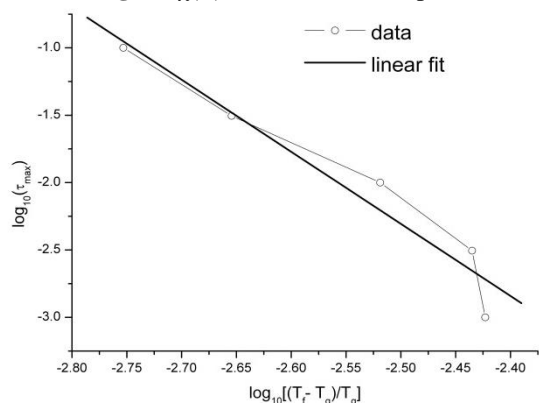


Fig.11. the $\log_{10}((T_f - T_g)/T_g)$ dependence of the $\log_{10}(\tau)$. In order to study the critical temperature for spin glass nature in this system, we utilized the conventional critical slowing-down law [21-23]. This dependence of $T_f(w)$ on frequency (f) is well described by the conventional critical “slowing down” of the spin dynamics as described by

$$\frac{\tau}{\tau_0} \propto \left(\frac{T_f - T_g}{T_g}\right)^{-z\nu} \quad (1)$$

where $\tau \propto 1/\omega$, T_g is the critical temperature for spin glass ordering which is equivalent to the $T_{f(w)}$ ($w \rightarrow 0$), $z\nu$ is a constant component, which fall within the range typical value for different spin-glass materials^[21-22], τ is the average relaxation time corresponding to the frequency of the ac

measurement and τ_0 is the relaxation times for the spin dynamics.

The agreement with Eq.(1) is shown in Fig. 11, where $\log_{10} f$ is plotted as a function of $\log_{10}((T_f - T_g)/T_g)$. The best fit to the form shown in Eq.(1) is obtained by choosing the value of critical temperature for spin glass ordering $T_g = 19\text{K}$, which minimized the least square deviation from a straight line fit.

In fact, the temperature value of the maximum of χ at a given frequency (ω) corresponds to the blocking temperature ($T_N = T_{\max}$), whereby it is assumed that the switching of the oscillating AC field matches the relaxation rate of the magnetization. Both in the real and in the imaginary components the peaks shift to lower temperatures with decreasing frequencies. However the intensities of the peaks behave differently; While for the real component the intensity of the peaks increase with decreasing frequencies, in the imaginary component the peaks decrease with decreasing frequencies. This behaviour of χ'' and χ' is typical of a spin glass state.

4.3. Field-dependent of magnetization and hysteresis behavior

In order to understand further regarding the nature of magnetic ordering, the ferrimagnetic behavior is characterized by the measurements of field-dependent magnetization and hysteresis behavior, as shown in Fig. 12. The observed M_s value is $2.82 \mu_B$, at 50 kOe, but the compound does not reach full saturation.

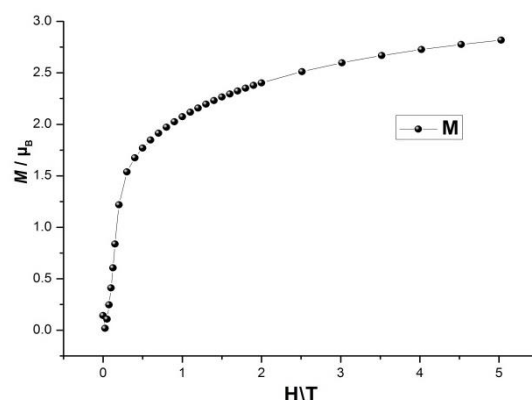


Fig.12. Field-dependent magnetization curves.

The hysteresis curves is measured at 4K, shown in the Fig. 13. The coercive field (H_c) value of 1.12 kOe and remanent magnetization (M_r) value of $0.92 \mu_B$ for the compound. The observed value of H_c is an order of magnitude higher than that for many

other hexacyano analogues [7]. For example, the observed value of H_C for $CsNi[Cr(CN)_6] \cdot 2H_2O$ [6]

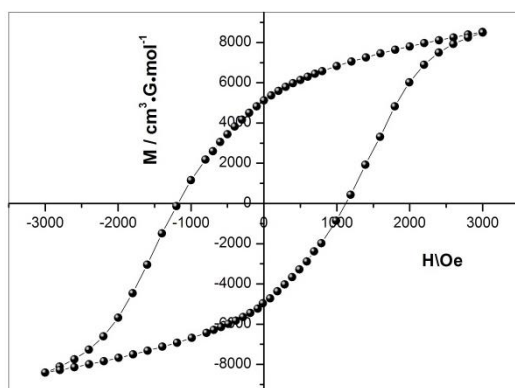


Fig.13. The hysteresis loop for the compound.

is 71 Oe (at 3 K), for $V[Cr(CN)_6]_{0.86} \cdot 2.8H_2O$ [8] is 25 Oe (at 10 K) and for $Cu_{1.5}[Fe(CN)_6] \cdot 6H_2O$ is 240 Oe, (at 4K) [17]. Magnetic parameters like saturation magnetization (M_s), coercive field (H_c), Curie constant (C), Weiss paramagnetic Curie temperature (θ), transition temperature (T_c), are different from the those of the bimetallic cyanide-bridged compounds $Ni_{1.5}[Fe(CN)_6] \cdot xH_2O$ [18] and $Cu_3[Fe(CN)_6]_2 \cdot 11.6H_2O$ [10]. Therefore, synthesis ideas of molecular alloy magnet can be regarded as a synthesis method to expand a new type of magnetic functional materials, which magnetic properties can be tuned and controlled by changing the composition of different transition metal cations [15,17,19].

5. CONCLUSIONS

In the present work we have reported a detailed investigation of magnetic properties of multi-metallic compound $Ni_{0.75}Cu_{0.75}[Fe(CN)_6] \cdot 6.3H_2O$ in which local ferromagnet order coexists with spin-glass behavior. The temperature-dependent magnetic susceptibilities of the compound were measured. The Curie-Weiss constants are $C=1.79 \text{ cm}^3 \cdot \text{K} \cdot \text{mol}^{-1}$, $\theta=21.53 \text{ K}$. These results indicate that there exist a ferromagnetic exchange interaction in the complexes. It undergoes a paramagnetic to ferromagnetic transition at 20K. The observed value of coercive field (H_c) and remanent magnetization (M_r) for the compound are 1.12 KOe and $0.92 \mu_B$. This value of H_c is much higher than that for reported most Prussian blue analogues. In addition, there exist a spin-glass behaviour in the compound. This behaviour of χ' and χ'' is typical of a spin glass state, both the in-phase and out-of-phase signals, χ' and χ'' , go through a maximum with strong frequency

dependence. We thus believe that the Ni-Fe Prussian blue analogue is one of the best examples of molecule-based magnets for the rational design of the magnetic properties.

Acknowledgements: This work was supported by the National Natural Science Foundation of China (NO.11164002, 11364004); Natural Science Foundation of Guangxi (NO.0991092).

REFERENCES

1. S. Ohkoshi, S. Yorozu, O. Sato, T. Iyoda, A. Fujishima, K. Hashimoto, *Appl. Phys. Lett.*, **70**, 1040 (1997).
2. S. Ohkoshi, T. Iyoda, A. Fujishima, K. Hashimoto, *Phys. Rev. B*, **56**, 11642 (1997).
3. S. Ohkoshi, O. Sato, T. Iyoda, A. Fujishima, K. Hashimoto, *Inorg. Chem.*, **36**, 268 (1997).
4. S. Ohkoshi, Y. Abe, A. Fujishima, K. Hashimoto, *Phys. Rev. Lett.* **82**, 1285 (1999).
5. S. Ohkoshi, T. Hozumi, K. Hashimoto, *Phys. Rev. B*, **64**, 132404 (2001).
6. V. Gadet, T. Mallah, I. Castro, M. Verdaguer, *J. Am. Chem. Soc.*, **114**, 9213 (1992).
7. A. Kumar, S.M. Yusuf, *Physica B*, **362**, 278 (2005).
8. S. Ferlay, T. Mallah, R. Ouahes, P. Veillet, M. Verdaguer, *Nature*, **378**, 701 (1995).
9. O. Kahn, *Molecular magnetism*. New York: VCH Publishers, 1993.
10. He Yun, Dai Yao-Dong, Huang Hong-Bo et al. *Chin. Phys. Lett.*, **20**, 1630 (2003).
11. He Yun, Dai Yao-Dong, Huang Hong-Bo, Lin Jun, Hsia Yuan-Fu, *Chin. Phys.*, **13**, 746 (2004).
12. J.A. Mydosh, *Spin Glasses: An Experimental Introduction*, Taylor & Francis, London (1993).
13. M.K. Singh, W. Prellier, M.P. Singh, R.S. Katiyar, J.F. Scott, *Phys. Rev. B*, **77**, 144403 (2008).
14. A. Kumar, S.M. Yusuf, L. Keller, *Physica B*, **386-386**, 444 (2006).
15. Kou H.Z., Gao S., Jin X., *Inorg. Chem.*, **40**, 6295 (2001).
16. J.S. Miller, A.J. Epstein, *Angew. Chem. (Int. Edtn. Engl.)*, **33**, 385 (1994).
17. Ng C.W., Ding J, Shi Y, et al., *J. Phys. Chem. Solids*, **62**, 767 (2001).
18. S. Juszczak, C. Johansson, M. Hanson, A. Ratuszna, G. Małeck, *J. Phys. Condens. Matter*, **6**, 5697 (1994).
19. J.S. Miller, A.J. Epstein, W.M. Reiff, *Chem. Rev.*, **88**, 201 (1988).
20. S. Ohkoshi, K. Hashimoto, *Phys. Rev. B*, **60**, 12820 (1999).
21. K. Binder, A.P. Young, *Rev. Mod. Phys.*, **58**, 801 (1986).
22. J.A. Mydosh, *Spin Glasses: An Experimental Introduction*, Taylor & Francis, London (1993).
23. M.K. Singh, W. Prellier, M.P. Singh, R.S. Katiyar, J.F. Scott, *Phys. Rev. B*, **77**, 144403 (2008).

SPIN-GLASS ПОВЕДЕНИЕ И ИЗСЛЕДВАНЕ НА МАГНИТНИТЕ СВОЙСТВА НА
МНОГОМЕТАЛНИ (НИКЕЛ-ЖЕЛЯЗО) КОМПЛЕКСИ С ФЕРОЦИАНИД
 $\text{Ni}_{0.75}\text{Cu}_{0.75}[\text{Fe}(\text{CN})_6]\cdot 6.3\text{H}_2\text{O}$

Кинг Лин^{1,2}, Джимин Джи¹, Хайфу Хуанг^{1,3}, Юн Хе^{1,*}, Джианмей Ксу²

¹Колеж по физика и технология, Университет Гуанкси, Гуилин, Китай

²Департамент по информационни технологии, Медицински колеж в Хайнан, Найкоу, Китай

³Департамент по физика, Университет в Нанджинг, Нанджинг, Китай

(Резюме)

Постъпила на April 22, 2014

Многометалното съединение $\text{Ni}_{0.75}\text{Cu}_{0.75}[\text{Fe}(\text{CN})_6]\cdot 6.3\text{H}_2\text{O}$ е приготвено чрез съутаяване. Измерен е неговия температурно-зависим магнитен susceptibilitет. Константите на Curie-Weiss са съответно $C = 1.79\text{cm}^3\cdot\text{K}\cdot\text{mol}^{-1}$, $\Theta = 21.53\text{K}$. Тези резултати показват, че в тези комплекси е налице феромагнитно-обменно взаимодействие. Преходът от парамагнитни към феромагнитни свойства става при 20 K. Наблюдаваната коерцетивна сила (H_c) и остатъчното намагнетизиране (M_r) за съединението са съответно 1.12 KOe и 0.92 μ_B . Стойността на H_c е много по-висока от съобщаваната за повечето аналози на фери-фероцианида. Освен това налице е spin-glass поведение на това съединение. Това поведение за χ'' и χ''' е типично за spin glass-състоянието, минавайки през максимум със силна честотна зависимост.

Capillary pressure effect on vacuum drying process of porous medium modeling

Zhijun Zhang^{1*}, Yuekai Zhang¹, Shiwei Zhang¹, Tianyi Su¹, Wenhui Zhang¹,
Yuanhua Xie¹, Lili Zhao²

¹*School of Mechanical Engineering and Automation, Northeastern University,
Shenyang 110004, China*

²*School of Mechanical Engineering, Shenyang University, Shenyang 110044, China*

Submitted April 22, 2014

Drying is the key process in chemical, food and other related industry process. A lot of modeling methods and simulation technology has been used to reveal the heat and mass transfer process. The parameters of modeling are very important because the simulation results are decided by them. The capillary Pressure is condition boundary that is very difficult to gotten. Based on the theory of heat and mass transfer, a coupled model for the porous medium vacuum drying process is constructed. The model is implemented and solved using COMSOL software. The parameter sensitivity analyses of capillary pressure were then examined. The temperature, and moisture characteristics were shown.

Key words: heat and mass transfer, porous medium, vacuum drying, capillary pressure, COMSOL

INTRODUCTION

As the basic unit operation in chemical engineering, drying is the key process in chemical, food and other related industry process. The vacuum drying has been used to corn in china [1–3]. However, the corn vacuum drying theory remains unclear. Hypothesized that corn is a porous medium, the vacuum drying is a complicated heat and mass transfer process that has been the subject of intensive research [4–7]. All vacuum drying models have to address the water phase change during numerical solving. In one method, the vapor pressure is equal to its equilibrium value [8–11]. Another method is non-equilibrium method [12–16]. As the porous medium, the heat and mass transfer in vacuum drying process has been studied with non-equilibrium method by us [17, 18]. In fact, the parameters of modeling are very important because the simulation results are decided by them. But most of the modeling is gotten by the reference [8-11]. It must be clarify the impact of model parameters on

the model predictions [19]. The intrinsic permeability and mass transfer coefficient has been studied by us, it is shown the obviously effect on simulation results [20,21]. Another parameter, capillary pressure also has the very important parameter [22], the details effect should be given.

In this paper, heat and mass transfer of porous medium in the vacuum drying process is implemented by using a non-equilibrium method. The parameter sensitivity analyses of capillary pressure were then examined.

MODEL DEVELOPMENT

Problem Description

A physical one-dimensional (1D) model that explains the drying process is shown in Fig. 1. The heat and mass transfer is considered only in the y direction. The total height of the porous medium is 1cm. The bottom is the heat surface, and the mass is out of from the top surface.

* To whom all correspondence should be sent.
E-mail: zhj_zhang@126.com

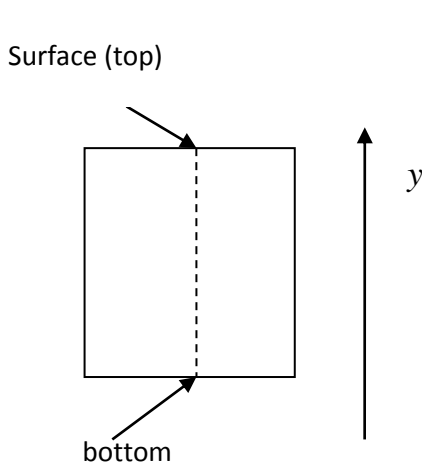


Fig. 1. 1D model of porous medium

Assumption

The porous medium consists of a continuous rigid solid phase, an incompressible liquid phase (free water), and a continuous gas phase that is assumed to be a perfect mixture of vapor and dry air, considered as ideal gases. For a mathematical description of the transport phenomenon in a porous medium, we adopt a continuum approach, wherein macroscopic partial differential equations are achieved through the volume averaging of the microscopic conservation laws. The value of any physical quantity at a point in space is given by its average value on the averaging volume centered at this point.

The moisture movement of the inner porous medium is liquid water and vapor movement; that is, the liquid water could become vapor, and the vapor and liquid water are moved by the pressure gradient. The heat and mass transfer theory could be found in everywhere [8].

The compressibility effects of the liquid phase are negligible, and the phase is homogeneous:

$$\bar{\rho}_w = cste \quad (1)$$

The solid phase is rigid and homogeneous:

$$\bar{\rho}_s = cste \quad (2)$$

The gaseous phase is considered an ideal gas.

This phase ensures that

$$\bar{\rho}_a = \frac{m_a P_a}{RT} \quad (3)$$

$$\bar{\rho}_v = \frac{m_v \bar{P}_v}{RT} \quad (4)$$

$$\bar{P}_g = \bar{P}_a + \bar{P}_v \quad (5)$$

$$\bar{\rho}_g = \bar{\rho}_a + \bar{\rho}_v \quad (6)$$

The assumption of the local thermal equilibrium between the solid, gas, and liquid phases involves

$$\bar{T}_s = \bar{T}_g = \bar{T}_w = \bar{T} \quad (7)$$

Governing Equations

Mass conservation equations are written for each component in each phase. Given that the solid phase is rigid, the following is given:

$$\frac{\partial \bar{\rho}_s}{\partial t} = 0 \quad (8)$$

The averaged mass conservation of the dry air yields

$$\frac{\partial(\varepsilon \cdot S_g \bar{\rho}_a)}{\partial t} + \nabla \cdot (\bar{\rho}_a \bar{V}_a) = 0 \quad (9)$$

For vapor,

$$\frac{\partial(\varepsilon \cdot S_g \bar{\rho}_v)}{\partial t} + \nabla \cdot (\bar{\rho}_v \bar{V}_v) = \dot{i} \quad (10)$$

For free water,

$$\frac{\partial(\varepsilon \cdot S_w \bar{\rho}_w)}{\partial t} + \nabla \cdot (\bar{\rho}_w \bar{V}_w) = -\dot{i} \quad (11)$$

For water, the general equation of mass conservation is obtained from the sum of the conservation equations of vapor (v) and free water (l). The general equation is written as follows:

$$\frac{\partial W}{\partial t} + \nabla \cdot \left\{ \frac{1}{\bar{\rho}_s} (\bar{\rho}_w \bar{V}_w + \bar{\rho}_v \bar{V}_v) \right\} = 0 \quad (12)$$

$$W = \frac{\varepsilon \cdot S_w \bar{\rho}_w + \varepsilon \cdot S_g \bar{\rho}_v}{(1 - \varepsilon) \bar{\rho}_s} \quad (13)$$

For the Darcy flow of vapor,

$$\bar{\rho}_v \bar{V}_v = \bar{\rho}_v \bar{V}_g - \bar{\rho}_g D_{eff} \cdot \nabla \bar{\omega} \quad (14)$$

For the Darcy flow of air,

$$\bar{\rho}_a \bar{V}_a = \bar{\rho}_a \bar{V}_g + \bar{\rho}_g D_{eff} \cdot \nabla \bar{\omega} \quad (15)$$

The vapor fraction in mixed gas is given by

$$\bar{\omega} = \frac{\rho_v}{\rho_g} \quad T_{bottom} = T_h \quad (16) \quad (28)$$

The saturation of free water and gas is

$$S_g + S_w = 1 \quad (17)$$

Where the gas and free water velocity is given by

$$\bar{V}_g = -\frac{k_{m,g} \cdot k_{r,g}}{\mu_g} \cdot (\nabla \bar{P}_g - \rho_g \bar{g}) \quad (18)$$

$$\bar{V}_w = -\frac{k_{m,w} \cdot k_{r,w}}{\mu_w} \cdot (\nabla \bar{P}_w - \rho_w \bar{g}) \quad (19)$$

For bound water,

$$\rho_w \bar{V}_w = -\rho_s \cdot D_b \nabla \left(\frac{\rho_w}{\rho_s} \right) \quad (20)$$

The pressure moving the free water is given by

$$\bar{P}_w = \bar{P} - \bar{P}_c \quad (21)$$

By considering the hypothesis of the local thermal equilibrium, the energy conservation is reduced to a unique equation:

$$\frac{\partial \bar{\rho} \bar{T}}{\partial t} + \nabla \cdot (\bar{\rho}_a \bar{V}_a C_a \bar{T}_a + \bar{\rho}_v \bar{V}_v C_v \bar{T}_v \quad (22)$$

$$+ \bar{\rho}_w \bar{V}_w C_w \bar{T}_w) = \nabla (k_e \cdot \nabla \bar{T}) - \lambda \cdot \dot{i} \quad (23)$$

$$k_e = (1 - \varepsilon)k_s + \varepsilon(S_w + S_g(\omega k_v + (1 - \omega)k_a))$$

$$\bar{\rho} \bar{T} = \bar{\rho}_s \bar{T}_s + \varepsilon \cdot S_g \bar{\rho}_a \bar{T}_a + \varepsilon \cdot S_g \bar{\rho}_v \bar{T}_v \quad (24)$$

$$+ \varepsilon \cdot S_w \bar{\rho}_w \bar{T}_w$$

BOUNDARY AND INITIAL CONDITIONS

The model was run for different parameters. It was heated from the bottom, and the air and vapor was escaped from the top surface. The other boundaries of the model are insulated and impermeable. The boundary conditions are then given as:

B.C. for Eq. (9):

$$\rho_{a,top} = \rho_{a,dryer} \quad (25)$$

B.C. for Eq. (10) [15]:

$$n_{v,top} = -h_m \varepsilon S_g (\rho_{v,top} - \rho_{v,dryer}) \quad (26)$$

B.C. for Eq. (15):

$$n_{w,top} = -h_m \varepsilon S_w (\rho_{v,top} - \rho_{v,dryer}) \quad (27)$$

B.C. for Eq. (21) in bottom:

B.C. for Eq. (21) in top:

$$q_{top} = h(T_{ext} - \bar{T}) + (\lambda + C_w \bar{T}) n_{w,top} + C_v \bar{T} n_{v,top} \quad (29)$$

The initial moisture of the porous medium is represented by the liquid water saturation; different initial water saturation values are used. To compare the effects, drying base moisture content (d. b.) was also used, as shown in Eq. (12). The water phase change rate is used as 1000 that has been studied before [17].

I.C. for Eq. (9):

$$\rho_a = \rho_{a,0} = \frac{P_{amb,0} M_a}{RT_0} \quad (30)$$

I.C. for Eq. (10):

$$\rho_v = \rho_{v,0} = \frac{P_{sat,0} M_v}{RT_0} \quad (31)$$

I.C. for Eq. (11):

$$S_w = S_{w,0} \quad (32)$$

I.C. for Eq. (21) :

$$\bar{T} = T_0 \quad (33)$$

PHASE CHANGE

The evaporation rate is a complex function of drying process in porous medium. The phase change can be formulated in two ways, equilibrium and non-equilibrium. Evaporation of water has been implemented using an equilibrium formulation where water in the solid matrix is assumed to be in equilibrium with water-vapor in the surrounding air. However, recent studies have shown that evaporation is not instantaneous and non-equilibrium exists during rapid evaporation between water-vapor in gas phase and water in solid phase [15]. Furthermore, the equations resulting from an equilibrium formulation cannot be implemented in any direct manner in the framework of most commercial software. The more general expression of non-equilibrium evaporation rate used for modeling of phase change in porous media that is consistent with studies on pure water just mentioned, is given by [14,15],

$$\dot{i} = K_r \frac{m_v (a_w P_{sat} - P_v) S_g \varepsilon}{RT} \quad (34)$$

Here k is a parameter signifying the rate constant of evaporation. The non-equilibrium formulation, given by equation (35), allows precisely this, i.e., k can express the evaporation rate explicitly and therefore would be preferred in a commercial software and is therefore used in our model.

The phase change rate of water could not be decided by any method for porous medium drying [13, 14]. The rate constant parameter k has the dimension of reciprocal time in which phase change occurs. A large value of k signifies that phase change occurs in a small time. For the assumption of equilibrium, k is infinitely large or phase change occurs instantaneously. A very high value of k , however, makes the convergence of the numerical solution difficult.

NUMERICAL SOLUTION

COMSOL Multiphysics 3.5a was used to solve the set of equations. COMSOL is advanced software used for modeling and simulating any physical process described by partial derivative equations. The set of equations introduced above was solved using the relative initial and boundary conditions of each. COMSOL offers three possibilities for writing the equations: (1) using a template (Fick Law, Fourier Law), (2) using the coefficient form (for mildly nonlinear problems), and (3) using the general form (for most nonlinear problems). Differential equations in the coefficient form were written using an unsymmetric-pattern multifrontal method. We used a direct solver for sparse matrices (UMFPACK), which involves significantly more complicated algorithms than solvers used for dense matrices. The main complication is the need to handle the fill-in in factors L and U efficiently.

A two-dimensional (2D) grid was used to solve the equations using COMSOL Multiphysics 3.5a. Given the symmetry condition setting at the left and the right sides, the 2D is applied to the 1D model shown in Fig. 1. The mesh consists of 2×200 elements (2D), and time stepping is 1 (0 s to 100 s of solution), 5 (100 s to 200 s of solution), 20 (200 s to 1000 s of solution), 30 (1000 s to 2000 s of solution), 40 (2000 s to 4000 s of solution), 50

(4000 s to 20000 s of solution) and 100 (20000 s to 50000 s of solution). Several grid sensitivity tests were conducted to determine the sufficiency of the mesh scheme and to ensure that the results are grid-independent. The maximum element size was established as $1e^{-4}$. A backward differentiation formula was used to solve time-dependent variables. Relative tolerance was set to $1e^{-3}$, whereas absolute tolerance was set to $1e^{-4}$. The simulations were performed using a Tongfang PC with Intel Core 2 Duo processor with 3.0 GHz processing speed, and 4096 MB of RAM running Windows 7.

INPUT PARAMETER

For capillary pressure, it has some different presentation,

It was as [8],

$$\bar{P}_{c1} = (aS_w \exp(-bS_w) + c(1-S_w)S_w^{-d})(1 - 2.79 \times 10^{-3}(T - 273.16)) \times 10^5$$

$$a = 1.937, b = 3.785, c = 0.093, d = 1.400 \quad (35)$$

it also was as [11],

$$\bar{P}_{c2} = 1.24 \times 10^4 (S_w + 1 \times 10^{-4})^{-0.61} \quad (36)$$

In the reference [12],

$$\bar{P}_{c3} = 56.75 \times 10^3 (1 - S_w) \exp\left(\frac{1.062}{S_w}\right) \quad (37)$$

The air pressure in the surface or dryer,

$$P_{a,dry} = \begin{cases} (101325 - 1700t) + 2400 & t < 61s \\ 25 & t \geq 61s \end{cases} \quad (38)$$

The parameter details are given in Table 1 and Table 2.

Table 1. Boundary and initial condition

<i>Initial temperature</i>	T_0	273+25	K
<i>Initial air pressure</i>	$P_{atm,0}$	101325	Pa
<i>Initial saturation</i>	$S_{w,0}$	0.3	
<i>Vapor pressure of dryer</i>	$P_{v,dry}$	2000	Pa
<i>Air pressure of dryer</i>	$P_{a,dry}$	Eq.(45)	Pa
<i>Temperature of dryer</i>	T_{ext}	273+28	K

RESULTS AND DISCUSSION

Fig.1 is the results of different capillarity pressure parameter effect moisture and temperature

Table 2. Parameters used in the simulation process

Parameter	Value or Source	Unit
ρ_l	998 [12]	kg m ⁻³
ρ_v	Ideal gas	kg m ⁻³
ρ_a	Ideal gas	kg m ⁻³
ρ_s	476 [8]	kg m ⁻³
C_w	4187 [12]	J kg ⁻¹ K ⁻¹
C_v	1840 [12]	J kg ⁻¹ K ⁻¹
C_a	1000 [12]	J kg ⁻¹ K ⁻¹
C_s	1400 [8,12]	J kg ⁻¹ K ⁻¹
k_w	[15]	W m ⁻¹ K ⁻¹
k_v	0.026 [15]	W m ⁻¹ K ⁻¹
k_a	0.026 [15]	W m ⁻¹ K ⁻¹
k_s	0.21	W m ⁻¹ K ⁻¹
$k_{n,w}$	4×10^{-14}	m ²
$k_{in,g}$	4×10^{-14}	m ²
$k_{in,l}$	[14]	
$k_{r,g}$	[14]	
μ_l	0.988×10^{-3} [15]	
μ_g	1.8×10^{-5} [15]	Pa s
h	2.5 [11]	Pa s
h_m	10 [15]	W m ⁻² K ⁻¹
λ	2.26×10^6 [15]	m s ⁻¹
ε	0.615 [8]	J kg ⁻¹
D_{eff}	[8]	m ²
Sr	0.08 [14]	
D_b	[8]	m ² s ⁻¹
M_a	29×10^{-3} [12]	kg mol ⁻¹
M_v	18×10^{-3} [12]	kg mol ⁻¹
P_c	[8],[11],[12]	Pa

curves when intrinsic permeability = 4×10^{-13} . The drying time is obviously different with different capillarity pressure model. The drying time is longest when capillarity pressure model Pc-2 used, and the drying time is lest when capillarity pressure model Pc-3 used. The moisture change is almost in direct proportion to the time when Pc-3 used in most drying time. But other capillarity pressure models are not

The temperature curve is also shown the obviously different. The temperature is increased at the drying initial stage because the heat and mass transfer is from bottom to up more than phase change. But model Pc-3 is with longer time temperature maintains and Pc-1 is with shorter time temperature maintains. The model Pc-1 is no obviously maintains time. Fig.3 is the results of different capillarity pressure parameter effect moisture and temperature curves when intrinsic permeability = 4×10^{-14} . The drying time is obviously different with different capillarity pressure model.

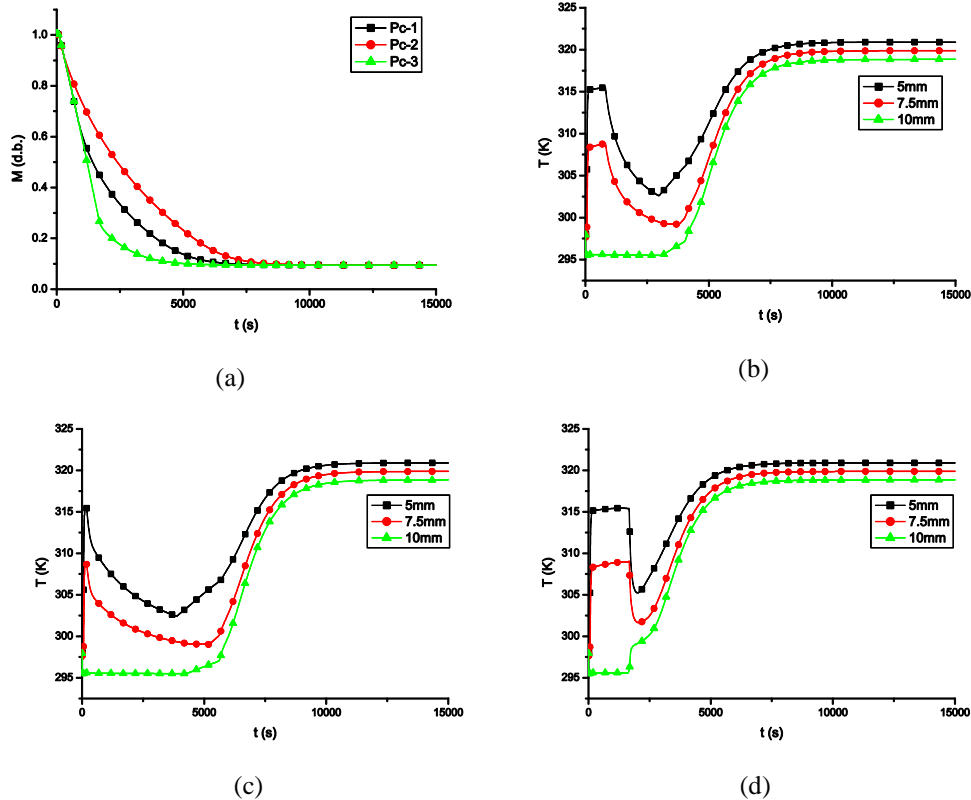


Fig.2. Capillarity pressure model effect when intrinsic permeability $k = 4 \times 10^{-13}$, (a) Moisture vs. time, (b) Temperature vs. time for model Pc-1, (c) Temperature vs. time for model Pc-2, (d) Temperature vs. time for model Pc-3.

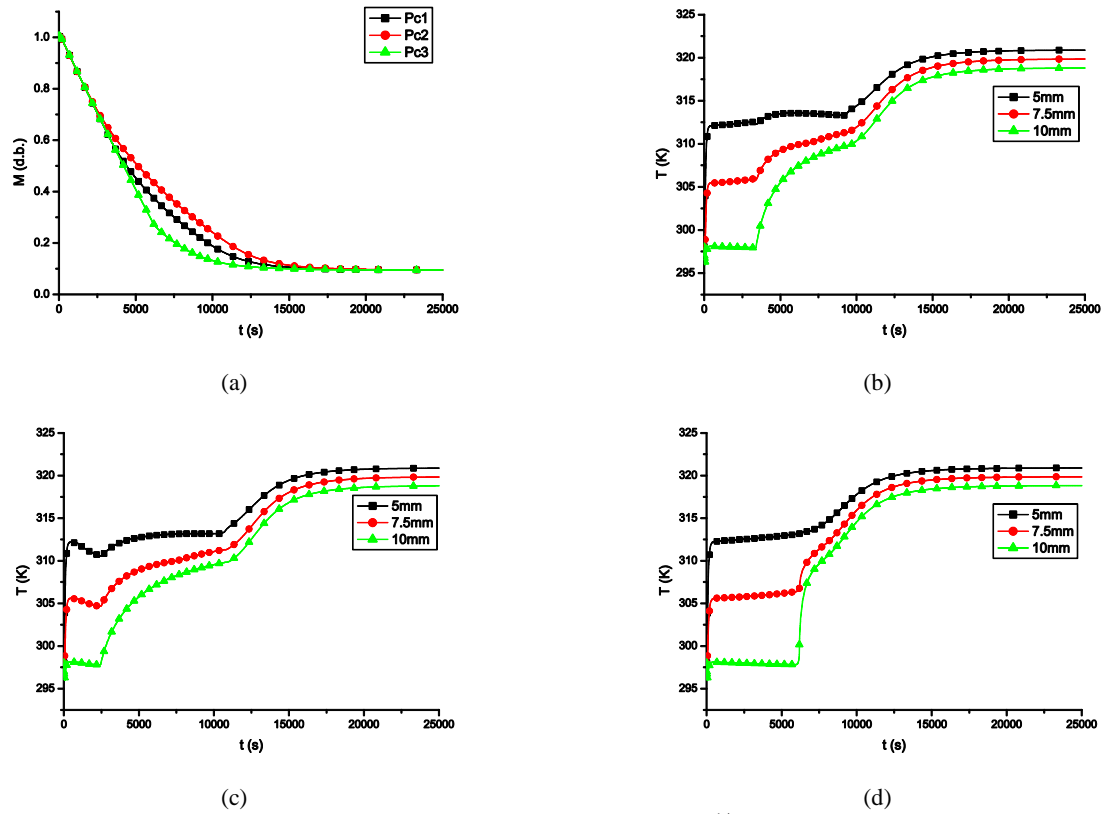


Fig.3. Capillarity pressure model effect when intrinsic permeability $k = \times 10^{-14}$, (a) Moisture vs. time, (b) Temperature vs. time for model Pc-1, (c) Temperature vs. time for model Pc-2, (d) Temperature vs. time for model Pc-3.

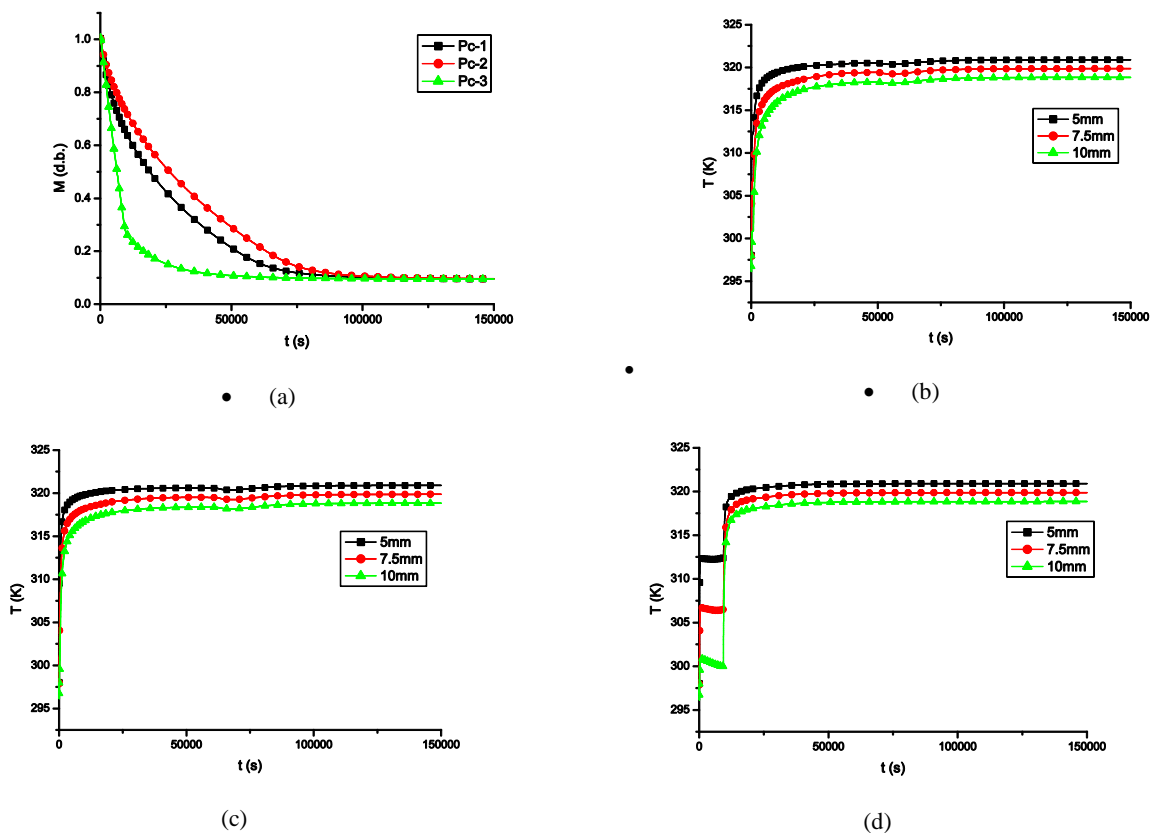


Fig. 4. Capillarity pressure model effect when Intrinsic permeability $k = 4 \times 10^{-15}$, (a) Moisture vs. time, (b) Temperature vs. time for model Pc-1, (c) Temperature vs. time for model Pc-2, (d) Temperature vs. time for model Pc-3.

The drying time is longest when capillarity pressure model Pc-2 used, and the drying time is lest when capillarity pressure model Pc-3 used. The moisture change is almost in direct proportion to the time when Pc-3 used in most drying time. But other capillarity pressure models are only in drying initial stage. It is different with Fig. 2. The temperature is increased and then maintains some time, and then increased. The different is the capillarity pressure model Pc-2 is with second temperature maintains time.

Fig.4 is the results of different capillarity pressure parameter effect moisture and temperature curves when Intrinsic permeability $=4 \times 10^{-15}$. The drying time is obviously different with different capillarity pressure model.

The drying time is longest when capillarity pressure model Pc-2 used, and the drying time is lest when capillarity pressure model Pc-3 used. The moisture change is almost in direct proportion to the time when Pc-3 used in most drying time. The

temperature is increased and then maintains some time, and then increased only for model Pc-3.

Fig.5 is the results of different capillarity pressure parameter effect moisture and temperature curves when Intrinsic permeability $=4 \times 10^{-16}$. The drying time is obviously different with different capillarity pressure model. In our simulation time, the drying is not gotten end for model Pc-1 and Pc-1.

The moisture change is almost in direct proportion to the time when Pc-3 used in most drying time. The temperature is increased and then maintains some time, and then increased only for model Pc-3.

The difference above is because the mass and heat transfer process different when used different capillarity pressure model. From Eq. (21), the mass of free water transfer is decided by capillarity pressure. The effect is not only shown in moisture change but also shown in temperature characterizes.

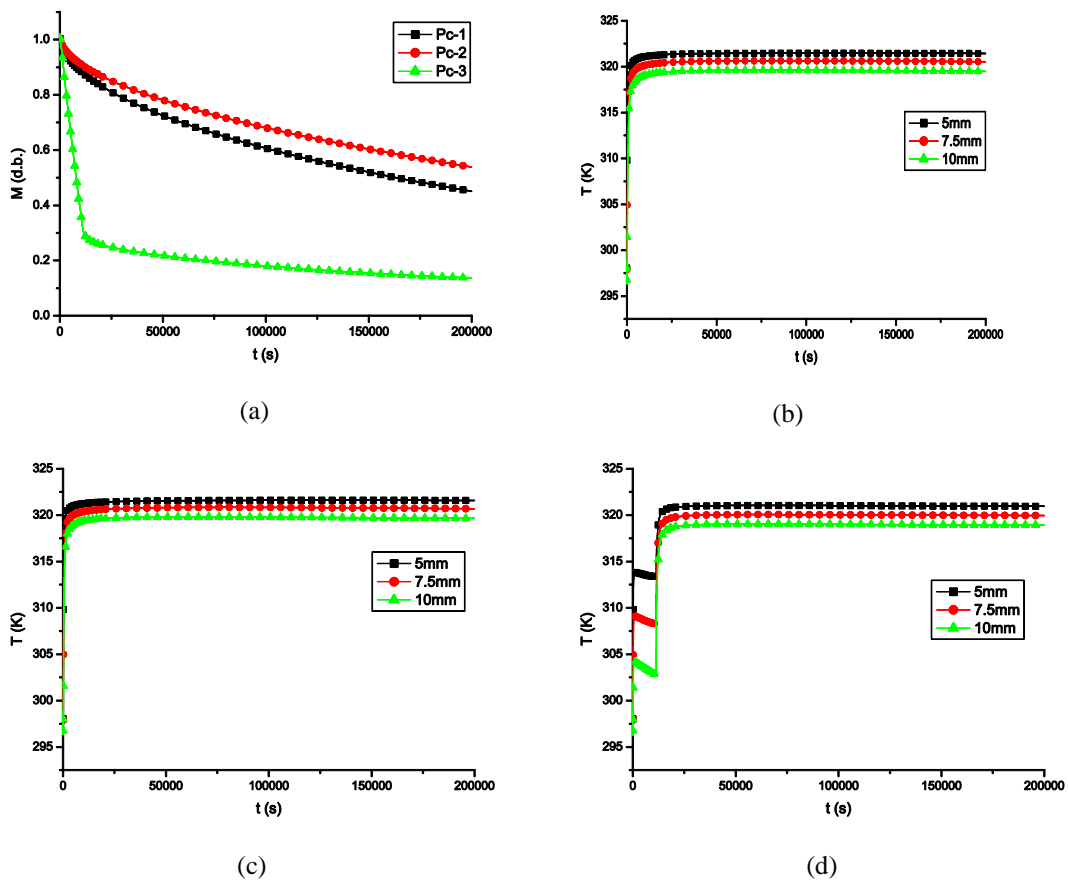


Fig.5. Capillarity pressure model effect when Intrinsic permeability $k = 4 \times 10^{-16}$, (a) Moisture vs. time, (b) Temperature vs. time for model Pc-1, (c) Temperature vs. time for model Pc-2, (d) Temperature vs. time for model Pc-3.

CONCLUSION

A coupled model of porous medium vacuum drying based on the theory of heat and mass transfer was implemented in this paper. The parameter sensitivity analyses of capillarity pressure model were then examined. The moisture and temperature characteristic is gotten. The results are shown that the capillarity pressure model has obviously effect on drying process. It would be affect the mass and heat transfer, and then the temperature curve is shown obviously different. The results has some meaningful for vacuum drying of food and chemical material for heat sensitivity.

NOMENCLATURE

B	diagonal tensor
D	diffusivity (m^2s^{-1})
D_{eff}	diffusion tensor (m^2s^{-1})
g	gravity vector (m s^{-2})
h	intrinsic averaged enthalpy (J kg^{-1})
I	water phase rate ($\text{kg s}^{-1}\text{m}^{-3}$)
k	intrinsic permeability (m^2)
k_r	relative permeability
m	mass (kg)
n	outer unit normal to the product
P	pressure (Pa)
P_c	capillary pressure (Pa)
R	universal Gas constant ($\text{J kmol}^{-1}\text{K}^{-1}$)
S	saturation
t	time (s)
T	temperature (K)
W	moisture content (in dry basis)
<i>Greek letters</i>	
ΔH	latent of phase change (J kg^{-1})
λ_{ef}	effective thermal conductivity tensor ($\text{W m}^{-1}\text{K}^{-1}$)
μ	viscosity ($\text{kg m}^{-1}\text{s}^{-1}$)
ρ	density (kg m^{-3})
ω	vapor fraction
<i>Subscripts</i>	
a	dry air
g	gas
w	water
s	solid
v	vapor
sat	vapor saturation
in	intrinsic
r	relative

Mathematical operators

Δ	gradient operator
∇	divergence operator

Acknowledgments: This research was supported by the National Natural Science Foundation of China (Grant No. 31000665, No. 51176027, No. 31371873 and 31300408).

REFERENCES

1. CH Xu, ZJ Zhang, SW Zhang and X He, Proc. 5th Asia-Pacific Drying, 2007, 1261-1267.
2. Z.J. Zhang, C.H. Xu, S.W. Zhang, X. He, Proc. 5th Asia-Pacific Drying Conference, 2007, 330-337.
3. Z.J. Zhang, C.H. Xu, S.W. Zhang, Proc. International Conference on Computer Science and Information Technology, 2008, 534-538
4. Y. Ichikawa, A.P.S. Selvadurai, Transport Phenomena in Porous Media, Aspects of Micro/ Macro Behaviour, 2012.
5. A.K. Haghi, *Theor. Found. Chem. Eng.*, **40**, 14 (2006).
6. S.J. Kowalski, Drying of porous materials, Springer, 2007.
7. J. Bear, Y. Bachmat, Introduction to Modeling of Transport Phenomena in Porous Media, Springer, 1990.
8. A. Erriguible, P. Bernada, F. Couture, M.A. Roques, *Chem. Eng. Process.*, **46**, 1274 (2007).
9. A. Erriguible, P. Bernada, F. Couture, M.A. Roques, *Drying Technol.*, **23**, 455 (2005).
10. K. Murugesan, H.N. Suresh, K.N. Seetharamu, P.A. Aswatha Narayana, T. Sundararajan, *Int. J. Heat Mass Transfer.*, **44**, 4075 (2001).
11. P. Perré, I.W. Turner, *AIChE J.*, **52**, 3109 (2006).
12. S.S. Torres, W. Jomaa, J.R. Puiggali, S Avramidis, *Appl. Math. Model.*, **35**, 5006 (2011).
13. S.S. Torres, J.R. Ramirez, L.L. Méndez-Lagunas, *Chem. Biochem Engin. Quart.*, **25**, 327 (2011).
14. A. Warning, A. Dhall, D. Mitrea, A.K. Datta, *J. Food Engin.*, **110**, 428 (2012).
15. A. Halder, A. Dhall, A.K. Datta, *Food Bioprod. Process.*, **85**, 209 (2007).
16. A. Halder, A. Dhall, A.K. Datta, *Food Bioprod. Process.*, **85**, 220 (2007).
17. Z.J. Zhang, N.H. Kong, *Math. Probl. Engin.*, Article ID 347598 (2012).
18. Z.J. Zhang, S.W. Zhang, T.Y. Su, S.S. Zhao, *Math. Probl. Engin.*, Article ID 120736 (2013).
19. M. Jalili, A. Anca-Couce, N. Zobel, *Energ. Fuel.*, **27**, 6705 (2013).
20. Z.J. Zhang, Y.K. Zhang, S.W. Zhang, T.Y. Su, Y.H. Xie, L.L. Zhao, *J. Chem. Pharm. Res.*, **5**, 1429 (2013).
21. L.L. Zhao, Z.J. Zhang, S.W. Zhang, W.H. Zhang, *J. Chem. Pharm. Res.*, **6**, 654 (2014).
22. G.A. Spolek, O.A. Plumb, *Wood Sci. Technol.*, **15**, 189 (1981).

МОДЕЛИРАНЕ НА ЕФЕКТА НА КАПИЛЯРНОТО НАЛЯГАНЕ ВЪРХУ ВАКУУМ-СУШЕНЕТО В ПОРЪОЗНА СРЕДА

Жиджун Жанг*, Юекай Жанг, Шиуей Жанг, Тяньй Су, Уенху Жанг, Юанхуа Ксие, Лили Жао

Департамент по механо-инженерство и автоматизация, Североизточен университет, Шенянг, Китай

(Резюме)

Постъпила на April 22, 2014 г.

Сушенето е ключов процес в химичната, хранителната и други сходни индустрии. Използвани са много методи за моделиране и симулиране за изучаване на топло и масообменните процеси при сушенето. Капилярното налягане трудно се определя в тези случаи. Съставен е модел на процеса на вакуум-сушенето на базата на теорията на топло-масообмена. Моделът е приложен с помощта на софтуер COMSOL. Изследвана е параметричната чувствителност спрямо капилярното налягане. Показани са температурните характеристики и влажността.

Development of a novel thermal storage molten-salt filled with nanoparticles for concentration solar plants

Dongxiao Niu, Yan Lu, Di Wu*

North China Electric Power University, No.2, Beinong Road, Huilongguan, Changping District, 102206 Beijing, China

Submitted April 22, 2014

Solar thermal power generation technology is the most feasible technology to compete with fossil fuels in the economy, and is considered to be one of the most promising candidates for providing a major share of the clean and renewable energy needed in the future. The appropriate heat transfer fluid and storage medium is a key technological issue for the future success of solar thermal technologies. Molten salt is one of the best heat transfer and thermal storage fluid for both parabolic trough and tower solar thermal power system. It is very important that molten salt heat transfer mechanisms are understood and can be predicted with accuracy. But studies on molten salts heat transfer are rare.

This study will lay a foundation for the application of carbon nanotubes in molten salt which can remarkably improve the stability and capacity of thermal storage. Preliminary experiments found that adding nanoparticles provided an anomalous enhancement to the specific heat capacity of molten salt. According to the experiments, multi-walled carbon nanotubes and Au nanoparticles both can enhance the specific heat capacity of molten salt by a factor approaching 100%.

In this paper, the interface thermal resistance theory is used to explain the phenomenon of the significantly improved heat capacity, then investigate the factors which affect the mechanism of specific heat capacity enhancement, such as the concentration, the size, the attributes, the stability of the nanoparticles, and dispersion behavior of the nanoparticles in the eutectic composition. The microstructure was confirmed by scanning electron microscope (SEM) and transmission electron microscope (TEM).

Key words: Molten Salt, Nanoparticles, Concentration Solar Plants, Interfacial Thermal Resistance

INTRODUCTION

Solar thermal techniques are especially promising since these platforms can provide uninterrupted power supply during off peak times. Solar thermal power plants rely on high temperature thermal storage facilities and require the storage medium to have high heat capacity and thermal conductivity. Hence, there is a need to find better performing thermal-energy storage technologies and materials that are cost effective. It should be noted that novel materials (such as nano-

material additives) can become cost-effective if they can increase the operating range of the storage facilities to a higher range of temperatures. High-temperature molten salt acting as the heat storage medium has the following advantages:

(1) The heat transfer coefficient of the molten salt is twice that of other organic heat carriers, making the thermal stability of the molten salt relatively high.

(2) The upper temperature limit of the molten salt which is put into practical applications is at present 600°C.

Therefore, in order to improve the operating

* To whom all correspondence should be sent.

E-mail: woodncepu@163.com

parameters and efficiency of solar concentrating systems and reduce the cost of electricity, approaches to enlarge the thermal capacity, enhance the heat transfer characteristics and increase the thermal stability higher of molten salt, are urgently needed. Many related research works have shown that nanoparticles can enhanced heat transfer characteristics, most of these research works focus on how to improve the thermal conductivity. This paper sets out to study the change in specific heat capacity in molten salt after mixing it with nanoparticles, as well as to find the main factors causing this change. Chiefly, the motivation of this study was to synthesize novel nanomaterials for TES in CSP applications. The experiments preliminarily validate that, nanoparticles strongly enhance the heat capacity of molten salt. Moreover, much to our surprise, endothermic and exothermic characteristics of molten salt change significantly after mixing in multi-walled carbon nanotubes during a certain temperature period.

THEORETICAL ANALYSIS

There are few related research works about the mechanisms by which nanoparticles improve the specific heat.

Three independent thermal transport mechanisms were proposed to explain the unusual enhancement of the specific heat capacity: (1) Mode I: enhanced specific heat capacity through nanoparticles due to higher specific surface energy (compared with the bulk material); (2) Mode II: additional thermal storage mechanisms due to interfacial interactions between nanoparticles and the adhering liquid molecules due to the extremely high specific surface area of the nanoparticles; and (3) Mode III: the existence of a semi-solid liquid layer adhering to the nanoparticles, which are likely to have enhanced specific heat capacity due to the smaller inter-molecular spacing similar to the nanoparticle lattice structure on the surface.

However, the three theoretical models are not fully proved by theory and experiments research is still at the speculation stage. The objective of the

study is to explore the effect of the addition of nanoparticles on the specific heat capacity of eutectic salt. And the influence factor and mechanical of the synthesis protocol on the specific heat capacity of the nanomaterials is also explored in this study.

In this study, multi-walled carbon nanotubes are selected as the main object of study, Au nanoparticles are also selected for comparison.

First of all, when the state of mixture of salt and nanoparticle is unclear, we have to analyse the simple mixing state in which the salt and nanoparticles are separated exist in molten state. The state is considered whether it can anomalous enhance the specific heat capacity of eutectic.

A simple mixing rule (Equation 1) was used to estimate the property values of the mixture (nanomaterials), as follows:

$$C_{p,t} = \frac{m_{np}C_{p,np} + m_bC_{p,b}}{m_{np} + m_b} \quad (1)$$

Where C_p is specific heat and m is mass of the sample. Subscripts t , np , b denote property values of the mixture (nanomaterial), the nanoparticles, and a pure solvent material (eutectic). This equation is frequently used in the nano-fluids literature.

The specific heat capacity of the eutectic is easy to determine, but the specific heat capacity at constant pressure of nanoparticles is difficult to calculate quantitatively.

The Debye theory is used to calculate the specific heat capacity of carbon nanotubes. The Debye theory assumes that a crystal is an isotropic continuous elastic medium where the thermal motion of atoms is sent in the form of elastic waves, Each elastic wave vibration mode is equivalent to an harmonic oscillator, the energy is quantized, and specifies a maximum elastic wave frequency ω_D , called the Debye frequency. Since the Debye temperature for carbon nanotube is expected to be 2500K as high as that for diamond, the quantum effect for the heat capacity is very important even at room temperature.

The degrees of freedom in a crystal which is composed of N atoms is $3N$, therefore there can only be $3N$ vibration modes, so:

$$\int_0^{\omega_D} g(\omega)d\omega = 3N \quad (2)$$

Substitution into the state density of elastic wave:

$$g(\omega) = \frac{3V\omega^2}{2\pi^2v_s^3} \quad (3)$$

The Debye frequency values can be determined:

$$\omega_D = \left(\frac{6N\pi^2v_s^3}{V} \right)^{\frac{1}{3}} = \left(6\pi^2n \right)^{\frac{1}{3}} v_s \quad (4)$$

n is the number of atoms per unit volume.

The Debye crystal vibration theory is the basis of traditional crystal molar heat capacity theory, which is suitable for the calculation of molar volume heat capacity for macro crystalline materials $C_V(T)$. Through the relation between $C_V(T)$ and $C_P(T)$, $C_P(T)$ can be calculated. The $C_V(T)$ formula in the Debye model theory is :

$$C_V(T) = 9R \left(\frac{T}{\theta_D} \right)^3 \int_0^{\theta_D/T} \frac{e^x x^4}{(e^x - 1)^2} dx \quad (5)$$

Where $C_V(T)$ is the Moore constant volume heat capacity of the material, with units of $J/(mol K)$; T is the thermodynamic temperature, with units of K ; θ_D is Debye temperature of material, with units of K ; R is the molar gas constant, which equals to $8.314 J/(mol K)$.

In order to conveniently calculate $C_P(T)$, a semi-empirical relation from the literature is used.

Where T_m is the melting point of carbon nanotubes, with units of K ; A_0 is a universal constant, equal to $3.9 \times 10^{-3} mol K/J$.

This is the modified Nernst-Lindermann equation, which is a widely used semi-empirical formula. The formula is used to calculate the $C_P(T)$ of carbon nanotubes. The melting point of carbon nanotubes

T_m is substituted into formula (6):

$$C_P(T) = C_V(T) \left(1 + 3RA_0 \frac{T}{T_m} \right) \quad (6)$$

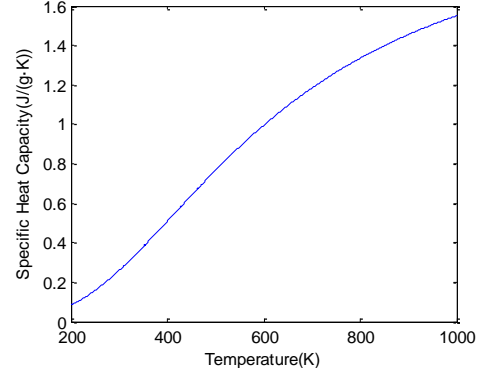


Fig 1. The variation of specific heat capacity with temperature for carbon nanotubes by simulation

The simulation curve shows that in the work temperature segment, carbon nanotubes are not enough to improve the value of the heat capacity of nanomaterial reached 100%. It can be concluded that the nanoparticles and the salt do not form an independent simple mix in the eutectic compound but form a composite structure, which can anomalously enhance the specific heat capacity of the eutectic.

By research, it can found that the influencing factors of carbon nanotubes/molten salt composite material thermodynamics performance mainly include: the degree of carbon nanotubes dispersion, carbon nanotube content percentage by mass, morphology and diameter of carbon nanotubes, carbon nanotube/molten salt two-phase interface thermal resistance.

Of these factors, the interface thermal resistance is regarded as the most important one. Interface thermal resistance causes the blockage of heat flow because of the difference of two phase phonon spectra, and the weakness of interface interaction. Interfacial thermal resistance has an intensity rejection effect to the heat transfer between nanoparticles and salt molecules, which makes the heat conduction rate slow, thus greatly enhancing the heat capacity. Phonon heat conduction is the main mechanism in multi-walled carbon nanotubes.

However, in molten salt/multi-walled carbon nanotube composite materials, the phonon heat conduction between the multi-walled carbon nanotubes have to through salt molecules.

The impact of heat capacity caused by dispersion, mass percentage, morphology and diameter are all contributed by the interfacial thermal resistance, it will be analysed below.

EXPERIMENTAL ANALYSIS

Experimental procedure

In this paper, the molten salt samples are nitrate salts. Nitrate salts were selected for Solar Two use because of their favorable properties compared with other candidates. In particular, these nitrate salts have low corrosion rates with common piping materials, are thermally stable in the upper temperature range required by steam Ranking cycles, have very low vapor pressures, are widely available, and are relatively inexpensive.

The general protocol for preparing the nanofluid eutectic is as follows: 600mg of Sodium nitrate, 400mg of Potassium nitrate were mixed and heated to a molten state. After cooling, the mixture is ground to powder and called the molten salt. 5mg multi-walled carbon nanotubes and 50mg gum arabic (GA) is dissolved in 20ml of Ultrapure water. After ultrasonically vibrating the water solution for one hour by an ultra sonicator (PS-20, Shenzhen Yida Corporation), 495mg of the new salt is added. This water solution, which now contains 1% of eutectic nanofluid, was ultrasonicated again for one hour to obtain a homogeneous dispersion of the nanofluid. This is the reference group called the nanofluid. The water solution was then rapidly evaporated in a drying oven, which was maintained at 100°C. A portion of the dry sample was put into a differential scanning calorimetry (DSC) measurements to test the heat capacity. The temperature was then ramped up to 500°C at 20°C/min.

What is more, to discover the reasons that result in the enhancement of specific heat capacity of nanofluid, six groups of comparative experiments were designed. Each of them altered one property

that had a great impact on nanoparticles, such as the size, the mass percentage and so on to explore the reasons that result in the enhancement of nanofluid's heat capacity. The experimental group is listed as follow:

Sample A: 1.5% concentration of multi-walled carbon nanotubes in nanofluid.

Sample B: 0.5% concentration of multi-walled carbon nanotubes in nanofluid.

Sample C: half an hour ultrasonication time.

Sample D: 50°C evaporating temperature.

Sample E: 10 μ L gold particle (Ted pella) of 5nm diameter to substitute the multi-walled carbon nanotubes.

Sample F: 10 μ L gold particle (Ted pella) of 10nm diameter to substitute the multi-walled carbon nanotubes.

Results and data analyses

According to the data obtained from six sets of comparative experiments, curves that reflect the specific heat capacity coefficient of the comparative groups under ambient conditions were obtained. As is shown in the graphs, nanoparticles enhance the specific heat capacity of a water solution significantly, but not to the same level. Properties of nanoparticles, volume fraction, particle diameter and suspension stability of the nanofluid are important factors that influence the thermal conductivity of nanofluid. The impact of various factors are analysed as follow:

Adding nanoparticles to the in pure eutectic.

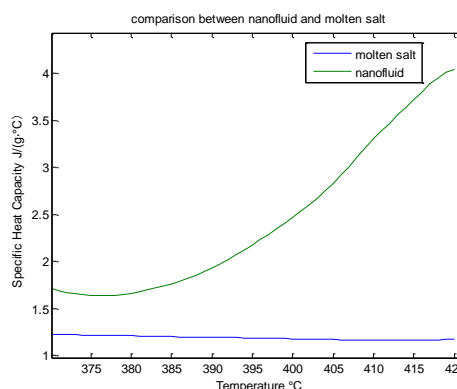


Fig 2. The variation of specific heat capacity with temperature for the pure eutectic and the nanofluid in liquid phase.

It shows that the heat capacity of the pure molten salt eutectic is about 1.25 J/(g K) , which is the same as given in the literature. In the $370\sim 420^\circ\text{C}$ high temperature work section, the specific heat capacity of sample nanofluid has been improved nearly 100% by adding 1% of multi-walled carbon nanotubes compared to that of the pure molten salt. What is more, the specific heat capacity is increasing by temperature. When the temperature is 420°C , the specific heat capacity is about 4.2 J/(g K) , which is nearly 332% of pure molten salt. The mechanism and influence factors will discuss below.

volume fraction. The sample nanofluids in Fig 3 and 4 are the same as the one in Fig 2, but they choose the different work temperature. Fig 2 is $370\sim 420^\circ\text{C}$, and Fig 3 and 4 is $365\sim 410^\circ\text{C}$, this is mainly determined by the stability of thermal

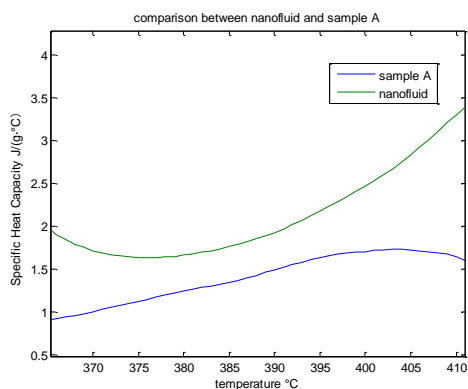


Fig 3. The variation of specific heat capacity with temperature for sample A and the nanofluid in liquid phase.

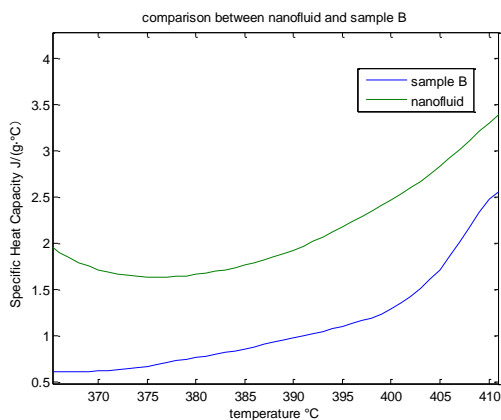


Fig 4. The variation of specific heat capacity with temperature for sample B and the nanofluid in liquid phase.

analysis base line in DSC graphic. The specific heat capacity of sample A and B are both less than nanofluid. The value of sample A is approach to the pure molten salt and has a small enhancement which is $1\sim 1.5 \text{ J/(g K)}$. Sample B has a similar variation tendency with nanofluid which has an obvious enhancement effect. But the value of sample B is smaller than nanofluid all the time. So the two conditions of volume fraction have different mechanisms.

There are two mechanisms of heat transfer in the composite structure:(1) nanotube-molten salt heat transfer; (2) nanotube -nanotube heat transfer. They are respectively restricted to the interfacial thermal resistance and thermal contact resistance. The concentration of carbon nanotubes is low, interfacial thermal resistance is the main influence factor of composite materials ; The concentration is high, nanotube-nanotube heat transfer is remarkably improved, the interfacial thermal is weakend which causes a reduction of specific heat capacity.

It can be seen that the concentration of carbon nanotubes does not have a linear relationship with specific heat capacity, but there is an ideal concentration range for nanomaterial. Too high or too low a concentration are both a disadvantage for the formation of the interfacial thermal resistance .

suspension stability of nanofluid

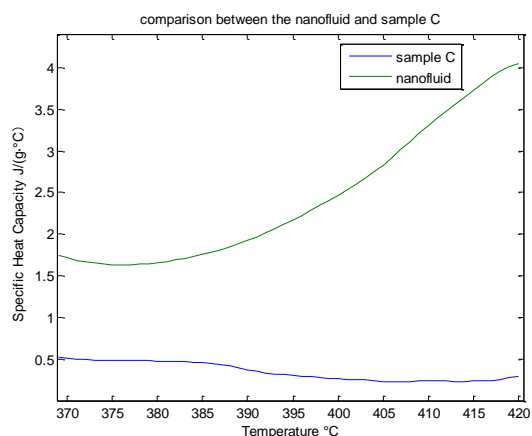


Fig 5. The variation of specific heat capacity with temperature for sample C and the nanofluid in liquid phase.

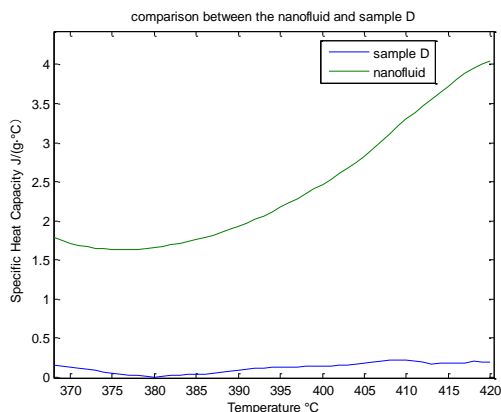


Fig 6. The variation of specific heat capacity with temperature for sample D and the nanofluid in liquid phase.

Fig 5 and 6 shows the specific heat capacity of sample C and D is not enhanced but has a large reduction which are both less than 1 J/(g K) . Moisture and shortage of ultrasonic sonication all lead to the agglomeration of carbon nanotubes, which are then unable to form the effective interfacial thermal resistance. It caused the salt molecules absorb more heat in the same temperature region that leads to the reduction of specific heat capacity.

Properties of nanoparticles

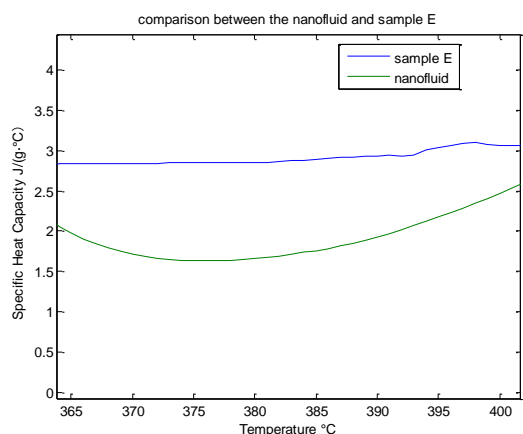


Fig 7. The variation of specific heat capacity with temperature for sample E and the nanofluid in liquid phase.

Gold nanoparticles have stable physical and chemical properties which enhance the specific heat capacity of the solution. What is more, in a high-temperature section, the specific heat capacity of the

eutectic composition is more stable and changes little.

Compared with multi-walled carbon nanotubes, nanometer gold particles have the shape of a ball, which makes the surface area large enough to scatter phonons. Therefore, the nanofluid containing gold nanoparticles has a very high interfacial thermal resistance, and the enhancement of the specific heat capacity is significant.

Fig 7 shows the comparison between sample E and sample nanofluid. In work temperature, sample E has the better effect of specific heat capacity enhancement than sample nanofluid, and the enhancement effect of sample E is more stable. Gold particles have the shape of a ball, which makes the surface area large enough to scatter phonons, due to many two-phase interfaces increased. Therefore, the nanofluid containing gold nanoparticles has a very high interfacial thermal resistance.

Particle diameter

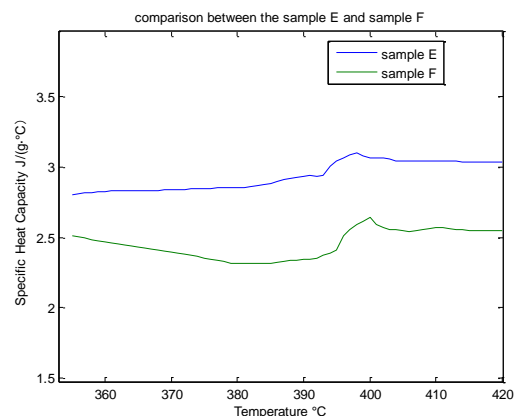


Fig 8. The variation of specific heat capacity with temperature for sample E and the sample F in liquid phase.

Gold nanoparticles which have large particle size are less effective than smaller ones in enhancing the specific heat capacity of a nanofluid. According to the research, nanoparticles of large size can increase the density of low-frequency vibrational phonon modes, however, they reduce the interfacial thermal resistance and coupling loss of heat conduction from the interior of the nanoparticles to the surrounding salt molecules with phonons of different vibration frequencies. Therefore, nanoparticles of small size

have the advantage in terms of improving heat capacity.

Fig 8 shows the specific heat capacity of sample E and F have the same variation tendency and stability in work temperature. They all can enhance the specific heat capacity to 100%, and sample E is more effective than sample F, which can reach to 220%. According to the research, nanoparticle of large size can increase the density of low-frequency vibrational phonon modes, however, reduce the interfacial thermal resistance. Therefore, nanoparticles of small size have the advantage in terms of improving heat capacity.

CONCLUSIONS AND DISCUSSION

There are many reasons that contribute to the change of the specific heat capacity, like the degree of dispersion of nano particles, the mass percentage of nanoparticles or the morphology or type of nanoparticles. In this paper, a speculation is made that all those reasons mentioned above are effected through the two-phase interfacial thermal resistance of nanoparticles and molten salt, which in turn changes the value of the specific heat capacity. The improvement of interfacial thermal resistance of nanoparticles and salt molecules forms a good two-phase interface, so that lots of heat is absorbed by nanoparticles and the heat transfer speed of salt molecules is reduced. This causes the overall hybrid system to absorb or release heat with slower temperature fluctuations, resulting in a significant enhancement of specific heat capacity.

Transmission electron microscopy (TEM) and scanning electron microscope (SEM) are utilized to observe the microstructure of the samples which have finished the test on DSC. Compared with Fig.9, the images Fig.10 from the TEM show that multi-walled carbon nanotubes can still present a good dispersion in molten state, and formed a complex heat conduction network structure between salt molecules which can anomalously enhance the heat conduction between nanoparticles; Through the observation of SEM images, it can be found that the original salt eutectic has a smooth surface, however after adding nanoparticles, a lot of the punctation

structures appear at the surface which is formed by gold-nanoparticles due to enhance the interfacial thermal resistance.

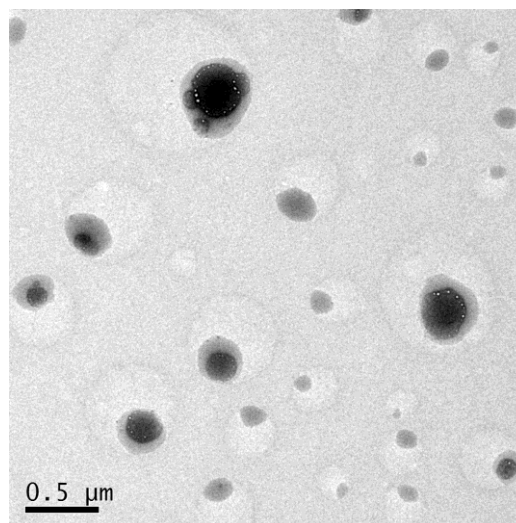


Fig 9. Transmission electron micrograph (TEM) of pure eutectic mixture after testing.

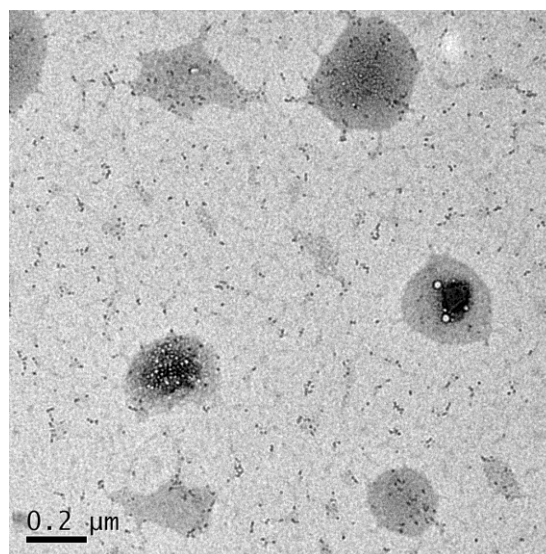


Fig 10. Transmission electron microscope (TEM) of nanofluid after testing. Multi-walled carbon nanotubes present good dispersion, and formed a complex heat conduction network structure.

In this paper, specific heat capacity of molten salt is anomalously enhanced by adding nanoparticles, we explore the mechanism and impact factors of this phenomenon by theoretical analysis and experiments. We hope that it can attract the attention of other researchers to do further research in this field and to improve the theoretical and

experimental research, our research group aims to explore this method for industrial applications.

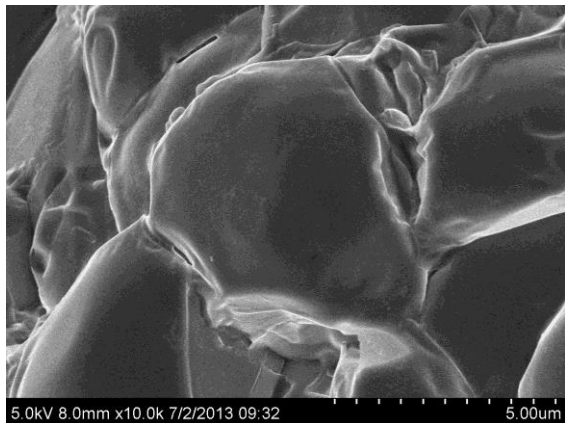


Fig 11. Scanning electron micrograph (SEM) of pure eutectic mixture after testing.

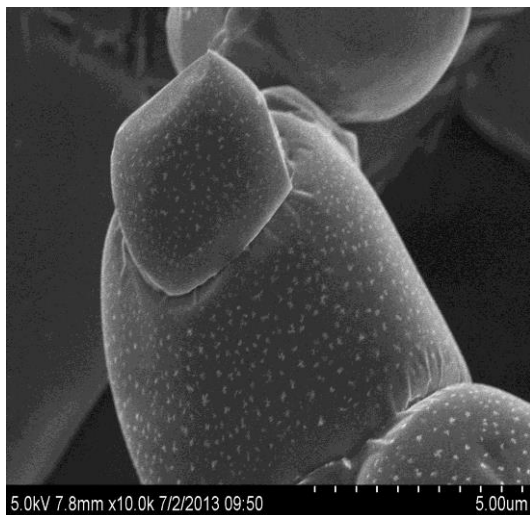


Fig 12. Scanning electron micrograph (SEM) of Sample F after testing. Special punctation structures are formed all over the nanomaterial (gold nanoparticle).

REFERENCES

- 1.S. Choi, Enhancing thermal conductivity of fluids with nanoparticles, in: D.A. Siginer, H.P. Wang (Eds.), *Developments and Applications of Non-Newtonian Flows*, ASME,1995,pp.99-105. FED-231/MD-66.
- 2.Shin, D., and Banerjee, D., Enhancement of specific heat of high-temperature silica nanofluids synthesized in alkali chloride salt eutectics for solar thermal-energy storage applications, *International*

- Journal of Heat and Mass Transfer*, 2011, Volume 54, Issues 5-6, Pages 1064-1070, February 2011.
- 3.Shin, D., and Banerjee, D., Effects of silica nanoparticles on enhancing the specific heat capacity of carbonate salt eutectic (work in progress), *International Journal of Structural Change in Solids – Mechanics and Applications*, Vol. 2, No. 2, pp. 25-31, November, 2010.
- 4.W.Yu, S.U.S Choi, The role of interfacial layers in the enhanced thermal conductivity of nanofluids: a renovated Maxwell model, *J. Nanopart. Res.* 5(1-2)(2003) 167-171.
- 5.D. Shin, D. Banerjee, Enhanced specific heat of nanofluid, *ASME J. Heat Transfer* 133(2) (2001) 024501.
- 6.D. Wen, G. Lin, S. Vafaei, K. Zhang, Review of nanofluids for heat transfer applications, *Particuology* 7 (2009) 141-150.
- 7.P. Keblinski, J.A. Eastman, D.G. Cahill, Nanofluids for thermal transport, *Mater. Today* 8 (2005) 36-44.
- 8.W. Evans, R. Prasher, J. Fish, P. Meakin, P. Keblinski, Effect of aggregation and interfacial thermal resistance on thermal conductivity of nanocomposite and colloidal nanofluids, *Int. J. Heat Mass Transfer* 51 (2008) 1431-1438.
- 9.S.Q. Zhou, R. Ni, Measurement of the specific heat capacity of water-based nanofluid, *Appl. Phys. Lett.* 92(2008) 093123.
- 10.B.X. Wang, L.P. Zhou, X.F. Peng, Surface and size effects on the specific heat capacity of nanoparticles, *Int. J. Thermophys.* 27(2006) 139-151.
- 11.Shin, D., and Banerjee, D., Enhancement of specific heat of high-temperature silica nanofluids synthesized in alkali chloride salt eutectics for solar thermal-energy storage applications, *International Journal of Heat and Mass Transfer*, 2011, Volume 54, Issues 5-6, Pages 1064-1070, February 2011.
- 12.L. Xue, P. Keblinski, S.R. Phillpot, S.U.-S. Choi, J.A. Eastman, Effect of liquid layering at the liquid-solid interface on thermal transport, *Int. J. Heat Mass Transfer* 47 (2004) 4277-4284.
- 13.S.H. Oh, Y. Kauffmann, C. Scheu, W.D. Kaplan, M. Ruhle, Ordered liquid aluminum at the interface with sapphire, *Science* 310 (2005) 661-663.

РАЗРАБОТВАНЕ НА НОВА, ТОПЛО-СЪХРАНЯВАЩА СТОПИЛКА ЗА СОЛАРНИ ИНСТАЛАЦИИ, ЗАПЪЛНЕНА С НАНО-ЧАСТИЦИ

Донгсяо Ню, Ян Лу, Ди У*

Севернокитайски електротехнически университет, Хуилонггуан, район Чангпинг, Бейджин, Китай

(Резюме)

Постъпила на 22 април, 2014 г.

Соларните термични станции са най-конкурентноспособните спрямо основаните на изкопаеми горива. Те се смятат за най-обещаващите из технологиите с чисти и възобновяеми енергийни източници в бъдеще. Подходящият флуид за топлообмена и за съхраняване на топлината е от ключово значение за успеха на соларните енерго-технологии. Солевите стопилки са най-добрите флуиди при параболичните и колонните соларни системи. От голямо значение е да се познаят механизмите на топлообмена при тези стопилки. Такива изследвания са рядкост.

Настоящото изследвания поставя основата на приложението на въглеродни нанотръби в солеви стопилки, които могат значително да подобрят стабилността и капацитета на топлинното съхранение. Предварителни експерименти показаха, че добавянето на наночастици води до аномално повишаване на специфичния топлинен капацитет на солевата стопилка. Според тези експерименти многостенните въглеродни нанотръби и златните наночастици заедно може да повишат специфичния топлинен капацитет на солевата стопилка с близо 100%.

В настоящата работа е използвана теорията на междуфазното съпротивление за да се обясни явлението на значително повишения топлинен капацитет. След това са изследвани факторите, които влияят на механизма на повишения топлинен капацитет (концентрация, размери, състав, стабилност на наночастиците, дисперсионни отношения на наночастиците в евтектичния състав). Микроструктурата е потвърдена чрез сканираща електронна микроскопия (SEM) и трансмисионна микроскопия (ТЕМ).

The effect of flame retardant additives on the combustion performance of flexible polyurethane foam

Chen Yingjie^{1*}, Liu Zhipeng¹, Dai Peigang¹, Liu Lan²

¹Guangdong Testing Institute of Product Quality Supervision, 510330 Guangzhou, China

²School of Chemistry and Chemical Engineering Sun Yat-sen University, 510275, Guangzhou, China

Submitted April 12, 2014

In this work, flexible polyurethane foams (FPUFs) were prepared by a one-step method with different flame retardant additives. Then, the combustion performances of the FPUFs were tested by evaluating their oxygen indices and smoke toxicities (OI) and by cone calorimetry (Cone). The results showed that the flame retardant performances of FPUFs prepared with 10% wt brominated flame retardant and 10% wt triazine triamine phosphate (MPOP) were improved. At an irradiance of 30 kW/m² with a sample thickness of 50 mm, the peak heat release rates of these two samples were 284.0 Kw/m² and 270.8 Kw/m², respectively. However, the smoke toxicity of the former showed greater harmful, and when the FPUF contained more than 4% wt brominated flame retardants, the smoke toxicity reached the WX level.

Key words: FPUF, Brominated Flame Retardants, Combustion Performance

INTRODUCTION

Due to accelerated industrialization and urbanization, the market for building materials has undergone dramatic growth in China. Polyurethane (PU) has a special structure and excellent performance, so it has been very extensively used. Meanwhile, because polyurethane (PU) is the product of a polyhydric alcohol compound (R-OH) and isocyanates (RN=C=O), the combustion process releases large amounts of toxic gases. Thus, PU materials incur a high fire risk [1]. Flexible polyurethane foam (FPUF) is a part of the polyurethane molding material with a porous structure and is the most flammable portion of the polyurethane material.

The flammability of FPUF limits its applications in many fields, and therefore, enhancing the flame retardant properties of FPUF would be invaluable

[2]. Flame retardants for FPUF include reactive flame retardants and additive flame retardants, defined by the relationship between the flame retardant and the base material. A reactive flame retardant affects the thermal stability, but its use is difficult in industrial production. In contrast, additive flame retardants are easy to use with simple production processes; thus, they have been widely used to date [3]. In this paper, FPUFs were prepared by a one-step method with different foam flame retardant additives. Then, the combustion performances of the FPUFs were tested by evaluating their oxygen indices (OI) and smoke toxicities and by the use of a cone calorimeter (Cone). We have tried to provide a reference work for the appropriate selection of flame retardants.

TEST

Materials

Polyether glycol (PPG-5623, hydroxyl value of 28.0 KOH mg/g with a degree of functionality of 3,

* To whom all correspondence should be sent.

E-mail: jietchen@126.com

CSPC); polyether polyol (POP CHF-628, hydroxyl value of 28.0 KOH mg/g with a degree of functionality of 3, Jiangsu Changhua Polyurethane Science & Technology Co., Ltd); toluene diisocyanate (TDI 80/20, degree of functionality of 3, Shanghai Basf Coating Co., Ltd); dibutyltin dilaurate (PUCAT L-33, Foshan City Puhui New Material Co., Ltd); stannous octoate (YOKE T-9, Jiangsu Yoke Technology Co., Ltd.); niac silicone L-540/STL DR; melamine (BK69 Macro Wei Chemical Co., Ltd); chloroalkyl poly phosphate (RDT-9, Guangzhou Yue Peng Chemical Technology Co., Ltd); 2,2',4',4',5,5-hexabromodiphenyl ether (HBB); 1,1,2-dibromo-4-(1,2-dibromoethyl)-cyclohexane (TBECH, J&K Scientific Ltd); triazine triamine phosphate (MPOP, Hefei Fine Collection Institute of Chemical Industry); and deionized water (self-made).

Apparatus

Oxygen index measuring instrument (Fire Testing Technology, FTT); cone calorimeter (Fire Testing Technology, FTT); smoke toxicity test device (Nanjing Shangyuan Fenxi Yiqi CO., LTD); and a mechanical agitator.

Preparation of FPUF

According to the formula found in Table 1, the PPG, POP and deionized water were all combined in a 1000 ml plastic beaker.

Table 1. Formulation of FPUF

Material	Ingredient/g
PPG	75~90
POP	10~25
TDI 80/20	31.5~40
Stannous octoate	0.2~1.5
Dibutyltin dilaurate	0.1~0.5
Niac silicone	0.6~1.0
Flame retardants	2.0~15.0
Deionized water	1.8~2.0

Dibutyltin dilaurate, niac silicone, stannous octoate and the corresponding flame retardant were then added and stirred with a mechanical mixer for 2 h with the material temperature kept at 25 °C. Finally, TDI 80/20 was added, and the mixture was

stirred at high speed for 4 to 5 s and then immediately poured into the natural foaming mold [4] with the temperature maintained at 25 °C for 24 h. The densities of the prepared materials were controlled to be 50 ± 2 kg/m³.

Test Method

Oxygen Index tested According to ISO 4589-2:1996, with test temperature 23 ± 2 °C, humidity at 50 ~ 55 % and sample size 100×10×10 mm.

Heat release rate tested according to ISO 5660-1:20 with irradiance setting at 30kW/m² and sample size 100×100×50 mm.

Smoke toxicity tested according to GB/T 20285-2006.

RESULTS

Oxygen Index (OI)

Figure 1 compares the oxygen indices for different flame retardant additives with mass fractions of 10%. Due to the flame retardant properties of POP itself, even without the addition of a flame retardant, the oxygen index of blank FPUF still reached 21.6%. The oxygen index of FPUF with RDT-9 (10%) added was higher than when MA (10%) was added. Phosphorus flame retardants act as a barrier between the air and the combustion products. Chlorine flame retardants work by the radical dilution of the oxygen in the air. Thus, the cooperative effect of these two flame retardant classes can achieve better performance than only MA. Among halogen flame retardants, brominated flame retardants are particularly prominent. The oxygen index reached 24.6% with the addition of HBB (5%) and TBECH (5%). However, the oxygen index achieved by adding MPOP (10%) was the best, reaching 25.2%, which can be attributed to the cooperation of N and P. The charring of the solid phase and the isolation of the air phase achieved a better flame retardant effect.

Heat Release Rate (HRR)

The heat release rate refers to the thermal radiation intensity of presupposition, i.e., the rate of heat release per unit area after ignition in kW/m². The heat release rate can be divided into the

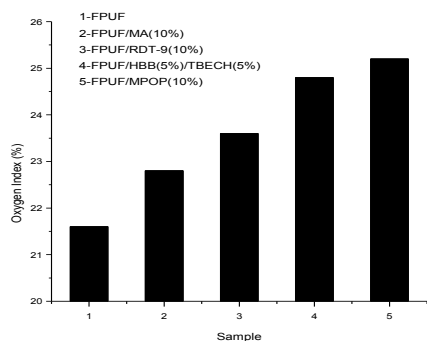


Fig. 1. Oxygen index of FPUF adding additive flame retardants.

average heat release rate and the peak heat release rate (pHRR). The average heat release rate has a practical function in the early evaluation of the contribution of the material itself as well as in early flame retardant and fire safety design [5]. The peak heat release rate (pHRR) is one of the most important parameters in evaluating the fire characteristics of materials. An irradiance of 30 kW/m² approximates actual fire conditions. Therefore, 30 kW/m² was used in the cone calorimeter test. Figure 2 shows the heat release rate curves of the four specimens at an irradiance of 30 kW/m². Among them, the heat release rate of blank FPUF reached the highest value. The pHRRs of the FPUFs with RDT-9 and MA additives were more or less the same, and both exceeded 500 kW/m². Meanwhile, the FPUFs with HBB (5%) and TBECH (5%) additives exhibited a pHRR reduced to 284 kW/m². The pHRR of the FPUF with the MPOP (10%) additive reached

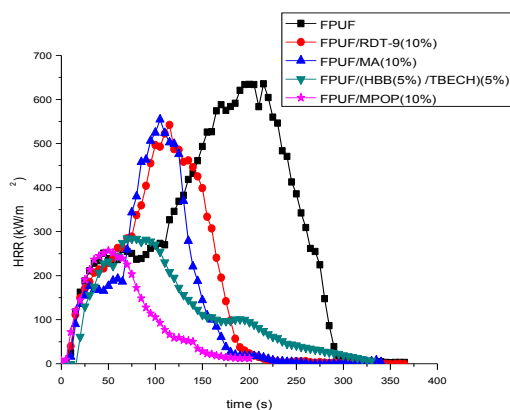


Fig. 2. The heat release rate curve of the four specimen in the irradiance of 30kW/m².

the lowest value, which was 5% lower than for the brominated flame retardant.

Total Heat Release (THR)

The total heat release of the cone calorimeter test refers to the total heat release per unit of sample area after complete combustion in MJ/m². The total heat release is an important parameter for evaluating the thermal hazard of the actual material. The greater the total heat release of the material, the more potential fire danger the material poses. According to Figure 3, the THR of blank FPUF is far greater than for the other four types of FPUFs prepared with flame retardant additives. During the combustion process of FPUF with a MPOP additive, the surface expansion phenomenon was clearly observed. The isolation of the charring increases the effect of the flame retardant, which leads to the minimum total heat release among the tested samples.

Mass loss rate (MLR)

The weight sensor supporting the sample pool in the cone calorimeter records the masses automatically. The mass loss rate was

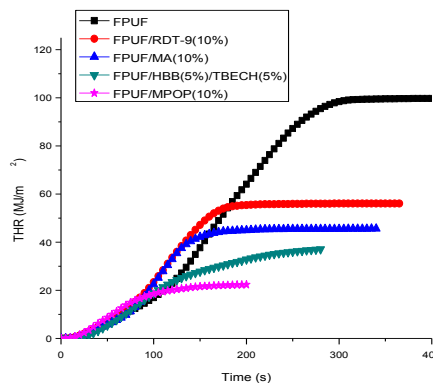


Fig. 3. The total heat release curve of the four specimen in the irradiance of 30kW/m²

calculated using the five point finite-difference method. This parameter is closely related to the heat release rate, the ratio of the extinction area and the formation rate of CO. The larger the mass loss rate, the more violent the burning of the sample that occurs. Figure 4 shows the mass loss rate curves of

the FPUFs with various flame retardant additives at mass fractions of 10%. Among these samples, the one with the MPOP (10%) additive showed the smallest mass loss rate and thus burned relatively slowly. By observation of the combustion processes of all of the samples, it was found that all of the specimens ignited within 5 s. Furthermore, the entire sample surface participates in the combustion process, resulting in rapid shrinking. The carbonization qualities of the residues after combustion ranged from 3% to 5%. The addition of a flame retardant changes the mass loss rate, but in the high irradiance used in this study, the samples show few differences. The charring rate of FPUF with the MPOP additive is the highest.

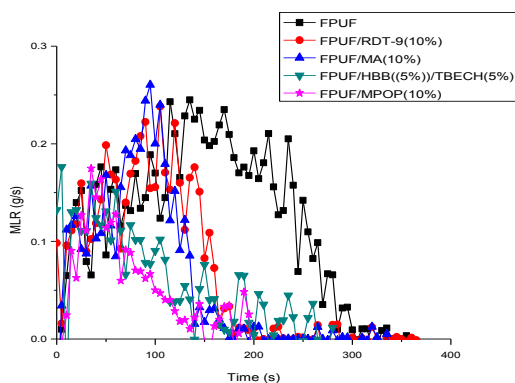


Fig. 4. The mass loss rate curve of different of FPUF adding different flame retardants

Specific extinction area (SEA)

The specific extinction area refers to the smoke production capacity per mass unit after the decomposition and evaporation of the combustible sample in m^2/kg . As shown in Figure 4, the FPUFs with the HBB and TBECH additives demonstrate strong smoke producing abilities due to incomplete combustion. This phenomenon demonstrates the smoke hazard from the use of brominated flame retardants, which pose high health risks to humans[6]. The FPUF with a MPOP additive produced less smoke, showing its ideal flame retardancy.

Smoke toxicity

The same materials in the same smoke concentrations show maximum toxicities under the

conditions of no flame and complete smoke production. For each material, we tested the animal toxicity under the above conditions. The smoke concentration when the experimental animals reach the test

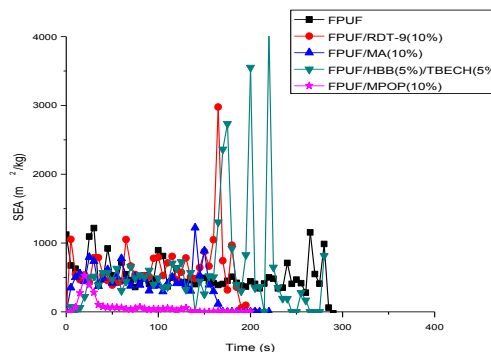


Fig. 5. Specific Extinction Area curve of different of FPUF adding different flame retardants.

termination point is taken as the basis of the smoke toxicity levels of the materials. The smoke concentrations and smoke toxicities show opposite trends. The results are shown in Figure 6. The blank specimen as well as the FPUFs with the flame retardant additives MA, RDT-9 and MPOP up to 10% wt all reached class ZA3, in which reaction phenomena that included tears and closed eyes were observed. The smoke toxicities of the FPUFs with HBB and TBECH additives varied gradually. When the concentration of these flame retardants reached 4%, the smoke toxicities reached class WX, in which the mice were comatose.

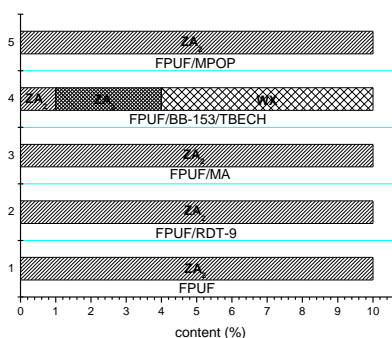


Fig. 6. Smoke concentrations and smoke toxicities.

CONCLUSIONS

FPUFs were prepared by a one step method using different flame retardant additives. The

combustion performances of the FPUFs were then tested by evaluating their oxygen indices (OI) and smoke toxicities and by the use of a cone calorimeter (Cone). The results showed that the flame performances of FPUFs prepared with 10% wt brominated flame retardants and 10% wt MPOP were superior. However, the smoke toxicity of the former showed a greater risk, and the smoke toxicity reached the WX level when brominated flame retardants of more than 4% wt were added. In the coordination of N and P, the FPUF with the MPOP additive showed ideal flame retardant properties. It is worth noting that when the content of MPOP exceeds 10%, the physical performance of the FPUF decreases rapidly due to increased brittleness and hardness.

Halogenated flame retardants have high smoke risk, and therefore, they have been gradually phased out. The flame retardant capabilities of non-halogen and coordinative flame retardants are promising, and thus, these additives have become the future direction in the development of flame retardant

products. For the preparation of FPUF composite materials with excellent comprehensive performances, the development of coordinative flame retardants and functional research on organic and inorganic additive types, intumescent flame retardants and reactive halogen-free flame retardants will represent the general trend.

REFERENCES

1. N. Usta, *J. Appl. Polymer Sci.*, **124**, 3372 (2012).
2. M. Ravey, E.M. Pearce, *J. Appl. Polymer Sci.*, **63**, 47 (1997).
3. Zhang Xiaoguang, Wang Lieping, *Chem. Ind. Eng. Progr.*, **31**, 1521 (2012).
4. Liu Yijun, *The Synthesis and Application of Polyurethane*. Beijing: Chemical Industry Press, 2012, pp.122-138.
5. Shu Zhongjun, Xu Xiaonan, Li Xiang. *Fire Performance Evaluation of Polymer Materials*, Beijing: Chemical Industry Press, 2007, pp. 61-62.
6. Tian Shi, She-Jun Chen., *Chemosphere*, **74**, 910 (2009).

ЕФЕКТ НА ДОБАВКИ, ЗАБАВЯЩИ ОГЪНЯ ВЪРХУ ГОРЕНЕТО НА ГЪВКАВА ПОЛИУРЕТАНОВА ПЯНА

Чен Ыингджи^{1*}, Лю Жипенг¹, Дай Пенганг¹, Лю Лан²

¹ *Институт за изпитания и наблюдение качеството на продукти Гуангдонг, Гуангдзю, Китай*

² *Колеж по химия и инженерна химия „Сун Ят-сен“, Гуангдзю, Китай*

Постъпила на 12 април, 2014 г.

(Резюме)

В настоящата работа се изследва горенето на гъвкава полиуретанова пяна (FPUFs), приготвена в едностадийен метод с различни добавки, забавящи огъня. Режимът на горене на FPUF е изпитан оценявайки кислородния индекс (OI) и токсичността на дима чрез конична калориметрия (Cone). Резултатите показват, че полиуретаните, приготвени с 10% бромирани забавители и 10% триазин триамин фосфат (MPOP) имат подобрени качества. Максималните скорости на топло-поглъщане са съответно 284.0 Kw/m² и 270.8 Kw/m², при излъчване от 30 kW/m² на проби с дебелина 50 mm. Обаче токсичността на дима показва по-големи вреди, а когато FPUF съдържа повече от 4% бромован забавител, токсичността достига WX-ниво.

Innovative prediction model of carbon monoxide emission from deep mined coal oxidation

Y. M. Wang¹, W. Z. Wang¹, Z. L. Shao², D. M. Wang³, G. Q. Shi^{1*}

¹ School of Safety Engineering, China University of Mining and Technology,
221116Xuzhou, China

² Key Laboratory of Gas and Fire Control for Coal Mines, 221116Xuzhou, China

³ State Key Laboratory of Coal Resources and Safe Mining, 221116Xuzhou, China

Submitted April 13, 2014

Due to great impacts to air pollution caused by residual coal oxidation in underground mine gob, monitoring and forecasting of hazardous gases emissions have become important topics in mining engineering and environmental research today. This paper presents a robot monitoring system for carbon monoxide emission from coal oxidation in spontaneous combustion condition. According to the terahertz-wave absorption spectrum, the CO concentrations are measured by using terahertz time-domain spectroscopy (THz-TDS) technique. Based on the measured values, an innovative method of CO concentration prediction has been developed by using least square support vector machine (LSSVM) with a novel hyper-parameter selection. The hourly CO concentrations have been predicted using the SVM and the hybrid LSSVM models respectively. Results show that the hybrid LSSVM has better accuracy. Statistic estimators have been employed to compare performances of the models. It has been concluded that the errors decrease and coefficients of determination increase for hybrid LSSVM model, hence it has definite practice significance and application value.

Key words: Coal oxidation, hazardous gas, terahertz spectroscopy technique, support vector machine

INTRODUCTION

Coal is the prime energy resource in most countries, 60% of them located in three countries: the United States, Russia, and China. Uncontrolled coal fires are a serious problem in many coal-producing countries and become an environmental and economic problem of international magnitude [1].

Although written accounts of coal fires date back to at least the time of Alexander the Great, the worldwide spread of coal fires has increased dramatically since the industrial revolution. Currently, thousands of coal fires are burning—some for centuries and many uncontrollably, with

flames up to 20 m and temperatures exceeding 1000°C—from eastern Asia and northern China into the coal basins of Russia, Europe, Africa, north and south America, and Australia [2,3].

Coal fire is a global catastrophe, some of its prime impacts are [4,5]: (a) Emission of many toxic gases, such as carbon monoxide (CO), carbon dioxide (CO₂), sulfur oxides (SO_x), methane (CH₄), and nitrogen oxides (NO_x). Among these noxious gases, CO₂ and CH₄ contribute to global warming. (b) Geomorphic effects include land subsidence, surface cracks, faults, and other geologic structures. This paper also presents an innovative method of CO concentration prediction using a novel hyper parameter selection for Least Square Support Vector Machine (LSSVM) [19] regression combined with particle swarm optimal

* To whom all correspondence should be sent.

E-mail: cumtwangym@126.com

algorithm (PSO) [20]. The CO concentrations of hazardous gas monitoring station in coal mine gob have been used to test the effectiveness of this method. Statistic estimators including mean absolute percentage error (MAPE), mean absolute error (MAE) and root mean square error (RMSE) and coefficient of determination (R2) have been employed to compare performances of the models.

EXPERIMENTAL

Hazardous gas samples were collected from the gob in an actual coal mine and analyzed by terahertz measurement to obtain the carbon monoxide concentration.

The monitoring system for CO concentration detection is shown in Fig. 1. To collect these samples, multiple sample collection tubes were placed in the gob behind the scraper conveyor. The gas from the gob was collected through these tubes using a pump, and pumped into a ball sample vessel. This full sample vessel was transferred to the laboratory for analysis. The pump system to remove gas from the gob using suction was an electric rotary vane vacuum pump with an explosion-proof motor.

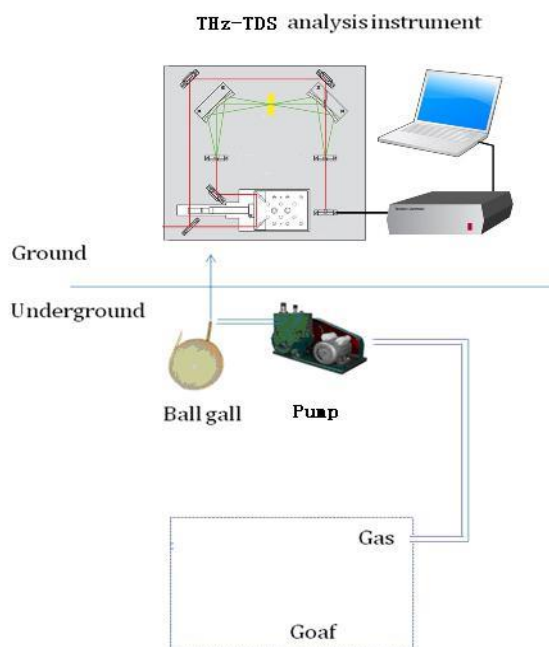


Fig. 1. Monitoring system for CO concentration detection.

Gas samples were collected at different points in the mine. Collection tubes were placed in the gob

near the air return roadway. Boundaries for the model were based on a workplace in a coalmine in northern China, which has a U-type ventilation mode. The intake airflow and return airflow are on the top and bottom, respectively, of the front of this model.

The gas samples were analyzed using a THz-TDS system which is used to measure THz absorption of carbon monoxide following the pioneering works [21].

According to the principle of radiation transfer [22-24], the radiation emitted from the source and traveling through the gas cell can be absorbed by the CO gas. The spectra of absorption coefficient for CO gas are presented in Fig. 2 at three different concentration levels, i.e., 0.5%, 1%, and 2%. CO gas is known to have a number of equispaced signature spectral lines that are at very precise frequency locations.

It can be seen that the frequency positions of the spectral lines did not change for the different concentration conditions; however, there was a significant change in the intensity of the lines from one concentration level to another. As concentration increases, so does the intensity of the rotational transition lines. There is evidently a near linear relationship between the pressure and the change in intensity of the absorption peaks. This is also true for all rotational lines in CO gas.

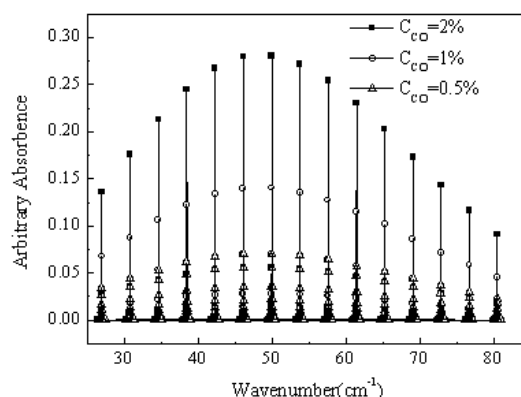


Fig. 2. Absorption spectrum of CO at different concentrations.

The measurements in this study demonstrate that varying the concentration of the gas affects only the amplitude of the absorption lines and not their exact

position. This is critical in air pollution studies when trying to single out a specific gas (such as CO) from a field sample with unknown constituents.

PREDICTION MODEL

Support vector machine (SVM) has been used in many applications, for example, the pattern recognition problem and fault diagnose with high dimension and nonlinearity [25, 26]. The hybrid Least square support vector machine (LSSVM) [27] as a novel approach for CO concentration prediction has been applied to data from the hazardous gas monitoring system. LSSVM is reformulations to the standard support vector machines which result in a set of linear equations instead of a quadratic programming problem of SVM.

LSSVM is a learning algorithm. It uses a hypothesis space of linear function in a high dimensional feature space by using the kernel theory. In this paper, this algorithm is trained by optimization theory. Consider a given training set $(x_i, y_i), i = 1, 2, \dots, n$, where x_i and y_i are the input and the output of the i th example, n denotes the number of samples. The support vector method approach aims at constructing a regression function of the following form:

$$y = \omega^T \varphi(x_i) + b \tag{1}$$

where $\varphi(x_i)$ is a nonlinear function which maps the feature space of input into a higher dimension feature space and can be reached by the kernel strategy, $\omega \in R^n$ is coefficient vector and $b \in R$ is bias term. These unknown coefficients ω and b can be obtained through solving the following optimization problem:

$$\begin{aligned} \min J(\omega, \mathbf{e}) &= \frac{1}{2} \omega^T \omega + \frac{\gamma}{2} \sum_{i=1}^N e_i^2 \\ \text{s.t.} \quad y_i [\omega^T \varphi(x_i) + b] &= 1 - e_i \quad i = 1, \dots, N \end{aligned} \tag{2}$$

where $J(\omega, \mathbf{e})$ is structure risk, In equation (2), the first term, measures the inverse of the margin distance. In order to obtain the minimum structural risk, the first term should be minimized. γ is the regularization parameter, determining the trade-off

between the fitting error minimization and smoothness. \mathbf{e} is a slack variable, which ensures classification validity under linear non-separable case. This optimization problem including the constraints can be solved by using the Lagrange function as following:

$$\begin{aligned} L(\omega, e_i, b, \alpha_i) &= \frac{1}{2} \omega^T \omega + \frac{\gamma}{2} \sum_{i=1}^N e_i^2 \\ &- \sum_{i=1}^N \alpha_i \{ y_i [\omega^T \varphi(x_i) + b] + e_i - 1 \} \end{aligned} \tag{3}$$

where α_i is the Lagrange multipliers. Considering the optimization conditions by Karush-Kuhn-Tucker (KKT), the optimal condition about (2) can be obtained as following:

$$\begin{cases} \frac{\partial L}{\partial \omega} = 0 \Rightarrow \omega = \sum_{i=1}^N \alpha_i y_i \varphi(x_i) \\ \frac{\partial L}{\partial b} = 0 \Rightarrow \sum_{i=1}^N \alpha_i y_i = 0 \\ \frac{\partial L}{\partial \alpha_i} = 0 \Rightarrow y_i [\omega^T \varphi(x_i) + b] + e_i - 1 = 0 \\ \frac{\partial L}{\partial e_i} = 0 \Rightarrow \gamma e_i = \alpha_i \end{cases} \tag{4}$$

where $i = 1, 2, \dots, N$.

Eliminating the parameter ω and \mathbf{e} in equation (4), these equality constraints can be transformed as following:

$$\begin{bmatrix} 0 & \mathbf{y}^T \\ \mathbf{y} & \mathbf{\Omega} + \frac{\mathbf{I}}{\gamma} \end{bmatrix} \begin{bmatrix} b \\ \mathbf{\alpha} \end{bmatrix} = \begin{bmatrix} 0 \\ \mathbf{Q} \end{bmatrix} \tag{5}$$

where \mathbf{I} is the identity matrix,

$$\Omega_{ij} = y_i y_j \varphi(x_i)^T \varphi(x_j).$$

The solution of $\mathbf{\alpha}$ and b can be obtained by solving (5) and substitute to (1). (1) is presented as:

$$f(x) = \sum_n \alpha_i \varphi(x_i)^T \varphi(x_j) + b \tag{6}$$

According to the Mercer rule, the kernel function $K(x_i, x_j)$ is introduced, thus the kernel function is expressed as:

$$K(x_i, x_j) = \varphi(x_i)^T \varphi(x_j) \tag{7}$$

In LSSVM, quadratic programming problem is changed as the problem of solving linear equation groups, which simplifies the calculation quantity. Combining equation (6) with equation (7), equation (6) is expressed as:

$$f(x) = \sum_n \alpha_i K(x_i, x_j) + b \quad (8)$$

There are various kernels used in the LSSVM. Different kernel function presents the different mapping from the input space to the feature space. As a result, LSSVM model changes with the different kernel function selections. The radial basis function (RBF) is used as the kernel function of the LSSVM because RBF kernel tends to give good performances under general smoothness assumptions. RBF-kernel function is presented as following:

$$K(x, y) = \exp\left(-\frac{\|x - y\|^2}{2\sigma^2}\right) \quad (9)$$

where σ is the kernel parameter and controls the LSSVM's regression or classification ability. In equation (2), γ is the regularization parameter determining the fitting error minimization and smoothness. They are important parameters in the LSSVM algorithm.

In LSSVM model, the parameter γ and parameter σ of the RBF function are chosen according to experience. In this way, for different sample sets, the optimal parameter values are difficult to be found, which affects the fault diagnosis efficiency and accuracy. However, it needs an exhaustive search over the space of hyper-parameters, which must be time consuming. This procedure needs to locate the interval of feasible solution and a suitable sampling step. In order to acquire the better classification accuracy, the particle swarm optimization algorithm (PSO) is used to find the optimal solution of these parameters in LSSVM.

The basic idea of particle swarm optimization can be described in an explicit way: each individual in particle swarm, referred to as a 'particle', represents a potential solution; each particle moves

its position in search domain and updates its velocity according to its own flying experience and neighbors' flying experience, aiming at a better position for itself.

According to the simple PSO model, the velocity V_i for each dimension of the i th particle can be updated as follow:

$$V_{i+1} = wV_i + c_1r_1(P_i - X_i) + c_2r_2(P_g - X_i) \quad (10)$$

where w is the inertia weight coefficient; c_1 and c_2 are two positive constants called acceleration coefficients; P_1 and P_2 P_i and P_g are the local individual best location and the global best location; r_1 and r_2 are random numbers in the range of [0,1]. The new position X_i for i th particle can be expressed as:

$$X_{i+1} = X_i + V_{i+1} \quad (11)$$

In the standard PSO, if $0 < w < 1$ and $V_{i+1} < V_i$, there exists a certain number that when the generation number is more than it, the current global best position P_g of the swarm does not vary, and consequently, all components of V_i , will be smaller than a given error, and the particle will stop evolution. Even if a better solution exists in this direction, the particle swarm may stop evolution before finding this position and fall into premature convergence. This is the reason why the standard PSO may fall into local optimum solution.

To solve the problem of premature convergence, we use the stochastic particle swarm optimization (SPSO) algorithm [28, 29]. Here set the inertia weight $w = 0$, substituting equation (10) into equation (11), the following equation can be obtained:

$$X_{i+1} = X_i + c_1r_1(P_i - X_i) + c_2r_2(P_g - X_i) \quad (12)$$

In order to improve the global searching ability, P_g is maintained to be the historic best position, and an extra particle j with the position X_j is generated randomly in the searching domain. In this way, the following updating procedure is obtained:

$$\begin{cases} P_j = X_j \\ P_g = \arg \min(P_i, P_j) \end{cases} \quad (13)$$

This means that if $P_g = P_j$, the random particle j locates at the best position and the new random particle will be searched repeatedly, therefore at least one particle is generated in the searching domain randomly to improve the global searching ability.

In the SPSO-LSSVM model, the appropriate parameters are selected by the SPSO algorithm, which can find the optimal parameter value quickly. As what has been mentioned above, γ and σ^2 become the swarms, then the dimension of the swarms is two. These swarms can be expressed as following:

$$\begin{aligned} \gamma_i &= [\gamma_{i1}, \gamma_{i2}, \dots, \gamma_{id}] \\ \sigma^2_i &= [\sigma^2_{i1}, \sigma^2_{i2}, \dots, \sigma^2_{id}] \end{aligned} \quad (14)$$

The key factor to determine the optimized hyper-parameters using SPSO is how to define the fitness function which evaluates the goodness of individual. The fitness function can evaluate the objective values of all particles. The choice of the fitness function is very important because it is on this basis that the SPSO evaluates the goodness of each particle solution for the LSSVM regression system. In function regression, the fitness function is the sum square error between the real output data of the system and the output data of the LSSVM model in the same input. In this study, the fitness function used is expressed as follows:

$$F(\gamma, \sigma^2) = \sum_{i=1}^N \left\{ \left[\frac{y_{ireg} - y_i}{y} \right]^2 \right\} \quad (15)$$

where y_i is real output data and y_{ireg} is the output data of the LSSVM model in the same input.

RESULTS AND DISCUSSION

Having constructed both the SVM and hybrid LSSVM models, the parameters would have had to be calibrated and evaluated. CO levels have been predicted by both SVM and LSSVM models for the field measurements.

The data taking part in the learning and testing steps of the models have been those collected from a period of 40 days in 2010 and 2011 respectively. In those days, the CO concentration was measured every 1 h so the CO level was predicted on hourly basis for each day. In both SVM and LSSVM models, 80 percent of the data were used for training the models and the rest were used for testing the models.

Optimization of these parameters has been done by a systematic grid search of the parameters using leave-one-out cross validation on the training set. First, a broad range of parameters settings are investigated with large steps. Second, after identifying a promising region, this region is searched in more details. The test set is used as an independent set to calculate the final prediction error. Furthermore, the test error is not used to select the optimal model but its size is compared to test set errors with other settings to identify possible overtraining.

The results are further analyzed using statistical indices. The statistical indices used in the analysis are mean absolute percentage error (MAPE), mean absolute error (MAE) and root mean square error (RMSE) and coefficient of determination (R^2). These parameters have been defined as below:

$$MAPE = \frac{1}{N} \sum_{i=1}^N \left| \frac{y'_i - y_i}{y_i} \right| \times 100\% \quad (16)$$

$$MAE = \frac{1}{N} \sum_{i=1}^N |y'_i - y_i| \quad (17)$$

$$RMSE = \sqrt{\frac{\sum_{i=1}^N [y'_i - y_i]^2}{N}} \quad (18)$$

$$R^2 = 1 - \frac{\sum_{i=1}^N [y'_i - y_i]^2}{\sum_{i=1}^N [\bar{y}_i - y_i]^2} \quad (19)$$

Where y_i is the observation value, \bar{y}_i is the average value and y' is the predicted value. The MAE and the MAPE correct the 'canceling out' effects; moreover, MAPE takes into account the different scales at which this measure can be computed. RMSE gives a relatively high weight to large errors. This means the RMSE is most useful

when large errors are particularly undesirable. The MAR and the RMSE can be used together to diagnose the variation in the errors in a set of forecasts. The RMSE will always be larger or equal to the MAE; the greater difference between them, the greater the variance in the individual errors in the sample. All errors are negatively oriented scores, so lower values are better. The computations were made with the Windows XP operating system and MATLAB.

Hourly CO concentrations predicted by SVM model have been shown in Fig. 3.

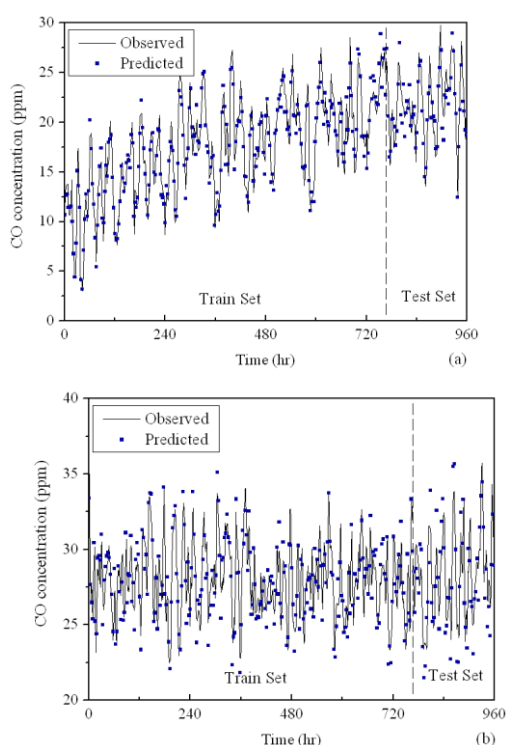


Fig. 3. Hourly CO concentrations predicted by SVM model in (a) 2010 and (b) 2011.

Correlations between prediction and measured values in the test stage have been determined using R^2 as shown in Fig. 4. Coefficients of determination for each period were 0.767 and 0.683 respectively. This means that the SVM model can predict CO concentration fluctuations within an acceptable limit. However, grid search and modeling was found to be very much time consuming. Also, there as been a significant amount of multicollinearity among the CO concentration predictors. Multicollinearity can make it difficult to correctly

identify the most important contributors to a physical process. Also the large number of the predictors, reduce the earning rate of the prediction process, hence, size reduction methods like LSSVM, can be useful solution for this predicament.

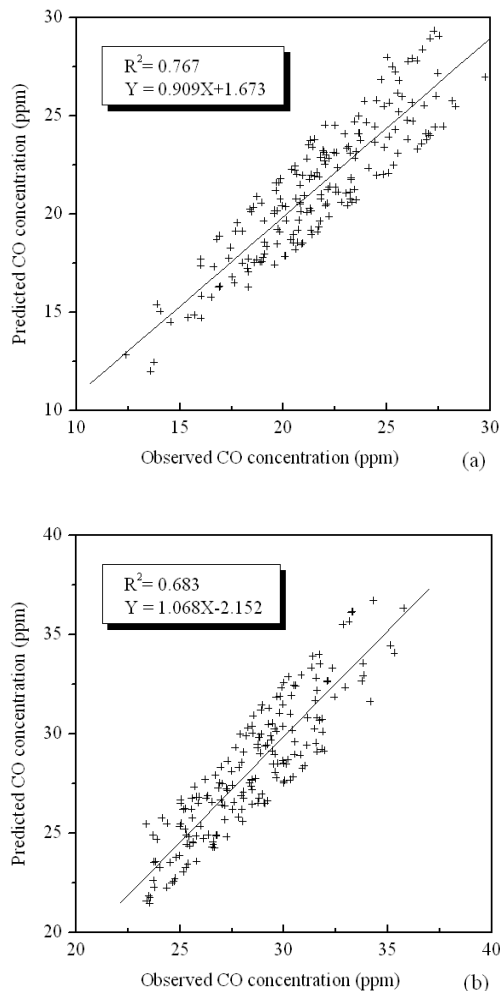


Fig. 4. Correlation between measured CO concentrations and SVM predictions predicted by SVM model during testing stages in (a) 2010 and (b) 2011.

The LSSVM method has been used in this research to reduce the size of the input data. Hourly prediction results of hybrid LSSVM model are shown in Fig. 5. Similar to the SVM model, correlations between prediction and measured values in the test stage have been determined for LSSVM model as shown in Fig. 6. Coefficients of determination for each period were found to be 0.838 and 0.78 respectively.

Results of the two SVM and hybrid LSSVM models have been compared and discussed

statistically and their respective computation times are illustrated in Table 1. It can be seen that the hybrid LSSVM model has higher coefficient of determination and fewer errors than the SVM model. Thus, the hybrid LSSVM model produced more accurate results and size reduction had positive effect on the model performance. Moreover, the hybrid LSSVM model achieves faster training speed and grid search. As it was observed, the total calculation time obviously is saved. The reduction of the input vector dimensions is resulted in the reduction of the SVM calculations and shortening the SVM training periods. Due to the effects of many factors on air pollution concentrations, a small error has remained. However in this case, the hybrid LSSVM has been found a better and faster predictive model.

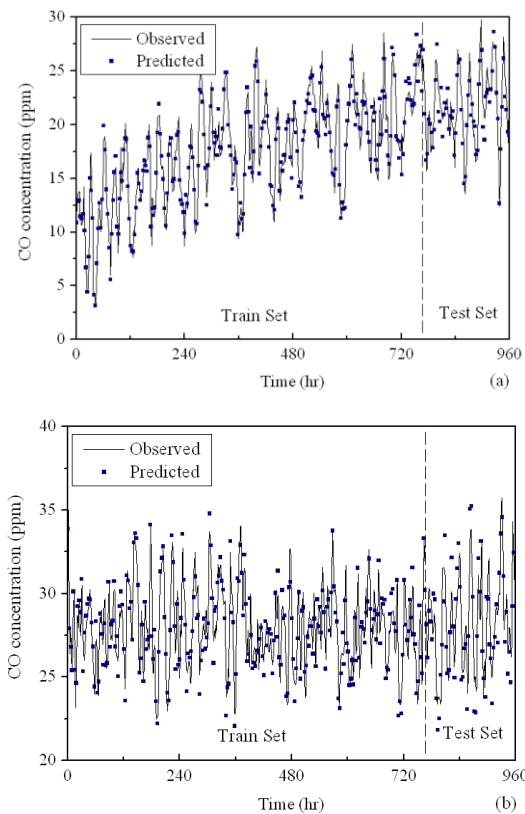


Fig. 5. Hourly CO concentrations predicted by LSSVM model in (a) 2010 and (b) 2011.

As seen in Table 1, the RMSE and MAR have decreased by using LSSVM method. This means that LSSVM is able to remove unqualified variables and noises, hence, the positive effect of the LSSVM

is more sensible. Also, the MAPE has decreased in both the testing and training processes by using hybrid LSSVM. In other words, LSSVM method can increase model prediction efficiency.

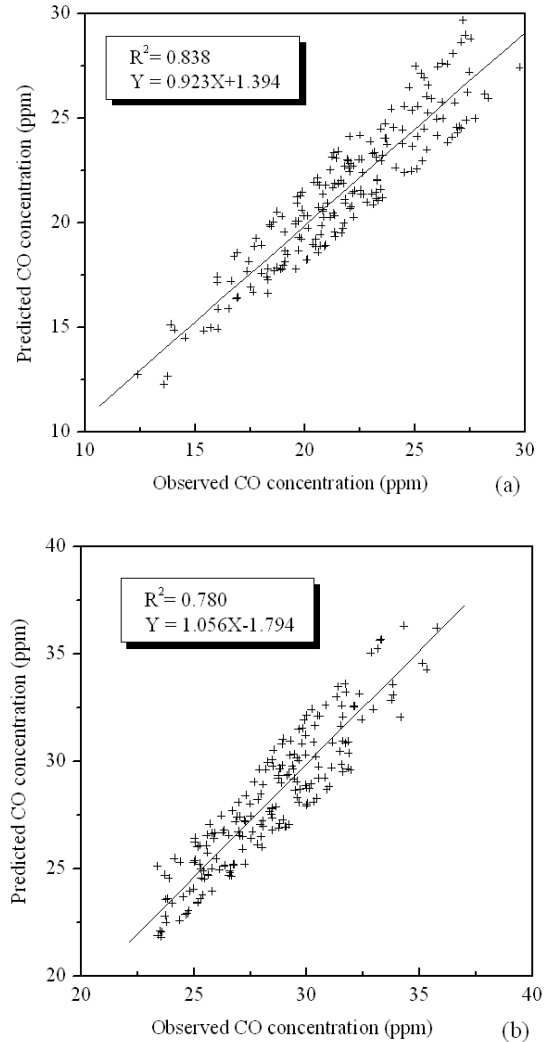


Fig. 6. Hourly CO concentrations predicted by LSSVM model in (a) 2010 and (b) 2011.

Table 1. Comparison of SVM and LSSVM models by statistics estimators.

		MAE	RMSE	MAPE	R ²	Time (s)
P ₁	LSSV Train	0.683	0.811	0.039	0.972	68
	M Test	1.173	1.358	0.054	0.838	
	SVM Train	0.856	1.028	0.049	0.956	
	M Test	1.408	1.630	0.064	0.767	
P ₂	LSSV Train	0.725	0.832	0.026	0.877	63
	M Test	1.143	1.305	0.040	0.780	
	SVM Train	0.943	1.081	0.034	0.792	
	M Test	1.371	1.566	0.048	0.683	

CONCLUSIONS

In this paper, a robot monitoring system for carbon monoxide emission from underground coal fires has been presented. The CO concentrations were measured by using terahertz time-domain spectroscopy (THz-TDS) technique according to the absorption characteristics of CO. This paper has also presented the prediction method of hourly hazardous gas emission from coal mine gob by applying the Support Vector Machine (SVM) and Least Square Support Vector Machine (LSSVM).

It can be concluded that such models provide a more promising alternative to time series forecasting. However, the important point of this approach is the data size reduction by LSSVM. The proposed hybrid LSSVM model provides a considerable improvement in the forecasting of CO concentrations over the SVM model based on the same set of input variables. Besides, the LSSVM implementation for size reduction obviously saved time of the SVM training and grid search method.

Statistical error estimators have been used to compare performance of the SVM and the hybrid LSSVM models. Errors estimated by the MRE, MSRE and MAPE decreased as R² decreased by implementing the LSSVM. Generally, the hybrid LSSVM models have good ability to predict air pollution in different time intervals.

Acknowledgements: This research was supported by the National Natural Science Foundation of China (Grant no. 51134020, 51106175 and 51104154), and A Project Funded by the Priority Academic Program Development of Jiangsu Higher Education Institutions.

REFERENCES

1. G.B. Stracher, *Int. J. Math. Geol.*, **27**, 499 (2009).
2. A.E. Whitehouse, A.A.S. Mulyana, *Int. J. Coal Geol.*, **59**, 91 (2004).
3. G.B. Stracher, T.P. Taylor, *Int. J. Coal Geol.*, **59**, 7 (2004).
4. M.A. Nolter, D.H. Vice, *Int. J. Coal Geol.*, **59**, 99 (2004).
5. E.L. Heffem, D.A. Coates, *Int. J. Coal Geol.*, **59**, 25 (2004).
6. S. Porada, *Fuel*, **83**, 1191 (2004).
7. X. Li, G. Matuschek, M. Herrera, H. Wang, A. Kettrup, *J. Anal. Appl. Pyrolysis*, **67**, 393 (2003).
8. M.V. Gil, D. Casal, C. Pevida, J.J. Pis, F. Rubiera, *Bioresour. Technol.*, **101**, 5601 (2010).
9. L. Liu, F.B. Zhou, *Int. J. Coal Geol.* **82**, 27 (2010).
10. L.M. Yuan, A.C. Smith, *Fuel*, **87**, 3409 (2008).
11. S. Wessling, C. Kuenzer, W. Kessels, M. W. Wuttke, *Int. J. Coal Geol.*, **7**, 175 (2008).
12. R.N. Singh, J. A. Shonhardt, N. Terezopoulos, *Miner. Resour. Eng.*, **11**, 2, 147 (2002).
13. K.H. Wolf, H. Bruining, *Fuel*, **86**, 2761 (2007).
14. A. Rosema, H.Y. Guan, H. Veld, *Fuel*, **80**, 7 (2001).
15. A.K. Singh, R.V.K. Singh, M.P. Singh, *Int. J. Coal Geol.*, **69**, 192 (2007).
16. J.J. Huang, H. Bruining, K.H. Wolf, *Fire Safety J.*, **36**, 477 (2001).
17. J.C. Hower, K.R. Henke, J.M.K. O'Keefe, M.A. Engle, D.R. Blake, G.B. Stracher, *Int. J. Coal Geol.*, **80**, 63 (2007).
18. F. Hindle, A. Cuisset, R. Bocquet, G. Mouret, C.R. Physique, **9**, 262 (2008).
19. J.A.K. Suykens, J. Vandewalle, *Neural Process. Lett.*, **9**, 293 (1999).
20. R. Poli, J. Kennedy, T. Blackwell, *Swarm Intell.*, **1**, 33 (2007).
21. N.N. Almoayed, M.N. Afsar, *IEEE T. Instrum. Meas.*, **55**, 1033 (2006).
22. Y. Yuan, F. Xie, H.L. Yi, S. K. Dong, H.P. Tan, *J. Infrared Millim. Wav.*, **30**, 439 (2011).
23. Y. Shuai, S.K. Dong, H.P. Tan, *J. Quant. Spectrosc. Radiat. Transfer*, **95**, 231 (2005).
24. Y. Shuai, X.L. Xia, H.P. Tan, *ASME J. Sol. Energy Eng.*, **130**, 021001 (2008).
25. Y. Guo, A.G. Song, J.T. Bao, H.R. Tang, J.W. Cui, *Int. J. Adv. Rob. Syst.*, **6**, 207 (2009).
26. X.J. Zeng, X.H. Huang, M. Wang, *Int. J. Adv. Rob. Syst.*, **6**, 59 (2009).
27. J.A.K. Suykens, J. De Brabanter, L. Lukas, J. Vandewalle, *Neurocomput.*, **48**, 85 (2002).
28. Y. Yuan, H.L. Yi, Y. Shuai, B. Liu, H.P. Tan. *Atmos. Environ.*, **45**, 4892 (2011).

29. Y. Yuan, H.L. Yi, Y. Shuai, F.Q. Wang, H.P. Tan, J. (2010).
Quant. Spectrosc. Radiat. Transfer, **111**, 2106

ИНОВАТИВЕН МОДЕЛ ЗА ПРЕДСКАЗВАНЕ НА ЕМИСИИ ОТ ВЪГЛЕРОДЕН МОНОКСИД ПОЛУЧЕНИ ПРИ ОКИСЛЕНИЕ НА ВЪГЛИЩА НА ГОЛЕМИ ДЪЛБОЧИНИ

Я.М. Уанг¹, У.З. Уанг¹, З.Л. Шао², Д.М. Уанг³, Г.К. Ши^{1*}

¹ Колеж по сигурността, Китайски минно-технологически университет, Ксуджоу, Китай

² Лаборатория на противопожарен контрол във въгледобивните мини, Ксудхоу, Китай

³ Държавна лаборатория по въглищни ресурси и безопасен добив, Ксиджоу, Китай

(Резюме)

Постъпила на 13 април, 2014 г.

Мониторингът и прогнозирането на емисиите на опасни газове вече е важна тема в минното инженерство и изследването на околната среда. Това се дължи на замърсяването на въздуха поради остатъчното окисление в подземните минни хоризонти. В настоящата работа се представя роботизирана мониторингова система за емисиите от въглероден моноксид от спонтанното горене на въглища в мини. Концентрациите на въглеродния моноксид се измерват чрез терахерц-вълнова спектроскопия (THz-TDS). На основата на измерените стойности е разработен иновативен метод, използващ „least square support vector machine“ (LSSVM) с хипер-параметричен подбор. Часовите концентрации са предсказвани чрез моделите SVM и хибридният LSSVM. Резултатите показват, че хибридният LSSVM- модел дава по-висока точност. Направен е изводът, че грешките намаляват, а корелационните коефициенти нарастват при хибридният LSSVM-модел, поради което той определено има практическа стойност и приложимост.

QSAR study on the pheromone of the turnip moth *Agrotis segetum* used as RDF descriptor

D.Z. Yang^{1,2*}, F.D.Chen², Y.B. Zhou², Z.L. Xiu¹

¹ College of Life science and Technology, Dalian University of Technology, Dalian 116021, P. R. China

² Key Laboratory of Marine Bio-resources Restoration and Habitat Repairation in Liaoning Province, Dalian Ocean University, Dalian 116023, P. R. China

Submitted April 13, 2014

Quantitative information on bioactive biological pheromone analogs from the turnip moth *Agrotis segetum* was studied, and the best prediction model was determined. The data set contained 45 organic molecules, of which 35 chemical compounds were selected as test set, and the other 10 were selected as the training set to build a quantitative structure–activity relationship model. For each analog, 150 molecular parameters were calculated, and multiple linear regression analysis was used to build the best model (used in the training and test sets, with correlation coefficients of $R^2 = 0.898$ and 0.869 , respectively). The linear relationship between biological activity and $\log P$ was also tested ($R^2 = 0.245$). Our results can serve as a reference for the quantitative prediction of pheromone activity and for the design of a new pesticide.

Key words: *Agrotis segetum* pheromone, molecular parameter, multiple linear regression, QSAR

INTRODUCTION

Communication between individuals comes in a variety of ways, such as by sound, sight, scent, and so on. The oldest way to communicate is through chemical signal substances released by individuals. from simple single-celled organisms (such as bacteria, algae, and fungi) to the highly developed humans, chemical signals are essential and apparent. Nobel Prize awardee A. Butenandt [1] first extracted a sexually stimulating compound from the gonads of a female aphid, which is stimulated by mating and makes them attract each other. He ultimately determined the existence of sexually stimulating compounds through his continuous research in 1959. In the same year, Karlson and Luscher [2] first proposed the use of

term pheromone to define the compounds and method of exchanging information between individuals through chemical signals, and established a new field of study. Study of insect pheromones is widely practiced as it does not only elucidate the chemical structure, biosynthetic pathway, molecular basis of pheromones, but it also supports the extensive research involving receptor structure and biological function.

Pheromones are sexual compounds of higher forms of living organism that are used to recognize each other. These substances can make the female and the male attract and mate with one another. Generally, pheromones are released by passive females to generate excitement and lure males. However, some species males also release pheromones. A. Butenandt [3] isolated bombyxin alcohol from the female silkworm, and determined

* To whom all correspondence should be sent.

E-mail: cumtwangym@126.com

that it is a trans-10,cis-12,16-carbon diene-1-alcohol, and also researched Lepidoptera. Pheromones contain straight-chain alcohols or acetyl with 12 to 16 carbon atoms and have one or two double bonds. In addition, chemical structures of some pheromones of *Coleoptera* and *Orthoptera* have been identified, but only show slight differences. Mammals also have pheromones, which are as studied in the fields of biology and chemistry. Many examples have been shown such as the relationship of spousal behaviors with a number of pheromones. Pheromone chemical structures are identical among heterologous animals, and their similarities have been studied for pest control.

Quantitative structure–activity relationship (QSAR) is used to describe the relationship between molecular structure and biological activity. The basic assumption is that the molecular structure helps determine physical, chemical, and biological nature of the compound, which then determine its biological activity. QSAR is a reliable and time- and labor-saving method that can be used in study of pheromones, which provides a means of predicting the functions and activities of chemical signaling compounds using available information on their molecular structures. These have important theoretical and practical roles in the in-depth study of the relationship between these biological signaling compounds and their biological activities. The purpose of this study is to create a new linear QSAR model to predict the biological activity of pheromones. With a reasonable choice of physical, and chemical, and molecular structure parameters. A better model with excellent reliability and predictability will be proposed using multiple linear regression method.

DATE SETS AND METHODS

Date sets

All the data regarding pheromone activities used in this article were from the literature. Compounds 1 to 7 were from Liljefors et al. [4], compounds 8 to 12 were from Wenqui et al.[5], compounds 13 and

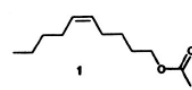
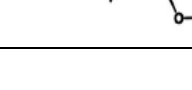
14 were from Johnson et al.[6], compounds 15 to 18 were from Gustavsson et al.[7], compounds 19 to 29 were from Johnson et al.[8-10], compounds 30 to 34 were from Bengtsson et al.^[11], compounds 35 and 36 were from an unpublished study (B. Hansson, Lund University), compounds 37 to 39 were from Ge Siwen et al. [12], compounds 40 to 43 were from Johnson et al.[9-10], and compounds 44 and 45 were from Johnson et al. [13].

In the modeling process, 75% of the sample data were included in the training set and used to create a training model, while the remaining data were included in the test set. The best prediction results were obtained by repeated training and testing, and statistical verification. The chemical structures and biological activity data of the training and validation sets are shown in Tables 1 and 2, respectively.

Parameter calculation

All compounds in the present study were first converted into 2D structures using Chemdraw from Chemoffice. These were then converted into SMILES format and entered into a molecular descriptor calculation software called The Dragon (<http://www.taletе.mi.it/>) to simulate the compound molecules, and obtain the most

Table 1. Chemical structures and biological activities including the octanol/water partition coefficients of the pheromones in training set.

No	STRUCTURE	SMILES	logP	Log(ELog(P _{re}))	re
1		<chem>CCCC\C=C/C/C/C/COC(C)=O</chem>	3.38	7.0	6.33
3		<chem>CCCCCCC\C=C/C/C/COC(C)=O</chem>	5.05	2.5	3.42
4		<chem>CCCCCCC\C=C/C/C/COC(C)=O</chem>	5.89	4.8	4.36
6		<chem>CCCC\C=C/C/C/C/C/C/COC(C)=O</chem>	5.05	2.0	2.36
8		<chem>CCCC\C=C/C(F)C/COC(C)=O</chem>	3.26	4.9	4.98

9		<chem>CCCC(F)(F)\C=C/CCC COC(C)=O</chem>	3.26	5.1	4.86
10		<chem>CCC(F)(F) C(F)(F)C=C/CCCCO C(C)=O</chem>	3.44	5.1	5.11
11		<chem>CC(=O)OC CCC\C=C/ C(F)(F)C(F) (F)C(F)(F) C(F)(F)F</chem>	4.37	2.0	1.88
12		<chem>CC(=O)OC CCC\C=C/ CCCC(F)(F) F</chem>	3.68	4.9	4.36
13		<chem>CC1CCC(C1)\C=C/ CCCCOC (C)=O</chem>	3.54	4.9	3.89
14		<chem>CC(=O)O CCCC\C=C/ C/C1=CC =CC(=C1)C</chem>	3.81	4.0	4.59
15		<chem>CCCCO\C =C/CCCC OC(C)=O</chem>	2.15	4.8	5.41
16		<chem>CCCCCO \C=C/CC CCOC(C) =O</chem>	2.98	5.0	5.00
17		<chem>COCC\C =C/CCCC OC(C)=O</chem>	1.71	6.2	5.94
18		<chem>COCCCC \C=C/CC CCOC(C) =O</chem>	2.54	4.3	3.93
19		<chem>CCCC\C=C/ C/CCC(C))COC(C) =O</chem>	3.78	4.8	5.46
21		<chem>CCCC\C=C/C C(C)CCOC(C) =O</chem>	3.71	4.6	4.99
22		<chem>CCCC\C=C/ C/CC(C) CCOC(C) =O</chem>	3.71	5.4	4.99
23		<chem>CCCC\C=C/ C(C)CC CCOC(C) =O</chem>	3.56	4.1	4.02
24		<chem>CCCC\C(C) C=C/CC CCOC(C) =O</chem>	3.56	6.0	5.64
26		<chem>CCCC(C) \C=C/CC CCOC(C) =O</chem>	3.71	4.1	4.14
27		<chem>CCC(C)C \C=C/CC CCOC(C) =O</chem>	3.71	5.1	5.24

29		<chem>CC(C)CC \C=C/CC CCOC(C) =O</chem>	3.71	6.0	6.06
30		<chem>CCCC\C=C/ C/C=C/C/ COC(C)= O</chem>	3.20	5.0	5.18
31		<chem>CCCC\C=C/ C/C=C/C COC(C)= O</chem>	3.06	5.8	5.30
32		<chem>CC(C=C)\ C=C/CCC COC(C)= O</chem>	3.06	4.1	4.76
33		<chem>C\C=C\C\ C=C/CCC COC(C)= O</chem>	3.06	6.2	6.15
34		<chem>CC(=O)O CCCC\C=C/ C/CCC=C</chem>	3.11	6.0	5.70
35		<chem>CCCC\C=C/ C/CCCC OC=O</chem>	3.12	4.6	4.50
36		<chem>CCCC\C=C/ C/CCCC OC(=O)C C</chem>	4.04	5.6	4.73
39		<chem>CCCC\C=C/ C/CCC(C) (O)=C(C) C)=O</chem>	3.23	5.4	5.83
40		<chem>CCCC\C=C/ C/CCC(C) (C)COC(C)=O</chem>	4.32	4.2	4.80
41		<chem>CCCC\C=C/ C/CC(C) (C)COC(C)=O</chem>	4.18	3.8	4.03
42		<chem>CCC(C)(C)C=C/ CCCCOC (C)=O</chem>	4.18	5.0	4.55
44		<chem>CC(=O)O CCCC\C=C/ C/CCCCI</chem>	2.99	5.3	6.06

Table 2. Chemical structure, biological activity, and octanol/water partition coefficient of the pheromone in test set.

No	STRUCTURE	SMILES	logP	Log(ELog(P _{re}))	
2		<chem>CCCCC \C=C/CC CCOC(C) =C</chem>	4.22	4.2	4.15
5		<chem>CCCC\C=C/ C/CCCC CCOC(C) =O</chem>	4.22	4.5	4.95
7		<chem>CCCC\C=C/ C/CCCC CCCCC OC(C)=O</chem>	5.89	4.0	5.19

20		<chem>CCCC\C=C/C/CCC(C)COC(C)=O</chem>	3.78	4.6	5.46
25		<chem>CCCC(C)\C=C/CCOC(C)=O</chem>	3.71	5.3	4.14
28		<chem>CCC(C)C\C=C/CCOC(C)=O</chem>	3.71	5.1	5.24
37		<chem>CCCC\C=C/C/CCCC(=O)OCC</chem>	3.55	3.5	5.58
38		<chem>CCCC\C=C/C/CCCC(=O)OC(C)=O</chem>	2.92	4.7	5.92
43		<chem>CC(=O)OCCCC\C=C/C/CCC(C)C(C)C</chem>	4.18	5.1	4.73
45		<chem>CC(=O)OCCCC\C=C/C/CCCBBr</chem>	3.11	5.6	6.13

commonly used 150 molecular Radial Distribution Function (RDF) series of the structural parameters. In accordance with the requirements of the prediction method, all the structural parameters 0 and 999 were deleted, and 158 parameters were streamlined. These parameters and the biological activity of the compounds were associated using multiple linear regression method. RDF parameters include: (1) RDF***u index: (Radial Distribution Function - *** / unweighed); (2) RDF***m index: (Radial Distribution Function*** / weighed by atomic masses); (3) RDF***v index: (Radial Distribution Function - *** / weighed by atomic van der Waals volumes); (4) RDF015e index: (Radial Distribution Function - *** / weighed by atomic Sanderson electronegativities); and (5) RDF***p index: (Radial Distribution Function - *** / weighed by atomic polarizabilities) and other descriptor.

Mathematical tools

This study was based on the molecular parameters of multiple linear regression (MLR) analysis. MLR is based on statistical analysis and is used to calculate regression equation. It also the earliest computational modeling method used to study QSAR. The basic assumptions in in MLR are based on the changes in the molecular structures

and biological activities, which are related to the physical and chemical parameters. The MLR equation is as follows:

$$Y = \beta_0 + \beta_1 X_1 + \beta_2 X_2 + \dots + \beta_k X_k \quad (1)$$

where $\beta_1, \beta_2, \dots, \beta_k$ are the regression coefficients. β_i is the average change in the dependent variable Y arising from the variation of X_k , ($i = 1, 2, \dots, k$), in the case where other independent variable remain unchanged.

RESULTS

Results of multiple linear regression analysis

In this paper, a stepwise method was chosen and used to calculate and establish the predictive model, which had a better statistical result ($R = 0.948$) and a better predictability ($R^2 = 0.898$). The linear regression relationship was significant between the structural parameters of the compound molecules and their corresponding biological activities.

A mathematical model based on six parameters (Table.3) was obtained when stepwise regression analysis was conducted. The model can be defined by the equation:

$$Y = 6.756 - 0.559RDF145m - 0.176RDF060u + 0.151RDF080e - 0.919RDF125m + 2.821RDF150m - 0.102RDF090u \dots \dots \dots (2)$$

$$n = 35, R^2 = 0.898, S = 0.528, F = 19.695, P < 0.001.$$

where n is the number of samples, R^2 is the regression coefficient, S is the standard deviation, and F is Fischer test value of the model ($P < 0.001$), which is statistically significant.

Table 3 shows the parameters that include RDF145m[1272], RDF060u[1225], RDF080e[1319], RDF125m[1268], RDF150m[1273], and RDF090u[1231].

Detection of the model

Figure.1 shows the comparison of experimental data of the stepwise and predicted values, where the triangle and square pertain to the training set and the test set molecules respectively. The results show that the predicted and

experimental values are in good agreement. The abscissa refers to the test values, and the ordinate refers to the predicted values.

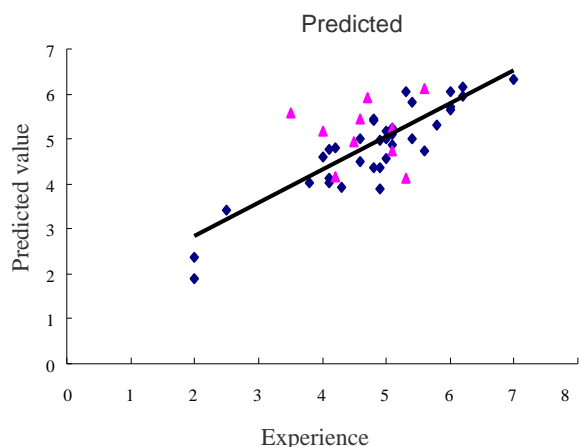


Fig.1. Experimental and predicted values of the stepwise method.

Relationship between the biological activity and sim/water coefficient (logP)

In this study, each sim/water coefficient ($\log P$) was tested for a linear relationship with the biological activity of the pheromones. The biological activity and $\log P$ relations were analyzed using statistics, and the results show that there was no significant linear relationship between the two ($R = 0.49$ and $R^2 = 0.245$). The results of statistical analysis were shown in Figure 2.

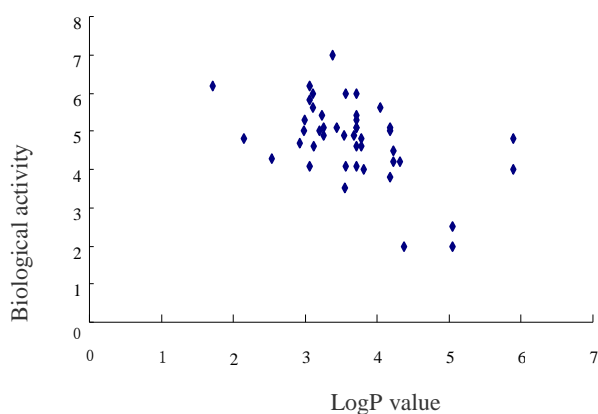


Fig.2. Relationship between biological activity and $\log P$.

DISSCUSSION

Pheromone binding proteins (PBPs) have a double role of carrying and deactivating in the insect antennae. PBPs dissolve and transport fat-

Table 3. Definition of model descriptors using the stepwise method.

Descriptors	Definition	Unstandardized Coefficients
RDF145m[1272]	Radial Distribution Function - 14.5 / weighed by atomic masses	-0.559
RDF080e[1319]	Radial Distribution Function - 8.0 / weighed by atomic Sanderson electroneg activities	0.151
RDF060u[1225]	Radial Distribution Function - 6.0 / unweighed	-0.176
RDF080e[1319]	Radial Distribution Function - 8.0 / weighed by atomic Sanderson electroneg activities	0.151
RDF125m[1268]	Radial Distribution Function - 12.5 / weighed by atomic masses	-0.919
RDF150m[1273]	Radial Distribution Function - 15.0 / weighed by atomic masses	2.821
RDF090u[1231]	Radial Distribution Function - 9.0 / unweighed	-0.102

soluble pheromones through the sensor's hydrophilic lymph to reach the dendritic membrane, and then deactivate the pheromones. A reduced PBP first combines with the pheromone and is oxidized once the pheromone and receptor membrane combine. The oxidized PBP then combines and deactivates odor molecules.

Therefore, reduced PBP may be used as a pheromone carrier, providing a binding ligand for the receptors of the dendritic membranes. Oxidized pheromone-PBP complexes do not stimulate the receptor cells. Receptor-mediated pheromone-PBP complexes may be the first step in the deactivation. The three main functions of PBP are as follows: First, it transports pheromone molecules in the lymph via the sensor micropores; second, it participates in the removal of the pheromone metabolites; third and last, it complexes with pheromone molecules to play a role in the G-protein coupled receptors of the dendritic membranes to activate the signaling pathway. The PBP complexes and pheromones combine with the receptors in the dendritic membrane, and activate the receptor-mediated G-protein, which sequentially activates the key enzyme in the second messenger cascade reaction. Adenylate cyclase catalyzes the conversion of ATP to cAMP. Phospholipase C hydrolyzes the membrane phosphatidylinositol, thereby releasing 1,4,5-inositol triphosphate) and diacylglycerol. Ion channels in plasma membranes are activated as the media concentration rapidly increase, and nerve impulses and sensor potential emerge.

A recent study of involving PBP [17,18] could provide another explanation, which estimates their activities 3D QSAR model. PBP complexes pheromone molecules and transports them to the receptors. Recent studies showed that PBP combined with the natural pheromone component have a higher affinity than the analog [16]. Even having the same concentration as with the analog, the pheromone component may have a significantly higher concentration in the receptors. Experimental receptor activity is based on a numbers contest for the same receptor, and because the relative quantity is not certain, the experimental receptor activity may overestimate the high-affinity PBP ligand. If the PBP ligand binding have better affinity data, this problem may be solved.

QSAR is based on the traditional structure–activity relationship, and combines the physical,

chemical, and mathematical methods. The history of the theory can be traced back to Crum-Brown's equation in 1868. The equation states that the physiological activity of compounds could be expressed using the function of the chemical structure. However it did not establish a clear functional model. The earliest implemented QSAR method was the Hansch equation. The Hansch equation grew out of the Hamiltonian equation and improved Taft equation. Hamiltonian equation is an empirical equation which was used in calculating the dissociation constant of a substituted benzoic acid. The equation was also used in establishing a linear relationship between the logarithm of dissociation constant of a substituted benzoic acid and the electrical parameters of substituents. Taft equation is an improvement if the Hamiltonian equation and it was used in calculating the hydrolysis reaction rate constant of aliphatic esters. The equation was also used in establishing a linear relationship between the logarithm of rate constants and electrical parameters, and the three-dimensional parameter.

As the 2D quantitative analysis could not accurately describe the relationship between the 3D molecular structure and its physiological activity, people began to explore the feasibility using 3D QSAR based on molecular conformation in the 1980s. Crippen [14] studied the 3D QSAR of distance geometry in 1979, while Hopfinger et al. [15] studied the molecular shape analysis method in 1980. Moreover, Cramer et al. [16] studied CoMFA in 1988. CoMFA swept the field of drug design when it was first released, and became the most widely used method in drug design that is based on QSAR. In the 1990s, some new 3D QSAR methods, such as CoMSIA (an improvement of CoMFA) and virtual receptor methods based on the 3D QSAR of distance geometry, appeared. However, CoMFA was still the most widely used QSAR method whatever 2D or 3D descriptor methods become available. The essence of a descriptor method is to collect better information on the chemical compounds and obtain better

mathematical models. In this present work, the RDF descriptors were used to describe the chemical information of pheromone analogs, and were fitted to the QSAR study.

Acknowledgements: This work was funded by the National Marine Public Welfare Research Project (No. 201305002, 201305043), and National Natural Science Foundation of China (No. 30901107).

REFERENCES

1. P. Karlson, A. Butenandt, *Entomology*, **4**, 39 (1959)
2. P. Karlson, M. Luscher, *Nature*, **183**, 55 (1959).
3. A. Butenandt, R. Beckmann, D. Stamm, *Chemie*, **324**, 84 (1961)
4. T. Liljefors, M. Engtsson, B.S. Hansson, *J. Chem. Ecol.*, **13**, 2023 (1987).
5. W.W. Qi, M. Bengtsson, B.S. Hansson, T. Liljefors, C. Löfstedt, G.D. Prestwich, W.C. Sun, M. Svensson, *J. Chem. Ecol.*, **19**, 143 (1993).
6. S. Jönsson, B.S. Hansson, T. Liljefors, *Bioorg. Med. Chem.*, **4**, 499 (1996).
7. A.L. Gustavsson, T. Liljefors, B.S. Hansson, *J. Chem. Ecol.*, **21**, 815 (1995).
8. S. Jönsson, T. Liljefors, B.S. Hansson. *J. Chem. Ecol.*, **17**, 103 (1991a).
9. S. Jönsson, T. Liljefors, B.S. Hansson, *J. Chem. Ecol.*, **18**, 637 (1992).
10. S. Jönsson, T. Malmström, T. Liljefors, B.S. Hansson, *J. Chem. Ecol.*, **19**, 459 (1993).
11. M. Bengtsson, T. Liljefors, B.S. Hansson, *Bioorg. Chem.*, **15**, 409 (1987).
12. A.L. Gustavsson, M. Tuvevsson, M.C. Larsson, W.W. Qi, B.S. Hansson, T. Liljefors, *J. Chem. Ecol.*, **23**, 2755 (1997).
13. S. Jönsson, T. Liljefors, B.S. Hansson, *J. Chem. Ecol.*, **17**, 1381 (1991b).
14. G.M. Crippen, *J. Chem. Ecol.*, **22**, 988 (1979).
15. A.J. Hopfinger, *J. Amer. Chem. Soc.*, **102**, 7196 (1980).
16. R.D. Cramer, D.E. Patterson, J.D. Bunce, *J. Amer. Chem. Soc.*, **110**, 5959 (1988).
17. G.D. Prestwich, G. Du. S.L. Forest, *Chemical Senses*, **20**, 461 (1995).
18. G. Schiavo, Q.M. Gu, G.D. Prestwich, T.H. Söllner, J.E. Rothman, *Proc. National Acad. Sci. USA*, **93**, 13327 (1996).

QSAR-ИЗСЛЕДВАНЕ НА ФЕРОМОНИ ОТ МОЛЕЦА *AGROTIS SEGETUM*, ИЗПОЛЗВАНИ КАТО RDF ДЕСКРИПТОРИ

Д.З. Янг^{1,2*}, Ф.Чен², И.Б. Жу², З.Л. Ксю¹

¹ Колеж за науките за живота и технологиите, Технологичен университет в Далян, Далян, Китай

² Лаборатория по възстановяване на морски биоресурси и възстановяване на хабитати в провинция Ляонинг, Океанографски университет в Далян, Китай

Постъпила на 13 април, 2014 г.

(Резюме)

Изследвани са биологично-активните аналози на феромона от молеца *Agrotis segetum* и са намерени най-добрите модели за прогнозиране. Наборът от данни съдържа 45 молекули, от които са подбрани 35 молекули, а десет от тях са избрани като аналози за съставяне на модела „количествена структура-активност“ (QSAR). За всеки аналог за изчислени 150 параметра и е използван множествен линеен регресионен анализ за съставянето на най-добрия модел (с корелационен коефициент съответно $R^2 = 0.898$ and 0.869). Линеината зависимост между биологична активност и $\log P$ също е изпробвана ($R^2 = 0.245$). Нашите резултати може да се използват като мярка за количествено предсказване на феромонната активност и синтезирането на нови пестициди.

Effect of thermophysical properties on forced convective hot air drying of multi-layered porous materials

Wei Cai ^{1*}, Guo Zhen Xie ², Jun Ming Li ³, Le Xian Zhu ¹, Shi Lin Ddong ¹

¹ Institute of Building Energy Conservation, Ningbo University of Technology, Ningbo 315016, China

² School of Energy and Environment Engineering, Beijing University of Civil Engineering and Architecture, Beijing 100044, China

³Department of Thermal Engineering, Tsinghua University, Beijing 100084, China

Submitted April 13, 2014

The convective drying kinetics of porous medium was investigated numerically. A mathematical model for forced convective drying was established to estimate the evolution of moisture content and temperature inside multi-layered porous medium. The set of coupled partial differential equations with the specified boundary and initial conditions were solved numerically using a MATLAB code. An experimental set-up of convective drying had been constructed and validated the theoretical model. The temperature and moisture content of the potato samples were dynamic measured and recorded during the drying process. Results indicate that thermal diffusion coefficient has significant positive impact on temperature distribution and mass diffusion coefficient might directly affect on the moisture content distribution. Soret effect has a significant impact on heat flux and temperature distribution in the presence of large temperature gradient.

Key words: porous materials; heat and mass transfer; thermophysical properties; convective drying

INTRODUCTION

Drying is one of the basic techniques for preserving wide variety of products, from raw materials to finished goods, from cereals to fruits. It is a highly complex transient process involving conjugated transfer phenomena of water content and heat. Drying controls to a large extent the final quality of the dried products and consumes a comparatively large amount of latent heat to eliminate the water content within the various perishable products [1-2]. In order to make the better dried products, improve dryer efficiency, reduce the operating expenses and time, the mathematical modelling tools have been one of the most important areas in modern drying technology

[3].

In recent years, many investigators like Mujumdar, Tsotsas and Rahman, have devoted their research to drying mathematical model of conjugated transport of moisture content and heat flux through porous medium [4-7]. Bennamouna *et al.* developed a transient model to evaluate the convective drying curve and the product temperature with introduction of shrinkage [8]. Ranjan *et al.* reported a two-dimensional diffusion model describing the heat and mass, momentum transfer to predict the drying rate of bananas. They reported that the experimental results were in good agreement with predicted results [9]. Morais *et al.* investigated the diffusion coefficient and drying curves of cowpea grains based on different mathematical models [10]. Although numerous studies have been published concerning heat and

* To whom all correspondence should be sent.

E-mail: zlcawei@163.com

moisture transfer model under different dimensions, mostly in mathematical analysis of the drying rate, and the dynamic characteristic of temperature and water content distribution within different porous materials, little literature is available on the effect of thermophysical properties of porous medium on the convective drying kinetics by taking the thermal-diffusion and diffusion-thermo effects into account [11-14].

In this work, a dynamic model with the third boundary condition for describing the transient heat and mass diffusion process inside the moist porous medium during forced hot air drying was proposed. An experimental method for forced convective drying was investigated and fresh potato was used as the sample. The measured values in different running conditions were compared with the calculated results to validate the effectiveness of the theoretical model developed. Effects of using different thermophysical properties of potato samples on the convective drying rate by taking into account the thermal-diffusion and diffusion-thermo effects were then investigated with numerical method.

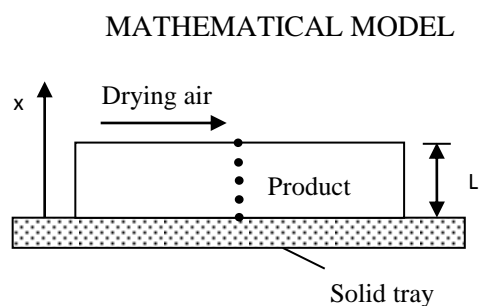


Fig. 1. Physical model of porous medium subjected to drying

A physical model that explains the sliced porous material is exposed to the hot air drying process used is shown in Fig. 1. The physical mechanisms of heat and mass transfer involved in the convective drying as follows: conductive heat transfer from the high-temperature region to the low-temperature region; forced convection takes place between the external surface of porous medium and the drying air surrounding it; mass transfer in the product is one dimensional process, which takes place only at

the surface level of the sliced porous solid; the gradients of temperature and relative moisture content are considered as the driving force of mass diffusion.

The physical model that involves the simultaneous heat and mass transfer process, as a consequence, is a very complicatedly model [15]. In order to simplify the model, the hypotheses listed below have been made:

- The flat porous slab is unsaturated, homogeneous and isotropic.
- At time zero, the products are assumed to be at uniform temperature and moisture content distributions.
- The side and bottom surfaces of the product had been insulated, and dimensions in the other directions are sufficiently large that heat transfer and moisture diffusion may be considered as one-dimensional only through x axis.
- The porous bodies are continuous slab during the drying period and compressibility effects are negligible.

According to Luikov's theory and the non-equilibrium thermodynamics using the above assumptions [16], the one-dimensional governing equations with coupled energy transfer and mass diffusion within moist medium subjected to hot air drying can be given as follows:

$$\frac{\partial T(x, \tau)}{\partial \tau} = a_q \frac{\partial^2 T(x, \tau)}{\partial x^2} + a_q \xi \frac{\partial^2 M(x, \tau)}{\partial x^2} \quad (1)$$

$$\frac{\partial M(x, \tau)}{\partial \tau} = a_m \delta \frac{\partial^2 T(x, \tau)}{\partial x^2} + a_m \frac{\partial^2 M(x, \tau)}{\partial x^2} \quad (2)$$

Where T is the local temperature of different thickness within the porous medium ($^{\circ}\text{C}$); M is the materials moisture content (kg water/kg solid, dry basis); a_q and a_m are the thermal diffusivity (m^2s^{-1}) and effective moisture diffusion coefficient (m^2s^{-1}), respectively; δ and ξ are the thermogradient coefficient (K^{-1}) and moisture gradient coefficient of the material (K); τ is the drying time (s).

Initially, the moisture content and temperature are assumed to be homogeneous within the porous material.

$$T(x, 0) = T_0 \tag{3}$$

$$M(x, 0) = M_0 \tag{4}$$

The boundary conditions of partial differential equations are given as follows:

$$\frac{\delta T}{\delta x} = 0, \quad \frac{\delta M}{\delta x} = 0 \text{ at } x = 0 \tag{5}$$

$$-\lambda \frac{\delta T(x, \tau)}{\delta x} \Big|_{x=l} = h_t [T(l, \tau) - T_a] \tag{6}$$

$$-D \frac{\delta M(x, \tau)}{\delta x} \Big|_{x=l} = h_m [M(l, \tau) - M_a] \tag{7}$$

Where λ , D , h_t and h_m are the heat-transfer coefficient ($\text{Wm}^{-2}\text{K}^{-1}$), mass-transfer coefficient (ms^{-1}), convective heat and mass transfer coefficient, respectively; l is the thickness of the multi-layered porous materials (m), x is the vector dimension in the direction of the thickness (m).

The coupled partial differential equations were discretized with the specified boundary and initial conditions. Equations (1) ~ (7) were integrated numerically by using a LU decomposition scheme, and a MATLAB 7.0 procedure code was developed to solve the system of partial equations. Fig. 2 is the flow chart of the detailed solution procedure.

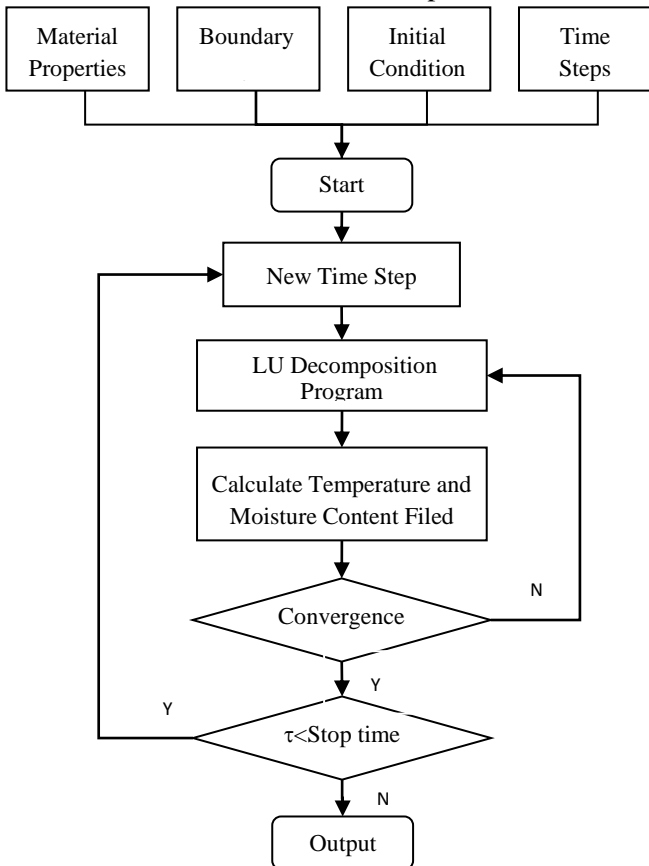


Fig. 2. Flow chart of the numerical calculation.

EXPERIMENTAL PROCEDURES

In order to validate the theoretical model, drying tests were carried out to investigate the coupled heat and mass transport in moist materials. Fig. 3 shows the convective drying experimental set-up scheme. A whole include a hot air drying chamber, a humidifier, an air heater, an analytical balance and a hygrometer and a fan. Before each new test, the drying apparatus is set to the experiment conditions required and then is left running for 90 min to ensure and maintain the steady-state operating conditions.

Fresh potato, which was used as the sample, was obtained from a market under the same brand. At the beginning of each drying test, the drying samples were stabilized at ambient air temperature, then peeled and cut into slices approximately 8 mm thick. The samples were put in the drier, where air was circulated through the top surface of drying material. As Fig.1 shows, the local temperatures of different thickness within the potato samples were measured by five T-type thermocouples, then recorded and stored in a digital data logger at an interval of 30 s. To obtain the drying rate, the

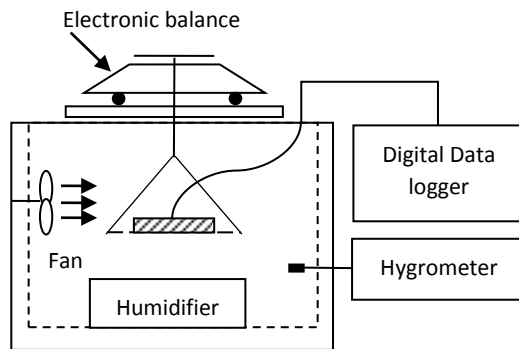


Fig. 3. Overall sketch of the experimental apparatus

weight change of the potato specimen during drying was dynamic measured and recorded with an electronic balance (Fig.3). At the end of each drying test, the potato specimens were put in a hot air circulation oven at 120°C for 24 h and weight again to determine the bone-dry weight.

Table 1. Estimated parameters of the contact drying experiment

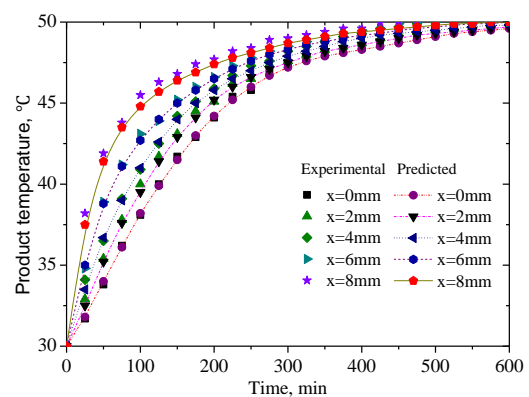
Temp. °C	RH, %	Vel., m/s	$\frac{\partial T}{\partial \tau}$, $\times 10^4 \text{ } ^\circ\text{C}/\text{s}$	$\frac{\partial M}{\partial \tau}$, $\times 10^4 \text{ } \%/ \text{s}$	$\frac{\partial T}{\partial x} _{x=l}$, $^\circ\text{C}/\text{s}$	$\frac{\partial M}{\partial x} _{x=l}$, $\%/ \text{s}$
55	40.0	0.276	6.94	-3.375	175.3	290.9
60	40.0	0.276	8.61	-4.785	218.3	145.6
60	58.6	0.276	4.19	-2.146	103.9	187.7
55	58.6	0.192	5.79	-2.548	145.0	220.7

To investigate the force convective drying process, a number of drying experiments were conducted using the same samples under different conditions, as Table 1 shows. By inverse problem method [17-18], the thermophysical parameters were estimated, the heat and mass transfer coefficients were $a_q = 2.54 \times 10^{-7} \text{ m}^2\text{s}^{-1}$, $a_m = 6.95 \times 10^{-8} \text{ m}^2\text{s}^{-1}$, $\delta = 0.0124 \text{ K}^{-1}$ and $\xi = 0.0185 \text{ K}$. Figure 4 shows the comparison of the simulated and experimental values of temperature and average moisture content within the potato sample during forced convective drying. Fig. 4(a) illustrates the local temperature of every layer of the sample will become higher as drying time goes by. The temperature difference between the top and bottom surfaces of the sample is become decrease with the drying time. There were no significant differences between the predicted and experimental temperature values at about 5% level. The drying rates are compared in Fig. 4(b). It is observed that the higher temperature and lower water content in the top surface of the sample than those in the bottom surface. This model could predict the temperature and moisture content variations in close agreement with the experimental data.

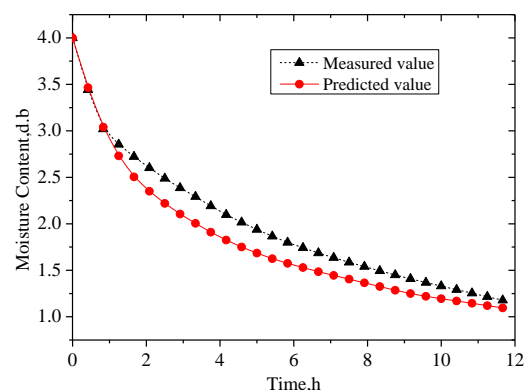
RESULTS AND DISCUSSION

Different phenomena linked to local temperature variation and moisture content loss with drying time are observed in the course of modern drying

technology [19-20]. Fig. 5 shows local temperature and moisture content distributions profile in the sample under real parameters. As shown in Fig. 5(a), the transient temperature of the upper part of the sample was increased rapidly and close to the hot air temperature near the end of drying. As shown in Fig. 5(b), the water content of the upper exposed surface layer of the product gradually decreased with the drying process, and the accumulation phenomenon of local humidity was found in deeper part of the product. As time goes on, the increased range of local moisture content of the deep layer would decrease, and the value would rise steadily. Subsequently the water content of the product was gradually diminished and nearly equal to the hot air humidity as the drying running toward the end. This is attributed to the fact that the mass flux migrate along the temperature gradient under Soret effect.



(a) temperature distribution



(b) average moisture content

Fig. 4. Comparison of simulative and experimental values with drying time.

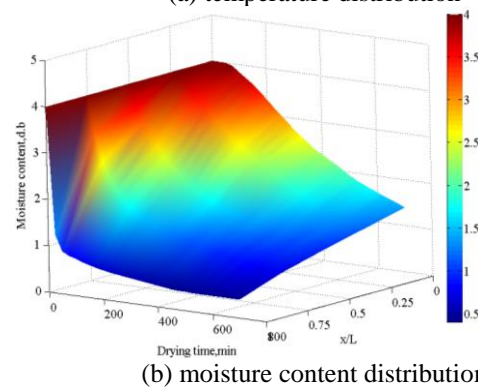
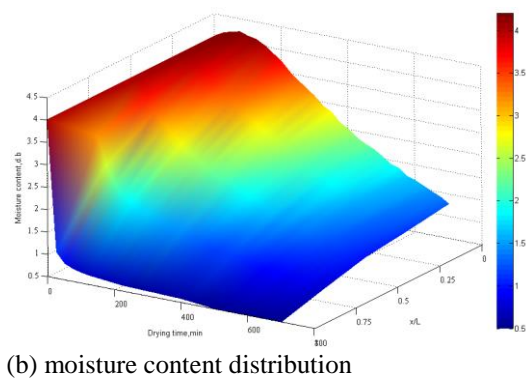
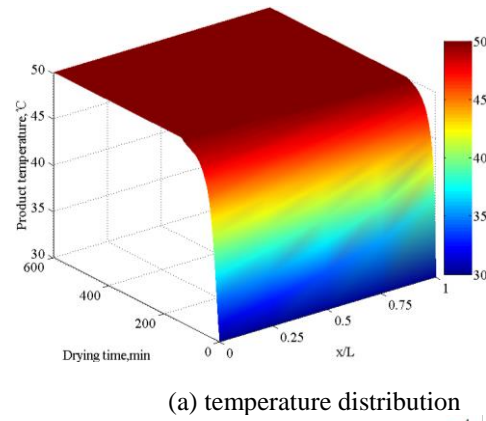
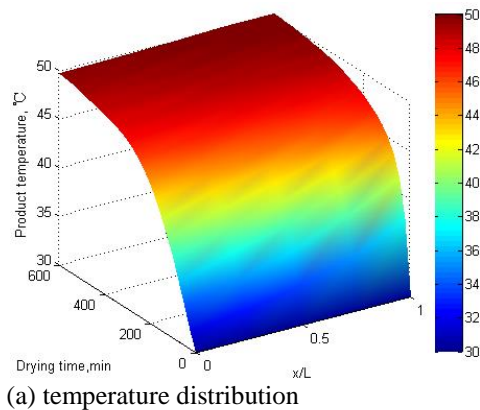


Fig. 5. Temperature and moisture content distributions in the product under real condition.

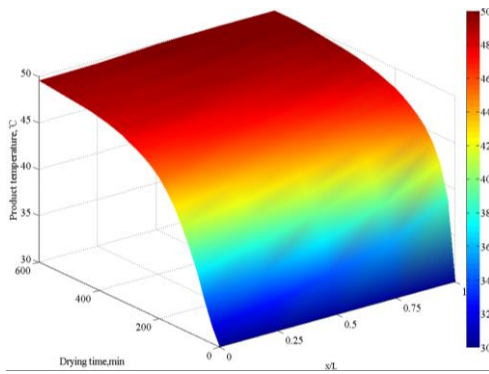
In order to describe heat and moisture transfer within potato product due to thermal diffusion, the simulation was repeated with thermogradient coefficient $a_q=2.54 \times 10^{-6} \text{ m}^2\text{s}^{-1}$ and the numerical simulation results are presented in Fig. 6. Fig. 6(a) shows that heat flow from hot air to the porous product is a process of energy transfer tending to equalize temperature in a very short time. These findings confirm that thermal diffusion coefficient has significant positive impact on heat flux and temperature distribution. However, there is no obvious difference between Fig. 5(b) with Fig. 6(b). One reason for this could be that the thermal diffusion behaviour has no significantly affect on moisture content distribution and dehydration in the product during conventional drying process.

Fig. 7 shows the local water content and temperature distributions profile within the moist product as the effective mass diffusion coefficient increasing by 10 times. Compared Fig. 5(a) with Fig. 7(a), one can easily find that it is no obvious difference, this may be due to the effective water

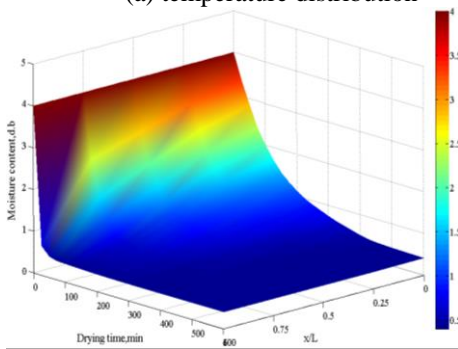
Fig. 6. Effect of heat diffusion coefficient on temperature and moisture content distribution in the product

vapour diffusion coefficient is very small and its influence on the temperature gradient and heat flow is less weak. It can be found in Fig. 7(b) that the humidity of the product is rapidly decreasing, the bulk of the water vapour migrate much easily through the upper exposed surface of the material and then quickly evaporated into the atmosphere. These findings imply that diffusion coefficient affects mass transfer and moisture content distribution.

As the thermogradient coefficient of the material increasing by ten times, the local temperature and moisture content distribution profiles are Fig.8 shows. It can be concluded from Fig. 8(a) that the thermogradient coefficient of the moist material has relatively less affect on the heat flux. As shown in Fig. 8(b), the accumulation phenomena of moisture content in that deep part of the product will be become more marked, this is due to the fact that water content diffuse towards the lower part of the product under Soret effect to the maximum extent. Also note that the growth of local moisture content

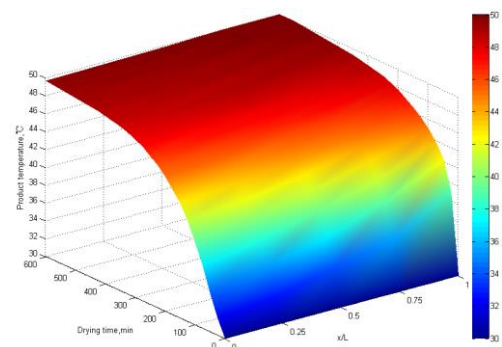


(a) temperature distribution

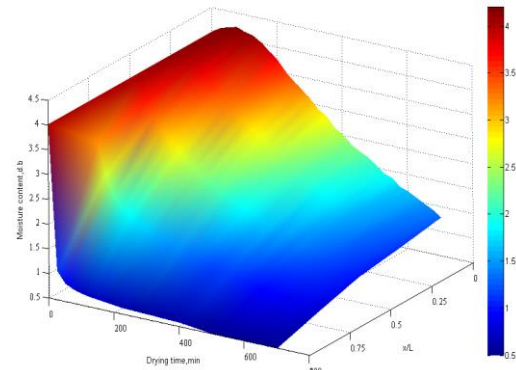


(b) moisture content distribution

Fig. 7. Effect of mass diffusion coefficient on temperature and moisture content distribution in the product

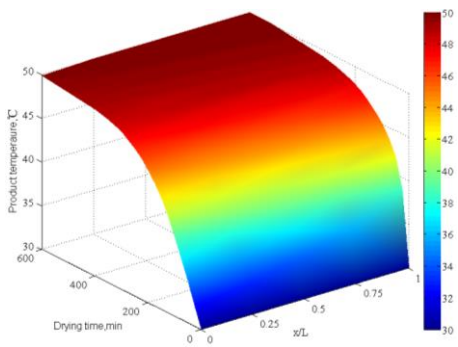


(a) temperature distribution

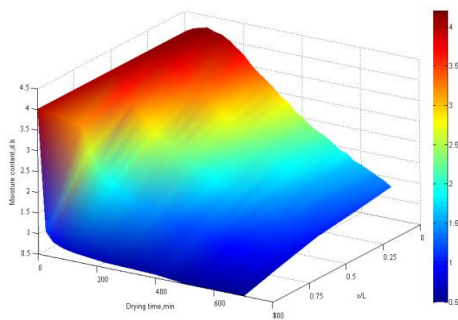


(b) moisture content distribution

Fig.9. Effect of moisture gradient coefficient on temperature and moisture content distribution in the product.



(a) temperature distribution



(b) moisture content distribution

Fig. 8. Effect of thermogradient coefficient on temperature and moisture content distribution in the product

of the deep part of the product reduces constantly and the humidity amount would reach a maximum. Variation of moisture content coefficient inside the product with drying time is shown in Fig. 9. It can be seen that moisture content coefficient has no obvious influence on the temperature distribution in the product. This shows that Duffour effect has relatively weak effect on temperature distribution in convective drying. The results indicate that the effect of mass transfer on heat transfer is very weak in conventional drying.

4. CONCLUSIONS

This paper proposes a theoretical model of coupled heat and moisture transport to evaluate the effects of thermophysical properties on the moisture content and temperature distributions within the porous materials during convective drying. An experimental system for analyzing the convective drying characteristic was developed to investigate the coupled heat and mass transport in the moist materials. The predicted temperature and

moisture content were compared with the experimental data.

Effects of using different thermophysical properties of potato samples on the convective drying rate by taking into account the thermal-diffusion and diffusion-thermo effects were investigated. The predicted results show that thermophysical parameters of the product has significant influence on the combined moisture content and heat transport inside the potatoes subjected to forced convective dried, and the accumulation phenomena of moisture content is found in the deep part of the moist product. Thermal diffusion coefficient has significant positive impact on heat transfer, and effective mass diffusion coefficient might directly affect on the moisture content distribution and convective drying rate. Soret effect has a significant impact on heat transfer in the presence of large temperature gradient during convective drying.

For further work, it would be desirable to estimate the thermophysical parameters of different porous materials and extend the modelling to multi-dimensional heat and moisture transfer process within moist media during forced convective drying.

Acknowledgements: Programs Supported by Ningbo Natural Science Foundation under Grant No. 2011A610073 and Beilun Science and Technology Innovation Foundation, Ningbo University of Technology. This material was also funded by National Undergraduate Innovation and Entrepreneurship Training Program (201311058005) and Wang Weimin Innovation Foundation (2013014).

REFERENCES

- 1.S.M.A. Rahman, M.R. Islam, A.S. Mujumdar, *Drying Technology*, **25**, 1359 (2007).
- 2.L. Sun, M.R. Islam, J.C. Ho, A.S. Mujumdar, *Bioresource Technology*, **96**, 1551(2005).

- 3.C. Lamnatou, E. Papanicolaou, V. Belessiotis, N. Kyriakis, *Numerical Heat Transfer Part A-Applications*, **56**, 379 (2009).
- 4.V.P.C. Mohan, P. Talukdar, *Int. J. Heat Mass Transfer*, **53**, 4638 (2010).
- 5.T. Defraeye, B. Blocken, J. Carmeliet, *Int. J. Heat Mass Transfer*, **53**, 112 (2012).
6. R. Prommas, *Int. Commun. Heat Mass Transfer*, **38**, 900 (2011).
- 7.B. Zecchi, L. Clavijo., J.M. Garreiro, P. Gerla, *J. Food Eng.*, **104**, 49 (2011).
- 8.L. Bennamouna, L. Fraikina, A. Leonarda, *Drying Technol.*, **32**, 13 (2014).
- 9.R. Ranjan, J. Irudayaraj, J.N. Reddy, A.S. Mujumdar, *Numerical Heat Transfer Part A-Applications*, **45**, 997 (2004).
10. IS.J.D. Morais, I.A. Devilla, D.A. Ferreira, I.R. Teixeira, *Revista Ciencia Agronomica*, **44**, 455 (2013).
11. T.W. Wong, W.H.N.S. Ashikin, C.L. Law, *Drying Technol.*, **32**, 117 (2014).
12. T. Defraeye, B. Blocken, J. Carmeliet, *Int. J. Heat Mass Transfer*, **55**, 112 (2012).
13. C.A. Perussello, V.C. Mariani, A.C.C. do Amarante, *Int. J. Food Properties*, **17**, 891(2014).
14. B.K. Jha, U. Mohammed, A.O. Ajibade, *J. Appl. Math*, 2013 (2013).
15. I. Bialobrzeski, *Drying Technol.*, **24**, 551 (2006).
16. D. Jou, J. Casas-Vazquez, G. Lebon *Extended irreversible thermodynamics* (4th ed.), Springer, Berlin, (2010) pp. 36-43).
17. G. T. Santos, M. Fortes, J.H. Martins, P.M.D. Monteiro, *Drying Technol.*, **31**, 1979 (2013).
18. U. Akyol, A. Cihan, R. Shaliyev, *Inverse Problems in Science and Engineering*, **18**, 227, (2010).
19. L.P. Wang, M. Zhang, S.B. Huang., L.Q. Lu, S.M. Roknul Azam, *Drying Technol.*, **32**, 190 (2014).
20. S.W. Zhang, N.H. Kong, Y.F. Zhu, Z.J. Zhang, C.H. Xu, *Mathematical Problems in Engineering*, 2013.

ЕФЕКТ НА ТЕРМОФИЗИЧНИТЕ СВОЙСТВА ВЪРХУ ПРИНУДЕНИТЕ КОНВЕКЦИИ ПРИ СУШЕНОТО НА МНОГО-СЛОЙНИ ПОРЪОЗНИ МАТЕРИАЛИ

Уей Кай^{1*}, Гуо Жен Ксие², Джун Минг Ли³, Ле Ксианг Жу¹, Ши Лин Донг¹

¹ *Институт по съхранение на енергията в строителството, Технологичен университет в Нингбо, Нингбо, Китай*

² *Колеж за енергетика и екологично инженерство, Пекински университет по строителство и архитектура, Пекин, Китай*

³ *Департамент по термично инженерство, Университет Цинхуа, Пекин, Китай*

Постъпила на 13 април, 2014 г.

(Резюме)

Изследвано е числено конвективното сушене на порьозна среда. Съставен е математичен модел за принуденото конвективно сушене за да се оцени изменението на важността и температурата в многослоен порьозен слой. Числено е решена система от свързани частни диференциални уравнения с начални и гранични условия с помощта на софтуера MATLAB. Математичният модел е изпитан експериментално. Изследвано е сушенето на проби от картофи в динамични условия (като температура и влажност). Резултатите показват, че коефициентът на термична дифузия и значителен положителен ефект върху температурния профил, а коефициентът на молекулярна дифузия може да влияе директно на разпределението на влажността. Ефектът на Soret има значително влияние върху топлинния поток и разпределението на температурата при големи температурни градиенти.

Photocatalytic oxidation of gaseous acetone and ethanol mixtures over titanium dioxide powders

Wei Cai^{1,2*}, Wei Gu¹, Lexian Zhu¹, Wen Lv¹, Chunli Xia², Bo Ding²

¹ School of Civil Engineering and Architecture, Ningbo University of Technology, Ningbo 315016, China

² School of Energy and Power Engineering, Xi'an Jiaotong University, Xi'an 710049, China

Submitted April 13, 2014

A gas-plate reactor coated with a commercial titanium dioxide (TiO₂) was used to investigate the performance of ultraviolet photocatalytic oxidation (UV-PCO) of ethanol and acetone contained in air. The device was challenged with organic compound mixtures: ethanol and acetone. The influence of the interaction, temperature, air flow rate on the conversion rate has been studied for the compounds. The result shows that the presence of ethanol reduces the initial degradation rate of acetone, the inhibition increases with increasing of ethanol in the system. This could not be interpreted by classic Langmuir-Hinshelwood (L-H) model. Acetone also inhibits the degradation of ethanol but it still can be described by L-H model. Acetaldehyde in the system comes from the degradation of ethanol, the behaviour of production and consumption of which is affected by the amount of ethanol and acetone in the mixture. Temperature significantly affects the degradation of organic compounds. Increasing the temperature accelerates the degradation of ethanol and acetone as well as the degradation of acetaldehyde, an intermediate produced in the system. Conversion efficiency generally diminished with increased airflow rate. The surface reaction mainly controls the oxidation rate while the gas-phase mass transfer effect is negligible.

Key words: photocatalytic degradation; VOCs; ethanol; acetone

INTRODUCTION

Indoor air quality (IAQ) can significantly impact human health, comfort, satisfaction, and productivity. Volatile organic compounds (VOCs) are an important group of air pollutants widely present in indoor environment [17]. Since VOCs emitted from buildings materials can attack human organs for a long period of time, thus causing various diseases, numerous attempts have been made to remove them from the atmosphere using several methods such as adsorption on activated carbon, thermal treatment, catalytic oxidation technologies, and so on [6, 8].

Ultraviolet photocatalytic oxidation (UV-PCO), as a convenient innovative and promising advanced oxidation technology, has been suggested as an alternative and energy efficient method to improve IAQ through the photocatalytic degradation of volatile organic compounds [3,16,21,25]. In the past decades, numerous studies have been carried out by researchers from all over the world on the application of PCO process to decompose and mineralize many VOCs. For example, formaldehyde [4,13,19], benzene [3,17,25], ethanol [7,14], acetone [14,18], toluene [9,11,15,17,20], trichloroethylene [10], dichloromethane were successfully degraded using UV-PCO technique. The previous study on the PCO process mainly focuses on the purification of a single type of pollutants, but little attention is paid to the interaction between organic compounds during photocatalytic decomposition [5].

In this work, the photocatalytic oxidation of acetone,

ethanol and the interaction between them during photocatalysis process have been investigated using a Fourier-transform infrared spectroscopy (FTIR). Ethanol is a typical organic compound indoors, and acetone is a popular indoor air pollutant. Indoor air, the presence of acetone and ethanol are due to the use of domestic materials and products as paints and cleaning products. Thus, in this present paper, ethanol and acetone were chosen as target pollutant species. This paper presents the experimental results and discusses the influence of the interaction between acetone and ethanol on photocatalytic activity of TiO₂.

MATERIALS AND METHODS

2.1 Catalyst preparation

Titanium dioxide (TiO₂) exhibits high activity and stability, was selected as the most active metal oxide semiconductor among heterogeneous photocatalysts and now it plays an important role in many industrial and technological processes, environmental and biomedical application (Tang and Yang, 2012). A commercial TiO₂ powder catalyst, without pretreatment, was supplied by Degussa (P-25, composed of 75% anatase and 25% rutile). The mean size and specific surface area of the catalyst particle was 21 nm and 50m²/g, respectively, measured by Micromeritics ASAP 2020 (Micromeritics, USA) nitrogen adsorption and desorption equipment.

TiO₂ powders were dispersedly deposited on a glass tube using the dip-coating method. TiO₂

* To whom all correspondence should be sent.
E-mail: zlcawei@163.com

powder was put into distilled water and dispersed fully in a magnetic stirring apparatus to get 2.5wt% TiO₂ slurry in advance. The glass tube was loaded with TiO₂ slurry, impregnated for 30 min and then dried at 373 K for 2 h in a loft drier heated by electricity. It was soaked and dried again and again until 2.05g TiO₂ was coated, i.e., the loaded TiO₂ on the tube was $3.24 \times 10^{-3} \text{g/cm}^2$. The total mass of TiO₂ loaded was determined by the weight difference before and after the coating procedure. By the way, when the density of TiO₂ on the side of the tube is over $3.2 \times 10^{-3} \text{g/cm}^2$ no light could permeate it.

Experimental apparatus

To develop a methodology for evaluating the performance of UV-PCO, an innovative system was built up, and the schematic diagram of the test apparatus employed a recycling loop is shown in Fig.1. It consists of a stainless steel UV-PCO reactor and an air stream circulation system. The reactor includes a 20-W lamp with 98% of the UV lamp radiation emitted at 254 nm and a glass tube (6.6 cm i.d. \times 62 cm long) that coated with TiO₂ powder in advance. They are located concentrically with 5 mm radial clearance. The ports on the left are used to put in the air containing reactants before each experimental run. The fan in the system is used to control the flux of the air. Fig.1 presents the system to generate the air containing the ethanol, acetone or the mixture of them. Compressed synthetic air (mixture of nitrogen and oxygen with volume ratio 79:21) was supplied by a gas cylinder. The compressed air was divided into three streams. Two of the ways are used to produce the air containing pollutants and one is used for cleaning the set-up before experiment. The bottles in the ways were filled with ethanol and acetone solutions

respectively. The mass percentage of the solution of ethanol is 99.7% and that of acetone is 99.5%. Ethanol and acetone sol were mixed with the compressed air and then was supplied through different mass flow controllers to the PCO reactor.

Procedure

The PCO experiments were carried out following a standard procedure. Before experiment the set-up is washed for 10 min by fresh air at the rate of 500 ml/min and then the air with pollutants is pressed in the set-up. After valves No.1 is turned off the No. 2 is turned on. The fan in the system starts to work and No. 3 and No. 5 on the sample ports are open. After the system is stable the UV-lamp is turned on and the photocatalytic degradation of organic compounds is enabled. During experiment the valve No.1 is closed and the valve No.2 is open. Sampling ports are on the right. They are connected with a FTIR (Perkin Elmer, UK) spectroscopy apparatus which is used to monitor the reactants and products. The valve No. 4 is closed while No. 3 and No. 5 are open for air to go into FTIR monitoring system during experiment. The data is recorded by a FTIR per 10 min, which has been quantified in advance by a gas chromatographic analysis (SP2100, made in Beijing, China). Temperature in the reactor is regulated through the water temperature in the water bath. The flux of air in the system is adjusted through the fan

RESULTS AND DISCUSSION

Developing an effective PCO reactor for IAQ purpose requires the ability to predict the performance of the device over the range of variability of the appropriate atmospheric variables

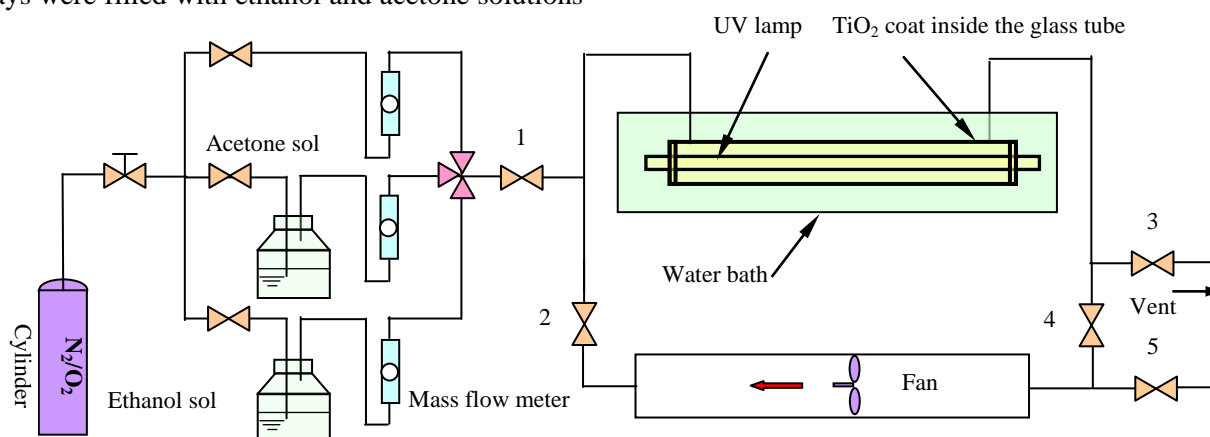


Fig.1. Schematic diagram of the experimental set-up.

(e.g. temperature, relative humidity, and initial concentration) and design variables (e.g. flow rate, UV-light intensity, and catalyst surface area) (Zero et al., 2010).

Degradation of acetone in the presence of ethanol

Fig.2 demonstrates the degradation of acetone in the presence or absence of ethanol. The experiments were carried out at the average temperature of 14°C and the flow rate of 500 ml/min. The slope of the short dash lines drawn in Fig.3 denotes the mean reaction rate of acetone, the values of which are given in Table 1.

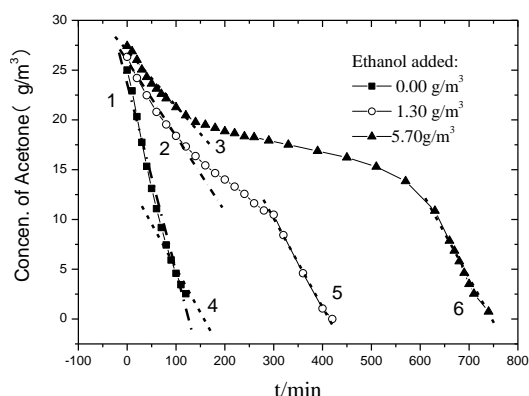


Fig. 2. Degradation of acetone in the presence and the absence of ethanol.

Table 1. Mean slope rate of the lines in Fig.2.

No.	1	2	3	4	5	6
Values	0.210	0.080	0.064	0.100	0.100	0.100
	Error ±0.005					

It is clear that during the degradation of single acetone the reaction rate can be described approximately by the rate of slope of dash line 1, while it can be characterized by the slope coefficient of line 4 when the concentration of acetone in the system is less than 8g/m³. The rate of slope of line 1 is the steepest among lines 1, 2 and 3 indicating that the initial degradation rate of acetone in single case is the fastest. The presence of ethanol reduces the initial degradation rate of acetone and the inhibition of ethanol increases with increasing the amount of ethanol in the system.

With the development of the photocatalytic degradation, acetone concentration decreases

against time gradually. Before it reaches 8g/m³ the inhibitory action of ethanol has existed. It can be seen from Fig. 2 that the higher the concentration of ethanol the lower the degradation rate of acetone. After the concentration of acetone falls to 8g/m³, the degradation rate can be expressed by the slope coefficient of parallel lines 4, 5 and 6, which is less than that of line 1. This result indicates the effect of ethanol disappear hereafter. In a word, compared with the degradation of acetone alone, it cannot be explained by Langmuir-Hinshelwood (L-H) model in presence of ethanol. The presence of ethanol reduces the initial degradation rate of acetone and the inhibition is increased with the increase of ethanol in the system.

Degradation of ethanol in the presence of acetone

Fig. 3 presents the concentration of the ethanol against time with and without acetone. The average initial concentration of ethanol is 6.14 g/m³. The initial concentration of acetone is 0, 12.54 g/m³ and 27.42 g/m³ respectively, the temperature is 4°C, and the flow rate is 500 ml/min.

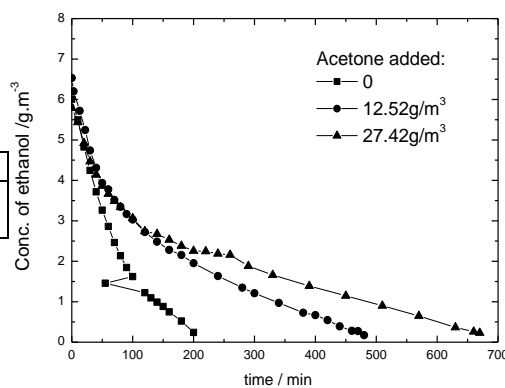


Fig. 3. Ethanol concentration against time in the presence and the absence of acetone.

As shown in Fig. 3, the concentration of the ethanol decreases gradually against time. The presence of acetone inhibits the degradation of ethanol. The higher the initial concentration of acetone is, the stronger the inhibition is. Nevertheless, the degradation of ethanol still can be described by L-H model. The existence of acetone makes the time for degradation of ethanol longer.

Production of acetaldehyde

Fig.4 shows the acetaldehyde concentration produced during the degradation of ethanol, acetone and the mixture of them. It can be observed that only two acetaldehyde curves appear. There is no acetaldehyde produced during the photo-catalytic degradation of acetone. It is concluded that the acetaldehyde comes from the degradation of ethanol, which was in accordance with the conclusion reported by Ding *et al.* [2].

The behaviour of production and consumption of acetaldehyde is affected by the amount of ethanol in the mixture. With the increase of the initial concentration of ethanol the peak concentration of acetaldehyde increases and the time for acetaldehyde to be exhausted is prolonged.

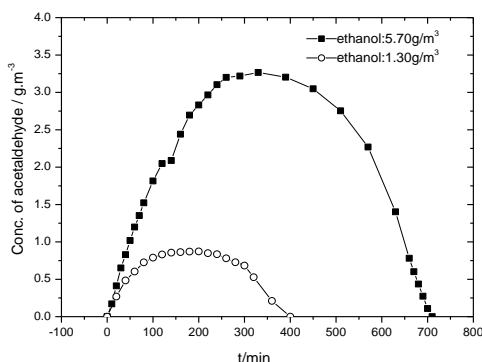


Fig. 4. Acetaldehyde produced during the degradation of ethanol in presence of acetone of 26g/m³

The behavior of production and consumption of acetaldehyde is affected by the amount of ethanol in the mixture. With the increase of the initial concentration of ethanol the peak concentration of acetaldehyde increases and the time for acetaldehyde to be exhausted is prolonged.

Acetone affects the production and consumption of acetaldehyde (See Fig. 5). The amount of acetone in the system also affects the behavior of production and consumption of acetaldehyde. Increasing the initial concentration of acetone in the system can raise the peak concentration of acetaldehyde and extend the subsistence time of acetaldehyde. It can be understood since the acetaldehyde concentration in the reaction system results from the balance of the two reactions: one is the reaction that ethanol is oxidized to acetaldehyde

and the other one is that acetaldehyde is photo-catalytically degraded. The results above indicate that the presence of acetone inhibits the degradation of acetaldehyde, resulting that the increase of peak concentration acetaldehyde and the prolongation of the subsistence time.

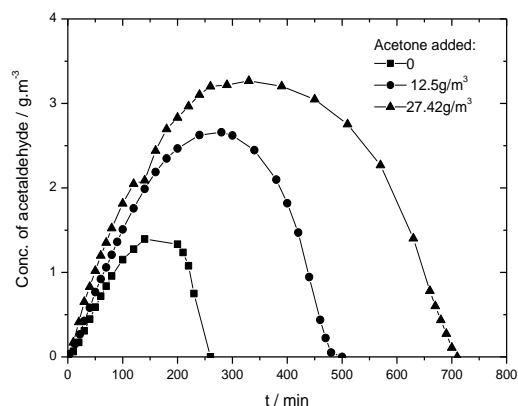


Fig. 5. Effect of the acetone in presence of ethanol of 6g/m³.

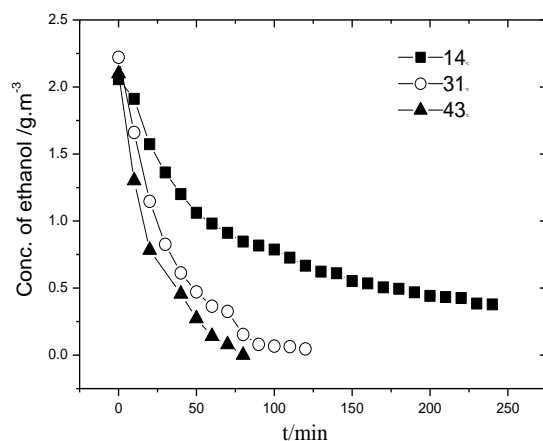


Fig. 6. Effect of temperature on the ethanol degradation.

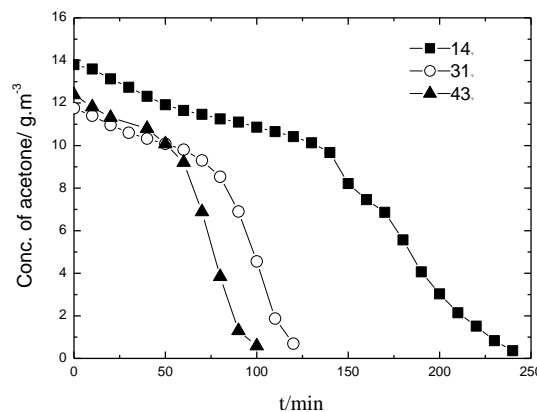


Fig.7. The effect of temperature on acetone degradation.

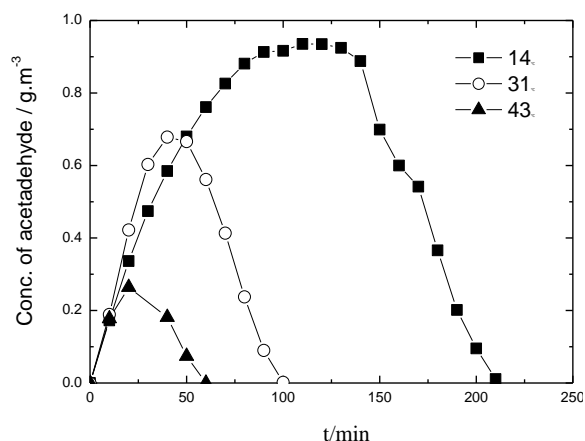


Fig.8. The effect of temperature on acetaldehyde produced.

Effect of temperature

Temperature is usually considered a key factor that influence of UV-PCO process based on the widely accepted mechanism [4]. Fig. 6, 7 and 8 illustrate the ethanol, acetone and acetaldehyde concentrations against time at the temperature of 14, 31 and 43°C respectively. The flow rate is 500 ml/min.

Fig.6 shows the higher the temperature is, more quickly the ethanol concentration decreases. It is demonstrated that temperature significantly influences the degradation rate. In Fig.7, the degradation rate of acetone in the system is also found to increase with increasing temperature. With the increasing of temperature the peak concentration and the time for acetaldehyde to be exhausted are reduced (See Fig. 8). The results indicate that temperature affects greatly the degradation of organic compounds. It can also be noted that the optimal temperature may be varied with different compound. It is applicable in this work, raising the temperature of the reaction system can accelerate the degradation of ethanol, acetone as well as the degradation of acetaldehyde, an intermediates produced in the system.

Effect of flow rate

Changes in flow rate will affect the PCO reaction rate by changing the convective mass transfer and the adsorption of ethanol and acetone

molecules onto the photocatalyst surface. To verify the effect of flow rate on the PCO of ethanol and acetone, two different flow rates were evaluated with degradation. Fig.9, 10 and 11 present the concentration of ethanol, acetone and acetaldehyde against time in the reaction system at the flow rate of 0.5 and 0.25 L/min. Temperature is 14°C.

As can be seen from Fig.9, 10 and 11, the curves between the two flow rates are overlapped and trends almost in the same way. The degradation efficiency decreased consistently when increasing flow rate from 0.25 L/min to 0.5 L/min and became stable when flow rate increased further. The results indicate that the degradation rates of ethanol, acetone and acetaldehyde at the different flow rates are proximal or the oxidation rate does not change significantly with a higher flow rate. It

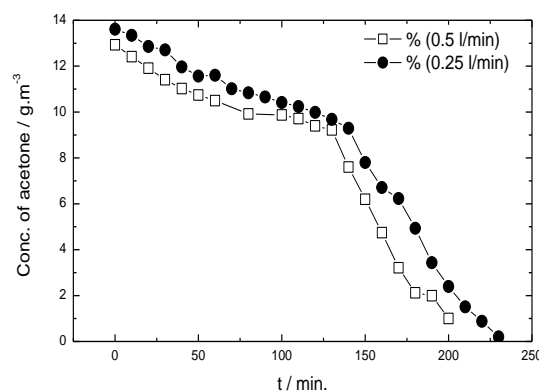


Fig. 9. Effect of flow rate on the degradation of acetone.

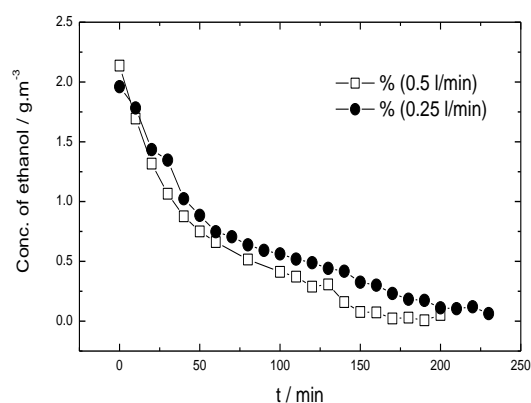


Fig.10. Effect of flow rate on the degradation of ethanol.

can be easily understood that although increasing the flow rate in the batch reactor means the increase of the circling times of the gas, it decreases the contact time of gas with TiO₂ film at every circling.

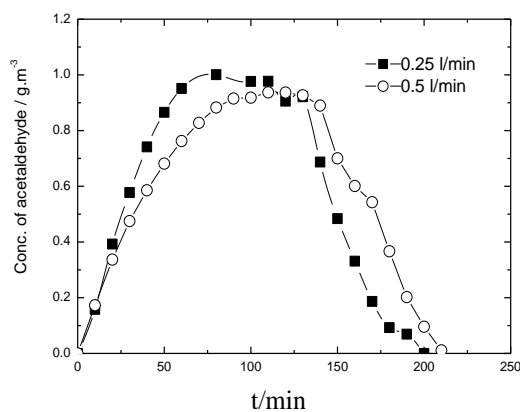


Fig. 11. Effect of flow rate on the degradation of acetaldehyde.

This is in line with the result of Yu *et al.* (2007) where they found that too high a flow rate resulted in shorter residence time and reduced the amount of formaldehyde degraded. Similar finding was also reported by Yu and Brouwers (2009) where they found that the lower the flow rate was, the faster the conversion increase speed was obtained. This indicates the surface reaction mainly control the oxidation rate under this condition while the gas-phase mass transfer effect is negligible.

CONCLUSIONS

- An UV-PCO experimental set-up for VOCs removal was designed and constructed. The photocatalytic oxidation of acetone, ethanol and the interaction between them during photocatalysis process were investigated using a FTIR. The following conclusions can be drawn based on the results obtained in this study.

- Compared with the degradation of acetone alone, it cannot be described by L-H model in presence of ethanol. The presence of ethanol reduces the initial degradation rate of acetone and the inhibition increases with increasing the amount of ethanol in the system. Acetone also inhibits the degradation of ethanol while it still can be described by L-H model.

- Acetaldehyde in the system comes from the degradation of ethanol, the behavior of production and consumption of which is affected by the amount of ethanol and acetone in the mixture.

- Temperature is a key factor of UV-PCO

process and affects greatly the degradation of organic compounds. Raising temperature accelerates the degradation of ethanol, acetone as well as the degradation of acetaldehyde, an intermediate produced in the system.

- Conversion efficiency generally diminished with increased airflow rate. The surface reaction mainly controls the oxidation rate while the gas-phase mass transfer effect is negligible.

Acknowledgment: This work was supported by Beilun Science and Technology Innovation Foundation, Ningbo University of Technology, with additional support from National Undergraduate Innovation and Entrepreneurship Training Program (201311058005) and Zhejiang Provincial Undergraduate Science and Technology Innovation Program (2012R422002).

REFERENCES

1. C.H. Ao, S. C. Lee, C. L. Mak, L.Y. Chan, *Appl. Catal. B*, **42**, 119 (2003).
2. B. Ding, Y. H. Liu, Z. W. Li, S. X. Zhang, *J. Fuel Chem. Tech.*, **34**, 226 (2006).
3. J.J. Du, W. Chen, C. Zhang, Y Li Liu, C X. Zhao, Y. Dai, *Chem. Eng. J.*, **170**, 53 (2011).
4. Z.N. Han, W.C. Chang, X P. Wang, T T. Lim, L. Hildemann, *Chem. Eng. J.*, **218**, 9 (2013).
5. Hodgson A.T., H. Destailats, D.P. Sullivan, W.J. Fisk, *Indoor Air*, **17**, 305 (2007).
6. H.B. Huang, D.Y.C. Leung, G.S. Li, M.K.H. Leung, X.L. Fu, *Catal. Today*, **175**, 310 (2011).
7. P.A. Kolinko, T.N. Filippov, D.V. Kozlov, V.N. Parmon, *J. Photochem. Photobiol. A*, **250**, 72 (2012).
8. D.M. Lee, H.J. Yun, S.J. Yu, S.J. Yun, S.Y. Lee, S. H. Kang, J. Yi, *Chem. Eng. J.*, **187**, 203 (2012).
9. X.Y. Li, Z.R. Zhu, Q.D. Zhao, L.Z. Wang, *J. Hazard. Mater.*, **186**, 2089 (2011).
10. T.H. Lim, S.D. Kim, *Chemosphere*, **54**, 305 (2004).
11. A. Maudhuit, C. Raillard, V. Hequet, L. L. Coq, J. Sablayrolles and L. Molins: Adsorption phenomena in photocatalytic reactions: The case of toluene, acetone and heptane. *Chem. Eng. J.*, **170**, 464-470 (2011).
12. J.H. Mo, Y.P. Zhang, Q.J. Xu, *Appl. Catal. B*, **132**-

- 133, 212 (2013).
13. J.H. Mo, Y.P. Zhang, R. Yang, Q.J. Xu, *Build. Environ.*, **43**, 238 (2008).
14. M.A. Nasalevich, E.A. Kozlova, T.P. Lyubina, A.V. Vorontsov, *J. Catal.*, **287**, 138 (2012).
15. L. Sun, G.Y. Li, S.G. Wan, T.C. An, *Chemosphere*, **78**, 313 (2010).
16. K. Suwannahong, W. Liengcharernsit, W. Sanograj, J. Krueenate, *J. Environ. Biol.*, **33**, 955 (2012)
17. F. Tang, X. D. Yang, *Build. Environ.*, **56**, 329 (2012).
18. G. Vincent, P.M. Marquaire, O. Zahraa, *J. Photochem. Photobiol A*, **197**, 177 (2008).
19. L.P. Yang, Z.Y. Liu, J.W. Shi, Y.Q. Zhang, H. Hu, W.F. Shangguan, *Sep. Purif. Technol.*, **54**, 204 (2007).
20. P.C. Yao, S.T. Hang, C.W. Lin, D.H. Hai, *J. Taiwan Inst. Chem. Eng.*, **42**, 470 (2011).
21. B.F. Yu, Z.B. Hu, M.Liu, H.L. Yang, Q.X. Kong, Y.H. Liu, *Int. J. Refrig.*, **32**, 3 (2009).
22. H. Yu, K. Zhang, C. Rossi, *Indoor Built Environ.*, **16**, 529 (2007).
23. Q.L. Yu, H. Brouwers, *Appl. Catal. B*, **92**, 454 (2009).
24. L. Zhong, F. Haghghat, C.S. Lee, N. Lakdawala, *J. Hazard. Mater.*, **261C**, 130 (2013).
25. J.B. Zhong, Y. Lu, W.D. Jiang, Q.M. Meng, X.Y. He, J.Z. Li, Y.Q. Chen, *J. Hazard. Mater.*, **168**, 1632 (2009).
26. M.E. Zorn, S.O. Hay, M.A. Anderson, *Appl. Catal. B*, **99**, 420 (2010).

ФОТОКАТАЛИТИЧНО ОКИСЛЕНИЕ НА ГАЗООБРАЗНИ СМЕСИ ОТ АЦЕТОН И ЕТАНОЛ ВЪРХУ ПРАХОВЕ ОТ ТИТАНОВ ДИОКСИД

Уей Кай^{1,2*}, Уей Гу¹, Лексиан Жу¹, Уен Лв¹, Чунли Ксиа², Бо Динг²

¹ Колеж по строително инженерство и архитектура, Технологичен университет в Нингбо, Нингбо, Китай

² Колеж по енергетика, Университет Кси'ан Джиаотонг, Кси'ан, Китай

(Резюме)

Постъпила на 13 април, 2014 г.

Изследвано е фотокаталитичното окисление на газообразни смеси от ацетон и етанол в двуфазен реактор с титанов диоксид (TiO₂) при ултравиолетово лъчение (UV-PCO). Изследвани са влиянието на концентрациите, температурата, дебита на газовете върху скоростта на реакциите. Резултатите показват, че наличието на етанол понижава началната скорост на разлагането на ацетона, като инхибирането се усилва с повишаване концентрацията на етанола. Това не може да се обясни с класическия модел на Лангмюир-Хиншелвуд (L-H). Ацетонът също инхибира окислението на етанола, и този ефект се интерпретира с (L-H) модела. В системата се натрупва и разлага ацеталдехид като продукт на окислението на етанола, като ходът на този процес зависи от количествата ацетон и етанол в сместа. Температурата влияе значително върху разлагането на тези органични съединения-повишаването ѝ води ускоряване на разлагането на ацетона, етанола и ацеталдехида и другите междинни съединения. Степента на превръщане намалява с повишаване дебита на газовата смес. Скоростта на реакциите се контролира т скоростта на повърхностната реакция, докато масопреенасянето в газовата фаза не оказва забележимо влияние.

ERRATUM

The authors of the paper

Removal of divalent heavy metal ions from aqueous solutions by Dowex HCR-S synthetic resin

B.A. Fil*, A. E. Yilmaz, R. Boncukcuoğlu, S. Bayar

Ataturk University, Faculty of Engineering, Department of Environmental Engineering, 25240, Erzurum-Turkey

published in Vol. 44, No.3, 201-207, 2012 have informed the *Journal* that affiliations of the authors should read as follows:

Removal of divalent heavy metal ions from aqueous solutions by Dowex HCR-S synthetic resin

B.A. Fil*^{1,2}, A.E. Yilmaz¹, R. Boncukcuoğlu¹, S. Bayar¹

¹ *Ataturk University, Faculty of Engineering, Department of Environmental Engineering, 25240, Erzurum, Turkey.*

² *Balikesir University, Faculty of Engineering, Department of Environmental Engineering, 10145, Balikesir-Turkey*

The corrected paper has been published online.

AUTHOR INDEX

- Abbas M., Rasool N., Riaz M., Zubair M., Abbas M., Noor-ul-Haq, Hayat N., GC-MS profiling, antioxidant, and antimicrobial studies of various parts of *Carissa grandiflora* 831
- Abbas M., See Abbas et al. 831
- Abbas W., See Attia et al. 535
- Abd El-Meged W., Attia H., Elbarawy M., Analytical solution of a transient Hartmann flow with Hall current and ion slip using finite Fourier transform..... 611
- Abdeen M. A. M., See Attia et al. 320, 535
- Abdelmaksoud I. H., See Attia et al. 508
- Abedian F., See Abedian et al. 431
- Abedian Z., Khosravi A.R., Mesbah A.R., Abedian F., Investigation of Trichophyton verrucosum proteins by sodium dodecyl sulfate polyacrylamide gel electrophoresis (SDS-PAGE) 431
- Aberomand-Azar P., See Khodadadi et al. 624
- Aboul-Hassan A. L., See Attia et al. 320
- Adinew B., Biodiesel production from *Trichilia emetica* seeds using in-situ transesterification 334
- Adinew B., Physico-chemical properties of *Trichilia emetica* seeds oil and its comparison with some selected oilseed oils 330
- Aghajanjpour Mir S. M., See Moradinejad et al. 687
- Ahmadi A., Khalili M., Asadi A., Nahri-Niknafs B., New morpholine and piperazine derivatives of ketamine: synthesis and anti-nociceptive effects. 556
- Ahmadi A., See Hajikhani et al. 731
- Ahmadi A., Synthesis, characterization and biological evaluation of new benzimidazoles 503
- Ahmadi A., Synthesis, characterization and biological evaluation of some novel Benzimidazole derivatives 245
- Ahmadi S., See Gharib et al. 215, 223
- Ahmed W. A., See Attia et al. 508
- Akbari A., Azami-Sardooei Z., Simple method for the synthesis and antibacterial activity of 2-amino-3-cyano-1,4,5,6-tetrahydropyrano[3,2-c] quinolin-5-one derivatives 757
- Akhavan H. R., See Gharib et al. 479
- Aladjadjijyan A., See Nikolova et al. 473
- Alaeiyan M., See Nejati et al. 462
- Ali Beyramabadi S., DFT Study on the Fe, Cu and Zn Complexes of 4-(2-Thiazolylazo) Resorcinol 31
- Alinezhad H., Zare M., A convenient synthesis of benzimidazoles using sulfonated ordered nanoporous carbon as efficient solid catalyst 347
- Amani A.M., Synthesis, characterization and biological activities of some novel isatin derivatives 795
- Amarowicz R., See Janiak et al. 640
- Amiri A., See Ghorbani-Choghamarani et al. 384
- Amrollahi M. A., See Shahabi et al. 264
- Anchev B., See Uzunova et al. 184
- Andić Z., See Dimitrijević et al. 814
- Angelova D., See Uzunova et al. 184
- Angelova-Romova M. Y., See Teneva et al. 465
- Ansari N. H., See Ataur Rahman et al. 750
- Antova G. A., See Teneva et al. 465
- Antova G., See Nikolova et al. 473
- Asadi A., See Ahmadi et al. 556
- Aslam M. A., See Bokhari et al. 788
- Aslan N., Erden P. E., Canel E., Kilic E., Development and validation of a potentiometric titration method for the determination of montelukast sodium in a pharmaceutical preparation and its protonation constant 497
- Atanasov V. N., Stoykova S. S., Goranova Y. A., Nedzhib A. N., Tancheva L. P., Ivanova Ju. M., Pantcheva I. N., Preliminary study on in vivo toxicity of monensin, salinomycin and their metal complexes 233
- Atashrouz S., Mirshekar H., Phase equilibrium modeling for binary systems containing CO₂ using artificial neural networks 104
- Ataur Rahman M., Shakya A. K., Wahab S., Ansari N. H., Synthesis of some new thiadiazole derivatives and their anticonvulsant activity 750
- Athare G.S., See Pattan et al. 125
- Attia H. A., Abbas W., Abdeen M. A. M., El-Din Abdin A., Effect of porosity on the flow and heat transfer between two parallel porous plates with the Hall effect and variable properties under constant pressure gradient 535
- Attia H. A., Abdelmaksoud I. H., Ahmed W. A., Elbarawy M. M., Effect of porosity on the flow with heat transfer of a non-Newtonian power law fluid due to a rotating disk with uniform suction and injection 508
- Attia H. A., Aboul-Hassan A. L., Abdeen M. A. M., El-Din Abdin A., MHD flow of a dusty fluid between two infinite parallel plates with temperature dependent physical properties under exponentially decaying pressure gradient 320
- Attia H. A., Essawy M. A. I., Khater A. H., Ramadan A. H., Unsteady non-Darcian flow between two stationary parallel plates in a porous medium with heat transfer subject to uniform suction or injection. 616
- Attia H., See Abd El-Meged et al. 611
- Azadi G., See Ghorbani-Choghamarani et al. 700
- Azami-Sardooei Z., See Akbari et al. 757
- Bachvarova-Nedelcheva A. D., Gegova R. D., Stoyanova A. M., Iordanova R. S., Copicia V. E., Ivanova N. K., Sandu I., Synthesis, characterization and properties of ZnO/TiO₂ powders obtained by combustion gel method 585
- Badiee A., See Mohammadi Ziaran et al. 719
- Baei M. T., Mohammadian H., Hashemian S., B₁₂N₁₂ nanocage as a potential adsorbent for the removal of aniline from environmental systems 735
- Baghernejad B., See Heravi et al. 397
- Bahari A., See Moradinejad et al. 687
- Bakhtiari L., See Gharib et al. 165, 215, 223

- Balkanska R., Karadjova I., Ignatova M., Comparative analyses of chemical composition of royal jelly and drone brood 412
- Bamoniri A., Mirjalili B. F., Nazemian S., Yaghmaeiyan Mahabadi N., Nano silica phosphoric acid as an efficient catalyst for one-pot synthesis of 2,4,5-tri-substituted imidazoles under solvent free condition 79
- Bangov I. P., See Naneva et al. 389
- Bastani D., See Mirzazadeh ghanadi et al. 652
- Bayhan Y. K., See Tekin et al. 117
- Belagali S.L., See Vadiraj et al. 447
- Bo Ding, See Wei Cai et al. 911
- Bock W., See Nikolova et al. 473
- Bocker C., See Harizanova et al. 56
- Boiadjeva Chr., See Glavcheva et al. 409
- Bokhari T. H., Aslam M. A., Hina S., Rizvi N. B., Rasool N., Saif M. J., Zubair M., Hussain A. I., Shahid Chatha S. A., Riaz M., Mineral composition, phenolic profile, antioxidant and antimicrobial activities of *Corchorus depressus* roots extracts... 788
- Bozorgmehr M. R., Housaindokht M. R., Study of the interference effect of propranolol and amlodipine drugs on their interaction with human serum albumin based on molecular dynamics simulation method..... 516
- Budinova T. K., See Tsyntsarski et al. 157, 353
- Cai Q., See Feng et al. 253
- Canel E., See Aslan et al. 497
- Chamarthi N. R., See Shaik et al. 724
- Chaulia S, N., See Mahapatra et al. 339
- Chen F. D., See Yang et al. 896
- Chen J., See Huang et al. 192
- Chen Yingjie, Liu Zhipeng, Dai Peigang, Liu Lan, The effect of flame retardant additives on the combustion performance of flexible polyurethane foam 882
- Chennamsetty S., See Shaik et al. 724
- Chermahini A. N., See Abedian et al. 523
- Chernev G. E., See Kabaivanova et al. 50
- Chunli Xia, See Wei Cai et al. 911
- Ckhakaia E., See Marsagishvili et al. 423
- Constantin V., See Popescu et al. 452
- Copcia V. E., See Bachvarova-Nedelcheva et al. 585
- Dai Peigang, See Chen Yingjie et al. 882
- Dardas G., See El-Sharkawy et al. 691
- Dass D., See Kumar et al. 238
- Dehury S. N., See Mahapatra et al. 339
- Detcheva A. K., See Georgieva et al. 840
- Devineni S. R., See Shaik et al. 724
- Di Wu, Yan Lu, Dongxiao Niu, Development of a novel thermal storage molten-salt filled with nanoparticles for concentration solar plants 873
- Dighe N.S., Saudagar R.B., Jain D.A., Design, synthesis and pharmacological screening of some [3-benzoyl-5-(4-substituted)-2, 3-dihydro-1,3,4-oxadiazol-2-yl] and [5-(4-substituted)-4H-1, 2, 4-triazol-3-yl] derivatives 85
- Dimitrijević S. B., See Dimitrijević et al. 814
- Dimitrijević S. B., Mirić M. B., Trujić V. K., Madić B. N., Dimitrijević St. P., Recovery of precious (Au, Ag, Pd, Pt) and other Metals by e-scrap processing 417
- Dimitrijević S. P., Andić Z., Kamberović Ž., Dimitrijević S. B., Vuković N., Recycling of silver-plated brass for production of high purity copper and ultrafine silver powder for electric contacts..... 814
- Dimitrijević St. P., See Dimitrijević et al. 417
- Dimitrov I. D., See Naneva et al. 389
- Dimitrova B., See Ivanov et al. 294, 306
- Dimov V., See Mouhovski et al. 68
- Djordjevic D., See Djordjevic et al. 277
- Djordjević M. G., See Djordjević et al. 771
- Djordjević M., Radivojević A. R., Pavlović M. A., Djordjević M. G., Stanković M. N., Filipović I. M., Filipović S. I., Preliminary geochemical investigation of karst barré from eastern Serbia Sokobanja basin..... 771
- Djordjevic N., Djordjevic D., Miljkovic M., Urosevic S., Activated carbon from cotton waste as an adsorbent in the purification process of azo-dyes..... 277
- Dobрева E., See Stoychev et al. 283
- Dobrudzhaliev D., See Ivanov et al. 294, 306
- Donath C., See Popescu et al. 452
- Dongxiao Nui, See Di Wu et al. 873
- Doytchinova I. A., See Naneva et al. 389
- Draeger G., See Mikhova et al. 135
- Dyankova Sv. M., Solak A.O., Preparation and characterization of composite hydrocolloid films from sodium alginate and high methoxyl pectin.. 368
- Eftimov T., See Nikolova et al. 473
- Elbarawy M. M., See Attia et al. 508
- Elbarawy M., See Abd El-Meged et al. 611
- El-Din Abdin A., See Attia et al. 320, 535
- El-Sharkawy K. A., Said M. M., Dardas G., Synthesis and antitumor activity of some fused heterocyclic compounds based on cyclohepta[b]thiophene derivatives..... 691
- Erden P. E., See Aslan et al. 497
- Essawy M. A. I., See Attia et al. 616
- Farahani Z., See Mohammadi Ziaran et al. 719
- Fattah M. A., See Ossman et al. 629
- Feng Sh., Sun T., Lu B., Cai Q., Synthesis of dimethyl carbonate from urea and methanol catalyzed by iron-chloride ionic liquid..... 253
- Ferhat Yardim M., See Tsyntsarski et al. 157
- Fil B. A., Özmetin C., Korkmaz M., Characterization and electrokinetic properties of montmorillonite 258
- Fil B. A., See Korkmaz et al. 594
- Filipović I. M., See Djordjević et al. 771
- Filipović S. I., See Djordjević et al. 771
- Furmaniak S., Multitemperature fitting of isotherms as a simple method of insight into the thermodynamics of water sorption on building materials 563
- Ganghoffer J.-F., See Hadzhilazova et al. 62

Gechev S., See Mouhovski et al.	68	free oxidizing media for the oxidation of 1,4-dihydropyridine and urazole derivatives.....	384
Gegova R. D., See Bachvarova-Nedelcheva et al.	585	Ghorbani-Choghamarani A., See Hajjami et al.	458
Georgieva R. H., Detcheva A. K., Karadjov M. G., Mitsiev S. E., Jordanov J. H., Ivanova E. H., Determination of the trace element content in Bulgarian bottled potable waters by total reflection X-ray fluorescence analysis	840	Gigova A., See Uzunova et al.	184
Gharib A., Hashemipour Khorasani B. R., Jahangir M., Roshani M., Bakhtiari L., Mohadeszadeh S., Ahmadi S., Preyssler heteropolyacid supported on nano-SiO ₂ , H ₁₄ [NaP ₅ W ₃₀ O ₁₁₀]/SiO ₂ : a green and reusable catalyst in the synthesis of polysubstituted quinolines.....	223	Glavchev I., See Glavcheva et al.	409
Gharib A., Hashemipour Khorasani B. R., Jahangir M., Roshani M., Bakhtiari L., Mohadeszadeh S., Synthesis of 2,4,5-trisubstituted and 1,2,4,5-tetrasubstituted-1H-imidazole derivatives and or 2,4,5-Triaryloxazoles using of Silica-Supported Preyssler Nanoparticles.....	165	Glavcheva Z., Lalev G., Boiadjieva Chr., Glavchev I., Effect of sulfate containing admixture on C ₃ A hydration.....	409
Gharib A., Noroozi Pesyan N., Jahangir M., Roshani M., Scheeren J. (Hans) W., Bakhtiari L., Mohadeszadeh S., Lagzian Sh., Ahmadi S., Heteropolyacids accelerated multi-component synthesis of N-phenylquinazolin-4-amines by using silica-supported Preyssler nanoparticles in green solvent.....	215	Goranova Y. A., See Atanasov et al.	233
Gharib A., Noroozi Pesyan N., Vojdanifard L., Jahangir M., Roshani M., Moghadasi S., Akhavan H. R., Catalytic synthesis of 1,3-diaryl-2-propene-1-ones by using heteropolyacids as heterogeneous recyclable green catalysts.....	479	Gugov I., See Harizanova et al.	56
Gharib A., Noroozi Pesyan N., Vojdanifard L., Jahangir M., Roshani M., Moghadasi S., Synthesis of β-amino carbonyl compounds using ZnO nanoparticles as a green, effective and reusable catalyst.....	486	Guo Jj., Zhang Jy., Yue Y., Guo Y., Mechanism of mercury removal by a novel hydrazine hydrate-modified pectin.....	801
Gharib A., Noroozi Pesyan N., Vojdanifard L., Roshani M., Silica-bonded N-propyl sulfamic acid: a recyclable catalyst for microwave-assisted synthesis of various dihydropyrano[3,2-c]chromenes	18	Guo Y., See Guo et al.	801
Gharib A., Vojdanifard L., Noroozi Pesyan N., Hashemi Pour Khorasani B. R., Jahangir M., Roshani M., Synthesis of bis-2,3-dihydroquinazolin-4(1H)-ones and 2,3-dihydroquinazolin-4 (1H)-ones derivatives with the aid of silica-supported Preyssler nanoparticles (SPNP).....	667	Guo Zhen Xie, See Wei Cai et al.	903
Ghasemi M., Mirjalili M. H., Hadian J., Chemical profiles of the essential oil of wild and in vitro regenerated Zataria multiflora Boiss. (Lamiaceae)	362	Hadian J., See Ghasemi et al.	362
Gholami Orimi A., See Hajinasiri et al.	825	Hadizadeh M. H., Hamadani M., Adsorption of toxic gases by an open nanocone coupled with an iron atom.....	576
Ghorbanian L., See Abedian et al.	523	Hadzhilazova M., Ganghoffer J.-F., Membrane fusion based on the stalk model.....	62
Ghorbani-Choghamarani A., Azadi G., Mallakpour Sh., Simple and efficient heterogeneous media for the oxidation of urazole derivatives to their corresponding triazolinediones via in situ generation of Cl ⁺	700	Haghi A. K., See Mohammadian et al.	530, 545
Ghorbani-Choghamarani A., Hajjami M., Norouzi M., Amiri A., Poly-(4-vinylpyridinium nitrate) and silica sulfuric acid (SiO ₂ -OSO ₃ H): an efficient and metal-		Haifu Huang, See Qing Lin et al.	857
		Hajikhani R., Ahmadi A., Nahri-Niknafs B., Microwave assisted synthesis and antimicrobial evaluation of phosphonohydrazone derivatives.....	731
		Hajinasiri R., Gholami Orimi A., Solvent-free (Neat) synthesis of stable phosphorus ylides using alkyl phenylcarbamates	825
		Hajjami M., Ghorbani-Choghamarani A., Norouzi M., Poly (4-vinylpyridinium tribromide): an efficient catalyst for the synthesis of 1, 1-diacetates from aldehydes	458
		Hajjami M., See Ghorbani-Choghamarani et al.	384
		Hamadani M., See Hadizadeh et al.	576
		Harizanova R., Vladislavova L., Bocker C., Rüssel C., Gugov I., Phase composition and microstructure of sodium - alumoborosilicate glasses and glass-ceramics in the system Na ₂ O/BaO/TiO ₂ /Al ₂ O ₃ /B ₂ O ₃ /SiO ₂ /Fe ₂ O ₃	56
		Hashemi Pour Khorasani B. R., See Ghabib et al.	667
		Hashemian S., See Baei et al.	735
		Hashemipour Khorasani B. R.,.....	165, 223
		Hayat N., See Abbas et al.	831
		Heravi M. M., Javanmardi N., Oskooie H. A., Baghernejad B., Methanesulfonic acid catalyzed one-pot synthesis of pyrano[2,3-c] pyrazole derivatives in water.....	397
		Heydari nasab A., See Mirzazadeh ghanadi et al.	652
		Hina S., See Bokhari et al.	788
		Hodjaoglu G. A., Ivanov I. S., Metal recovery of solid metallurgical wastes. Galvanostatic electroextraction of copper from sulphate electrolytes containing Zn ²⁺ and Fe ²⁺ ions.....	150
		Hormozi F., See Sarafraz et al.	645
		Housaindokht M. R., See Bozorgmehr et al.	516
		Huang G.-L., See Huang et al.	192

Huang H.-L., Liu F., Chen J., Huang G.-L., Liquid-phase synthesis of N,N'-diacetyl- β -chitobiosyl allosamizoline	192	Khater A. H., See Attia et al.	616
Huiping Deng, See Xu Han et al.	847	Kheiri S., See Montazerzohori et al.	96
Hussain A. I., See Bokhari et al.	788	Khodabakhshi S., See Jafari et al.	36
Hussain S. M., See Seth et al.	704	Khodadadi B., Sabeti M., Nahri-Niknafs B., Moradi-Dehaghi S., Aberomand-Azar P., Raeis-Farshid S., Preparation, characterization and photocatalytic activity of TiO ₂ /CoO nanocomposite	624
Ignatova M., See Balkanska et al.	412	Khosravi A.R., See Abedian et al.	431
Ilic M. D., See Mitic et al.	269	Kilic E., See Aslan et al.	497
Iordanova R. S., See Bachvarova-Nedelcheva et al.	585	Kilic E., See Öztürk et al.	764
Itoua Bl. V., Vladov C., Ongoka P., Petrov L., Hydrodesulfurization of thiophene on the CoMo/Al ₂ O ₃ catalyst modified by coking pretreatment	120	Kiros Y., See Ossman et al.	629
Ivanov B., Dimitrova B., Dobrudzhaliev D., Optimal design and planning of biodiesel supply chain considering crop rotation model. Part 1. Mathematical model formulation of the problem.	294	Korkmaz M., Fil B. A., Özmetin C., Yaşar Y., Full factorial design of experiments for boron removal from Colemanite mine wastewater using Purolite S 108 resin	594
Ivanov B., Dimitrova B., Dobrudzhaliev D., Optimal design and planning of biodiesel supply chain considering crop rotation model. Part 2. Location of biodiesel production plants on the Bulgarian scale	306	Korkmaz M., See Fil et al.	258
Ivanov I. S., See Hodjaoglu et al.	150	Kostova B., See Mouhovski et al.	68
Ivanova E. H., See Georgieva et al.	840	Kostov-Kytin V., See Lihareva et al.	569
Ivanova Ju. M., See Atanasov et al.	233	Koteva N., See Stoychev et al.	283
Ivanova N. K., See Bachvarova-Nedelcheva et al.	585	Koyuncu Zeybek D., See Öztürk et al.	764
Jafari F., Khodabakhshi S., MnSO ₄ .H ₂ O: A highly efficient and inexpensive catalyst for the synthesis of benzo-2-pyrones and benzopyrazines	36	Kuchekar S. R., See Zaware et al.	180
Jagannadham V., See Sanjeev et al.	375	Kumar A., See Kumar et al.	238
Jagnar A.B., See Pattan et al.	125	Kumar D., Kumar A., Dass D., Syntheses, structural and biological studies of Mn(II), Cu(II), Zn(II), Fe(III) and MoO ₂ (VI) complexes of a tridentate OOS donor thiazolidin-4-one	238
Jahangir M., See Gharib et al.	165, 215, 223, 479, 486, 667	Kumar J., See Mukesh Kumar et al.	743
Jain D.A., See Dighe et al.	85	Kumar N., See Meena et al.	141
Janevska V., See Mikhova et al.	135	Kumar S., See Sharma et al.	175
Janiak M., Slavova-Kazakova A., Kancheva V., Amarowicz R., Sephadex LH-20 column chromatography of the hydrolysed lignan macromolecule of flaxseed	640	Lagzian Sh., See Gharib et al.	215
Javanmardi N., See Heravi et al.	397	Lalev G., See Glavcheva et al.	409
Jianmei Xu, See Qing Lin et al.	857	Lashgari N., See Mohammadi Ziaran et al.	719
Joohar S., See Montazerzohori et al.	96	Le Xian Zhu, See Wei Cai et al.	903
Jordanov J. H., See Georgieva et al.	840	Lei Cai, See Xu Han et al.	847
Jun Ming Li, See Wei Cai et al.	903	Lexian Zhu, See Wei Cai et al.	911
Jun Shi, See Xu Han et al.	847	Lihareva N., Kostov-Kytin V., Sorption of Cs ⁺ by nano-sized microporous titanium silicates with pharmacosiderite structure	569
Kabaivanova L. V., Chernev G. E., Markov P. V., Miranda Salvado I. M., Hybrid materials parameters influencing the enzyme activity of immobilized cells	50	Lili Zhao, See Zhijun Zhang et al.	864
Kadir H. A., See Zaroog et al.	602	Liu F., See Huang et al.	192
Kaleem S., See Muralikrishna et al.	580	Liu Lan, See Chen Yingjie et al.	882
Kamberović Ž., See Dimitrijević et al.	814	Liu Zhipeng, See Chen Yingjie et al.	882
Kancheva V., See Janiak et al.	640	Lu B., See Feng et al.	253
Karadjov M. G., See Georgieva et al.	840	Machavariani M., See Marsagishvili et al.	423
Karadjova I., See Balkanska et al.	412	Madić B. N., See Dimitrijević et al.	417
Khalili M., See Ahmadi et al.	556	Mahapatra B. B., Dehury S. N., Chaulia S. N., Polymetallic complexes part CIV synthesis, characterization and potential antibacterial study of dimeric & tetrameric complexes of Co(II), Ni(II) Cu(II), Zn(II), Cd(II) and Hg(II) with azodye ligands	339
		Mahendra K.N., See Raghavendra Rao et al.	11
		Makedonski L., See Stancheva et al.	195
		Mallakpour Sh. See Ghorbani-Choghamarani et al.	700
		Manolov I., See Stanchev et al.	5
		Mansour M. S., See Ossman et al.	629
		Marcheva M. P., See Teneva et al.	465
		Markov P. V., See Kabaivanova et al.	50

Marsagishvili T., Machavariani M., Tatishvili G., Ckhakaia E., Thermodynamic analysis of processes with the participation of zeolites	423	Mouhovski J., Vitov O., Dimov V., Kostova B., Gechev S., High vacuum phase transformation of fluorspar vapors to crystal aggregates.....	68
Meena A. S., See Meena et al.	141	Mousavi Kani S. N., See Moradinejad et al.	687
Meena K. S., See Meena et al.	141	Mukesh Kumar P. C., Kumar J., Sendhilnathan S., Tamarasan R., Suresh S., Heat Transfer and Pressure Drop Analysis of Al ₂ O ₃ Nanofluid as Coolant in Shell and Helically Coiled Tube Heat Exchanger	743
Meena P. L., Kumar N., Meena A. S., Meena K. S., Comparative Studies on Russell-Saunders Atomic Term Symbols (Terms) for Equivalent Electrons of nf^4 and nf^{10} Configurations	141	Mundla N. D., See Shaik et al.	724
Mesbah A.R., See Abedian et al.	431	Muralikrishna G., Pillai S.K., Kaleem S., Shakeel F., Inhibition of glycolysis and respiration of sarcoma-180 cells by cyclophosphamide	580
Mikhova B., Janevska V., Stamboliyska B., Draeger G., Popovski E., Synthesis and structure of some novel dicoumarinamines	135	Musavi S. A., See Montazerzohori et al.	96
Miljkovic M., See Djordjevic et al.	277	Muvvala S.S., Ratnakaram V.N., Antibacterial activity of some newer 1,2,3 – benzotriazole derivatives synthesized by ultrasonication in solvent – free conditions	25
Miranda Salvado I. M., See Kabaivanova et al.....	50	Naderi F., A computational study on the smallest exohedrally functionalized fullerenes, C ₂₀ X ₈ (X = H, F, Cl, Br, NH ₂ , OH and CN).....	680
Mirić Ml. B., See Dimitrijević et al.	417	Nahri-Niknafs B., See Ahmadi et al.	556
Mirjalili B. F., See Bamoniri et al.....	79	Nahri-Niknafs B., See Hajikhani et al.	731
Mirjalili M. H., See Ghasemi et al.	362	Nahri-Niknafs B., See Khodadadi et al.	624
Mirshekar H., See Atashrouz et al.	104	Naneva L. H., Dimitrov I. D., Bangov I. P., Doytchinova I. A., Allergenicity prediction by partial least squares-based discriminant analysis..	389
Mirzazadeh ghanadi A., Heydari nasab A., Bastani D., Numerical simulation and experimental investigation of mass transfer in liquid-liquid jets	652	Nazemian S., See Bamoniri et al.	79
Mitić V. D., Stankov-Jovanovic V. P., Ilic M. D., Vasiljevic P. J., Zabar A. Lj., Stojanovic G. S., The antioxidant, hemolytic and cholinesterase inhibition properties of Galium verum L. and Tragopogon pratensis subsp. pratensis	269	Nedzhib A. N., See Atanasov et al.	233
Mitsiev S. E., See Georgieva et al.	840	Nejati A., Alaeiyan M., The edge version of MEC index of one-pentagonal carbon nanocones.....	462
Mobinikhaledi A., See Shahabi et al.....	264	Nikolova K., Perifanova-Nemska M., Uzunova G., Eftimov T., Antova G., Aladjadjian A., Plachkova V., Bock W., Physico-chemical properties of sunflower oil enriched with ω-3 fatty acids.....	473
Moghadasi S., See Gharib et al.....	479, 486	Nirmal S.A., See Pattan et al.	125
Moghanian H., Mohamadi A., Imine-enamie tautomerism in bicyclic systems in gas phase and solution: a computational study	43	Noor-ul-Haq, See Abbas et al.....	831
Mohadeszadeh S., See Gharib et al.....	165, 215, 223	Noroozi Pesyani N., See Gharib et al.	18, 215, 479, 486, 667
Mohamadi A., See Moghanian et al.....	43	Norouzi M., See Hajjami et al.	458
Mohammadi Ziarani G., Badiei A., Lashgari N., Pourjafar T., Farahani Z., Silica-based sulfonic acid (SiO ₂ -Pr-SO ₃ H): an efficient catalyst in the green one-pot synthesis of 3,4-dihydropyrimidinones/thiones	719	Norouzi M., See Ghorbani-Choghamarani et al.	384
Mohammadian H., See Baei et al.	735	Ongoka P., See Itoua et al.	120
Mohammadian M., Haghi A. K., Study on the production of a new generation of electrospun nanofiber webs	530	Oskooie H. A., See Heravi et al.	397
Mohammadian M., Haghi A. K., Systematic parameter study for nano-fiber fabrication via electrospinning process.....	545	Ossman M. E., Mansour M. S., Fattah M. A., Taha N., Kiros Y., Peanut shells and talc powder for removal of hexavalent chromium from aqueous solutions	629
Montazerzohori M., Tavakol H., Kheiri S., Musavi S. A. and Joohar S., Synthesis, spectral characterization and theoretical investigation of some new mercury four coordinated complexes	96	Özmetin C., See Korkmaz et al.	594
Moradi-Dehaghi S., See Khodadadi et al.....	624	Özmetin C., See Fil et al.	258
Moradinejad Z., Bahari A., Aghajanpour Mir S. M., Mousavi Kani S. N., Synthesis and structural investigation of La ₂ O ₃ doped anthracene nanocrystallites as an advanced dielectric material....	687	Öztürk F., Koyuncu Zeybek D., Kilic E., Voltammetric behavior of lercanidipine and anodic adsorptive stripping voltammetric method for assay in pharmaceutical dosage forms and biological fluids	764
		Padhi P., Rout S. K., Panda D., Effect of modification of zeolite A using sodium carboxymethylcellulose (CMC)	777

Panda D., See Padhi et al.	777	375
Pantcheva I. N., See Atanasov et al.	233	Sarafraz M. M., Hormozi F., Qualitative investigation of the convective boiling heat transfer of dilute Al ₂ O ₃ -water/glycerol solution inside the vertical annuli	645
Patel P.V., See Pattan et al.	125	Sarbu A., See Tsyntarski et al.	157
Pattan J.S., See Pattan et al.	125	Sarkar S., See Seth et al.	704
Pattan S.R., Patel P.V., Athare G.S., Jagnar A.B., Nirmal S.A., Pattan J.S., Synthesis and evaluation of some substituted pyrazole derivatives of biological interest	125	Saudagar R.B., See Dighe et al.	85
Pavlović M. A., See Djordjević et al.	771	Scheeren J. (Hans) W., See Gharib et al.	215
Perifanova-Nemska M.,	473	Sendhilnathan S., See Mukesh Kumar et al.	743
Petrov K. K., See Tsvetanova et al.	784	Seth G. S., Hussain S. M., Sarkar S., Effects of Hall current and rotation on an unsteady MHD natural convection flow with heat and mass transfer past an impulsively moving vertical plate in the presence of radiation and chemical reaction	704
Petrov L., See Itoua et al.	120	Shahabi D., Amrollahi M. A., Mobinikhaledi A., Synthesis of some novel and water-soluble 2,4,6-substituted 3,5-dihydroxymethylpyridines	264
Petrov N. V., See Tsyntarski et al.	157, 353	Shahid Chatha S. A., See Bokhari et al.	788
Petrova B. N., See Tsyntarski et al.	157, 353	Shaik N. R., See Shaik et al.	724
Peycheva K., See Stancheva et al.	195	Shaik T. B., Chennamsetty S., Devineni S. R., Shaik N. R., Mundla N. D., Rajkumari J. P., Chamarthi N. R., Catalyst-free green synthesis of urea and thiourea derivatives of tetramethylguanidine (TMG) and evaluation of biological activity	724
Pillai S.K., See Muralikrishna et al.	580	Shakeel F., See Muralikrishna et al.	580
Plachkova V., See Nikolova et al.	473	Shakya A. K., See Aatur Rahman et al.	750
Popescu A.-M., Donath C., Constantin V., Density, viscosity and electrical conductivity of three choline chloride based ionic liquids	452	Shao Z. L., See Wang et al.	887
Popovski E., See Mikhova et al.	135	Sharma D., Kumar S., A facile synthesis of 1-(2, 4-dihydroxyphenyl)-3-aryl-propane-1,3-diones via Baker-Venkataraman rearrangement under solvent free conditions at room temperature	175
Pourjafar T., See Mohammadi Ziaran et al.	719	Shi G. Q., See Wang et al.	887
Qing Lin, Zhimin Ji, Haifu Huang, Yun He, Jianmei Xu, Spin-glass behavior and magnetic studies of nickel-iron multi-metal Prussian blue complexes Ni _{0.75} Cu _{0.75} [Fe(CN) ₆] _{•6.3} H ₂ O	857	Shi Lin Dong, See Wei Cai et al.	903
Radivojević A. R., See Djordjević et al.	771	Shiwei Zhang, See Zhijun Zhang et al.	864
Raeis-Farshid S., See Khodadadi et al.	624	Sirkecioglu A., See Tsyntarski et al.	157
Raghavendra Rao, Ramakrishna Reddy K., Mahendra K.N., Synthesis, characterization, antibacterial, antifungal and anthelmintic activities of a new 5 - nitroisatin Schiff base and its metal complexes	11	Slavova-Kazakova A., See Janiak et al.	640
Rajkumari J. P., See Shaik et al.	724	Solak A.O., See Dyankova et al.	368
Ramadan A. A., See Attia et al.	616	Stamboliyska B., See Mikhova et al.	135
Ramakrishna Reddy K., See Raghavendra Rao et al. ..	11	Stanchev S., Manolov I., Aldol condensation of 3-acetyl coumarin derivatives and extraordinary side reactions	5
Rasool N., See Abbas et al.	831	Stancheva M., Makedonski L., Peycheva K., Determination of heavy metal concentrations of most consumed fish species from Bulgarian Black Sea coast	195
Rasool N., See Bokhari et al.	788	Stanković M. N., See Djordjević et al.	771
Ratnakaram V.N., See Muvvala et al.	25	Stankov-Jovanovic V. P., See Mitic et al.	269
Razkazov N., See Stoychev et al.	283	Stojanovic G. S., See Mitic et al.	269
Riaz M., See Abbas et al.	831	Stoyanova A. M., See Bachvarova-Nedelcheva et al.	585
Riaz M., See Bokhari et al.	788	Stoychev D., Dobрева E., Razkazov N., Stoycheva M., Koteva N., Electroless deposition of composite Co-P-diamond layers and their polishing properties	283
Rizvi N. B., See Bokhari et al.	788	Stoycheva M., See Stoychev et al.	283
Rončević S., Svedružić L. P., Determination of selected elements in freshwater sponge tissue, natural water and sediments by inductively coupled plasma optical emission spectrometry	401	Stoykova S. S., See Atanasov et al.	233
Roshani M., See Gharib et al.	18, 165, 215, 223, 479, 486, 667	Sun T., See Feng et al.	253
Rout S. K., See Padhi et al.	777	Suresh S., See Mukesh Kumar et al.	743
Rüssel C., See Harizanova et al.	56	Svedružić L. P., See Rončević et al.	401
Sabeti M., See Khodadadi et al.	624		
Said M. M., See El-Sharkawy et al.	691		
Saif M. J., See Bokhari et al.	788		
Sandu I., See Bachvarova-Nedelcheva et al.	585		
Sandu T., See Tsyntarski et al.	157		
Sanjeev R., Jagannadham V., Veda Vrath R., Attenuation effect through methylene group: Part II			

Taha N., See Ossman et al.	629	887
Tamilarasan R., See Mukesh Kumar et al.	743		
Tancheva L. P., See Atanasov et al.	233		
Tatishvili G., See Marsagishvili et al.	423		
Tavakol H., See Montazerzohori et al.	96		
Tayyab S., See Zaroog et al.	602		
Teimouri A., Chermahini A. N., Ghorbanian L., Synthesis of functionalized piperidines by one-pot multicomponent reaction using nano-crystalline solid acid catalysts	523		
Tekin D., Yörük S. and Bayhan Y. K., The Effect of Temperature on Rate of Bacterial Oxidation of Fe(II)	117		
Teneva O. T., Zlatanov M. D., Antova G. A., Angelova- Romova M. Y., M. P. Marcheva, Lipid composition of flaxseeds	465		
Teodosiev D. K., See Tsyntsarski et al.	353		
Tianyi Su, See Zhijun Zhang et al.	864		
Trujić V. K., See Dimitrijević et al.	417		
Tsvetanova F. V., Petrov K. K., Influence of pH and aeration on 2,3-butanediol production from glucose by <i>Klebsiella pneumoniae</i> G31	784		
Tsyntsarski B. G., Petrova B. N., Budinova T. K., Petrov N. V., Teodosiev D. K., Removal of phenol from contaminated water by activated carbon, produced from waste coal material	353		
Tsyntsarski B., Petrova B., Budinova T., Petrov N., Sarbu A., Sandu T., Ferhat Yardim M., Sirkecioglu A., Removal of detergents by zeolites and membranes	157		
Tzaneva B. R., The influence of temperature on the corrosion behaviour of high nitrogen austenitic stainless steel in chloride media	378		
Urosevic S., See Djordjevic et al.	277		
Uzunov I., See Uzunova et al.	184		
Uzunova G., See Nikolova et al.	473		
Uzunova S., Angelova D., Anchev B., Uzunov I., Gigova A., Changes in structure of solid pyrolysis residue during slow pyrolysis of rice husk	184		
Vadiraj K.T., Belagali S.L., Spectrophotometric determination of copper (II) in industrial effluent samples using sulfanilic acid as a ligand system..	447		
Vasiljevic P. J., See Mitic et al.	269		
Veda Vrath R., See Sanjeev et al.	375		
Vitov O., See Mouhovski et al.	68		
Vladislavova L., See Harizanova et al.	56		
Vladov C., See Itoua et al.	120		
Vojdanifard L., See Gharib et al.	18, 479, 486, 667		
Vuković N., See Dimitrijević et al.	814		
Wahab S., See Aatur Rahman et al.	750		
Wang D. M., See Wang et al.	887		
Wang W. Z., See Wang et al.	887		
Wang Y. M., Wang W. Z., Shao Z. L., Wang D. M., Shi G. Q., Innovative prediction model of carbon monoxide emission from deep mined coal oxidation			
Wei Cai, Guo Zhen Xie, Jun Ming Li, Le Xian Zhu, Shi Lin Dong, Effect of thermophysical properties on forced convective hot air drying of multi-layered porous materials.....	903		
Wei Cai, Wei Gu, Lexian Zhu, Wen Lv, Chunli Xia, Bo Ding, Photocatalytic oxidation of gaseous acetone and ethanol mixtures over titanium dioxide powders	911		
Wei Gu, See Wei Cai et al.	911		
Weicheng Zhou, See Xudong Jiang et al.	852		
Wen Lv, See Wei Cai et al.	911		
Wenhui Zhang, See Zhijun Zhang et al.	864		
Xiong Yu, See Xudong Jiang et al.	852		
Xiu Z. L., See Yang et al.	896		
Xu Han, Lei Cai, Huiping Deng, Jun Shi, The study of TiO ₂ -ZrO ₂ preparation and its elimination efficiency on triclosan	847		
Xudong Jiang, Zhedong Yuan, Xiong Yu, Weicheng Zhou, Synthesis and antimicrobial activity of some new 1β-methylcarbapenem derivatives having pyrrolidine or piperidine moieties	852		
Yaghmaeiyan Mahabadi N., See Bamoniri et al.	79		
Yan Lu, See Di Wu et al.	873		
Yang D. Z., Chen F. D., Zhou Y. B., Xiu Z. L., QSAR study on the pheromone of the turnip moth <i>Agrotis</i> <i>segetum</i> used as RDF descriptor.....	896		
Yaşar Y., See Korkmaz et al.	594		
Yörük S., See Tekin et al.	117		
Yuanhua Xie, See Zhijun Zhang et al.	864		
Yue Y., See Guo et al.	801		
Yuekai Zhang, See Zhijun Zhang et al.	864		
Yun He, See Qing Lin et al.	857		
Zabar A. Lj., See Mitic et al.	269		
Zare M., See Alinezhad et al.	347		
Zaroog M. S., Kadir H. A., Tayyab S., Structural transitions in the acid-denatured ficin induced by halogenols and alkanols.....	602		
Zaware B. H., Kuchekar S. R., Kinetic study for formation of thiazole by cyclisation	180		
Zhang Jy., See Guo et al.	801		
Zhedong Yuan, See Xudong Jiang et al.	852		
Zhijun Zhang, Yuekai Zhang, Shiwei Zhang, Tianyi Su, Wenhui Zhang, Yuanhua Xie, Lili Zhao, Capillary pressure effect on vacuum drying process of porous medium modeling.....	864		
Zhimin Ji, See Qing Lin et al.	857		
Zhou Y. B., See Yang et al.	896		
Zlatanov M. D., See Teneva et al.	465		
Zubair M., See Abbas et al.	831		
Zubair M., See Bokhari et al.	788		

АВТОРСКИ УКАЗАТЕЛ

Абас М., Расул Н., Риаз М., Зубаир М., Аббас М., Нур-ул-Хак, Хаят Н., GC-MS профилиране, антиоксидантно и антимиembroно изследване на различни части на растението <i>Carissa grandiflora</i>	472
Абас У., Виж Атия и др.	191
Аббас М., Виж Абас и др.	824
Абд Ел-Мегед У., Атия Х., Елбарауи М., Аналитично решение на задачата за преходно течение на Hartmann с ток на Hall и йонно приплъзване с помощта на крайна трансформация на Fourier.....	756
Абделмаксуд И.Х., Виж Атия и др.....	478
Абдийн М. А. М., Виж Атия и др.....	472
Абедиан З., Кхосрави А.Р., Месбах А.Р., Абедиан Ф., Изследване на протеини от <i>Trichophyton verrucosum</i> чрез електрофореза в натриев додецил сулфат -полиакриламиден гел (SDS-PAGE).....	191
Абедиан Ф., Виж Абедиан и др.	562
Абероманд-Азар П., Виж Холадади и др.....	794
Абул-Хасан А. Л., Виж Атия и др.	502
Агаджанпур Мир С. М., Виж Морадинеджад и др.	502
Адиню Б., Получаване на биодизел от семена на <i>Trichilia emetica</i> чрез in-situ трансестерификация	502
Адиню Б., Физико-химични свойства на маслодайни семена от <i>Trichilia emetica</i> и сравняване с някои избрани растителни масла.....	237
Азади Г., Виж Горбани-Чогамарани и др.	237
Азами-Сардуеи З., Виж Акбари	237
Акбари А., Азами-Сардуеи З., Прост метод за синтеза и антибактериална активност на 2-амино-3-циано-1,4,5,6-тетрахидропирано[3,2-с] хинолин-5-он производни	116
Акхаван Х. Р., Виж Гариб и др.....	116
Аладжаджиян А., Виж Николова и др.	116
Алаеян М., Виж Неджати.....	116
Аланази Ф. К., Радуан А. А., Хак Н., Алсарра И. А., Шакийл Ф., Валидиран UHPLC-DAD метод за количествено определяне на холестерил-сукцинил-5-флуороацилови конюгати.....	329
Али Бейрамабади С., DFT-изследване на комплексите на желязото, медта и цинка с 4-(2-тиазолилazo)резорцинол.....	329
Алинежад Х., Заре М., Удобна синтеза на бензимидазоли със сулфониран подреден нанопорьозен въглерод като ефикасен твърд катализатор.....	623
Алсарра И. А., Виж Аланази и др.	623
Амани А. М., Синтеза, охарактеризиране и биологична активност на някои нови изатинови производни	544
Амарович Р., Виж Яниак и др.....	544
Амири Ар., Виж Горбани-Чогамарани и др.	544
Амролахи М. А., Виж Шахаби и др.	544
Ангелова – Ромова М., Виж Тенева и др.	544
Ангелова Д., Виж Узунова и др.	544
Андийч З., Виж Димитриевич и др.....	544
Ансари Н. Х., Виж Атаур Рахман и др.	544
Антова Г., Виж Николова и др.	544
Антова Г., Виж Тенева и др.	544
Анчев Б., Виж Узунова и др.	544
Асади А., Виж Ахмади и др.	544
Аслам М. А., Виж Бохари и др.....	544
Аслан Н., Ерден П. Е., Джанел Е., Килич Е., Метод за потенциометрично титруване за определяне на натриева сол на монтелукаст във фармацевтични препарати и на константата му на протониране	544
Атанасов В. Н., Стойкова С. С., Горанова Я. А., Неджиб А. Н., Танчева Л. П., Иванова Ю. М., Панчева И. Н., In vivo токсичност на монензин, салиномицин и техни метални комплекси (предварително изследване)	544
Атаур Рахман М., Шакия А. К., Уахаб Ш., Ансари Н. Х., Синтеза на някои нови тиadiaзолови производни тяхното анти-конвулсивно действие.	544
Аташруз С., Мишекар Х., Моделиране чрез изкуствени невронни мрежи на бинарни системи, съдържащи въглероден диоксид	544
Атия Х. А., Абделмаксуд И.Х., Ахмед В.А., Елбарави М. М., Ефект на порьозността върху поток с пренос на топлина на ненютонов флуид, дължащ се на въртящ се диск с постоянно всмукване и инжектиране	544
Атия Х. А., Абул-Хасан А. Л., Абдийн М. А. М., Ел-Дин Абдин А., Магнитохидродинамично течение на запрашен флуид между две безкрайни успоредни плоскости с температурно зависими физични свойства при експоненциално затихващ градиент на налягането	544
Атия Х.А., Есави М.А.И., Хатер А.Х., Рамадан А.А., Нестационарен не-Darcian-ов поток между две стационарни успоредни плочи в порьозна среда с пренос на топлина, предмет на постоянно всмукване или инжектиране	544
Атия Х.А., Абас У., Абдийн М. А. М., Ел-Дин Абдин А., Ефект на порьозността върху течението и топлопренасянето между две порьозни плочи с ефект на Хол и променливи свойства при постоянен градиент на налягането	544
Атия Х., Виж Abd El-Meged и др.	544
Атхар Г. С., Виж Патан и др.	544
Ахмади А., Синтеза, охарактеризиране и биологична оценка на нови бензимидазоли.....	544
Ахмади А., Синтеза, характеристики и биологична оценка на някои нови производни на бензимидазола.....	544
Ахмади А., Халили М., Асади А., Нахри-Никнафс Б., Нови производни на кетамин с морфолин и пиперазин: синтези и анти-ноцисептивен ефект ..	544

.....	562	Рошани М., Синтеза на бис-2,3-дихидрохиназолин-4(1H)-они и тяхни производни с помощта на Preyssler'ови наночастици (SPNP) върху подложка от силициев диоксид.....	679
Ахмади С., Виж Гариб и др.	222, 232	Гариб А., Норузи Песян Н., Вожданифард Л., Джахангир М., Рошани М., Могадаси С., Акхаван Х. Р., Каталитична синтеза на 1,3-диарил-2-пропен-1-они използвайки хетерополикиселини като рециклируем зелен катализатор.....	485
Ахмед В.А., Виж Атия и др.	515	Гариб А., Норузи Песян Н., Вожданифард Л., Джахангир М., Рошани М., Могадаси С., Синтеза на β -амино-карбонилни съединения използвайки наночастици от ZnO като зелен, ефективен и многократно употребяван катализатор.....	496
Багернаджад Б., Виж Херави и др.	400	Гариб А., Норузи Песян Н., Вожданифард Л., Рошани М., N-пропил-сулфаминова киселина върху носител от силициев диоксид: рециклируем катализатор за синтези на различни дихидропропанол [3,2-c] – хромени при микровълново лъчение.....	24
Бадиеи А., Виж Мохамеди Зиарани и др.	723	Гариб А., Песян Н. Н., Джахангир М., Рошани М., Схеерен Й. (Ханс) В., Бахтиари Л., Мохадезаде С., Лагзян Ш., Ахмади С., Ускорена многокомпонентна синтеза на N-фенилхиназолин-4-амини използвайки Preyssler'ови наночастици върху носител от силициев диоксид и хетерополикиселини в “зелен” разтворител.....	222
Баеи М. Т., Мохамедиан Х., Хашемиан С., $V_{12}N_{12}$ -наноклетка като потенциален адсорбент за отстраняването на анилин в околната среда....	742	Гариб А., Хашемипур Хорасани Б.Х., Джахангир М., Рошаниа М., Бахтиари Л., Мохадесзаде С., Синтеза на 2,4,5-тризаместени и 1,2,4,5-четиризаместени-1H-имидазолони производни и/или 2,4,5-триарилоксазоли с помощта на наночастици от Preyssler'ов катализатор върху подложка от силициев диоксид.....	174
Байхан Й. К., Виж Текин и др.	119	Гариб А., Хоразани Б.Р.Х., Джахангир М., Рошани М., Бахтиари Л., Мохадесзаде С., Ахмади С., Preyssler'ови хетерополикиселини $H_{14}[NaP_5W_{30}O_{110}]$, нанесени върху наночастици от силициев диоксид: зелен и рециклируем катализатор за синтезата на поли-заместени хинолини.....	232
Балканска Р., Караджова И., Игнатова М., Сравнителни анализи на химичния състав на пчелно млечиче и пило от търтеи.....	416	Гасеми М., Мирджалили М. Х., Хадян Дж., Химически профили на етерично маслона диворастящи и ин-витро регенерирани <i>Zataria multiflora</i> BOISS. (LAMIACEAE).....	367
Бамонири А., Мирджалили Б.Ф., Наземиан С., Махабади Н.Я., Нано-силициево-фосфорна киселина като ефективен катализатор при едностепенната синтеза на 2,4,5-три-заместени имидазоли в отсъствие на разтворител.....	84	Гегова Р.Д., Виж Бъчварова-Неделчева и др.	593
Бангов И. П., Виж Нанева и др.	396	Георгиева Р. Х., Дечева А. К., Караджов М. Г., Мициев С. Е., Йорданов Ю. Х., Иванова Е. Х., Определяне на следи от елементи в български бутилирани питейни води с помощта на рентгенофлуоресцентен анализ с пълно вътрешно отражение.....	844
Бастани Д., Виж Мирзадеганани и др.	657	Гечев С., Виж Муховски и др.	78
Бахари А., Виж Морадинаджад и др.	690	Гигова А., Виж Узунова и др.	191
Бахтиари Л., Виж Гариб и др.	174, 222, 232	Главчев И., Виж Главчева и др.	411
Беллагали С.Л., Виж Вадирадж.....	451	Главчева З., Лалев Г., Бояджиева Хр., Главчев И., Влияние на сулфатсъдържаща добавка върху хидратацията на C_3A	411
Бо Динг, Виж Уей Кай и др.	917		
Бозоргмехр М. Р., Хусаиндокхт М. Р., Изследване на ефекта на интерференция на пропанолол и амлодипин върху взаимодействието с албумин от човешки серум чрез метода на синамично симулиране.....	522		
Бок В., Виж Николова и др.	478		
Бокър Кр., Виж Харизанова и др.	61		
Бохари Т. Х., Аслам М. А., Хина С., Ризви Н. Б., Расуул Х., Саиф М. Дж., Зубаир М., Хусаин А. И., Шахид Чатха Ш. А., Риаз М., Минерален състав, фенолен профил, антиоксидантна и антимикробна активност на екстракти от корени на <i>Cochorus depressus</i>	794		
Бояджиева Хр., Виж Главчева и др.	411		
Будинова Т., Виж Цинцарски и др.	164, 361		
Бъчварова-Неделчева А. Д., Гегова Р. Д., Стоянова А. М., Йорданова Р. С., Копчия В. Е., Иванова Н. К., Санду И., Синтеза, характеризирание и свойства на прахове от ZnO/TiO_2 , получени по метода на изгаряне в гел.....	593		
Вадирадж К.Т., Беллагали С.Л., Спектрофотометрично определяне на мед (II) в проби от промишлени отпадъци с помощта на сулфанилова киселина като лиганд.....	451		
Васильевич П. Й., Виж Митич и др.	276		
Веда Вратх Р., Виж Санджеев и др.	377		
Витов О., Виж Муховски и др.	78		
Владиславова Л.,.....	61		
Владов Ч., Виж Итуа и др.	124		
Вожданифард Л., Виж Гариб и др. ...	24, 485, 496, 679		
Вукович Н., Виж Димитриевич и др.	824		
Гангхофер Ж.-Фр., Виж Хаджилазова.....	67		
Гариб А., Вожданифард Л., Норузи Песян Н., Хашеми Пур Хорасани Б. Р., Джахангир М.,			

Голами Орими А., Виж Хаджинасири	830	[3-бензоил-5-(4-заместени)-2, 3-дихлоро-1,3,4-оксадиазол-2-ил] и [5-(4-заместени)-4Н-1,2,4-триазол-3-ил] производни	95
Горанова Я. А., Виж Атанасов и др.	237	Димитриевич С. Б., Виж Димитриевич и др.	824
Горбаниан Л., Виж Теимури и др.	529	Димитриевич С. Б., Мирич Мл. Б., Тружич Вл. К., Мадич Б. Н., Димитриевич С. П., Добиване на ценни (Au, Ag, Pd, Pt) и други метали чрез е-скап процес	422
Горбани-Чогамарани А., Азади Г., Малакпур Ш., Прости и ефективни хетерогенни среди за окислението на уразолови производни до съответните триазолиндиони чрез in situ генериране на Cl ⁺	703	Димитриевич С. П., Виж Димитриевич и др.	422
Горбани-Чогамарани А., Виж Хаджами и др.	461	Димитриевич С. П., Андийч З., Камберович Ж., Димитриевич С. Б., Вукович Н., Рециклиране на посребрен месинг за получаването чиста мед и свръх-фин сребърен прах за електрически контакти	824
Горбани-Чогамарани А., Хаджами М., Нороузи М., Амири Ар., Поли-(4-винилпиридиниев нитрат) и силициев диоксид-сярна киселина (SiO ₂ -OSO ₃ H): ефективна и безметална среда за окисление на 1,4-дихидропиридин и производни на уразола	388	Димитров И. Д., Виж Нанева и др.	396
Гугов И., Виж Харизанова и др.	61	Димитрова Б., Виж Иванов и др.	305, 319
Гуо Дж., Жанг Дж., Юе И., Гуо И., Механизъм за отстраняване на живак чрез един нов, модифициран с хидразин хидрат- пектин	805	Димов В., Виж Муховски и др.	78
Гуо Жен Ксие, Виж Уей Кай и др.	910	Добрева Е., Виж Стойчев и др.	293
Гуо И., Виж Гуо и др.	805	Добруджалиев Д., Виж Иванов и др.	305, 319
Дай Пенганг, Виж Чен Йингджи и др.	886	Дойчинова И. А., Виж Нанева и др.	396
Дардас Г., Виж Ел-Шаркауи и др.	699	Донат К., Виж Попеску и др.	457
Дас Д., Виж Кумар и др.	244	Донгсяо Ню, Виж Ди У и др.	881
Девинени С. Р., Виж Абедиан и др.	730	Дрегер Г., Виж Михова и др.	140
Дехури С. Х., Виж Махапатра и др.	346	Дянкова Св. М., Солак А. О., Приготвяне и охарактеризиране на композитни филми от натриев алгинат и метоксилиран пектин	374
Дечева А. К., Виж Георгиева и др.	844	Евтимов Т., Виж Николова и др.	478
Джаванмарди Н., Виж Херави и др.	400	Елбарави М., Виж Абд Ел-Мегед и др.	615
Джаганнадхам В., Виж Санджеев и др.	377	Елбарави М. М., Виж Атия и др.	515
Джангар А. Б., Виж Патан и др.	134	Ел-Дин Абдин А., Виж Атия и др.	329, 544
Джанел Е., Виж Аслан и др.	502	Ел-Шаркауи К. А., Саид М. М., Дардас Г., Синтеза и антитуморна активност на някои степени хетероциклени съединения основани на циклохепта[b]тиофенови производни	699
Джафари Ф., Ходабахши С., MnSO ₄ .H ₂ O: високоефективен и евтин катализатор за синтеза на бензо-2-пирони и бензопиразини	42	Ерден П. Е., Виж Аслан и др.	502
Джахангир М., Виж Гариб и др.	174, 222, 232, 485, 496, 679	Есави М.А.И., Виж Атия и др.	623
Джейн Д.А., Виж Дигхе и др.	95	Есави М.А.И., Виж Атия и др.	622
Джианмей Ксу, Виж Кинг Лин и др.	863	Жанг Дж., Виж Гуо и др.	805
Джимин Джи, Виж Кинг Лин и др.	863	Жедонг Юан, Виж Ксудонг Джианг, и др.	856
Джорджевич Д. М., Радожоевич А. Р., Павлович М. А., Джорджевич М. Г., Станкович М. Н., Филипович И. М., Филипович С. И., Предварително геохимично изследване на карстова котловина в басейна на Сокобаня в Източна Сърбия	776	Жиджун Жанг, Юекай Жанг, Шиуей Жанг, Тяньй Су, Уенху Жанг, Юанхуа Ксие, Лили Жао, Моделиране на ефекта на капилярното налягане върху вакуум-сушенето в порьозна среда	872
Джорджевич Д., Виж Джорджевич и др.	282	Жу И. Б., Виж Янг и др.	902
Джорджевич М. Г., Виж Джорджевич и др.	776	Забар А. Л., Виж Митич и др.	276
Джорджевич Н., Джорджевич Д., Милькович М., Урошевич С., Активен въглен от памучни отпадъци като адсорбент при пречистването от азо-багрила	282	Заре М., Виж Алинежад	352
Джун Минг Ли, Виж Уей Кай и др.	910	Заруг М. С., Кадир Х. А., Тайяб С., Структурни преходи в киселинно денатуриран фицин, индуцирани от халогеноли и алканоли	610
Джун Ши, Виж Ксу Хан и др.	851	Зауаре Б.Х., Кучекар С.Р., Кинетично изследване на образуването на тиазол чрез циклизация	183
Джухари С., Виж Монтезозохори и др.	103	Златанов М., Виж Тенева и др.	472
Ди У, Ян Лу, Донгсяо Ню, Разработване на нова, топло-съхраняваща стопилка за соларни инсталации, запълнена с нано-частици	881	Зубаир М., Виж Абас и др.	839
Дигхе Н.С., Саудагар Р.Б., Джейн Д.А., Дизайн, синтеза и фармакологичен скрийнинг на някои		Зубаир М., Виж Бохари и др.	794
		Иванов Б., Димитрова Б., Добруджалиев Д., Оптимално проектиране и планиране на	

ресурсно осигурителната верига за производство и доставки на биодизел с отчитане на сеитбообращението. Част 1. Формулировка на математичния модел	305	Костова Б., Виж Муховски и др	78
Иванов Б., Димитрова Б., Добруджалиев Д., Оптимално проектиране и планиране на ресурсно осигурителната верига за производство и доставки на биодизел с отчитане на сеитбообращението. Част 2. Определяне на местоположението на биорафинериите за територията на България	319	Костов-Китин В., Виж Лихарева	575
Иванов Ив. С., Виж Ходжаоглу	156	Котева Н., Виж Стойчев и др.	293
Иванова Е. Х., Виж Георгиева и др.	844	Коюнджу Зейбек Д., Виж Йозтюрк и др.	770
Иванова Н.К., Виж Бъчварова-Неделчева и др.	593	Ксионг Ю, Виж Ксудонг Джианг, и др.	856
Иванова Ю. М., Виж Атанасов и др.	237	Ксу Хан, Лей Кай, Хуипинг Денг, Джун Ши, Изследване на препарат от TiO_2-ZrO_2 и определяне неговата ефективност спрямо триклозан	847
Игнатова М., Виж Балканска и др.	416	Ксудонг Джианг, Жедонг Юан, Ксионг Ю, Уейченг Жу, Синтеза и анти-микотична активност на някои нови 1β -метил-карбапенем'ови производни с пиролидинови или пиперидинови половици	856
Илич М. Д., Виж Митич и др.	276	Ксю З. Л., Виж Янг и др.	902
Итуа Бл. В., Владов Ч., Онгока П., Петров Л., Хидроочистка на тиофен върху $CoMo/Al_2O_3$ катализатор, модифициран чрез предварителна коксуваща обработка	124	Кумар А., Виж Кумар и др.	244
Йозметин Дж., Виж Коркмаз и др.	601	Кумар Д., Кумар А., Дас Д., Синтези, сруктурни и биологични изследвания на комплекси на $Mn(II)$, $Cu(II)$, $Zn(II)$, $Fe(III)$ и $MoO_2(VI)$ с донор от тридентат-4-он	244
Йозметин Дж., Виж Фил и др.	263	Кумар Дж., Виж Мукеш Кумар и др.	749
Йозтюрк Ф., Коюнджу Зейбек Д., Килич Е., Волтамперометрични отнасяния на лерканидипин и анодно-адсорбционен волтамперометричен метод за анализ на фармацевтични дозировки и биологични флуиди	770	Кумар Н., Виж Меена и др.	149
Йорданов Ю. Х., Виж Георгиева и др.	844	Кумар С., Виж Шарма	179
Йорданова Р. С., Виж Бъчварова-Неделчева и др.	593	Кучекар С. Р., Виж Зауаре	183
Йорюк С., Виж Текин и др.	119	Кхосрави А. Р., Виж Абедиан и др.	434
Кабаиванова Л. В., Чернев Г. Е., Марков П. В., Миранда Салвадо И. М., Параметри на хибридни материали, влияещи върху ензимната активност на имобилизирани клетки	55	Кънчева В., Виж Яниак и др.	644
Кадир Х. А., Виж Заруг и др.	610	Лагзян Ш., Виж Гариб и др.	222
Калеев С., Виж Мулаликришна и др.	584	Лалев Г., Виж Главчева и др.	411
Камберович Ж., Виж Димитриевич и др.	824	Лашгари Н., Виж Мохамади Зиарани и др.	723
Караджов М. Г., Виж Георгиева и др.	844	Ле Ксионг Жу, Виж Уей Кай и др.	910
Караджова И., Виж Балканска и др.	416	Лей Кай, Виж Ксу Хан и др.	851
Килич Е., Виж Аслан и др.	502	Лексиан Жу, Виж Уей Кай и др.	917
Килич Е., Виж Йозтюрк и др.	770	Лили Жао, Виж Жиджун Жанг и др.	872
Кинг Лин, Джимин Джи, Хайфу Хуанг, Юн Хе, Джианмей Ксу, Spin-glass поведение и изследване на магнитните свойства на многометални (никел-желязо) комплекси с фероцианид $Ni_{0.75}Cu_{0.75}[Fe(CN)_6] \cdot 6.3H_2O$	863	Лиу Ф., Виж Хуанг и др.	194
Кирос И., Виж Осман и др.	639	Лихарева Н., Костов-Китин В., Сорбция на Cs^+ от наноразмерни микропорьозни титанови силикати със структура на фармакосидерит	575
Кирос И., Виж Осман и др.	638	Лу Б., Виж Фенг и др.	257
Константин В., Виж Попеску и др.	457	Лю Жипенг, Виж Чен Йингджи и др.	886
Копция В.Е., Виж Бъчварова-Неделчева и др.	593	Лю Лан, Виж Чен Йингджи и др.	886
Коркмаз М., Виж Фил и др.	263	Месбах А.Р., Виж Абедиан и др.	434
Коркмаз М., Фил Б. А., Йозметин Дж., Яшар И., Пълен факторен експеримент за отстраняването на бор от отпадъчните води от мината Колеманит с йонообменната смола Purolite S 108	601	Мадич Б. Н., Виж Димитриевич и др.	422
		Македонски Л., Виж Станчева и др.	203
		Малакпур Ш., Виж Горбани-Чогамарани и др.	703
		Манолов И., Виж Станчев	10
		Мансур М. С., Виж Осман и др.	638
		Мансур М.С., Виж Осман и др.	639
		Марков П. В., Виж Кабаиванова и др.	55
		Марсагишвили Т., Мачавариани М., Татишвили Г., Цхакария Е., Термодинамичен анализ на процеси с участие на зеолити	430
		Марчева М., Виж Тенева и др.	472
		Махабади Н.Я., Виж Бамонири и др.	84
		Махапатра Б. Б., Дехури С. Х., Чаулиа С. Н., Полимерни комплекси част CIV синтеза, охарактеризиране и антибактериално изследване на димерни и тетрамерни комплекси на $Co(II)$,	

Ni(II), Cu(II), Zn(II), Cd(II) и Hg(II) с азобагрилни лиганди.....	346
Махендра К.Н., Виж Рао и др.	17
Мачавариани М., Виж Марсагишвили и др.	430
Меена А.С., Виж Меена и др.	149
Меена К.С., Виж Меена и др.	149
Меена П.Л., Кумар Н., Меена А.С., Меена К.С., Сравнителни изследвания на атомните термови символи (термове) на Russell-Saunders за електрони от nf^4 и nf^{l0} - конфигурации.....	149
Милькович М., Виж Джорджевич и др.	282
Миранда Салвадо И. М., Виж Кабаиванова и др. ...	55
Мирджалили Б. Ф., Виж Бамонири и др.	84
Миржалили М. Х., Виж Гасеми и др.	367
Мирзазадеганад А., Хейдаринасаб А., Багани Д., Числено симулиране и експериментално изследване на масопренасянето в течно-течни струи.....	657
Мирич Мл. Б., Виж Димитриевич и др.	422
Митич В. Д., Станков-Йованович В. П., Илич М. Д., Васильевич П. Й., Забар А. Л., Стоянович Г. С., Антиоксидантни и хемолитични свойства и инхибиране на холинестераза чрез <i>Galium vegum L.</i> и <i>Tragopogon pratensis subsp. pratensis</i>	276
Михова Б., Яневска В., Стамболийска Б., Дрегер Г., Поповски Е., Синтеза и структура на някои нови дикумарин-амини.....	140
Мициев С. Е., Виж Георгиева и др.	844
Мишекар Х., Виж Аташруз.....	116
Мобинихаледи А., Виж Шахаби и др.	268
Могадаси С., Виж Гариб и др.	485, 496
Моганиан Х., Мохамеди А., Имино-енаминна тавтомерия при би-циклични системи в газова фаза: изчислително изследване.....	49
Монтезозохори М., Тавакол Х., Хеири С., Мусави С.А., Джухари С., Синтеза, спектрално охарактеризиране и теоретично изследване за някои живачни комплекси с координационно число четири.....	103
Моради-Дехаги С., Виж Холадади и др.	628
Морадинеджад З., Бахари А., Агаджанпур Мир С. М., Мусави Кани С. Н., Синтез и структурни изследвания на антраценови нанокристали, дотирани с La_2O_3 , като съвременен диелектричен материал	690
Мохадесзаде С., Виж Гариб и др.	174, 222, 232
Мохамеди А., Виж Моганиан	49
Мохамеди Зиарани Г., Бадиен А., Лашгари Н., Пурджафар Т., Фарахани З., Ефективен катализатор (SiO_2 -Pr- SO_3H) за едностайдийна зелена синтеза на 3,4-дихидропиримидинони/ тиони	723
Мохамедиан М., Хаги А.К., Изследване върху получаването на ново поколение тъкани от електропредени нановлакна.....	534
Мохамедиан М., Хаги А.К., Систематично параметрично изследване на получаването на нановлакна чрез електропредене	555
Мохамедиан Х., Виж Баеи и др.	742
Муввала С.С., Ратнакар В.Н., Антибактериална активност на някои нови производни на 1,2,3 – бензотриазола, синтезирани при ултразвуково въздействие без разтворители	30
Мукеш Кумар П. К., Кумар Дж., Сендинатан С., Тамилаасан Р., Суреш С., Анализ на топлообмена и хидравличното съпротивление на нанофлуид от Al_2O_3 като охладител в кожухотръбни и спирални топлообменници	749
Мулалкришна Г., Пилаи С.К., Калеем С., Шакеел Ф., Инхибиране на гликолизата и дишането на клетки на саркома-180 чрез циклофосфамид ...	584
Мундла Н. Д., Виж Абедиан и др.	730
Мусави Кани С. Н., Виж Морадинеджад и др.	690
Мусави С.А., Виж Монтезозохори и др.	103
Муховски Й., Витов О., Димов В., Костова Б., Гечев С., Високовакуумни фазови превръщания на флуоритови пари в кристални агрегати.....	78
Надери Ф., Числено изследване на най-малките ексодрични функционализирани фулерени, $C_{20}X_8$ ($X = H, F, Cl, Br, NH_2, OH$ и CN).....	686
Наземиан С., Виж Бамонири и др.	84
Нанева Л. Х., Димитров И. Д., Бангов И. П., Дойчинова И. А., Оценка на алергенност чрез дискриминантен анализ по метода на парциалните най-малки квадрати.....	396
Нахри-Никнафс Б., Виж Ахмади и др.	562
Нахри-Никнафс Б., Виж Хаджихани и др.	734
Нахри-Никнафс Б., Виж Холадади и др.	628
Неджати А., Алаеян М., Ребрено модифициран индекс на ексцентрична свързаност на еднопентагоналнен наноконус	464
Неджиб А. Н., Виж Атанасов и др.	237
Николова К., Перифанова-Немска М., Узунова Г., Евтимов Т., Антова Г., Аладжаджиян А., Бок В., Физико-химични свойства на сляночгледово масло, обогатено с ω -3 мастни киселини	478
Нороузи М., Виж Горбани-Чогамарани и др.	388
Норузи М., Виж Хаджами и др.	461
Норузи Песян Н., Виж Гариб и др. ..	24, 485, 496, 679
Нур-ул-Хак, Виж Абас и др.	839
Онгока П., Виж Итуа и др.	124
Оскойе Х. А., Виж Херави и др.	400
Осман М.Е., Мансур М.С., Фатах М.А., Таха Н., Кирос И., Използване на черупки от фъстъци и прах от талк за отстраняване на шест-валентен хром от водни разтвори.....	639
Павлович М. А., Виж Джорджевич и др.	776
Падхи А. П., Рут С. К., Панда Д., Ефект на модификацията на зеолит А с натриева сол на карбоксиметилцелулоза (СМС).....	783
Панда Д., Виж Падхи и др.	783
Панчева И. Н., Виж Атанасов и др.	237
Патан Дж. С., Виж Патан и др.	134
Патан С. А., Виж Патан и др.	134
Патан С. Р., Пател П. В., Атар Г. С., Джангар А. Б., Патан С. А., Патан Дж. С., Синтеза и	

охарактеризиране на някои заместени производни на пиразола с биологично приложение.....	134
Пател П. В., Виж Патан и др.....	134
Пейчева К., Виж Станчева и др.....	203
Перифанова-Немска М.,.....	478
Песян Н. Н., Виж Гариб и др.....	222
Петров К. К., Виж Цветанова.....	787
Петров Л., Виж Итуа и др.....	124
Петров Н., Виж Цинцарски и др.....	164, 361
Петрова Б., Виж Цинцарски и др.....	164, 361
Пилаи С.К., Виж Мулаликришна и др.....	584
Попеску А.-М., Донат К., Константин В., Плътност, вискозитет и електропроводност на три йонни течности на основата на холин-хлорид.....	457
Поповски Е., Виж Михова и др.....	140
Пурджафар Т., Виж Мохамеди Зиарани и др.....	723
Раджкумари Дж. П., Виж Абедиан и др.....	730
Радожоевич А. Р., Виж Джорджевич и др.....	776
Радуан А. А., Виж Аланази и др.....	813
Раеис-Фаршид С., Виж Холадади и др.....	628
Разказов Н., Виж Стойчев и др.....	293
Рамадан А.А., Виж Атия и др.....	623
Рамадан А.А., Виж Атия и др.....	622
Рао Р., Реди К.Р., Махендра К.Н., Синтеза, охарактеризиране, антибактериални, противогъбични и антихелминтни свойства на 5-нитроизатин шифова база и нейните комплекси.....	17
Расул Н., Виж Абас и др.....	839
Расуул Х., Виж Бохари и др.....	794
Ратнакарм В.Н., Виж Муввала.....	30
Реди К.Р., Виж Рао и др.....	17
Риаз М., Виж Абас и др.....	839
Риаз М., Виж Бохари и др.....	794
Ризви Н. Б., Виж Бохари и др.....	794
Рончевич С., Сведружич Л. П., Определяне на избрани елементи в тъкан от сладководни гъби, природни води и утайки чрез оптична емисионна спектрометрия с индуктивно свързана плазма.....	408
Рошани М., Виж Гариб и др.....	24, 174, 222, 232, 485, 496, 679
Рут С. К., Виж Падхи и др.....	783
Рюсел Кр., Виж Харизанова и др.....	61
Сабети М., Виж Холадади и др.....	628
Саид М. М., Виж Ел-Шаркауи и др.....	699
Саиф М. Дж., Виж Бохари и др.....	794
Санджеев Р., Джаганнадхам В., Веда Вратх Р., Ефект на ослабване на метиленови групи: Част II.....	377
Санду И., Виж Бъчварова-Неделчева и др.....	593
Санду Т., Виж Цинцарски и др.....	164
Сарафраз М. М., Хормози Ф., Качествено изследване на конвективното топлопренасяне с кипене в разреждени суспензии на Al_2O_3 във водно-глицеролови смеси във вертикално пръстеновидно пространство.....	651
Сарбу А., Виж Цинцарски и др.....	164
Саркар С., Виж Сет и др.....	718
Саудагар Р.Б., Виж Дигхе и др.....	95
Сведружич Л. П., Виж Рончевич.....	408
Сендинатан С., Виж Мукеш Кумар и др.....	749
Серкичиоглу А., Виж Цинцарски и др.....	164
Сет Г. С., Хусаин С. М., Саркар С., Ефекти на токовете на Hall и на въртенето в нестационарно магнито-хидродинамично течение с естествени конвекции и топло и масопренасяне зад импулсивно движеща се вертикална плоскост при излъчване и химична реакция.....	718
Славова-Казакова А., Виж Яниак и др.....	644
Солак А. О., Виж Дянкова.....	374
Стамболийска Б., Виж Михова и др.....	140
Станков-Йованович В. П.,.....	276
Станкович М. Н., Виж Джорджевич и др.....	776
Станчев Ст., Манолов И., Алдолна кондензация на производни на 3-ацетилкумарина с неочаквани странични реакции.....	10
Станчева М., Македонски Л., Пейчева К., Определяне на концентрациите на тежки метали в най-консумираните рибни видове в българското черноморско крайбрежие.....	203
Стойкова С. С., Виж Атанасов и др.....	237
Стойчев Д., Добрева Е., Разказов Н., Стойчева М., Котева Н., Безелектролизно отлагане на композитни слоеве от кобалт, фосфор и диаманти и техните полиращи свойства.....	293
Стойчева М., Виж Стойчев и др.....	293
Стоянова А.М., Виж Бъчварова-Неделчева и др.....	593
Стоянович Г. С., Виж Митич и др.....	276
Сун Т., Виж Фенг и др.....	257
Суреш С., Виж Мукеш Кумар и др.....	749
Схеерен Й. (Ханс) В., Виж Гариб и др.....	222
Тавакол Х., Виж Монтезрозохори и др.....	103
Тайяб С., Виж Заруг и др.....	610
Тамилаисан Р., Виж Мукеш Кумар и др.....	749
Танчева Л. П., Виж Атанасов и др.....	237
Татишвили Г., Виж Марсагишвили и др.....	430
Таха Н., Виж Осман и др.....	639
Таха Н., Виж Осман и др.....	638
Теимури А., Чермахини А. Н., Горбаниан Л., Синтеза на функционализирани пиперидини чрез единестепенна многокомпонентна реакция с използване на нано-кристални киселинни катализатори.....	529
Текин Д., Йорюк С., Байхан Й. К., Влияние на температурата върху скоростта на бактериално окисление на Fe(II).....	119
Тенева О., Златанов М., Антова Г., Ангелова – Ромова М., Марчева М., Липиден състав на ленени семена.....	472
Теодосиев Д. К., Виж Цинцарски и др.....	361
Тружич Вл. К., Виж Димитриевич и др.....	422
Тяньй Су, Виж Жиджун Жанг и др.....	872
Уанг Д. М., Виж Уанг и др.....	895
Уанг У. З., Виж Уанг и др.....	895

Уанг Я. М., Уанг У. З., Шао З. Л., Уанг Д. М., Ши Г. К., Иновативен модел за предсказване на емисии от въглероден моноксид получени при окисление на въглища на големи дълбочини.....	895	Хадизаде М.Х., Хамаданиан М., Адсорбция на токсични газове с отворен наноконус свързан с железен атом.....	579
Уахаб Ш., Виж Атаур Рахман и др.	756	Хайфу Хуанг, Виж Кинг Лин и др.....	863
Уей Гу, Виж Уей Кай и др.	917	Хак Н., Виж Аланази и др.	813
Уей Кай, Гуо Жен Ксие, Джун Минг Ли, Ле Ксианг Жу, Ши Лин Донг, Ефект на термофизичните свойства върху принудените конвекции при сушенето на много-слоини порьозни материали ..	910	Халили М., Виж Ахмади и др.	562
Уей Кай, Уей Гу, Лексиан Жу, Уен Лв, Чунли Ксиа, Бо Динг, Фотокаталитично окисление на газообразни смеси от ацетон и етанол върху прахове от титанов диоксид.....	917	Хамаданиан М., Виж Хадизаде.....	579
Уейченг Жу, Виж Ксудонг Джианг, и др.	856	Харизанова Р., Владиславова Л., Бокър Кр., Рюсел Кр., Гугов И., Фазов състав и микроструктура на натриево-алумоборосиликатни стъкла и стъклокерамики в системата $\text{Na}_2\text{O}/\text{BaO}/\text{TiO}_2/\text{Al}_2\text{O}_3/\text{B}_2\text{O}_3/\text{SiO}_2/\text{Fe}_2\text{O}_3$	61
Уен Лв, Виж Уей Кай и др.	917	Хатер А.Х., Виж Атия и др.....	623
Уенху Жанг, Виж Жиджун Жанг и др.	872	Хатер А.Х., Виж Атия и др.....	622
Узунов И., Виж Узунова и др.	191	Хашеми Пур Хорасани Б. Р., Виж Гариб и др.	679
Узунова Г., Виж Николова и др.....	478	Хашемиан С., Виж Баеи и др.	742
Узунова С., Ангелова Д., Анчев Б., Узунов И., Гигова А., Изменения в структурата на твърдите остатъци от бавната пиролиза на оризови люспи .	191	Хашемипур Хорасани Б.Х., Виж Гариб и др.	174, 679
Урошевич С., Виж Джорджевич и др.	282	Хаят Н., Виж Абас и др.....	839
Фарахани З., Виж Мохамеди Зиарани и др.	723	Хейдаринасаб А., Виж Мирзазадеганади и др.....	657
Фатах М. А., Виж Осман и др.....	638	Хеири С., Виж Монтезрозохори и др.	103
Фатах М.А., Виж Осман и др.....	639	Херави М. М., Джаванмарди Н., Оскойе Х. А., Багернаджад Б., Метансулфонова киселина катализираща едностадийна синтеза на пирано [2,3-С] пиразолни производни във вода.....	400
Фенг Ш., Сун Т., Лу Б., Цай К., Синтеза на диметилкарбонат от карбамид и метанол, катализирана от йонна течност и железен трихлорид.....	257	Хина С., Виж Бохари и др.	794
Ферхат Ярдим М., Виж Цинцарски и др.	164	Ходабахши С., Виж Джафари.....	42
Фил Б. А., Виж Коркмаз и др.....	601	Ходадади Б., Сабети М., Нахри-Никнафс Б., Моради-Дехаги С., Абероманд-Азар П., Раеис-Фаршид С., Получаване, охарактеризиране и фотокаталитична активност на нанокompозити от TiO_2/CoO	628
Фил Б. А., Йозметин Дж., Коркмаз М., Охарактеризиране и електрокинетични свойства на монтморилонит.....	263	Ходжаоглу Г. А., Иванов Ив. С., Извличане на метали от твърди металургични отпадъци. Галваностатична електроекстракция на мед от сулфатни електролити, съдържащи Zn^{2+} и Fe^{2+} йони.....	156
Филипович И. М., Виж Джорджевич и др.....	776	Хоразани Б.Р.Х., Виж Гариб и др.	232
Филипович С. И., Виж Джорджевич и др.....	776	Хормози Ф., Виж Сарафраз.....	651
Фурманяк С., Много-температурно напасване на изотерми като прост метод за изучаване на термодинамиката на сорбцията на вода в строителни материали.....	568	Хормози Ф., Виж Сарафраз.....	645
Хаги А. К., Виж Мохамедиан.....	534, 555	Хуанг Г.-Л., Виж Хуанг и др.	194
Хаджами М., Виж Горбани-Чогамарани и др.	388	Хуанг Х.-Л., Лиу Ф., Чен Дж., Хуанг Г.-Л., Течнофазна синтеза на N,N' -диацетил- β -хитобиозил алозамизолин.....	194
Хаджами М., Горбани-Чогамарани А., Норузи М., Поли (4-винилпиридин трибромид): ефективен катализатор за синтезата на 1,1-диацетати от алдехиди.....	461	Хуипинг Денг, Виж Ксу Хан и др.....	851
Хаджилазова М., Гангхофер Ж.-Фр., Стеблови модел на сливане на мембрани.....	67	Хусаин А. И., Виж Бохари и др.....	794
Хаджинасири Р., Голами Орими А., Синтез на стабилни фосфорни илиди с алкил-фенилкарбамати без разтворител.....	830	Хусаин С. М., Виж Сет и др.	718
Хаджихани Р., Ахмади А., Нахри-Никнафс Б., Микровълнова синтеза и антимикробна активност на производни на фосфонохидразона ..	734	Хусаиндокхт М. Р., Виж Бозоргмехр.....	593
Хадян Дж., Виж Гасеми и др.	367	Цай К., Виж Фенг и др.	257
		Цанева Б. Р., Влияние на температурата върху корозионното поведение на аустенитна неръждаема стомана с високо съдържание на азот в хлоридни среди.....	383
		Цветанова Ф. В., Петров К. К., Влияние на рН и аерацията върху получаването на 2,3-бутандиол от глюкоза чрез <i>Klebsiella pneumoniae</i> G31.....	787
		Цинцарски Б. Г., Петрова Б. Н., Будинова Т. К., Петров Н. В., Теодосиев Д. К., Извличане на фенол от замърсени води чрез активен въглен,	

получен от отпадни продукти от преработката на въглища.....	361	Шакия А. К., Виж Атаур Рахман и др.	756
Цинцарски Б., Петрова Б., Будинова Т., Петров Н., Сарбу А., Санду Т., Ферхат Ярдим М., Серкичиоглу А., Извличане на детергенти чрез зеолити и мембрани	164	Шао З. Л., Виж Уанг и др.	895
Цхакария Е., Виж Марсагишвили и др.	430	Шарма Д., Кумар С., Проста синтеза на 1-(2,4- дихидроксифенил)-3-арил-пропан-1,3-диони чрез прегрупиране на Baker-Venkataraman при обикновени температури без разтворител.....	179
Чамартхи Н. Р., Виж Абедиан и др.	730	Шахаби Д., Амролахи М. А., Мобинихаледи А., Синтеза на някои нови водо-разтворими 2,4,6- заместени 3,5-дихидрометил-пиридини	268
Чаулиа С. Н., Виж Махапатра и др.	346	Шахид Чатха Ш. А., Виж Бохари и др.	794
Чен Дж., Виж Хуанг и др.	194	Ши Г. К., Виж Уанг и др.	895
Чен Йингджи, Лю Жипенг, Дай Пенганг, Лю Лан, Ефект на добавки, забавящи огъня върху горенето на гъвкава полиуретанова пяна.....	886	Ши Лин Донг, Виж Уей Кай и др.	910
Чен Ф., Виж Янг и др.	902	Шиуей Жанг, Виж Жиджун Жанг и др.	872
Ченнамсети С., Виж Абедиан и др.	730	Юанхуа Ксие, Виж Жиджун Жанг и др.	872
Чермахини А. Н., Виж Теимури и др.	529	Юе И., Виж Гуо и др.	805
Чернев Г. Е., Виж Кабаиванова и др.	55	Юекай Жанг, Виж Жиджун Жанг и др.	872
Чунли Ксия, Виж Уей Кай и др.	917	Юн Хе, Виж Кинг Лин и др.	863
Шаик Н. Р., Виж Абедиан и др.	730	Янг Д. З., Чен Ф., Жу И. Б., Ксю З. Л., QSAR- изследване на феромони от молеца <i>Agrotis</i> <i>segetum</i> , използвани като RDF дескриптори....	902
Шаик Т. Б., Ченнамсети С., Девинени С. Р., Шаик Н. Р., Мундла Н. Д., Раджкумари Дж. П., Чамартхи Н. Р., Зелени, безкаталитични технологии за синтез на производни на карбамида и тиокарбамида с тетраметилгванидин (TMG) и оценяване на биологичната им активност	730	Ян Лу, Виж Ди У и др.	881
Шакеев Ф., Виж Мулаликришна и др.	584	Яневска В., Виж Михова и др.	140
Шакийл Ф., Виж Аланази и др.	813	Яниак М., Славова-Казакова А., Кънчева В., Амарович Р., Колонна хроматография със Sephadex LH-20 на хидролизирана лигнанова макромолекула от ленено семе.....	644
		Яшар И., Виж Коркмаз и др.	601

SUBJECT INDEX

1-(2,4-dihydroxyphenyl)-3-aryl-propane-1,3-diones .	175	Beer's Law.....	447
1,1-Diacetate.....	458	benzil	79, 165
1,2,3 - benzotriazole derivatives	25	Benzimidazole	245, 347, 503
1,2-phenylenediamine.....	347	Benzo-2-pyrones.....	36
1,3-diaryl-2-propene-1-ones	479	Benzopyrazine	36
1,4-Dihydropyrano[2,3-c] pyrazole	397	Bicyclic.....	43
1,4-Dihydropyridines.....	384	biochemical indices	233
1 β -Methylcarbapenem.....	852	Biodiesel.....	334
2,4,5-trisubstituted imidazole	79	Biodiesel Supply Chain	294, 306
2-aryloxy-4-hydroxyacetophenones	175	bioisostere.....	135
3-acetylcoumarins.....	5	biscoumarins.....	5
4-(2-Thiazolylazo) resorcinol	31	Black Sea.....	195
Acetic anhydride.....	458	Boron Removal.....	594
acetone.....	913	Brominated Flame Retardants	882
Acetophenone	479	BSSE-CP	576
acid-denatured state	602	building materials	563
Acidic medium	447	Bulgaria	195
Acidithiobacillus ferrooxidans.....	117	Bulgarian bottled potable waters	840
activated carbon.....	277, 353	Bulgarian scale	306
activity	120	C3A	409
acute toxicity.....	233	capillary pressure.....	864
Acyal	458	carbon dioxide	104
adsorption	157, 277, 353	carbon nanocones	462
Ag 417		Carbon tax	294
Agrotis segetum pheromone	896	carbonylation	253
Al ₂ O ₃	645	Catalyst.....	36, 120, 223, 479
alcohol-induced state	602	Chemical composition	412
aldehyde.....	347, 458	choline chloride	452
aldol reaction	5	cholinesterase inhibition.....	269
alginate	368	chromatography.....	640
allergens.....	389	chromenes.....	18
aminocoumarins.....	135	Cluster analysis.....	412
anodic polarisation.....	378	Coal oxidation	887
antibacterial	85, 125	coal tar-pitch.....	353
antibacterial activity.....	11, 25, 245, 852	Cobalt-molybdenum/alumina	120
anticoagulant.....	135	coking pretreatment.....	120
antifungal.....	85	Combustion Performance	882
antifungal activity	11, 245, 503	composite Co-P-Diamond layers.....	283
Anti-inflammatory	125	composite films	368
anti-inflammatory activity	85	composite powders	585
Anti-nociceptive effect	556	COMSOL	864
antioxidant activity	269	Concentration Solar Plants	873
antitubercular	85, 125	conducting fluid.....	611
arenium ions	375	convective drying	905
aromatic aldehyde.....	165, 479	copper.....	150
artificial neural network.....	104	Copper (II).....	447
attenuation effect	375	corrosion resistance	378
Au 417		Crop rotation.....	294, 306
auto- and cross-covariance.....	389	crystal structure	68
Azo-compound	31	Cs ⁺ uptake.....	569
azo-dye	277	Cyclisation.....	180
Azodye complexes.....	339	Cyclophosphamide	580
bacterial oxidation	117	deep eutectic solvents	452
Baker-Venkataraman rearrangement	175	density	452
barium titanite.....	56	Density functional theory	31
Bee brood.....	412	Dermatophyte	431

detergent	157	Gram-negative bacteria.....	245
DFT.....	135	Gram-positive bacteria	245
DFT study	43	Green	215
dicoumarols	135	grinding technique	175
dihydropyrano[3,2-c]chromenes	18	Hall current.....	611
dimethyl carbonate.....	253	Hammett reaction constant (ρ).....	375
discriminant analysis	389	Hartmann flow	611
dissolution.....	368	hazardous gas.....	887
Drone brood.....	412	heat and mass transfer.....	864, 905
drug interaction.....	516	heat transfer	320, 508, 535
eccentricity.....	462	heavy metals	195
economy.....	417	hemiacetal.....	5
edge modified eccentric connectivity index.....	462	hemolytic activity	269
effect of temperature.....	117	Heterogeneous	479
electrical conductivity.....	452	heterogeneous catalyst.....	79, 347
electrodeposition.....	150	Heteropolyacids.....	215, 223, 479
electroextraction	150	hexavalent chromium	629
Electrokinetic.....	258	Hexokinase	580
Electroless deposition	283	high methoxyl pectin	368
Electrospinning.....	545	hybrids	50
Enamine	43	hydromagnetics.....	535
Energy crops	294	ICP-OES.....	401
enzyme activity.....	50	Imine.....	43
e-scrap processing.....	417	in vitro culture	362
essential and toxic elements.....	840	Industrial effluent	447
essential oil	362	in-situ transesterification	334
Esters	264	Interfacial Thermal Resistance	873
ethanol	913	invert glass.....	56
ethanol-water mixture.....	497	investigation	417
ethylene glycol.....	452	ion exchange.....	569, 594
fatty acid content.....	473	Ion slip	611
fatty acids.....	465	ionic liquids	253, 452
Fe (II).....	117	IR Assignment.....	31
ferromagnetic.....	857	iron.....	150
Fiber diameter.....	545	Irradiation microwave.....	18
ficin.....	602	Isatin	11
finite difference.....	535, 616	Isophthalic aldehyde.....	486
Finite Fourier sine transform (FFST).....	611	Isotherm.....	594
fish	195	jetting mode.....	652
Fixed Bed.....	594	Ketamine	556
flax oil.....	473	Kinetics.....	180
flaxseed.....	640	Lactate dehydrogenase	580
flaxseed glyceride oil.....	465	Lamiaceae.....	362
Flow between two parallel plates.....	535	lamination	530
fluorescence	473	Laplace transform (LT)	611
forced convection.....	645	ligand binding	516
Forchheimer equation	616	lignan	640
Formalin test	556	lipid membranes	62
FPUF.....	882	liquid- liquid extraction	652
free energies.....	423	liquid-phase synthesis.....	192
frequency dispersion.....	423	Lithium aluminum hydride.....	264
freshwater sponge	401	macromolecule	640
FTIR	258	magnetic susceptibility	238
Full Factorial Design	594	magnetic transition	857
fungicides.....	503	Malignant tumor	580
furfural.....	353	mass transfer	68, 652
Galium verum L.....	269	mechanical properties	368
GDW model.....	563	membrane	157
Geometry optimization	31	Mercury	96
gram positive	238	metal complexes	233

metal content.....	401	piperidines	523
metal production	417	pitting.....	378
methanesulfonic acid	397	PLS	389
methanol	253	polar medium.....	423
Microstate	141	Polishing properties	283
microstructure	56	Poly-(4-vinylpyridinium nitrate)	384
MILP.....	294	Poly(4-vinylpyridinium tribromide)	458
MnSO ₄ xH ₂ O.....	36	polyether ionophores	233
modeling	104	Polymetallic complexes	339
molecular alloys magnet	857	Polysubstituted quinoline	223
molecular parameter	896	porosity	184
Molten Salt	873	porous materials.....	905
monomeric	238	porous medium	508, 535, 864
Montelukast sodium.....	497	potentiometric titration	497
Montmorillonite.....	258	power law fluid.....	508
Morpholine derivative	556	Preyssler	223
morphology.....	184	Processing variables	545
Multi-component	215	Production cost	294
multicomponent reaction	165	protective clothing	530
multiple linear regression	896	Protein extraction.....	431
N,N'-diacetyl- β -chitobiosyl allosamizoline.....	192	Prussian blue analogue	857
Nanocone	576	purification	68
nanocrystallisation	56	Purolite S 108	594
Nanofiber	530, 545	Pyrazoles	125
Nanoparticles	486, 645, 873	Pyridine derivatives	264
nano-silica phosphoric acid	79	pyrolysis	184
Nano-SiO ₂ -supported	223	QSAR	85, 896
nano-structured ZnO.....	523	quaternary ammonium salt	452
nano-sulfated zirconia.....	523	Quinolines	223
nano-ZSM-5 zeolites	523	Recyclable catalysts.....	215
nano- γ -alumina	523	Reduction.....	264
NBO analysis	43	re-esterification.....	5
nodoid surfaces	62	refrigerant	104
non-allergens	389	removal.....	629
Non-Darcian flow	616	Response surface methodology	545
non-Newtonian fluid.....	508	rice husk	184
N-phenylquinazolin-4-amines	215	Rotating disk flow	508
nucleate boiling.....	645	Royal jelly	412
numerical simulation	652	Russell-Saunders term	141
numerical solution	320, 508, 616	Sarcoma-180 cells	580
one-pot synthesis	397	Schiff base	11, 96
optical medium	68	SEM.....	258
Optimization	96	Sephadex LH-20.....	640
Optimum design	306	Silica-bonded N-propyl sulfamic acid (SBNPSA)	18
oxalic acid.....	452	silica-supported Preyssler nanoparticle (SPNP)	165, 215
Oxidation	384	Singlet.....	141
parallel plates	320, 616	sodium chloride	378
parameters.....	50	sol-gel	50, 624
Pd 417		sol-gel chemistry	585
peanut shell	629	solvent-free	486
pharmaceutical dosage.....	497	solvent-free conditions	79, 175
phase equilibrium.....	68	solvent-free synthesis	25
phenol	353	spatial dispersion	423
phospholipids.....	465	specific surface area.....	184
photocatalysis	847	Spectroscopic.....	96
Photocatalytic activity	624	spectroscopic techniques	503
photocatalytic degradation	913	spin glass	857
physico-chemical parameters.....	334	stainless steel	378
physico-chemical properties	330	stalk model	62
Piperazine derivative	556	sterols.....	465

strong field and covalent character	238	Triazolinedione	384
structural transition	602	trichilia emetica seeds	334
substituted imidazole	165	Trichilia emetica seeds oil	330
Sulfanilic acid (SA)	447	trichloroacetimidate donors	192
sulfate containing polymer	409	Trichophyton verrucosum	431
sulfonated ordered nanoporous carbon	347	triclosan	847
sunflower oil	473	triethanolamine	452
supercritical fluid extraction	104	Triplet and Quintet	141
support vector machine	887	Two-phase flow	320
synthesis	852	ultrasound irradiation	25
Tail immersion test	556	Urazole	384
Talc powder	629	urea	253
Tautomerism	43	vacuum drying	864
technology	417	vapor liquid equilibria	104
temperature	378	variable properties	320
temperature-dependent properties	535	viscosity	452
terahertz spectroscopy technique	887	VOCs	913
Term symbol	141	warfarin	516
tertiary structure	516	waste cotton fibers	277
Theoretical	96	wastewater	629
thermodynamic analysis	423	water	157
thermodynamics of sorption	563	water sorption	563
thermophysical properties	905	water/glycerol	645
Thiazole	180	XRD	258, 409
thiazolidin-4-one	238	Zataria multiflora Boiss.	362
thiophene hydrodesulfurization	120	z-descriptors	389
thymol	362	zeolite	157, 423
TiO ₂ /CoO Nanocomposite	624	Zero charge point	258
TiO ₂ -ZrO ₂	847	zinc	150
titanosilicate framework	569	ZnO	486
tocopherols	465	β1,β2-Diamino diketone	486
total reflection X-ray fluorescence analysis	840	β-Amino carbonyl	486
Toxic gases	576	ω-3 fatty acids	473
Tragopogon pratensis subsp. pratensis	269		
triaryloxazoles	165		

ПРЕДМЕТЕН УКАЗАТЕЛ

1-(2,4-дихидроксифенил)-3-арил-пропен-1,3-диони	175	Preyssler'ови наночастици върху носител от силициев диоксид	165, 215
1,1-диацетат	458	Purolite S 108	594
1,2,3-бензотриазолни производни	25	Sephadex LH-20	640
1,2-фенилендиамин	347	TiO ₂ /CoO нанокмозит	624
1,3-диарил-2-пропен-1-они	479	Tragopogon pratensis subsp. pratensis	269
1,4-дихидропирано[2,3-с]пиразол	397	Trichilia emetica - семена	334
1,4-дихидропиридини	384	Trichophyton verrucosum	431
1β-метил-карбапенем	852	Zataria multiflora Boiss.	362
2,4,5-три-заместени имидазоли	79	β1,β2-диамино дикетон	486
2-ароилокси-4-хидроксиацетофенони	175	β-амино карбонил	486
3-ацетилкумарини	5	ω-3 мастни киселини	473
4-(2-тиазолилазо)резорцинол	31	адсорбция	157, 277, 353
Acidithiobacillus ferrooxidans	117	азобагрилни комплекси	339
С3А (трикалциев алуминат)	409	азо-багрило	277
Galium verum L.	269	азо-съединение	31
MnSO ₄ ·xH ₂ O (манганов сулфат монохидрат)	36	активен въглен	277, 353
N,N'-диацетил-β-хитобиозил алозамизолин	192	активност	120
N-пропил-сулфаминова киселина (SBNPSA)	18	алгинат	368
N-фенилхиназолин-4-амини	215	алдехид	347, 458
		алдолна реакция	5

алергени.....	389	електрична проводимост.....	452
алкохолно-индуцирано състояние.....	602	електроекстракция.....	150
аминокумарин.....	135	електроотлагане.....	150
анодна поларизация.....	378	електропредене.....	545
антибактериален.....	85, 125	електрохиметика.....	258
антибактериална активност.....	11, 25, 245, 852	енамин.....	43
антикоагулант.....	135	ензимна активност.....	50
антиноциептивен ефект.....	556	е-скрап процес.....	417
антиокислителна активност.....	269	естери.....	264
арениеви йони.....	375	етанол.....	913
ароматен алдехид.....	165, 479	етанол/вода смеси.....	497
атомно-емисионна спектроскопия с индуктивно свързана плазма (ICP-EOS).....	401	етерично масло.....	362
ацеталдехид.....	458	етилен гликол.....	452
ацетон.....	913	ефект на отслабване.....	375
ацетофенон.....	479	ефект на температура.....	117
ацилал.....	458	желязо (II).....	117
бактериално окисление.....	117	задържане на Cs+.....	569
бариев титанид.....	56	закон на Beer.....	447
без разтворител.....	486	заместен имидазол.....	165
безелектролизно отлагане.....	283	зародиш на кипене.....	645
бензил.....	79, 165	защитно облекло.....	530
бензимидазол.....	245, 347, 503	з-дискриптори.....	389
бензо-2-пирони.....	36	зелен.....	215
бензопиразин.....	36	зеолит.....	157, 423
биодизел.....	334	злокачествен тумор.....	580
био-изостерен.....	135	зол-гел.....	50, 624
биохимични индекси.....	233	зол-гел химия.....	585
бискумарини.....	5	изатин.....	11
би-цикличен.....	43	изкуствена невронна мрежа.....	104
бромиран забавител на огън.....	882	изотерма.....	594
България.....	195	изофталов алдехид.....	486
българска бутилирана вода.....	840	изследване.....	417
вакуумно сушене.....	864	икономика.....	417
взаимодействие на лекарства.....	516	имин.....	43
вискозитет.....	452	ин-витро регенерирани.....	362
високометоксилиран пектин.....	368	ин-ситу трансестерификация.....	334
вода.....	157	йонни течности.....	253, 452
вода/глицерол.....	645	йонно приплъзване.....	611
водна сорбция.....	563	йонообмен.....	569, 594
въглероден диоксид.....	104	каменовъглен пек.....	353
въглеродни наноконуси.....	462	капиларно налягане.....	864
въглищно окисление.....	887	катализатор.....	36, 120, 223, 479
въртящ се диск.....	508	кетамин.....	556
геометрична оптимизация.....	31	кинетика.....	180
Грам-отрицателна бактерия.....	245	киселинен медиум.....	447
Грам-положителна.....	238	киселинно-денатурирано състояние.....	602
Грам-положителна бактерия.....	245	клъстерен анализ.....	412
гъвкава полиуретанова пяна (ГПУП).....	882	кобалт-молибден/алуминии.....	120
двуфазен поток.....	320	композитни прахове.....	585
дерматофит.....	431	композитни словата от Co-P-диамант.....	283
детергент.....	157	композитни филми.....	368
диаметър на нишки.....	545	конвективно сушене.....	905
дикумароли.....	135	корозионна устойчивост.....	378
диметил карбонат.....	253	крайна трансформация на Fourier.....	611
дискриминационен анализ.....	389	кристална структура.....	68
дихидропирано[3,2-с]хромени.....	18	лактат-дехидрогеназа.....	580
едностадийен синтез.....	397	ламиниране.....	530
екстракция на протеини.....	431	ленено глицеридно масло.....	465
ексцентричност.....	462	ленено семе.....	640
		лигандно свързване.....	516

лигнан	640	параметри	50
липидни мембрани	62	пило от търтеи	412
литиево алуминиев хидрид	264	пиперазин производни	556
магнитен сусцептибилитет	238	пиперазини	523
макромолекула	640	пиразоли	125
маслодайни семена на <i>Trichilia emetica</i>	330	пиридинови производни	264
масов трансфер	68, 652	пиролиз	184
мастни киселини	465	плътност	452
мастни киселини - съдържание	473	поли-(4-винилпирадин нитрат)	384
мед	150	поли-(4-винилпирадин трибромид)	458
мед (II)	447	полиетерни йонофорни антибиотици	233
мембрана	157	поли-заместени хинолини	223
метални комплекси	233	полиметални комплекси	339
метанол	253	пираци свойства	283
метансулфонова киселина	397	полярен медиум	423
механични свойства	368	порьозен медиум	508, 535, 864
микровълново облъчване	18	порьозни материали	905
микроструктура	56	порьозност	184
микро-състояние	141	потенциометрично титруване	497
многокомпонентна	215	поток между две паралелни порьозни плочи	535
многокомпонентна реакция	165	прегрупиране на Baker-Venkataraman	175
множество от суперпозиционни грешки	576	предварително коксуване	120
модел на D'Arcy и Watt (GDW)	563	преестерификация	5
моделиране	104	Прейслер	223
молекулен параметър	896	премахване	629
мономер	238	пречистване	68
монтморилонит	258	проводяща течност	611
морфолин производни	556	производство на метали	417
морфология	184	променливи на процес	545
нано-ZMS-5-зеолити	523	промишлени отпадъци	447
нано- γ -алуминии	523	пространствено разпределение	423
нановлакна	530, 545	противовъзпламенителна	125
наноконус	576	противовъзпламенителна активност	85
нанокристализация	56	противогъбичен	85
нано-силициево-фосфорна киселина	79	противогъбична активност	11, 245, 503
наноструктуриран ZnO	523	противотуберкулозен	85, 125
наносульфатиран цирконии	523	пчелно млечице	412
наночастици	486, 645, 873	пълнен факторен експеримент	594
натриев хлорид	378	равновесие пари-течност	104
натриева сол на монтелукаст	497	разтворимост	368
не-Darcsian-ов поток	616	реакционна константа на Хамет (ρ)	375
неалергени	389	ребрено модифициран индекс на ексцентрична свързаност	462
ненютонова течност	508	регенерируем катализатор	215
неподвижен слой	594	редукция	264
неръждаема стомана	378	рентгенофлуоресцентен анализ с пълно вътрешно отражение	840
нодоидни повърхности	62	ресурсно-осигурителна верига	294, 306
окисление	384	риба	195
оксалова киселина	452	ротация на биокултури	294, 306
опасен газ	887	саркома - 180 клетки	580
оптимален дизайн	306	свободна енергия	423
оптимизация	96	свойства на променливите	320
оптичен медиум	68	свърхкритична екстракция	104
оризови люспи	184	СЕМ	258
остра токсичност	233	синглет	141
отпадни води	629	синтез	852
отстраняване на бор	594	синтез без разтворител	25
охлаждащ агент	104	синтез в течна среда	192
паладий (Pd)	417	сладководни гъби	401
памучни отпадъци	277		
паралелни плочи	320, 616		

слънчогледово масло	473	уравнение на Forchheimer (разширение)	616
смилане	175	уразол.....	384
солева стопилка.....	873	урея	253
спектроскопия	96	Устноцветни (Lamiaceae)	362
спектроскопски техники	503	фазово равновесие	68
специфична повърхност	184	фармацевтична доза	497
стероли.....	465	фенол	353
строителни материали	563	ферромагнитни	857
струен модел	652	физикохимични параметри.....	334
структурна трансформация.....	602	физикохимични свойства.....	330
сулфанилова киселина.....	447	фицин.....	602
сулфат съдържащ полимер	409	флуоресценция.....	473
сулфунуиран подреден нанопорест въглерод	347	формалинов тест	556
съдържание на метали	401	фосфолипиди.....	465
тавтомеризъм	43	фотокатализ.....	847
талков прах	629	фотокаталитична активност.....	624
тежки метали	195	фотокаталитично разграждане	913
температура	378	ФТИР	258
температурно-зависими свойства.....	535	фунгициди	503
теоретичен	96	фурфурол.....	353
терахерц-въннова спектроскопия	887	фъстъкова черупка.....	629
територия на България	306	Хартманов поток.....	611
термове на Russell-Saunders	141	хексавалентен хлорен атом.....	629
термови символи.....	141	хексокиназа	580
термодинамика на сорбция	563	хемиацетал	5
термодинамичен анализ	423	хемолитична активност	269
термофизични свойства.....	905	хетерогенен	479
технология.....	417	хетерогенен катализ	79, 347
течно-течна екстракция.....	652	хетерополикиселини.....	215, 223, 479
тиазол	180	хибриди.....	50
тиазолидин-4-он.....	238	хидродесулфунизация на тиофен.....	120
тимол.....	362	хидромагнитно	535
титаносиликатен скелет	569	химичен състав	412
ток на Hall.....	611	хинолини	223
токоферол	465	холинестеразно инхибиране	269
токсични газове.....	576	холин-хлорид	452
топлинен и масов трансфер	864, 905	хроматография	640
топлинен трансфер	320, 508, 535	хромени	18
трансформация на Лаплас	611	цена на продукт (продуктова цена).....	294
третична структура	516	циклизация	180
триазолиндион	384	циклофосфамид	580
триарилоксазоли	165	цинков оксид	486
триетаноламин	452	Черно море	195
триколзан	847	четвъртична амониева сол	452
триплет и квинтет	141	числено решение.....	320, 508, 616
трихлороацетамидни донори	192	числено симулиране	652
уарфарин.....	516	Шифова база	11, 96
ултразвуково облъчване.....	25		

BULGARIAN CHEMICAL COMMUNICATIONS

Instructions about Preparation of Manuscripts

General remarks: Manuscripts are submitted in English by e-mail or by mail (in duplicate). The text must be typed double-spaced, on A4 format paper using Times New Roman font size 12, normal character spacing. The manuscript should not exceed 15 pages (about 3500 words), including photographs, tables, drawings, formulae, etc. Authors are requested to use margins of 3 cm on all sides. For mail submission hard copies, made by a clearly legible duplication process, are requested. Manuscripts should be subdivided into labelled sections, e.g. **Introduction, Experimental, Results and Discussion, etc.**

The title page comprises headline, author's names and affiliations, abstract and key words.

Attention is drawn to the following:

a) **The title** of the manuscript should reflect concisely the purpose and findings of the work. Abbreviations, symbols, chemical formulas, references and footnotes should be avoided. If indispensable, abbreviations and formulas should be given in parentheses immediately after the respective full form.

b) **The author's** first and middle name initials, and family name in full should be given, followed by the address (or addresses) of the contributing laboratory (laboratories). **The affiliation** of the author(s) should be listed in detail (no abbreviations!). The author to whom correspondence and/or inquiries should be sent should be indicated by asterisk (*).

The abstract should be self-explanatory and intelligible without any references to the text and containing not more than 250 words. It should be followed by key words (not more than six).

References should be numbered sequentially in the order, in which they are cited in the text. The numbers in the text should be enclosed in brackets [2], [5, 6], [9–12], etc., set on the text line. References, typed with double spacing, are to be listed in numerical order on a separate sheet. All references are to be given in Latin letters. The names of the authors are given without inversion. Titles of journals must be abbreviated according to Chemical Abstracts and given in italics, the volume is typed in bold, the initial page is given and the year in parentheses. Attention is drawn to the following conventions:

a) The names of all authors of a certain publications should be given. The use of “*et al.*” in

the list of references is not acceptable.

b) Only the initials of the first and middle names should be given.

In the manuscripts, the reference to author(s) of cited works should be made without giving initials, e.g. “Bush and Smith [7] pioneered...”. If the reference carries the names of three or more authors it should be quoted as “Bush *et al.* [7]”, if Bush is the first author, or as “Bush and co-workers [7]”, if Bush is the senior author.

Footnotes should be reduced to a minimum. Each footnote should be typed double-spaced at the bottom of the page, on which its subject is first mentioned.

Tables are numbered with Arabic numerals on the left-hand top. Each table should be referred to in the text. Column headings should be as short as possible but they must define units unambiguously. The units are to be separated from the preceding symbols by a comma or brackets.

Note: The following format should be used when figures, equations, *etc.* are referred to the text (followed by the respective numbers): Fig., Eqns., Table, Scheme.

Schemes and figures. Each manuscript (hard copy) should contain or be accompanied by the respective illustrative material as well as by the respective figure captions in a separate file (sheet). As far as presentation of units is concerned, SI units are to be used. However, some non-SI units are also acceptable, such as °C, ml, l, etc.

The author(s) name(s), the title of the manuscript, the number of drawings, photographs, diagrams, etc., should be written in black pencil on the back of the illustrative material (hard copies) in accordance with the list enclosed. Avoid using more than 6 (12 for reviews, respectively) figures in the manuscript. Since most of the illustrative materials are to be presented as 8-cm wide pictures, attention should be paid that all axis titles, numerals, legend(s) and texts are legible.

The authors are asked to submit **the final text** (after the manuscript has been accepted for publication) in electronic form either by e-mail or mail on a 3.5” diskette (CD) using a PC Word-processor. The main text, list of references, tables and figure captions should be saved in separate files (as *.rtf or *.doc) with clearly identifiable file names. It is essential that the name and version of

the word-processing program and the format of the text files is clearly indicated. It is recommended that the pictures are presented in *.tif, *.jpg, *.cdr or *.bmp format, the equations are written using "Equation Editor" and chemical reaction schemes are written using ISIS Draw or ChemDraw programme.

The authors are required to submit the final text with a list of three individuals and their e-mail addresses that can be considered by the Editors as potential reviewers. Please, note that the reviewers should be outside the authors' own institution or organization. The Editorial Board of the journal is not obliged to accept these proposals.

EXAMPLES FOR PRESENTATION OF REFERENCES

REFERENCES

1. D. S. Newsome, *Catal. Rev.–Sci. Eng.*, **21**, 275 (1980).
2. C.-H. Lin, C.-Y. Hsu, *J. Chem. Soc. Chem. Commun.*, 1479 (1992).
3. R. G. Parr, W. Yang, *Density Functional Theory of Atoms and Molecules*, Oxford Univ. Press, New York, 1989.
4. V. Ponec, G. C. Bond, *Catalysis by Metals and Alloys* (Stud. Surf. Sci. Catal., vol. 95), Elsevier, Amsterdam, 1995.
5. G. Kadinov, S. Todorova, A. Palazov, in: *New Frontiers in Catalysis* (Proc. 10th Int. Congr. Catal., Budapest, 1992), L. Guzzi, F. Solymosi, P. Tetenyi (eds.), Akademiai Kiado, Budapest, 1993, Part C, p. 2817.
6. G. L. C. Maire, F. Garin, in: *Catalysis. Science and Technology*, J. R. Anderson, M. Boudart (eds), vol. 6, Springer-Verlag, Berlin, 1984, p. 161.
7. D. Pocknell, *GB Patent 2 207 355* (1949).
8. G. Angelov, PhD Thesis, UCTM, Sofia, 2001.
9. JCPDS International Center for Diffraction Data, Power Diffraction File, Swarthmore, PA, 1991.
10. *CA* **127**, 184 762q (1998).
11. P. Hou, H. Wise, *J. Catal.*, in press.
12. M. Sinev, private communication.
13. <http://www.chemweb.com/alchem/articles/1051611477211.html>.

CONTENTS

A. Gharib, L. Vojdanifard, N. Noroozi Pesyan, B. R. Hashemi Pour Khorasani, M. Jahangir, M. Roshani, Synthesis of bis-2,3-dihydroquinazolin-4(1H)-ones and 2,3-dihydroquinazolin-4 (1H)-ones derivatives with the aid of silica-supported Preyssler nanoparticles (SPNP)	667
F. Naderi, A computational study on the smallest exohedrally functionalized fullerenes, C ₂₀ X ₈ (X = H, F, Cl, Br, NH ₂ , OH and CN).....	680
Z. Moradinejad, A. Bahari, S. M. Aghajanpour Mir, S. N. Mousavi Kani, Synthesis and structural investigation of La ₂ O ₃ doped anthracene nanocrystallites as an advanced dielectric material	687
K. A. El-Sharkawy, M. M. Said, G. Dardas, Synthesis and antitumor activity of some fused heterocyclic compounds based on cyclohepta[b]thiophene derivatives	691
A. Ghorbani-Choghamarani, G. Azadi Sh. Mallakpour, Simple and efficient heterogeneous media for the oxidation of urazole derivatives to their corresponding triazolinediones <i>via in situ</i> generation of Cl ⁺ ...	700
G. S. Seth, S. M. Hussain, S. Sarkar, Effects of Hall current and rotation on an unsteady MHD natural convection flow with heat and mass transfer past an impulsively moving vertical plate in the presence of radiation and chemical reaction	704
G. Mohammadi Ziarani, A. Badiei, N. Lashgari, T. Pourjafar, Z. Farahani, Silica-based sulfonic acid (SiO ₂ -Pr-SO ₃ H): an efficient catalyst in the green one-pot synthesis of 3,4-dihydropyrimidinones/thiones	719
T. B. Shaik, S. Chennamsetty, S. R. Devineni, N. R. Shaik, N. D. Mundla, J. P. Rajkumari, N. R. Chamarthi, Catalyst-free green synthesis of urea and thiourea derivatives of tetramethylguanidine (TMG) and evaluation of biological activity	724
R. Hajikhani, A. Ahmadi B. Nahri-Niknafs, Microwave assisted synthesis and antimicrobial evaluation of phosphonohydrazone derivatives	731
M. T. Baei, H. Mohammadian, S. Hashemian, B ₁₂ N ₁₂ nanocage as a potential adsorbent for the removal of aniline from environmental systems	735
P.C. Mukesh Kumar , J. Kumar, S. Sendhilnathan, R.Tamilarasan, S.Suresh, Heat Transfer and Pressure Drop Analysis of Al ₂ O ₃ Nanofluid as Coolant in Shell and Helically Coiled Tube Heat Exchanger	743
M. Ataur Rahman, A. K.Shakya , S. Wahab, N. H. Ansari , Synthesis of some new thiadiazole derivatives and their anticonvulsant activity	750
A. Akbari, Z. Azami-Sardooui, Simple method for the synthesis and antibacterial activity of 2-amino-3-cyano-1,4,5,6-tetrahydropyrano[3,2-c] quinolin-5-one derivatives	757
F. Öztürk, D. Koyuncu Zeybek, E. Kilic, Voltammetric behavior of lercanidipine and anodic adsorptive stripping voltammetric method for assay in pharmaceutical dosage forms and biological fluids	764
M. Djordjević, A. R. Radivojević, M. A. Pavlović, M. G. Djordjević, M. N. Stanković, I. M. Filipović, S. I. Filipović, Preliminary geochemical investigation of karst barré from eastern Serbia Sokobanja basin ...	771
P. Padhi, S. K. Rout, D. Panda, Effect of modification of zeolite A using sodium carboxymethylcellulose (CMC)	777
F. V. Tsvetanova, K. K. Petrov, Influence of pH and aeration on 2,3-butanediol production from glucose by <i>Klebsiella pneumoniae</i> G31	784
T. H. Bokhari, M. A. Aslam, S. Hina, N. B. Rizvi, N. Rasool, M. J. Saif, M. Zubair, A. I. Hussain, S. A. Shahid chatha, M.Riaz, Mineral composition, phenolic profile, antioxidant and antimicrobial activities of <i>Corchorus depressus</i> roots extracts	788
A.M. Amani, Synthesis, characterization and biological activities of some novel isatin derivatives	795
Jj. Guo, Jy. Zhang, Y. Yue, Y. Guo, Mechanism of mercury removal by a novel hydrazine hydrate-modified pectin	801
F. K. Alanazi ¹ , A.A. Radwan ¹ , N. Haq ^{2,3} , I. A. Alsarra ^{2,3} , F.Shakeel, Validated UHPLC-DAD method for quantification of cholesteryl-succinyl-5-fluorouracil conjugate	806
S. P. Dimitrijević, Z. Anđić, Ž. Kamberović, S. B. Dimitrijević, N. Vuković, Recycling of silver-plated brass for production of high purity copper and ultrafine silver powder for electric contacts	814
R. Hajinasiri, A. Gholami Orimi, Solvent-free (Neat) synthesis of stable phosphorus ylides using alkyl phenylcarbamates	825
M. Abbas, N. Rasool, M. Riaz, M. Zubair, M. Abbas, Noor-ul-Haq, N. Hayat, GC-MS profiling, antioxidant, and antimicrobial studies of various parts of <i>Carissa grandiflora</i>	831
R. H. Georgieva, A. K. Detcheva, M. G. Karadjov, S. E. Mitsiev, J. H. Jordanov, E. H. Ivanova, Determination of the trace element content in Bulgarian bottled potable waters by total reflection X-ray fluorescence analysis	840
The 2nd Asia-Pacific Conference on Engineering Technology (APCET 2014)	845
Xu Han, Lei Cai, Huiping Deng, Jun Shi, The study of TiO ₂ -ZrO ₂ preparation and its elimination efficiency on triclosan	847
Xudong Jiang, Zhedong Yuan, Xiong Yu, Weicheng Zhou, Synthesis and antimicrobial activity of some new 1β-methylcarbapenem derivatives having pyrrolidine or piperidine moieties	852
	943

<i>Qing Lin, Zhimin Ji, Haifu Huang, Yun He, Jianmei Xu</i> , Spin-glass behavior and magnetic studies of nickel-iron multi-metal Prussian blue complexes $\text{Ni}_{0.75}\text{Cu}_{0.75}[\text{Fe}(\text{CN})_6]\cdot 6.3\text{H}_2\text{O}$	857
<i>Zhijun Zhang, Yuekai Zhang, Shiwei Zhang, Tianyi Su, Wenhui Zhang, Yuanhua Xie, Lili Zhao</i> , Capillary pressure effect on vacuum drying process of porous medium modeling	864
<i>Dongxiao Niu, Yan Lu, Di Wu</i> , Development of a novel thermal storage molten-salt filled with nanoparticles for concentration solar plants	873
<i>Chen Yingjie, Liu Zhipeng, Dai Peigang, Liu Lan</i> , The effect of flame retardant additives on the combustion performance of flexible polyurethane foam	882
<i>Y. M. Wang, W. Z. Wang, Z. L. Shao, D. M. Wang, G. Q. Shi</i> , Innovative prediction model of carbon monoxide emission from deep mined coal oxidation	887
<i>D.Z. Yang, F.D.Chen, Y.B. Zhou, Z.L. Xiu</i> , QSAR study on the pheromone of the turnip moth <i>Agrotis segetum</i> used as RDF descriptor	896
<i>Wei Cai, Guo Zhen Xie, Jun Ming Li, Le Xian Zhu, Shi Lin Ddong</i> , Effect of thermophysical properties on forced convective hot air drying of multi-layered porous materials	903
<i>Wei Cai, Wei Gu, Lexian Zhu, Wen Lv, Chunli Xia, Bo Ding</i> , Photocatalytic oxidation of gaseous acetone and ethanol mixtures over titanium dioxide powders	911
<i>Erratum</i>	918
<i>AUTHOR INDEX</i>	919
<i>AUTHORS INDEX (IN BULGARIAN)</i>	926
<i>SUBJECT INDEX</i>	934
<i>SUBJECT INDEX (IN BULGARIAN)</i>	937
<i>INSTRUCTIONS TO THE AUTHORS</i>	941

СЪДЪРЖАНИЕ

<i>А. Гариб, Л. Вожданифард, Н. Норузи Песян, Б. Р. Хашеми Пур Хорасани, М. Джакхангир, М. Рошани</i> , Синтеза на бис-2,3-дихидрохиназолин-4(1H)-они и тяхни производни с помощта на Preyssler ^o ви наночастици (SPNP) върху подложка от силициев диоксид	679
<i>Ф. Надери</i> , Числено изследване на най-малките ексоедични функционализирани фулерени, C ₂₀ X ₈ (X = H, F, Cl, Br, NH ₂ , OH и CN).....	686
<i>З. Морадинеджад, А. Бахари, С. М. Агаджанпур Мир, С. Н. Мусави Кани</i> , Синтез и структурни изследвания на антраценови нанокристали, дотирани с La ₂ O ₃ , като съвременен диелектричен материал	690
<i>К.А. Ел-Шаркауи, М.М. Саид, Г. Дардас</i> , Синтеза и антитуморна активност на някои стопени хетероциклени съединения основани на цикло-хепта[<i>b</i>]тиофенови производни	699
<i>А. Горбани-Чогамарани, Г. Азади, Ш. Малакпур</i> , Прости и ефективни хетерогенни среди за окислението на уразолови производни до съответните триазолиндиони чрез <i>in situ</i> генериране на Cl ⁺	703
<i>Г.С. Сет, С.М. Хусаин, С. Саркар</i> , Ефекти на токовете на Hall и на въртенето в нестационарно магнитохидродинамично течение с естествени конвекции и топло и масопренасяне зад импулсивно движеща се вертикална плоскост при излъчване и химична реакция	718
<i>Г.Мохамеди Зиарани, А. Бадиен, Н. Лаишари, Т. Пурджафар, З. Фарахани</i> , Ефективен катализатор (SiO ₂ -Pt-SO ₃ H) за едностадийна зелена синтеза на 3,4-дихидропиримидинони/тиони	723
<i>Т.Б. Шаик, С. Ченнамсети, С.Р. Девинени, Н.Р. Шаик, Н.Д. Мундла, Дж.П. Раджкумари, Н.Р. Чамартхи</i> , Зелени, безкаталитични технологии за синтез на производни на карбамида и тиокарбамида с тетраметилгванидин (TMG) и оценяване на биологичната им активност	730
<i>Хаджихани, А. Ахмади, Б. Нахри-Никнафс</i> , Микровълнова синтеза и антимикуробна активност на производни на фосфонохидраза.....	734
<i>М.Т. Баеи, Х. Мохамедиан, С. Хашемиан, В₁₂N₁₂-наноклетка</i> като потенциален адсорбент за отстраняването на анилин в околната среда	742
<i>П. К. Мукеш Кумар, Дж. Кумар, С. Сендинатан, Р. Тамилаасан, С. Суреш</i> , Анализ на топлообмена и хидравличното съпротивление на нанофлуид от Al ₂ O ₃ като охладител в кожухо-гръбни и спирални топлообменници	749
<i>М. Атаур Рахман, А.К. Шакия, Ш. Уахаб, Н.Х. Ансари</i> , Синтеза на някои нови триадиазолови производни тяхното анти-конвулсивно действие	756
<i>А. Акбари, З. Азами-Сардуеи</i> , Прост метод за синтеза и антибактериална активност на 2-амино-3-циано-1,4,5,6-тетрахидропирано[3,2-с] хинолин-5-он производни	763
<i>Ф. Йозторк, Д. Коюнджу Зейбек, Е. Килич</i> , Волтаперометрични отнасяния на лерканидипин и анодно-адсорбционен волтаперометричен метод за анализ на фармацевтични дозировки и биологични флуиди	770
<i>Д.М. Джорджевич, А.Р. Радожоевич, М.А. Павлович, М.Г. Джорджевич, М.Н. Станкович, И.М. Филипович, С.И. Филипович</i> , Предварително геохимично изследване на карстова котловина в басейна на Сокобана в Източна Сърбия	776
<i>А. П. Падхи, С.К. Рут, Д. Панда</i> , Ефект на модификацията на зеолит А с натриева сол на карбоксиметилцелулоза (СМС).....	783
<i>Ф.В. Цветанова, К.К. Петров</i> , Влияние на рН и аерацията върху получаването на 2,3-бутандиол от глюкоза чрез <i>Klebsiella pneumoniae</i> G31	787
<i>Т.Х. Бохари, М.А. Аслам, С. Хина, Н.Б. Ризви, Х. Расуул, М. Дж. Саиф, М. Зубаир, Ш.А. Шахид Чатха, М. Риаз</i> , Минерален състав, фенолен профил, антиоксидантна и антимикуробна активност на екстракти от корени на <i>Corchorus depressus</i>	794
<i>А.М. Амани</i> , Синтеза, охарактеризиране и биологична активност на някои нови изатинови производни ...	800
<i>Дж. Гуо, Дж. Жанг, И. Юе, И. Гуо</i> , Механизъм за отстраняване на живак чрез един нов, модифициран с хидразин хидрат- пектин	805
<i>Ф.К. Аланази, А.А. Радуан, Н. Хак, И.А. Алсарра, Ф. Шакийл</i> , Валидиран UHPLC-DAD метод за количествено определяне на холестерил-сукцинил-5-флуороацилови конюгати	813
<i>С.П. Димитриеви, З. Андийч, Ж. Камберович, С.Б. Димитриеви, Н. Вукович</i> , Рециклиране на посребрен месинг за получаването чиста мед и свръх-фин сребърен прах за електрически контакти	824
<i>Р. Хаджинасири, А. Голами Орими,</i> , Синтез на стабилни фосфорни илиди с алкил-фенилкарбамати без разтворител	830
<i>М. Аббас, Н. Расул, М. Риаз, М. Зубаир, М. Аббас, Нур-ул-Хак, Н. Хаят</i> , GC-MS профилиране, антиоксидантно и антимикуробно изследване на различни части на растението <i>Carissa grandiflora</i>	839
<i>Р. Х. Георгиева, А. К. Дечева, М. Г. Караджов, С. Е. Мицев, Ю. Х. Йорданов, Е. Х. Иванова</i> , Определяне на следи от елементи в български бутилирани питейни води с помощта на рентгенофлуоресцентен анализ с пълно вътрешно отражение	844

<i>Ксу Хан, Лей Кай, Хуитинг Денг, Джун Ши</i> , Изследване на препарат от TiO_2-ZrO_2 и определяне неговата ефективност спрямо триклозан	851
<i>Ксудонг Джиаанг, Жедонг Юан, Ксионг Ю, Уейченг Жу</i> , Синтеза и анти-микотична активност на някои нови 1β -метил-карбапенем-ови производни с пирролидинови или пиперидинови половини	856
<i>Кинг Лин, Джимин Джи, Хайфу Хуанг, Юн Хе, Джиаанмей Ксу</i> , Spin-glass поведение и изследване на магнитните свойства на многометални (никел-желязо) комплекси с фероцианид $i0.75Cu_{0.75}[Fe(CN)_6]\cdot 6.3H_2O$	863
<i>Жиджун Жанг, Юекай Жанг, Шиуей Жанг, Тяньй Су, Уенху Жанг, Юанхуа Ксие, Лили Жао</i> , Моделиране на ефекта на капилярното налягане върху вакуум-сушенето в порьозна среда	872
<i>Донгсяо Ню, Ян Лу, Ди У</i> , Разработване на нова, топло-съхраняваща стопилка за соларни инсталации, запълнена с нано-частици	881
<i>Чен Йингджди, Лю Жипенг, Дай Пенганг, Лю Лан</i> , Ефект на добавки, забавящи огъня върху горенето на гъвкава полиуретанова пяна	886
<i>Я.М. Ванг, У.З. Ванг, З.Л. Шао, Д.М. Ванг, Г.К. Ши</i> , Иновативен модел за предсказване на емисии от въглероден монооксид получени при окисление на въглища на големи дълбочини	895
<i>Д.З. Янг, Ф.Чен, И.Б. Жу, З.Л. Ксю</i> , QSAR-изследване на феромони от молеца <i>Agrotis segetum</i> , използвани като RDF дескриптори	902
<i>Уей Кай, Гуо Жен Ксие, Джун Минг Ли, Ле Ксианг Жу, Ши Лин Донг</i> , Ефект на термофизичните свойства върху принудените конвекции при сушенето на много-слойни порьозни материали	910
<i>Уей Кай, Уей Гу, Лексиан Жу, Уен Лв, Чунли Ксиа, Бо Динг</i> , Фотокаталитично окисление на газообразни смеси от ацетон и етанол върху прахове от титанов диоксид	917
<i>Поправка</i>	918
<i>АВТОРСКИ УКАЗАТЕЛ НА АНГЛИЙСКИ</i>	919
<i>АВТОРСКИ УКАЗАТЕЛ НА БЪЛГАРСКИ</i>	926
<i>ПРЕДМЕТЕН УКАЗАТЕЛ НА АНГЛИЙСКИ</i>	934
<i>ПРЕДМЕТЕН УКАЗАТЕЛ НА БЪЛГАРСКИ</i>	937
<i>ИНСТРУКЦИЯ ЗА АВТОРИТЕ</i>	941